Argonne NATIONAL LABORATORY

ANL-07/29

Physics Division Annual Report 2006

About the Cover

Students and teachers from the first "Rickover High School Experience", a week long summer camp for top academic students from the Rickover Naval Academy, a magnet school in downtown Chicago. The school was held in the Physics Division and covered "hands on" experiments, lectures, tours, and career discussions. In future years the school will expand to cover Chemistry and Biology, and have participation from other schools.

About Argonne National Laboratory

Argonne is a U.S. Department of Energy laboratory managed by UChicago Argonne, LLC under contract DE-AC02-06CH11357. The Laboratory's main facility is outside Chicago, at 9700 South Cass Avenue, Argonne, Illinois 60439. For information about Argonne, see www.anl.gov.

Availability of This Report

This report is available, at no cost, at http://www.osti.gov/bridge. It is also available on paper to the U.S. Department of Energy and its contractors, for a processing fee, from:

U.S. Department of Energy
Office of Scientific and Technical Information
P.O. Box 62
Oak Ridge, TN 37831-0062
phone (865) 576-8401
fax (865) 576-5728
reports@adonis.osti.gov

ANL-07/29

ARGONNE NATIONAL LABORATORY
9700 S. Cass Avenue
Argonne, Illinois 60439-4801

PHYSICS DIVISION ANNUAL REPORT 2006

Robert V. F. Janssens
Director

December 2007

Preceding Annual Reports
ANL-04/22 2003
ANL-05/61 2004
ANL-06/53 2005

Edited by Jeannie Glover

FOREWORD

This report highlights the activities of the Physics Division of Argonne National Laboratory in 2006. The Division's programs include the operation as a national user facility of ATLAS, the Argonne Tandem Linear Accelerator System, research in nuclear structure and reactions, nuclear astrophysics, nuclear theory, investigations in medium-energy nuclear physics as well as research and development in accelerator technology. The mission of nuclear physics is to understand the origin, evolution and structure of baryonic matter in the universe – the core of matter, the fuel of stars, and the basic constituent of life itself. The Division's research focuses on innovative new ways to address this mission.

The cover of this report illustrates a new initiative in the Division: the one-week summer school for high school students from the Rickover Naval Academy, a magnet school in the Chicago Public Schools system. This one-week program was organized by members of the Division with the aim of exposing the students to the potential and the excitement of a scientific career through active participation in a number of activities. The opportunities ranged from hands on experiments to lectures about contemporary physics issues, from presentations by scientists about their careers to tours of some of Argonne's main research facilities. The Division views education as a key part of its mission and as such is involved in many other programs at the undergraduate, graduate and post-doctoral levels, mostly coordinated by Argonne's Division of Educational Programs. This report also highlights efforts towards increasing the number and quality of minority students in science.

During 2006, progress towards the Californium Rare Ion Breeder Upgrade (CARIBU) has been brisk. This project, with a 2009 completion date, will enhance the research potential at ATLAS by making hundreds of neutron-rich nuclei available for research at energies in the vicinity of the Coulomb barrier. As this report shows, the design of most major components has been completed and the project is moving into the production phase.

Argonne also continues to lead in the development of new technical concepts required for an advanced exotic beam facility. Highlights of developments during 2006 are too numerous to be listed here, but include the initial operation of a new clean room and surface processing facility for superconducting cavities, a joint venture with Fermilab, full power tests of the prototype module of a cw RFQ for the high-power driver linac, and the construction of a dedicated facility for high-intensity tests of a large-scale prototype gas catcher.

Notable results from ATLAS include the discovery of the first excited state in ^{101}Sn, which provides the first experimental information on the energy separation between the neutron $d_{5/2}$ and $g_{7/2}$ single-particle orbits outside doubly-magic ^{100}Sn, and the completion of work related to the determination of the E1 component of the $^{12}C(\alpha,\gamma)^{16}O$ reaction rate at energies essential for nuclear astrophysics. The impact of the hindrance of fusion at extreme sub-barrier energies, a phenomenon discovered at ATLAS a few years ago, on reactions of importance in astrophysics such as $^{12}C + ^{12,13}C$, $^{12}C + ^{16}O$, and $^{16}O + ^{16}O$ has been quantified. High-precision mass measurements of neutron-rich fission fragments in the A ~ 140 region with the Canadian Penning Trap suggest that the neutron drip line may not be located as far out in neutron number as previously thought.

In medium-energy physics, preparations to search for an electric dipole moment in ^{225}Ra have advanced considerably: not only were ^{225}Ra atoms optically trapped, but the beneficial effect of blackbody radiation on the trap was discovered. Preparations are well underway for a super-Rosenbluth measurement of electron-proton elastic scattering. The ultimate goal of this program is the elucidation of the existing discrepancies between the results obtained with this technique and those derived from polarization transfer for the charge and magnetization distributions of the proton. Preliminary results from experiment E03-103 at Jefferson Laboratory indicate that the EMC effect in ^{4}He is nearly identical to that in ^{12}C, suggesting that the nuclear dependence of this effect scales with density rather than mass.

In nuclear theory, Green function quantum Monte Carlo calculations of the rms radii of the helium isotopes were extended to ^{8}He in preparation for an upcoming experiment. In an effort to account for the hindrance of fusion between complex nuclei, it was shown that this phenomenon can be understood in a coupled-channels approach by using an ion-ion potential in the entrance channel that has a shallow pocket, linked to nuclear incompressibility. At the level of quantum chromodynamics, important progress continues to be made using the Dyson-Schwinger equations. For example, a constraint on the convergence radius of chiral perturbation theory was developed and a prediction made for the ratio of the neutron electric and magnetic form factors. At the level of meson and baryon degrees of freedom, efforts to develop a dynamical coupled-channels model have progressed to the point where hadronic interactions have been determined from the fitting of pion-nucleon scattering data up to 2 GeV. The group also continues to play the lead role in directing the Excited Baryon Analysis Center at Jefferson Laboratory.

The progress that has been made in meeting the exciting intellectual challenges of modern Nuclear Physics reflects the talents and dedication of the staff of the Physics Division as well as that of the many visitors and students who bring so much to the research. The year 2006 was a particularly challenging one from the fiscal point of view, and this report is testimony to the resourcefulness of everyone. In particular, the Division owes a debt of gratitude to its Director during these challenging times, Don Geesaman. With vision and enthusiasm he kept the focus of everyone on the physics issues at hand.

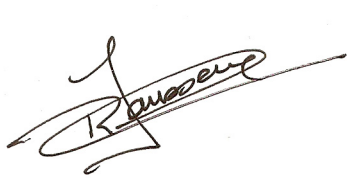

Robert V. F. Janssens, Director

TABLE OF CONTENTS

I. LOW-ENERGY NUCLEAR PHYSICS RESEARCH

OVERVIEW

The low-energy nuclear research program is focused on the fundamental study of the many-body quantum system that is the atomic nucleus. Much recent interest in this field derives both from the many and strong interrelations this field has with fundamental studies of astrophysics and cosmology, as well as applications in medicine, energy generation, national security and defense. The nuclear physics is constantly evolving and recently a stronger emphasis has been placed on the study of nuclei far from stability – both on the neutron and proton-rich sides of the line of stability. The Argonne nuclear physics program is, therefore, concerned with many of the most pressing questions in the field. Some highlights are listed below:

- The study of reactions and nuclear structure of importance for the nucleosynthesis in stellar environments is a central part of the program, which for many studies uses the radioactive beams from the ATLAS in-flight facility. Recent work in this area includes studies of the $^{12}C(\alpha,\gamma)$ reaction – one of the most important reactions in nucleosynthesis – as well as the triple α-reaction, which produces the carbon that is essential for all known life forms.

- In weak interaction physics, a central question is whether the neutrino – now known to have mass – is its own antiparticle, which would allow neutrinoless double beta decays, $0\nu\beta\beta$, in $0^+ \rightarrow 0^+$ transitions. Such transitions have not yet been conclusively identified, but even if they were, the interpretation of the transition strength in terms of the neutrino mass depends sensitively on the occupation of valence orbits in both the parent and daughter nucleus. A program to experimentally determine these properties in the relevant nuclei near ^{76}Ge has been undertaken in collaboration with Yale University and the Research Center for Nuclear Physics, Osaka.

- Efforts in the study of heavy elements are aimed at understanding the single particle structure in transfermium nuclei, in particular the orbits that are associated with the expected spherical shell gaps in super-heavy nuclei. Two recent studies have identified the location of the [521]½ proton orbital and the 2-qp {[734]9/2,[624]7/2} neutron configuration in ^{254}No and ^{252}No, respectively. These findings provide important experimental information for improving theoretical models used to predict the stability of nuclei in the super-heavy region.

- The study of nuclei far from the stability is a central theme in modern nuclear structure research. The neutron-rich nuclei offer a rich area for studies of possible changes in the spin-orbit strength, the development of a new "sub-shell" at $N = 32$-34, and the use of the deep-inelastic reaction to reach very neutron-rich nuclei, *e.g.,* the doubly-magic ^{78}Ni.

- The nuclei along the $N = Z$ line offers the opportunity to study *n-p* pairing and the isospin mirror symmetry, and recently a glimpse of the single neutron structure outside the ^{100}Sn doubly-closed shell has been obtained – a long anticipated achievement.

- Interesting dynamical features in the continuum γ-ray emission during the spin-down of super-deformed ^{152}Dy and ^{194}Hg have been discovered, which give rise to rotational damping in these systems and as well as ergodic rotational bands in ^{194}Hg.

- A small, but successful, effort is devoted to the study of heavy-ion fusion at deep sub-barrier energies, where a hindrance of the fusion probability was previously discovered. The present focus in this work is on the characterization of this phenomenon and extension of experiments to lighter systems, some of which play a strong role in carbon and oxygen burning in Type Ia supernovae explosions. The study of relativistic heavy-ion collisions with the PHOBOS collaboration at RHIC is in the process of phasing out with the publications of the final results from this work.

- A number of exciting technical developments have been progressing over the past year. Chief among them is the construction of the CARIBU radioactive ion injector at the ATLAS facility. When complete, this system will provide a wide range of very neutron-rich beams derived from ^{252}Cf fission fragments, albeit at low intensity, which will enable the study of, *e.g.*, the single particle structure near doubly-magic ^{132}Sn as well as a wide range of both lighter and heavier neutron-rich nuclei. In order to take advantage of these beams, a novel, high-acceptance spectrometer, HELIOS, is being constructed, which is designed for studying light-ion transfer reactions in inverse kinematics with such beams.

- Other important technical developments include the Argonne contribution to the GRETINA γ-tracking array, completion of the Argonne Implantation – Decay Array (AIDA), using planar HPGe detectors for polarization measurements, and the development of portable γ-ray detector systems for Homeland Security applications.

A. REACTIONS OF ASTROPHYSICAL IMPORTANCE

The study of nuclear processes and quantum states which are of relevance for the energy production and the synthesis of heavier elements in stars and explosive stellar processes, such as Type Ia supernovae, gamma-ray bursts, etc., are critical components of the ATLAS research program.

a.1. Expectations for ^{12}C and ^{16}O Induced Fusion Cross Sections at Energies of Astrophysical Interest (C. L. Jiang, K. E. Rehm, B. B. Back, and R. V. F. Janssens)

Fusion reactions between light heavy-ions such as ^{12}C and ^{16}O play an important role in the history of stellar evolution, especially in the interior of highly developed stars (like carbon and oxygen burnings, type Ia supernovae, etc.), where these reactions are important routes for the production of heavier nuclei. Although these processes occur in explosive scenarios at high temperatures, the Gamow energies are still extremely low, resulting in very small cross sections, which in many cases are not yet experimentally accessible. One has, therefore, to rely on phenomenological extrapolation methods, *e.g*., optical model calculations, which are often used to analyze fusion reactions of light heavy-ion systems. Extrapolations based on the optical model analysis give astrophysical *S* factors that increase continuously while the energy decreases. This result is somewhat at variance with the data. Instead, a maximum of the *S* factor has been recently observed in many medium-heavy systems where it was interpreted as a new fusion hindrance effect occurring at extreme sub-barrier energies.[1] It was concluded in a systematic study (see Ref. 2) that there may be a hindrance behavior for light heavy-ion fusion reactions too. We have, therefore, studied the effect of the hindrance behavior for lighter systems, using the systematics obtained from the fusion reactions of both heavier and lighter nuclei.[2] This effect will introduce a substantial change in the extrapolated *S* factor and consequently also in the calculated astrophysical reaction rates. The extrapolations for three reactions $^{12}C + ^{12}C$, $^{12}C + ^{16}O$ and $^{16}O + ^{16}O$ are reexamined in the present study.

For example, the fusion reaction $^{16}O + ^{16}O$, a temperature of $T_9 = 3$ corresponds to an effective energy of ~7 MeV, which is about the energy of the lowest data point measured so far. The calculated reaction rates for three extrapolations are presented in Fig. I-1a, *i.e.,* Hulke *et al.,* (dot-dashed line[3]), Fowler *et al.* (dashed line[4]) and the present analysis (solid line). Here the rate of Hulke *et al.* is higher than that of Fowler *et al*. reflecting the fact that Hulke's *S(E)* factor is always higher. The difference between the two rates is about a factor of 5 at lower temperatures, and decreases to a factor of 2 at higher temperatures. The results from the present extrapolation which includes the fusion hindrance behavior, are much smaller than the other two, except at temperatures above $T_9 \sim 2$, consistent with the difference in the *S* factors discussed above.

The relations of reaction rates calculated for the fusion reactions $^{12}C + ^{16}O$ and $^{12}C + ^{12}C$ for the previous and present extrapolation are similar to $^{16}O + ^{16}O$.

The ratios of reaction rates calculated from the present extrapolation to Fowler's compilation[4] for the three fusion reactions $^{12}C + ^{12}C$, $^{12}C + ^{16}O$ and $^{16}O + ^{16}O$ are summarized in Fig. I-1b as red, black and light-blue bands, respectively. Obviously, the influence of fusion hindrance is more pronounced for the reaction $^{16}O + ^{16}O$. At a temperature of $T_9 \sim 1.0$ the ratios differ by factors of up to 100. For the reactions $^{12}C + ^{16}O$ and $^{12}C + ^{12}C$, the differences of the ratios are in the range 1.5-3 and 1-5, respectively. At lower temperatures, the differences increase rapidly.

Since the physical nature of fusion hindrance at extreme low energies is still a matter of debate, many questions need to be answered by future experiments and better theoretical treatments. The extrapolation method presented in this paper is only a first step which hopefully will trigger future fusion measurements as well as theoretical studies of these important light heavy-ion systems and improves our understanding of the reaction mechanism at extremely low energies. The detailed result of the present study has been published in Ref. 5.

[1]C. L. Jiang *et al*., Phys. Rev. Lett. **89**, 052701 (2002); Phys. Rev. C **69**, 014604 (2004); Phys. Rev. Lett. **93**, 012701 (2004); Phys. Rev. C **71**, 044613 (2005); Phys. Lett. **B540**, 18 (2006).
[2]C. L. Jiang *et al.,* Phys. Rev. C **73**, 014613 (2006).
[3]G. Hulke *et al.,* Z. Phys. **A297**, 161 (1980).
[4]W. Fowler, G. Caughlan, and B. Zimmerman, Annu. Rev. Astrophys. **13**, 69 (1975).
[5]C. L. Jiang *et al.,* Phys. Rev. C **75**, 015803 (2007).

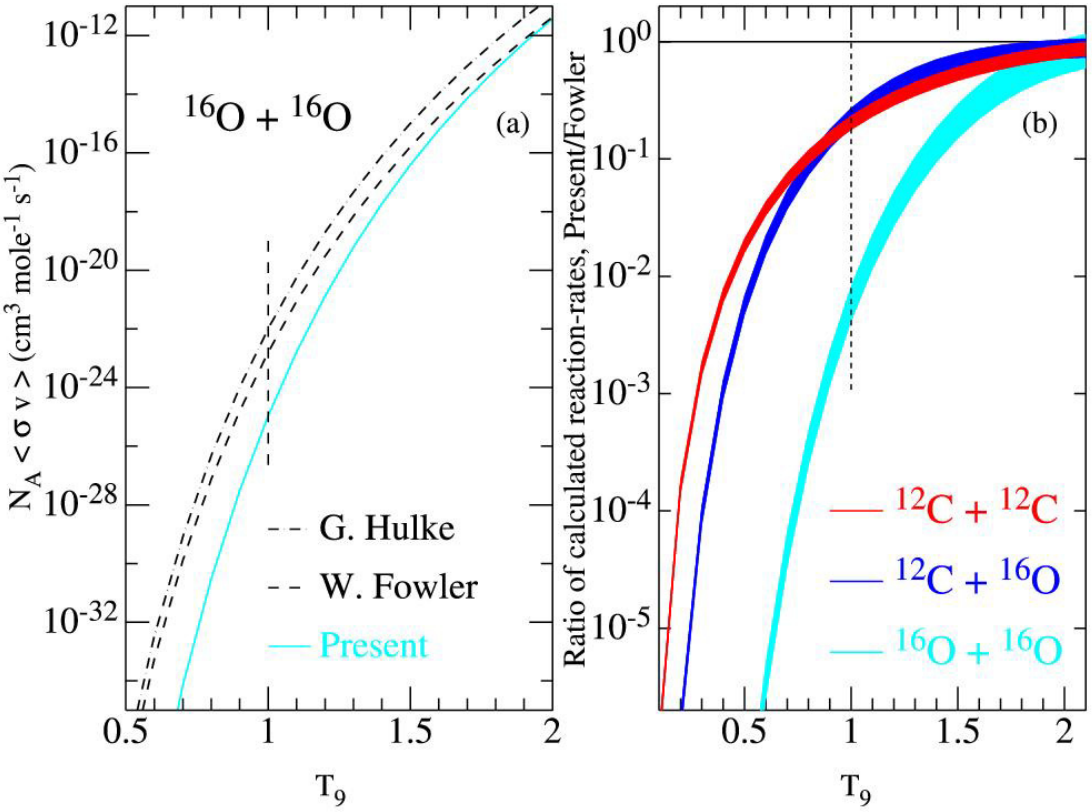

Fig. I-1. (a) Calculated fusion reaction rates for the system $^{16}O + ^{16}O$. (b) Ratio of calculated reactions rates (present to Fowler's) for systems $^{16}O + ^{16}O$, $^{12}C + ^{16}O$ and $^{12}C + ^{12}C$.

a.2. A New Measurement of the E1 Component of the $^{12}C(\alpha,\gamma)^{16}O$ Cross Section at Low Energies

(X. D. Tang, K. E. Rehm, I. Ahmad, J. Greene, A. Hecht, D. Henderson, R. V. F. Janssens, C. L. Jiang, D. Kahl, F. Moore, M. Notani, R. C. Pardo, N. Patel, G. Savard, J. P. Schiffer, S. Sinha, B. Shumard, M. Paul,* A. Champagne,† C. Brune,‡ L. Jisonna,§ R. E. Segel,§ and A. Wuosmaa¶)

Measurements of the β-delayed α decay of ^{16}N provide the tightest constraints for determining the E1 component of the α-capture reaction $^{12}C(\alpha,\gamma)^{16}O$. In these experiments S_{E1} is extracted from the height of a small satellite peak in the α-energy spectrum. This peak, which originates from the interference between the subthreshold 1^- state at E_x = 7.117 MeV and the higher-lying 1^- state at E_x = 9.585 MeV, has been studied by several groups in the past,[1,2] all of them using Si surface barrier detectors. These detectors are sensitive to β particles, have dead layers and are prone to deterioration effects during long measurements.

Because of the importance of the $^{12}C(\alpha,\gamma)^{16}O$ reaction in nuclear astrophysics, we have remeasured the ^{16}N decay using a different approach. To reduce the

sensitivity to electrons from the beta decay we have developed an array of high acceptance ionization chambers of minimal thickness to be used for the coincident detection of ^{12}C and α particles following the ^{16}N decay. Special emphasis has been put on measuring backgrounds simultaneously using the identical geometry. A schematic of the setup and a description of the procedure used in the experiments were given in last year's annual report.

Figure I-2 shows the coincident events measured in the upstream and downstream parts of the detector. On the left the decay events of ^{16}N implanted into a 17 $\mu g/cm^2$ thick carbon foil are presented, while on the right a background spectrum for the same detector is shown. The two groups with the highest count rate seen in the left part of Fig. I-2 correspond to ^{12}C-α coincidences in the up- and down-stream detectors, respectively. The two groups exhibit a tail caused by energy-loss straggling of the low energy ^{12}C particles in the carbon foil. The groups observed close to the y-axis are caused by ^{16}N decays, where either the ^{12}C or the α particle is stopped in the target frame, so that only part of the corresponding energy is detected. In a first pass of the analysis we discuss the events in the lower right part of the spectrum which are not effected by the target frame. The resulting α spectrum is shown in Fig. I-3. The insert in Fig. I-3 shows a comparison of the low-energy part of our spectrum with the results from earlier experiments, given by the dashed[1] and solid[2] lines.

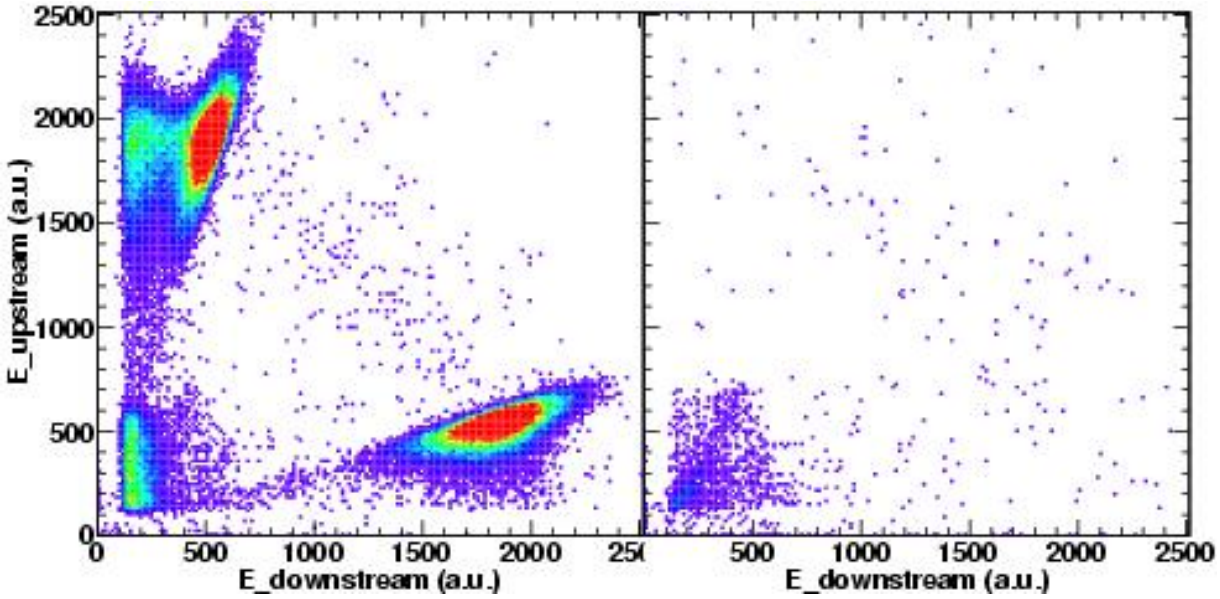

Fig. I-2. (Left) coincident energy spectrum, measured with one of the twin-ionization chambers for a foil with implanted ^{16}N particles. (Right) same as above, but for a non-implanted foil.

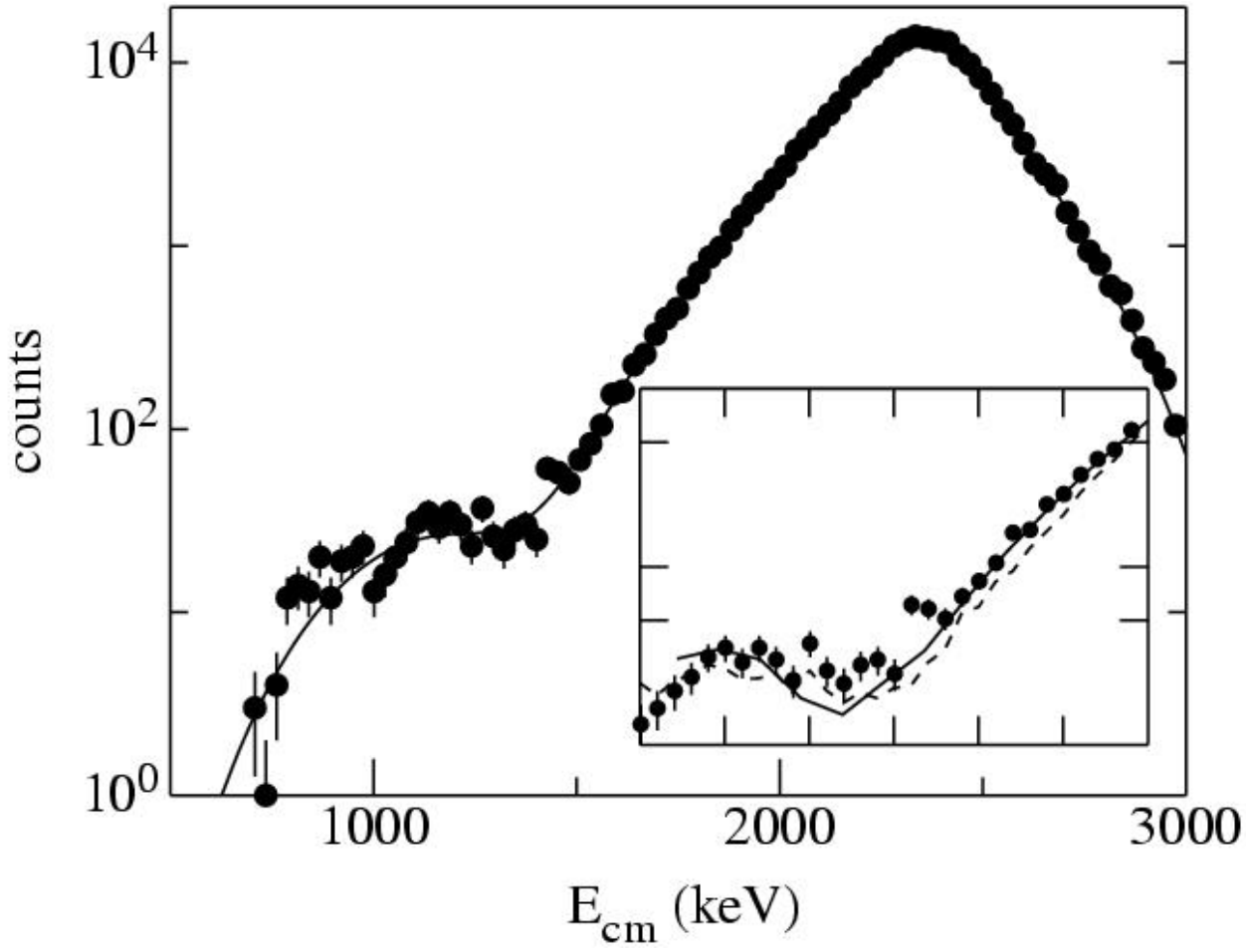

Fig. I-3. Summed α spectrum in comparison with an R-matrix fit. The insert shows the low-energy part of the spectrum together with the previous results. (dashed line: Ref. 1, solid line: Ref. 2).

Extracting the relevant *S*-factor S_{E1} from the data is usually done using the R-matrix formalism with a least-squares fit to data from the β-delayed α decay of ^{16}N, in combination with experimental results of the capture reaction $^{12}C(\alpha,\gamma)^{16}O$, performed at higher energies, as well as with phase shift parameters obtained from elastic scattering $^{12}C(\alpha,\alpha)$. There are a large number of free parameters (~14) which in some cases show strong correlations. We have used the R-matrix program from Ref. 2 together with the same phase shift and capture data. From this fit we obtain S_{E1} = 74 ± 21 keVb, including a systematic uncertainty of 10 keVb, which is dominated by the ±5 keV uncertainty of the energy calibration.

There are new data available for some of the other inputs used in the fits. With the phase shifts of Ref. 3, which are not yet available in tabulated form, the S_{E1} value increases to about 88 ± 18 keVb. A similar sensitivity of S_{E1} was observed when the β-branching ratio of the sub-threshold 1^- state was increased by about 10%, as suggested by a recent experiment (see following contribution). Using the newest set of α capture data,[4-6] however, does not change S_{E1} appreciably. The results of the fits are summarized in Table I-1. A paper describing these results has been published in Phys. Rev. Lett.[7]

We are presently analyzing the full data set, which requires a cut in the emission angle of the ^{12}C and α particles. A paper with the whole data set, including a detailed description of the twin-ionization chambers is under preparation. The strong sensitivities to the fit parameters indicate that improved measurements for all input parameters as well as a better theoretical description are needed in order to reduce the uncertainties in the $^{12}C(\alpha,\gamma)^{16}O$ reaction rate.

Table I-1. S_{E1} values obtained from R-matrix fits with different input parameters. See text for details.

Source of ^{16}N data	S_{E1} (keVb)	χ^2	Other data used in fit
Ref.1	79 ± 21	1.6	
This work	74 ± 21	2	Standard input
	88 ± 18	2.9	Phase shift from [3]
	70 ± 20	2	New β-branching ratio
	73 ± 21	1.7	(α,γ) data from [4-6]
	85 ± 18	2.7	Data from [3-6]

*The Hebrew University of Jerusalem, Israel, †University of North Carolina, ‡Ohio University, §Northwestern University, ¶Western Michigan University.

[1]R. Azuma *et al*., Phys. Rev. C **50**, 1194 (1994), L. Buchmann *et al*., Phys. Rev. Lett. **70**, 726 (1993).
[2]Z. Zhao *et al*., Phys. Rev. Lett. **70**, 2066 (1993).
[3]L. Buchmann and C. Barnes, Nucl. Phys. **A777**, 254 (2006).
[4]R. Kunz *et al*., Phys. Rev. Lett. **86**, 3244 (2001).
[5]R. Kunz *et al*., Astrophys. J. **567**, 643 (2002).
[6]M. Assunção *et al*., Phys. Rev. C **73**, 055801 (2006).
[7]X. D. Tang *et al*., Phys. Rev. Lett. **99**, 052502 (2007).

a.3. The Branching Ratio of the Subthreshold 1$^-$ State in the β-Decay of ^{16}N

(K. E. Rehm, X. D. Tang, G. Savard, M. P. Carpenter, J. P. Greene, R. V. F. Janssens, C. L. Jiang, T. Lauritsen, C. J. Lister, M. Notani, N. Patel, R. C. Pardo, J. P. Schiffer, S. Zhou, and M. Paul*)

In the last three years we have been involved in an experiment to study the $^{12}C(\alpha,\gamma)^{16}O$ reaction, which has often been called the most important reaction in nuclear astrophysics. In this experiment we measured the beta-delayed α decay of ^{16}N, using a new setup of high-efficiency twin-ionization chambers. The final error in determining the astrophysically important S_{E1} of the $^{12}C(\alpha,\gamma)^{16}O$ reaction has contributions coming from the statistics as well as from systematic uncertainties. The three main contributions to the systematic uncertainties originate from the energy calibration of the α spectrum, from the ^{17,18}N contaminations in the beam and from the β-branching ratio, populating the two 1$^-$ states in ^{16}O.

Because of the strong dependence on the α energy calibration, special emphasis has been put in our experiment on obtaining good energy calibrations. In order to bracket the main alpha peak from the decay of ^{16}N, we have produced a "sandwich" source consisting of layers of 10 μg/cm^2 thick ^{6}LiF and ^{10}B, evaporated on the two sides of a 17 μg/cm^2 thick carbon target. From this, alpha lines of 2.056,1.776 and 1.472 MeV were obtained, with thermal neutrons from a PuBe source, through the (n,α) reaction. The thickness of these foils was determined with a ^{228}Th source using the split pole spectrograph. The stability of the ionization chamber calibration during a two-week long run was checked during the experiment with daily ^{10}B calibrations and was found to be better than ±2 keV. In addition, pulser calibrations and linearity tests have been performed before and after the experiment. With all these tests we obtained for the whole run an energy calibration with an accuracy of ±5 keV, which is a factor of four better than the energy calibration obtained in Ref. 1. Because of the ^{16}N production technique used in this experiment, we do not have to apply a correction for the presence of ^{17,18}N components in the beam.

The next highest systematic uncertainty comes from the branching ratio populating the two 1$^-$ states in ^{16}O. We have, therefore, performed an experiment at Gammasphere to reduce the uncertainty of the β-branching ratio of the sub-threshold 1$^-$ state in ^{16}O at 7116.9 keV that was previously measured to be 4.8(4)%.

The β-decay of ^{16}N proceeds mainly to the 3$^-$ state at 6129.9 keV, which has a precisely determined beta branching ratio of 66.2(6)%. The 3$^-$ as well as the sub-

threshold 1^- states decay almost exclusively by emission of a single high-energy gamma ray and the beta branching ratio to the 7116.9 keV state can then be determined from the relative intensities of the 7116.9 keV and 6129.9 keV gamma rays emitted in the decay of ^{16}N:

$$\frac{BR(6129)}{BR(7116)} = \frac{N_\gamma(6129)}{N_\gamma(7116)} \frac{\varepsilon_\gamma(7116)}{\varepsilon_\gamma(6129)} \quad (1)$$

where *BR(E)* is the direct beta feeding to the state at excitation energy, E, $N_\gamma(E)$ is the number of gamma rays detected at that energy and $\varepsilon_\gamma(E)$ is the detector efficiency at that gamma ray energy.

For the case of ^{16}N the efficiencies, ε_γ can be obtained from the ratio between the coincident counts $N_{\gamma\gamma}$ populating and depopulating the level of interest and the number of counts N_γ, populating the level, *e.g.*,

$$\frac{N_{\gamma\gamma}(6129-2741)}{N_\gamma(2741)} = \frac{\varepsilon_\gamma(6129)\varepsilon_\gamma(2741)}{\varepsilon_\gamma(2741)} = \varepsilon_\gamma(6129) \quad (2)$$

Combining equations (1) and (2) we obtain

$$\frac{BR(6129)}{BR(7116)} = \frac{N_\gamma(6129)}{N_\gamma(7116)} \frac{N_{\gamma\gamma}(7116-1754)}{N_{\gamma\gamma}(6129-2741)} \frac{N_\gamma(2741)}{N_\gamma(1754)} \quad (3)$$

Corrections to equation (3) due to side feeding and angular correlation effects are smaller than 1%.

The experiment was performed with a 1-2 nA 28 MeV ^{15}N beam bombarding a 10 mg/cm2 thick Ti foil, which was loaded with deuterium. The ^{16}N products, produced via the d(^{15}N,^{16}N)p reaction, were stopped in the target. A measurement cycle consisted of a 7 s long production period followed by a 7 s counting period. The gamma decays were detected with the 100 individual detectors of Gammasphere. From the analysis of the spectra and using Eq. 3 a new preliminary value for the beta branching ratio of the sub-threshold 1^- state of *BR* = 5.1(1)% has been obtained.

*The Hebrew University of Jerusalem, Israel.

[1]R. E. Azuma *et al*., Phys. Rev. C **50**,1194 (1994).

a.4. Experiments to Further the Understanding of the Triple-Alpha Process in Hot Astrophysical Scenarios (N. Patel, U. Greife, K. E. Rehm, C. L. Jiang, D. Henderson, M. Notani, and X. D. Tang)

The elements beyond the stability gaps at A = 5 and A = 8 rely in their production on the triple-alpha process, which in two steps *via* the reactions $\alpha(\alpha,\gamma)^8$Be (through the short-lived ^{8}Be ground state) and ^{8}Be$(\alpha,\gamma)^{12}$C synthesizes one crucial element of life. The great story of the universe would not have produced Carbon-based life forms if the latter reaction had not conveniently located in the Gamow window of the Helium burning Red Giant stars, an s-wave resonance combining the three alpha particles to ^{12}C. Considering the importance of Carbon nucleosynthesis, it is quite surprising how unexplored the region of excited states above the ^{8}Be$(\alpha,\gamma)^{12}$C threshold has been (since the early experiments in the 1950's – 60's)[1-6] until recently the Aarhus/Jyväskylä group has undertaken and published[7-11] several experiments looking at the alpha emission from states in ^{12}C populated by beta decay of ^{12}B and ^{12}N. These new measurements require a rethinking of the level structure in ^{12}C above the astrophysically most relevant level at 7.654 MeV (0^+).

In addition to the 1990 edition of Ajzenberg-Selove[12] of excited states, the recent NACRE compilation[13] assumes a 2^+ resonance at 9.117 MeV (Γ_α = 0.56 MeV)[14] for which no experimental evidence exists. Other publications [*e.g.* 15] prefer to limit their

range of astrophysical temperatures to where they think that only the well known 7.65 MeV level is relevant. In explosive scenarios like supernovae, where the temperatures up to several 10^9 K are achieved, taking only the 7.65 MeV resonance into account is not sufficient and the inclusion of either the theoretically predicted 2^+ state[13] or experimentally inferred states[7] has a significant effect. The ^{12}N and ^{12}B decay experiments performed at Jyväskylä and CERN/ISOLDE clearly show a broad resonance structure above the 7.65 MeV state. The group performed detailed R-matrix calculations of the different ways this resonance could interfere with the state at 7.65 MeV and conclude that their spectrum could not be explained by the 2^+ resonance theoretically predicted[14] and used in the NACRE compilation.[13] The assumption of a 0^+ state and its interference with the 7.65 MeV level is shown to yield a more satisfactory fit.

In order to improve the earlier experiments we have developed a new detector system that will be used for the studies of the triple alpha decay of high-lying states in ^{12}C. Stopping the ^{12}B(^{12}N) beam in a catcher foil and measuring the triple α decay in an array of Si strip detectors suffers from efficiency corrections that need to be applied especially for decays with lower energies. Stopping the beam in a Si detector and measuring the subsequent α decay, as done, *e.g.*, in our earlier ^{8}B experiment, results in "β-summing effects" that need to be corrected in the analysis. We have, therefore, developed a new detector system consisting of a pair of twin-ionization chambers (IC), filled with P10 counting gas. The system is shown in Fig. I-4.

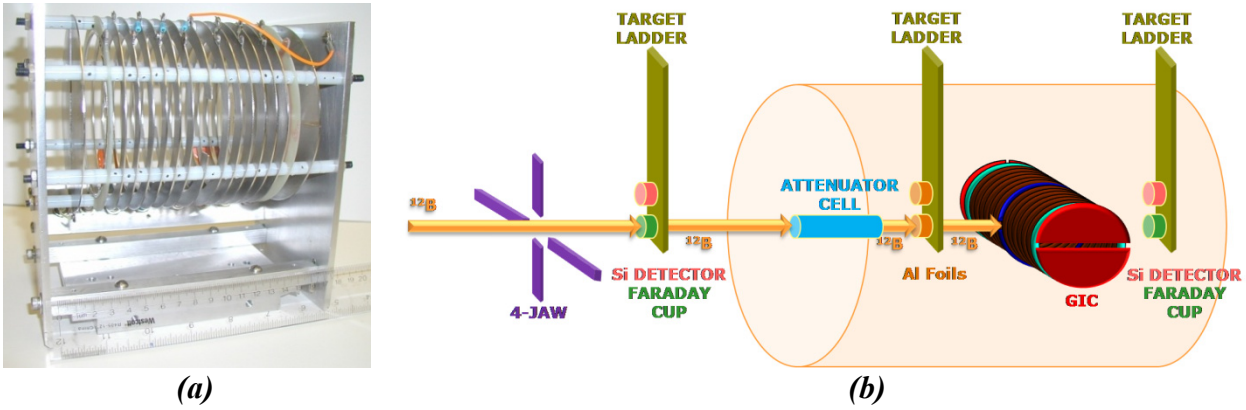

Fig. I-4. (a) Twin Frisch gridded ionization chamber (GIC) and (b) the schematic of the experimental setup.

A 72 MeV ^{12}B beam, produced *via* the d(^{11}B,^{12}B)p reaction in a cryogenically cooled gas cell, enters the ionization chamber after passing through an attenuator cell where its energy is reduced so that the ^{12}B ions are stopped in the center of the IC. The short half-life of ^{12}B (~20 ms) eliminates the need for a stopping foil and, thus, no energy corrections are needed. In phase I of the experiment we have investigated the technique of stopping the ^{12}B ions in the center of the IC. For this the beam-left anode of the IC was subdivided into an upstream and a downstream part. At a low pressure in the attenuator most of the energy from the triple α decay of ^{12}C is deposited in the downstream half of the anode, while at a higher pressure the energy is mainly deposited in the upstream half. The results are shown in Fig. I-5. In this experiment the optimum pressure for the attenuator was found to be 100 Torr. Experiments to use this detector system for measuring the triple α decay are under way.

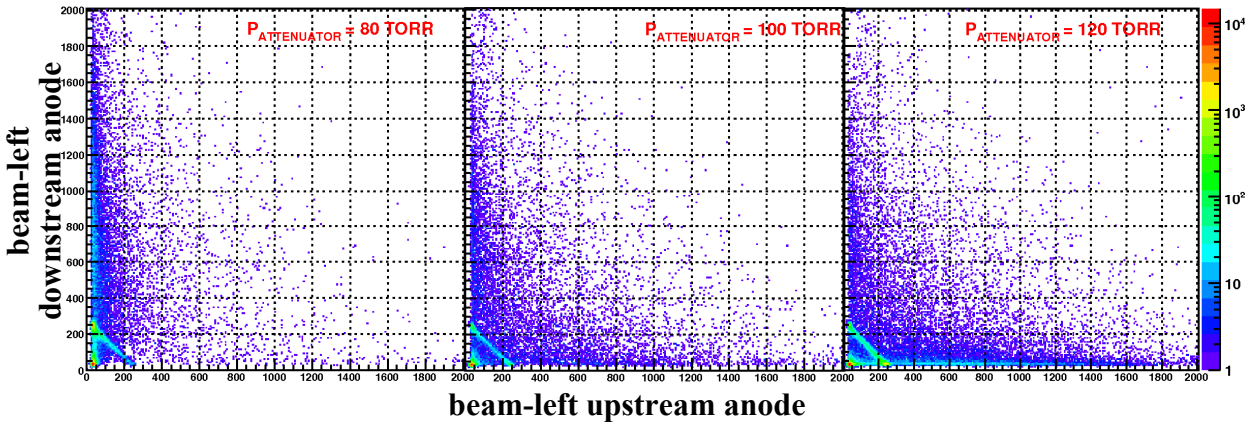

Fig. I-5. Spectra of the energy deposited in the upstream and downstream part of the twin-ionization chamber for different pressures in the attenuator cell. The pressure in the IC was 250 Torr.

[1]D. N. F. Dubar *et al.*, Phys. Rev. **92**, 649 (1953).
[2]C. W. Cook *et al.*, Phys. Rev. **107**, 508 (1957).
[3]C. W. Cook *et al.*, Phys. Rev. **111**, 567 (1958).
[4]R. W. Peterson and N. W. Glass, Phys. Rev. **130**, 292 (1963).
[5]W. C. Olsen *et al.*, Nucl. Phys. **61**, 625 (1965).
[6]D. Schwalm and B. Povh, Nucl. Phys. **89**, 401 (1966).
[7]H. O. U. Fynbo *et al.*, Nature **433**, 136 (2005).
[8]C. Au. Diget *et al.*, Nucl. Phys. **A760**, 3 (2005).
[9]H. O. U. Fynbo *et al.*, Nucl. Phys. **A718**, 541c (2003).
[10]H. O. U. Fynbo *et al.*, Phys. Rev. Lett. **91**, 082502 (2003).
[11]H. O. U. Fynbo *et al.*, Eur. J. Phys. **A15**, 135 (2002).
[12]F. Ajzenberg-Selove, Nucl. Phys. **A506**, 1 (1990).
[13]C. Angulo *et al.*, Nucl. Phys. **A656**, 3 (1999).
[14]P. Descouvemont and D. Baye, Phys. Rev. C **36**, 54 (1987).
[15]K. Langanke, M. Wiescher, and F. K. Thielemann, Z. Phys. **A324**, 147 (1986).

a.5. Study of the ^{57}Fe(*d,p*)^{58}Fe Reaction in Inverse Kinematics as Surrogate to an (*n,γ*) Reaction

(K. E. Rehm, X. D. Tang, I. Ahmad, J. P. Greene, D. J. Henderson, C. L. Jiang, R. C. Pardo, R. Scott, D. Seweryniak, R. Vondrasek, M. Paul,* P. Collon,† B. Ingel,* Y. Kashiv,*,‡ H. Nassar,* and A. Wuosmaa§)

The nuclide ^{60}Fe is thought to be predominantly produced in core-collapse supernovae (CCSN) by an (*n,γ*) reaction on the radioactive nucleus ^{59}Fe ($t_{1/2}$(*g.s.*) = 45.1 days). The observation of two lines (1173 keV and 1333 keV) in the decay of ^{60}Fe through ^{60}Co (1173 keV and 1333 keV) has been very recently reported by the Integral mission.[1] Further measurements are hoped to reveal subtle differences in the sources of the two isotopes (mass, metallicity of star, depth within the star and effect of the final explosion). Independently, a signal of live ^{60}Fe measured in a deep-sea crust[2] was interpreted as resulting from the direct deposition on Earth of ejecta from a close-by supernova (estimated to have been ~20 pc away and ~3 Myr ago). These first experimental results emphasize the importance of ^{60}Fe as an observable from CCSN's and of the understanding of its nucleosynthesis. No experimental information exists on the ^{59}Fe(*n,γ*)^{60}Fe reaction at stellar temperatures.

In order to study the possible relation between *(d,p)* and (*n,γ*) reactions in this region of nuclides (see *e.g.* Ref. 3), we investigated the reaction ^{57}Fe(*d,p*)^{58}Fe in inverse kinematics with a ^{57}Fe beam at a laboratory incident energy of 500 MeV on a CD_2 target. The

energy allows us to populate neutron unbound states in ^{58}Fe, also available in the neutron capture reaction ^{57}Fe(n,γ)^{58}Fe (Fig. I-6). The detection system is illustrated in Fig. I-7. A thick absorber (Au) had to be used in order to slow down forward-recoiling ^{58}Fe ions so as to match the electric rigidity acceptance of the FMA (Fig. I-7).

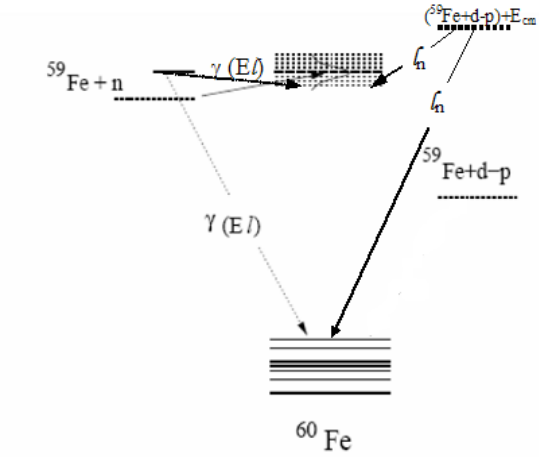

Fig. I-6. Schematic diagram of (n,γ) and (d,p) reactions.

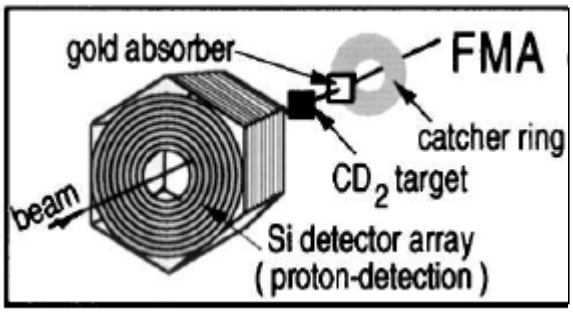

Fig. I-7. Schematic diagram of the detection system for the study of the d(^{57}Fe,p)^{58}Fe. Protons are detected at back angles in a double-sided Si strip detector and forward recoils in the FMA.

Figure I-8 shows the proton singles spectrum measured in the Si detector, showing population of discrete low-lying states; interestingly, most of the states identified are 2^+ states. Population of highly-excited states near and above the neutron separation energy (S_n = 6.1 MeV) are also strongly populated. However, owing to the thick absorber and the resulting angular scattering, the efficiency of coincidences between forward recoils (FMA) and protons (DSSD) was very low in this experiment and did not allow us to collect significant statistics on high-lying states. Moreover, the detection of neutron-unbound states requires the detection of a ^{57}Fe forward recoil and its discrimination from the high-intensity scattered beam. Use of a Ti absorber instead of Au is expected to improve the conditions. Alternative methods of detection of the forward-recoils (magnetic spectrograph, gas-filled magnet) are being also considered.

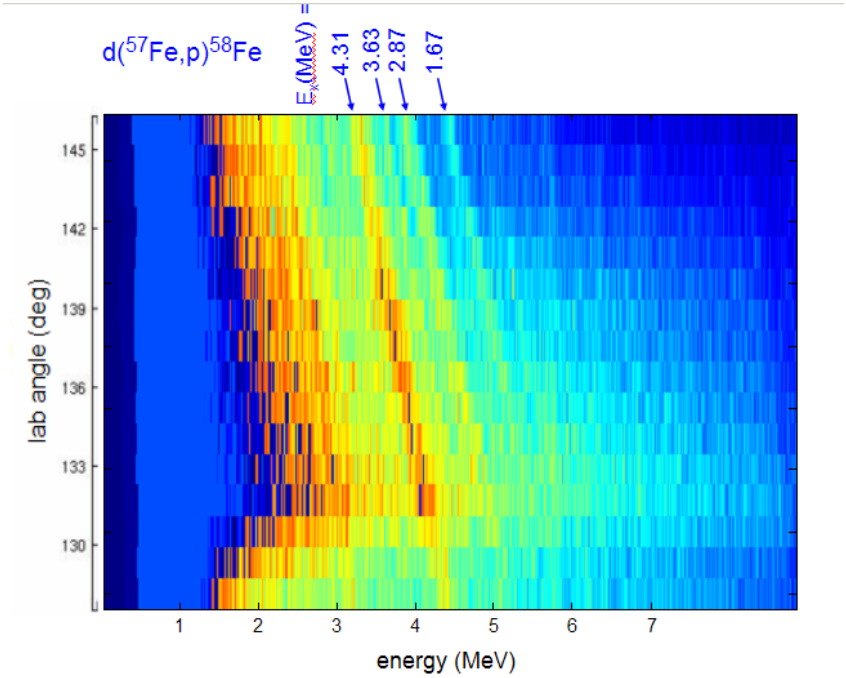

Fig. I-8. Angle vs. energy of protons detected in the backward double-sided Si strip detector. Kinematic lines corresponding to states identified in ^{58}Fe are shown.

*The Hebrew University of Jerusalem, Israel, †University of Notre Dame, ‡University of Chicago, §Western Michigan University.

[1]M. J. Harris *et al*., arXiv: astro-ph/0502219, (2005).
[2]K. Knie *et al*., Phys. Rev. Lett. **93** 171103, (2004).
[3]P. G. Hansen and J. A. Tostevin, Ann. Rev. Nucl. Part. Sci. **53**, 219 (2003).

a.6. The Spin of the 2.645 MeV State in ^{20}Na

(K. E. Rehm, J. Greene, D. Henderson, R. V. F. Janssens, C. L. Jiang, M. Notani, R. C. Pardo, J. P. Schiffer, X. D. Tang, L. Jisonna,* R. E. Segel,* M. Paul,† and A. Wuosmaa‡)

The 2.645-MeV state in ^{20}Na, the first level above the ^{19}Ne + p threshold, plays an important role in the ^{19}Ne(p,γ)^{20}Na reaction rate and, thus, in the breakout from the hot CNO cycle into the *rp*-process, which occurs in various hydrogen-rich stellar environments. However, this reaction rate is still uncertain by 2-3 orders of magnitude. This uncertainty has its origin in the two possible spin-parity assignments that have been proposed for this state in the literature. In Ref. 1, this state has been given a 1^+ assignment based on measurements of angular distributions of the ^{20}Ne(^{3}He,t) reaction. The 1^+ assignment, however, has been questioned[2] because it requires an unusually large Coulomb shift and, therefore, the authors of Ref. 2 have assigned a spin-parity of 3^+ to this level.

Because of its importance for the breakout from the hot CNO cycle in novae, several attempts have recently been made to determine the spin-parity of this state.[3,4] In Ref. 3, the structure of ^{20}Na was studied using a heavy ion fusion reaction (^{10}B + ^{12}C), but only the level structure below the proton threshold could be measured. A recent direct study of the ^{19}Ne(p,γ)^{20}Na reaction using a recoil mass separator could only give an upper limit for the resonance strength.[4]

We have performed a coincidence experiment to determine the branching ratio Γ_p/Γ_γ for the 2.645 MeV and 2.849 MeV states. These states, which lie above the proton threshold and can, therefore, decay either by γ or by proton emission, were populated *via* the ^{3}He(^{20}Ne,t)^{20}Na reaction with a 160 MeV ^{20}Ne beam

bombarding a ~50 μg/cm^2 gas cell target filled with ^{3}He and cooled to LN_2 temperatures. The outgoing tritons were detected in a 40 × 40 mm^2 double-sided Si strip detector. The coincident heavy recoils ^{20}Na (following γ-decay) or ^{19}Ne (following proton decay) were identified according to mass and nuclear charge in the focal plane detector of the Enge split-pole spectrograph. Due to the advantages of inverse kinematics this technique has a high detection efficiency.

Figure I-9 shows *Q*-value spectra obtained from the angle and energy of the tritons detected in the position-sensitive Si detector, in coincidence with ^{20}Na (blue) and ^{19}Ne (magenta) detected in the spectrograph. Because of the particle threshold at 2.199 MeV, the tritons in coincidence with ^{20}Na mainly populate states below 2 MeV, while the spectrum in coincidence with ^{19}Ne shows only states above E_x ~ 2.5 MeV. The locations of various levels in ^{20}Na are indicated by the arrows. Considerable effort has been devoted to study the backgrounds in these spectra. The requirement of a triton-heavy-recoil coincidence leads to a background suppression of three orders of magnitude. This is sufficient for the ^{20}Na spectrum which gives us confidence that the events above E_x ~ 2 MeV are free of background. A source of background in the ^{19}Ne *Q*-value spectrum is proton-^{19}Ne coincidences from the decay of proton-unbound ^{20}Na excited states. The Si strip detector could not distinguish protons from tritons and because the protons are from a three-body final state they are spread over a wide range of energy and angle. This, in turn, leads to events scattered throughout the ^{19}Ne *Q*-value spectrum including the region in ^{20}Na where proton decay to ^{19}Ne is energetically forbidden.

From the spectra shown in Fig. I-9 we can obtain estimates for the ratio Γ_p/Γ_γ. Predictions for Γ_p/Γ_γ for the states at E_x = 2.646 MeV and 2.849 MeV taken from the literature are given in Table I-2. While the restrictions on Γ_p/Γ_γ are of little help in choosing between the 1^+ and 3^+ possibilities for the 2.645 MeV state, the ratio for the two spin possibilities (3^+ and 3^-) for the 2.849 MeV state differ by almost a factor of 200. Even with the limited statistics that were achieved in this experiment the experimental ratios obtained in this measurement favor a 3^+ assignment for the 2.849 MeV state, leaving the spin-parity of 1^+ for the 2.645 MeV state. In order to finalize the limits which can be given to Γ_p/Γ_γ the efficiency of the experimental setup needs to be calculated. For this Monte Carlo calculations are presently being performed.

Table I-2. Calculated branching ratios Γ_p/Γ_γ from the reported resonance parameters taken from the literature for the 2.645 MeV and the 2.849 MeV states in ^{20}Na.

E_x (MeV)	E_r (keV)	J^π	Γ_p/Γ_γ
2.645	0.446	1^+	8.9[1]
		3^+	≤ 28.9[5]
2.849	0.650	3^+	2445[1]
		3^-	13.5[2]

*Northwestern University, †The University of Jerusalem, Israel, ‡Western Michigan University.

[1]L. O. Lamm *et al.*, Nucl. Phys. **A510**, 503(1990).
[2]B. A. Brown *et al.*, Phys. Rev. C **48**, 1456(1993).
[3]D. Seweryniak *et al*., Phys. Lett. **B590**, 170(2004).
[4]M. Couder *et al*., Phys. Rev. C **69**, 022801 (2004).
[5]T. Fortune *et al*., Phys. Rev. C **61**, 057303 (2000).

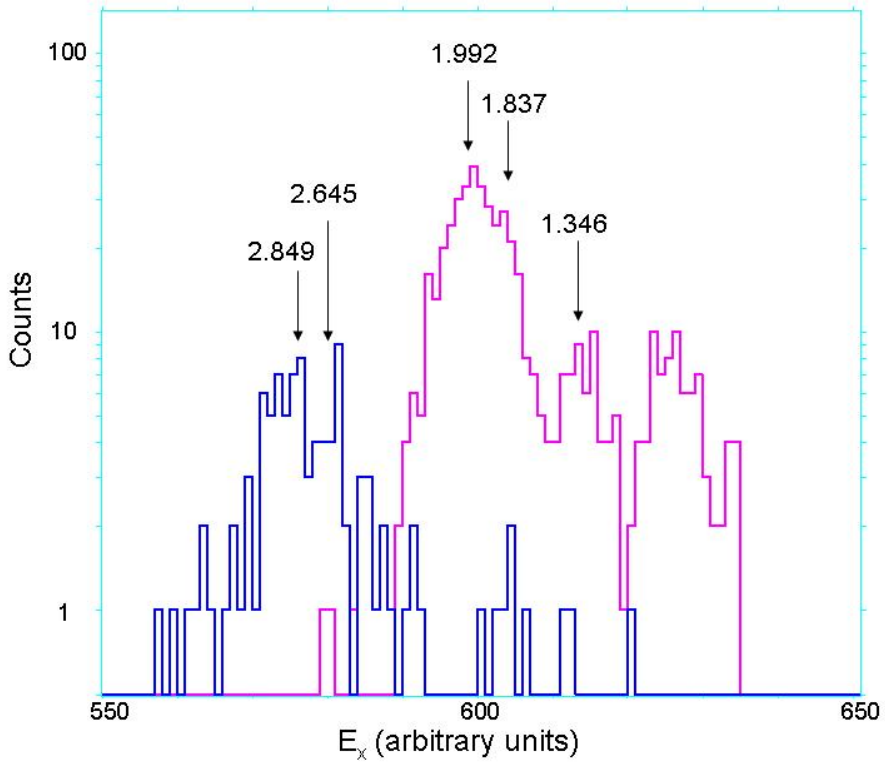

Fig. I-9. Q-value spectra for tritons coincident with ^{20}Na (magenta) and ^{19}Ne (blue) for ^{20}Na states in the excitation energy region E_x = 0.5-3 MeV.

a.7. Improved Measurement of the ^{44}Ti Half-Life from a 14-Year Long Study

(I. Ahmad, J. P. Greene, E. F. Moore, S. Ghelberg,* A. Ofan,* M. Paul,* and W. Kutschera†)

The half-life of ^{44}Ti has been determined by following the decay of ^{44}Ti and ^{60}Co for 14 years. Mixed sources containing ^{44}Ti and ^{60}Co, and pure sources of ^{44}Ti and ^{60}Co were prepared and their gamma-ray spectra were measured with Ge spectrometers once or twice a year. Measurements were performed at Argonne and at The Hebrew University of Jerusalem. Special efforts were made to check for systematic errors and these were found to be negligible within the quoted uncertainty.

The half-life values at Argonne were determined from the ratios of the counts in the 1157.0 keV peak and the 1173.2- and 1332.5 keV gamma ray peaks. These ratios were fitted as a function of the time since the beginning of the experiment with an exponential function. The slope of the fit gives the difference between the decay constants of ^{60}Co and ^{44}Ti ($\lambda\ ^{60}$Co - $\lambda\ ^{44}$Ti). The half-life was determined by using 5.2711 ± 0.0004 yr for the ^{60}Co half-life. An example of the fit is shown in Fig. I-10. The data obtained from spectra measured at source-to-detector distances of 5.2 cm and 10.2 cm were used. In addition, half-life values were determined from the spectra of the mixed source and the spectra of the pure ^{44}Ti and ^{60}Co sources. At The Hebrew University of Jerusalem, only the mixed source was used and the measurements were made at one distance. The half-life values determined from these measurements are given in Table I-3. The weighted average of all the data set gives a half-life of 58.9 ± 0.2 yr. In order to include possible systematic uncertainty, we have increased the error to 0.3 yr giving a final value of 58.9 ± 0.3 yr. The results of this study were published.[1]

Table I-3. Summary of ^{44}Ti half-life measurements. All values except those given in the last line were measured at Argonne.

Source	Distance	Number of data points	Half-life from 1157/1173 ratio[a]	χ^2/DOF[b]	Half-life from 1157/1333 ratio[a]	χ^2/DOF[b]
Measurements at Argonne						
Mixed ^{44}Ti + ^{60}Co	5.2 cm	22	58.8 ± 0.4 yr	0.97	59.0 ± 0.3 yr	1.03
Mixed ^{44}Ti + ^{60}Co	10.2 cm	19	58.7 ± 0.5 yr	1.5	58.8 ± 0.4 yr	0.95
Pure ^{44}Ti and pure ^{60}Co	5.2 cm	18	59.0 ± 0.5 yr	2.1	59.4 ± 0.6 yr	3.5
Pure ^{44}Ti and pure ^{60}Co	10.2 cm	15	58.5 ± 0.6 yr	1.8	59.2 ± 0.6 yr	2.3
Measurements at HU						
Mixed ^{44}Ti + ^{60}Co	6.7 cm	18	58.4 ± 0.5 yr	1.2	59.0 ± 0.7 yr	0.8

[a] 1σ uncertainties are given. The weighted average of all above numbers give a value of 58.9 ± 0.2 yr.
[b] DOF = degree of freedom.

*The Hebrew University of Jerusalem, Israel, †University of Vienna, Austria.
[1] I. Ahmad *et al*., Phys. Rev. C **74**, 065803 (2006).

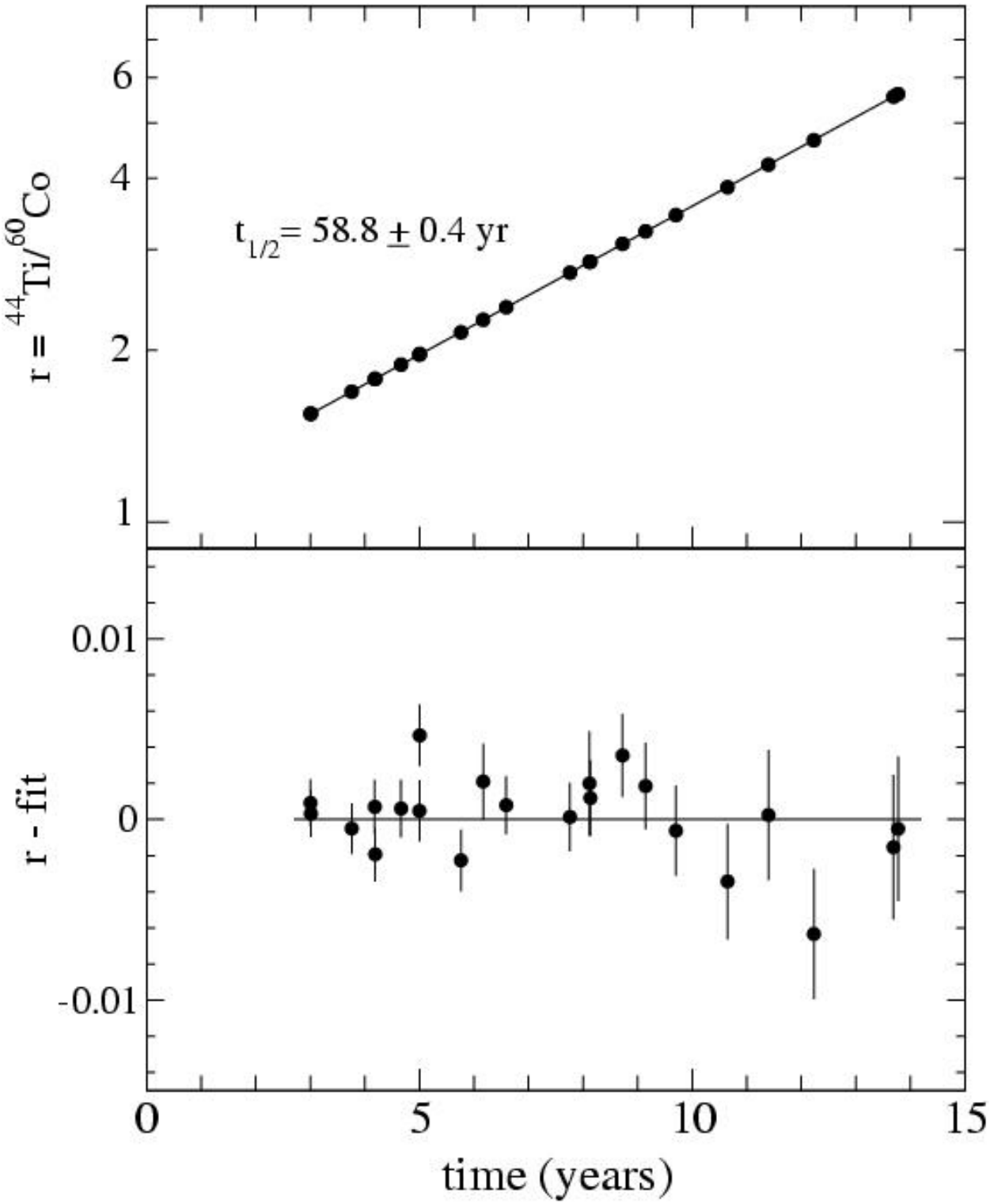

Fig. I-10. Semi-logarithmic plot of the ratios of the areas of the 1157.0 keV peak of ^{44}Ti and the 1173.2 keV of ^{60}Co peak against the time of measurement for the Argonne data. The line represents the best fit to data points and gives a half-life value of 58.8 ± 0.4 yr. The bottom figure shows the difference between the measured data points and the values calculated by the fit.

a.8. Ultra-Sensitive Detection of the *p*-Process Nuclide ^{146}Sm

(I. Ahmad, J. P. Greene, D. J. Henderson, C. L. Jiang, M. Notani, R. C. Pardo, N. Patel, K. E. Rehm, R. Scott, R. Vondrasek, N. Kinoshita,* T. Hashimoto,* T. Nakanishi,* A. Yokoyama,* H. Amakawa,† T. Mitsugashira,‡ T. Ohtsuki,§ N. Takahashi,¶ L. Jisonna,|| P. Collon,** D. Robertson,** C. Schmitt,** X. D. Tang,** Y. Kashiv,†† H. Nassar,†† and M. Paul††)

Among the very few *p*-process nuclides (see Ref. 1 for a review), ^{146}Sm is especially interesting in view of its half-life ($t_{1/2} = 1.03 \times 10^8$ yr)[2-5] and evidence for live ^{146}Sm in the Early-Solar System, established by isotopic anomalies of Nd in meteoritic material.[6] Earth crust samples themselves display an interesting anomaly in their ^{142}Nd/Nd isotopic abundance compared to bulk meteoritic material (chondrites), tentatively interpreted as resulting from fractionation between Sm and Nd due to subtle differences in their geochemical properties during planet differentiation.[7,8] The α decay of ^{146}Sm to ^{142}Nd constitutes in this case a Solar-System clock for such planetary processes, enhancing the importance of an accurate knowledge of the ^{146}Sm half-life value. This work is devoted to the development of a high-sensitivity direct detection method based on accelerator mass spectrometry (AMS). A first application will be a new determination of the ^{146}Sm half-life. The measurement will be performed using the relation $t_{146} = (A_{147}/A_{146})(N_{146}/N_{147})t_{147}$, where N_{146} (N_{147}) represent respectively the number of ^{146}Sm (^{147}Sm) atoms in a sample measured by AMS (ICP-MS), A_{146} (A_{147}) their respective α activities and t_{147} the accurately known ^{147}Sm α half-life ($(1.17 \pm 0.02) \times 10^{11}$ yr).[9]

^{146}Sm samples were produced by activation of enriched ^{147}Sm targets *via* (γ,*n*), (*n*,2*n*) and (*p*,2*n*) reactions, the latter followed by electron capture. Sm was then purified and ^{147}Sm and ^{146}Sm α-counted at Kanazawa University (Japan). The experimental method used involves: (*i*) use of sputter cathodes (reduced Sm metal) in the ECR-II ion source; (*ii*) tuning of the accelerator system with $^{80}Kr^{12+}$ (pilot beam) and/or $^{147}Sm^{22+}$ and scaling the ATLAS beam line components by the small ratio of *m*/*q*'s for $^{146}Sm^{22+}$; and (*iii*) detection of ^{146}Sm in the gas-filled Enge split-pole spectrograph (10 Torr N_2) used to disperse the isobaric ^{146}Sm and ^{146}Nd (and other background) components.[10] Figure I-11 shows α-radioactivity and AMS identification spectra measured in our experiment.

Figure I-11 demonstrates for the first time the successful identification of ^{146}Sm and its separation from stable ^{146}Nd by AMS. Efforts towards the measurement of the ^{146}Sm/^{147}Sm absolute isotopic ratios in the irradiated targets and a new determination of the ^{146}Sm half-life are underway.

*Kanazawa University, Ishikawa, Japan, †The University of Tokyo, Japan, ‡Tohoku University, Ibaraki, Japan, §Tohoku University, Miyagi, Japan, ¶Osaka University, Japan, ||Northwestern University, **University of Notre Dame, ††The Hebrew University of Jerusalem, Israel.

[1] M. Arnould and S. Goriely, Phys. Rep. **384**, 1-84 (2003).
[2] D. C. Dunlavey and G. T. Seaborg, Phys. Rev. **92**, 206 (1953).
[3] M. Nurmia *et al*., Ann. Acad. Sci. Fenn. A **VI**, 148 (1964).
[4] A. M. Friedman *et al.*, Radiochim. Acta **5**, 192-194 (1966).
[5] F. Meissner *et al*., Z. Phys. **A327**, 171-174 (1987).
[6] S. B. Jacobsen and G. J. Wasserburg, Earth Planet. Sci. Lett. **67**, 137 (1984).
[7] M. Boyet and R. W. Carlson, EPSL **250**, 254-268 (2006).
[8] R. Andreasen and M. Sharma, Science **314**, 806 (2006).
[9] N. Kinoshita *et al*., J. Nucl. Radiochem. Sci. **4**, 5 (2003).
[10] M. Paul *et al.,* Nucl. Phys. **A746**, 613 (2004), Nucl. Instrum. Methods **A277**, 418 (1989).

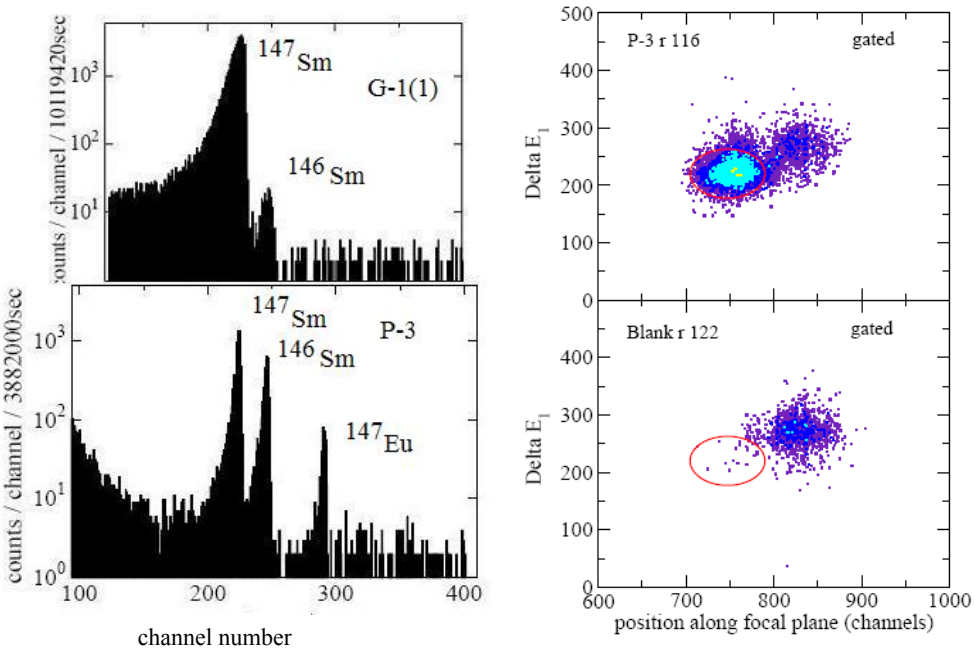

Fig. I-11. Left: α-spectra measured for the (γ,n) (top) and (p,2n) followed by electron capture (bottom) irradiated ^{147}Sm target. The groups corresponding to ^{147}Sm and ^{146}Sm (and an additional ^{147}Eu group produced in the proton activation) are observed; Right: spectra of energy-loss signal (ΔE1) vs. position gated by a software window on ^{146}Sm events. The counts observed for the blank spectrum (right bottom) are attributed to a memory effect in the ion source and correspond to a ratio ^{146}Sm /^{147}Sm of 3 × 10^{-12}. Interestingly, Sm is observed to have a stopping power smaller than Nd in the measured energy range, in agreement with a SRIM 2006 calculation.

B. WEAK INTERACTIONS

Nuclear decays constitute an essential tool for studying the fundamental properties of the weak interaction. Several studies relating to this work are carried out at ATLAS and at other laboratories. One study involves a search for scalar currents in weak decays – in violation of the Standard Model – in the super-allowed 0+ 0+ transitions by measuring the βν angular correlation of ^{14}O nuclei stored in a Paul trap. Another important study is the determination of the nuclear structure relevant for the interpretation of potential observation of neutrino-less double beta in ^{76}Ge. The observation of this decay mode would establish the Majorana nature of neutrinos and their mass could be derived once the nuclear structure is sufficiently well known to compute the relevant transition matrix elements.

b.1. β-Decay of ^{69,70,71}Kr (C. J. Lister, S. M. Fischer, M. P. Carpenter, S. Gros, G. Savard, J. Clark,* and B. Blank†)

The β-decays of $N < Z$ Krypton isotopes are all interesting. ^{71}K → ^{71}Br tests Mirror Symmetry. It is known already to have the largest non-analog branch known between mirror pairs. ^{70}Kr → ^{70}Br is ideal for seeking low-lying J = 0,1 states in ^{70}Br which are key for quantifying the difference in T = 1 and T = 0 pairing. ^{69}Kr → ^{69}Br is a "Trojan Horse" as the subsequent ^{69}Br → ^{68}Se + p breakup allows the mass of ^{69}Br to be inferred from the known ^{68}Se mass and the observation of the decay proton. This experiment cannot be done at ANL as the production cross sections in fusion-evaporation are too small. It is also not possible at MSU using fragmentation, as a velocity filter (which is still under construction) is needed to remove very strong contaminants from the cocktail beam. However, at GANIL in France, this experiment is feasible using the LISE spectrometer. In collaboration with Bertram Blank from Bordeaux, we proposed the study in 2006 and now have got the beam time allocated for a run in November 2007.

*Yale University, †University of Bordeaux, France.

b.2. Progress at the Beta-Decay Paul Trap (N. D. Scielzo,* G. Savard,† S. Caldwell,† J. Fallis,‡ L. Gang,§ A. A. Hecht,¶ D. Lascar,|| A. Levand, H. Sharma,‡ I. Tanihata, A. Villari,** B. J. Zabransky, J. A. Clark,†† S. Gulick,‡‡ R. Segel,§§ and K. S. Sharma¶¶)

The development of the BPT program has continued with initial loadings with ^{14}O isotopes and test measurements of the beta-gamma correlation in its decay for the planned scalar current search experiment to be performed. The ^{14}O isotopes were produced with the $p(^{14}N,^{14}O)$ reaction, transported through the Enge spectrograph and stopped in the gas catcher where they were cooled and extracted for transport and accumulation in the gas cooler modified to operate at the higher frequencies required for very light ions. The ^{14}O ions extracted from the cooler were transported to the new isobar separator where they were purified and accumulated before transfer to the BPT where further accumulation was implemented. Although issues with lifetime of the ions in the traps and the gas catcher were encountered because of vacuum failures occurring at short intervals before the runs, it was possible to obtain first beta-gamma angular correlation data from trapped radioactive ions inside the BPT. A spectra of beta-coincident gamma rays detected in the high-purity germanium detectors surrounding the BPT is shown in Fig. I-12. The spectra is extremely clean with only the 2313 keV gamma ray of interest and 511 keV annihilation radiation detected.

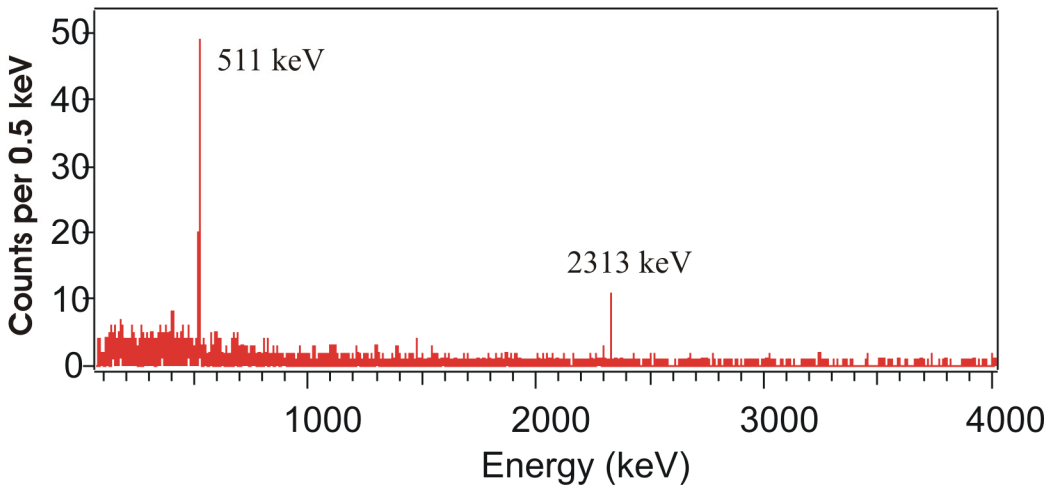

Fig. I-12. Gamma ray energy spectrum observed in coincidence with betas from the pure ^{14}O radioactive ion sample trapped in the BPT.

This initial correlation measurement was hampered by the limited lifetime of the radioactive ions inside the BPT which resulted in part of the sample decaying from the walls of the trap, not the trap centered. After determining experimentally that this was a gas purity issue and not an ion optical injection issue, it was still possible to subtract this contribution (at a severe loss in statistics) and observe the effect of the beta-neutrino correlation as shown in Fig. I-13. The observed energy shifts are in agreement with the expected values in the Standard Model for a pure vector transition. This measurement was performed with only part of the silicon array in operation and under poor vacuum conditions. Both conditions have been cured and a higher statistics run is expected to follow.

*Argonne National Laboratory and Lawrence Livermore National Laboratory, †Argonne National Laboratory and University of Chicago, ‡Argonne National Laboratory and University of Manitoba, Canada, §Argonne National Laboratory and McGill University, Quebec, Canada, ¶Argonne National Laboratory and University of Maryland, ||Argonne National Laboratory and Northwestern University, **GANIL, Caen, France, ††Yale University, ‡‡McGill University, Quebec, Canada, §§Northwestern University, ¶¶University of Manitoba, Canada

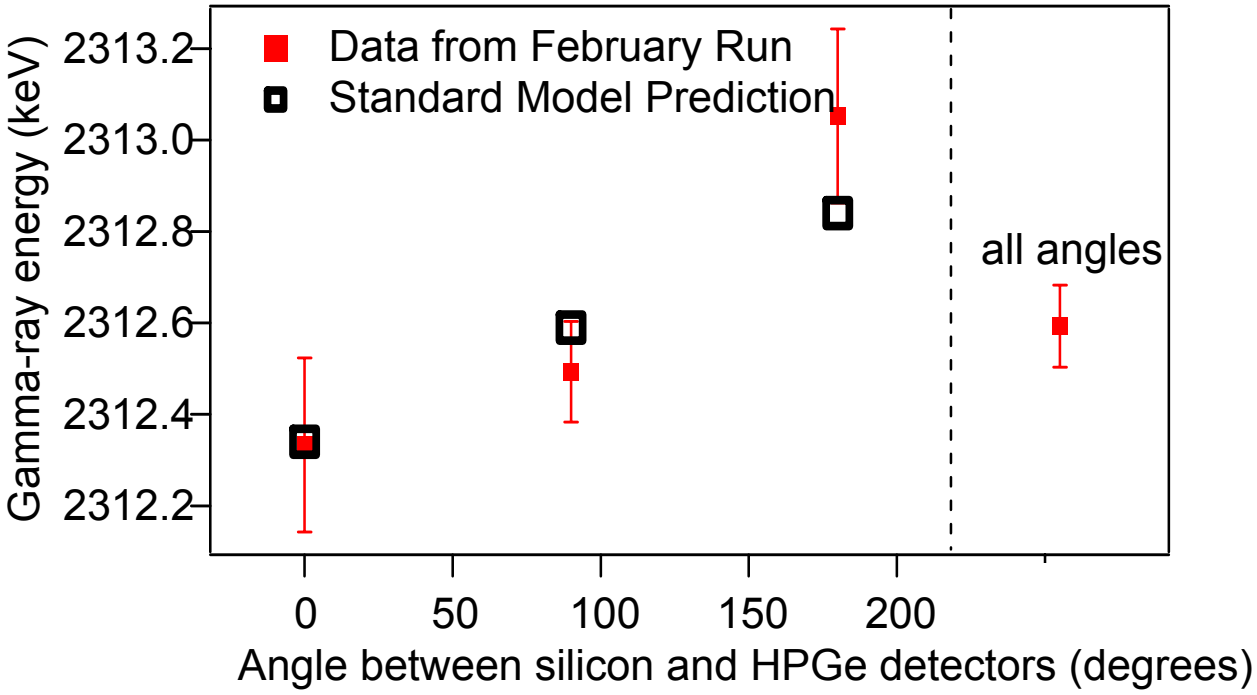

Fig. I-13. Doppler shifted gamma-ray energies as a function of the angle between the beta and gamma ray detected. The black squares are the shifts expected using the Standard Model predictions for a pure Fermi decay.

b.3. Nuclear Structure Relevant to Neutrinoless Double Beta Decay: ^{76}Ge and ^{76}Se

(J. P. Schiffer, S. Gros, C. L. Jiang, K. E. Rehm, X. D. Tang, S. J. Freeman,* J. A. Clark,† C. Deibel,† C. R. Fitzpatrick,* A. Heinz,† D. Hirata,§ B. P. Kay,* A. Parikh,† P. D. Parker,† A. C. C. Villari,‡ V. Werner,† and C. Wrede†)

The possibility of observing neutrinoless 2β decay[1] would offer the opportunity of determining the neutrino mass *if* the nuclear matrix element were known. Because theoretical calculations are uncertain, measurements of the occupations of valence orbits with nucleons active in the decay can be important. The occupation of valence neutron orbits in ^{76}Ge and ^{76}Se were determined by precisely measuring cross sections for both neutron-adding and removing transfer reactions. Our results indicate that the Fermi surface is much more diffuse than in theoretical (QRPA) calculations and that the populations of at least three orbits change significantly in the process -- by contrast in the calculations the changes are confined primarily to one orbit.

What unquestionably matters to the matrix element is knowing the population of the valence orbits of nucleons that switch from neutrons to protons. We have, therefore, undertaken a set of measurements to determine this quantity experimentally, and report here on results focusing on the valence neutron populations and the differences in these populations for ^{76}Ge and ^{76}Se. In a previous experiment we determined that the neutron pair correlations in these two nuclei are quantitatively very similar.[2]

In the present measurement the Macfarlane-French sum rules were used with the measured sums of spectroscopic factors for neutron-adding and neutron-removing reactions. The active orbits for neutrons in these nuclei, with 42 and 44 neutrons, are $p_{3/2}$, $f_{5/2}$, $p_{1/2}$, and $g_{9/2}$. We took care to measure the absolute cross sections for the neutron-adding (d,p) and (α,^{3}He), as well as for the neutron-removing (p,d) and (^{3}He,α) reactions at or near the peaks of the angular distributions for each *l*-value.

The measurement was carried out at the Yale tandem accelerator with the particles identified with the Enge spectrograph and gas-filled focal-plane detector backed by a scintillator. The target thicknesses together with

the spectrometer solid angle and beam current measurements were calibrated by measuring Rutherford scattering at an energy low enough to assure pure Coulomb scattering. Most of these reactions have been measured previously, but we show the angle-dependence in Fig. I-14, where all the ratios indicate consistency with previously determined spins. While our primary purpose was to obtain accurate relative cross sections, a possible candidate for the missing $5/2^-$ state in ^{77}Ge was identified. The finite-range DWBA program PTOLEMY was used in the extraction of spectroscopic factors.

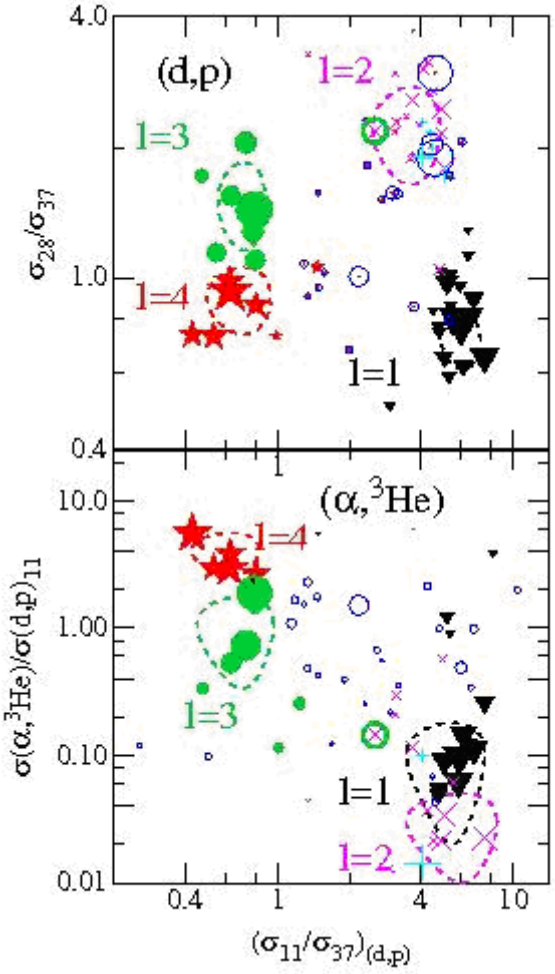

Fig. I-14. The ratios of cross sections are shown for different angles and reactions. The data on top are from (d,p) reactions. The data in the bottom panel are from a combination of the (α,^{3}He) and the (d,p) experiments. The symbols, one for each state, indicate the l-value assignments from previous work: triangles (black) are l = 1, circles (green) are l = 3, and stars (red) are l = 4. In addition, states not included in the analysis, are l = 2 transitions indicated by x's and l = 0 by + signs. States with unknown l-values are indicated by hollow circles (in blue). The size of the symbols is a rough measure of the cross sections. The dashed lines indicate the loci of the ratios for well-established l-values. The x surrounded by a (green) circle in the lower box, between the l = 2 and 3 islands is the 500-keV 5/2 ± 5/2- doublet ^{77}Ge.

To circumvent the issue of absolute spectroscopic factors we normalized the sums by requiring that the summed strengths for neutron-adding and neutron-removing spectroscopic factors, the vacancies and occupancies can, therefore, add up to the (2J + 1) degeneracy of the orbits. The normalization factors for the l = 1, 3, and 4 transitions are 0.56, 0.55, and 0.62 respectively with rms fluctuations among the targets of 1, 12, and 6%. These values are consistent with the spectroscopic factors expected from short-range

correlations.

The results are summarized in Table I-4. Data with ^{74}Ge and ^{78}Se were obtained in parallel as a check. The constancy of the sums is a measure of the validity of the procedure. The occupancy is determined both from the neutron adding and the neutron removing reactions, but since the latter is smaller it is likely to be more accurate. The weighted mean of the two numbers is given in the last column.

While the estimates of uncertainties depend on some ambiguities in the DWBA sensitivity to distorting parameters and the possibility of missed states, and, therefore, need to be taken with caution, there are several checks that give us some confidence in them.

- The normalization factors obtained for each target separately are relatively constant, and so are those obtained for l = 3 and 4 transitions separately.
- The summed neutron-removal and adding strengths for ^{74,76}Ge ^{76,78}Se are consistent with the expected value of 22.0 using two overall normalization numbers for all four targets.
- As an independent result, the neutron vacancies expected for the four nuclei are 8, 6, 8, and 6 respectively, while the observed values are 7.3, 6.1, 8.1 and 5.8, in very good agreement.

Table I-4. Summary of results.

l-value Target	Holes	Particles	Holes + Particles	Adopted Occupancy
l = 1 ($1/2^- + 3/2^-$)				
^{74}Ge	1.10			4.9
^{76}Ge	1.07	4.94	6.06	**4.95(.2)**
^{76}Se	1.56	4.63	5.93	**4.42(.2)**
^{78}Se	0.90			5.1
l = 3 ($5/2^-$)				
^{74}Ge	1.93	4.25	6.18	4.1
^{76}Ge	1.13	3.82	4.95	**4.5(0.4)**
^{76}Se	2.13	3.46	5.60	**3.7(0.4)**
^{78}Se	2.37	4.43	6.80	3.9
l = 4 ($9/2^+$)				
^{74}Ge	4.43	5.88	10.31	5.67
^{76}Ge	3.45	6.34	9.80	**6.47(0.3)**
^{76}Se	4.41	6.11	10.53	**5.76(0.3)**
^{78}Se	2.84	7.36	10.20	7.23

As to orbits beyond the closed shell at N = 50 that may have some occupancy, we have some limits from the neutron-removal reaction on ^{76}Se, which suggests that perhaps about 0.2 neutrons are in the $1d_{5/2}$ orbit. The difference in the occupancy of orbits in ^{76}Ge and ^{76}Se is 0.4 ± 0.2 in *1p*, 0.7 ± 0.3 in $0g_{9/2}$ and 0.7 ± .4 in $0f_{5/2}$, and is plotted in Fig. I-15 along with the QRPA calculations[3] in the figure.

There are significantly more vacancies in the *1p* and especially in the $0f_{5/2}$ orbits in the data than in the calculations. For the neutrinoless double-beta decay experiments it is the ***changes*** in occupancy that are important and so, in the lower part of Fig. I-15 we show the differences between^{76}Ge and ^{76}Se. From this it is very clear that while the QRPA results indicate that the predicted changes between the two nuclei are mostly in the $0g_{9/2}$ orbit, the experiment shows quite clearly that the changes in the *1p* and $0_{5/2}$ orbits are much larger than predicted.

*University of Manchester, United Kingdom, †Yale University, ‡GANIL, Caen, France, §GANIL, Caen, France and The Open University, Milton Keynes, United Kingdom.

[1]S. R. Elliott and P. Vogel, Ann. Rev. Nucl. Part. Sci. **52**, 115 (2002).
[2]S. J. Freeman *et al*., Phys. Rev. C **75**, 051301 (2007).

[3]V. A. Rodin and A. Faessler, private communication, calculated within the method of QRPA and RQRPA as described in V. A. Rodin, A. Faessler, F. Simkovic, and P. Vogel, Phys. Rev. C **68**, 044302 (2003) and Nucl. Phys. A**766**, 107 (2006).

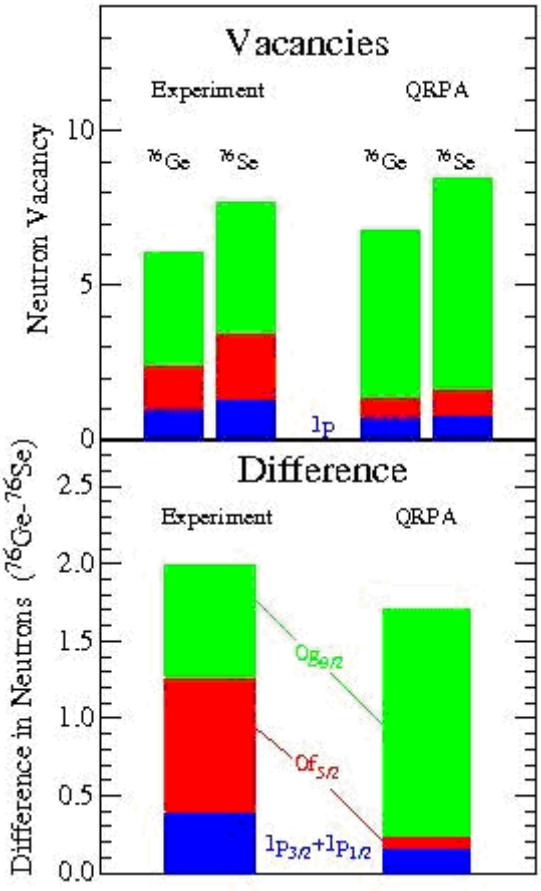

Fig. I-15. The deduced neutron vacancies for ^{76}Ge and ^{76}Se are shown in the three active valence orbits and compared to those from the QRPA calculations of Ref. 3. The naive shell closure should give 6 and 8 vacancies for these two nuclei. The lower part of the figure shows the differences in these occupations (expected to be 2.0), again compared to the QRPA calculation.

C. SPECTROSCOPY OF VERY HEAVY ELEMENTS

Recent improvements in detection efficiency and production rate have enabled an important experimental program on the spectroscopy of trans-fermium nuclei. The aim of this program is to determine the location of single particle and 2-quasiparticle states in deformed No nuclei in order to help pin down the level spacing and, therefore, the stability of spherical super-heavy nuclei. Detailed nuclear structure properties of slightly lighter nuclei are also studied.

c.1. Two-Quasiparticle States in ^{254}No and the Stability of Superheavy Nuclei

(T. L. Khoo, D. Seweryniak, I. Ahmad, B. Back, R. Blinstrup, M. P. Carpenter, J. Chapman, C. N. Davids, R. V. F. Janssens, F. G. Kondev, T. Lauritsen, C. J. Lister, E. F. Moore, D. Peterson, S. F. Zhu, S. K. Tandel,* G. Mukherjee,*,† P. A. Butler,‡ P. Chowdhury,* P. T. Greenlees,§ A. A. Hecht,†,¶ A. Heinz,|| R.-D. Herzberg,‡ P. Ikin,‡ G. D. Jones,‡ P. Reiter,** U. S. Tandel,* and X. F. Wang†,††)

A central question in the study of superheavy nuclei is the location of the magic gaps. Models predict gaps with significantly different locations in Z and N as a consequence of different single-particle energies. Hence, discriminating tests of the models can be made by checking the predicted energies against experimental values. In this manner, 2-quasiparticle (qp) states in shell-stabilized nuclei probe the levels that govern the stability of superheavy nuclei, test 2-qp energies from theory and, thereby, check their predictions of magic gaps.

We have identified in ^{254}No (Z = 102) 2- and 4-qp isomers, with quantum numbers $K^{\pi} = 8^{-}$ and (14^{+}), and a low-energy 2-qp $K^{\pi} = 3^{+}$ state. It is significant that a constituent of the $K^{\pi} = 3^{+}$ configuration is the [521]1/2 orbit, from the spherical $f_{5/2}$ shell, which lies above a Z = 114 gap that appears with Woods-Saxon (WS) single-particle energies. The use of WS single-particle energies reproduces the experimental proton 2-qp energies in ^{254}No. The WS potential also systematically reproduces the 1-qp energies in odd-A heavy nuclei.[1] These results indicate that WS energies are valid for Z up to 102 and suggest that a proton gap would occur at Z = 114 -- if the WS potential continues to describe the proton energy levels of nuclei with Z > 102. In contrast, there are shortcomings in the 2-qp energies from self-consistent mean-field theories, with corresponding deviations in 1-qp energies in neighboring odd-A nuclei. Therefore, their predictions of magic gaps at Z = 120 and 126 should be viewed with reservations. The parameters of the interactions used in self-consistent mean-field SHFB and RMF models have been adjusted to fit bulk properties of closed-shell nuclei. Thus, the success of their single-particle energies is impressive, but definitely do require improvements,[2] *e.g.* a lowering of the proton $i_{13/2}$ orbit, to reproduce *all* measured 1- and 2-qp energies. To preserve the virtue of self-consistency when extrapolating to the heaviest nuclei, there is a need for a new interaction designed for this purpose.

In summary, spectroscopic measurements of 2-qp states in ^{254}No provide the first experimental information on the proton magic shell gap for superheavy nuclei by discriminating among the theories that make predictions on the gap. This work has been published in Physical Review Letters.[2]

*University of Massachusetts-Lowell, †Argonne National Laboratory, ‡University of Liverpool, United Kingdom, §University of Jyväskylä, Finland, ¶University of Maryland, ||Yale University, **Universität zu Köln, Germany, ††University of Notre Dame.

[1]R. Chasman *et al*., Rev. Mod. Phys. **49**, 833 (1978); A. Parkhomenko and A. Sobiczewski, Acta Phys. Pol. **B35**, 2447 (2004), *ibid.* **B36**, 3115 (2005).

[2]S. K. Tandel *et al*., Phys. Rev. Lett. **97**, 082502/1-4 (2006).

c.2. $K = 8^-$ Isomers and $K = 2^-$ Octupole Bands in ^{252}No and $N = 150$ Isotones

(A. Robinson, T. L. Khoo, I. Ahmad, D. Seweryniak, S. Gros, D. Peterson, B. B. Back, M. P. Carpenter, C. N. Davids, J. P. Greene, A. Hecht, R. V. F. Janssens, F. G. Kondev, T. Lauritsen, C. J. Lister, E. F. Moore, S. Zhu, S. K. Tandel,* P. Chowdhury,* U. Tandel,* A. Heinz,† X. Wang,‡ P. A. Butler,§ R. Herzberg,§ G. Jones,§ S. Eeckhaudt,¶ P. T. Greenlees,¶ R. Julin,¶ M. Leino,¶ J. Uusitalo,¶ P. Reiter,|| and G. Mukherjee**)

In shell-stabilized heavy nuclei around ^{254}No, many of the orbitals around the Fermi level have large projections of their spin along the symmetry axis so that high-K isomers should be common. The isomers, which can be studied in a quiet environment far from the target, provide opportunities to investigate the excited configurations of nuclei populated with sub-microbarn cross sections, not only of the isomers, but also of lower-lying rotational bands fed in the isomeric decays. The occurrence of K isomers reveals the applicability of K-selection rules, indicating that K is a good quantum number and that the nucleus has a prolate shape with axial symmetry. The energies of 2-quasiparticle states provide incisive tests of theories. An example is the $K = 8^-$ isomer at 1296 keV in ^{254}No which decays to a $K = 3^+$ band. The energies of the $K = 3^+$, 8^- states, which are built on proton configurations, reveal that Woods-Saxon proton single-particle energies are accurate for Z up to at least 102. In ^{252}No, 2-quasiparticle energies calculated with the Woods-Saxon potential also suggest a $K = 8^-$ isomer, but built instead on neutron states, at a lower energy of 1.01 MeV. Hence, detection of this predicted isomer constitutes a test of the Woods-Saxon single-particle energies.

The ^{206}Pb(^{48}Ca,2n) reaction was used to populate states in ^{252}No. The nuclides were transported and uniquely identified by the Fragment Mass Analyzer (FMA). The nuclides were implanted into individual 1×1 mm^2 pixels of a double-sided Si strip detector. Time and spatial correlations then identified the decay of an isomer, *i.e.*, in each pixel, a delayed coincidence between the implant and an electron signal, with sum energy 100-500 keV. Gamma rays from the isomer were detected in prompt coincidence with the delayed electron signal. In this manner, an isomer was discovered in ^{252}No, with a half-life of 109 ms and quantum numbers $I,K^\pi = 8,8^-$. It decays *via* multiple pathways into a $K^\pi = 2^-$ octupole vibrational band. The decay scheme of the isomer is shown in Fig. I-16, together with that of the isotone ^{246}Cm.[1-2] The two decay schemes are very similar.

The energies of $IK^\pi = 22^-$ and 88^- states in the $N = 150$ isotones are displayed in Fig. I-17. They span an impressively wide range of $Z = 94$-102, especially for such heavy nuclei. The 8^- energies are rather constant (within 75 keV), which suggests that the 8^- state has a neutron configuration – as expected. Similarly, the energies of the 2^- octupole band head are constant within 90 keV. A striking exception is the 2^- energy in ^{248}Cf, where there is a pronounced minimum. For the 8^- states, we propose a neutron 2-qp configuration {[734]9/2, [624]7/2}. The calculated energies for this configuration, based on Woods-Saxon single-particle energies and a Lipkin-Nogami prescription for pairing, are 170-260 keV lower than the measured ones, but within the model uncertainty of ~300 keV. The deep minimum at $Z = 98$ is due to the nearly degenerate proton orbitals 7/2[633] and 3/2[521] (Ref. 5), which constitute a low-lying 2-qp proton state. Only in ^{248}Cf is there a confluence of low-lying proton and neutron 2^- 2-qp states, increasing the octupole collectivity and, thereby, lowering the vibrational energy. Quasiparticle (QRPA) calculations for octupole vibrations have been performed using single-particle energies given by a modified Nilsson potential, which approximate those from the Woods-Saxon potential. The trend with Z of the $K = 2^-$ energies, including the minimum at $Z = 98$, is reproduced by the QRPA calculations. All calculated energies are higher by ~200 keV. This difference is not significant since the calculated energies are very sensitive to the magnitude of the octupole force, *e.g.*, a 2% reduction would give agreement with the experiment.

---

*University of Massachusetts-Lowell, †Yale University, ‡University of Notre Dame, §University of Liverpool, United Kingdom, ¶University of Jyväskylä, Finland, ||Universität zu Köln, Germany, **Variable Energy Cyclotron Center, Kolkata, India.

[1]K. Moody *et al*., Z. Phys. A - Atomic Nuclei **328**, 417 (1987).

[2]I. Ahmad, in Proc. Frontiers in Nuclear Physics, Dubna, p. 31 (1995).

[3]S. W. Yates, A. M. Friedman, and I. Ahmad, Phys. Rev. C **12**, 442 (1975).
[4]T. Greenlees *et al*., private communication (2006).
[5]I. Ahmad *et al*., Phys. Rev. C **71**, 054305 (2005).

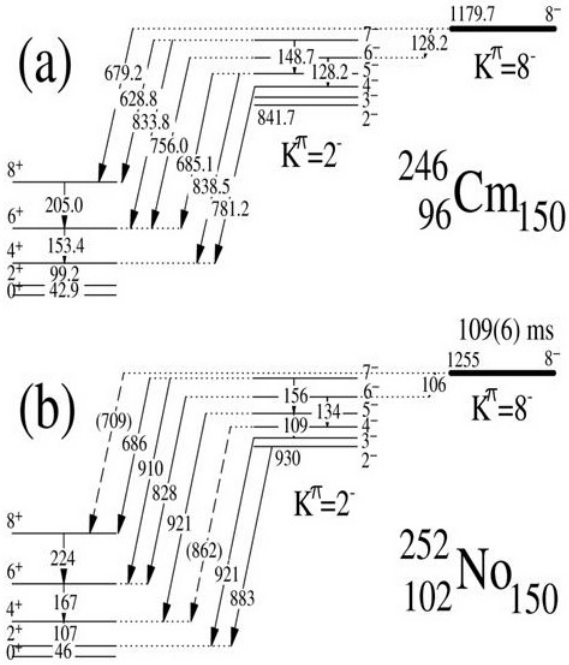

Fig. I-16. Decay schemes of the $K^{\pi} = 8^-$ isomers in the N = 150 isotones, ^{246}Cm and ^{252}No.

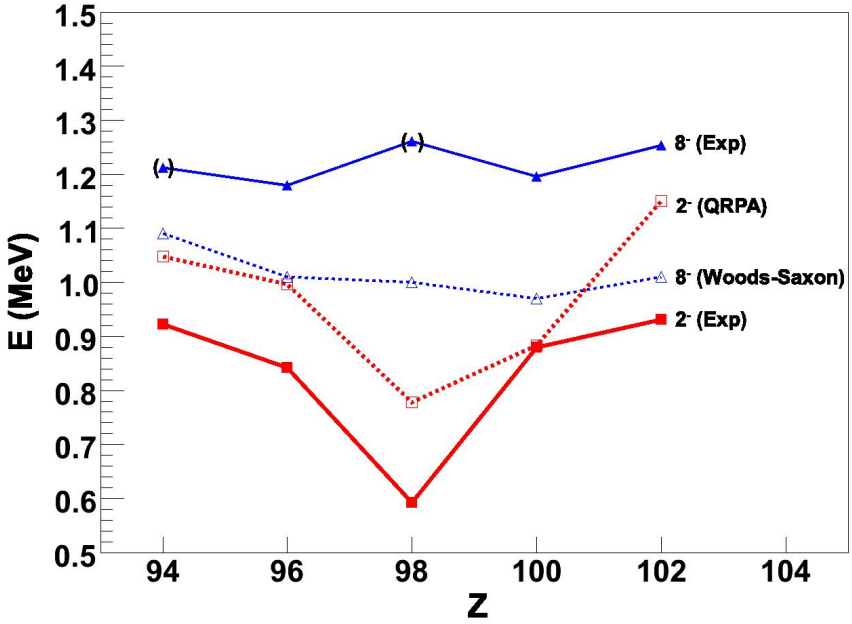

Fig. I-17. Energies of the $K^{\pi} = 8^-$ isomers (blue) and 2^- octupole bands (red) in N = 150 isotones with Z = 94-102 from experiment (filled symbols) and theory (open symbols). The data for ^{244}Pu, ^{246}Cm, ^{248}Cf and ^{250}Fm are from Ref. 1-4. Based on the published data[1,3] we have made assignments of 8^- states in ^{244}Pu and ^{248}Cf.

c.3. Octupole Strength in the ^{238,240,242}Pu Nuclei

(R. V. F. Janssens, S. Zhu, M. P. Carpenter, I. Ahmad, J. P. Greene, T. L. Khoo, T. Lauritsen, C. J. Lister, D. Seweryniak, F. G. Kondev,* X. Wang,† U. Garg,† I. Wiedenhöver,‡ A. Bernstein,‡ P. Wilson,‡ E. Diffenderfer,‡ C. Teal,‡ A. Larabee,§ B. Meredith,§ and S. Freeman||)

Octupole correlations have attracted much attention over the years, and the actinide nuclei remain an interesting source of information because they offer the possibility to investigate the interplay between collective rotation and octupole degrees of freedom. Sheline and Riley[1] recently pointed out that a deep depression of the excitation energies of the lowest 1^- states occurs in the region of neutron numbers from 132 to 140 for Ra and Th nuclei, where strong octupole correlations lead to the stable octupole deformation. Moreover, a smaller depression was found at neutron numbers of 144 and 146 for Pu isotopes, *i.e.* ^{238,240}Pu. This observation is consistent with an earlier suggestion by I. Wiedenhöver *et al*.[2] that, in the lightest Pu isotopes, strong octupole correlations lead to the absence (239, 240) or delay in frequency (238) of the strong proton alignment observed in the heavier (241, 242, 243, 244) Pu isotopes.

The present work focuses on the octupole correlations in 3 even even (A = 238, 240, 242) Pu nuclei. A series of "unsafe" Coulomb excitation experiments as well as 1 neutron transfer measurements has been carried out with Gammasphere at ATLAS. The so called "unsafe" Coulomb excitation technique (beam energy is about 15% above Coulomb barrier) was used in order to enhance the feeding of the highest spin states. Billions of events with fold 3 or higher were collected. In the subsequent data analysis, the raw data were converted into both the traditional RADWARE format (Cube and Hypercube) and the latest BLUE database format.

For ^{238}Pu, only the yrast and octupole vibrational bands are seen in the level scheme resulting from our data analysis (see Fig. I-18) since this data is from the weak 1 neutron pick up channel in reactions of a ^{207}Pb beam with a ^{239}Pu target. Both bands are extended towards higher spin by 2 more levels, which are critical, therefore, the obtained alignment plot better indicates that the expected "back bending" is delayed at least up to $\hbar\omega$ ~0.3 MeV. It is also noteworthy that the levels in the yrast and octupole bands are interleaved at the highest spins.

In ^{240}Pu, the key $(I + 1)^+ \rightarrow I^-$ E1 linking transitions have been established at high spin. This can be viewed as solid evidence for an octupole rotor. The investigation of the branching ratios, between the inter- and in-band transitions, also supports the conclusion of a stable octupole deformation at high spin. This is in agreement with theoretical predictions by Jolos and von Brentano.[3,4]

In ^{242}Pu, the yrast and 5 excited bands (1 of positive and 4 of negative parity) were observed. One of the most notable differences between ^{242}Pu and ^{240}Pu is that in ^{242}Pu all excited bands decay to the yrast band. The so called "back bending" occurs at $\hbar\omega$ ~0.25 MeV, and no pattern of interleaved states with alternating spin and parity is observed.

Detailed calculations are being performed currently, hence, a complete interpretation of the experimental results is still under discussion.

---

*Nuclear Engineering Division, Argonne National Laboratory, †University of Notre Dame, ‡Florida State University, §Greenville College, ||University of Manchester, United Kingdom.

[1]R. K. Sheline and M. A. Riley, Phys. Rev. C **61**, 057301 (2000).
[2]I. Wiedenhöver *et al*., Phys. Rev. Lett. **83**, 2143 (1999).
[3]R. V. Jolos and P. von Brentano, Phys. Rev. C **49**, R2301 (1994).
[4]R. V. Jolos and P. von Brentano, Nucl. Phys. **A587**, 377 (1995).

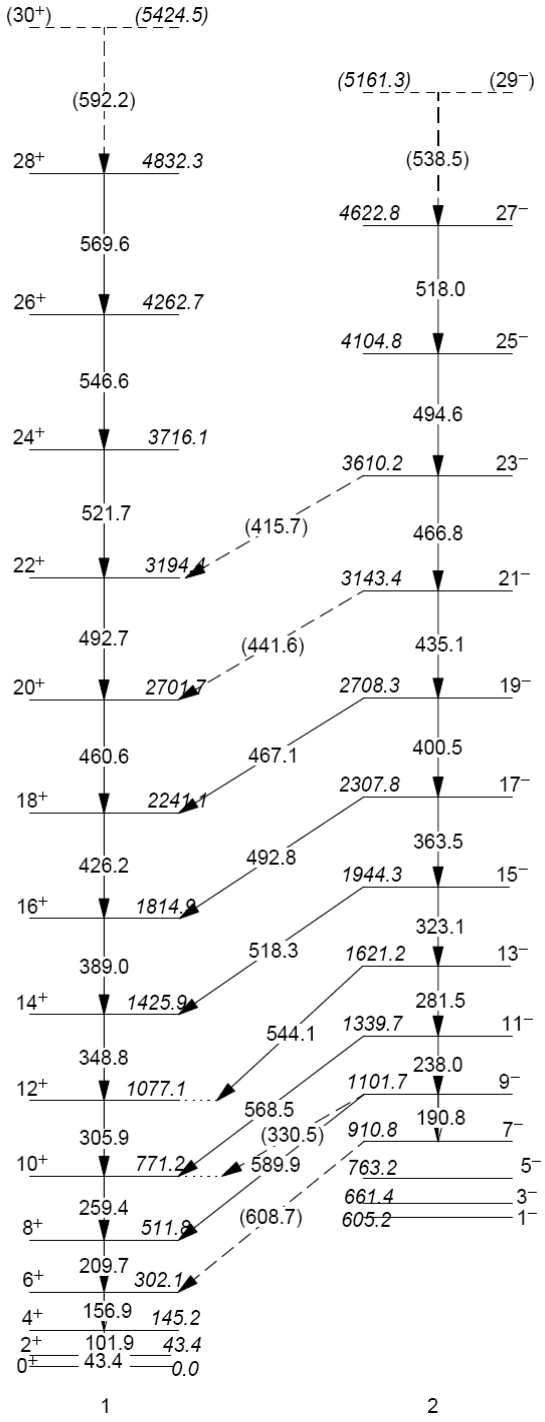

Fig. I-18. Partial level scheme of ^{238}Pu.

c.4. Measurements of the ^{246}Cm Half-Life (I. Ahmad, F. G. Kondev, J. P. Greene, M. A. Kellett,* and L. L. Nichols*)

Precise half-life values of actinide nuclei and their decay properties are needed for proper handling of the radioactive waste generated in reactors. Long half-lives are difficult to measure and, hence, it is important to use different techniques to reduce systematic uncertainties. One method which has not been much used in the past is the measurement of the daughter activity in the presence of the parent. We have determined the ^{246}Cm half-life by measuring the activity of ^{246}Cm in a sample of ^{250}Cf after it has decayed several half-lives. A thin source of ^{250}Cf was prepared in the 1970s with an electromagnetic isotope separator and allowed to decay. The alpha spectra of this source was measured with a PIPS Si detector. An example of the alpha spectrum is shown in Fig. I-19. Using the ratio of the alpha activities of ^{246}Cm and ^{250}Cf and the decay time and the half-life of ^{250}Cf (13.08 ± .09 yr), the half-life of ^{246}Cm was determined to be 4706 ± 40 yr. This is in agreement with previously measured precise values of ^{246}Cm. The results of this study were published.[1]

*International Atomic Energy Agency, Vienna, Austria.

[1]F. G. Kondev *et al*., Appl. Radiat. Isot. **65**, 335 (2007).

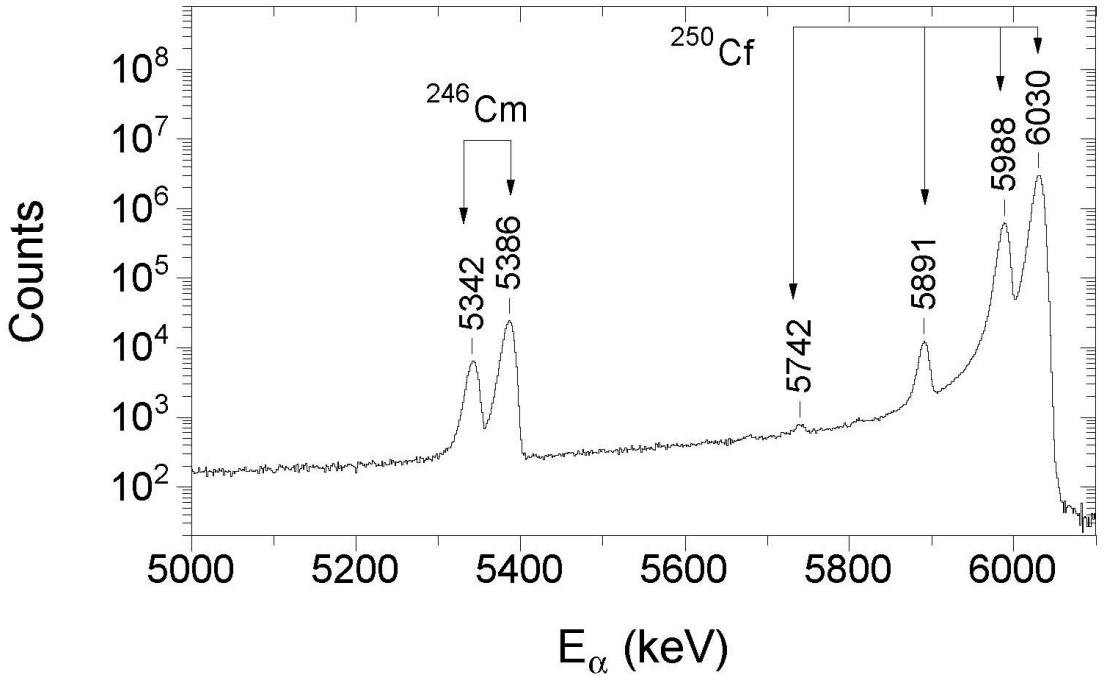

Fig. I-19. The α-particle spectrum of a mass-separated ^{250}Cf source measured with a 25-mm^2 PIPS detector at a source-to-detector geometry of 0.23%.

D. STRUCTURE OF NUCLEI FAR FROM STABILITY

The study of nuclei far from stability is a central focus of modern nuclear physics research. A recent success was the identification of the first excited state in ^{101}Sn, which represents a single neutron orbit outside the doubly-magic ^{100}Sn core. Other studies are attempting to reach the doubly-magic ^{78}Ni nucleus on the neutron-rich side using the deep-inelastic reaction mechanism. A wide range of studies are pursued which aim to reveal the changes in shell structure and shapes of nuclei away from the line of β-stability using beams from ATLAS and other facilities.

d.1. Neutron-Rich Nuclei

d.1.1. Is the Nuclear Spin-Orbit Interaction Changing with Neutron Excess?

(J. P. Schiffer, K. E. Rehm, B. P. Kay,* S. J. Freeman,* J. A. Clark,† C. Deibel,* A. Heinz,† A. Parikh,† P. D. Parker,* and C. Wrede*)

The single-particle character of nuclei underlies much of our understanding of nuclear structure. The states formed by a proton outside the closed shell of 50 protons, the $g_{7/2}$-$h_{11/2}$ separation in particular, was studied with the (α,t) reaction on all the stable, even Sn isotopes in 2004 to demonstrate that the difference between major single-particle states was changing drastically with neutron excess.[1] This result has been explained by Otsuka[2] by the effect of the tensor part of the nucleon-nucleon interaction as the $h_{11/2}$ neutron orbit is filling in the Sn isotopes. This explanation also seems to account, at least qualitatively, for the observed changes in single-particle states, and even shell structure, in light nuclei away from the region of stability.[3]

An experiment to obtain quantitative information on neutron single-particle states in heavy nuclei, outside $N = 82$, was carried out on the separation between the $i_{13/2}$ and $h_{9/2}$ single-neutron states. The measurement was carried out at the Yale tandem using the (α,^{3}He) reaction, that is particularly suited for measurements with high orbital-angular-momentum transfer. Targets were a problem because the available stable $N = 82$ targets are ^{136}Xe, ^{138}Ba, ^{140}Ce, ^{142}Nd, and ^{144}Sm. Xenon is a gas and, therefore, difficult to use as a target, while the metallic targets all oxidize quickly. With some care these difficulties have been overcome.

The single-particle states are all fragmented into two components, apparently due to the proximity of the $9/2^-$ and $13/2^+$ states formed by coupling an $f_{7/2}$ neutron to the 2^+ or 3^- vibration in these nuclei. The centroids of the single-particle states were observed, and the trends in the separation show a behavior that is similar to that predicted by the tensor matrix elements, when the protons are filling the $0g_{7/2}$ and $1d_{5/2}$ orbits.[3] The results are shown in Fig. I-20.

In addition, from the spectroscopic factors, the mixing matrix elements to the weak coupling states could be extracted, and these were found to be remarkably constant. These are listed in Table I-5.

Table I-5. Mixing Matrix Elements in $N = 83$ Nuclei.

	$h_{9/2} - 2^+ \otimes f_{7/2}$	$i_{13/2} - 3^- \otimes f_{7/2}$
^{139}Ba	162 ± 6 keV	629 ± 17 keV
^{141}Ce	151 ± 5 keV	632 ± 34 keV
^{143}Nd	145 ± 2 keV	686 ± 16 keV
^{145}Sm	162 ± 4 keV	725 ± 9 keV
Average (rms)	**150 keV (9)**	**698 keV (50)**

*University of Manchester, United Kingdom, †Yale University.

[1] J. P. Schiffer *et al*., Phys. Rev. Lett. **92**, 162501 (2004).

[2]T. Otsuka *et al*., Phys. Rev. Lett. **95**, 232502 (2005).
[3]A. Ozawa *et al*., Phys. Rev. Lett. **84**, 5493 (2000).
[4]B. H. Wildenthal *et al*., Phys. Rev. C **3**, 1199 (1971).

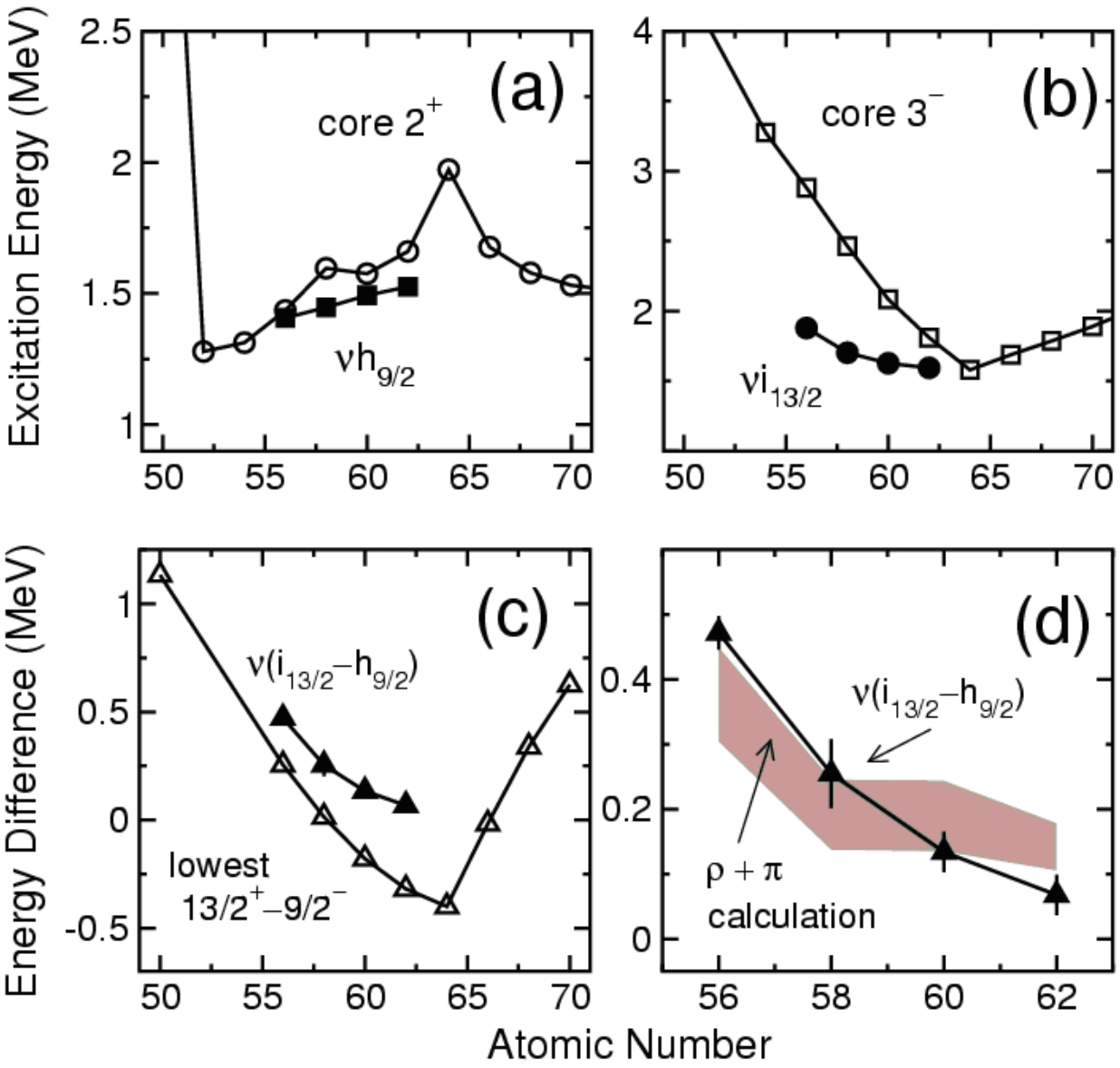

Fig. I-20. The top two boxes show the energy dependence of the single-particle states determined in the present experiment for N = 83 systems (solid symbols), compared to the energies of the vibrational states in the core N = 82 nuclei (open symbols), for the $h_{9/2}$ and $i_{13/2}$ states respectively in (a) and (b). In (c) the energy splitting between these two centroid energies from the present work is shown in solid symbols while the open symbols show the separation between the lowest states with these quantum numbers in all N = 83 nuclei. In (d) the present results are again shown with the colored band representing the results with the tensor interaction. The width of this band represents the experimental uncertainty[4] in the proton occupation numbers.

d.1.2. Excited States in the Ca Isotopes Towards "Doubly-Magic" ^{54}Ca: β Decay of $^{51-53}$K

(R. V. F. Janssens, S. Zhu, M. P. Carpenter, F. G. Kondev, X. Wang, R. Broda,* B. Fornal,* P. Mantica,† J. Pereira,† J. Stoker,† J. Pinter,† G. C. Ball,‡ G. Hackman,‡ A. Andreyev,‡ A. C. Morton,‡ C. Pearson,‡ S. C. Ravuri,‡ C. Svensson,§ P. E. Garrett,§ D. Bandyopadhyay,§ G. F. Grinyer,§ B. Hyland,§ A. A. Phillips,§ M. A. Schumaker,§ J. C. Waddington,¶ R. A. E. Austin,|| J. J. Ressler,** J. Kozemczak,†† and A. Larabee††)

Shell model calculations with the new GXPF1 *pf* shell interaction[1] have suggested the development of significant sub-shell gaps at $N = 32$ and $N = 34$ in the Ca isotopes. These new gaps in these neutron-rich nuclei are believed to be the result of a reduced proton $f_{7/2}$ – neutron $f_{5/2}$ monopole interaction as protons are removed from the $f_{7/2}$ orbital, when the proton number decreases from $Z = 28$ (Ni) to $Z = 20$ (Ca). Confirmation of the $N = 32$ sub-shell gap has already been achieved in the Ti and Cr isotopic chains, based on the results of beta-decay measurements, high-spin state studies following deep inelastic reactions and B(*E2*) transition strengths through Coulomb excitation of intermediate energy fragments.[2-4] However, there is no evidence for a $N = 34$ shell closure in ^{56}Ti and ^{58}Cr. For example, the energy of the first excited 2^+ state in ^{56}Ti[5] falls midway between the shell model predictions with the GXPF1 Hamiltonian, where a shell closure is expected, and those with the KB3G interaction, where this gap is absent. However, the presence of a $N = 34$ shell gap at ^{54}Ca, where the proton $f_{7/2}$ shell is empty, cannot be ruled out. In fact, the latest calculations with a modified GXPF1 interaction, labeled GXPF1A, still predict a gap at $N = 34$ in the Ca isotopic chain.[3,6] Systematic data on the approach to the proposed ^{54}Ca "doubly-magic" nucleus are critical to test the latest shell model predictions. To put it simply, with the $Z = 20$ proton shell closed, the neutron-rich calcium isotopes provide a unique opportunity to delineate neutron shell structure above $N = 28$. Specifically, information on the ordering and on the location of the $p_{3/2}$, $p_{1/2}$ and $f_{5/2}$ orbitals is highly desirable. In order to address the issue, a study of the $^{51-53}$Ca isotopes through the beta decay of mass selected $^{51-53}$K nuclei was undertaken at the ISAC facility located at TRIUMF in Vancouver.

The neutron-rich $^{51-53}$K isotopes were produced by spallation of a Ta target by 500 MeV protons, and extracted from a surface ionization source as singly-charged ions. The desired isotopes, following mass separation, were implanted into a moving tape collector located at the center of the 8π spectrometer, which comprises 20 Compton suppressed HPGe detectors. The SCEPTAR array of plastic scintillator detectors was used to detect the beta particles. The event-by-event coincidence data recorded for subsequent analysis included beta-γ and beta-γ-γ coincidences. Beta-gated, γ-single spectra and γγ coincidence matrices have been analyzed for all three cases ($^{51-53}$K). Figure I-21 is a spectrum obtained for ^{51}K. The detailed analysis is ongoing.

*Niewodniczanski Institute, Krakow, Poland, †Michigan State University, ‡TRIUMF, Vancouver, British Columbia, §University of Guelph, Ontario, ¶University of McMaster, Hamilton, Ontario, ||St. Mary's University, Halifax, Nova Scotia, **Simon Fraser University, Burnaby, British Columbia, ††Greenville College.

[1]M. Honma *et al.*, Phys. Rev. C **65**, 061301(R) (2002).
[2]R. V. F. Janssens *et al.*, Phys. Lett. **B546**, 55 (2002).
[3]D.-C. Dinca *et al.*, Phys. Rev. C **71**, 041302(R) (2005).
[4]S. Zhu *et al.*, Phys. Rev. C **74**, 064315 (2006).
[5]S. N. Liddick *et al.*, Phys. Rev. Lett. **92**, 072502 (2004).
[6]A. Gade *et al.*, Phys. Rev. C **74**, 021303(R) (2006), T. Otsuka, private communication.

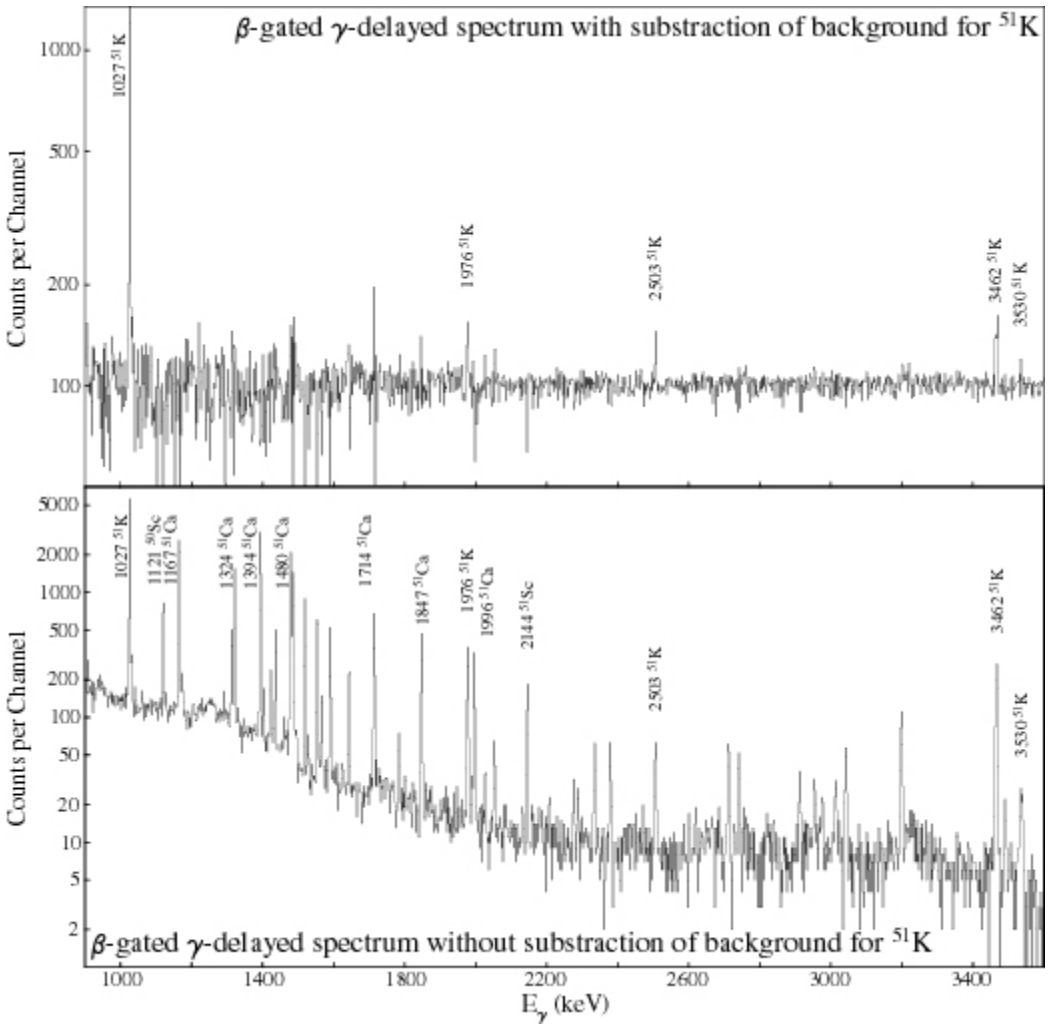

Fig. I-21. Sample spectra from the beta decay measurements on ^{51}K under the conditions given with the data.

d.1.3. Shell Model States in Neutron-Rich Potassium Isotopes (S. Zhu, R. V. F. Janssens, M. Carpenter, R. Broda,* W. Królas,* B. Fornal,* A. Gadea,† N. Marginean,† L. Corradi,† A. M. Stefanini,† J. Wrzesiński,* T. Pawłat,* S. Beghini,‡ G. DeAngelis,† F. Della Vedova,† E. Farnea,† E. Fioretto,† B. Guiot,† S. Lunardi,‡ P. Mantica,‖ P. Mason,‡ G. Montagnoli,‡ D. R. Napoli,† R. Orlandi,† I. Pokrovskiy,† E. Sahin,† F. Scarlassara,‡ S. Szilner,¶ C. A. Ur,‡ M. Trotta,§ and J. J. Valiente-Dobon†)

We used the PRISMA spectrometer coupled with the CLARA gamma multi-detector array at the Legnaro National Laboratory to identify gamma rays in exotic neutron-rich nuclei produced in the ^{48}Ca + ^{238}U reaction. The spectrometer is able to provide the nuclear product *A* and *Z* identification. The precise determination of the product velocity vectors allowed to correct properly for the Doppler shift of gamma rays emitted in flight and associated with a given isotope. The analysis focused on the neutron-rich ^{48}K and ^{49}K isotopes, and revealed a number of gamma transitions de-exciting states populated in each isotope. Figure I-22 displays the gamma spectrum obtained for ^{48}K.

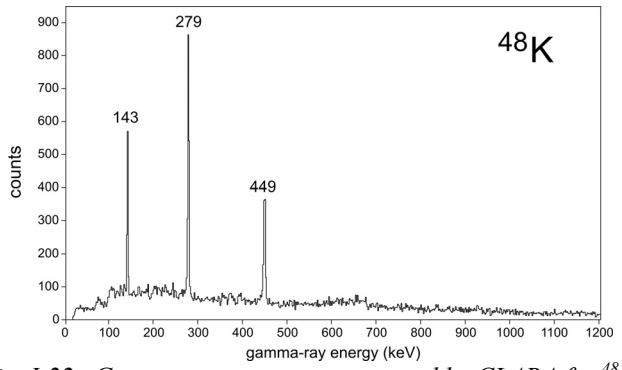

Fig. I-22. Gamma-ray spectrum measured by CLARA for ^{48}K.

The identified new gamma rays were used as the starting point in the analysis of the gamma coincidence data obtained for the same reaction in a thick target experiment performed earlier with the Gammasphere array at ANL in a series of experiments exploiting deep-inelastic heavy-ion reactions for the spectroscopy of neutron-rich nuclei.[1] In this experiment the identification of in-beam gamma transitions in exotic nuclei produced with very low cross-sections posed obvious difficulties, however, the presence of ^{48,49}K was clearly detected from the observed radioactive decays. The present PRISMA-CLARA results opened the way to establish the level schemes of both isotopes as shown in Fig. I-23. The assigned spins and parities are suggested based on the consideration of observed gamma decay features and simple shell model expectations.

The observed level structures of both isotopes contain essential information for improvements of the quantitative shell model description in this region of nuclei. The ^{48}K levels arise from the corresponding proton-neutron couplings and provide information on the two-body effective interactions of the $p_{3/2}$ neutron with $s_{1/2}$, $d_{3/2}$ proton-holes and a $f_{7/2}$ proton-particle. An important conclusion is that the ^{48}K ground state spin/parity is 1^- rather than the earlier accepted 2^- values which require some reinterpretation of the beta decay to the ^{48}Ca daughter. In the ^{49}K level scheme, the extra pair of $p_{3/2}$ neutrons increases the complexity, but the 771 keV state is assigned as the most probable lowest lying $3/2^+$ state. This indicates that just as in the ^{47}K, the $s_{1/2}$ proton-hole state is the ground state, but the $d_{3/2}$ level is located at much higher energy. Thus, in the present study of nuclear structure evolution with increasing neutron richness, one observes the continuation of the reordering trend of these proton-hole states as seen in a series of lighter potassium isotopes.

*Institute of Nuclear Physics, Krakow, Poland, †INFN, Laboratori Nazionali di Legnaro, Italy, ‡INFN, Padova and Universitá, Italy, §INFN, Sezione di Napoli, Italy, ¶Ruder Bošković Institute, Zagreb, Croatia, ||Michigan State University.

[1]R. Broda, J. Phys. G **32,** 151 (2006).

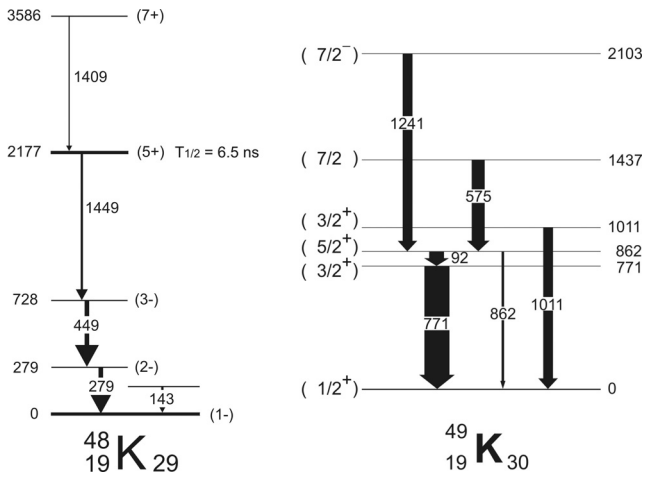

Fig. I-23. Established level schemes of ^{48}K and ^{49}K.

d.1.4. Yrast Structure of Neutron-Rich ^{51}Ca

(R. V. F. Janssens, M. P. Carpenter, S. Zhu, B. Fornal,* R. Broda,* N. Marginean,† L. Corradi,‡ G. De Angelis,† F. Della Vedova,† E. Farnea,† E. Fioretto,† A. Gadea,† M. Honma,‡ W. Królas,* S. Lunardi,§ P. F. Mantica,¶ P. Mason,|| G. Montagnoli,|| D. R. Napoli,† T. Otsuka,** T. Pawłat,* F. Scarlassara,|| A. M. Stefanini,† S. Szilner,†† C. A. Ur,|| M. Trotta,‡‡ J. J. Valiente-Dobon,† and J. Wrzesiński*)

Around doubly-magic ^{48}Ca, the neutron $\nu p_{3/2}$, $\nu p_{1/2}$ and $\nu f_{5/2}$ orbitals are significantly separated in energy. As evidenced in earlier studies, a $N = 32$ subshell closure in neutron-rich nuclei occurs,[1-3] reflecting the presence of an energy gap between the $\nu p_{3/2}$ orbital and the two other neutron states. This closure disappears when going towards the stability line due to the strong proton $\pi f_{7/2}$ - neutron $\nu f_{5/2}$ monopole interaction, primarily governed by the tensor force, which causes a decrease in energy of the $\nu f_{5/2}$ single-particle orbital with respect to the $\nu p_{3/2}$ and $\nu p_{1/2}$ levels as protons are added to the $\pi f_{7/2}$ shell.[4,5] It has been shown that the magnitude of this decrease is high enough to reduce a possible second gap, *i.e.*, between the $\nu p_{1/2}$ and $\nu f_{5/2}$ states, in the Ti and Cr isotopes.[6-8] In Ca nuclei, however, the $\nu p_{3/2}$, $\nu p_{1/2} - \nu f_{5/2}$ splitting may be sufficient to produce a subshell closure also at $N = 34$, but this feature is difficult to detect, as the states involving the $\nu f_{5/2}$ orbital in such species like $^{51-54}$Ca are hard to reach.

We investigated the yrast structure of ^{51}Ca by analyzing data from two complementary experiments. In the first measurement, γ-γ coincidence events, from neutron-rich species produced in deep-inelastic collisions of a ^{48}Ca beam on a thick ^{238}U target, were collected with the Gammasphere array at Argonne. The production rate of the ^{51}Ca nucleus was, however, too low to locate unambiguously new γ rays that weakly appeared in coincidence gates on the known (from the ^{51,52}K β-decay studies)[9] groundstate transitions in ^{51}Ca. In the second experiment the same system was investigated by employing the PRISMA spectrometer coupled with the CLARA γ-ray multi-detector array at the INFN, LNL Legnaro. A γ-ray spectrum from CLARA, gated on the ^{51}Ca products, showed a series of lines clearly belonging to ^{51}Ca (Fig. I-24). Out of those, three γ rays were known from the β-decay study.[9] Subsequent analysis of γ coincidence data taken with Gammasphere allowed us to establish coincidence relationships between the observed lines and to construct an extended level scheme for ^{51}Ca (Fig. I-25). Of special interest is a state located at 4320 keV with a tentative spin-parity assignment of 9/2 arising mostly from the $\nu p_{3/2}{}^2 f_{5/2}$ configuration, which involves an $f_{5/2}$ neutron. The energy of this state can be described quite well by shell-model calculations assuming a sizable energy gap between the $\nu p_{1/2}$ and $\nu f_{5/2}$ neutron orbitals at $Z = 20$.

*Institute of Nuclear Physics, PAN, Kraków, Poland, †INFN, Laboratori Nazionali di Legnaro, Italy,

‡University of Aizu, Japan, §Dipartimento di Fisica dell'Universita' di Padova, Italy, ¶Michigan State University,
||INFN, Sezione di Padova and Universitá di Padova, Italy, **University of Tokyo, Japan,
††Ruder Bošković Institute, Zagreb, Croatia, ‡‡INFN, Sezione di Napoli, Italy.

[1]A. Huck *et al.*, Phys. Rev C **31**, 2226 (1985).
[2]R. V. F. Janssens *et al*., Phys. Lett. **B546**, 55 (2002).
[3]A. Gade *et al*., Phys. Rev. C **74**, 021301(R) (2006).
[4]T. Otsuka *et al*., Phys. Rev. Lett. **87**, 082502 (2001).
[5]T. Otsuka *et al*., Phys. Rev. Lett. **95**, 232502 (2005).
[6]S. Liddick *et al*., Phys. Rev. Lett. **92**, 072502 (2004).
[7]B. Fornal *et al*., Phys. Rev. C **70**, 064304 (2004).
[8]S. Zhu *et al*., Phys. Rev. C **74**, 064315 (2006).
[9]F. Perrot *et al*., Phys. Rev. C **74**, 014313 (2006).

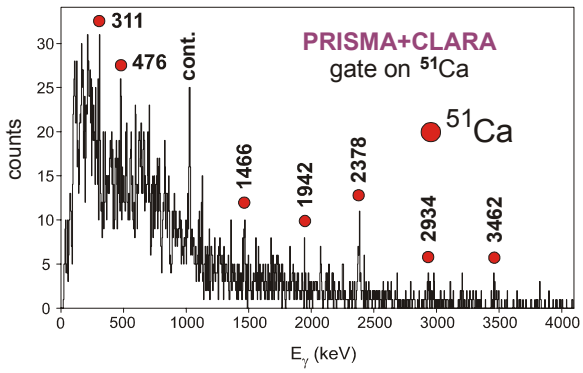

Fig. I-24. γ spectrum in coincidence with the ^{51}Ca products.

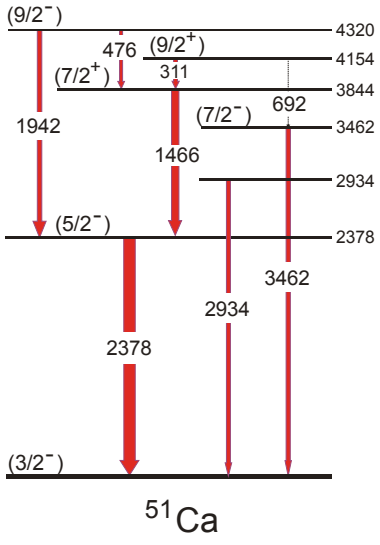

Fig. I-25. Proposed level scheme of ^{51}Ca.

d.1.5. One-Neutron Knockout in the Vicinity of the $N = 32$ Sub-Shell Closure: ^{9}Be(^{57}Cr,^{56}Cr + γ)X

(R. V. F. Janssens, M. P. Carpenter, S. Zhu, A. Gade,* D. Bazin,* B. A. Brown,* C. M. Campbell,* J. M. Cook,* A. N. Deacon,† D.-C. Dinca,* S. J. Freeman,† T. Glasmacher,* M. Horoi,‡ B. P. Kay,† P. F. Mantica,* W. F. Mueller,* J. R. Terry,* and J. A. Tostevin§)

The one-neutron knockout reaction ^{9}Be(^{57}Cr,^{56}Cr + γ)X has been measured in inverse kinematics with an intermediate-energy beam. Cross sections to individual states in ^{56}Cr were partially untangled through the detection of the characteristic γ-ray transitions in coincidence with the reaction residues. The experimental inclusive longitudinal momentum distribution and the yields to individual states were compared to calculations that combine spectroscopic factors from the full *fp* shell model and nucleon-removal cross sections computed in a few-body eikonal approach. The results of this study were published.[1]

*Michigan State University, †University of Manchester, United Kingdom, ‡Central Michigan University, §University of Surrey, United Kingdom.

[1]A. Gade *et al.*, Phys. Rev. C **74**, 047302 (2006).

d.1.6. One-Particle Excitations Outside the ^{54}Ti Semi-Magic Core: The ^{55}V and ^{55}Ti Yrast Structures

(S. Zhu, R. V. F. Janssens, M. P. Carpenter, F. G. Kondev, T. Lauritsen, C. J. Lister, A. Robinson, D. Seweryniak, X. Wang, B. Fornal,* S. J. Freeman,† M. Honma,‡ R. Broda,* A. N. Deacon,† B. P. Kay,† W. Króla,*§ J. Kozemczak,¶ A. Larabee,¶ S. N. Liddick,** P. F. Mantica,** T. Otsuka,†† T. Pawłat,* J. F. Smith,† D. Steppenbeck,† B. E. Tomlin,** and J. Wrzesiński*)

Our earlier work has clearly shown that the GXFP1 interaction is very successful in describing the yrast structure in the even-even ^{50,52,54}Ti isotopes and accounts for the $N = 32$ sub-shell closure, but fails in the case of ^{56}Ti ($N = 34$ sub-shell closure).[1,2,3] This led to a modified GXPF1 interaction, labeled GXPF1A, with a narrower $\nu p_{1/2}$-$\nu f_{5/2}$ gap in the effective single-particle energies. With five $T = 1$ matrix elements involving mainly the $\nu p_{1/2}$ and $\nu f_{5/2}$ single-particle orbitals modified, this interaction has provided a consistent description of the known low-lying structures along the entire chain of neutron-rich Ti isotopes, including ^{56}Ti. In order to provide new tests of full *pf*-shell calculations with the GXPF1A interaction, the level structures of ^{55}V and ^{55}Ti, the two nuclei with a single nucleon outside the semi-magic ^{54}Ti$_{32}$ core, have now been investigated. The excited states in ^{55}V and ^{55}Ti have been populated by utilizing both fusion-evaporation and deep-inelastic reactions. The level schemes obtained from these studies can be found in Figs. I-26 and I-27. Shell-model calculations with the GXPF1A Hamiltonian account for the data reasonably well. The addition of a proton does not appear to affect the $N = 32$ shell gap significantly, although comparisons between calculations and experiment at high spins ($I^{\pi} \geq 21/2^{-}$) indicate the need for a larger model space for an accurate description of the data in this regime. The energy separation between the $\nu p_{1/2}$ and $\nu f_{5/2}$ orbitals in neutron-rich Ti isotopes is not large enough to result in an $N = 34$ shell gap. However, comparisons between the ^{55}Ti data and the calculations argue for the presence of a sizable $N = 34$ gap in ^{54}Ca. The results of this study were published.[4]

*Institute of Nuclear Physics, Krakow, Poland, †University of Manchester, United Kingdom, ‡University of Aizu, Japan, §Joint Institute for Heavy Ion Research, ¶Greenville College, **Michigan State University, ††University of Tokyo, Japan.

[1]R. V. F. Janssens *et al.*, Phys. Lett. **B546**, 22 (2002).
[2]B. Fornal *et al.,* Phys. Rev. C **70**, 064304(2004).
[3]D.-C. Dinca *et al.,* Phys. Rev. C **71**, 041302(R) (2005).
[4]S. Zhu *et al.*, Phys. Lett. **B650**, 135 (2007).

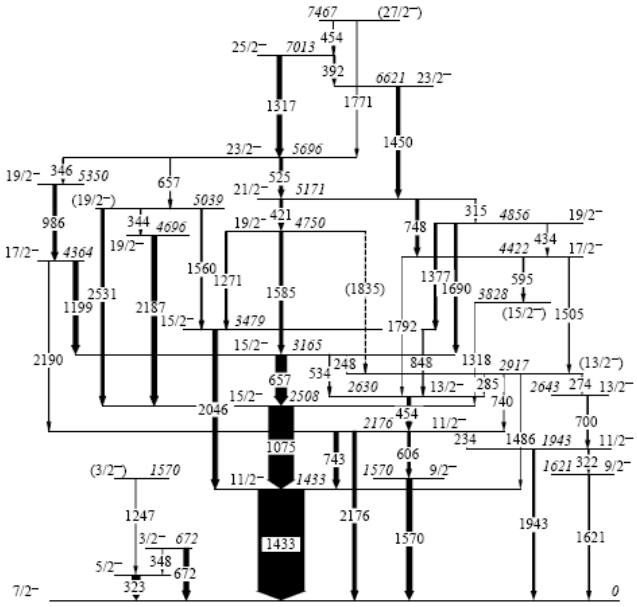

Fig. I-26. Proposed level scheme for ^{55}V.

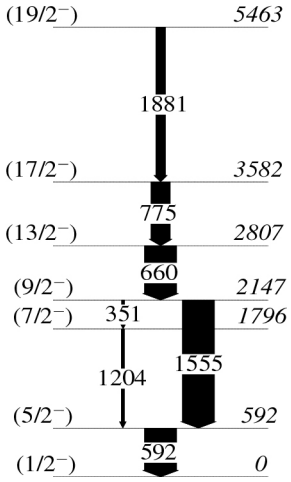

Fig. I-27. Proposed level scheme for ^{55}Ti.

d.1.7. Structure of the Even-Even Neutron-Rich ^{56,58,60}Cr Isotopes

(S. Zhu, R. V. F. Janssens, M. P. Carpenter, F. G. Kondev, T. Lauritsen, C. J. Lister, D. Seweryniak, A. N. Deacon,* S. J. Freeman,* R. Broda,† I. R. Calderin,‡ B. Fornal,† J. F. Smith,* S. L. Tabor,‡ B. J. Varley,* M. Honma,§ F. R. Xu,¶ P. Chowdhury,** W. Króla,† S. N. Liddick,†† P. F. Mantica,†† B. E. Tomlin,†† and J. Wrzesiński†)

The existence of the N = 32 sub-shell above doubly-magic ^{48}Ca has been firmly established in a series of recent experiments.[1,2] Shell model calculations with the GXPF1A effective interaction are able to account for this gap as resulting from a weakening of the $\pi 1f_{7/2}$-$\nu 1f_{5/2}$ proton-neutron monopole interaction as protons are removed from the $1f_{7/2}$ orbital, combined with a significant $\nu 2p_{1/2}$-$\nu 2p_{3/2}$ spin-orbit splitting.[3] With the $\pi f_{7/2}$ shell half-filled, Cr isotopes are among the nuclei best suited for studying the possible role of collectivity in the region. Recent studies of odd, neutron-rich Cr isotopes above N = 32 indicate an increasing involvement of the shape-driving $g_{9/2}$ orbital in the low-lying structure of neutron-rich Cr isotopes.[4] Experimental information on the excited states in the even-even, neutron-rich Cr nuclei provides further tests of the suitability of the *fp* shell-model space for the description of their level structure and of the possible shape-driving influence of the $\nu g_{9/2}$ orbital. The yrast states of the neutron-rich Cr isotopes were populated *via* two deep inelastic reactions of ^{48}Ca on 50 mg/cm^2 ^{208}Pb and ^{238}U targets at beam energies about 20% above the Coulomb barrier. Another approach used here for producing neutron-rich Cr isotopes involved fusion of ^{48}Ca projectiles with ^{14}C radioactive targets (thickness 100 μg/cm^2, ~90% enrichment). The beam energy was selected as 130 MeV to optimize two-proton evaporation producing ^{60}Cr. Reaction products were dispersed according to their charge-to-mass (A/q) ratio with the Fragment Mass Analyzer (FMA). An ion chamber behind the focal plane was used to provide Z resolution and separate ^{60}Cr residues from other isotopes with stronger yields.

The deduced level schemes of ^{56,58,60}Cr represent significant extensions over previous knowledge. Specifically, despite a low-spin structure reflecting the N = 32 sub-shell closure in ^{56}Cr, evidence was found at higher energy for a negative-parity sequence associated with prolate, collective rotation. This band exhibits striking similarities with those seen in the odd neighbors ^{55,57}Cr. The data collected for ^{58}Cr demonstrate unambiguously that the level scheme proposed recently by Marginean *et al.*[5] from a PRISMA + CLARA experiment is in error, raising considerable doubt about an interpretation in terms of an E(5) dynamical symmetry proposed in the latter work. In addition, the lowest observed negative-parity state in ^{58}Cr is ~1.1 MeV lower than that in ^{56}Cr, a trend similar to that exhibited by the $9/2^+$ ($\nu g_{9/2}$) bandheads in the odd Cr neighbors. Furthermore, the properties of the sequence built on this negative-parity state differ significantly from those seen in ^{56}Cr, consistent with the spherical or slightly oblate shape proposed for ^{59}Cr by Freeman *et al.*[6] The yrast sequence observed for the first time in ^{60}Cr is also consistent with an interpretation in terms of an oblate deformation. The results of this study have been published.[7]

*University of Manchester, United Kingdom, †Niewodniczanski Institute of Nuclear Physics, Krakow, Poland, ‡Florida State University, §University of Aizu, Japan, ¶Peking University, China, **University of Massachusetts, ††Michigan State University.

[1]R. V. F. Janssens *et al.*, Phys. Lett. **B546**, 55 (2002).
[2]D. C. Dinca *et al.*, Phys. Rev. C **71**, 041302(R) (2005), and references therein.
[3]M. Honma *et al.*, Phys. Rev. C **65**, 061301 (2002).
[4]A. N. Deacon *et al.*, Phys. Lett. **B622**, 151 (2005).
[5]N. Marginean *et al.*, Phys. Lett. **B633**, 696 (2006).
[6]S. J. Freeman *et al.*, Phys. Rev C **60**, 064301 (2004).
[7]S. Zhu *et al.*, Phys. Rev. C **74**, 064315 (2006).

d.1.8. Yrast Structures in the Neutron-Rich Isotopes ^{59,60}Fe and the Role of the $g_{9/2}$ Orbital

(R. V. F. Janssens, M. P. Carpenter, T. Lauritsen, C. J. Lister, D. Seweryniak, S. Zhu, A. N. Deacon,* S. J. Freeman,* M. Honma,† P. Chowdhury,‡ J. F. Smith,* S. L. Tabor,‡ B. J. Varley,* and F. R. Xu¶)

Neutron-rich *fp*-shell nuclei have been the subject of much recent investigation. Primarily, such work has been motivated by the increasing evidence for unexpected modifications to the single-particle structures of these exotic systems due to aspects of the nucleon-nucleon interaction not immediately apparent in near-stable systems. In understanding these developments a great deal of synergistic effort is occurring on both the theoretical and experimental fronts.[1-9] The Fe isotopes, with $Z = 26$, represent the next logical step in the investigation of neutron-rich *fp*-shell nuclei. The structure of the neutron-rich isotopes ^{59,60}Fe has been studied with the Gammasphere detector array using fusion-evaporation reactions. Level schemes for these nuclei have been extended to spins of ~20 ħ. Both isotopes exhibit regular, near-yrast γ-decay sequences which are generated by the intrusion of the $g_{9/2}$ orbital into the *fp* shell-model space. The yrast and near-yrast structures have been compared with the results of shell-model calculations using the GXPF1A interaction in the full *fp* model space, and the role of the $g_{9/2}$ orbital in the experimental data was assessed by comparison with total Routhian surface calculations. In both cases, shell-model calculations reproduce the low-lying, natural-parity states satisfactorily. TRS calculations indicate a very soft shape, becoming softer as the rotational frequency increases.

*University of Manchester, United Kingdom, †University of Aizu, Japan, ‡University of Massachusetts, ‡Florida State University, ¶Peking University, China.

[1]R. V. F. Janssens *et al*., Phys. Lett. **B546**, 55 (2002).
[2]T. Otsuka *et al*., Phys. Rev. Lett. **87**, 082502 (2001).
[3]M. Honma *et al*., Phys. Rev. C **65**, 061301 (2002).
[4]B. Fornal *et al*., Phys. Rev. C **70**, 064304 (2004).
[5]T. Otsuka *et al*., Phys. Rev. Lett. **95**, 232502 (2005).
[6]D.-C. Dinca *et al*., Phys. Rev. C **71**, 041302(R) (2005).
[7]A. N. Deacon *et al*., Phys. Lett. **B622**, 151 (2005).
[8]A. Gade *et al*., Phys. Rev. C **74**, 021301(R) (2006).
[9]S. Zhu *et al*., Phys. Rev. C **74**, 064315 (2006).

d.1.9. Deep Inelastic Reaction Studies with Gammasphere: The Structure of ^{61}Fe

(R. V. F. Janssens, M. P. Carpenter, T. Lauritsen, D. Seweryniak, S. Zhu, N. Hoteling,* W. B. Walters,* R. Broda,† B. Fornal,† A. A. Hecht,* M. Hjorth-Jensen,‡ W. Krolas,†§ T. Pawlat,† X. Wang,¶ A. Wohr,¶ and J. Wrzesinski†)

The recent identification of lowered 2^+ energy trends near $N = 40$ below ^{68}Ni has given rise to much discussion of a possible new region of deformation. This would appear to result from a growing influence from the $g_{9/2}$ neutron orbital as the neutron *pf* orbitals are filled. One way to study the effect of this orbital is to identify and study the positive parity states in odd-*A* isotopes near $N = 40$, where the *pf* shell is full. The location in energy and the structure of these levels will yield important information about the evolution of these isotopes toward $N = 40$, and can be used to further characterize the general features of nuclei in this region. In ^{61}Fe, an isomeric $9/2^+$ state representing a single neutron excitation into the $g_{9/2}$ orbital has already been identified, and characterized in terms of both magnetic and quadrupole moments. From the latter, a β_2 deformation of +0.26 or -0.24 has been suggested, indicating that this state is either prolate or oblate. To proceed further with such an interpretation, it is imperative that the bands and states above this isomer be established. Hence, in this experiment, data from the deep-inelastic reaction of ^{64}Ni + ^{238}U are used to identify new levels above the established isomer.

In this experiment, a pulsed beam of 450 MeV ^{64}Ni spaced by 410 ns was employed so that there would be time between pulses to allow for the decay of short-lived isomers, such as, for example, the ~0.25 μs state

in ^{61}Fe. Thus, it is possible to construct triple-coincidence cubes which utilize the time with respect to the beam pulse in order to separate "prompt" events from "delayed" events. With this technique, four coincidence cubes were produced: prompt-prompt-prompt (PPP), prompt-prompt-delayed (PPD), prompt-delayed-delayed (PDD), and delayed-delayed-delayed (DDD). Since there are two known transitions that decay, in sequence, from the 861 keV isomeric state, a double coincidence gate in the PDD cube yielded new transitions above the isomer. Once this was established, the PPD cube could be used to identify weaker transitions at higher energies in the level scheme.

New levels and gamma rays are presented in the level scheme in Fig. I-28. Also shown is a comparison with the shell model in which the calculated levels compare favorably with those determined from experiment. Since this agreement could only be achieved upon the lowering of the $g_{9/2}$ single particle energy by 1.7 MeV, these results appear to support an oblate deformation, as opposed to prolate, where one would expect more of a rotational character that is unlikely to be so well reproduced by the shell model.

A paper summarizing these results in currently in preparation.

*University of Maryland, †Niewodniczanski Institute of Nuclear Physics, Krakow, Poland, ‡University of Oslo, Norway, §Oak Ridge National Laboratory, ¶University of Notre Dame.

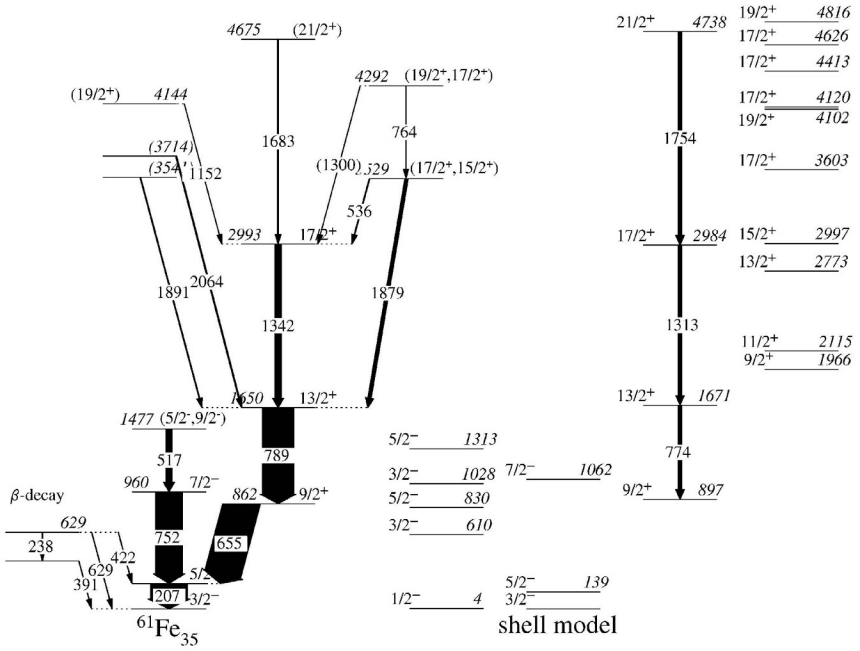

Fig. I-28. Level scheme determined for ^{61}Fe compared with shell model calculations.

d.1.10. Deep Inelastic Reaction Studies with Gammasphere: The Structure of ^{64}Fe

(R. V. F. Janssens, M. P. Carpenter, T. Lauritsen, D. Seweryniak, S. Zhu, N. Hoteling,* W. B. Walters,* R. Broda,† B. Fornal,† A. A. Hecht,* M. Hjorth-Jensen,‡ W. Krolas,†§ T. Pawlat,† D. X. Wang,¶ A. Wohr,¶ and J. Wrzesinski†)

The structure of ^{68}Ni and adjacent nuclei has been of considerable interest as neutron number 40 marks the filling of the $N = 3$ oscillator shell. Hence, there exists some remnant of a shell gap that has not been completely eroded away by the spin-orbit interaction, a fact that is evident in the 2^+ energy peak at $N = 40$ in ^{68}Ni. However, addition or subtraction of protons from the ^{68}Ni core leads to a very different behavior, as the 2^+ energies in, for example, the Fe isotopes, drops considerably as $N = 40$ is approached. Since such behavior is often associated with the onset of deformation, it is of special interest to investigate the

structure beyond the 2^+ energy in the Fe isotopes in this region. This additional data will, in turn, allow for a more complete and thorough analysis of the evolution of structure in this region, as well as a better understanding of the nucleon-nucleon interactions at play in these nuclei.

To investigate the neutron-rich Fe isotopes, an experiment was performed with the Gammasphere spectrometer in which the deep inelastic reaction of ^{64}Ni and ^{238}U was studied. A thick ^{238}U target was used so as to stop all reaction products at the target position centered in Gammasphere. Events were recorded under a three fold or higher condition. New levels in ^{64}Fe could be identified from a coincidence gate on the known 746 keV, $2^+ \rightarrow 0^+$ transition. Additional gamma rays with energies 582, 687, 781, 1005, 1017, 1078, and 1079 keV were identified and placed in the level scheme shown in Fig. I-29, which was compared to shell model calculations. The shell model results compared well for the 2^+ energy, but the excitation energy of higher-lying levels were increasingly over-predicted. A larger model space, in which the $g_{9/2}$ neutron orbital was included, gave more favorable results, emphasizing the increased importance of this state near $N = 40$.

Results from this work have been published in Physical Review C **74**, 064313 (2006).

*University of Maryland, †Niewodniczanski Institute of Nuclear Physics, Krakow, Poland, ‡University of Oslo, Norway, §Oak Ridge National Laboratory, ¶University of Notre Dame.

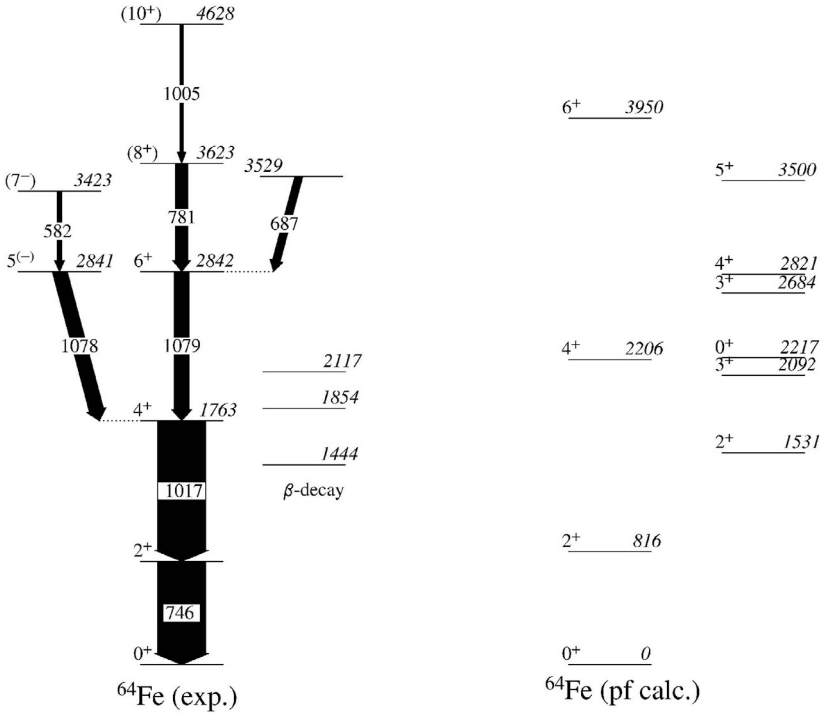

Fig. I-29. Level scheme adopted for ^{64}Fe, compared with shell model calculations.

d.1.11. Study of $N = 50$ Nuclei Near ^{78}Ni Using Deep Inelastic Reactions

(M. P. Carpenter, F. G. Kondev, R. V. F. Janssens, N. Hoteling, T. L. Khoo, T. Lauritsen, C. J. Lister, D. Seweryniak, X. Wang, S. Zhu, R. Broda,* B. Fornal,* A. Galindo-Uribarri,† A. Ibanez,‡ E. Padilla-Rodal,†,§ and J. P. Ureggo-Blanco§)

The study of doubly- and semi-magic nuclei have historically proven to be important in establishing for example the interaction strengths for the shell model. Until recently, these parameters were set by nuclei lying near the line of beta-stability, however, with the utilization of first and second generation radioactive beam facilities, studies of exotic neutron rich nuclei at and near closed shells have begun. What has motivated

many of these measurements from a nuclear structure standpoint is the fact that rearrangements of single-particle energies are observed in neutron rich systems. Such changes in the single-particle energies have been attributed to the attractive strength of the spin-isospin part of the effective nuclear interaction. As a result, one has observed the disappearance of certain magic numbers and the emergence of new closed shells.

While Gammasphere is not located at a traditional radioactive beam facility, one can still access neutron rich nuclei using techniques which do not require the acceleration of radioactive ions. For example, by studying the γ rays emitted after spontaneous fission of ^{248}Cm, important new information on excited states has been obtained for nuclei near ^{132}Sn. We have also studied neutron-rich nuclei using so-called deep inelastic reactions (DIC). In these studies, ^{208}Pb or ^{238}U targets are bombarded by a neutron rich stable beam at energies ~25% above the Coulomb barrier. By swapping protons and neutrons with the target, neutron-rich nuclei relative to the beam are produced, and their de-excitation by γ rays is studied with Gammasphere. Utilizing ^{48}Ca beams and DIC, we have studied the $N = 32$ and $N = 34$ isotopes ^{52,54}Ti to high spin and helped establish the presence of an $N = 32$ shell for $Z \leq 22$.[1,2]

With the success of the Gammasphere experiments utilizing a ^{48}Ca beam to explore the yrast sequences in the neutron rich Ti isotopes, we have extended our measurements into the region around $N = 50$ and $Z = 28$ (^{78}Ni). Neutron-rich nuclides in this region are of particular interest due to their role in the *r*-process, and in particular, their contribution to the peak in the solar elemental abundance near $A = 80$. While much is known with regards to the $N = 50$ isotones starting at ^{86}Kr and proceeding up towards ^{100}Sn, very little is known about the isotones approaching and including ^{78}Ni. In the Gammasphere measurement, data were collected using an ^{82}Se beam incident on both thick ^{208}Pb and ^{238}U targets. As a result, all products produced in these reactions are stopped in the target. Data were taken at two different beam energies - 525 and 630 MeV. In addition, the time between beam pulses was 400 ns allowing for the identification of isomers with lifetimes as long as several μsec.

One of the main purposes of this measurement was to identify the yrast structures for both ^{84}Se and ^{82}Ge to spins up to $\sim 12\ \hbar$. In addition, we hoped to develop detailed level structures for ^{81}Se, ^{83}Se, ^{83}As, ^{81}Ge, and possibly ^{83}Ge. Two separate blue data bases have been created from the data taken at 630 MeV which correspond to the ^{208}Pb and ^{238}U targets, respectively. Current results include a more extensive level scheme for ^{84}Se up to $I = 12\ \hbar$ and excited states in ^{82}Ge have been identified up to $I = 6\ \hbar$ (see Fig. I-30).

*Niewodniczanki Institute of Nuclear Physics, Cracow, Poland, †Oak Ridge National Laboratory, ‡National Autonomous University of Mexico, Mexico City, Mexico §University of Tennessee.

[1]R. V. F. Janssens *et al*., Phys. Lett. **B546**, 55 (2002).
[2]B. Fornal *et al*., Phys. Rev. C **70**, 064304 (2004).

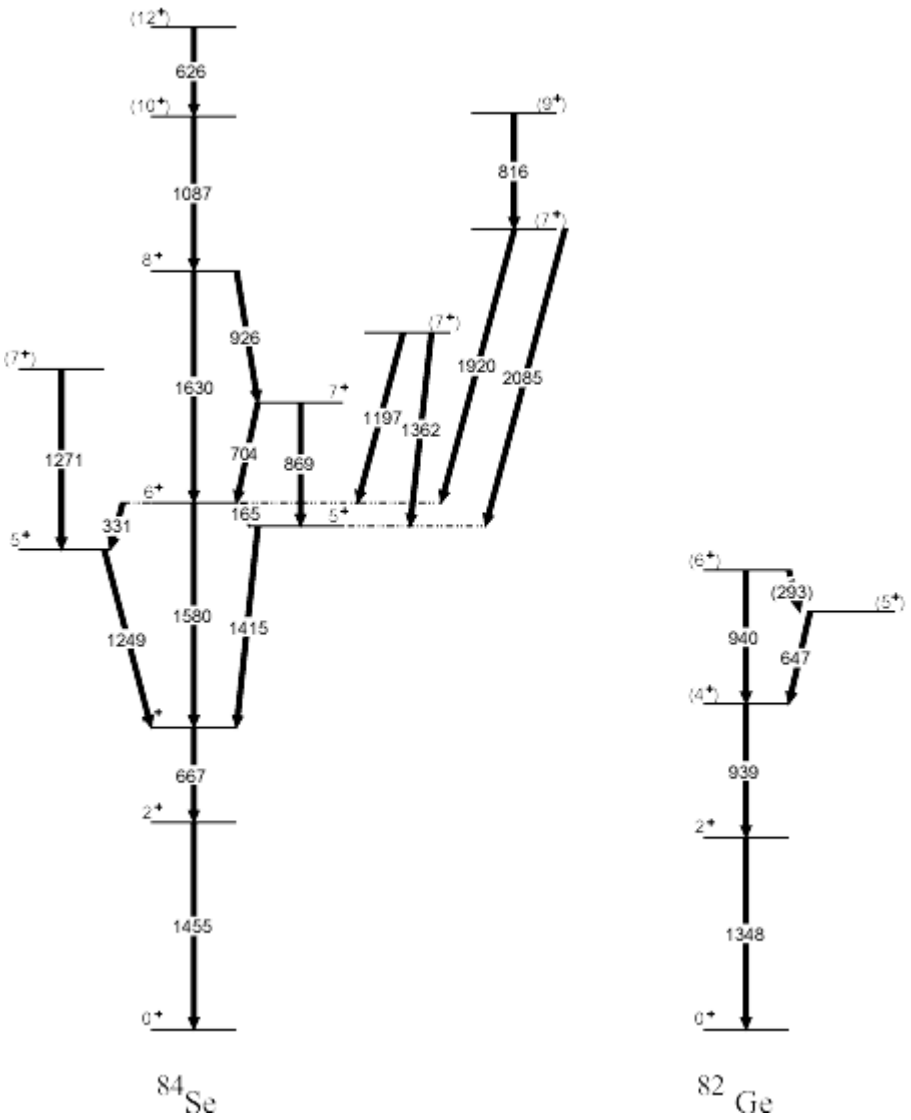

Fig. I-30. Partial level schemes for the N = 50 isotones deduced from this work.

d.1.12. Structure of Neutron-Rich Zn Isotopes (A. A. Hecht,* N. Hoteling,* M. P. Carpenter, R. V. F. Janssens, S. Zhu, F. G. Kondev, T. L. Khoo, T. Lauritsen, C. J. Lister, D. Seweryniak, X. Wang, W. B. Walters,† J. Stone,† R. Broda,‡ B. Fornal,‡ W. Krolas,‡ J. Wrzesinski,‡ A. Galindo-Uribarri,§ A. Ibanez,¶ E. Padilla-Rodal,§,|| J. P. Ureggo-Blanco,|| and A. F. Lisetskiy**)

The neutron rich region near doubly-magic ^{78}Ni is significant to both nuclear structure and nuclear astrophysics: as experimental input for models on shell structure far from stability and as the seed region for the beginning of the rapid neutron capture process of nucleosynthesis. This region is not easily accessible experimentally with most of the data on excited states coming from beta decay studies. Expanding this knowledge to high spin states, deep inelastic scattering (DIS) experiments were performed at the ATLAS accelerator center at Argonne National Laboratory using pulsed beams of ^{82}Se and of ^{64}Ni impinged on thick targets of ^{238}U and ^{208}Pb. Gamma-rays were detected by the Gammasphere array consisting of 101 Compton-suppressed HPGe counters.

Focusing on Zn, excited states in the even-even nuclei $^{66-78}$Zn were observed using γ–γ–γ coincidence matrices. Several new levels were found for $^{66-76}$Zn, and many previously known levels were confirmed. Levels were tentatively identified up to 12^+ in ^{66}Zn, 14^+ in ^{68}Zn, 12^+ in ^{70}Zn, 12^+ in ^{72}Zn, 10^+ in ^{74}Zn and 6^+ in ^{76}Zn. Using the angular sensitivity of Gammasphere, angular correlations were studied in order to deduce the spins for several of the new states, and fix the spins of levels that were previously tentatively assigned. The variation in energy of the positive parity yrast levels as a function of neutron number for the even Zn isotopes is plotted in Fig. I-31.

Of particular interest are the tentative observation of two 6^+ states lying below the first excited 8^+ states in ^{74}Zn with the yrast intensity flowing largely through the upper 6^+ level. It was found in Ref. 1 and 2 that due to the enhanced two-body interaction in the $(g_{9/2})^2_{I\,=\,2}$ channel, there is an unusual ordering of seniority $s = 4$ and $s = 2$ states ($s = 4$ is lower in energy than $s = 2$) for both the $I = 4^+$ and $I = 6^+$ states in ^{72}Ni with the $s = 2$ and $s = 4$ $I = 6^+$ levels lower than the $I = 8^+$, $s = 2$ state. The seniority symmetry imposes selection rules where *E2* transitions between the states with the same seniority are strongly hindered. The apparent observation of two low lying 6^+ levels in ^{74}Zn is a direct consequence of the phenomena studied in ^{72}Ni and the seniority selection rules. By adding two protons to ^{72}Ni, the $\nu g_{9/2}$ content of the high-spin states does not change much, but stronger mixing of $(g_{9/2})^n$ configurations occurs with different n values and a breaking of the seniority symmetry. The shell model predicts almost the same B(*E2*) value for the decay of the $I = 8^+$ to $I = 6^+_{1,2}$ for ^{74}Zn while experiment shows the larger intensity for the transition to the $I = 6^+_2$ state. The shell model predicts a similar lowering of the $I = 6^+_{1,2}$ in ^{76}Zn, put predicts different results for ^{78}Zn, where the small B(*E2*) and small energy gap between the $I = 8^+$ and $I = 6^+_1$ states lead to and isomeric lifetime for the $I = 8^+$ level.

A manuscript reporting both the experimental data and shell model calculations is currently under preparation.

*University of Maryland and Argonne National Laboratory, †University of Maryland, ‡Niewodniczanki Institute of Nuclear Physics, Cracow, Poland, §Oak Ridge National Laboratory, ¶Autonomous University of Mexico, Mexico City, Mexico ||University of Tennessee, **University of Arizona.

[1]A. F. Lisetskiy, AIP Conference Proceedings **725(1)**, 231 (2004).
[2]M. Horoi, AIP Conference Proceedings **764**, 170 (2005).

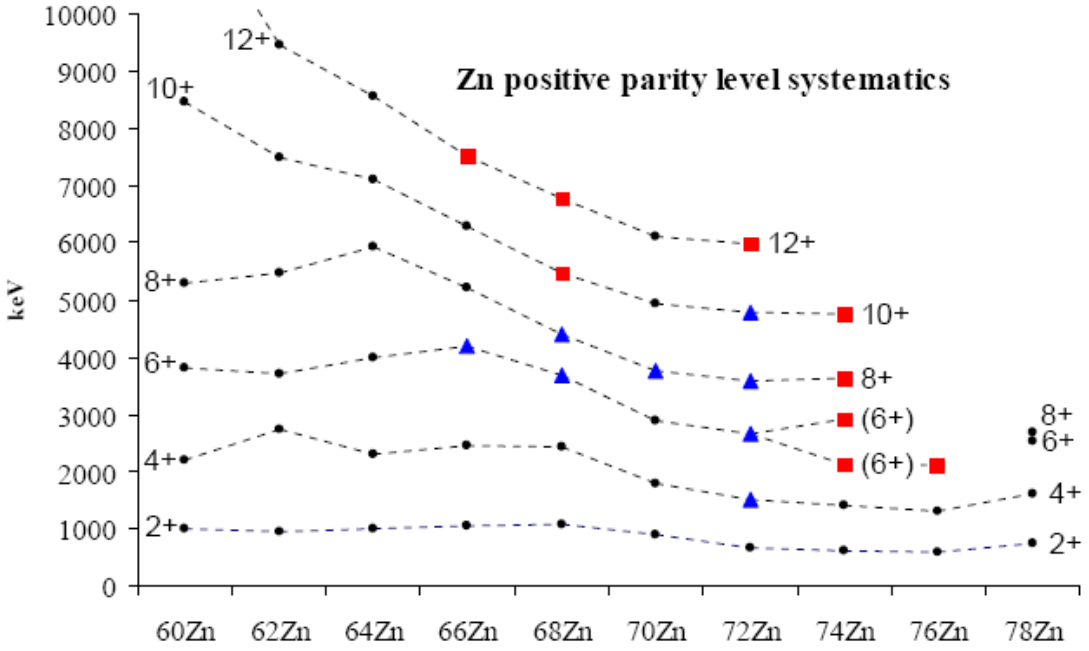

Fig. I-31. Even parity yrast level energies for Zn isotopes as a function of neutron number. Red squares represent new levels found in this work. Blue triangles represent levels with previously unsure level spins and parities which were fixed in this work.

d.1.13. Beta-Decay Studies of Neutron-Rich Fission Products for Advanced Fuel Cycle Applications (C. J. Lister, F. G. Kondev,*and P. Chowdhury†)

The DOE Office of Science issued a call for proposals for projects which allowed research into the physics of advanced fuel cycles while remaining inside the core mission of the Office. The call was entitled "Nuclear Physics Research and Development for the Advanced Fuel Cycles, LAB 07-05". The physics division at ANL appears well positioned for this type of research, especially in the light of the CARIBU upgrade and the available equipment. A joint ANL/PHY, ANL/NE, University of Massachusetts-Lowell proposal was prepared and submitted. The proposals are expected to be reviewed in the summer of 2007 with funding from FY2008-2010.

The proposal abstract reads:

Beams of mass-separated neutron-rich isotopes that are important for Advanced Fuel Cycle (AFC) research will be extracted from the CARIBU source at the Argonne ATLAS accelerator and will be studied with our existing suite of high quality spectroscopic tools (Penning Traps, the Fragment Mass Analyzer, Gammasphere, Total Absorption Gamma Spectrometer, the X-Array). The Nuclear Engineering program at Argonne will collaborate in this research and provide insight into the most important measurements for AFC and will rapidly disseminate results into the appropriate databases. The University of Massachusetts-Lowell will add their expertise in applied nuclear physics, and draw new young scientists into this research. Together, these resources offer a unique opportunity for significantly improved β-decay measurements of fission fragments that are relevant not only for AFC reactor design, but also for nuclear structure studies and astrophysics. We propose to strengthen the infrastructure for β-decay studies at ATLAS immediately, with short-term nuclear structure physics goals, and then start a program of detailed decay measurements on key isotopes for AFC research as soon as CARIBU is operational.

*Nuclear Engineering Division, Argonne National Laboratory. †University of Massachusetts-Lowell.

d.1.14. Multi-Quasiparticle K-Isomers in ^{174}Lu and Neutron-Rich ^{172,174}Er

(M. P. Carpenter, F. G. Kondev, R. V. F. Janssens, T. Lauritsen, D. Seweryniak, S. Zhu, G. D. Dracoulis,* G. J. Lane,* A. P. Byrne,* R. O. Hughes,* P. Nieminen,* H. Watanabe,* P. Chowdhury,† and F. R. Xu‡)

Deep inelastic reactions on a series of rare earth targets have been performed at Gammasphere utilizing a ^{136}Xe beam with a beam energy of ~6 MeV/nucleon. The targets used have been thick in order that the excited nuclei are stopped in the target before they decay. Beam pulsing has also been utilized in order to search for high-K isomers which are plentiful in this mass region ($70 \leq Z \leq 82$). Two papers were published in 2006 reporting results from these measurements.

In the first publication, two-quasiparticle, isomeric states have been identified in the neutron rich isotopes ^{172,174}Er. In the case of ^{172}Er, a candidate for the $K^{\pi} = 6^{+}$ two-quasineutron state is found at 1500 keV. In ^{174}Er, a nuclide whose level scheme was previously unknown, a long-lived isomer at 1112 keV decaying *via* an inhibited E1 transition and revealing the yrast sequence of ^{174}Er. This isomer is proposed to be a $K^{\pi} = 8^{-}$, two-quasineutron state, defining a sequence in the $N = 106$ isotones extending from the well-deformed neutron-rich isotope ^{174}Er to the neutron-deficient isotope ^{188}Pb, where the presence of the isomer signifies a prolate minimum in an otherwise spherical well. Configuration-constrained potential-energy surface calculations are used to predict the excitation energy of the 6^{+} and 8^{-} intrinsic states and as a basis for extracting the pairing force strength, G_n, in the $N = 104$ and $N = 106$ isotones. These results are published in Ref. 1.

The second publication reports on a $K^{\pi} = 13^{+}$, 280 ns four-quasiparticle isomer identified in the odd-odd nucleus ^{174}Lu. The isomer decays to both $K^{\pi} = 7^{+}$ and $K^{\pi} = 0^{+}$ rotational bands obtained from the parallel and antiparallel coupling of the proton $7/2^{+}[404]$ and neutron $7/2^{+}[633]$ orbitals. K mixing caused by particle-rotation coupling explains the anomalously fast transition rates to the 7^{+} band but those to the 0^{+} band are caused by a chance degeneracy between the isomer and a collective state, allowing the mixing matrix element for a large K difference to be deduced. Details can be found in Ref. 2.

*Australian National University, Canberra, Australia, †University of Massachusetts-Lowell, ‡Peking University, Beijing, China.

[1]G. D. Dracoulis *et al*., Phys. Lett. **B635**, 200 (2006).
[2]G. D. Dracoulis *et al*., Phys. Rev. Lett. **97**, 122501 (2006).

d.2. Proton-Rich Nuclei

d.2.1. Single-Neutron States in ^{101}Sn

(D. Seweryniak, M. P. Carpenter, S. Gros, R. V. F. Janssens, T. L. Khoo, T. Lauritsen, C. J. Lister, D. Peterson, A. P. Robinson, S. Zhu, X. Wang,* A. A. Hecht,† N. Hoteling,† G. Lotay‡, W. B. Walters†, and P. J. Woods‡)

Doubly-magic nuclei are the cornerstones of the nuclear landscape. Studying the properties of exotic doubly-magic nuclei such as ^{48}Ni, ^{78}Ni, ^{100}Sn and ^{132}Sn is essential for understanding the evolution of the nuclear structure far from the line of stability. Single-particle energies are important characteristics of doubly-magic nuclei. They provide a stringent test of nuclear mean field models and are essential ingredients in shell-model calculations of multi-nucleon configurations.

Due to low population cross sections the ^{100}Sn nucleus and its neighbors are not known very well. A search for γ-ray transitions in ^{101}Sn, which contains only one neutron outside of the ^{100}Sn core, was carried out at ATLAS. ^{101}Sn nuclei were produced using the ^{46}Ti(^{58}Ni,3n)^{101}Sn reaction with the cross section of only ~50 nb. Beta-delayed protons with energies and decay times consistent with previous ^{101}Sn decay studies[1] were observed at the focal plane of the FMA. In-beam γ rays were detected in Gammasphere and were correlated with the ^{101}Sn β-delayed protons using the Recoil-Decay Tagging method.

The resulting ^{101}Sn γ-ray spectrum is shown in Fig. I-32 (top) along with the spectrum of γ rays randomly correlated with long-lived β-particles (bottom). A γ-ray line at 172 keV can be seen in the ^{101}Sn spectrum, which is absent in the background spectrum. Based on the systematics of N = 51 isotones this line was interpreted as a transition between the neutron $g_{7/2}$ and $d_{5/2}$ orbitals.

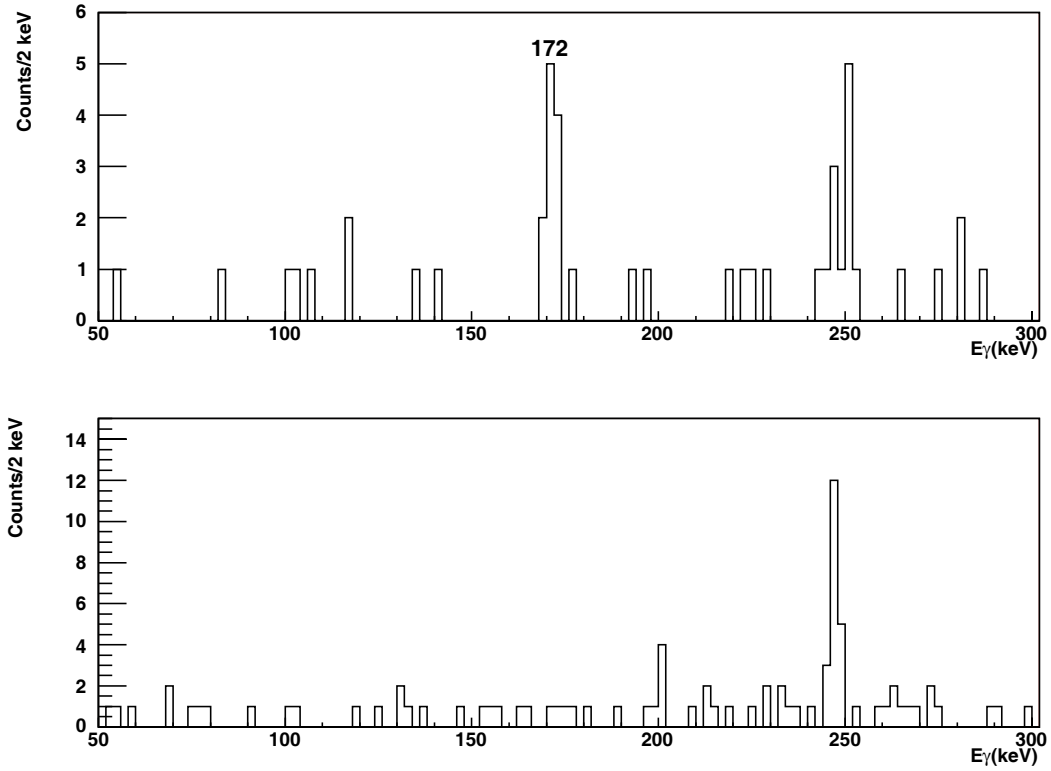

Fig. I-32. (top) Gamma rays tagged with ^{101}Sn β-delayed protons and (bottom) randomly correlated with long lived β emitters.

The separation energy between the $d_{5/2}$ and $g_{7/2}$ neutron states calculated using various mean-field potentials are widely spread and are on average larger than the measured value. Inclusion of tensor effects might help to reconcile the data and theory. The measured $d_{5/2}$-$g_{7/2}$ energy difference was used to calculate excited states in light $^{102\text{-}109}$Sn isotopes in the shell-model framework. Excellent agreement between the calculations and the data was obtained after attenuating the $(g_{7/2})_{0+}$ interaction by about 30%.

A search for core-excited states in ^{101}Sn is planned using the existing implantation station. The same method can be used to learn about proton-neutron interactions in the β-delayed proton emitter ^{100}In although a high granularity DSSD will be required in this case.

More experimental details and full discussion can be found in Ref. 2.

*Argonne National Laboratory and University of Notre Dame, †University of Maryland, ‡University of Edinburgh, United Kingdom.

[1]O. Kavatsyuk *et al.*, Eur. Phys. J. A **31**, 319 (2007).
[2]D. Seweryniak *et al.*, Phys. Rev. Lett. **99**, 022504 (2007).

d.2.2. Isospin Symmetry of Odd-Odd Mirror Nuclei: Identification of Excited States in ^{48}Mn and a Comparison to the Mirror Nucleus ^{48}V

(M. P. Carpenter, C. N. Davids, R. V. F. Janssens, C. J. Lister, D. Seweryniak, M. A. Bentley,* C. Chandler,† M. J. Taylor,* J. Brown,* J. Ekman,‡ S. J. Freeman,§ P. E. Garrett,¶ G. Hammond,† S. M. Lenzi,|| and R. du Rietz‡)

The fact that the attractive nuclear force acting between all neutrons and protons is approximately charge symmetric yields some startling and beautiful symmetries in nuclear behavior. The classic example is mirror symmetry, where two nuclei with interchanged numbers of protons and neutrons exhibit near-identical energy-level schemes. The Coulomb interaction lifts this degeneracy, and energy shifts result. However, the underlying spatial symmetry of the wave functions of these analogue states is generally preserved, and the resulting energy differences can be interpreted in terms of Coulomb phenomena. The long-range and well-understood Coulomb force, thus, has the potential to provide an extremely sensitive probe of spatial correlations and distributions of the protons in the nucleus.

Over the last decade, experimental advances have allowed for the study of the proton-rich members of mirror pairs in the $A \sim 40$-60 region. Fortuitously, one of the most successful nuclear models - the large scale *pf* shell model - is now able to perform calculations in the whole *pf* shell, and has been applied to model Coulomb effects in this region. The differences in excitation energy [mirror energy differences (MED)] between analogue states have been shown to be remarkably sensitive to nuclear structure effects and, through detailed comparison with the shell model results, can now be interpreted with *quantitative* reliability. Mirror-pair spectroscopy in this region has so far been restricted to odd-A $T_Z = \pm ½$ or even-even $T_Z = \pm 1$ mirror pairs. We have recently measured for the first time a $T = 1$ odd-odd mirror pair with $A > 40$, namely, ^{48}Mn/^{48}V to high spin. The MED behavior is unlike any other observed in this region and, uniquely, is interpreted almost entirely in terms of a subtle shrinking of the nuclear radius as a function of angular momentum.

The experiment was performed at the ATLAS facility of the Argonne National Laboratory, where a beam of 110 MeV ^{40}Ca bombarded a self supporting ^{10}B target. The nuclei ^{48}Mn or ^{48}V were produced *via* the evaporation of two neutrons or protons, respectively. The γ rays were detected with the Gammasphere array, which comprised 98 large-volume Compton-suppressed Ge detectors. The cross section leading to ^{48}Mn is expected to be a few tens of microbarns, a factor of $\sim 10^4$ weaker than the expected intensity of the mirror, ^{48}V, and, thus, unique identification of the recoils is essential. The recoiling nuclei were analyzed using the Fragment Mass Analyzer (FMA) which separates the residues as a function of M/q at the focal plane. Z identification is achieved using a split-anode isobutane-filled ionization chamber located behind the focal plane.

Figure I-33a shows the MED for the yrast positive parity sequence for the ^{48}Mn/^{48}V mirror pair along with the result of a full *pf* shell-model calculation based on the ANTOINE code[1] with Coulomb effects determined by the method described by Zuker *et al.*[2] In the odd-A and even-even mirror pairs of this region, the dominant Coulomb effect observed is a multipole effect associated with the angular-momentum recoupling of pairs of $f_{7/2}$ protons as a function of angular momentum. For these odd-odd nuclei, this effect is blocked by the occupation in both ^{48}Mn and ^{48}V of both $f_{7/2}$ protons and $f_{7/2}$ neutrons in the positive parity sequence. Despite the obvious restrictions placed on the shell model by limits on the valence space, and, hence, the need to assume a significant inert core, the full-*pf* shell model gives a remarkably accurate state-by-state account of the spin dependence of energy differences throughout the entire yrast sequence. In order to understand the behavior of the MED observed and calculated in Fig. I-33a, a single-*j* shell scenario, where only $f_{7/2}$ configurations are allowed is considered. The results of this calculation are shown in Fig. I-33b, and illustrates that the rise in MED results nearly entirely from radial effects, *i.e*. the shrinking of the nucleus with increasing spin.

A more complete account of these results can be found in a recent publication in Physical Review Letters.[3]

*University of York, United Kingdom, †Keele University, Straffordshire, United Kingdom, ‡Lund University, Sweden, §University of Manchester, United Kingdom, ¶University of Guelph, Ontario, ||INFN, Padova, Italy

[1] E. Caurier *et al*., Phys. Rev. C **50**, 225 (1994).

[2]A. P. Zuker *et al*., Phys. Rev. Lett. **89**, 142502 (2002).
[3]M. A. Bentley *et al.,* Phys. Rev. Lett. **97**, 132501 (2006).

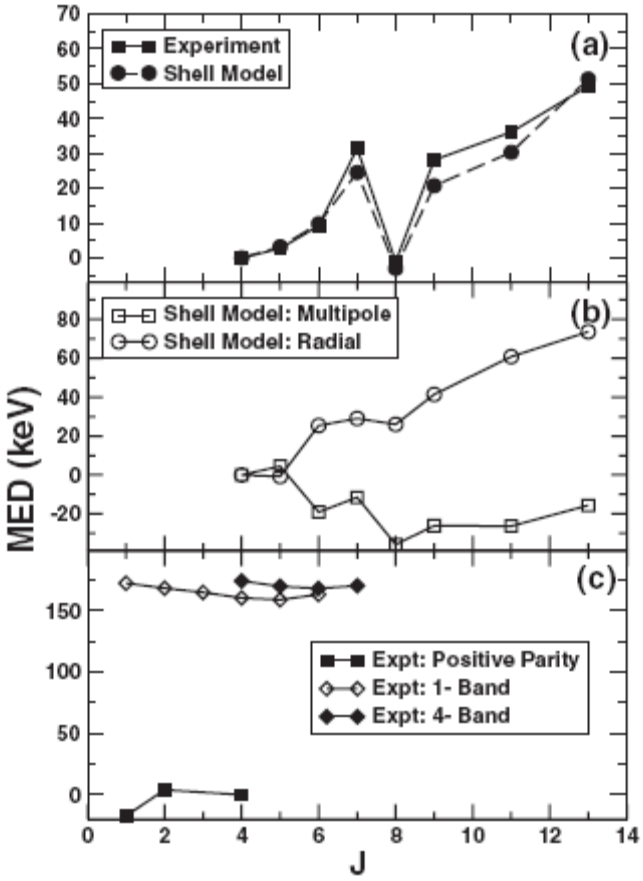

Fig. I-33. Mirror energy differences (MED) for the T = 1 states of ^{48}M/^{48}V. (a) The experimental MED, along with the predictions of the shell model, for the positive-parity states. (b) The calculated multipole and radial contributions to the MED (see Ref. 3 for details). (c) The MED for the negative-parity structures based on the $J^{\pi} = 1^-, 4^-$ states and the MED for the non-yrast positive-parity states into which they feed.

d.2.3. Coulomb Shifts and Shape Changes in the Mass 70 Region

(C. J. Lister, B. S. Nara Singh,* A. N. Steer,* D. G. Jenkins,* R. Wadsworth,* M. A. Bentley,* P. J. Davies,* R. Glover,* N. S. Pattabiraman,* T. Grahn,† P. T. Greenlees,† P. Jones,† R. Julin,† S. Juutinen,† M. Leino,† M. Nyman,† J. Pakarinen,† P. Rahkila,† J. Sarén,† C. Scholey,† J. Sorri,† J. Uusitalo,† P. A. Butler,‡ M. Dimmock,‡ D. T. Joss,‡ J. Thomson,‡ B. Cederwall,§ B. Hadinia,§ and M. Sandzelius§)

The odd-odd nucleus ^{78}Y was studied at ATLAS (using Gammasphere) and at Jyväskylä (using Juroball and RITU) by a York-ANL-Jyväskylä collaboration. *T = 1* excited states were found for the first time in the Jyväskylä experiment, while the ANL data set was contaminated by reactions on light impurities. Even with the knowledge of the locations of the states, no useful coincidence information could be extracted from the Gammasphere data set, despite lengthy investigation. The unusual negative Coulomb shifts were interpreted as arising from the nuclear shape smoothly increasing with spin.

This work has now been published.[1]

*University of York, United Kingdom, †University of Jyväskylä, Finland, ‡University of Liverpool, United Kingdom, §Royal Institute of Technology, Stockholm, Sweden.
[1]Phys. Rev. C **75**, 061301(R) (2007).

d.2.4. Shapes and Triaxiality of ^{74}Kr (C. J. Lister and S. M. Fischer)

Shape coexistence in light krypton isotopes is providing an exquisite test of current nuclear theories. Recently, Coulomb excitation of ^{74,76}Kr at GANIL has added detailed information on the shapes and their excitation modes. From a variety of "in-beam" Gammasphere experiments we have found relevant new additional information which compliments the inelastic excitation studies. In particular, the role of triaxial shapes can be delineated. In fusion reactions producing ^{74}Kr, a triaxial shape band appears to be the main path for populating the known low-lying oblate shape isomer.

A paper is being written and will be submitted in FY2007.

d.2.5. *T = 1* States in ^{74}Rb and Their ^{74}Kr Analogs (S. M. Fischer,* C. J. Lister, N. J. Hammond, R. V. F. Janssens, T. L. Khoo, T. Lauritsen, E. F. Moore, D. Seweryniak, S. Sinha, D. P. Balamuth,† P. A. Hausladen,† D. G. Sarantites,‡ W. Reviol,‡ P. Chowdhury,§ S. D. Paul,¶ C. Baktash,¶ and C.-H. Yu¶)

^{74}Rb was investigated in connection with the issue of the strength of the *np*-pairing field and also because of its significance in testing the wavefunctions needed for inferring the structure-free decay rate of the superallowed ^{74}Rb - ^{74}Kr β-decay. The *T = 1* analogs of the ^{74}Kr groundstate band were found, revealing rather small Coulomb shifts, but a candidate for the important low-lying J = 0 state was not found.

This work was published.[1]

*DePaul University and Argonne National Laboratory, †University of Pennsylvania, ‡Washington University, §University of Massachusetts-Lowell, ¶Oak Ridge National Laboratory.
[1]Phys. Rev. C **74**, 054304 (2006).

d.2.6. Mapping the Periphery of Deformation in the *A* ~ 80 Region: A Study of ^{83}Nb (S. M. Fischer, C. J. Lister, M. P. Carpenter, N. J. Hammond, R. V. F. Janssens, E. F. Moore, G. Mukherjee, D. Seweryniak, S. Sinha, S. J. Freeman,* J. Carney,† D. P. Balamuth,‡ and Y. Sun§)

The upper edge of the highly deformed region near *A* ~ 80 has been investigated at ATLAS using a conventional fusion-evaporation reaction. Large deformation was found for ^{83}Nb. Analysis suggests the conditions are right for K-isomers. The results have now been published.[1] This research has proven timely, as new experiments have recently revealed isomers in *N* = *Z* ^{82}Nb and ^{86}Tc and observed their decays. The isomers were produced at GSI following fragmentation experiments. The understanding of these isomers critically depends on the deformation inferred for ^{83}Nb. A possible interpretation is that they are two-quasiparticle K-isomers, relative to a *T = 1 np*-paired vacuum groundstate.

*University of Manchester, United Kingdom, †DePaul University, ‡University of Pennsylvania, §University of Notre Dame.
[1]S. M. Fischer *et al*., Phys. Rev. C **75**, 064310 (2007).

d.2.7. Effect of a Triaxial Nuclear Shape on Proton Tunneling in ^{145}Tm

(D. Seweryniak, C. N. Davids, M. P. Carpenter, N. Hammond, R. V. F. Janssens, T.-L. Khoo, G. Mukherjee, S. Sinha, S. J. Freeman,* A. Woehr,† A. Robinson,‡ P. J. Woods,‡ B. Blank,§ T. Davinson,‡ N. Hoteling,¶ Z. Liu,‡ J. Shergur,¶ A. A. Sonzogni,|| and W. B. Walters¶)

Proton decay is an important source of information on nuclear structure beyond the proton drip line. Transitional ^{145,146,147}Tm proton emitters are situated between spherical nuclei along the $N = 82$ shell closure and an island of prolate deformation. In fact, proton-rich $N = 76,77,78$ isotones are predicted to be triaxial or γ-soft. This offers a unique opportunity to shed light on the role of triaxiality on the proton emission. In order to learn more about the structure of the proton emitter ^{145}Tm, a search for in-beam γ rays with Gammasphere and the Fragment Mass Analyzer was carried out using the Recoil-Decay Tagging method. The ^{145}Tm ground-state rotational band was found to exhibit the properties expected for a $h_{11/2}$ proton decoupled band. In addition, coincidences between protons feeding the 2^+ state in ^{144}Er and the 2^+-0^+ γ-ray transition were detected, the first measurement of this kind, leading to a more precise value for the 2^+ excitation energy of 329(1) keV.

As shown in Fig. I-34, calculations using the Particle-Rotor model indicate that the properties of the $\pi_{11/2}$ band are consistent with the presence of triaxiality with an asymmetry parameter $\gamma \sim 20^o$ if the calculated value of $\beta_2 = 0.25$ is used.

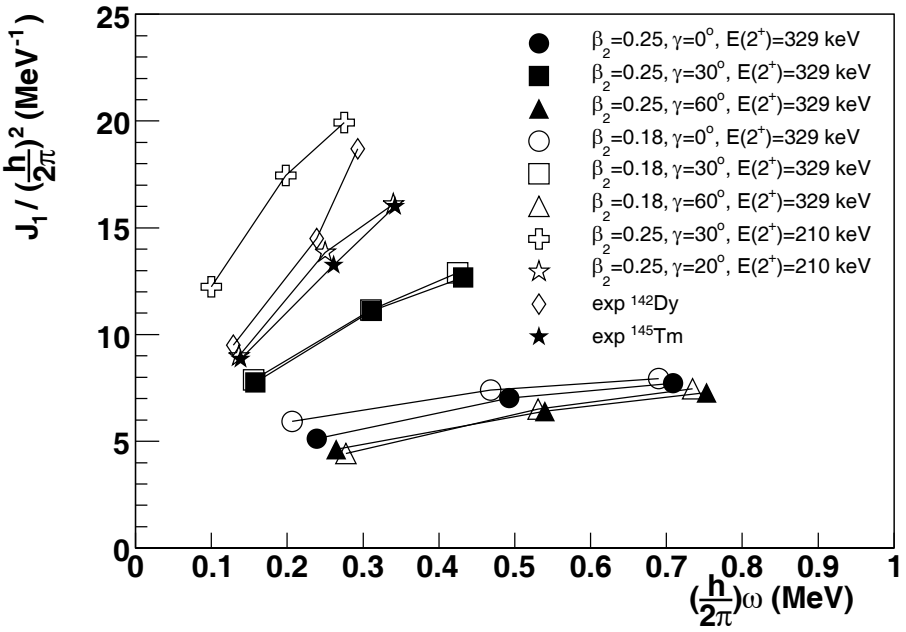

Fig I-34. The moment of inertia as a function of the rotational frequency extracted for the ^{145}Tm $\pi h_{11/2}$ band and the values calculated with the Particle Rotor model using different quadrupole deformations β_2, asymmetry parameters γ, and moments of inertia (obtained from the 2^+ energies). Smaller $E(2^+) = 210$ keV takes into account increase in the moment of inertia as a function of the rotational frequency similar to the lighter $N = 76$ isotones. The moment of inertia for the even-even $N = 76$ isotone ^{142}Dy is plotted for comparison.

The ground state wave function components $0^+ \otimes h_{11/2}$ and $2^+ \otimes f_{7/2}$ calculated using the Core Quasi-Particle Coupling model for $\beta_2 = 0.25$ and $\gamma = 20^o$ are also consistent with that deduced from the proton decay rate and proton decay branching ratio to the 2^+ state in the daughter measured for the ^{145}Tm ground state.

The experimental details and complete theoretical discussion can be found in Ref. 1.

*Argonne National Laboratory and University of Manchester, United Kingdom, †Argonne National Laboratory and University of Maryland, ‡University of Edinburgh, United Kingdom, §CEN Bordeaux-Gradignan, IN2P3-CNRS, France, ¶University of Maryland, ||Brookhaven National Laboratory.
[1]D. Seweryniak *et al*., Phys. Rev. Lett. **99**, 082502 (2007).

d.2.8. Multiple Band Structures in ^{169}Ta

(M. P. Carpenter, R. V. F. Janssens, A. A. Hecht, T. Lauritsen, E. F. Moore, S. Zhu, F. G. Kondev, D. J. Hartley,* W. H. Mohr,* J. R. Vanhoy,* M. A. Riley,† A. Aguilar,† C. Teal,† M. K. Djongolov,‡ M. Danchev,‡ L. L. Riedinger,‡ G. B. Hagemann,§ G. Sletten,§ P. Chowdhury,¶ S. K. Tandel,¶ W. C. Ma,|| and S. W. Odegard**)

The intruder proton orbitals of the mass-170 region have recently drawn attention because of their anomalous behavior. Collective structures based on the $i_{13/2}$ proton orbital have been the focus of many studies of Lu nuclei, as wobbling excitations have been observed in ^{161,163,165,167}Lu. This collective mode indicates that stable triaxial deformation is present in these nuclei over a wide range of spin and energy. However, no examples of wobbling have been identified, thus far, outside the Lu nuclei, raising the following questions: Are these Lu nuclei unique? Or will stable triaxial deformation be observed in a broader region of nuclei? In order to answer this question, an investigation of the high-spin properties of ^{169,171}Ta was undertaken with the Gammasphere spectrometer.

Rotational structures in the ^{169}Ta nucleus were studied *via* the ^{124}Sn(^{51}V, 6n) reaction, where the ^{51}V beam was accelerated to 228 MeV by the Argonne Tandem-Linac Accelerator System (ATLAS) facility at Argonne National Laboratory. These data were obtained as a side channel of an experiment focusing on ^{171}Ta,[1] but the sensitivity provided by the Gammasphere spectrometer proved sufficient for a significant extension of the level scheme of this rare-earth nucleus. Over 170 new transitions and four new band structures were placed in ^{169}Ta, including the one associated with the [404]7/2 configuration. This sequence mixes strongly with the [402]5/2 band as should be expected for pseudospin partners. The intruder [660]1/2 sequence was also identified for the first time in ^{169}Ta. This configuration has drawn considerable attention recently as wobbling bands have been observed in Lu nuclei based on this orbital intruder.

As was the case for ^{171}Ta, no wobbling structures were observed in ^{169}Ta. The moment of inertia and the band crossing behavior of the $i_{13/2}$ sequence indicate that it likely has enhanced deformation with respect to the other configurations. However, a lifetime measurement is required to verify this assertion. The new data allowed the excitation energies of all the configurations to be determined for the first time. In general, good systematic agreement is observed between the Ta bandhead energies and the calculated values of Ref. 2. The results of this study have recently been published in Physical Review C.[3]

*U. S. Naval Academy, †Florida State University, ‡University of Tennessee, §Niels Bohr Institute, Copenhagen, Denmark, ¶University of Massachusetts-Lowell, ||Mississippi State University, **University of Oslo, Norway.
[1]D. J. Hartley *et al*., Phys. Rev. C **72**, 064325 (2005).
[2]W. Nazarewicz, M. A. Riley, and J. D. Garrett, Nucl. Phys. **A512**, 61 (1990).
[3]D. J. Hartley *et al*., Phys. Rev. C **74**, 054314 (2006).

d.2.9. Reflection-Asymmetric Tidal Waves in ^{220}Th

(M. P. Carpenter, R. V. F. Janssens, T. L. Khoo, T. Lauritsen, C. J. Lister, D. Seweryniak, S. Zhu, W. Reviol,* C. J. Chiara,* M. Montero,* D. G. Sarantites,* O. L. Pechenaya,* and S. G. Frauendorf†)

In a recent experiment at ATLAS, using the ^{26}Mg + ^{198}Pt reaction at 128 MeV, multiple octupole-type band structures in ^{220}Th have been observed.[1] The evaporation residues were selected with the HERCULES device and residue-gated γ rays were measured with Gammasphere. HERCULES is

particularly suitable for very asymmetric reactions and targets with thicknesses in excess of 0.5 mg/cm^2.

The ^{220}Th level scheme has the following features: (1) The pattern of alternating-parity levels persists up to the highest spins observed (s = +1 simplex), but the nucleus exhibits a more vibrational-like behavior than the heavier thorium isotopes. (2) A rather large parity-splitting and a related staggering of the *B(E1)/B(E2)* ratios is observed. (3) Two negative-parity, odd-spin sequences are present. (4) A short sequence of negative-parity states with even spins (presumably s = -1 simplex) is present as well.

As shown in Fig. I-35, the yrast states of ^{220}Th have an approximately constant rotational energy $\hbar\omega \sim E_\gamma$ (the transition energies fluctuate around $E_\gamma \sim 420$ keV). The isotone ^{218}Ra shows a very similar behavior[2] (in contrast to the $N \geq 132$ isotones), a behavior that implies that the $N = 130$ nuclei do not rotate faster to acquire angular momentum. Multiple band crossings taking place over a broad range of spin values I, at the same value in two isotones, are considered to be a highly unlikely explanation of the described behavior and an interpretation in a "traditional" nuclear rotation framework seems difficult. On the other hand, the near-equal spacing of transitions in the yrast structure cannot reflect the presence of spherical vibrational phonons either, as it extends over a large spin range. In Ref. 1, we propose a new approach which considers collectivity arising from reflection-asymmetric nuclear tidal waves with a constant angular velocity ω, hereby retaining the simplex structure. The nuclear shape in the rotating frame of reference is a combination of quadrupole and octupole deformations which both increase with I. The analogous I behavior was seen in "signature-partner" band structures built on K-isomers in ^{182,183}Os,[3,4] which the authors interpreted in terms of tidal waves[5] on a triaxial nuclear surface. Another example may be the $K^\pi = 33/2^+$ band in ^{179}Re.

The concept of tidal waves accounts also for the staggering feature: the vibrational-like motion implies tunneling between the two shapes related to each other by the operation of space inversion which restores the parity. Nuclear tidal waves may well represent a common high-spin phenomenon in so-called transitional regions where the nuclear shape is deformation soft.

*Washington University, †University of Notre Dame.

[1]W. Reviol *et al*., Phys. Rev. C **74**, 044305 (2006).
[2]N. Schulz *et al*., Phys. Rev. Lett. **63**, 2645 (1989).
[3]J. F. Smith *et al*., Phys. Rev. Lett. **75**, 105 (1995).
[4]L. K. Pattison *et al*., Phys. Rev. Lett. **9**1, 182501(2003).
[5]D. M. Cullen, R. Glover, L. K. Pattison, P. M. Walker, S. Frauendorf, and D. Almehed, J. Phys. G **31**, S1709 (2005).

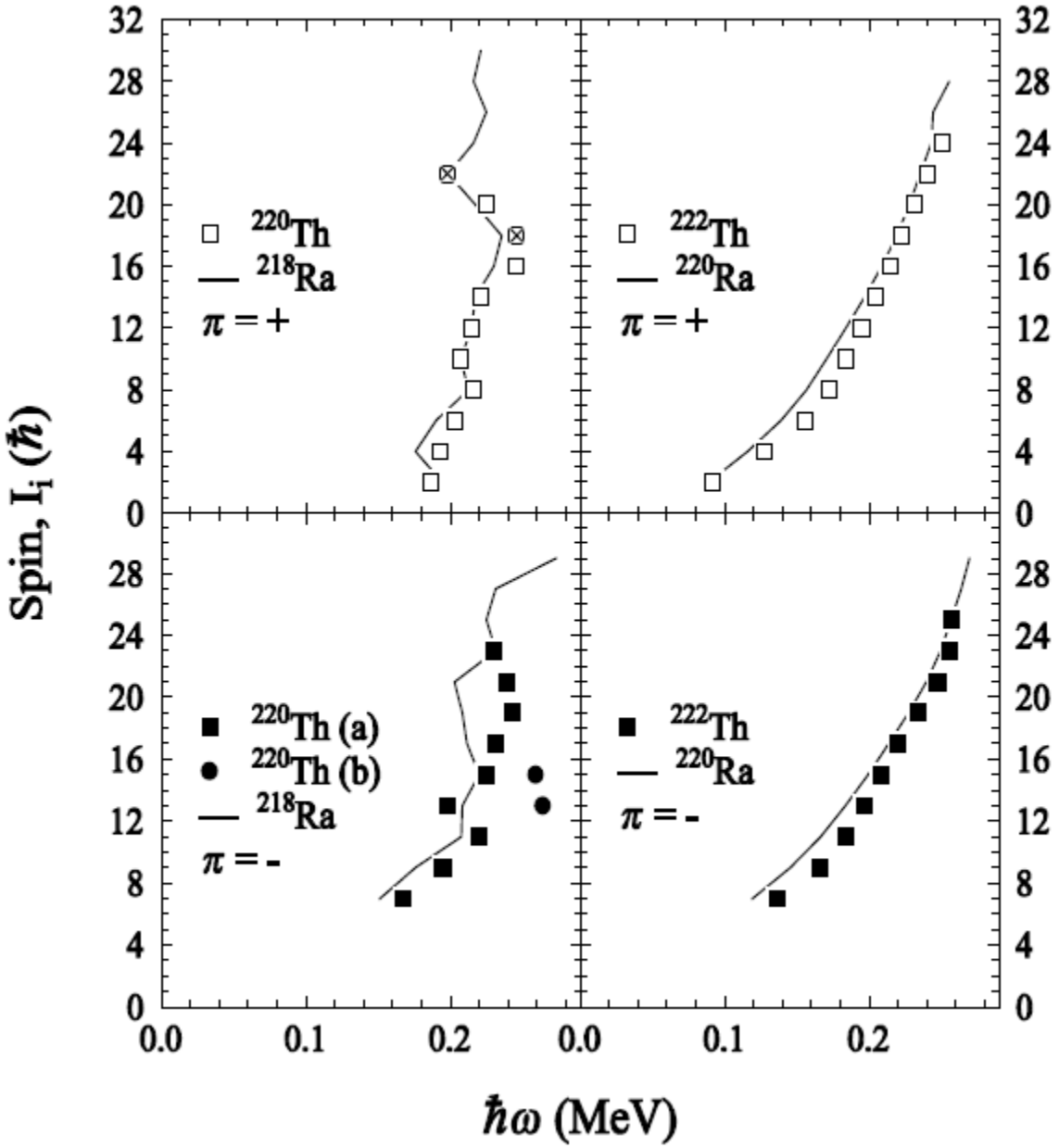

Fig. I-35. Spin I_i versus rotational energy $\hbar\omega$ for the yrast E2 transitions in ^{220}Th[1] and ^{218}Ra[2] (left panels) and in ^{222}Th[3] and ^{220}Ra[3] (right panels). The data points marked with crosses are derived from level-energy differences rather than from γ-ray energies. For ^{220}Th, both yrast (a) and yrare (b) states are shown.

E. OTHER NUCLEAR STRUCTURE RESEARCH

The efficiency of data collection with Gammasphere allows for studies of the gamma-decay pathways along excited, very high-spin superdeformed nuclei. These studies include the rotational damping observed in both the A = 150 and A = 190 region.

e.1. Rotational Damping, Ridges and the Quasicontinuum of γ Rays in ^{152}Dy

(T. Lauritsen, R. V. F. Janssens, T. L. Khoo, I. Ahmad, M. P. Carpenter, F. G. Kondev, C. J. Lister, D. Seweryniak, S. Zhu, P. Fallon,* A. O. Macchiavelli,* B. Herskind,† T. Døssing,† A. Korichi,‡ and A. Lopez-Martens‡)

The quasicontinuum of γ rays from the feeding and decay of superdeformed and normal bands in ^{152}Dy have been extracted in 1- and 2-dimensional spectra. The E_γ-E_γ correlations in the latter reveal strong ridges associated with superdeformed and normal states in this nucleus (see Fig. I-36). The entry distributions for normal and superdeformed bands have been extracted from measured fold and sum-energy distributions. A Monte Carlo model was developed to (simultaneously) describe all the quasicontinuum and ridge spectra as well as the feeding intensity of the superdeformed bands. The rotational damping widths in the normal and superdeformed wells were derived based on a comparison of the data with model calculations of the continuum of γ rays at finite temperatures.

A comprehensive, detailed paper describing both the techniques used and results obtained has been published.[1]

*Lawrence Berkeley National Laboratory, †Niels Bohr Institute, Copenhagen, Denmark, ‡C.S.N.S.M., IN2P3-CNRS, Orsay, France.

[1]T. Lauritsen *et al*., Phys. Rev. C **75**, 064309 (2007).

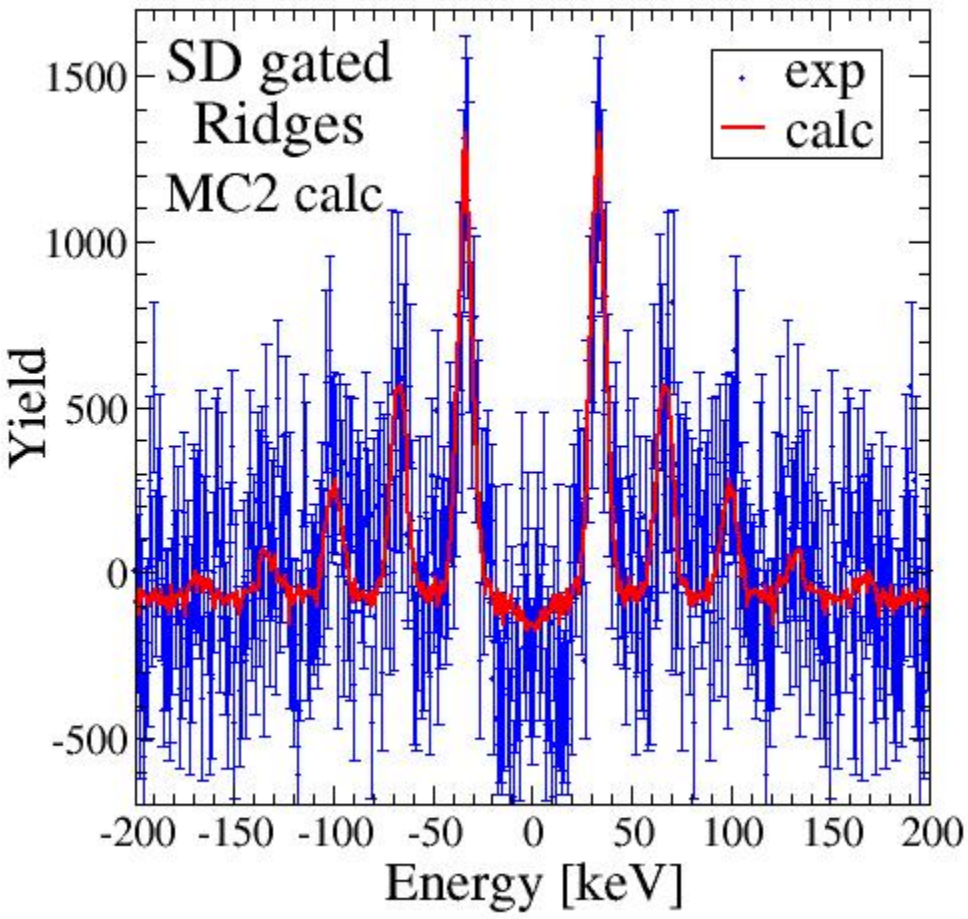

Fig. I-36. The ridges seen in a gamma-gamma matrix when double gates are placed on clean gamma rays of SD band 1 in ^{152}Dy.

e.2. Rotational Damping, Ridges and the Quasicontinuum of γ Rays in ^{194}Hg

(T. Lauritsen, T. L. Khoo, R. V. F. Janssens, I. Ahmad, M. P. Carpenter, F. G. Kondev, C. J. Lister, D. Seweryniak, S. Zhu, P. Fallon,* A. O. Macchiavelli,* B. Herskind,† T. Døssing,† A. Korichi,‡ and A. Lopez-Martens‡)

The ridges in gamma-gamma matrices, when double gates are placed on clean super-deformed (SD) transitions in ^{194}Hg, have been extracted. Ridges out to third order are clearly visible in Fig. I-37. These ridges, in conjunction with the quasicontinuum of gamma rays in ^{194}Hg that were extracted earlier,[1] will be used to determine the rotational damping parameters in ^{194}Hg in the same type of analysis that was performed recently for ^{152}Dy.[2]

The Monte Carlo code KL_sd/kla will be used to simultaneously reproduce the super-deformed ridges as well as the super-deformed area normal-deformed γ-ray quasi-continuum spectra. Via the renormalization of the rotational damping parameters necessary to reproduce the data, the strength of the rotational damping in the normal-deformed and super-deformed wells of ^{194}Hg will be inferred.

*Lawrence Berkeley National Laboratory, †Niels Bohr Institute, Copenhagen, Denmark, ‡C.S.N.S.M, IN2P3-CNRS, Orsay, France.

[1]T. Lauritsen *et al.*, Phys. Rev. C **62**, 044316 (2000).
[2]T. Lauritsen *et al.*, Phys. Rev. C **75**, 064309 (2007).

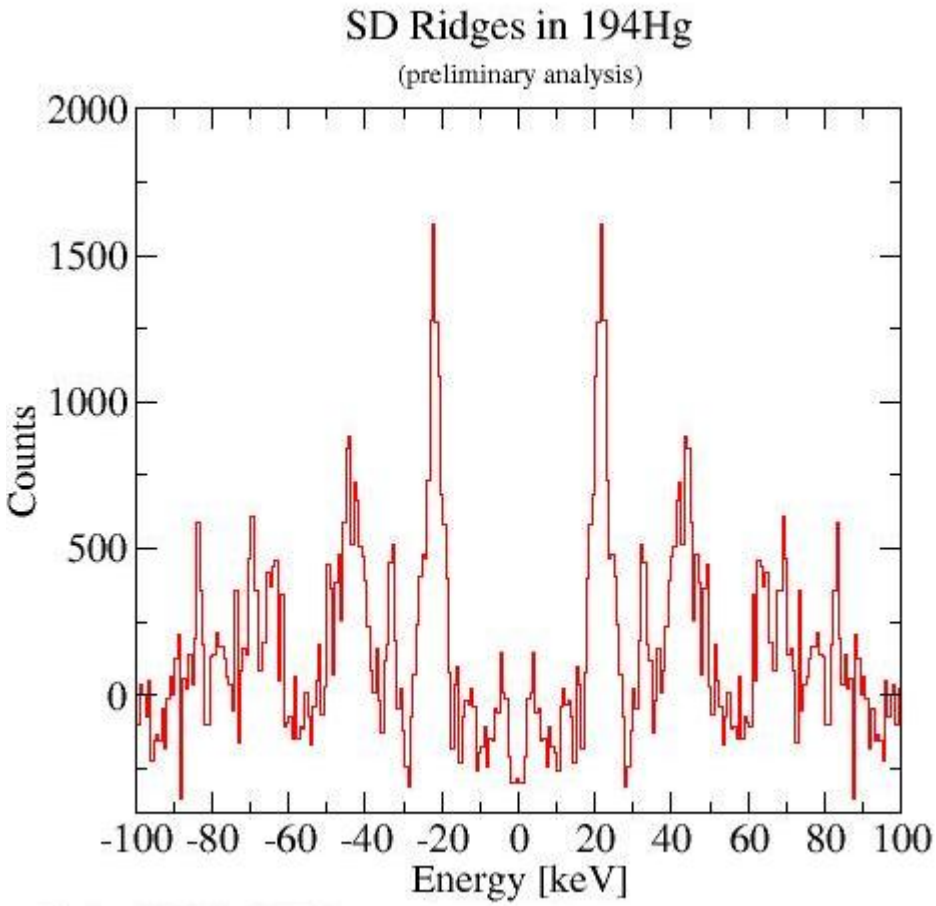

Fig. I-37. The ridges seen in a gamma-gamma matrix when double gates are placed on clean gamma rays of SD band 1 in ^{194}Hg.

e.3. Understanding the Origin of Ergodic Superdeformed Bands

(T. L. Khoo, T. Lauritsen, A. Lopez-Martens,* T. Døssing,† M. Matsuo,‡ B. Herskind, and K. Yoshida§)

The excited states in the super-deformed (SD) potential well in ^{194}Hg exhibit a new phenomenon in nuclei. Very narrow ridges (FWHM ~ 10 keV) are observed in E_γ-E_γ matrices and fluctuations in the counts reveal that a large number of bands (~150) contribute. From the data, we can deduce that excited SD bands decay in almost the same manner as discrete bands, *i.e.*, an initial state with initial spin I decays to one final state with spin I-2. This occurs despite the fact that the ~150 excited bands represent complicated mixed states with 2-8 mean-field basis states. Thus, the γ transitions would be expected to have fluctuating transition strengths following Porter-Thomas distributions. Yet, the collective flow remains almost intact, revealing the preservation of rotational coherence even in mixed chaotic states. In sharp contrast, normal deformed nuclei, which have smaller deformation, exhibit weak (~10%) narrow ridges with only ~30 bands, with the remaining collective strength spread over a very wide energy interval of ~200 keV.

The highly-correlated SD E2 flow was, in fact, predicted[1] by theory. We have sought to understand the origin of the new phenomenon by examining the results of this theory, with the assistance of new calculations. The narrowly confined E2 strength and the large

number of participating bands are found to be related. They arise due to two reasons: (a) the basis (mean-field) states in the SD well of Hg nuclei have an exceptionally small dispersion in rotational frequencies $\Delta\omega$ (~25 keV) and (b) the basis states mix through the 2-body residual interaction. (N.B. $2\Delta\omega = E_\gamma$). The onset of mixing ($n_{mix} \geq 2$, where n_{mix} is the number of components in the wave function) occurs at a lower heat energy (U ~ 1.2 MeV) than the onset of damping ($n_{branch} \geq 2$, where n_{branch} is the number of decay branches) at U ~ 1.6 MeV. When damping sets in the rotational strength normally becomes widely dispersed. In all other cases investigated so far, mixing and damping are simultaneous. Therefore, for excited SD Hg states, there exists a "golden" region, which sustains the unusually large number (~150) of rotational bands and where the dispersion in rotational strength Γ_{E2} remains exceedingly small (~10 keV). The spread Γ_{E2} (10 keV) is smaller than the estimated average spacing D (10-30 keV) between the excited levels, *i.e.*, $\Gamma_{E2} < D$. Mottelson[2] has pointed out that, when this condition is satisfied, rotational bands with unusual properties would arise, with exactly the characteristics that we have now observed. Following Mottelson,[2] we call these ergodic bands. Figure I-38 shows the variation of n_{mix} and n_{branch} as a function of U for transitions from states with $I^\pi = 40^+$. It can be seen that n_{branch} remains close to 1 even after mixing occurs ($n_{mix} > 2$), before it gradually increases and then exceeds 2.

When $n_{branch} > 2$, damping sets in. For our excited SD states, the spread in E2 strength, usually called Γ_{rot}, is not expected to be as large as the ~200 keV normally observed in normal nuclei. The reason is that, as soon as mixing sets, motional narrowing also occurs, given by the condition $2\Delta\omega < \Gamma_\mu$; Γ_μ (40-55 keV) is the compound damping width. In this limit, $\Gamma_{rot} = 4\ \Delta\omega$ $(2\Delta\omega)/\Gamma_\mu$ = 15-30 keV, which is reduced with respect to the usual value $4\Delta\omega$. There is no clear evidence in our data for this slightly broader damped component in the E_γ-E_γ ridge structure since the narrow ridge stricture exhausts the full E2 strength. Motional narrowing, due to the small dispersion $2\Delta\omega$, is also responsible for the occurrence of these ergodic bands.

*C.S.N.S.M., Orsay, France, †The Niels Bohr Institute, Copenhagen, Denmark, ‡Niigata University, Japan, §Nara University, Japan, Lawrence Berkeley National Laboratory.

[1]K. Yoshida and M. Matsuo, Nucl. Phys. **A636**, 169 (1998).
[2]B. R. Mottelson, Nucl. Phys. **A557**, 717c (1993).

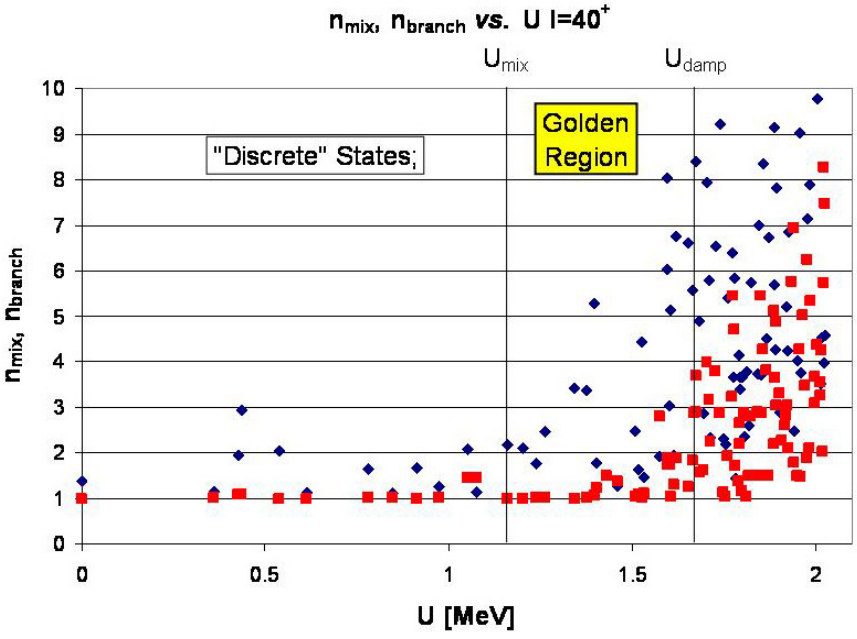

Fig. I-38. Variation of n_{mix} (blue diamonds) and n_{branch} (red squares) with U, the excitation energy above the yrast SD line for transitions from states with $I^\pi = 40^+$. Ergodic SD rotational bands occur in the golden region between the vertical lines, which mark the onset of mixing ($n_{mix} \geq 2$) and damping ($n_{branch} \geq 2$).

e.4. Triaxial Strongly Deformed Bands in ^{163}Tm

(R. V. F. Janssens, E. F. Moore, M. P. Carpenter, N. J. Hammond, T. Lauritsen, G. Mukherjee, D. Seweryniak, S. Zhu, X. Wang,* U. Garg,* Y. Gu,* S. Frauendorf,* T. Li,* B. K. Nayak,* N. S. Pattabiraman,† S. S. Ghugre,† R. S. Chakrawarthy,‡ M. Whitehead,‡ and A. O. Macchiavelli§)

Triaxiality in nuclei has been a longstanding prediction of theory, but has proved very difficult to establish experimentally. Triaxial strongly deformed (TSD) bands in the region of A ~ 160-175, predicted by theory,[1,2] have been observed in Lu, Hf and Ta nuclei.[3-12] Further, some of these observed TSD bands have been identified as so-called "wobbling bands". This wobbling mode of excitation is generally considered as one of the most unambiguous fingerprints for nuclear triaxiality. Nevertheless, the fact that wobbling bands have only been observed in several (*A* = 161, 163, 165, 167) Lu isotopes,[8-12] but not in any other element remained somewhat of a puzzle until very recently. A possible resolution of this issue has been proposed in our work of exploring the TSD band structures in the ^{163}Tm nucleus.[13]

A "thin" target experiment and a DSAM lifetime measurement were carried out with the reaction ^{130}Te (^{37}Cl, 4n) using Gammasphere at LBNL and at ANL, respectively. As can be seen in Fig. I-39, the level scheme resulting from our data analysis indicates four bands of interest: two known yrast bands and two proposed TSD bands. The structure of key transitions connecting the two TSD bands in ^{163}Tm is distinctly different from the one expected for wobbling bands. The measured quadrupole moments (Q_t) of TSD bands in ^{163}Tm (~7.5 eb) are essentially the same as the ones (of wobbling bands) in ^{163}Lu, while such values in Hf nuclei are larger by 4-6 eb (see Table III in Ref. 14), possibly pointing to a different nature. There is a discrepancy (~20-30%) between data and calculations for the Q_t moments of the TSD bands.[14] However, this seems to be a general feature in the region and requires further investigation.

The two new bands observed in the ^{163}Tm nucleus have been identified to be the TSD bands built on a TSD minimum: $\varepsilon_2 = 0.39$, $|\gamma| = 17^o$. It has been confirmed that these two TSD bands are associated with a larger deformation than the yrast (ND) bands, *i.e.*, Q_t (TSD) ~7.5 eb and Q_t (ND) ~6.4 eb. Within the framework of present calculations, the deformation of the TSD bands is driven mainly by a large neutron gap at $N = 94$ (see Fig. 5 in Ref. 14). The TSD bands in ^{163}Tm have been interpreted as structures associated with particle-hole excitations in a TSD well.[13] It is worth pointing out that the Tilted Axis Cranking (TAC)[15] calculations performed in the present work provide a natural explanation for the presence of wobbling bands in the Lu isotopes and the absence of such bands in all neighboring Tm, Hf and Ta nuclei. The explanation is related to: (I) the shape driving effects of the $i_{13/2}$ proton orbital; (II) the presence of a strong shell gap at $N = 94$; and (III) the level density around the Fermi surface. The results of this study have been published.[13,14]

*University of Notre Dame, †UGC-DAE Consortium for Scientific Research, Kolkata, India, ‡University of Manchester, United Kingdom, §Lawrence Berkeley National Laboratory.

[1]H. Schnack-Petersen *et al*., Nucl. Phys. **A594**, 175 (1995).
[2]R. Bengtsson, http://www.matfys.lth.se/~ragnar/TSD-defsyst.html.
[3]W. Schmitz *et al*., Phys. Lett. **B303**, 230 (1993).
[4]S. Törmänen *et al*., Phys. Lett. **B454**, 8 (1999).
[5]H. Amro *et al*., Phys. Lett. **B506**, 39 (2001).
[6]M. K. Djongolov *et al*., Phys. Lett. **B560**, 24 (2003).
[7]D. J. Hartley *et al*., Phys. Lett. **B608**, 31 (2005).
[8]P. Bringel *et al*., Eur. Phys. J. A **24**, 167 (2005).
[9]S. W. Ødegård *et al*., Phys. Rev. Lett. **86**, 5866 (2001).
[10]D. R. Jensen *et al*., Phys. Rev. Lett. **89**, 142503 (2002).
[11]G. Schönwaßer *et al*., Phys. Lett. **B552**, 9 (2003).
[12]H. Amro *et al*., Phys. Lett. **B553**, 197 (2003).
[13]N. S. Pattabiraman *et al*., Phys. Lett. **B647**, 243 (2007).
[14]X. Wang *et al*., Phys. Rev. C **75**, 064315 (2007).
[15]S. Frauendorf, Nucl. Phys. **A677**, 115 (2000).

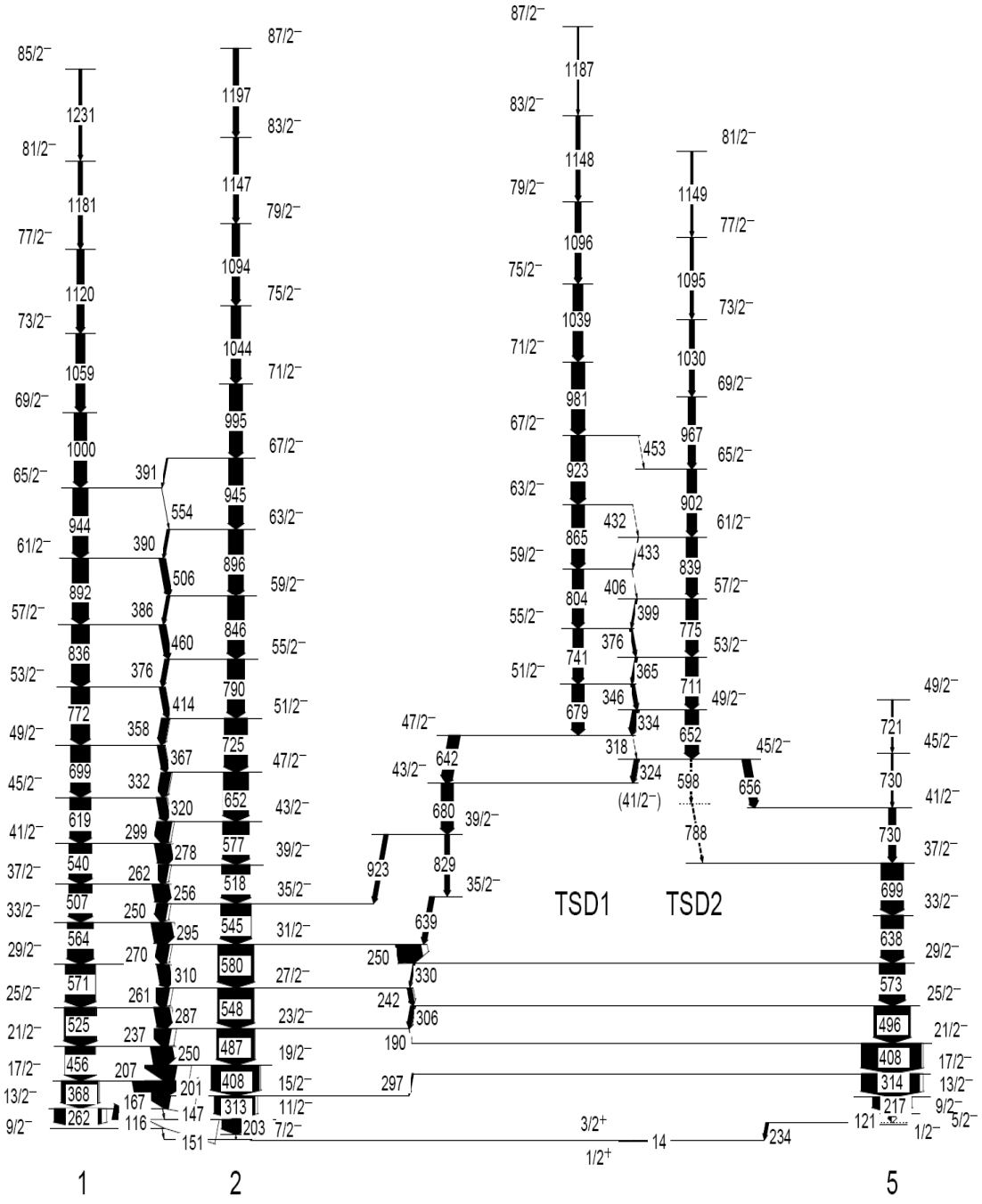

Fig. I-39. Partial level scheme of ^{163}Tm.

e.5. Quantifying the Level of Isospin Mixing in the $A = 31$ Mirror Nuclei

(C. J. Lister, M. P. Carpenter, R. V. F. Janssens, T. L. Khoo, T. Lauritsen, D. Seweryniak, S. Zhu, N. S. Pattabiraman,* D. G. Jenkins,* M. A. Bentley,* R. Wadsworth,* G. Lotay,† P. J. Woods,† and Krischichayan‡)

One of the outstanding questions in nuclear physics is the extent to which isospin symmetry is violated as a function of increasing Z and A. The focus of the present work is on isospin mixing and its impact on electromagnetic transition rates but such an investigation is not straightforward as the role of isospin mixing has to be disentangled from other nuclear structure effects. Stringent selection rules apply in $N = Z$ nuclei making them an excellent focus for searching for isospin mixing. Despite few striking examples, our knowledge of isospin mixing and its effect on electromagnetic decays is rather limited at the present time.

A new approach to the issue was recently highlighted by Ekman *et al*., who studied the $T = 1/2$ mirror nuclei, ^{35}Ar and ^{35}Cl.[1] They found that the decay branching of the lowest $7/2^-$ level was very different in the two nuclei. They found that in ^{35}Ar an E1 transition was present, while in the well-studied stable nucleus ^{35}Cl, the analogous transition was almost completely absent. Importantly, both $7/2^-$ states are particle bound, which rules out a lot of possibilities for perturbing the transition strengths. In general, it is expected that such E1 transitions in conjugate nuclei would be of very similar strength. Ekman *et al.*, advanced the explanation that the cancellation of the E1 matrix element in ^{35}Cl arose from isospin mixing, in this case between the dominant $T = 1/2$ and a weak $T = 3/2$ component.[1] They were unable, however, to quantify this suggestion since absolute transition strengths were not available for ^{35}Ar.

Recently, similar behavior to that reported for $A = 35$ was found in the $T = 1/2$ mirror nuclei,[2] ^{31}S and ^{31}P (see Fig. I-40). Again, the decay pattern of the first $7/2^-$ state was found to change dramatically between the mirror nuclei. In this case, a 2195 keV E1 transition clearly present in ^{31}P was found to have no counterpart in the decay scheme of ^{31}S. It is very difficult in the absence of lifetime measurements, and hence, absolute transition strengths, to speculate on the role that different mechanisms such as isospin mixing might have on the E1 transition strengths. Lifetimes are well known for states of interest in the stable isotope ^{31}P, but prior to the present work, lifetimes were only known for a few low-lying states in ^{31}S.

Lifetimes in ^{31}S were obtained using the Doppler Shift Attenuation Method (DSAM). The earlier study of the mirror nuclei ^{31}S and ^{31}P used the ^{20}Ne + ^{12}C reaction. It was found that it was difficult to get a reliable adhesion between a carbon foil and a thick target backing which was appropriate for a DSAM measurement. It was, therefore, decided to change to the ^{16}O + ^{16}O reaction and use metal oxide on metal targets. A ^{16}O beam at an energy of 29 MeV bombarded a target of nickel monoxide of 530 μg/cm^2 thickness backed by 3.5 mg/cm^2 nickel. The resulting gamma radiation was detected using the Gammasphere array consisting of 100 high-purity germanium detectors. Lineshape spectra were obtained by gating in an all detector verses specific angle matrices. The program "lineshape" was employed, in which the shell-corrected Northcliffe and Schilling stopping powers for the recoil nucleus in the target and backing material was used. The mean lifetime of the transition of interest 1166 keV in ^{31}S was estimated as 0.98(20) ps. Figure I-41 shows the lineshape of the 1166 keV transition at 70°, 90°and 110°.

Having obtained a lifetime for the $7/2^-$ level in ^{31}S, we are now able to calculate B(E1) transition rates for the transitions de-exciting both $7/2^-$ states in ^{31}S *and* ^{31}P (see Table I-6). In the case of the 2195/2215 keV mirror E1 transitions, it is striking that the latter is relatively much weaker. Theoretical analysis is underway to probe whether isospin mixing is responsible for this difference.

Table I-6. B(E1) transition rates obtained for ^{31}S from lifetimes measured in the present work and ^{31}P from the literature.

Nucleus	E_γ (keV)	$I_i \rightarrow I_f$	B(E1) W.u.
^{31}S	1166	$7/2^- \rightarrow 5/2^+_2$	5.9×10^{-4} W.u.
	2215	$7/2^- \rightarrow 5/2^+_1$	$<2.0 \times 10^{-6}$ W.u.
^{31}P	1136	$7/2^- \rightarrow 5/2^+_2$	$4.5(8) \times 10^{-4}$ W.u.
	2195	$7/2^- \rightarrow 5/2^+_1$	$8.2(6) \times 10^{-5}$ W.u.
	1481	$11/2^- \rightarrow 9/2^+_2$	$1.0(5) \times 10^{-3}$ W.u.

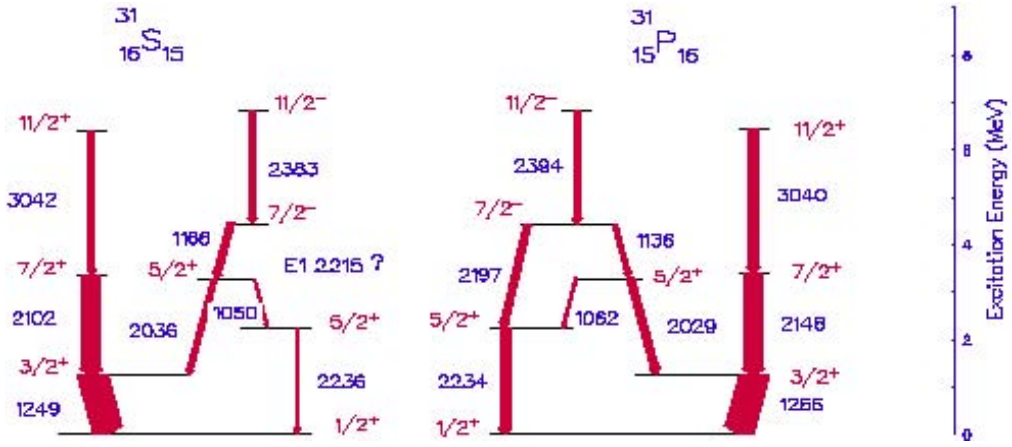

Fig. I-40. Comparison of the mirror level schemes for ^{31}S and ^{31}P. In ^{31}S, the transition between the $7/2^-$ state and the first excited $5/2^+$ state is missing, leading to the present investigation of isospin breaking in these nuclei.

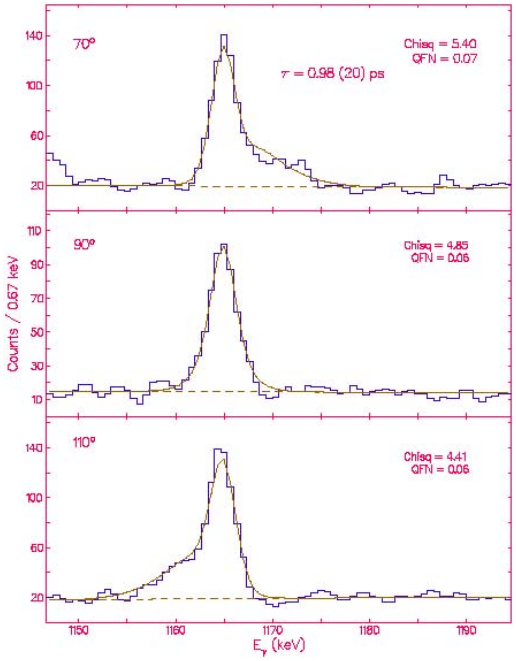

Fig. I-41. DSAM fit to the line shapes of the 1166 keV gamma ray from $7/2^-$ state in ^{31}S measured at three different angles.

*University of York, United Kingdom, †University of Edinburgh, United Kingdom, ‡UGC-DAECSR, Calcutta, India.

[1]J. Ekman *et al*., Phys. Rev. Lett. **92**, 132502 (2004).
[2]D. G. Jenkins *et al*., Phys. Rev. C **72**, 031303(R) (2005).

F. THE PHOBOS EXPERIMENT AT RHIC

Having completed its planned research program after six years of successful operation, the PHOBOS experiment at RHIC was disassembled in the fall of 2005. As one of the two "small" RHIC experiments, PHOBOS has played a disproportionately large role in the RHIC physics program with a main focus on charged particle multiplicity measurements, but also with central contributions to studies of flow, particle spectra, particle correlations, and anti-particle to particle ratios.

Although the PHOBOS data taking has been completed, a significant body of data is still under analysis. Recent results have been obtained including system size dependence of elliptic flow,[1] elliptic flow fluctuations in Au + Au collisions,[2] transverse momentum spectra of identified hadron spectra,[3] and an analysis of cluster properties seen in two-particle correlations in pp collisions at 200 and 410 GeV.[4]

Further analyses of PHOBOS data will be carried out and published over the next few years. Also, longer papers that summarize the PHOBOS results in more general categories will be written and published.

f.1. The PHOBOS Experiment at RHIC (B. B. Back for the PHOBOS Collaboration)

f.1.1. System Size, Energy, Pseudorapidity, and Centrality Dependence of Elliptic Flow

The elliptic flow, v_2, observed in relativistic heavy-ion collisions, provides important information on the hydrodynamic properties of the hot and dense medium formed in the participant region of such collisions. Until recently, the eccentricity of this region has been derived by using simple geometry such that the short transverse axis is assumed to coincide with the impact parameter. In recent studies of Cu + Cu collisions, surprisingly large values of v_2 were observed in near-central collisions, for which the geometrical model predicts very small values of the overlap eccentricity, Fig. I-42.

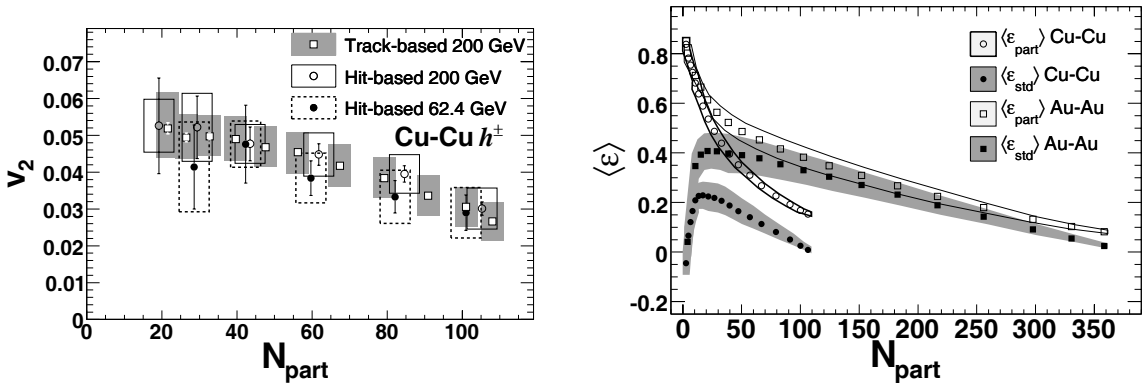

Fig. I-42. Left: The elliptical flow signal, v2 obtained from a hit-based analysis in the -1 < η < 1 range is shown as a function of N_{part} for 0-40% central CuCu collisions at 62.4 (solid points) and 200 (open circles) GeV and compared to results for a track-based analysis for the 200 GeV data. The boxes show 90% C.L. systematic errors whereas the error bars represent 1σ errors. Right: Glauber Monte Carlo calculations of the average eccentricity <ε> calculated by including (open symbols) or excluding (solid symbols) the co-variance term σ_{xy} of Eq. 1 for both CuCu and AuAu collisions at 200 GeV.

In a simple geometrical representation of the participant region one expects that v_2 approaches zero for the most central events. This discrepancy has been understood as event-by-event fluctuations of the orientation of the participant region because of the small number of nucleons involved for this system. Using the probabilistic distribution of nucleon-nucleon interaction points in a Glauber Monte Carlo calculation one may compute the "participant eccentricity" in the transverse x-y plane

$$\varepsilon_{part} = \frac{\sqrt{\left(\sigma_y^2 - \sigma_x^2\right)^2 + 4\sigma_{xy}^2}}{\sigma_y^2 + \sigma_x^2}, \qquad (1)$$

which corresponds to a principal component transformation that maximizes the eccentricity for each event. Here σ^2_x, σ^2_y, and σ_{xy} are the associated (co)variances of the participant region consisting of nucleon-nucleon interaction points. In Fig. I-42 (right panel) this quantity, obtained in Glauber Monte Carlo simulations, is compared to the standard method of calculating the eccentricity, ε_{std}, in which the co-variance term, σ_{xy} was excluded. We observe that for the light CuCu system the omission of the co-variance term has a substantial effect on the computed eccentricity of the participant region.[1]

f.1.2. Elliptic Flow Fluctuations in Au + Au Collisions at 200 GeV

A new analysis method for elliptic flow in heavy-ion collisions has recently been developed on the basis of a maximum likelihood method. This analysis is found to agree well with both the track-based and hit-based methods employed previously,[2] Fig. I-43 (left top panel).

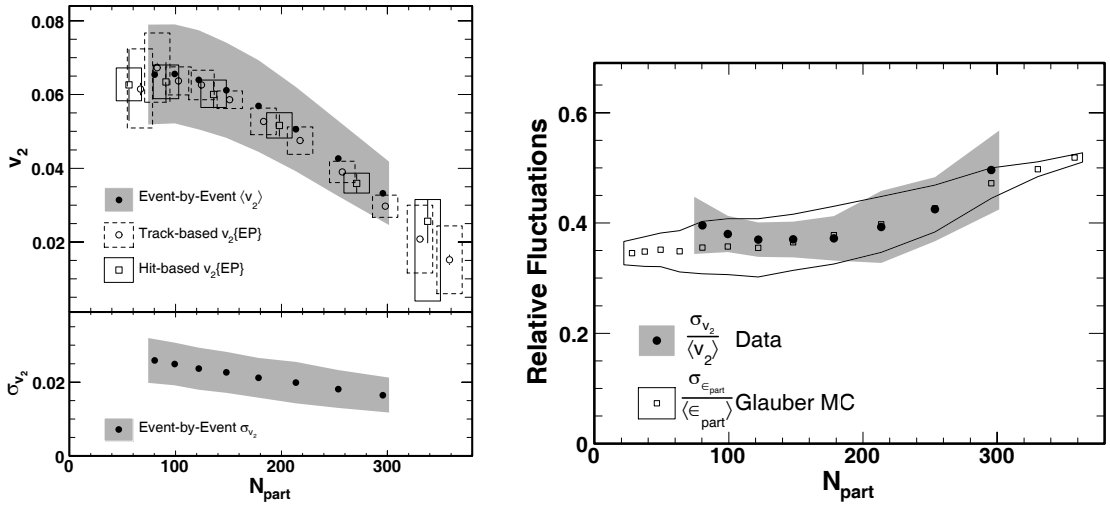

Fig. I-43. Left panel: The average elliptic flow <v2> (top) and its standard deviation σ_{v2} (bottom) is plotted vs. the number of participants, N_{part} for 200 GeV Au + Au collisions. Results of the present event-by-event analysis technique (solid points) are compared with previously published data (open symbols). Right panel: The normalized elliptic flow fluctuation $\sigma_{v2}/<v2>$ (solid points) is plotted as a function of N_{part} and compared to the normalized eccentricity fluctuation $\sigma_{\varepsilon part}/\varepsilon_{part}$ obtained from Glauber Monte Carlo simulations (open squares).

The event-by-event method allows for the determination of the fluctuation of the elliptic flow signal, σ_{v2}, for events of a certain centrality class as shown in Fig. I-43 (left bottom). The relative size of these fluctuations for AuAu collisions is found to depend only weakly on centrality, solid points in Fig. I-43 (right) in agreement with Glauber Monte Carlo simulations (open squares).[3]

f.1.3. Identified Hadron Transverse Momentum Spectra in AuAu Collisions at 62.4 GeV

Particles emitted in AuAu collisions at 62.4 GeV have been identified on the basis of their (1) time-of-flight, (2) energy-loss, and (3) residual energy of particles stopped in the first Si detector layers of the PHOBOS spectrometer. This analysis allows for the accumulation of identified particle spectra (pions, kaons and protons) over a wide range of transverse momentum with unique coverage for low p_T particles over a range of collision centralities. The resulting spectra were fit with the blast-wave model[4] which simulated thermal emission from a radially expanding source is shown in Fig. I-44 for the 0-15% centrality bin.

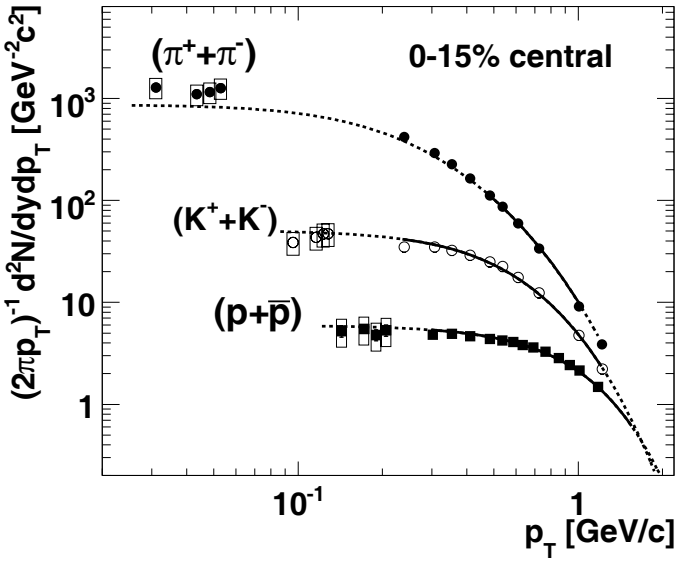

Fig. I-44. Blast-wave fits to identified spectra of pions (solid circles), kaons (open circles) and (anti)-protons (solid squares) for 0-15% central AuAu collisions at 62.4 GeV. The low pT data obtained by the stopped particle method are shown with systematic errors (boxes).

The parameters obtained from the blast-wave fits vary only slightly with collision centrality, with the temperature at kinetic freeze-out T = 103, 102, and 101 MeV and the radial expansion velocity β_s = 0.78, 0.76, and 0.72 (fraction of c), for the 0-15%, 15-30%, and 30-50% centrality bin, respectively. Here, a linear velocity profile is assumed, namely $\beta(r) = \beta_s(r/R)$, where R = 10 fm is the radius of the fireball at kinetic freeze-out. These fits were derived by excluding the stopped particle data points. Including these points into the fit changes the values of T and β_s by less than 6 MeV and 0.02, respectively.

[1]B. Alver *et al.*, accepted for publication in Phys. Rev. Lett.
[2]B. B. Back *et al.*, Phys. Rev. Lett. **95**, 122303 (2005).
[3]B. Alver *et al.*, submitted to Phys. Rev. Lett.
[4]E. Schnedermann, J. Sollfrank, and U. Heinz, Phys. Rev. C **48**, 2462 (1993).

G. REACTION MECHANISM STUDIES

Studies of the heavy-ion fusion reaction have recently experienced a renaissance with the discovery at Argonne of a substantial reduction of the fusion cross section at deep sub-barrier energies. Both systematic evaluations of the effect based on published data as well as the measurements in new systems are carried out.

g.1. Radius-of-Curvature of the *S* Factor Maximum in Sub-Barrier Fusion Hindrance

(C. L. Jiang, B. B. Back, R. V. F. Janssens, and K. E. Rehm)

It has recently been demonstrated that the appearance of sub-barrier fusion hindrance in heavy-ion fusion reactions is associated with a maximum in the astrophysical *S* factor.[1] The energy corresponding to the maximum is denoted E_s and the corresponding logarithmic derivative of the cross section is denoted L_s.

It was found that the *S* factor can be expressed approximately by the second-order Taylor expansions of *ln S(E)* around the maximum

$$S = S_0 e^{-(E-E_s)^2/2\rho}, \qquad (1)$$

where S_0 is the value of the *S* factor at its maximum and ρ is the radius-of-curvature, which can be formulated as

$$\frac{1}{\rho} = \left|\frac{d^2 \ln S}{dE^2}\right| = \left|\frac{dL}{dE} - \frac{d(\pi\eta/E)}{dE}\right| \text{ at } E = E_s. \qquad (2)$$

i.e., ρ is determined by the difference of derivatives from the logarithmic derivative of the experimental cross section, *L(E)*, and that corresponding to a constant *S* factor, $L_{cs}(E) = \frac{\pi\eta}{E}$.

Previously, we have found[2] that E_s follows an overall systematics over a wide range of projectile-target combinations as a function of the parameter $\zeta = Z_1 Z_2 \sqrt{\mu}$ where μ is the reduced mass number. In addition, E_s appears to depend sensitively on the nuclear structure of the interacting nuclei. Following this approach, we have examined the radius-of-curvature of the *S* factor maximum for a number of systems for which the fusion cross sections have been studied down to small cross sections. The radius-of-curvature is in all cases derived from the difference in logarithmic derivatives between the data and the constant *S* factor expression according to Eq. (2), either for which an *S* factor maximum has been observed, or where extrapolation methods have been used to obtain the slopes of the logarithmic derivatives near E_s.

The radius-of-curvatures, thus obtained, are shown in Fig. 45a as a function of the parameter ζ. With the aid of some other curves from systematics, a fit curve of ρ was obtained as the dashed curve shown in Fig. 45a (see Ref. 3 for details). There is a maximum of ρ, appearing at around ζ = 1000, near the data point for the system $^{16}O + ^{76}Ge$, *i.e.,* in a region where the data were mostly obtained by extrapolation. It would, therefore, be of interest to perform more detailed experimental studies of some systems with the parameter ζ in the range ζ < 1000 to determine whether a maximum value of ρ occurs in this region.

In Fig. 45b we show the same data, but normalized to the energy E_s. For the light fusion systems, from $^{10}B + ^{10}B$ to $^{16}O + ^{16}O$, the value of ρ is rather large relative to its centroid value E_s. Furthermore, the ratio ρ/E_s decreases by more than one order of magnitude, from about 0.35 to about 0.015 for heavier systems. If this ratio is large, the *S* factor maximum is not easily recognized visually. Thus, the determination of the sub-barrier hindrance effect in light systems represents a significant experimental challenge. An *S* factor representation is shown in Fig. 45c for the system $^{12}C + ^{13}C$. The solid curve is obtained with the description of the radius-of-curvature given by Eq. (1). In this case, it is difficult to recognize the *S* factor maximum. This is an important result with consequences for studying the extrapolation of the *S* factors to very low energies for reactions of astrophysical interest.[4]

Aside from the general trend discussed above and displayed in Fig. I-45a, large fluctuations of ρ around the average trend, represented by the dashed curve are seen for systems of colliding nuclei of the same element, but with different masses. In particular, the systems highlighted by vertical bands, namely $^{58}Ni + ^{58}Ni$, $^{58}Ni + ^{60}Ni$, $^{58}Ni + ^{64}Ni$, $^{64}Ni + ^{64}Ni$ and $^{90}Zr + ^{90}Zr$, $^{90}Zr + ^{89}Y$, $^{90}Zr + ^{92}Zr$, $^{90}Zr + ^{96}Zr$, show large deviations from the overall general trend. These systems range from "stiff" to "soft" colliding nuclei.

These deviations emphasize a strong dependence of ρ on nuclear structure.

The detailed result of the present study has been published in Ref. 3.

[1]C. L. Jiang, H. Esbensen, B. B. Back, R. V. F. Janssens, and K. E. Rehm, Phys. Rev. C **69**, 014604 (2004).
[2]C. L. Jiang, B. B. Back, H. Esbensen, R. V. F. Janssens, and K. E. Rehm, Phys. Rev. C **73**, 014613 (2006).
[3]C. L. Jiang, B. B. Back, R. V. F. Janssens, and K. E. Rehm, Phys. Rev. C **75**, 057604 (2007).
[4]C. L. Jiang, K. E. Rehm, B. B. Back, and R. V. F. Janssens, Phys. Rev. C **75**, 015803 (2007).

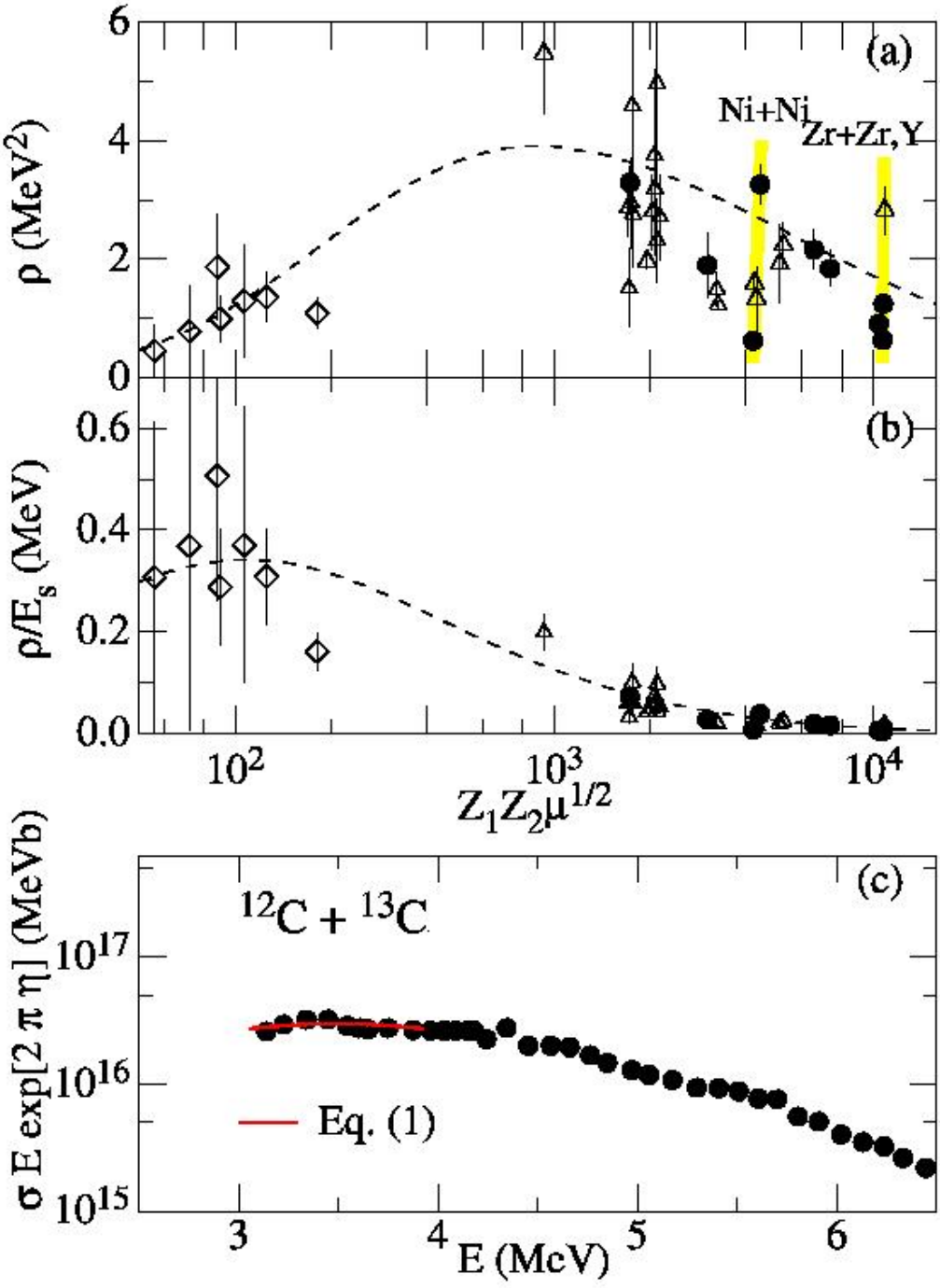

Fig. I-45. (a) Systematics of the radius-of-curvature of the S factor maximum. The value of the radius-of-curvature ρ is plotted versus $Z_1Z_2\mu^{1/2}$. The vertical bands highlight the location of the Ni + Ni and Zr + Zr,Y systems. (b) Same as (a) but the ordinate has been divided by the value E_s. (c) S (E) factor for the system $^{12}C + ^{13}C$. The solid curve was obtained from Eq. (1). See text for details.

H. HIGH-PRECISION AND HIGH-SENSITIVITY EXPERIMENTS

High precision measurements of nuclear masses for select systems of high importance for fundamental decay processes and astrophysical reactions remain a central focus of the research program at ATLAS.

h.1. High-Precision *Q*-Value Measurements on Superallowed Fermi Emitters

(G. Savard,*,† S. Caldwell,*,† J. Fallis,¶,* A. A. Hecht,*,** D. Lascar,*,††, A. Levand,* N. D. Scielzo,* H. Sharma,*,¶ K. S. Sharma,*,¶ I. Tanihata,* A. C. C. Villari,*,‡‡ F. Buchinger,‡ J. A. Clark,§ J. E. Crawford,‡ S. Gulick,‡ J. C. Hardy,‖ J. K. P. Lee,‡ and R. Segel††)

Superallowed $0^+ \rightarrow 0^+$ decays provide the most precise value for the weak vector coupling constant and the up-down mixing matrix element V_{ud}, and play a critical role in the test of the unitarity of the top row of the Cabibbo-Kobayashi-Maskawa (CKM) quark mixing matrix. The data on the superallowed Fermi decays used to obtain the most precise value of V_{ud} involves *Q*-value, lifetime and branching ratio measurements and comes from over 100 different experiments. And although they contribute less than 20% of the total uncertainty on V_{ud}, the remainder come from the small theoretical corrections that must be applied to the data. The recent measurement on ^{46}V performed at the CPT yielded a significant shift in that data set and resulted in a first statistically significant shift of the corrected *Ft* value from the mean value used to determine V_{ud}. To see if this is an isolated case or a first sign of a general trend, it is necessary to apply the high precision available with ion trap measurements to others emitters. This work was continued this year with precision *Q*-value measurements on the superallowed emitters ^{10}C and ^{38}K to complement the recent work we did on ^{14}O, ^{42}Sc, ^{26m}Al and ^{34}Cl. The results of these measurements, compared to the most recent tabulation on superallowed emitters (J. C. Hardy and I. S. Towner, Phys. Rev. C **71** 055501 (2005)), are shown in Fig. I-46.

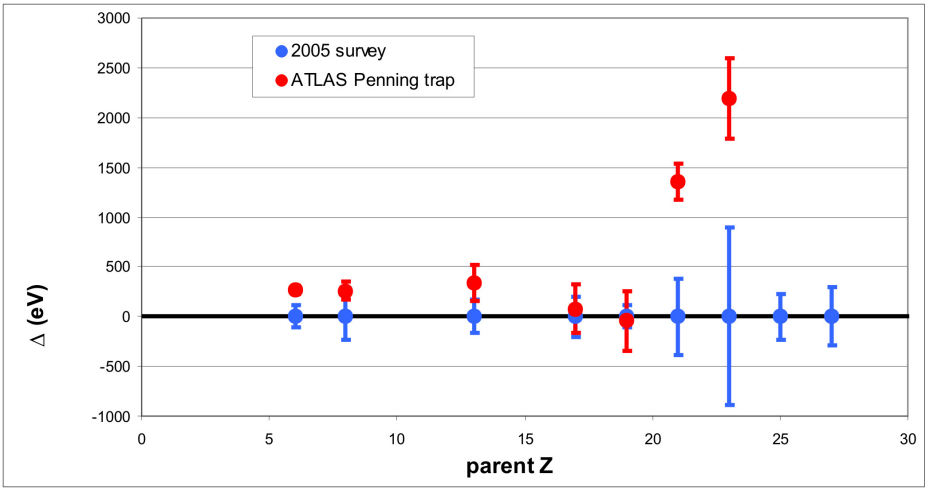

Fig. I-46. Q-values obtained at the CPT for the high-precision superallowed Fermi emitters compared to the tabulation of all previous precision measurements.

As can be seen from Fig. I-46, the precision obtained at the CPT equals or exceeds the combined precision of all previous measurements and our measurement of the *Q*-value in the decay of ^{10}C in particular has reached an accuracy below 40 eV, a record for Penning trap measurements on short-lived isotopes. Our

measurements were performed in triplets where possible systematic errors can be tested directly on-line and no effect outside of the stated error bars was observed. We find excellent agreement with the Chalk River *Q*-value difference measurements that are considered the most reliable components of the high-precision reaction *Q*-value data, but conclude that the experimental error bars on many single threshold or reaction measurements must have been underestimated. For the five lightest emitters measured we find fairly good agreement with previous results although our results are typically slightly higher. For the heavier emitters ^{42}Sc and ^{46}V, we find large shifts to higher *Q*-values which raise the corresponding *Ft* values accordingly. If all other inputs (lifetimes, branching ratios and theoretical corrections) are taken at face value, this would considerably worsen the CVC test and the limit on scalar currents obtained from superallowed decays. This first clear deviation from the CVC test is instead most likely an indication of a problem with the nuclear structure dependent corrections for these heavier cases where core excitations can play a more important role. Measurements on the remaining two cases in the high-precision set and complementary measurements of the excitation energy of the long-lived isomers in these nuclei should soon determine the extent of this effect.

*Argonne National Laboratory, †University of Chicago, ‡McGill University, Montreal, Quebec, §Yale University, ¶University of Manitoba, Winnipeg, Manitoba, ||Texas A&M University, **University of Maryland, ††Northwestern University, ‡‡GANIL, Caen, France.

h.2. Mass Measurements of Heavy Fission Fragments Using the CPT Mass Spectrometer

(H. Sharma,*,† G. Savard,*,‡ S. Caldwell,*,‡ J. Fallis,*,† L. Gang,*,§ A. A. Hecht,*,|| D. Lascar,*,** A. Levand,* N. D. Scielzo,* I. Tanihata,* A. C. C. Villari,*,†† Y. Wang,*,† K. S. Sharma,† F. Buchinger,§ L. Blomeley,§ J. A. Clark,¶ J. E. Crawford,§ S. Gulick,§ J. K. P. Lee,§ and R. Segel||)

With the addition of the new isobar separator to the CPT system, it was possible to extend the previous measurements on heavy fission fragments from ^{252}Cf with 17 new mass measurements. Of these, 8 are new measurements and the remainder are improvements to our previous results. The new data extend our knowledge of the masses of neutron rich nuclides to $N = 93$ for La and Ba isotopes, $N = 94$ for Ce isotopes and $N = 95$ for Pr isotopes, the farthest excursion from stability for these elements so far. The data analysis for these cases is now completed. Our results are in good agreement with the 2003 Atomic Mass Evaluation (AME 2003) in regions where it is anchored by previous experimental data. However, they reveal a trend for these neutron-rich isotopes to be less bound than the results of the AME 2003 as the neutron number increases (see Fig. I-47).

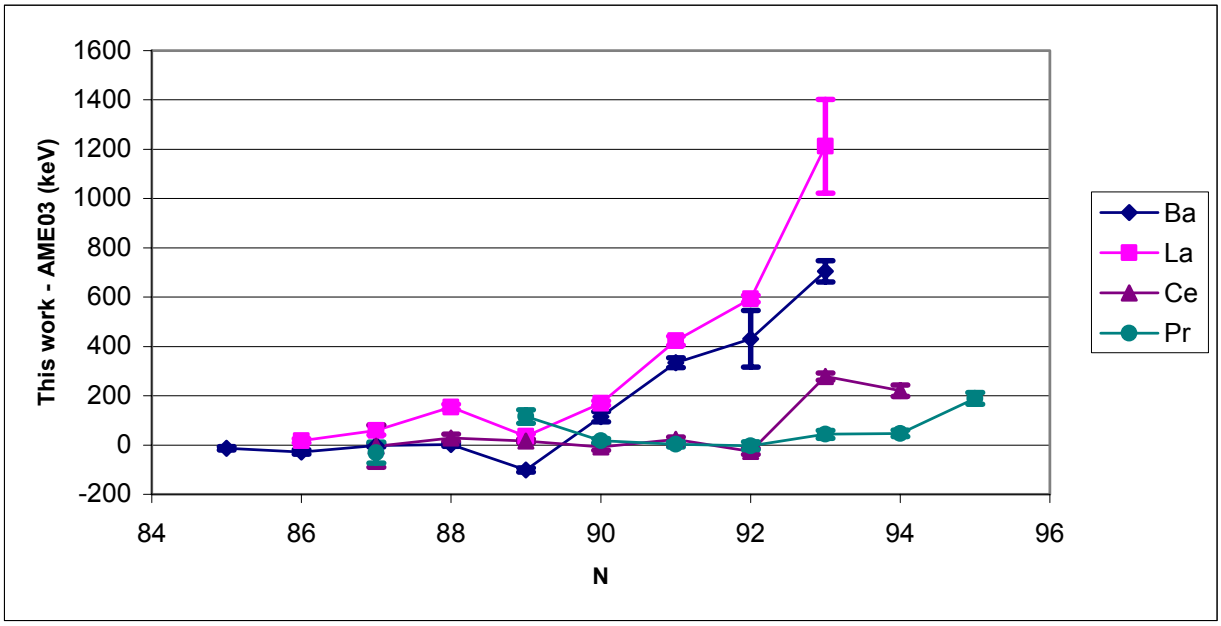

Fig. I-47. Comparison of the data from this work with the results of the AME2003.

Trends in the two-neutron separation energies for these nuclides are shown in Fig. I-48. The dotted lines show the results of the AME 2003 while the solid lines show the values calculated entirely from the results of our measurements. The plot clearly shows that the region of deformation starting at $N = 90$ for the Pr, Nd and heavier nuclides terminates with Ce and is not present for the Ba and La isotopic chains.

*Argonne National Laboratory, †University of Manitoba, Winnipeg, Manitoba, ‡University of Chicago, §McGill University, Montreal, Quebec, ¶Yale University, ||University of Maryland, **Northwestern University, ††GANIL, Caen, France.

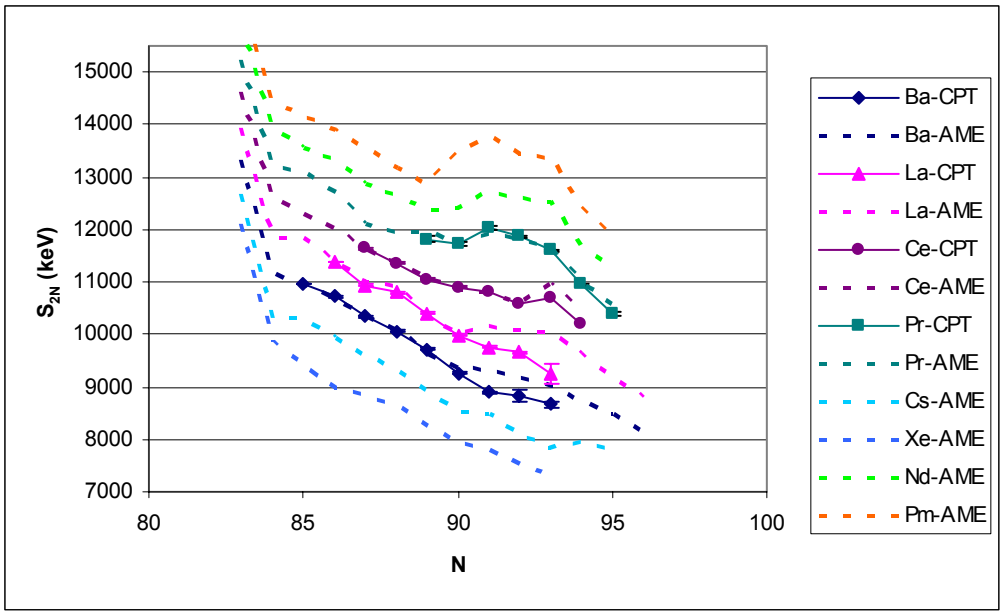

Fig. I-48. Two-neutron separation energies from this work and the AME 2003.

h.3. A Bragg Scattering Method to Search for the Neutron Electric Dipole Moment

(M. Peshkin, M. Arif,¶ T. W. Dombeck,* D. S. Hussey,¶ D. Jacobson,¶ H. Kaiser,† D. Koetke,‡ and R. K. Smither§)

The goal of this experiment is to search for the neutron electric dipole moment by observing the precession of the neutron's spin polarization in the atomic electric fields when neutrons are Bragg reflected from a perfect silicon crystal. The anticipated rotation in a single reflection is a few microradians. By causing the neutrons to undergo some 20,000 successive reflections as they drift down a slot cut into the crystal, we anticipate achieving a sensitivity of a few times 10^{-27} e-cm, comparable with the sensitivity sought in the next round of ultra-cold-neutron experiments, but with significantly different systematic errors. Our experiments are being carried at out the reactor at the NIST Center for Neutron Research, in Gaithersburg, MD.

In 2006, NIST commenced construction of a dedicated beam line and experimental area for this experiment. That construction is expected to be completed in early summer 2007. At that time, we will measure the reflectivity and geometrical properties of an improved slotted silicon crystal currently being prepared at Argonne. We have previously shown experimentally that the reflectivity of a properly prepared silicon surface is greater than 0.9999. In 2007, we plan to measure the reflectivity or raise its lower bound.

We are currently preparing for an experiment to measure the interaction of the neutron's magnetic dipole moment (MDM) with the atomic electric fields by the same technique, making use of the Schwinger interaction between an electric field and a moving MDM, the latter appearing as an effective EDM. The MDM experiment will serve as a proof of principle and exploration of systematic errors for the EDM experiment, and it will also serve as a necessary calibration of the effective electric fields experienced by the neutrons in the EDM experiment. Technical details of the MDM experiment will be given in a NIST report "Technical Report on the Status of the Measurement of Neutron Schwinger Scattering in Silicon," to be published in 2007. The MDM experiment is being done in collaboration with F. Wietfeldt of Tulane University.

We are currently procuring a set of Helmholtz coils to achieve the magnetic field quality needed for the Schwinger experiment. We have on hand, or on order, all of the necessary polarization handling equipment (polarizer, Heusler analyzer crystal, spin rotation coils, etc.). We expect to use these in 2007 to investigate the effects of neutron penetration into the crystal in Bragg scattering and begin preliminary measurements and

calibrations.

*University of Hawaii, †University of Indiana, ‡Valparaiso University, §APS User Program, Argonne National Laboratory, ¶National Institute of Standards and Technology.

I. DEVELOPMENT OF NEW EXPERIMENTAL EQUIPMENT

A vital program of development of new instrumentation and methods is carried out at ATLAS. Most prominent among these is the development of the HELIOS spectrometer to study transfer reactions in inverse kinematics and the development of the CARIBU facility, which will provide exotic neutron-rich beams of high quality for these and other studies. In addition, other existing instrumentation is being augmented and improved to increase the sensitivity and reach of the experimental program.

i.1. HELIOS – A Solenoidal Spectrometer for Inverse Reactions (B. B. Back, C. J. Lister, R. Pardo, K. E. Rehm, J. P. Schiffer, S. J. Freeman,* and A. H. Wuosmaa†)

The effort to design and build a spectrometer based on a large superconducting solenoid, HELIOS (HELIcal Orbit Spectrometer), is progressing rapidly. The spectrometer provides automatic particle identification and a very large solid angle for detecting light low-energy particles emitted in inverse kinematics reactions while preserving the energy dispersion corresponding to the center-of-mass system. The physics aim is to study single particle transfer, pick-up or inelastical scattering reactions on light targets (H, He) with heavy radioactive beams produced either at the ATLAS in-flight facility or at the future CARIBU radioactive ion injector. Details on the spectrometer concept and performance simulations are given in Ref. 1.

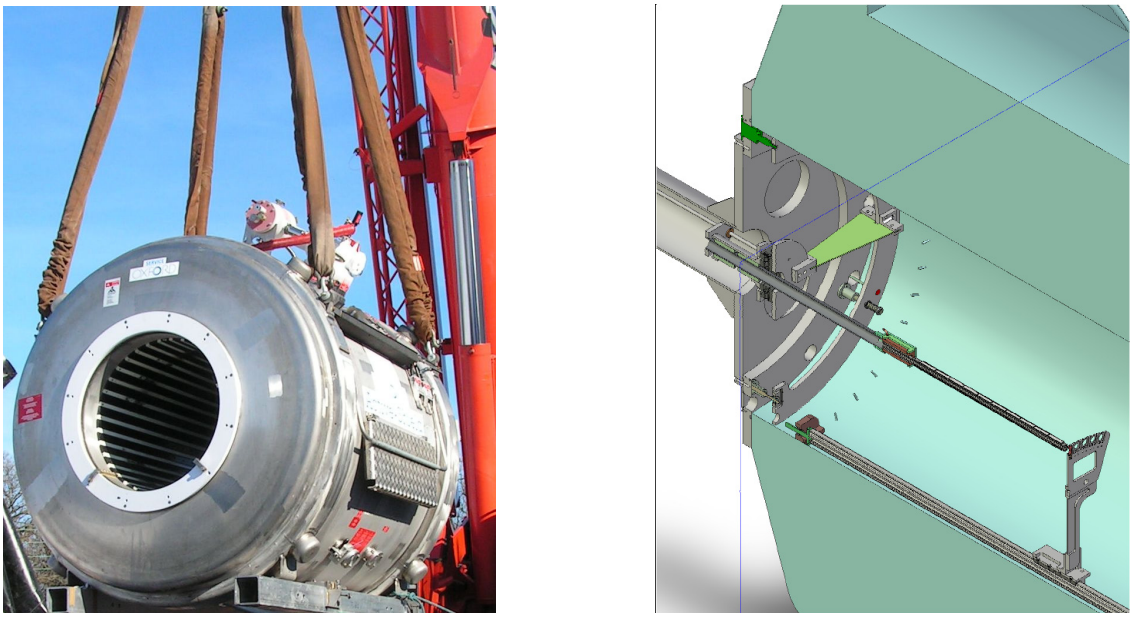

Fig. I-49. Left: Arrival of the Siemens solenoid at Argonne, December 8, 2006. Right: Cut-away schematics of the HELIOS spectrometer showing the target mechanism, the Piezo-electric cooled square cross section Si detector array, the alignment and positioning mechanism as well as the end-flanges that serve to make the solenoid bore into a vacuum chamber.

A superconducting solenoid magnet from a decommissioned MRI scanner was acquired from Siemens Medical. The magnet parameters, namely 3 *T* magnetic field strength in a 90 cm bore of length ~2 m, is well suited for the spectrometer design. The solenoid was transported from Tübingen, Germany to Argonne (Fig. I-49 left) at the end of 2006 and installed on a custom-designed support stand in its final location in

the former general purpose area at ATLAS. The mechanical design of end-flanges and the support structures for the Si-detector array and target mechanism is complete (Fig. I-49 right) and the components are presently at various stages of manufacturing. A jig for field mapping using a three axis Hall probe has been fabricated and is ready for use. It is planned to power up the magnet to a 2 *T* field and to carry out the field mapping late summer 2007. A set of legacy Si detectors have been tested. They will be mounted and wire-bonded to custom-designed PC boards, and incorporated into the 2 × 2 cm hollow detector array that will detect particles emitted into the backward hemisphere. First source tests are planned for the fall and the first stable beam test experiment will be carried out in the beginning of CY2008.

*University of Manchester, United Kingdom, †Western Michigan University.

[1]A. H. Wuosmaa, J. P. Schiffer, B. B. Back, C. J. Lister, and K. E. Rehm, Nucl. Instrum. Methods A.

i.2. A High Resolution Isobar Separator for the CARIBU Project (C. N. Davids and D. Peterson)

A high-resolution isobar separator for the CARIBU project has been designed. Its properties are: high transmission (> 95%), high first-order mass resolution (22,400:1), and compact size. The isobar separator uses only magnetic dispersive elements and all focusing elements are electrostatic.

3-dimensional simulations have been performed for the electrostatic quadrupoles, sextupoles, and multipole using the ion-optical program SIMION. From these we have obtained the physical lengths of the various electrodes, as well as realistic fringe-field distributions. The two 60º bending magnets have been ordered. Design of the focusing elements is proceeding, and they will be fabricated locally.

i.3. GRETINA Progress (C. J. Lister, J. Anderson,* and the GRETINA Collaboration)

Good progress was made in many areas of the GRETINA gamma-ray tracking project. In the physics direction, workshops were held at St. Louis (to discuss auxiliary detectors and interface issues), Berkeley (to discuss electronics) and Florida State University (to discuss science strategy and produce a white paper in preparation for the NSAC Long Range planning process).

In the hardware domain, the first "quad" module of tracking crystals was delivered. The mechanical design was refined and modified to be incorporated at various operation sites. The 10-channel primary digitizers were prototyped. In signal processing, great strides were made in better understanding electronic cross talk.

At Argonne, responsibility was taken for the trigger design, the signal routers and clock distribution system. John Anderson (ANL/HEP) has taken the lead role in this area. A Memorandum of Understanding (MOU) was signed between LBNL and ANL, and the first Statement of Work (SOW) issued. John has started design of the prototype board with a goal of integrating with digitizers by May 2007.

Kim Lister has continued on the GRETINA steering committee, which meets weekly for telephone conference calls.

*High Energy Physics Division, Argonne National Laboratory.

i.4. Polarization Experiment at Lawrence Berkeley National Laboratory (S. Gros, C. J. Lister, J. Pavin,* and I. Y. Lee*)

Using planar germanium detectors for linear polarization measurements of gamma rays has proven promising, with very high "Figure of Merit", *Q*.[1] The alpha-gamma fine structure decays from heavy nuclei provide a good method of calibration of polarization sensitivity "offline".[2] To date, our studies have been with analog electronics. However, digital pulse processing should allow better position determinations

of the interaction points, and thus, even higher polarization sensitivity.

In order to investigate this possibility, the ANL polarization setup was transferred to the 88" cyclotron at Berkeley, where the GRETINA data acquisition system was used. Figure I-50 shows the truck being loaded with equipment for shipping. Figure I-51 shows the experiment installed at LBNL. Data were collected for two weeks, amassing 1.5 Tbytes of digital data. A steep learning curve has been experienced in digital data analysis, due to formats which are very different from their analog counterparts, but generation of spectra has now started.

_____

*Lawrence Berkeley National Laboratory.

[1]N. Hammond, C. J. Lister, and G. D. Jones, Argonne National Laboratory Physics Division Annual Report 2003, Section h.13, page 106 (http://www.phy.anl.gov/div/ar04/index.html).

[2]G. D. Jones, Nucl. Instrum. Methods **A491**, 452 (2002).

Fig. I-50. Loading the germanium strip detector for shipping, along with its polarization setup and electronics.

Fig. I-51. The polarization experiment installed and running at LBNL. The rack of GRETINA digital electronics is on the left of the picture.

i.5. Digital Waveform Analysis of Signals from the Twin-Ionization Chamber (N. Patel, X. D. Tang, A. Lauro, and K. E. Rehm)

As was shown in our previous ^{16}N experiment, a twin-ionization chamber provides energy information as well as the emission angle for a particle is emitted from the cathode foil located in the center of the ionization chamber. The angle information is normally obtained from the shape of the Frisch-grid signal. In order to improve the angle resolution and collect information about multi-particle decays (*e.g.*, from the decay of ^{12}C into three alphas), we started to study the signals from a waveform digitizer.

A LeCroy 2262 Waveform digitizer was used to store the digitized signals from the grids and anodes on the computer. Figure I-52 shows some typical waveforms from the anode and Frisch grid for alpha particles produced *via* ^{10}B(n,α)^{7}Li and ^{6}Li(n,α)t reactions with neutrons from a Pu-Be source. The signal on the left side of Fig. I-52 corresponds to alphas emitted perpendicular to the cathode, while the right side corresponds to alphas emitted parallel to the cathode. Using a trapezoidal digital filter for the anode signal (see red curve in Fig. I-52), an energy resolution of 1.35% was obtained, which is very close to the value achieved with a standard ORTEC shaping amplifier. The blue curves show the digitized grid signals, whose shapes are close to what is expected for alphas emitted perpendicular (left) or parallel (right) to the cathode.

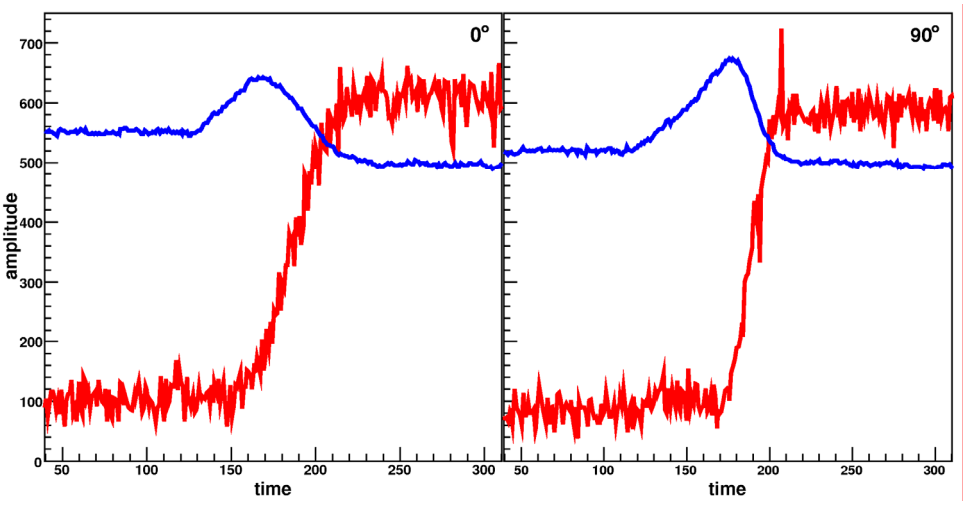

Fig. I-52. Grid (blue) and anode (red) waveform of alpha particle emitted at two different angles. Left: ~0° (perpendicular to cathode) and right: ~90° (parallel to cathode).

It is interesting to note that the rise time of the anode signal also shows an angle dependence, with the left signal exhibiting a longer rise time τ_r than the right signal. This correlation is shown in more detail in Fig. I-53 in a plot of τ_r^2 *vs.* the amplitude of the anode signal. For comparison, angle (grid) *vs.* the amplitude of the anode is also shown in Fig. I-53. This correlation allows us to obtain energy and angle information from an analysis of the anode signal alone. Improvements by using the digitized waveform from the Frisch grid are underway.

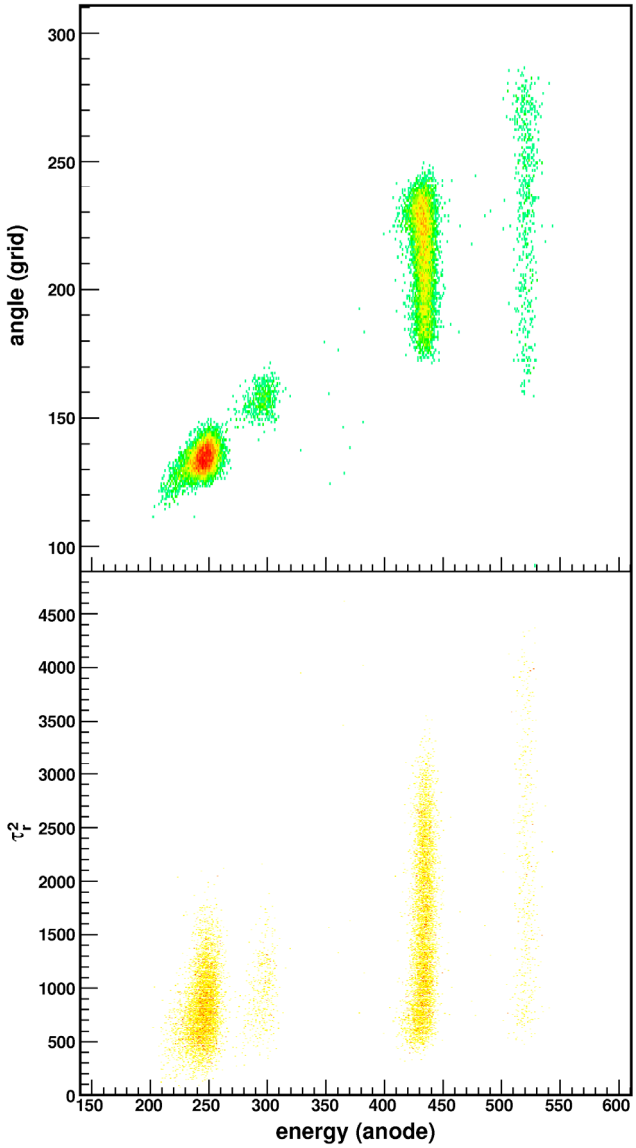

Fig. I-53. Top plot shows the angle (grid) vs. energy (anode) while the bottom plot shows the anode rise time squared, τ_r^2, vs. the energy (anode) signal.

i.6. Argonne Implantation-Decay Array – Status Report (D. Seweryniak, B. Shumard, D. Henderson, and A. P. Robinson)

In order to facilitate coincidence measurements between a Double-Sided Si Strip detector and the X-Array of Ge clover detectors a new thin and compact vacuum chamber was designed and built to house the DSSD behind the FMA focal plane. The chamber, together with one of the clover detectors and a LEPS, is shown in Fig. I-54.

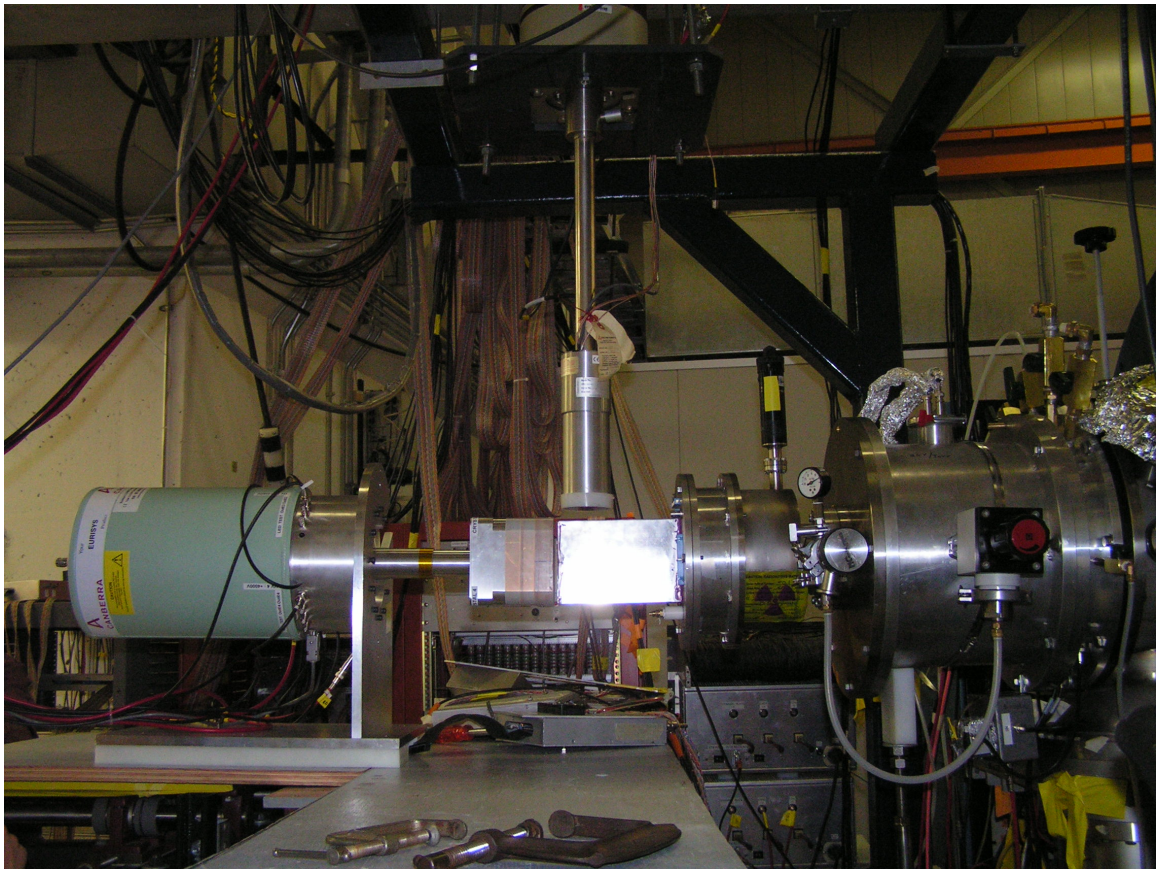

Fig. I-54. The compact DSSD chamber together with one of the clover detectors and a LEPS.

Figure I-55 contains a picture of the DSSD inside the chamber. The chamber walls are only 1/16'' thick. Thanks to the small size of the chamber, the DSSD can be surrounded by 5 clover detectors in "box" geometry. The chamber was already used in several experiments with the 40 × 40 and 80 × 80 DSSDs. The frame which will support the 5 clover detectors is currently under construction.

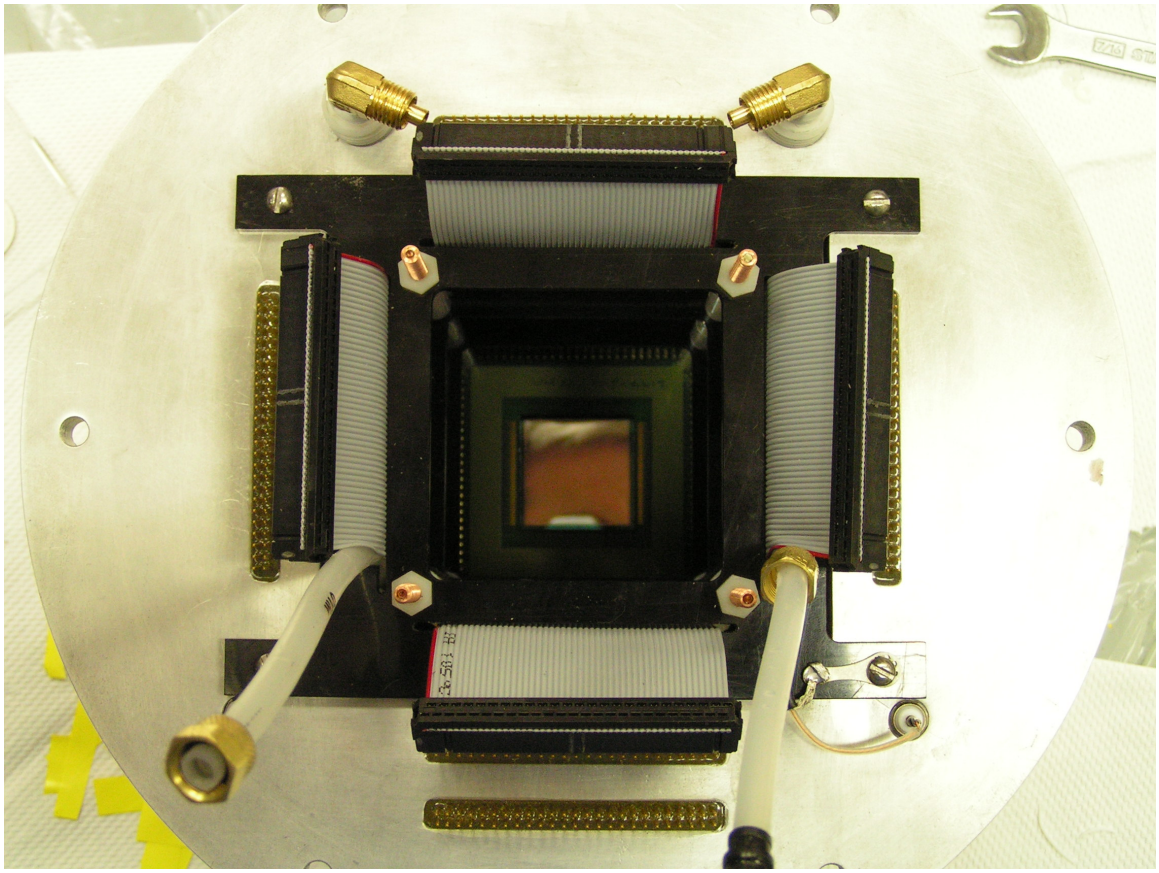

Fig. I-55. The 80 × 80 DSSD inside the chamber.

i.7. A Comparison of Performance of High Purity Germanium (HPGe) DSSDs with Different Electrode Technologies (S. Gros, C. J. Lister, N. Hammond, S. Fischer, S. Freeman,* and P. Chowdhury†)

Segmented planar Germanium (Ge) detectors are used in various nuclear sciences applications such as molecular imaging, gamma-ray telescopes on board satellites, detection of hidden radioactive material for national security and nuclear structure studies. Despite their excellent energy resolution, current planar Ge counters suffer from charge collection inefficiencies and cross talk induced between neighboring electrodes. These shortcomings arise particularly when the detectors are used in "multiple correlated" counting mode; for example, in the case of Compton cameras and γ-ray polarimeters. In these regards, the performance of these detectors could greatly be improved. Moreover, their extreme fragility and limited portability still restrict most of their operation to the safe laboratory environment. Recent advances in contact technology and electrode processing could potentially resolve some of these shortcomings and increase the robustness and longevity of planar HPGe detectors.

In order to identify the causes of charge collection inefficiencies and pinpoint the origin of cross talk, we tested and compared the performance of two planar HPGe DSSDs. Both detectors offered different crystal dimensions, electrode technologies and front-end electronics. The first prototype (MARK4) was manufactured by Ametek (ORTEC) with their traditional L.E.P.S. technology. The second detector (NP1) was acquired through an SBIR collaboration with PhDs Co. and was produced with new ultra thin sputtered amorphous germanium contacts. The dimensions and characteristics of the detectors are summarized in Table I-7.

The project also aimed to evaluate the properties of the

new amorphous germanium contacts. Although the initial energy resolution values were acceptable, the AC electrodes were subject to large random and microphonic noise, and the whole detector was oscillating when more than a few contacts were connected on either side. This behavior was found to result from improper grounding occurring at different sites (cryostat, signals connections, preamplifiers mother boards) and from a strong coupling of the preamplifiers through their bias voltage lines. The oscillatory problem was solved by perfecting the grounding of the detector casing, and decoupling the preamplifiers. An improved preamplifier design was also used, which reduced significantly the magnitude of the AC noise to an almost usable signal quality.

The comparison tests were identical for both detectors: a ^{137}Cs source was placed at ~20 cm from the center of the Ge crystal, illuminating the strips connected to the DC preamplifiers. Data consisting of time and energy, measured for each strip, were acquired through analog instrumentation with the SCARLET data acquisition system. A sorting algorithm extracted events with multiplicity 1 and 2, and the data analysis focused on comparing the energy distribution from the Compton scattering of 662 keV γ-rays for double hits between neighbor and next neighbor strips.

Figure I-56 shows a set of example energy distributions between 2 strips (sum energy *vs.* energy difference). Figure I-56a, b and c present the results for neighbor hits between Boron (B), Lithium (Li) and amorphous Germanium (a-Ge) strips respectively, while Fig. I-56b, d and f show the energy response for interactions between 2 next-neighbors in B, Li and a-G strips. For all cases involving interactions in neighbor strips (Fig. I-56a, c and e), the sum energy is higher than the incident photon energy. When next neighbor interactions are considered (Fig. I-56b, d, and f), the shift in sum energy is smaller, and in the case of 2nd next neighbor interactions (not shown here), the sum energy peak is almost at the right incident gamma-ray energy. This deviation in sum energy demonstrates the existence of cross talk in the detector. The capacitive coupling between the strips is large enough to induce a positive shift of the baseline for the B, Li and a-Ge electrodes signals. As the coupling between electrodes decreases with distance, the shift in sum energy reduces from interactions between neighbors to interactions between next neighbors, and becomes undetectable for events between electrodes separated by more than 2 strips. The cross talk is the largest between Li electrodes, and is of similar magnitudes between B and amorphous-Ge strips.

Figure I-57a shows a detailed energy distribution from 2 neighbor strips in the NP1 prototype (Fig. I-56c). Two regions are delimited by colored polygons. The top linear region corresponds to full energy events (FEE) having constant sum energies. The lower region with a curved shape corresponds also to FEE, but the amount of charges generated from the photon absorption is not recovered. The projections of intensity on the energy difference axis for both regions, shown in Fig. I-57b and c, help determine the origin of the second curved region. The intensity observed in the constant sum energy region shows two maxima at energies corresponding to forward scattering angles around 60°, which follows the Compton intensity profile expected for 662 keV γ-rays. The intensity projection observed for the second type of events does not follow the expected Compton profile. It peaks instead at small energy sharing – which mainly corresponds to single hits FEE, interacting either near a strip boundary or close to the gap separating the strips. At larger energy sharing, we believe that the loss of charges results from either the incident or scattered photon, interacting in an active region of the crystal that favors trapping and recombination, thus, reducing the lifetime of the charge carriers. These low electric field regions are usually located near the sides of the Ge crystals, or close to the gap between neighbor strips. We believe that a reduction of the inter-strip gap would reduce the amount of lost charges. We studied altering the bias voltage from 650 V to 800 V, but did not observe any improvement in charge collection efficiency.

Overall, the performance of the B strips compared to thick Li contacts and to the new a-Ge technology shows that thin contacts with a small inter strip gaps provides the best combination to limit the loss of charge and the amount of cross talk between strips. Despite the problems we had with the NP1 detector, it appeared that this detector has an electrode technology that is robust and that amorphous-Ge contacts are stable even after many thermal cycles. We have discussed some issues with the detector manufacturer regarding the design of the detector's cryostat, the scheme of grounding the electronics, and the design of the front-end preamplifiers, and have emphasized the need for a smaller gap between the strips. This should improve the performance of the NPX type of detectors. We anticipate that the present counter will be re-mounted in a superior cryostat and will be returned to us for further testing in FY2008.

A paper presenting some results is being prepared for Nucl. Instrum. Methods.

Table I-7. Characteristics of the MARK4 and of the NP1 Prototype Detectors.

Detector	*Crystal Dimensions*	*Depletion Voltage*	*Bias Voltage*	*Strips Width*	*Guard Ring Width*	*Anode Technology*	*Anode Strip Gap*	*Anode Readout*	*Cathode Technology*	*Cathode Strip Gap*	*Cathode Readout*
Mark 4	88 × 88 mm^2 20 mm thick	2 kV	2.2 kV	5 mm	5 mm	0.6 mm Lithium diffused	0.5 mm saw cut	AC coupled CSP/ warm FET	0.1 mm Boron ion implanted	0.15 mm	DC coupled CSP/ cold FET
NP1	100 mm ∅ 14 mm thick	500 V	-650 V	5 mm	2~5 mm	Sputtered a-Ge/ Al contacts	0.5 mm	DC coupled CSP/ warm FET	Sputtered a-Ge/ Al contacts	0.5 mm	AC coupled CSP/ warm FET

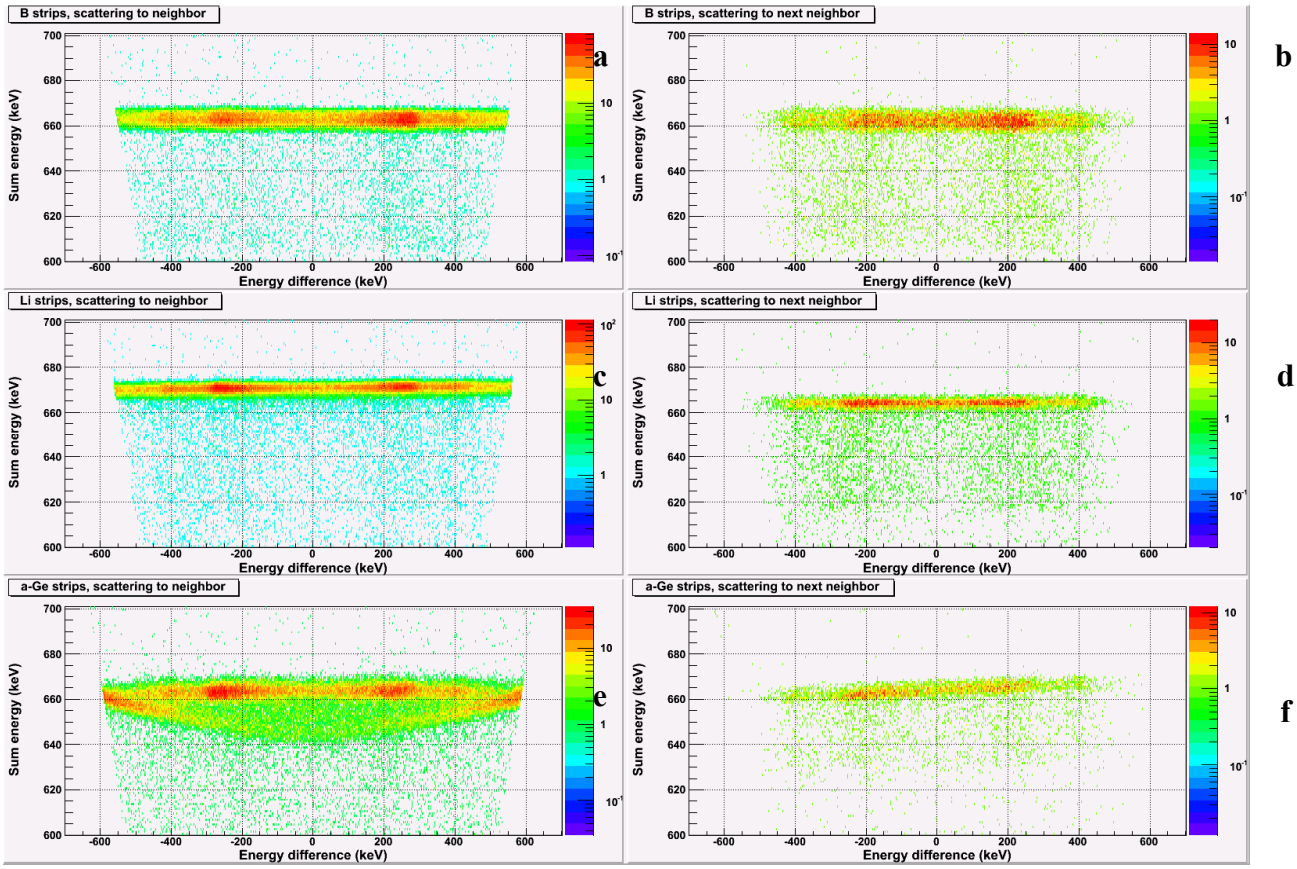

Fig. I-56. Example energy distributions for double hit interactions: between a) two neighbor and b) two next neighbor Boron strips; between c) two neighbor and d) two next neighbor Lithium strips; between e) two neighbor and f) two next neighbor for amorphous Germanium strips.

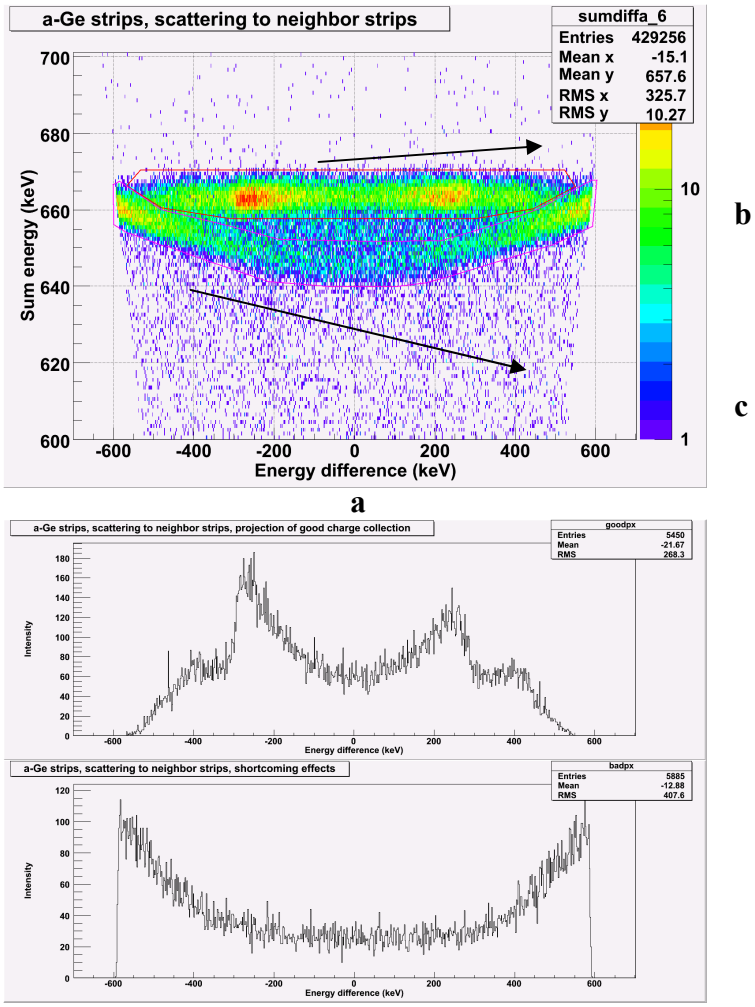

Fig. I-57. Energy distribution for neighbor a-Ge strips (a) and intensity projections of energy distributions for: b) good events with full collection of charge carriers; c) events with energies distorted by cross talk or charge losses.

*University of Manchester, United Kingdom, †University of Massachusetts-Lowell.

i.8. Development of a Portable Gamma Array, MISTI, for Homeland Security Use

(C. J. Lister and B. Phlips*)

The Domestic Nuclear Detection Office (DNDO) in the Department of Homeland Security (DHS) issued a call for proposals for an advanced technology demonstrator for "stand-off radiation detectors systems" DNDO-BAA07-010FP-018. The specification called for the detection, identification and location of a caesium-137 source at 100 m. An NRL/ANL collaboration has been formed to design and build a portable device with this capability.

At Argonne, we are involved in the design and procurement of the germanium array. This will consist of ~28 large volume hyper-pure p-type counters mounted in "Pop-Top" capsules, and attached to a purpose-built liquid nitrogen Dewar. We are initially involved in investigating the issue of mechanical ruggedness. A test will be made at NRL using a vibration stand usually employed for evaluating the robustness of satellites being prepared for rocket launches.

This work is expected to be carried out in FY2007-2008

and be completed early in FY2009.

*Naval Research Laboratory.

i.9. Gammasphere Operations (M. P. Carpenter, C. J. Lister, R. V. F. Janssens, T. L. Khoo, T. Lauritsen, J. Rohrer, E. F. Moore, D. Seweryniak, P. Wilt, S. Zhu, and F. G. Kondev*)

As reported last year, Gammasphere was moved in 2006 back to the FMA beam line in area IV allowing for measurements requiring Gammasphere to run in conjunction with the FMA to be performed. The move took place in the first week of March and experiments resumed by the end of the month. Even though the device was unavailable for approximately 1 month due to the move, twenty-four PAC approved experiments were performed with Gammasphere in 2006 which is 20% larger when compared to the number of experiments performed in 2005. Twenty of these experiments were performed on the FMA beam line.

By the end of 2006, Gammasphere had been operating at ATLAS for nearly four years, and it appears that the device will operate at our facility for the foreseeable future. In 1997, 2000 and 2002, Gammasphere was moved after approximately two years of operation at the host facility. In each instance, all Ge detectors were annealed and optimum energy resolution was restored to the array. Since Gammasphere is not scheduled to move from Argonne, we have undertaken a policy to anneal a detector once its resolution has degraded beyond 3 keV at 1.33 MeV.

Due to failures of resistors along the bias chain, we continue to see breakdowns on the BGO PMT bases. This results in a non-responsive channel. The PMT can be repaired by locating the failed resistor and replacing it, however, this is a very time consuming operation. While it is our plan to replace all of these bases with new components in the long run, we continue to repair the bases as they fail and as the schedule allows. For example, whenever a Ge detector is removed for annealing, its corresponding BGO shield is removed and repaired. A prototype replacement for the BGO bases has been constructed and is currently being tested for both gain stability and long term reliability.

The new data acquisition system has been commissioned and is now utilized in all Gammasphere experiments. With the new system, one is able to record the data to a hard drive. In this way, experimenters are able to bring their own USB hard drives to record data on and take with them at the end of an experiment. Along with the new acquisition system, a new online analysis program, GSSort, has been developed using the Root package from CERN. GSSort is rapidly replacing both the SCANU and DAPHNE sorting programs which were used previously. Detailed information about GSSort can be found on the Gammasphere web page.

It had been planned to modify the board in order to allow for the BGO energies to be available for readout ~2 μsec after they were hit by a γ ray. This same modification had been done for the Ge energies and times and the BGO times in 2003. This modification will allow for the BGO energy information to be available for FMA experiments where the recoiling residues have flight times greater than 1 μsec. This modification for each board will take 1 1/2 months to perform and has been postponed until 2007 when ATLAS will be down for upgrades and maintenance.

*Nuclear Engineering Division, Argonne National Laboratory.

i.10. Nuclear Target Development (J. P. Greene)

The Physics Division operates a target development laboratory that produces targets and foils of various thicknesses and substrates, depending on the requirements for experiments performed at the ATLAS and dynamitron accelerators. The targets are prepared from both naturally occurring materials and stable isotopes that are supplied either in pure, elemental form or as stable compounds. In addition to ATLAS experiments, targets and foils are provided for all staff members whether working within the Physics Division

or undertaking experiments at other facilities. Whenever possible, support is provided to other ANL divisions and, in particular, to requests from researchers at the University of Chicago as well as other universities (*e.g.*, Yale and Notre Dame).

In the past year, numerous targets were fabricated either as self-supporting foils, on various substrates or as "sandwich" targets. Targets produced included Al, ^{243}Am, Au, ^{10}B, Ba, ^{138}BaO, Be, ^{12}C, ^{40}Ca, CD_2, Ce, ^{140}CeO, ^{252}Cf, ^{50}Cr, Cu, Formvar, C/Ti/Gd, ^{76}Ge, Havar, HfH, ^{113}In, Kapton, ^{6,7}LiF, ^{24}Mg, MgO, ^{92}Mo, Mylar, ^{15}N(ammonium salt), ^{150}Nd, $^{142}Nd_2O_3$, ^{58}Ni, NiO, Os, Paraflint, ^{208}Pb, phosphor, Pt, SiC, ^{149}Sm, ^{120}Sn, Ta, $Ta^{18}O$, Ta_2O_5, ^{126,130}Te, $^{120,124,128}TeO_2$, Teflon, ^{229}Th, ^{46}Ti, TiC, $TiCl_4$, TiD, UC_2, UF_4, W and WC. Many of these target foils have been fabricated by mechanical rolling using our small rolling mill. A large fraction of these targets were prepared for experiments carried out at Gammasphere.

Beyond target development, thin plastic films and foils are produced for various detector systems used for experiments at ATLAS as well as energy degraders and windows for the Advanced Penning Trap. New materials and mounting technologies are being implemented with the gas cell needed for the CARIBU project and for astrophysics research using in-flight radioactive beams at SPS III and for gas targets at the FMA.

As part of ATLAS support, the target lab routinely produces carbon stripper foils of 2 $\mu g/cm^2$ for use in the tandem as well as other thickness for additional stripping throughout the accelerator. For the production of enriched beams at ATLAS, there continues to be a need for the preparation of various dilutions of isotopic source material into suitable form for introduction into the ion sources.

The target development laboratory includes state-of-the-art equipment used for thin-film fabrication. The addition of a new, multi-purpose, computer-controlled vacuum evaporation system extends our capabilities and provides a stable platform for the continued production of accelerator targets. The available techniques consist of multiple resistive heating, focused ion beam sputtering, ion assisted deposition, electron beam and electron bombardment evaporation, carbon arc evaporation, electrodeposition and mechanical rolling. The evaporators are maintained under high vacuum and each vessel contains a quartz-crystal film-thickness monitor with deposition rate indicators. Also included are movable shutters, quartz-lamp substrate heaters and thermocouple temperature sensors, allowing for complete process monitoring during target deposition.

Other auxiliary equipment used for target development includes electrodeposition apparatus, a small rolling mill, an alpha particle counting chamber, inert atmosphere glove box, laminar flow clean bench, pellet press, a reduction furnace, and a variety of precision balances. A turbo-pumped target storage facility is in operation for maintaining, under high vacuum, those targets that readily oxidize in air. This system utilizes computer-controlled circuitry to prevent targets from exposure to atmosphere during power interruptions. A second storage system employing a bank of vacuum desiccators and connected to a mechanically pumped manifold is available for use by individual experimenters. An additional set-up, consisting of two large plastic desiccator boxes, evacuated using a small turbo-pump system, is in operation for long-term material storage. This allows a separation of material storage from target storage, hence eliminating repeated exposure when transferring and retrieving targets.

A low-level radioactive source and target preparation laboratory exists at a separate location within the division that is dedicated to the production of these sources and targets. Available preparation techniques include multiple resistive heating employing a diffusion-pumped vacuum evaporator. A second, smaller evaporator system was constructed for close proximity evaporations of higher activity materials, to be used as targets as well as radioactive sources. Preparation and handling of actinide targets by electrodeposition as well as fission sources (mainly ^{252}Cf) has been done using this lab as well as high activity samples for source experiments at Gammasphere and EDM search experiments using ^{225,226}Ra.

An area of increased research effort has been toward development of ISOL targets for the RIA proposal involving a uranium compound production target. Toward this end, direct measurements of the thermal conductivity of uranium carbide have been made using a method developed at ANL. Sample material of small grain size uranium carbide has been obtained from several sources for these measurements and is being studied for radioactive release properties in collaboration with ORNL. This work is still in progress.

J. ATLAS USER PROGRAM

j.1. ATLAS User Program (E. F. Moore and R. V. F. Janssens)

During FY2006 ATLAS hosted strong “campaigns” involving radioactive beams, the CPT, and, of course, Gammasphere. In the spring of 2006, Gammasphere was moved back from its "stand alone" position to its location in front of the FMA.

Many of the experimental programs were driven by outside Users, and in all programs, there was considerable outside User involvement. Over 97% of all experiments performed in FY2006 included one or more outside Users and roughly 60% of the approved experiments had an outside User as the Principal Investigator. In July 2005, Frank Moore moved over to the Argonne SCD Division to work full time for the U.S. Department of Energy, Radiological Assistance Program (RAP). Nevertheless, he continued to provide limited assistance with scheduling, with essential User services and with the ATLAS web page. However, a large portion of the in-house scientific staff and members of the technical support staff spent substantial amounts of their time in experiment setup, preparation, and assistance for the many different experiments performed at ATLAS.

A total of 213 Users from 56 different institutions were present at ATLAS for experiments in FY2006. A total of 61 Users came from U.S. universities, while 77 originated from foreign universities, mostly from Canada and Europe. The number of Users from U.S. national laboratories was 55, while that for scientists from foreign similar institutions was 20. There were 75 students at ATLAS for experiments in FY2006, of which 13 were based at Argonne long-term.

The Program Advisory Committee met twice during the FY2006, on January 20-21 and on September 15-16 to recommend experiments for beam time allocation at ATLAS. In January 2006, the Program Advisory Committee members were:

Ani Aprahamian, University of Notre Dame
Birger Back, Argonne National Laboratory
Art Champagne, Univ. of North Carolina-Chapel Hill
Augusto Macchiavelli, Lawrence Berkeley Nat. Lab.
David Radford (*Chair*), Oak Ridge National Laboratory
Gene Sprouse, Stony Brook University
Piet Van Duppen, University of Leuven, Belgium

By the time of the September meeting, the term of two committee members had expired and the composition of the PAC was as follows:

Birger Back, Argonne National Laboratory
Sean Freeman, University of Manchester, U.K.
David Radford, Oak Ridge National Laboratory
Hendrik Schatz, Michigan State University
Gene Sprouse, Stony Brook University
Krzysztof Starosta (*Chair*), Michigan State University
Piet Van Duppen, University of Leuven, Belgium

At the January meeting, a total of 103 days of beam time were approved. The corresponding number for the September meeting is 127. In each instance, the request for beam time far exceeded the amount available: in January the total demand was for 273 days, while 253 days were requested in September. Due to the large demand for beam time, the PAC was asked to prioritize experiments into two categories; those that must be run at any cost (*priority I*), and those that should be granted beam time if at all possible (*priority II*). For each of the two PAC meetings, roughly 20% of the accepted proposals were ranked as priority II.

In FY2006, the ATLAS User Group Executive Committee consisted of Ani Aprahamian (University of Notre Dame), Krzysztof Starosta (Chair, Michigan State University), Ingo Wiedenhöver (Florida State University), and Alan Wuosmaa (Western Michigan University). The term of this committee expired at the end of calendar year 2006.

j.2. Experiments Involving Outside Users

All experiments in which outside Users directly participated during FY2006 are listed below. The spokesperson for each experiment is given in square brackets after the title, and the collaborators are given below each entry.

1. Investigation of the Ionization Density Limit of a Large Accelerated Gas Cell System [Savard]
   G. Savard, J. Clark, A. Levand, Z. Zhou, J. Wang, W. L. Trimble, M. Portillo, J. Vaz, B. Blank, L. Blomeley, D. J. Peng, D. Mackay, J. J. Letcher, N. D. Scielzo, H. Sharma, J. Fallis, D. Lascar, R. Segel, A. A. Hecht, S. Caldwell, G. Li, T. Sun, M. Sternberg, and J. van Scholt

2. Electromagnetic Decay Properties of the Tz = ± 1/2 A = 67 Mirror Pair: Isospin Symmetry From E1 Amplitudes [De Angelis]
   G. De Angelis, D. V. Tonev, D. R. Napoli, S. Lunardi, E. Farnea, C. A. Ur, D. G. Sarantites, C. J. Chiara, W. Reviol, O. Pechenaya, M. P. Carpenter, C. J. Lister, G. Mukherjee, N. Hammond, R. Orlandi, S. F. Gadea Raga, J. J. Valiente-Dobon, F. Della Vedova, A. Bracco, S. Leoni, S. M. Lenzi, R. Wadsworth, D. Seweryniak, S. Zhu, and S. N. S. Bondili

3. Request for Exploratory Time: The $k_{17/2}$ Orbital in the Heaviest Elements [Freeman]
   S. J. Freeman, R. Chapman, J. F. Smith, B. P. Kay, C. J. Lister, R. V. F. Janssens, M. P. Carpenter, S. Zhu, and X. Wang

4. Studies of Excited States in ^{101}Sn. Phase I: Search for ^{101}Sn β-Delayed Protons [Seweryniak]
   D. Seweryniak, S. Zhu, R. V. F. Janssens, C. J. Lister, M. P. Carpenter, N. Hammond, D. Henderson, A. A. Hecht, W. B. Walters, D. A. Peterson, C. Vaman, G. Lotay, K. Starosta, P. J. Woods, S. Gros, and N. Hoteling

5. The ^{44}Ti(^{3}He,p) Reaction and the Question of T = 0, T = 1 Pairing in N = Z Nuclei [Macchiavelli]
   A. O. Macchiavelli, R. M. Clark, P. Fallon, M. Wiedeking, K. E. Rehm, R. V. F. Janssens, S. Zhu, C. N. Davids, and C. J. Lister

6. Identification of Excited States in ^{107}Te with Recoil Decay Tagging Measurement [Starosta]
   K. Starosta, C. Vaman, D. Seweryniak, A. P. Robinson, D. A. Peterson, K. B. Lagergren, P. J. Woods, C. N. Davids, W. B. Walters, A. A. Hecht, S. Zhu, S. Gros, D. Henderson, G. Lotay, and N. Hoteling

7. The First Spectroscopic Study of the Odd-Odd N = Z ± 2 Mirror Pair ^{44}V/^{44}Sc [Bentley]
   M. A. Bentley, J. R. Brown, M. J. Taylor, E. K. Johansson, L. L. Andersson, P. E. Garrett, D. Seweryniak, C. J. Lister, M. P. Carpenter, T. Lauritsen, and R. V. F. Janssens

8. Transient-Field g Factor Measurements of Excited States in Fission Fragments [Smith]
   A. G. Smith, B. J. Varley, A. L. M. Thallon, G. S. Simpson, S. J. Freeman, B. P. Kay, R. Orlandi, I. Ahmad, M. P. Carpenter, R. V. F. Janssens, C. J. Lister, T. Lauritsen, and J. Greene

9. DSAM Lifetime Measurements for Fission Fragments using Hercules [Reviol]
   W. Reviol, D. G. Sarantites, C. J. Chiara, O. Pechenaya, S. A. Komarov, D. Seweryniak, M. P. Carpenter, R. V. F. Janssens, S. Zhu, T. L. Khoo, J. Greene, and M. Montero Diez

10. The Structure of Neutron-Rich sdf-Shell Nuclei using Multi-Nucleon Transfer Reaction Studies at Gammasphere [Fallon]
    P. Fallon, I.-Y. Lee, E. Rodriguez-Vieitez, M. Descovich, C.Y. Wu, D. Cline, S. Zhu, D. Seweryniak, M. P. Carpenter, R. V. F. Janssens, A. O. Macchiavelli, and M. Wiedeking

11. Beyond the N = Z Line: A Study of the T_z = -1 Nucleus ^{70}Kr [Wadsworth]
    R. Wadsworth, M. J. Taylor, S. N. S. Bondili, P. E. Kent, P. J. Davies, C. J. Lister, D. Seweryniak, M. P. Carpenter, S. Zhu, S. M. Fischer, D. G. Sarantites, and W. Reviol

12. High Spin States in the N = Z - 3 Nucleus ^{49}Fe - Coulomb Effects at Large Proton Excess [Bentley]
    M. A. Bentley, J. R. Brown, P. E. Kent, M. J. Taylor, R. Wadsworth, D. G. Jenkins, L. L. Andersson, E. K. Johansson, D. Rudolph, D. Seweryniak, S. Zhu, T. Lauritsen, C. J. Lister, M. P. Carpenter, R. V. F. Janssens, and M. B. Gomez-Hornillos

13. Identification of the Mixed-Symmetry One-Phonon $2^+_{1,ms}$ State of ^{136}Ce and ^{134}Xe in Inverse-Kinematics Coulomb Excitation [Ahn]
    T. Ahn, G. I. Rainovski, A. Costin, C. J. Lister, R. V. F. Janssens, M. P. Carpenter, S. Zhu, and N. Pietralla

14. Study of Excited States in ^{7}He through the d(^{8}Li,^{3}He)^{7}He Reaction [Wuosmaa]
    A. H. Wuosmaa, R. H. Siemssen, L. Jisonna, J. C. Lighthall, S. T. Marley, N. J. Goodman, D. Patel, K. E. Rehm, R. V. F. Janssens, R. C. Pardo, J. Greene, D. Henderson, J. P. Schiffer, and C. L. Jiang

15. Re-Examination of the ^{32S} + ^{96}Ru → ^{128}Nd* → ^{123}Pr + p4n Reaction Using the Fragment Mass Analyzer: Was Proton Decay Observed at Dubna in 1970? [Perajarvi]
    K. Perajarvi, H. T. Penttila, J. Cerny, A. P. Robinson, C. N. Davids, and D. Seweryniak

16. Accelerator Mass Spectrometry of ^{59}Ni at High Sensitivity [Paul]
    M. Paul, I. Ahmad, P. Collon, D. J. Robertson, C. J. P. Schmitt, D. Henderson, J. Greene, C. L. Jiang, R. C. Pardo, K. E. Rehm, X. Tang, N. Patel, R. H. Scott, R. Vondrasek, and L. Jisonna

17. Test of Nuclear Chirality in ^{104}Rh - Study of Electromagnetic Transitions and the Chiral Selection Rules via Lifetime Measurements using the Recoil Distance Method in Inverse Kinematics [Rainovski]
    G. I. Rainovski, A. Costin, T. Koike, R. Wadsworth, M. T. Danchev, A. Dewald, R. V. F. Janssens, M. P. Carpenter, C. J. Lister, S. Zhu, C. Vaman, and N. A. Pietralla

18. Distortion of Mirror Symmetry: The Special Case of A = 71:T_z ± 1/2 Mirror Nuclei ^{71}Br and ^{71}Kr [Fischer]
    S. M. Fischer, C. J. Lister, D. G. Sarantites, C. J. Chiara, O. Pechenaya, D. Seweryniak, S. Zhu, S. Gros, D. A. Peterson, R. A. Kaye, W. A. Yemington, D. J. McLaughlin, W. Reviol, D. P. Robinson, X. Wang, and Y. K. Ryu

19. Proton Decay below the ^{100}Sn Double Shell Closure [Robinson]
    A. P. Robinson, D. Seweryniak, P. J. Woods, C. N. Davids, S. Gros, S. Zhu, G. Lotay, A. A. Hecht, and B. Shumard

20. Measurement of the β-Delayed α Spectrum of ^{16}N with a New Technique-4 [Rehm]
    X. Tang, M. M. Notani, N. Patel, C. L. Jiang, J. P. Schiffer, J. Greene, S. Henderson, B. Shumard, K. E. Rehm, R. V. F. Janssens, L. Jisonna, R. E. Segel, D. M. Kahl, C. Brune, A. H. Wuosmaa, M. Paul, A. E. Champagne, A. A. Hecht, and G. Savard

21. Sub-Barrier Fusion of the Closed Shell ^{48}Ca + ^{48}Ca System [Back]
    B. Back, C. L. Jiang, C. J. Lister, R. V. F. Janssens, C. N. Davids, D. Seweryniak, K. E. Rehm, A. P. Robinson, X. Tang, S. Zhu, X. Wang, and D. A. Peterson

22. Structure of the Neutron-Rich Fe Isotopes via Deep-Inelastic Reactions [Walters]
    W. B. Walters, J. R. Stone, N. Stone, J. Wrzesinski, W. A. Krolas, R. J. Broda, B. Fornal, A. A. Woehr, N. Hoteling, A. A. Hecht, S. Zhu, M. P. Carpenter, R. V. F. Janssens, D. Seweryniak, C. N. Davids, and X. Wang

23. Precision Measurement of the Q-Value of the Superallowed Decays of ^{42}Sc, ^{50}Mn, ^{54}Co, ^{34}Cl, and ^{26m}Al with the CPT Mass Spectrometer [Savard]
    G. Savard, J. A. Clark, A. Levand, J. Fallis, H. Sharma, Y. Wang, N. D. Scielzo, A. C. Villari, P. J. Sloan, I. Tanihata, S. L. Gulick, R. E. Segel, A. A. Hecht, K. S. Sharma, J. C. Hardy, D. Lascar, M. Sternberg, C. L. Wrede, C. M. Deibel, D. Danaher, and C. Riviere

24. Quantifying the Level of Isospin Mixing in the A = 31 Mirror Nuclei [Pattabiraman]
    N. S. Pattabiraman, R. Wadsworth, D. G. Jenkins, R. Glover, Krishichayan, C. J. Lister, S. Zhu, M. P. Carpenter, C. J. Barton, P. E. Kent, P. J. Woods, T. Davinson, G. Lotay, R. V. F. Janssens, T. L. Khoo, T. Lauritsen, and D. Seweryniak

25. Gammasphere and Fragment Mass Analyzer Upgrades [Lister]
    C. J. Lister, S. M. Fischer, D. Seweryniak, S. Zhu, S. Gros, A. P. Robinson, T. L. Khoo, A. A. Hecht, M. P. Carpenter, B. Shumard, N. Hoteling, R. V. F. Janssens, and C. N. Davids

26. Effects of Heavy Ion Irradiation on Phase Transitions of the Vortex Matter in High Temperature Superconductors [Kwok]
    W. K. Kwok, U. Welp, L. Paulius, and R. Xie

27. Neutron-Proton Correlations in Odd-Odd N = Z ^{86}Tc: Characterization of the 1.6 ms Isomer [Regan]
    C. J. Lister, P. H. Regan, D. Henderson, I. J. Cullen, N. J. Thompson, G. D. Jones, A. B. Garnsworthy, S. J. Williams, Z. Liu, B. Blank, and B. Shumard

28. Lifetimes of Astrophysical Resonances in ^{19}Ne [Woods]
    P. J. Woods, G. Lotay, D. Seweryniak, D. G. Jenkins, T. Davinson, M. P. Carpenter, R. V. F. Janssens, A. P. Robinson, S. Gros, and S. Zhu

29. Lifetimes of Chiral Bands in ^{135}Nd [Garg]
    U. Garg, T. Li, S. Mukhopadhyay, F. G. Kondev, S. Zhu, M. P. Carpenter, T. Lauritsen, D. Seweryniak, X. Wang, R. V. F. Janssens, S. Gros, and A. A. Hecht

30. High-Spin Spectroscopy of ^{224}U [Reviol]
    W. Reviol, C. J. Chiara, O. Pechenaya, D. G. Sarantites, K. Hauschild, A. P. Lopez-Martens, T. L. Khoo, M. P. Carpenter, C. J. Lister, D. Seweryniak, and S. Zhu

31. Search for a High-K Isomer in ^{252}No [Khoo]
    T. L. Khoo, D. Seweryniak, A. P. Robinson, S. Gros, D. A. Peterson, I. Ahmad, B. Back, M. P. Carpenter, C. N. Davids, J. Greene, A. A. Hecht, R. V. F. Janssens, F. G. Kondev, T. Lauritsen, C. J. Lister, S. Zhu, P. Chowdhury, S. K. Tandel, U. S. Tandel, A. M. Heinz, J. Qian, X. Wang, R.-D. Herzberg, G. D. Jones, and S. Eeckhaudt

32. Search for Deformed States in ^{185}Pb [Carpenter]
    M. P. Carpenter, F. G. Kondev, R. V. F. Janssens, C. J. Lister, A. P. Robinson, S. Zhu, D. Seweryniak, T. L. Khoo, T. Lauritsen, X. Wang, N. Hoteling, A. A. Hecht, A. J. Larabee, W. Reviol, S. Gros, and M. Asai

33. High Spin States in the T = 3/2 Mirror Nuclei ^{37}Ca and ^{37}Cl, and the T = 1/2 Mirror Nuclei ^{37}K and ^{37}Ar [Williams]
    S. J. Williams, A. B. Garnsworthy, S. J. Steer, I. J. Cullen, G. A. Jones, P. E. Kent, J. R. Brown, M. J. Taylor, D. Rudolph, P. E. Garrett, G. A. Demand, D. Bandyopadhyay, M. A. Phillips, and K. L. Green

34. The Study of (p,p), (p,α) and (α,p) Reactions Using MUSIC and the Thick Target Technique-2 [Tang]
    X. Tang, K. E. Rehm, M. M. Notani, N. Patel, L. Jisonna, C. L. Jiang, D. Henderson, B. Shumard, and J. P. Schiffer

35. The Spin of the 2.643 MeV State in ^{20}Na, Studied via the ^{19}Ne(^{3}He,d)^{20}Na Reaction [Jisonna]
    L. Jisonna, X. Tang, M. M. Notani, N. Patel, C. L. Jiang, J. Greene, D. Henderson, B. Shumard, R. E. Segel, A. H. Wuosmaa, J. P. Schiffer, K. E. Rehm, R. C. Pardo, G. Zinkann, and J. O. Fernandez-Niello

36. A Study of np Interactions in Odd-Odd N = Z + 2 ^{112}Cs [Smith]
    J. F. Smith, S. J. Freeman, A. N. Deacon, B. P. Kay, D. Steppenbeck, E. S. Paul, A. N. Grint, B. M. McGuirk, M.-K. Petri, and C. J. Chiara

37. The Branching Ratio of the Subthreshold 1- State in the β-Decay of ^{16}N [Rehm]
    X. Tang, K. E. Rehm, M. M. Notani, C. J. Lister, M. P. Carpenter, R. V. F. Janssens, C. L. Jiang, J. P. Schiffer, G. Savard, N. Patel, L. Jisonna, R. E. Segel, A. H. Wuosmaa, and S. Zhu

38. Precision Measurement of the Q-Value of the Superallowed Decays of ^{10}C, ^{34}Cl, ^{38m}K, ^{50}Mn and ^{54}Co, and the Unitarity of the CKM Matrix [Savard]
    G. Savard, A. Levand, H. Sharma, A. A. Hecht, D. Lascar, J. A. Clark, J. Fallis, N. D. Scielzo, S. Caldwell, R. E. Segel, F. Buchinger, C. L. H. Wrede, and C. M. Deibel

39. K-Isomers in Trans-Plutonium Nuclei via Deep-Inelastic and Transfer Reactions [Chowdhury]
    S. K. Tandel, U. S. Tandel, C. Wilson, A. J. Knox, P. Chowdhury, M. P. Carpenter, C. J. Lister, S. Zhu, D. Seweryniak, T. Lauritsen, T. L. Khoo, F. G. Kondev, R. V. F. Janssens, A. P. Robinson, J. Greene, I. Ahmad, S. Gros, D. A. Peterson, and X. Wang

40. The p-Process ^{146}Sm Nuclide: Half-Life and Production [Paul]
    M. Paul, K. E. Rehm, R. C. Pardo, R. Vondrasek, R. H. Scott, P. Collon, D. Henderson, C. J. P. Schmitt, M. M. Notani, N. Patel, Y. Kashiv, N. Kinoshita, L. Jisonna, J. Greene, D. Robertson, and C. L. Jiang

41. Evolution of the One-Phonon Mixed-Symmetry $2^+_{1,ms}$ State from U(5) to O(6) Dynamical Symmetry Limits in Xe Isotopes from Inverse-Kinematics Coulomb Excitation [Pietralla]
    N. A. Pietralla, T. Ahn, L. Bettermann, W. Rother, V. R. Werner, M. T. Chamberlain, R. V. F. Janssens, C. J. Lister, M. P. Carpenter, and S. Zhu

42. Neutron Excitations at the Fermi Surface above the N = 32 Shell Gap: Structure of ^{55}Ti [Zhu]
    R. V. F. Janssens, S. Zhu, M. P. Carpenter, T. Lauritsen, A. P. Robinson, D. Seweryniak, B. Fornal, S. J. Freeman, A. N. Deacon, J. F. Smith, B. P. Kay, D. Steppenbeck, and A. J. Larabee

43. The Structure of ^{13}B [Schiffer]
    J. P. Schiffer, C. L. Jiang, X. Tang, R. C. Pardo, M. M. Notani, A. H. Wuosmaa, K. E. Rehm, D. Patel, R. E. Segel, I. Tanihata, J. C. Lighthall, and S. T. Marley

44. Preliminary Measurement of the β-ν Correlation in ^{14}O [Scielzo]
    N. D. Scielzo, G. Savard, H. Sharma, I. Tanihata, A. A. Hecht, A. Levand, J. A. Clark, K. S. Sharma, S. Caldwell, D. Lascar, J. Fallis, R. E. Segel, T. Wang, D. Donaher, and G. Li

45. Study of ^{92}Pd Through ^{40}Ca(^{54}Fe,2n) [Sarantites]
    D. G. Sarantites, W. Reviol, C. J. Chiara, O. Pechenaya, W. L. Mason, C. J. Lister, R. V. F. Janssens, D. Seweryniak, M. P. Carpenter, S. Zhu, and T. Lauritsen

j.3. Renovation of the ATLAS Data Room (C. J. Lister and J. Rohrer)

After 20 years, the ATLAS data room was looking tired. Moreover, the functionality of the room had changed over the years, with most experiments now having their electronics and acquisition computers located at the beam lines near the equipment. Finally, a new high speed data acquisition network needed to be installed, and the old VAX-based systems decommissioned.

During spring shutdown in 2006 a renovation took place. Redundant racks were removed, along with old cables, patch panels, furniture and computers. New partition walls were installed and new furniture acquired. The new data network came online, and new workstations running "Root" visualization packages became available to users. A new conference area was created (see Fig. I-58) with a refrigerator, chilled water, and a microwave oven. Wireless network access was installed. This has all proven very popular with the outside Users of our facility.

Fig. I-58. The conference area in the renovated data room.

II. OPERATION AND DEVELOPMENT OF ATLAS

OVERVIEW

Operational performance, work on improvement projects, and related accelerator physics R&D projects for the Argonne Tandem Linear Accelerator System (ATLAS), a DOE national user facility, are described in this chapter. ATLAS is funded to provide heavy-ion beams for basic research in nuclear physics but also serves other areas of research and development, including material science. In addition, ATLAS has a long-standing program in developing the tools of accelerator mass spectroscopy (AMS) applied to wide ranging research programs such as oceanography, nuclear physics, astrophysics, and geology. Over half of the beam time is allocated to experiments for which the spokesperson is an outside user. Recent ATLAS operating performance and related development projects are described in this section. ATLAS personnel are also involved in developing technology in support of a future advanced facility, based on ATLAS technologies, for beams of short-lived nuclei.

ATLAS continued to operate on a 5.3 day schedule through FY2006 and into FY2007 with some limited 7-day operation to accommodate runs approved for longer operation that would be disadvantaged by breaking into segments. Although not efficient use of the facility, this schedule has been brought about by budgetary constraints. In December 2006, ATLAS began a long maintenance period focused on replacing our smallest refrigerator with a larger unit to provide improved cooling capacity. This increased capacity will improve overall operation but will also improve the performance of the new resonators that are part of the Energy Upgrade project expected to be online in 2008. Construction of a new cryostat and resonators for a major energy upgrade of the facility, which will increase the overall voltage of ATLAS by ~25%, nears completion. Construction of the final six resonators is complete and electropolishing and surface preparations are underway.

For FY2006, ATLAS provided 38 beams of different isotopes to users. A total of 5358 hours of research beam time was provided for the research program, while the total scheduled operating hours for FY2006 was 5568 including startup time.

Since FY1995, ATLAS has made beams of short-lived rare isotopes (RIBs) available for nuclear physics research. A total of 19 different radioactive beams have been developed over those years and are generally available for use. Further development of RIBs is planned as required by the nuclear physics and nuclear astrophysics programs at ATLAS.

The proposal to create neutron-rich beams from fission fragments and accelerate those beams with the ATLAS accelerator, now known as CARIBU – CAlifornium Rare Ion Beam Upgrade –

was approved and the project began on January 1, 2006. The total project cost is $4.6M and the first beam is planned for the second quarter of FY2009.

Table II-1. Summary of ATLAS experiments and user statistics.

	FY2006 (actual)	FY2007 (extrap.)	FY2008 (pred.)	FY2009† (pred.)
Beam Use for Research (hr)				
Nuclear Physics	5202	3370	4450	4350
Accelerator R&D (CARIBU & ATLAS)	31	*350	200	300
Accelerator Mass Spectroscopy	75	85	100	100
Other	50	45	50	50
Total	5358	3850	4800	4800
Number of Experiments Receiving Beam	46	36	40	41
Number of Scientists Participating in Research	411	311	368	368
Institutions Represented				
Universities (USA)	21	15	18	18
DOE National Laboratories	3	3	3	3
Other	32	20	26	27
Usage of Beam Time (%)				
In-House Staff	36	35	35	35
Universities (USA)	36	40	40	40
Other DOE National Laboratories	5	5	5	5
Other Institutions	23	20	20	20
Total	100	100	100	100

*Includes tests of the prototype RIA gas catcher system.
†Does not include stopped beam experiments.

A. OPERATION OF THE ACCELERATOR

a.1. Operations Summary (R. C. Pardo, D. Barnett, L. Carlquist, A. Deriy, G. Devane, R. Jenkins, A. Krupa, E. Lindert, S. McDonald, F. H. Munson, Jr., D. R. Phillips, M. Power, A. Ruthenberg, R. H. Scott, S. Sharamentov, P. Strickhorn, R. C. Vondrasek, and G. P. Zinkann)

ATLAS provided a total of 5358 hours of beam available to the research program in FY2006 and 5714 hours were scheduled for all operational activities during that period. The facility ran with a reliability factor of 94.3% for the fiscal year. The beam time exceeded the planned value for this year because of a delay in a planned major maintenance shutdown to install a new cryogenic refrigerator, a project described in more detail below. This shutdown did not occur until FY2007 and regular operation continued instead.

A record total of 38 different isotopes were provided during this period; the species distribution is shown in Fig. II-1. The focus of the research program continues to be on the lighter elements with $A \leq 58$ accounting for ~80% of all beam time.

In-flight beams used in research for the first time included ^{12}B and ^{19}Ne. In FY2006, in-flight radioactive beams of ^{8}Li, ^{10}C, ^{12}B, ^{16}N, and ^{19}Ne as well as the longer-lived ^{44}Ti were provided. The total radioactive beam time provided for the year was 910 hours. Significantly improved transmission from the negative ion source to the Tandem allowed the available beam current for ^{44}Ti to increase to 2×10^{6} ions/s reliably. Work continues on the development of an RF chopper for improved beam purity of in-flight RIBs with installation of that system planned for late 2006.

The CARIBU project, a major new initiative for the facility, will provide a wide array of far-from-stability neutron-rich beams. The project is now into its second year and has made excellent progress in all major areas. It is discussed in more detail in another section of this report. Although the project will draw on a large number of ATLAS operations personnel to implement the project, we do expect normal ATLAS operations to continue, largely unaffected, until FY2008 when time will be required for early tests. A larger amount of time will be required when commissioning activities begin in FY2009.

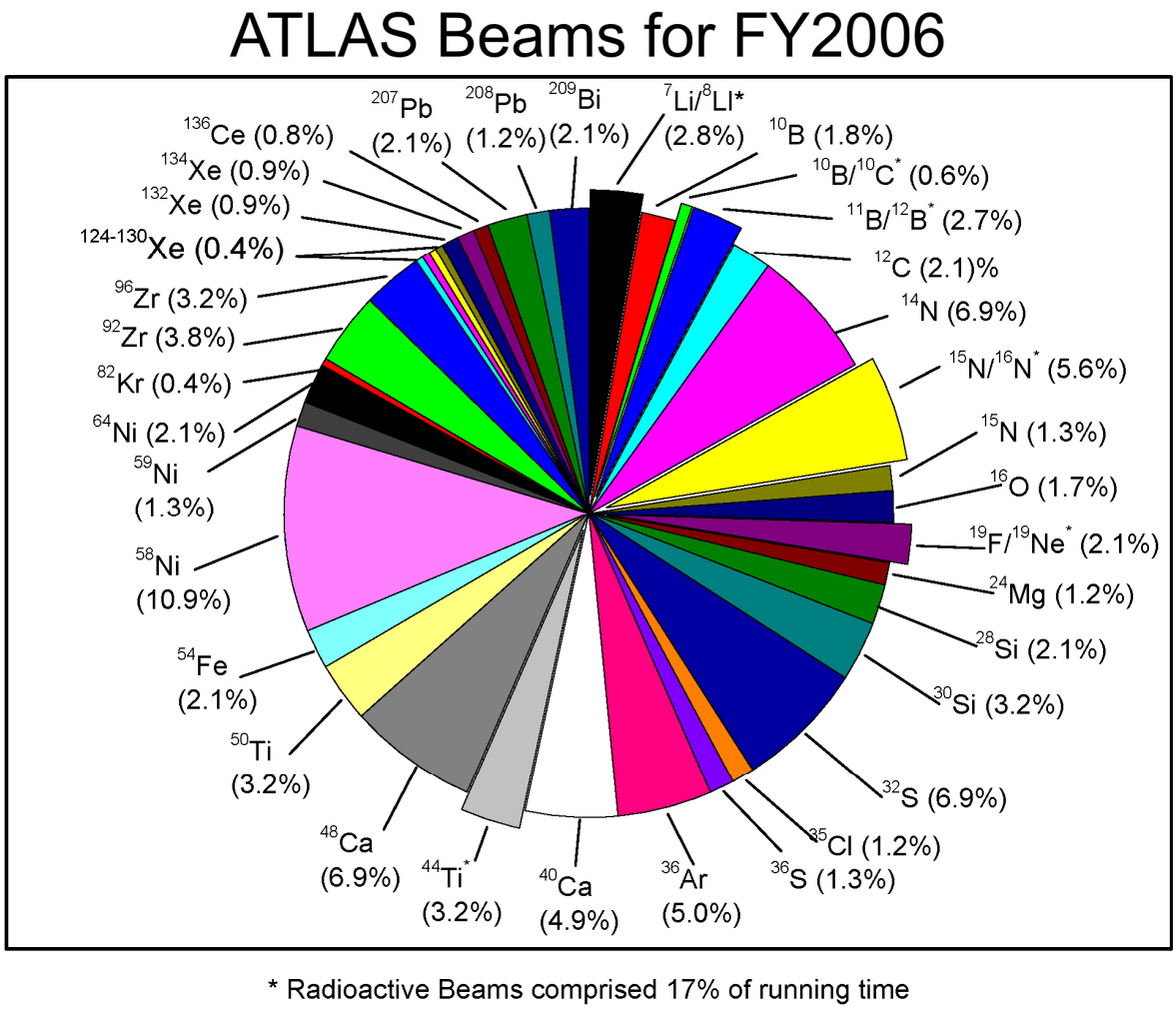

Fig. II-1. Distribution of beam time by isotope provided by ATLAS in FY2006. A record total of 38 different isotopes were provided to the research program. Radioactive beams (indicated by an asterisk) comprised 17% (910 hours) of all beam time in the fiscal year.

B. DEVELOPMENTS RELATED TO ATLAS

b.1. Status of the ECR Ion Sources (R. C. Vondrasek and R. H. Scott)

b.1.1. Refinement of the Sputter Technique

The sputter technique, which has been in use on the ATLAS ECR ion sources since 1994, has an inherent limiting factor in that it requires a relatively high gas pressure in the plasma chamber for adequate sputter yield. The high pressure limits the production of high-charge state ions as well as intense beams of the mid-charge states. When operating with the sputter probe for large beam currents (100 eμA of Pb^{23+}) the pressure increases to 3.0e-7 due to the higher sputter yield required, and this higher pressure negatively impacts overall source performance. When optimizing for high charge state production, the operating pressure is typically 1.0e-7 Torr, but then the sputter yield decreases due to an insufficient amount of gas in the region of the sputter probe and large beam currents (>10 eμA of Pb^{37+}) cannot be achieved. To mitigate this limitation, a technique has been developed to lower the overall pressure in the plasma chamber by introducing the working gas at the tip of the sputter sample. This has the effect of introducing the gas in the region it is most needed for a good sputter yield as opposed to diffusing throughout the entire plasma chamber.

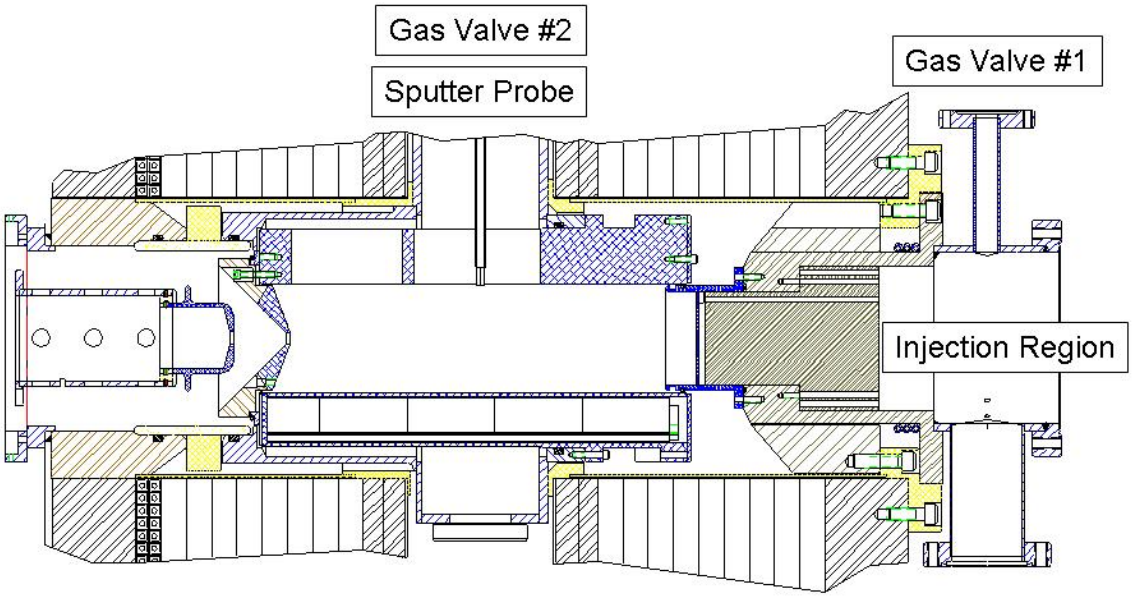

Fig. II-2. Sputter probe configuration on ECR2. The gas from Valve #1 diffuses into the plasma chamber via the injection region. The gas from the Valve #2 flows into the plasma chamber directly from the sputter probe.

In operation, the main plasma support gas is introduced through a valve mounted on the injection region tank. The sputter support gas is then introduced directly at the sputter probe tip using a second gas valve. This has the effect of decoupling the plasma support gas (Valve #1) and sputter support gas (Valve #2) levels and providing an increased local pressure at the probe tip where it is needed for an adequate sputter yield. The gas flows through a stainless steel tube which holds the sputter sample and is introduced into the plasma chamber through a 0.5 mm diameter hole in the sputter sample, shown in Fig. II-2.

The source was run in two-frequency heating mode (14 + 10.85 GHz) with the total RF power level kept constant at 500 W. The extraction voltage was 14 kV, and the solenoid coil currents were not varied between runs. A natural lead sample was used with the sputter

voltage kept constant at -0.28 kV (0.1 mA drain).

The results from the two operating modes are shown in Table II-2. With the gas flowing in only through the injection region (Valve #1), the total source drain current was 1.07 mA with a vacuum of 1.0e-7 Torr. With the gas flowing in only through the sputter sample (Valve #2), the total drain current decreased to 0.83 mA, reflecting the decrease in the amount of gas within the plasma chamber, and the vacuum increased to 1.4e-7 Torr in the plasma tank. This measurement is outside of the plasma chamber and at this level may not accurately reflect what is occurring within the plasma chamber itself.

Table II-2. Beam Intensities for ^{Nat}Pb.

Charge state	Intensity (eμA) using Valve #1	Intensity (eμA) using Valve #2
31+	6.75	9.67
32+	6.00	8.36
33+	4.88	6.88
34+	3.95	5.59
35+	3.00	4.22
36+	2.08	3.04

As can be seen in the table, the beam currents for the highly charged ions (HCI) of lead increased on average by 42%. This demonstrates that the technique of lowering the base pressure within the plasma chamber by introducing the working gas at the sputter sample location improves the HCI production. More tests are scheduled to determine the effect on the mid-charge state production.

b.1.2. Source Liner Development

The measurement of ^{39}Ar in ocean water samples has been an ongoing process hampered by the prevalence of potassium in the ion source. The potassium problem was addressed by installing a quartz liner in the ion source, thus, reducing the background level by a factor of 130. But this also had the detrimental effect of reducing the beam intensity due to the inadequacies of quartz as a plasma chamber material. In collaboration with a group at Princeton University, a new ultra-pure aluminum liner was fabricated with a measured bulk potassium contaminant of <10 ppb.

First, a baseline measurement of source performance for $^{40}Ar^{8+}$ was performed. After a few days of conditioning, 490 eμA of $^{40}Ar^{8+}$ was extracted from the source without a liner in place. Then the ultra-pure aluminum liner was installed and conditioned for several days. At 250 W of power, 340 eμA of $^{40}Ar^{8+}$ was achieved. This is a factor of 4 higher than the previous best beam current with a quartz liner. It is hoped that the potassium level in the source will be reduced by either the same amount or greater as when the quartz liner is in use.

b.2. ATLAS Control System (F. H. Munson and M. Power)

b.2.1. ATLAS Operations Databases and Communication Improvements

A project to provide a web-based ATLAS "bulletin board" is underway. With one of its planned primary displays located in the ATLAS control room, this bulletin board will be used to convey instructions and generally distribute information primarily regarding ATLAS operations to the ATLAS operators.

ATLAS maintains a relational database management system called Hercules. The system is comprised of three separate databases. These include the "operator shift log", an "equipment maintenance log", and a "mechanical and electrical drawing index". As part of an on-going project to retire this system, the functionality of the mechanical and electrical drawing index portion of the system has been replaced by a web-based application that interfaces to the open source MySQL relational database management system. This system has the added advantage of being able to link to the actual drawing indexed in the database for viewing if the drawing file exists. This feature was not available in the older Hercules system.

b.2.2. ATLAS Hardware Upgrade Project

CAMAC (Computer Automated Measurement and Control) is the I/O (Input-Output) hardware subsystem architecture historically used at ATLAS. Acquiring CAMAC modules used at ATLAS that provide a GPIB (General Purpose Interface Bus or IEEE488) interface or a Serial Line (RS-232) interface has become cost prohibitive. One solution is to replace the functionality of these particular CAMAC modules with an Ethernet "gateway" that provides a connection between the ATLAS control system LAN (Local Area Network) and devices that use the GPIB or RS-232 interface. Prototype software that interfaces this gateway to Vsystem has been written to test the feasibility of this approach.

In addition to the GPIB and RS-232 CAMAC modules mentioned previously, CAMAC modules in use at ATLAS in general are becoming unavailable from manufacturers, or are becoming too costly to acquire and repair. Motivated by the new CARIBU (Californium Rare Ion Breeder Upgrade) project, it has been decided that a CAMAC alternative should be found. The overall goal is to limit or eliminate the need for purchasing new CAMAC equipment except for some unexpected special need. This would be accomplished by replacing CAMAC equipment with alternatives in those systems that can be isolated, and operated more or less independently, retaining the replaced CAMAC equipment (crates and modules) as spares.

A significant amount of time has been devoted to researching an alternative. After much consideration it has been decided that one or more of the three architectures or bus structures that will be used for CARIBU, and future ATLAS projects, include a commercially available IOC (Input Output Controller), VME64x (Versa Module Eurocard 64-bit Extension), and cPCI (Compact PCI). Initial focus has been on the IOC and the VME64x approach. Both of these bus structures (as well as cPCI) support the pseudo IP (Industry Pack) standard.

Industry packs are self contained modules providing several different I/O options and typically come in two sizes. The size being considered for use at ATLAS is the standard 1.8 × 3.9 inch module.

The IOC is a 1U (1.75") high rack mount unit that employs a PC/104 CPU (Central Processing Unit) module that provides all of the typical SBC (Single Board Computer) features, such as an Ethernet controller, USB (Universal Serial Bus) controller, HDD (Hard Disk Drive) controller, graphics adapter controller, and keyboard and mouse interfaces. The IOC has provisions for supporting up to as many as six industry packs. This is approximately one third the I/O capability of the standard CAMAC crate currently used at ATLAS.

The VME64x approach utilizes a standard PC mounted in a 1U high rack mount chassis configured with a PCI module capable of interfacing to a VME64x crate controller. Through the use of "carrier modules" a single slot in a VME64x crate can accommodate up to four industry packs. With one slot being devoted to the crate controller, a seven slot crate could support up to four times the number of industry packs provided for by the IOC. This is almost equal to the I/O capability of the standard CAMAC crate currently used at ATLAS.

The current plan is to use IOCs in those applications where space is at a premium and required I/O is minimal, and use VME64x crates where use of the IOC is not suitable.

An IOC and a VME64x crate have been acquired. Analog I/O, digital I/O, RS-232 I/O, and stepper motor controller IPs have been acquired as well. Prototype software to interface to Vsystem for testing and evaluation purposes has been written. To date, Vsystem software handlers have been written to test monitoring or controlling devices requiring 16-bit ADC I/O, 16-bit DAC I/O, 48-bit digital I/O, RS-232, and stepper motors.

b.3. ATLAS Electronics (S. Sharamentov)

b.3.1. RF Amplifier Replacement

Sixteen new RF amplifiers (see Physics Division Annual Report 2005, page 113) were built and installed in two Booster RF racks, bringing the total number of modified RF racks to 3. Three more racks, one in the Booster and two in ATLAS, will be modified in 2007-2008. Additional improvement was the installation of 97 MHz band pass filters in the resonator's pick-up lines. These filters suppress the 104 MHz split ring resonator mode and the easing process of locking the self-exiting resonator oscillations to a master frequency.

b.3.2. Tandem Electronics Upgrade

The old electronics for the Tandem multi-harmonic buncher was replaced with new I and Q RF controller systems identical to the previously installed (see Physics Division Annual Report 2004, page 142) PII multi-harmonic buncher system.

A new four channel high voltage power supply chassis, replacing old power supplies, was designed and built. Each channel is based on Ultravolt A – 25A series high voltage DC-DC converters, covering the output voltage range positive or negative polarity from 0 to 25 kV, and up to 30 W of output power. This power supply features a flexible channel configuration design allowing for independent control of all four channels, two pairs of precisely tracking each other master-slave channels or combination of two independent channels and one pair of master-slave outputs, of plus or minus polarity. Figure II-3 shows the new chassis with four output channels

Fig. II-3. Front, rear and top view of the four channel power supply. The power supply was installed in the Tandem area as the QET002 quadrupole power supply.

b.4. Slow Tuner System with High Slew Rate (G. Zinkann and S. Sharamentov)

The Argonne Tandem Linear Accelerator System (ATLAS) superconducting cavities use a pneumatic system to maintain the cavity eigenfrequency at the master oscillator frequency. The present pneumatic slow tuner control has a limitation in the tuning slew rate. In some cases, the frequency slew rate is as low as 30 Hz/sec. The total tuning range for ATLAS cavities varies from 60 kHz to as high as 450 kHz depending on the cavity type. With the present system, if a cavity is at the extreme end of its tuning range, it may take an unacceptable length of time to reach the master oscillator frequency. We have designed a new slow tuner control system that increases the frequency slew rate by a factor of three hundred in the most extreme case.

A single channel slow tuner prototype system was developed two years ago. The single channel system was tested on an on-line superconducting cavity. The results of this test were used to develop a six channel

unit. This six channel unit, shown in Fig. II-4, is capable of controlling six SC cavities in one ATLAS cryostat.

In January 2007 we will install the final version of the six channel slow tuner system on the A-cryostat and a portion of the B-cryostat resonators, and we plan to expand this to the remainder of the system in subsequent years.

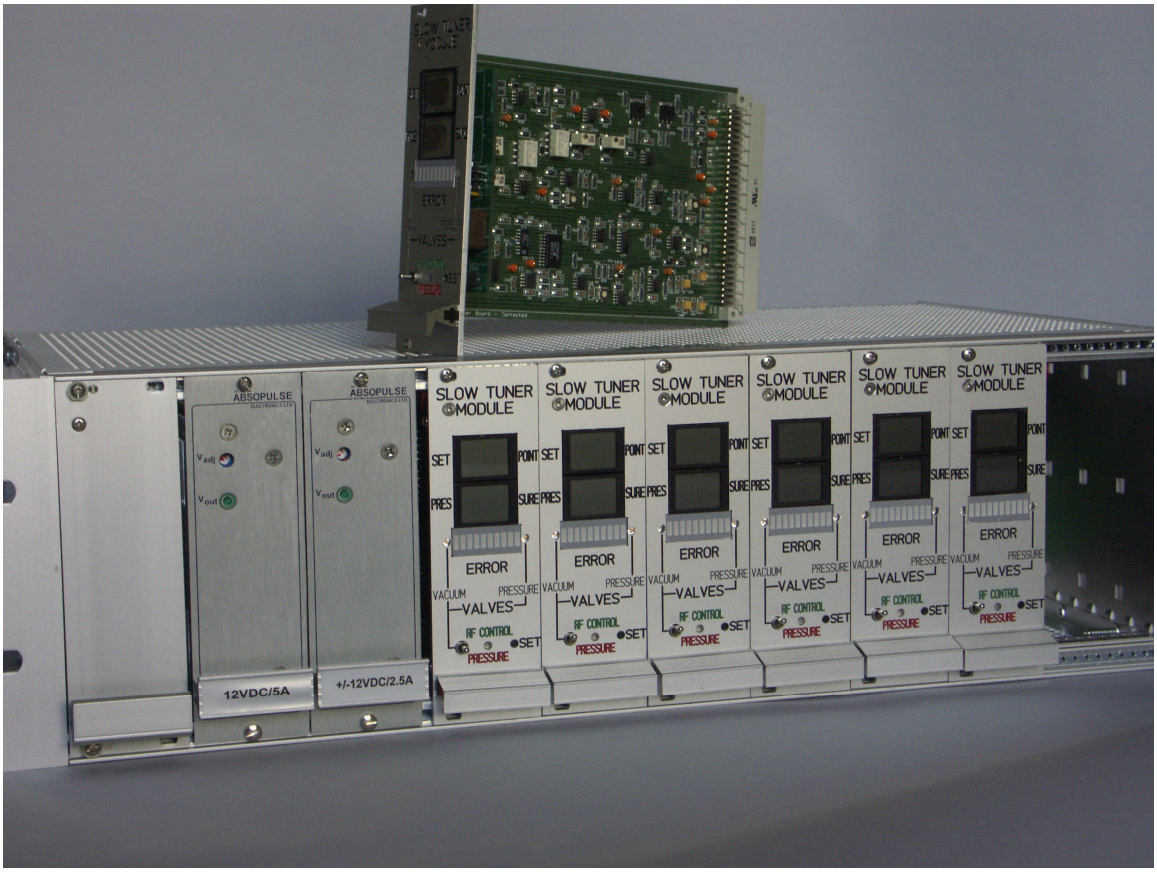

Fig. II-4. The electronic control system for the six channel control unit.

b.5. ATLAS Cryogenic System (S. MacDonald and R. Jenkins)

b.5.1. Installation of an Additional 2800 Refrigerator

An Accelerator Improvement Project (AIP) to increase the refrigeration capacity and improve reliability and overall performance of the ATLAS cryogenic system was undertaken in late 2006. The $173k project planned to use a CTI Model 2800 cold box that was acquired from Lawrence Livermore National Laboratory in late 2001. The project was to replace the Model 1630 refrigerator with this unit, which will increase the overall capacity of the cryogenic system by approximately 100 watts and to make other improvements to the helium distribution system for added reliability and capacity. This increase in capacity will allow the operation of the ATLAS upgrade cryostat at planned fields, as well as provide an increased operating margin which should decrease cryogenic downtime.

The refrigerator was removed from storage in April 2006 and found to have incurred extensive damage during shipment. This refrigerator was also found to have many leaks caused by poor fabrication techniques and corrosion. The repairs of these leaks consumed a period of seven months that was not planned for. Eventually, all leaks were repaired. The refrigerator was then rewired and outfitted with a remote wet engine operation device, a JT valve controller, new

thermometry readouts and a redesigned liquid nitrogen control system. The rebuilt refrigerator, shown in Fig. II-5, was then successfully tested using local utilities and one of the spare RS compressors in November and December 2006.

Fig. II-5. CTI Model 2800 – 300 Watt liquid helium refrigerator shown after installation in the ATLAS facility.

Engineering and planning of the 2800 installation was completed during the refrigerator repair period. Integration designs were finalized, the cold lines were fabricated and the procurement of high lead-time items was accomplished. A vacuum break to separate the PII and booster sections was also designed. This break, along with the 2800 installation, would effectively separate the insulating vacuum portions of the three accelerator sections. This separation will allow each of the sections to be warmed independently, allowing greater flexibility in maintenance, upgrades and operating.

In late December 2006 the facility entered a long maintenance period for the final installation. The first operation of the installed system began in February and ATLAS returned to operation in March. In the end, the installation was highly successful and the cryogenics system is operating extremely well.

b.6. A 50-kV RF Chopper for In-Flight RIB Beams (J. Bogaty, R. C. Pardo, and S. I. Sharamentov)

Work has continued on the RF Chopper project whose goal is to improve the in-flight RIB beam cleanliness by removing the primary beam tails. The vacuum chamber for the chopper is complete and work is now proceeding on completion of the RF control electronics and the resonant tuning circuits for the chopper. The system is expected to be ready for installation by November 2007.

b.7. Californium Rare Ion Breeder Upgrade Project (CARIBU) (R. Pardo, G. Savard, S. Baker,* C. Davids, T. Levand, D. Phillips, F. Munson, M. Power, A. Ruthenberg, S. Sharamentov, T. Sun, R. Vondrasek, B. Zabransky, and G. Zinkann)

The Californium Rare Ion Beam Upgrade (CARIBU) for the ATLAS facility is under construction. The facility will use ^{252}Cf fission fragments thermalized and collected into a low-energy particle beam by a helium gas catcher, mass analyzed by an isobar separator, and charge bred to higher charge states for acceleration in ATLAS. In addition, unaccelerated beams will be available for trap and laser probe studies. A 1Ci ^{252}Cf source will provide sufficient yield to deliver accelerated beams of up to ~5 × 10^5 (10^7 to traps) far-from-stability ions per second on target.

The CARIBU Project Implementation Plan was signed on December 23, 2005 and the project began formally on January 3, 2006. The project can be thought of as consisting of seven major activities, that in early stages largely can progress independently. Those activities are:

1. Source and shield cask
2. Gas catcher and RFQ system
3. Isobar separator
4. High voltage platform
5. Electron cyclotron resonance (ECR) charge breeder ion source
6. Weak beam diagnostics
7. Building enhancements required by the CARIBU project

This year the dominant effort has focused on design and engineering of these major components, safety reviews that provide input to the design and engineering effort, and R&D activities associated with designing a gas catcher system that can handle larger space charge forces than has been required in previous applications. The building footprint is being expanded by the construction of a new space (a separate project that is not part of CARIBU). Activities this year also include designing, procuring and installing enhancements to that space required by the CARIBU project. Good progress has been made in all of these major subsystems and we are now entering an intense construction and procurement phase for most of these systems.

A total of ten project milestones were scheduled to be met during the past year and 8 of those have been achieved. The remaining outstanding milestones are associated with completion of the design of the gas catcher, source holder, and cask. These reviews are planned to take place by late February 2007.

We are now entering a period of major procurement activity. Bids for two major procurements, the isobar separator dipole magnet systems and the high voltage platform, are now beginning solicitation. In addition, procurements associated with the ECR charge breeder (CB) project and the building facilities enhancements are well advanced.

Detailed Discussion of the Major Components of CARIBU

ECR Charge Breeder

This major activity institutes modifications to change an existing ECR ion source (ECR-I) into a charge breeder ECR source. Modifications include changes to the "injection region" iron, RF waveguides and other components to provide a pathway into the plasma for the low-charge-state ions from the isobar separator. The ions are then decelerated and trapped in the plasma, charge bred and extracted at higher charge states,

sufficient for acceleration in ATLAS. In addition to these changes, new 1+ stable beam sources are being constructed to serve as a source of stable beams for development and setup of the ECR CB. In addition, the beam transfer from the CARIBU isobar separator has been modeled and the beam deceleration optics into the CB has been studied resulting in a final design for ion transfer into the CB.

Early in the project a major change in the preliminary plans was made regarding source operating voltage. After significant internal review, discussion and preliminary tests, it was decided to redesign ECR-I with the goal of operating the source at 50 kV. By operating the source at this potential, a significantly simpler gas-catcher isobar-separator beam optics is possible. All tests indicate operation at this voltage should be possible. This decision is supported by noting that two other ECR source projects are operating at 60 kV bias voltage.

This year, the final design for the system was finalized and a design and safety review of the system was held on August 3-4. Comments from the review committee were incorporated into the final plans and procurement and construction activity was initiated. It appears that the rebuilt source will be able to turn on in a normal operating mode in May 2007 and charge breeder tests with stable beams should be initiated by summer 2007, approximately 3-4 months ahead of the project schedule.

Source and Shield Cask Assembly

The source and shield cask assembly provide shielding to the ^{252}Cf source as well as mechanisms to manipulate the source to move it from a storage position to the operating position at one end of the gas catcher system. In addition, the shield cask is designed to function as an on-site transportation cask for movement of the source from the Building 200 M-wing hot cell area over to the CARIBU facility. The design of the shielding system is intended to allow personnel access to the CARIBU building area and the area around the cask on the high-voltage platform.

The activity on this major subsystem has focused on understanding the safety requirements that must be met in order to handle a 1 Ci ^{252}Cf source and the design of the shielding and handling system. A laboratory ALARA review of the CARIBU Project was conducted on October 28, 2005. This was done at a very early stage before the project was approved by DOE. The trigger for the review was the concern that an airborne release of ^{252}Cf could result in a large radiation dose to an individual, primarily by inhalation. The maximum credible incident or worst case accident scenario was discussed and the mitigation measures were considered to prevent a large dose. The ALARA Committee Chair issued a memo with recommendations and with concurrence for specification of a sheet-metal building addition to the ATLAS accelerator. Local source shielding will be used rather than a concrete building.

This review was followed by an Integrated Safety Review of the project in January 2006 by an ad-hoc committee appointed by the Physics Division Director in response to a recommendation of the TCMS project review. The resulting report gave overall concurrence to the preliminary cask and shield design ideas and provided other recommendations giving guidance concerning various important issues to address as the design went forward.

In the ensuing months up to the present, the designs of the source mount and shielding cask have gone forward. That design effort is essentially finished with final design drawings for most of the system available. The system is now ready for a final design and safety review. This review is now planned for late February 2007.

In addition to the cask and source holder design, a storage can for the shipping cask to hold the source when it is shipped from Oak Ridge to ANL has been designed. The design has been reviewed by ORNL personnel. Although certification is not required, a can must be fabricated and pass ASME-specified testing. Fabrication and testing is planned for the second quarter of 2007. Preliminary plans and procedures have been developed for transfer of the ^{252}Cf source from the shipping cask to the local shield cask.

High Voltage Platform

In order to accelerate ions in the ATLAS linac, an ion must have a velocity of ~0.008c to match the velocity profile of the first resonator. This is achieved by mounting the ECR ion source on a high voltage platform. For fission fragments from CARIBU, a maximum total voltage of 250 kV is required. This

requirement means that the ^{252}Cf source and all associated equipment must also be biased to that voltage. Thus, the source, shield cask, isobar separator and associated equipment are mounted on a new HV platform designed for a maximum operating voltage of 200 kV (50 kV comes from the local additional bias of the ^{252}Cf source and the ECR charge breeder ion source). This new HV platform design is based on the design of the existing platforms, but the dimensions are set by the equipment required (shield cask, gas catcher, isobar separator and associated equipment). The platform height is constrained by the facility beamline height of 69" and the shielding requirements of the source. Thus, although the basic platform design was easily specified, the exact dimensions were strongly coupled to the designs of the other equipment occupying the platform. This was largely due to the large amount of shielding needed around the source constraining the platform elevation and the large space needed by the gas catcher system and isobar separator which made it desirable to build the platform without significant extra space.

Therefore, finalizing the platform design was delayed into December, beyond the anticipated date, when the final overall dimensions of the other equipment, including elevation, were agreed upon. In order to accommodate the necessary radiation shielding and the required diameter of the gas catcher, the platform floor is only 26.5" off the building floor, but this will be sufficient for the required 200 kV bias and is well within the rated standoff voltage of 275 kV for the insulated feet.

The design of the platform is now complete and is in the procurement process. The forecast for completion of the platform is early August 2007. Following completion of the platform, electrical distribution, chilled water and other utilities must be supplied to the platform.

Gas Catcher System

The gas catcher system must stop and thermalize the fission recoils and transform them into a cooled low-energy ion beam for injection into the isobar separator. The gas catcher must operate at large ionization density (similar to those that will be present at RIA/AEBL) and a major thrust early in the project was the completion of a (out of project but emphasized by the TCMS review) high-intensity test demonstrating operation under such conditions. The test was performed on a new beamline in experimental area II at ATLAS that was completed and commissioned during the year and performed using a gas catcher with RF focusing along the full body and the extraction cone. The gas catcher used had a length of 85 cm, similar to what will be used for the CARIBU gas catcher, an inside diameter of 25 cm, and was operated at pressures of 100-200 mbar as required for CARIBU. The activity extracted from the device was monitored as a function of primary beam current and showed essentially no loss in efficiency up to 10^8 incoming ions per second followed by a slow decrease with further increase in intensity and still about 10% efficiency at 10^9 ions per second. These tests, performed from October to December 2006, demonstrated successful efficient operation at 3 to 4 orders of magnitude higher intensity than previously achieved and confirmed the validity of the approach being developed for the CARIBU gas catcher. The high-intensity gas catcher used for these tests had additional features to improve the outgassing of the device and the uniformity of the RF fields and those are being implemented in the final design of the CARIBU gas catcher. Detailed simulations were performed to find the optimum size for the CARIBU gas catcher and we settled for the 85 cm stated above and a larger diameter of 50 cm. This yields sufficient stopping range to limit the number of required degraders to 3 to cover all fission fragments. Transfer of the source from the cask to the gas catcher will take place through an all-metal valve using a UHV compatible shielding plug that will not compromise the vacuum requirements. Transport of the radioactive ions extracted from the gas catcher must be performed through focusing structures to remove the remaining gas and form a low emittance beam. Simulations of this section were performed by a new CARIBU post-doc, Dr. Tao Sun, that started with the project in October 2006. Using two sections of RFQ separated by microRFQs, followed by acceleration to 50 keV and focusing through a 1 mm aperture, yields enough differential pumping to remove most of the gas before acceleration and form a low-emittance beam with properties suitable for the operation of the isobar separator. The whole RFQ-acceleration-focusing section is just under 1 m long and feeds directly into the matching section at the entrance of the isobar separator.

Isobar Separator

The isobar separator design relies on the extremely low transverse emittance expected from the gas catcher/RFQ system as well as the corresponding low energy spread for ions extracted. Because of these excellent beam properties it is possible to design a relatively simple, single stage, isobar separator which still is expected to achieve a mass resolution of approximately 1/20,000 without energy compensation.

The activity associated with the isobar separator this year has been to finalize the beam optics design of the separator, present that design in a design review corresponding to Project Milestone 8, and begin the procurement of the long lead-time dipole magnets. In addition, the detailed design of the multipole high-order correctors has been initiated and work on the vacuum chamber is now underway.

A design review of the isobar separator took place on October 11, 2006. This review focused on the detailed beam optics design of the system and the detailed choices made regarding focusing elements and corrector elements. Most importantly, the decision to use electrostatic quadrupoles for first order focusing and high order electrostatic multipole elements was endorsed.

The procurement specifications for the dipole magnets, power supplies and NMR gaussmeters were finalized in December and the procurement process has now been initiated. Delivery of the magnets is forecast for June 2008.

The beam optics into and out of the separator design use electrostatic focusing elements. Electrostatic quadrupoles form the entrance waist into the system and set the beam divergence into the dipole magnets as shown in Fig. II-6. A symmetric set of lenses reform the exit waist where the mass selection is made. Sextupoles in the entrance and exit region and a 48-element electrostatic high-order multipole corrector control aberrations sufficiently to achieve the design mass resolution. A design for the electrostatic quadrupole and sextupole systems has been developed and cost estimates for constructing these devices in local machine shops are being obtained. The design of the high order correcting multipole element between the two dipoles is continuing at this time. A final design for the multipole is expected by February 2007.

Weak Beam Diagnostics/ATLAS Facility Enhancements

We plan to install two tape stations in the low-energy region of the CARIBU facility to identify the isotopic species selected by the isobar separator. One tape station is planned on the unaccelerated beamline, after the isobar separator, and a second station will be installed after the ECR charge breeder to allow species confirmation at that location as well. No work on these systems has begun, but we plan to modify an existing design developed for the CPT existing trap facility.

In order to efficiently develop accelerated beams through the ATLAS facility, we plan to perform initial setups using similar m/q stable beams with intensities that allow use of existing diagnostics. After scaling to the desired beam, weak beam diagnostics are required to check that the correct species has been selected, to optimize transmission, and to check operating conditions periodically throughout a run. The planned diagnostics include weak beam profile monitors, particle counters, and energy and time detectors.

This year work has progressed by exploring diagnostics options and developing prototypes of those options. A secondary electron emission, MCP amplifier, and scintillator coupled to a CCD digitized camera previously developed at ATLAS has been installed and re-commissioned. The device, shown in Fig. II-7, had been demonstrated in live time down to approximately 1000 ions/s and is now being interfaced into a computer to allow signal integration and averaging to improve its sensitivity even further. This device has also been modified to provide a direct pulse for every ion detected to allow a rate to be extracted without computer analysis and provide live time response at almost any rate.

An alternative system, replacing the scintillator/CCD detector with a resistive-division two-dimensional anode to provide the X-Y beam profile, has been ordered for evaluation from Quantar Technology. This system will be very similar to one in use at Oak Ridge National Laboratory developed by D. Shapiro.

In addition, a simple phosphor screen coupled to an extremely sensitive CCD camera (without an MCP amplifier) will be tested for maximum sensitivity. This system has been purchased and will be tested when ATLAS resumes operation in February.

In addition to these weak beam diagnostics, silicon detectors will be mounted throughout the system to determine the energy and timing properties of the beam. A simple prototype diagnostics chamber has been designed and is under construction to be installed in the spectrograph beamline for testing in February.

We plan to finalize our diagnostic choices for the ATLAS system in the next 9 months and begin procurement and construction of all diagnostics in FY2008. The total procurement budget for this activity is $200k.

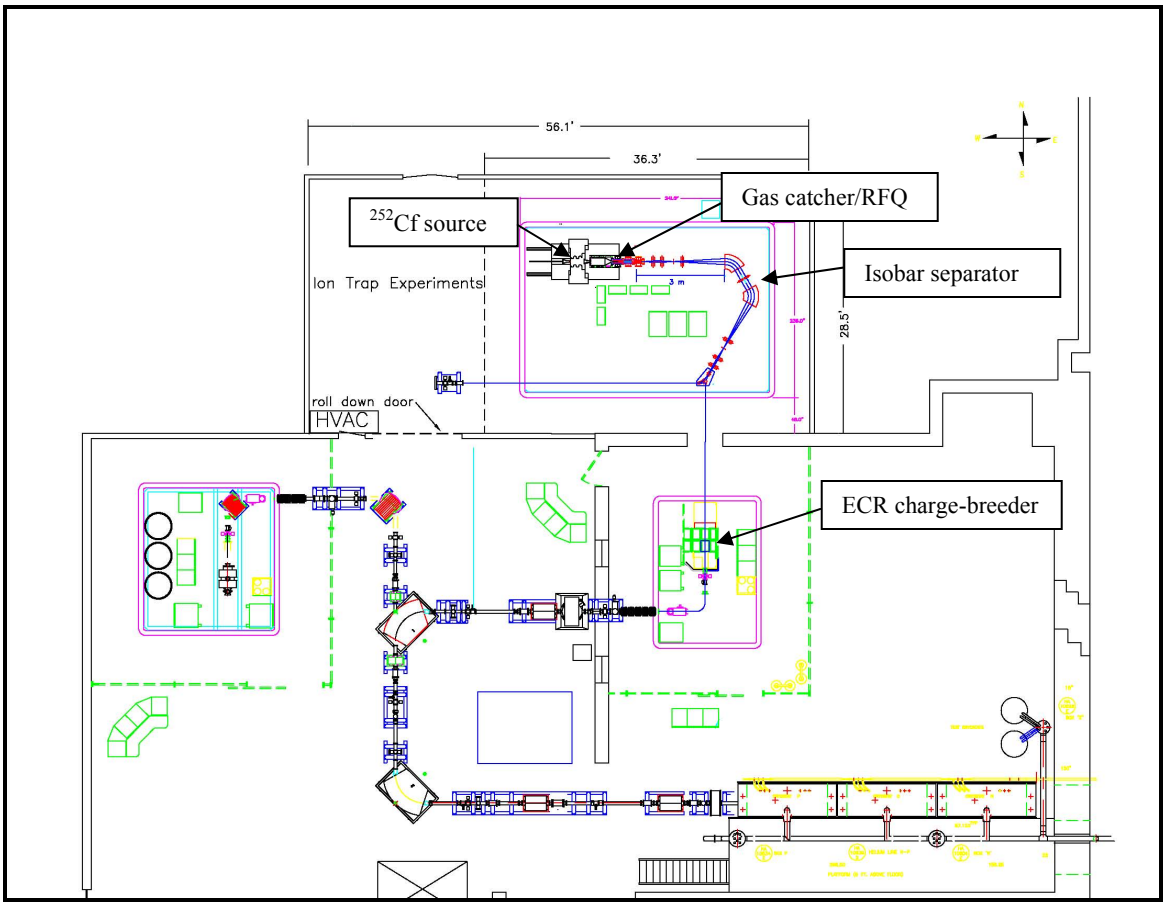

Fig. II-6. Layout of the major components of the CARIBU project. The relationship between the source and shielding, gas catcher/RFQ cooler, isobar separator, and ECR charge breeder is indicated. Not shown are the unaccelerated-beam trap equipment and the stable beam 1+ platform and sources that are used to develop the charge breeder performance.

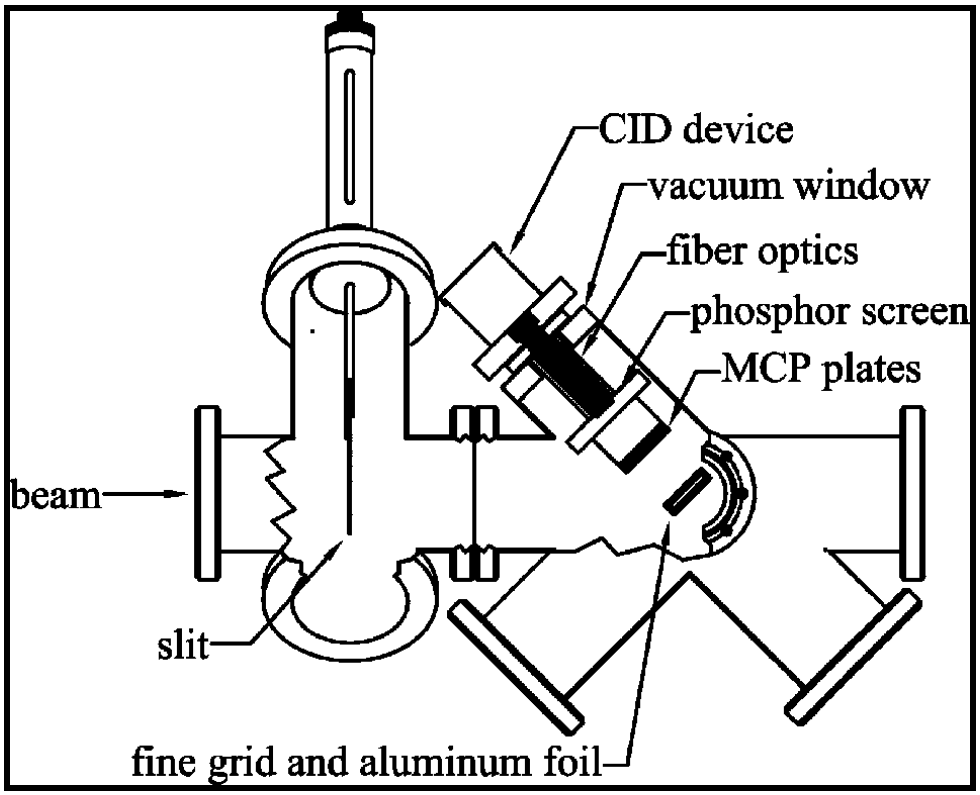

Fig. II-7. Sketch of the main components for a weak-beam diagnostics profile detector and beam counter under evaluation for CARIBU.

Building Expansion and Facility Enhancements

The californium source and other equipment on the new high-voltage platform will be housed in a new building addition, not part of the CARIBU project, which also will provide a small experimental area for the unaccelerated beam experiments. Certain facility enhancements are required in the new building for the operations of CARIBU. These enhancements include a 2-ton crane, additional electrical service of approximately 100 kVA, a HEPA exhaust and filter system, a roll-up door for room isolation, and a hole in the existing concrete wall for the connecting beamline between the CARIBU platform and the ECR charge breeder. The building is now complete and all of the facility enhancements are expected to be in place by February 15.

The building, shown in Fig. II-8, was largely completed by late November, approximately six weeks later than planned originally, but the remaining enhancements are delayed by approximately three additional months due to a variety of procurement snafus. The final feature, additional electrical power needed by the CARIBU, will be installed in January 2007. These delays have not caused any significant delay in the project, partly because of our own delays in finalizing the specifications for the high-voltage platform as previously discussed.

Safety reviews of the building expansion and facility enhancements have included considerations of possible scenarios associated with a worst case release of radioactive materials from the californium source. These reviews and analyses have included a NEPA analysis, fire hazard analysis, and a maximum credible incident analysis which envisioned the release of materials due to a plane crash into the building. The results of these analyses have been incorporated into the design of the various components surrounding the source – the shielding cask, the HEPA exhaust system, high voltage isolation and room isolation design.

Thus, the room containing the californium source will remain generally isolated from the rest of the ATLAS facility. A negative pressure will be maintained in the

new space. The space will be exhausted by the 1500 CFM HEPA exhaust system filtering out most radioactive particulates from the stack effluent. The HEPA exhaust stack is 30 feet high assuring adequate dispersal of radioactive noble gases as well as any accidental release.

_____

*EQO Division, Argonne National Laboratory.

Fig. II-8. Building addition for the CARIBU facility. The addition is funded as a separate laboratory project.

III. ACCELERATOR PHYSICS AND EXOTIC BEAM TECHNOLOGY

OVERVIEW

This chapter presents the results of R&D being carried out by the group at Argonne that was working on concepts for the U.S. Rare Isotope Accelerator Project (RIA). This R&D is now mostly directed towards components and concepts for a facility that is approximately half the cost of RIA, the Advanced Exotic Beam Laboratory (AEBL). That work has now also been generalized to projects related to advanced exotic beam facilities world-wide, and has also been extended to include work related to other accelerator projects such as the 8-GeV proton driver project at Fermi Lab and the International Linear Collider (ILC) Project.

The topics covered in this chapter are arranged in three main sub-sections: (A) Superconducting RF, (B) Beam Dynamics and Injectors, and (C) Rare Isotope Production and Separation.

Highlights of developments during 2006 include:

- Significant progress on the construction of a prototype RIA-type drift-tube cryomodule that will be used for an ATLAS Energy Upgrade Accelerator Improvement Project.

- Initial operation of the new clean room and surface processing facility in building 208 which was constructed as a joint FNAL/ANL project.

- Continued work on several aspects of the FNAL proton driver project including extensive studies of the beam dynamics of the full 8-GeV linac.

- Continued development of the beam dynamics for a high-power heavy-ion driver linac based on a 345-MHz triple-spoke resonator including studies to quantify the effects of misalignment and RF setting errors, and the development of algorithms for optimization and tuning of multiple-charge-state beams.

- Complete an updated design of the m/q = 240 injector for an exotic beam post accelerator.

- Full power tests of the prototype module of a cw RFQ for the high-power driver linac.

- Significant progress towards completion of a prototype two-charge-state low energy beam transport system.

- Construction of a prototype system to demonstrate a thin film liquid lithium stripper for use with high intensity uranium beams in the driver linac.

- Simulation tools for large acceptance fragment separator designs have been developed as extensions of the COSY Infinity high-order optics code.

- Significant progress has been made in the development of techniques for inclusion of full 3-D effects of large aperture magnets in COSY Infinity.

- Methods to prepare samples of UC_x with density over 5 g/cm^3 and thermal conductivity over 10 w/m-k have been developed.

- A beamline for high intensity tests of the large-scale prototype gas catcher has been constructed and used for first evaluations.

- Detailed simulations of an alternative gas catcher geometry, the "inverse-cyclotron" concept, have shown that there are several problems with the approach.

A. SUPERCONDUCTING RF

a.1. Joint ANL/FNAL Superconducting Cavity Surface Processing Facility (SCSPF)

(M. Kelly, S. Gerbick, and K. W. Shepard)

Cavity electropolishing at the joint ANL/FNAL SCSPF began in 2006 on a set of six new quarter-wave resonators as part of an energy upgrade to the ATLAS accelerator. Electropolishing, together with clean assembly, is a key to achieving the best possible performance in today's bulk niobium SRF cavities. Figure III-1 shows the two major sub-assemblies of the quarter-wave resonator that were electropolished separately and will be electron beam welded together to form the complete niobium cavity.

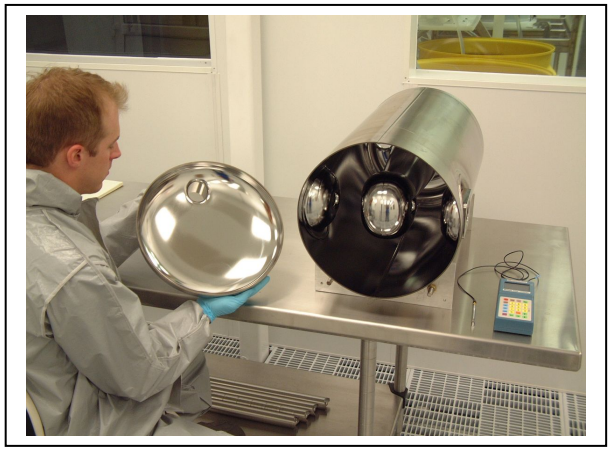

Fig. III-1. The two major sub-assemblies of an ANL quarter-wave cavity immediately after electropolishing and prior to the final electron beam closure weld.

The facility will also support R&D for the International Linear Collider. Shown in Fig. III-2 is a nearly complete engineering design for a new electropolishing system for 1.3 GHz elliptical cell cavities to be housed in the ANL portion of the joint facility. First operations are planned for the summer of 2007. The system is also planned to meet most of the electropolishing needs for ILC cavities in the U.S. for the next two years.

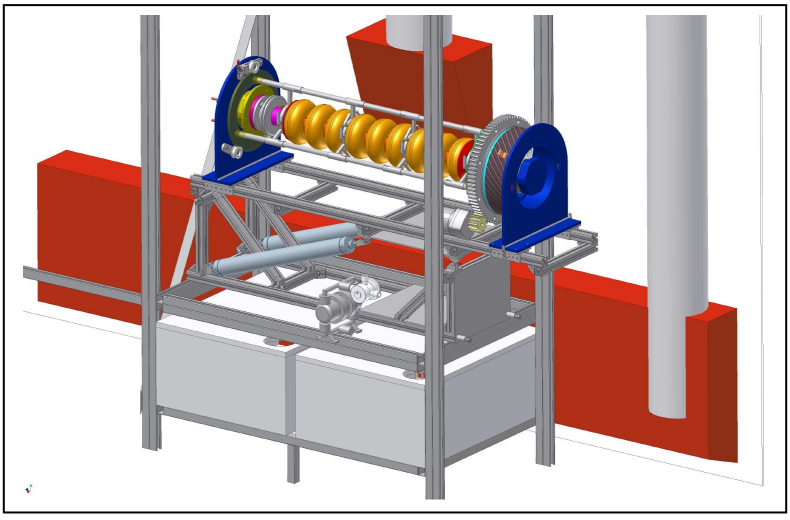

Fig. III-2. A 1.3 GHz elliptical cell cavity electropolishing system designed at ANL for the joint ANL/FNAL SCSPF.

a.2. Fast Mechanical Tuner Development for AEBL (Z. A. Conway, J. Fuerst, M. P. Kelly, S. I. Sharamentov, K. W. Shepard, and G. Zinkann)

The superconducting spoke cavities in the proposed Advanced Exotic Beams Laboratory (AEBL) driver linac will be highly sensitive to mechanical deformations due to their small beam-loaded bandwidth. RF eigenfrequency variations due to microphonics which are a large fraction of the loaded cavity bandwidth result in RF field phase and amplitude errors. The phase and amplitude control system must tolerate this RF frequency variation. This can be accomplished by increasing the output power from the RF power source, and/or controllably deforming the cavity with a fast mechanical tuner to introduce a controllable RF frequency variation. The sum of the microphonic and the controllable mechanical tuner induced RF frequency variations will be less than the total microphonic RF frequency variations, reducing the RF power required to control the cavity RF field amplitude and phase.

The performance of two prototype fast mechanical tuners was characterized by measuring the coupled tuner/cavity transfer function. The transfer function correlates the amplitude and frequency of the tuner drive signal with the cavity RF frequency modulation. This was done by sweeping the frequency of the signal driving the fast tuner and simultaneously recording the phase and amplitude of the resulting cavity RF frequency modulation.

The fast tuners were mounted on the spoke cavities by bolting the actuator assembly to a conflat flange on the integral stainless steel helium jacket. During operation the fast tuner actuator expands and contracts, pushing between the niobium wall of the cavity and the stainless-steel helium jacket.

The first mechanical tuner tested was a piezoelectric actuated fast tuner. The mechanical tuner incorporated an APC International Ltd. PSt 1000/25/100 actuator mounted in an ANL designed guide assembly. The transfer function for this tuner mounted on the $\beta = 0.5$ triple-spoke cavity is shown in Fig. III-3.

The second tuner tested was a magnetostrictive actuated fast tuner. The mechanical tuner incorporated an Energen Inc. actuator supplied to ANL under an SBIR grant. The actuator was mounted in an ANL designed guide assembly. The transfer function for this tuner mounted on the $\beta = 0.5$ triple-spoke cavity is shown in Fig. III-4.

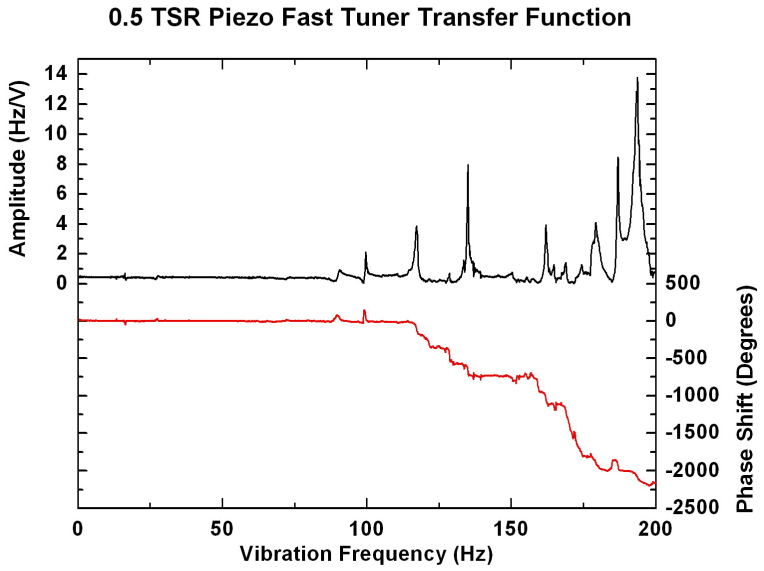

Fig. III-3. Transfer function amplitude and phase for the combined $\beta = 0.5$ triple spoke resonator and piezoelectric fast tuner system.

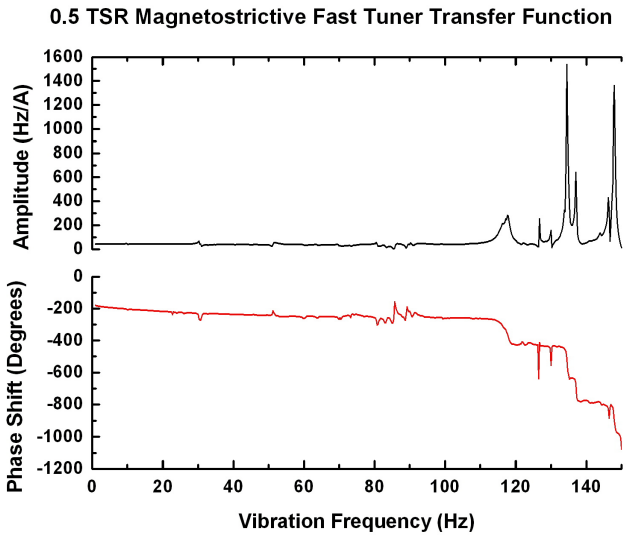

Fig. III-4. Transfer function amplitude and phase for the combined β = 0.5 triple spoke resonator and magnetostrictive fast tuner system.

The piezoelectric fast tuner was also used to damp the RF frequency variations due to microphonics in the β = 0.5 triple-spoke cavity. The piezoelectric fast tuner was operated in a negative feedback loop with the control signal proportional to the RF frequency deviation of the cavity from an external stable oscillator. The probability density and the spectrum of the RF frequency variations with and without the piezoelectric fast tuner negative feedback are shown in Figs. III-5 and III-6, respectively.

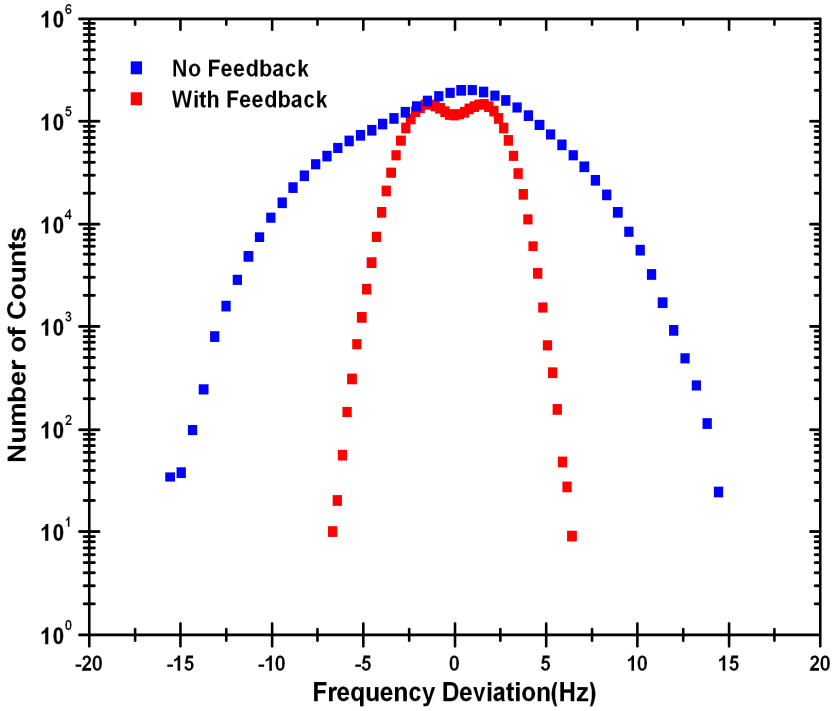

Fig. III-5. Probability density of the β = 0.5 triple spoke resonator microphonic induced RF frequency variations with and without negative feedback.

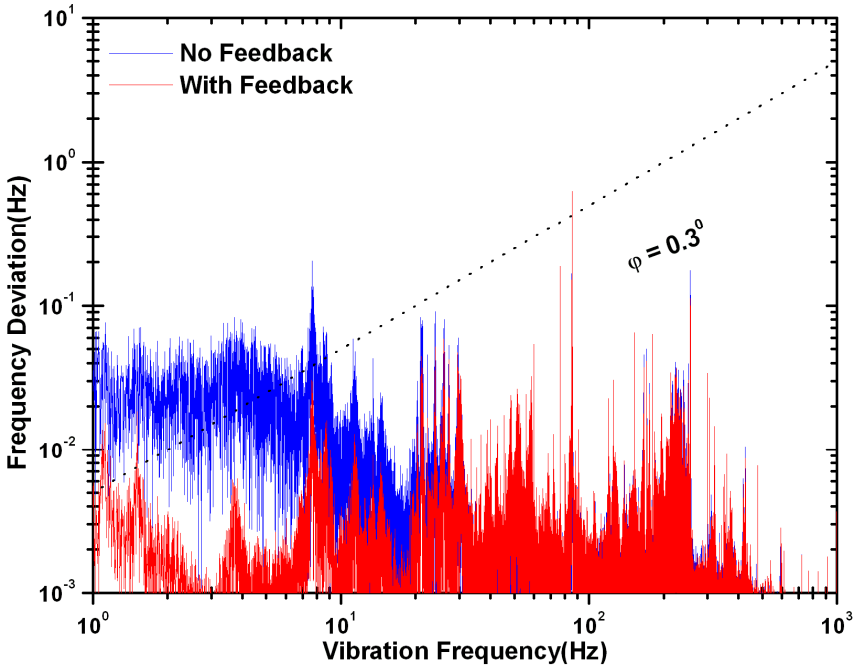

Fig. III-6. Frequency spectrum of the β = 0.5 triple spoke resonator microphonic induced RF frequency variations with and without negative feedback.

a.3. Cavities and Cryomodule for the ATLAS Upgrade (Z. Conway, J. Fuerst, M. Kedzie, M. Kelly, S. MacDonald, and K.W. Shepard)

The remaining six quarter-wave cavities for the ATLAS upgrade cryomodule are nearing completion. Major subassemblies have been electron beam welded together in preparation for final assembly. Figure III-7 (left) shows cavity housings and center conductors while (right) shows a center conductor and toroid end ready for electron beam welding.

Fig. III-7. Housing/re-entrant nose subassemblies together with center conductor subassemblies for six quarter-wave cavities (left). Center conductor and upper toroid subassemblies are fixtured in vacuum chamber for electron beam welding (right).

The cavities must resonate at the proper frequency to perform in the accelerator. During fabrication, frequency is tuned within one part in ten million by adjusting the cavity geometry. Major subassemblies are periodically clamped together to measure the resonant frequency, factoring in the predicted impact of future construction steps such as weld shrinkage and chemical processing. Figure III-8 (left) shows a typical frequency measurement setup. To save on fixturing costs and, more importantly, to avoid the possibility of tool bit inclusions which could lead to weld blowout, we have made extensive use of wire EDM to trim subassemblies to length during tuning. Figure III-8 (right) shows a housing and center conductor, together with trim rings cut off as part of the tuning process.

Fig. III-8. Cavity assembly clamped together for frequency measurement (left). Cavity housing and center conductor together with rings of material sliced off using wire EDM for frequency adjustment (right).

Cryomodule engineering tests have been performed to verify thermal shield performance. Future tests of the cryogenic systems are planned. Additional subsystems such as input couplers and mechanical slow tuners are approaching final design and will be fabricated next year.

B. BEAM DYNAMICS AND INJECTORS

b.1. Development and Test of a Grid-Less Multi-Harmonic Buncher (P. N. Ostroumov, V. N. Aseev, A. Barcikowski, B. Clifft, R. Pardo, S. I. Sharamentov, and M. Sengupta)

Currently, ATLAS is being upgraded with the Californium Rare Ion Breeder Upgrade (CARIBU). To avoid beam losses associated with the existing gridded multi-harmonic buncher (MHB), we have developed and built a grid-less four-harmonic buncher with a fundamental frequency of 12.125 MHz. The side cross-section and side view of the MHB are shown in Fig. III-9. This configuration allowed us to use the multi-harmonic RF electronics and vacuum box of the old buncher. The multi-harmonic buncher must produce a saw-tooth modulation of the beam energy which produces a short bunch width at the entrance of the first PII cavity. The energy gain of a charged particle passing through the grid-less MHB depends on the transit time factor which is a function of both the particle velocity and harmonic number. Determination of the exact harmonic mix and beam dynamics simulations has been performed using the TRACK code. The main concern in a grid-less bunching system is the uniformity of the longitudinal electric field over the radial direction. As follows from the TRACK simulations there is no noticeable effect of the beam size in the MHB on the quality of beam bunching.

The performance of the new MHB has been measured by studying the beam bunch width using a Fast Faraday Cup located at the first accelerating resonator in the ATLAS linac. Beams of $^{40}Ar^{9+}$, $^{58}Ni^{15+}$, and $^{16}O^{6+}$ were used in these bunching tests at an energy of 35 keV/u. Using the $^{40}Ar^{9+}$ beam, the performance of the buncher was compared to TRACK calculations. The bunch width was measured to be (0.7 ± 0.2) ns FWHM, as seen in Fig. III-10, in good agreement with TRACK predictions which is 1 nsec.

The harmonic buncher operates in conjunction with a 24.25 MHz spiral loaded 2-gap resonator which rebunches the beam to reduce the bunch width into the first resonator further and to reduce the sensitivity to space charge. Nominally, the additional "magnification" from this buncher was expected to be approximately 0.3. The two bunchers can operate such that the second buncher is presented with either a "virtual" or a "real" waist from the harmonic buncher. TRACK calculations predicted that the virtual waist would be the better operating mode. This was tested using a $^{58}Ni^{15+}$ beam at low (~1.5 eμA) beam current. The transmission through the first section of the linac (18 resonators accelerating the beam to approximately 1.5 MeV/u) was observed for both cases. For the virtual waist condition the best transmission achieved is 73% of the original DC beam and only 68% for the real waist configuration. TRACK calculations predicted 75% and 65% for the two situations respectively.

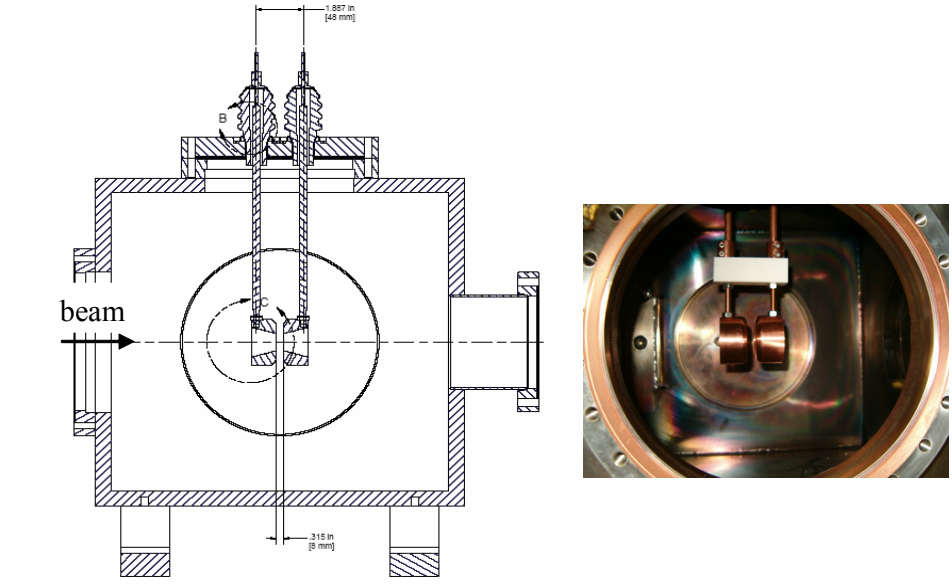

Fig. III-9. The side cross-section (left) and the side view (right) of the buncher.

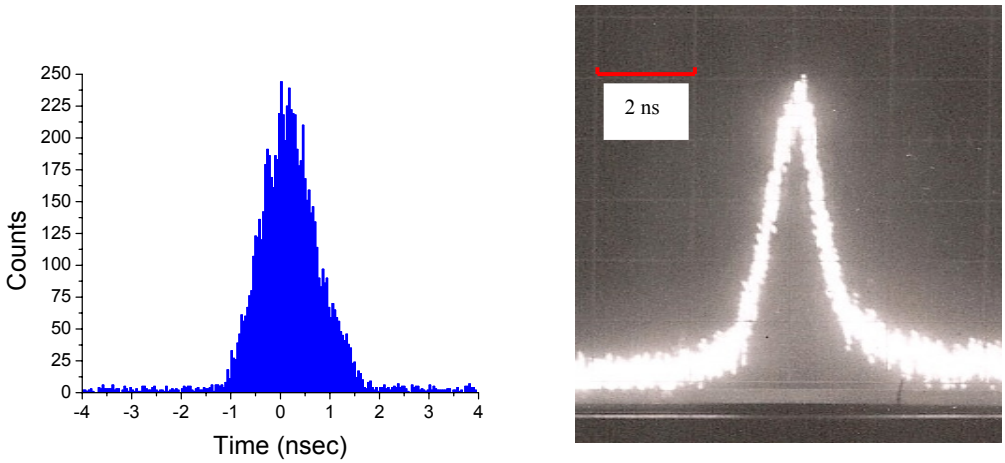

Fig. III-10. Simulated (on the left) and measured (on the right) bunch intensity distribution at the PII entrance for the low current (0.3 eμA) $^{40}Ar^{9+}$ ion beam.

b.2. High Power Tests of a 57-MHz CW RFQ (P. N. Ostroumov, A. Barcikowski, M. Bracken, B. Clifft, S. A. Kondrashev, and S. I. Sharamentov)

A Continuous Wave (CW) Radio Frequency Quadrupole (RFQ) accelerator has been designed for the RIA Driver Linac and reported previously. The high-power tests were performed using a 20-kW triode amplifier. After several hours of outgassing, the inter-vane voltage was increased to 75 kV, limited by the amplifier power. To increase available power, the triode circuit was tuned to the cavity frequency to produce 22 kW into a dummy load. When full RF power was applied, the cavity was operated with vacuum in the medium 10^{-6} Torr range. Due to the restricted capacity of the cooling system, the cavity can be operated at a high power level only in self-excited mode. At the highest available power the eigenfrequency of the cavity drops by 240 kHz and the cavity temperature increases by 20° C.

Inter-vane voltage calibration was performed by two methods: (a) using power-loss measurements and (b) X-ray end-point energy measurements. The pick-up loop power was measured directly by a power meter. The results are shown in Fig. III-11. So far, no sparking has been observed in the cavity when the available RF power is limited by the amplifier. Table III-1 shows the calculated and measured cavity parameters. Simulations by HFSS and MWS have been performed using exact 3D model of the cavity.

We observed multipacting in the cavity at 200-230 Watts power level. This level of RF power corresponds to the voltage required for acceleration of protons when the design voltage for the uranium beam is 68.5 kV. Our experiments suggest that the design voltage for uranium beams can be chosen to be at least ~85 kV, which makes the RF power required for proton acceleration equal to 320 W. We can, therefore, conclude that the RFQ cavity will provide stable acceleration of any ions, from hydrogen to uranium.

Currently, we are restricted in cavity cooling capacity: the design flow of the water is 50 GPM at 8 kW while we have operated at 9 GPM. As a consequence, there is an appreciable frequency shift which primarily occurs due to displacement of the vane tips. To observe vane tip displacement we have installed a CCD camera and taken images of the vane tips through a vacuum window as RF power is increased. Figure III-12 shows the intensity of the image signal taken in horizontal plane along the horizontal direction. We have detected ~120 μm change of the distance between the vane tips at 8.6 kW compared to the 40 μm design value. We expect that with increased cooling capabilities the displacement of the vane tips and frequency shift can be significantly reduced.

The basic design concepts, namely, 100% OFE copper structure machined prior to the assembly with high accuracy, and brazing in high temperature hydrogen atmosphere furnace have proven extremely successful, as evidenced by the voltages achieved and RF power requirements in initial tests of the RIA driver RFQ. So far, no sparking has been observed in the cavity when

operating up to the limit of available RFQ power.

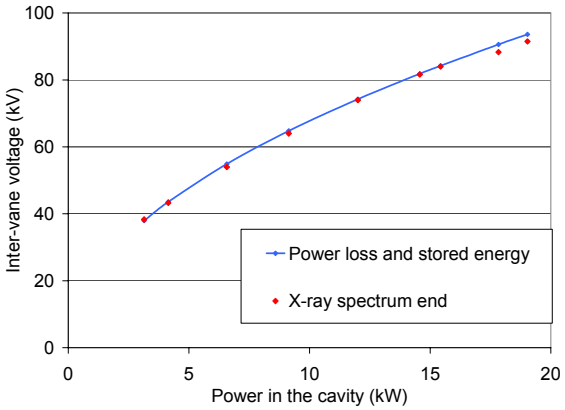

Fig. III-11. RFQ inter-vane voltage as a function of forward RF power measured by two methods.

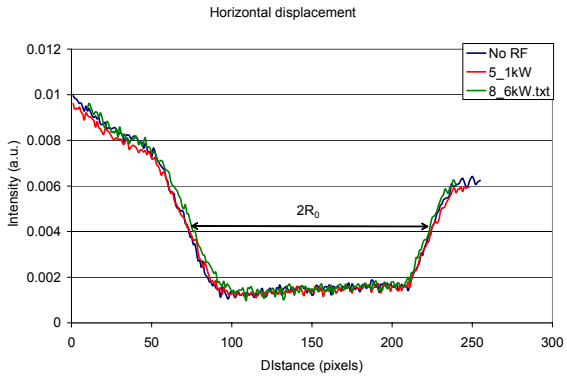

Fig. III-12. CCD image intensity along the horizontal plane. $2R_0$ is the distance between the vane tips.

Table III-1. Comparison of the simulated and measured parameters of one-segment RFQ cavity.

Parameter	Simulated	Measured
Frequency, MHz	55.62	55.863
Quality factor	9317	8688
Stored energy (V_0 = 68.5 kV), J	0.254	-
P (kW) to obtain V_0 = 68.5 kV, kW	9.5	10.2
P (kW) to obtain V_0 = 91.5 kV, kW	17.6	19.0

b.3. Production of a ^{209}Bi Beam in an All Permanent Magnet ECR Ion Source

(R. H. Scott, S. A. Kondrashev, and P. N. Ostroumov)

During the past year the 700 W, 12.75-14.5 GHz TWT RF amplifier has been repaired on the BIE-100 all permanent magnet (PM) ECR ion source.[1] When combined with the 2 kW, 14 GHz klystron, two frequency operation has been restored. An easily replaceable commercial oven[2] for production of metal ions was added to the source as well (Fig. III-13).

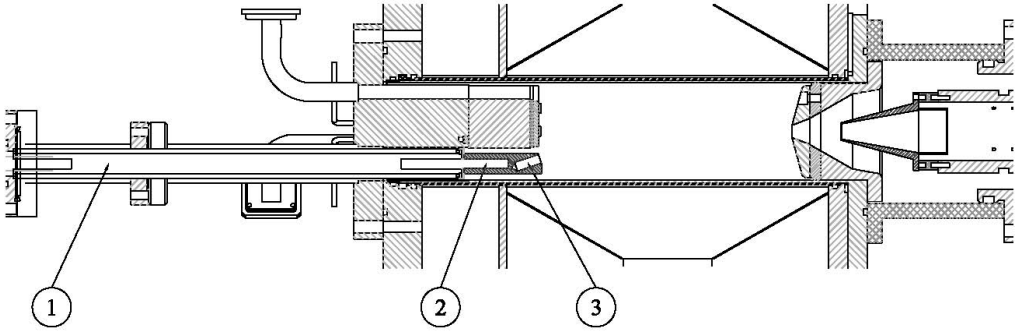

Fig. III-13. BIE-100 with (1) oven support assembly, (2) cartridge heater insertion point and (3) sample material.

The oven can operate up to a temperature of 800° C, which is enough to evaporate a wide range of metals. The frequency of TWT RF amplifier, biased disc potential and oven power are controllable from outside of the high voltage cage. Bismuth, with an operating temperature near 550° C, has been used for the tests. Only the bottom half of crucible was filled with bismuth to minimize material heating by RF and sputtering by plasma ions. Oxygen was used as a support gas to enhance charge states of ^{209}Bi ions.

The bismuth ion beam was first extracted by applying 15 kV potential and accelerated by 60 kV potential of the HV platform. The 20 mm input aperture Faraday cup (FC) equipped with a suppression ring was installed downstream of the 90° magnet to record the currents of different charge states. The distribution of ^{209}Bi ion currents for different charge states obtained after a few days of the source conditioning and tuning is shown in Fig. III-14.

One can see that $^{209}Bi^{19+}$ and $^{209}Bi^{20+}$ ions are the most abundant in the distribution. Intensities of the $^{209}Bi^{20+}$ - $^{209}Bi^{24+}$ ions are in the range of 1-2.5 pμA. The source also produces O^{1+} and O^{2+} ions with the current up to 350 eμA. The quality and intensity of bismuth ions are entirely adequate to verify multiple-charge state acceleration technique[3] using the new set-up of the multiple-charge state LEBT.[4]

[1]D. Z. Xie, Rev. Sci. Instrum. **73**, 531 (2002).
[2]National Electrostatics Corp., www.pelletron.com.
[3]P. N. Ostroumov *et al*., Phy. Rev. Lett. **86**, 2798 (2001).
[4]N. E. Vinogradov *et al.*, Proc. of LINAC-2006, Knoxville, TN, August 2006, p. 336.

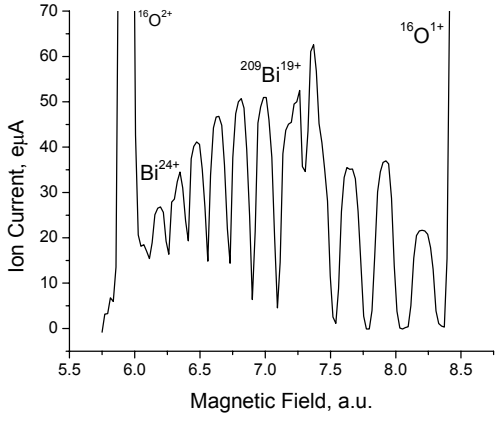

Fig. III-14. Bismuth beam intensities at different charge states.

b.4. High Current Regime of an All Permanent Magnet ECR Ion Source

(S. A. Kondrashev, A. Barcikowski, J. A. Nolen, P. N. Ostroumov, and R. H. Scott)

Stability tests of the windowless liquid lithium stripper for AEBL[1] require 400 W bunched light ion beams in the energy range from 100 keV/u to 200 keV/u. The multiple-charge-state LEBT being constructed in the Physics Division can be upgraded to obtain 150 keV/u beams by adding a second accelerating tube. A 3 mA dc beam current in a single charge state is required to achieve 400 Watts on the target. Helium and hydrogen were used as working gases to verify the performance of the BIE-100 all permanent magnet ECR ion source. The ion beams were extracted by 15 kV potential and accelerated by 60 kV potential of the HV platform. The 20 mm input aperture Faraday cup equipped with a suppression ring was used to record ion beam intensity downstream of the 90º magnet. The distributions of helium and hydrogen ion beam intensities obtained after two days of source conditioning and tuning are shown in Fig. III-15. A 3.3 mA dc proton beam was successfully generated which is entirely suitable to form a bunched and well focused beam on the target.

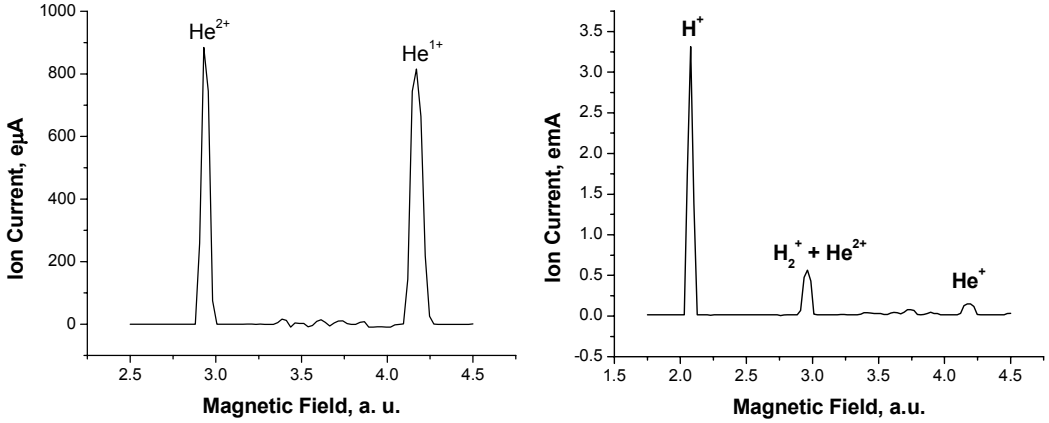

Fig. III-15. Helium (on the left) and hydrogen (on the right) ion beam intensities as a function of the magnet field.

[1]J. A. Nolen, C. B. Reed, V. J. Novick, J. R. Specht, and Y. Momozaki, Development of Windowless Liquid Lithium Stripper for RIA, Physics Division Annual Report 2005, p. 146.

b.5. Scintillator Screen Based CW Beam Emittance Measurements

(S. A. Kondrashev, A. Barcikowski, B. Mustapha, P. N. Ostroumov, and R. H. Scott)

Fast emittance measurements can be performed using a beam imaging system placed downstream of a "pepper pot" plate. The pepper pot method has the advantage of giving the possibility to extract emittances for both vertical and horizontal planes using the same single image. Micro channel plates (MCP) and scintillator screens are normally used as an imaging system. However, scintillator screens are preferable due to their simplicity and wide dynamic range. Such an approach was used to measure emittances of ion beams[1] with energy higher than 100 keV/u or intense (above 10 mA) pulsed low energy (below 100 keV/u) ion beams.[2] As far as we know, there are no data on scintillator screen sensitivities for low intensity (0.1-10 eμA/cm^2) low energy (below 100 keV/u) CW beams typically generated by ECR ion sources.

The main goal of this study is to find whether the pepper pot - scintillator screen (PPSS) method can be used to measure emittances of CW beams generated by ECR ion sources. The BIE-100 all permanent magnet ECR ion source was used to generate ion beams of various elements from hydrogen to bismuth. The PPSS assembly, shown in Fig. III-16, was placed downstream of the 90º magnet and movable faraday cup (FC). The pepper pot plate has 100 pinholes with 200 μm diameter and 4-mm spacing between the holes horizontally and vertically covering a working area of

36 × 36 mm^2. The CsI (Tl) crystal was chosen as a scintillator screen because it has shown the highest sensitivity for high energy proton beams.[3] The diameter and thickness of the crystal are 80 mm and 3 mm respectively. A grounded fine metal mesh with transparency above 50% is attached to the crystal surface irradiated by ions to prevent potential raise caused by ion beam charge. The distance between the pepper pot and scintillator screen is 100 mm. A COHU 2600 monochrome CCD camera connected to a PC was used to acquire and save beam images. The pepper pot plate is isolated from ground and its potential can be varied in the range of ±1 kV to study the effect of secondary electrons on the emittance. The FC was used as a shutter and detector of the ion beam current. In our measurements, the beam energy is 75 keV per unit charge for all elements used.

It was found that CsI (Tl) has a high sensitivity for a variety of ion species from protons to heavy ions. Pepper pot images were recordable for proton and bismuth beams with current densities below 1 eμA/cm^2. A typical image of a $^{129}Xe^{14+}$ ion beam with current density of 7 eμA/cm^2 is shown in Fig. III-16.

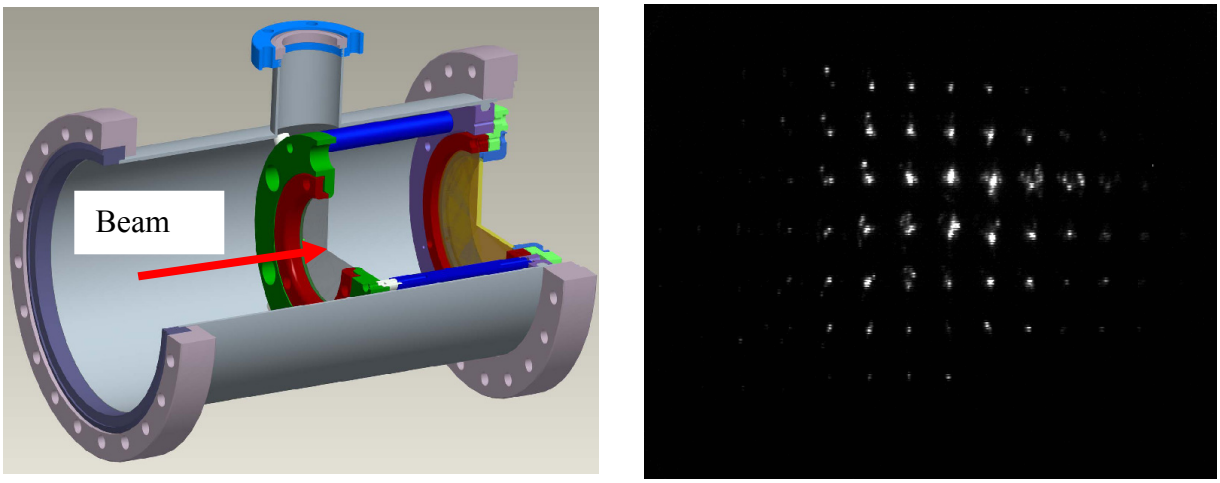

Fig. III-16. Cut-out view of pepper pot – scintillator screen assembly (on the left) and image of a $^{129}Xe^{14+}$ ion beam (on the right).

The analysis of captured images was performed using a software developed at Brookhaven National Laboratory for their emittance meter.[4] The results obtained for the $^{129}Xe^{14+}$ ion beam is presented in Fig. III-17.

The linearity of the CsI (Tl) crystal for different input current densities and its life-time under irradiation by CW ion beams will be studied in the near future. A new mask with 100 μm pinholes spaced by 3 mm in both directions is being developed to improve the resolution. A software for on-line emittance measurements is under development as well.

---

[1] M. Domke *et al*., A Single Shot Emittance Measuring System for Intense Heavy Ion Beams, GSI-Preprint-97-64, October 1997.
[2] A. Balabaev *et al*., Rev. Sci. Instrum. **73**, 1121-1124 (2002).
[3] R. Jung, G. Ferioli, and S. Hutchins, Single Pass Optical Profile Monitoring, Proceedings of the DIPAC 2003, Mainz, Germany.
[4] A. Pikin *et al*., Pepper Pot Emittance Meter, BNL note C-A/AP/#244, July 2006.

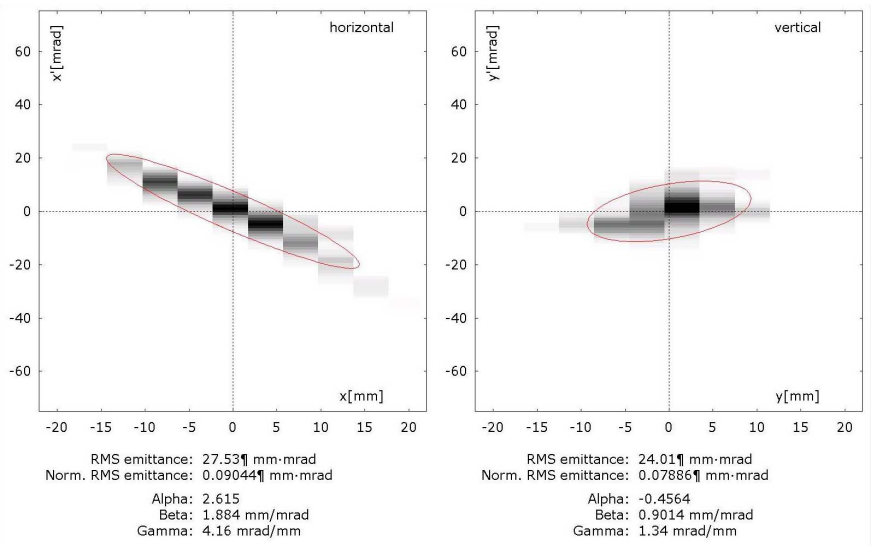

Fig. III-17. Horizontal and vertical emittances of $^{129}Xe^{14+}$ beam. The 4-rms emittance ellipses are plotted in red.

b.6. A Parallel 3D Poisson Solver in Cylindrical Coordinates (J. Xu, P. N. Ostroumov, and J.A. Nolen)

In beam dynamics simulations, the space charge effects due to electrostatic forces between charged particles, become prominent when the density of particles is high. Since many accelerator devices have cylindrical geometry, a 3D Poisson solver in the Cylindrical Coordinate System (CYLCS) has wide applications. Particularly, we are interested in a 3D solver in CYLCS for the parallel beam dynamics code PTRACK.[1] In these simulations, it is very important to accurately calculate beam halo which can produce beam losses along the accelerator. While it is relatively simple to solve Poisson's equation in the Cartesian Coordinate System (CARTCS), it is more complicated to develop a 3D Poisson solver in the CYLCS. In the CYLCS, Poisson's equation has the following form:

$$\nabla^2\phi(r,\theta,z)=\frac{\partial^2\phi}{\partial r^2}+\frac{1}{r}\frac{\partial\phi}{\partial r}+\frac{1}{r^2}\frac{\partial^2\phi}{\partial\theta^2}+\frac{\partial^2\phi}{\partial z^2}=-\frac{\rho}{\varepsilon_0}$$

Figure III-18 shows the 3D and 2D meshes used in the CYLCS. In order to avoid singularity at the center, Gauss-Lobatto-Radau integration points have been adopted.

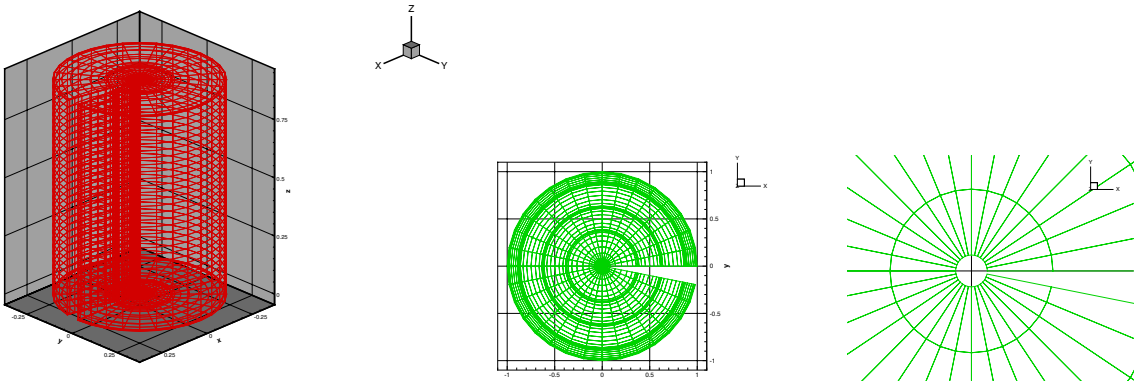

Fig. III-18. Cylindrical mesh (3D & 2D).

The new Poisson solver has been used to substitute the Cartesian Poisson solver implemented in the PTRACK last year. PTRACK is the parallel version of the beam dynamics code TRACK, which has been developed

during the past several years in the Physics Division.[2] The PTRACK algorithm for the space charge calculation is shown in Fig. III-19 and a particle-in-cell (PIC) method has been similarly implemented in the CYLCS, as shown in Fig. III-20.

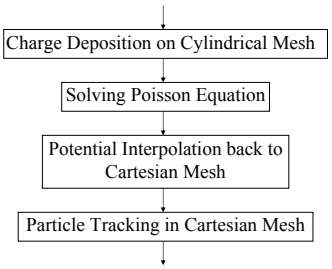

Fig. III-19. Algorithm for the Poisson solver in the CYLCS.

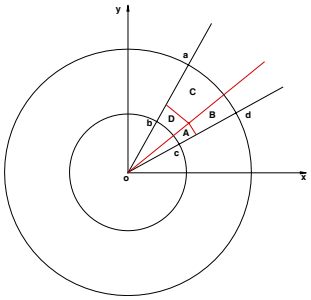

Fig. III-20. PIC in the CYLCS.

We have applied domain decomposition in the longitudinal (z) and circumferential (θ) directions, as shown in Fig. III-21. The particles have been distributed evenly to different processors. Figure III-22 shows the scaling of the parallel Poisson solver in the CYLCS on different platforms; good scaling can be achieved up to 256 processors. Super-linear scaling has been observed on IBM SP machines due to large cache and memory.

The new solver has been used for the simulation of a 8-GeV proton linac which includes the medium energy beam transport section between the RFQ and the first 4 superconducting accelerating cavities (MEBT4CAV). We have compared our parallel simulation results with the PTRACK using a Cartesian Poisson solver. The results in CARTCS and CYLCS (see Fig. III-23) are close for the particular application, as expected. In general, the Poisson solver in the CYLCS is more accurate, especially for the halo particles.

The new Poisson solver has nearly the same speed as the Cartesian Poisson solver on 64^3 mesh, and can be run on thousands of processors on BG/L.

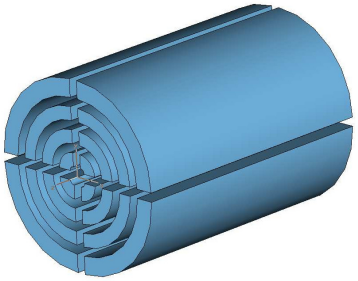

Fig. III-21. Parallel model for the code TRACK.

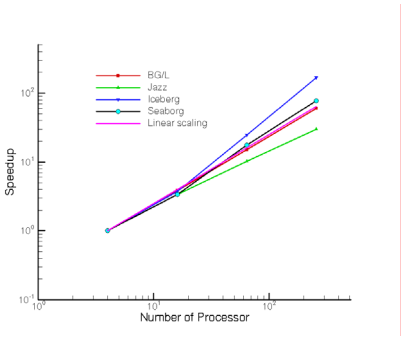

Fig. III-22. Scaling on different platforms.

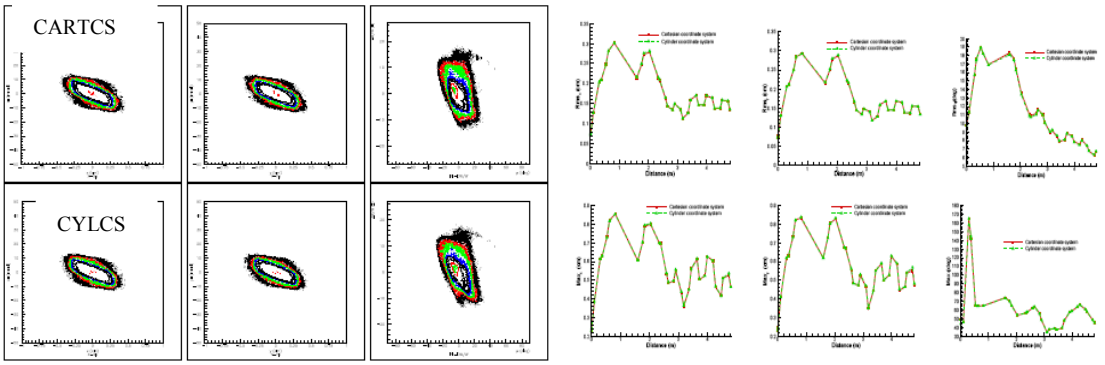

Fig. III-23. Comparison of the results obtained by the Cartesian and Cylindrical Poisson solvers. The left plots compare contours in phase space and the right plots compare beam rms and maximum envelopes.

[1]J. Xu, B. Mustapha, V. N. Aseev, and P. N. Ostroumov, Parallelization of a Beam Dynamics Code and First Large Scale RFQ Simulations, Phys. Rev. ST Accel. Beams **10**, 014201 (2007).
[2]P. N. Ostroumov and V. N. Aseev, TRACK-a Code for Beam Dynamics Simulations in SC Linac with 3D Electric and Magnetic Fields, ANL Technical Report (2003).
[3]P. N. Ostroumov, V. N. Aseev, and B. Mustapha, Beam Loss Studies in High-Intensity Heavy-Ion Linacs, Phys. Rev. ST. Accel. Beams **7**, 090101 (2004).

b.7. Concept for an Ion LINAC for the Future Electron-Ion Collider (P. N. Ostroumov)

Currently, the Jefferson Lab is leading the effort to develop a high-luminosity Electron-Ion Collider (ELIC) with variable center-of-mass energy in the range of 20 to 65 GeV.[1] The ELIC consists of a heavy-ion synchrotron and storage ring which requires a pulsed linear accelerator with the parameters listed in Table III-2. The linac is designed for acceleration of a wide variety of polarized and unpolarized ions from H^- (285 MeV) to $^{208}Pb^{67+}$ (100 MeV/u). The block-diagram of the proposed linac is given in Fig. III-24. Cost-effective acceleration of lead ions up to 100 MeV/u requires a stripper. The optimum stripping energy is 13 MeV/u.

Table III-2. Basic parameters of the linac.

	Parameter	Value
1	Ion species	From Hydrogen to Lead
2	Ion species for the reference design	^{208}Pb
3	Kinetic energy of lead ions	100 MeV/u
4	Maximum beam current averaged over the pulse	2 mA
5	Pulse repetition rate	10 Hz
6	Pulse length	0.25 msec
7	Maximum beam pulsed power	680 kW
8	Fundamental frequency	115 MHz
9	Total length	150 m

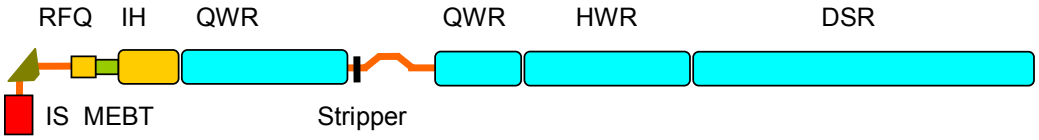

Fig. III-24. Block-diagram of the linac. IS is the ion source, RFQ is the NC radio frequency quadrupole accelerator, MEBT is the medium energy beam transport, IH is the NC interdigital structure, QWR is the RIA-type quarter-wave SC resonator operating at 115 MHz, β_G = 0.15, HWR is the RIA-type quarter-wave SC resonator operating at 230 MHz, β_G = 0.26, and DSR is the RIA-type double-spoke SC resonator operating at 345 MHz, β_G= 0.4.

The linac includes a normal conducting (NC) RFQ and an interdigital IH structure operating at a fixed velocity profile. These two structures are very effective up to ~5 MeV/u, especially for pulsed machines. In the proposed linac, the NC section provides 4.8 MeV/u beam energy for all ion species. This section of the linac is similar to the CERN Lead injector linac[2] and to BNL's pulsed heavy-ion injector being constructed.[3] The
4.8 MeV/u ion beams will be injected into the superconducting (SC) linac which comprises three different types of accelerating cavities to cover the velocity range from 0.1c to 0.5c similar to those developed at ANL for RIA. All these cavities have been built and tested providing excellent quality as is reported in Ref. 4 and later publications of the ANL SRF group.

The linac comprises 119 SC cavities. For the current application, 30 MV/m surface field in all SC cavities is proposed as a design parameter. The SC cavities will be combined into cryostats with the length of about 6 m together with SC focusing quadrupoles. After stripping, a dog leg system is necessary to clean ions with unwanted charge states. The linac is design to provide optimal voltage gain for lead ions (see Fig. III-25) and can be re-phased to accelerate any ions from hydrogen to lead.

The linac requires a total of 7 RF amplifiers: 4 amplifiers for the NC section and 3 amplifiers for the SC section. The SC section of the linac can be fed just from 3 RF amplifiers operating at three different harmonics of the fundamental frequency 115 MHz. The power will be distributed to the cavities through ferrite vector modulators (FVM) to adjust phase and amplitude of the accelerating fields in each cavity.

[1]A. Afanasev *et al*., Zeroth-Order Design Report for the Electron-Light Ion Collider at CEBAF, http://casa.jlab.org/research/elic/elic_report.shtml.
[2]H. D. Haseroth, Pb Injector at CERN, Proceedings of LINAC-1996, p. 283.
[3]J. Alessi *et al*., Status of the EBIS Project at Brookhaven, Proceedings of LINAC-2006, p. 385.
[4]K. W. Shepard, Status of Low and Intermediate Velocity Superconducting Accelerating Structures, Proceedings of PAC-2003, p. 581.

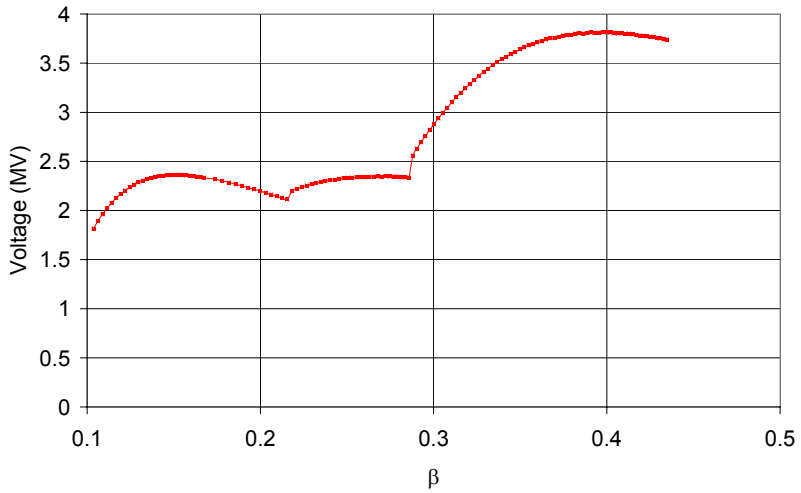

Fig. III-25. Voltage gain per resonator as a function of Lead ion velocity.

b.8. Developments Related to the Low-Q Post-Accelerator (P. N. Ostroumov, J. A. Nolen, and K. W. Shepard)

Both Super CARIBU and AEBL projects require acceleration of radioactive ions at a charge state 1+ or 2+. The post-accelerator includes a normal conducting (NC) section comprising three RFQs to provide 75 keV/u for all ion species and a superconducting (SC) section to achieve 1 MeV/u for heaviest ions.

We are developing NC prototype RFQ operating at 12.125 MHz for initial acceleration of ions with charge-to-mass ratio of 1/238 and higher. The new set of electrodes capable of accelerating $^{238}U^{+1}$ will be fabricated and installed into the vacuum enclosure of the existing 12 MHz split-coaxial RFQ resonator.[1] The design of the new RFQ vanes has the following features:

- Average radius of the RFQ is 7.0 mm, required inter-vane voltage is 82 kV.
- Water cooling of vanes will be provided.
- Higher accuracy of alignment will be implemented.

Figure III-26 shows the engineering model of the 12 MHz RFQ with a new electrode set. The existing 27 kW RF amplifier should be sufficient to achieve the design inter-electrode voltage of 82 kV. We have completed engineering design and development of fabrication drawings of the new set of RFQ vanes and will proceed with fabrication as soon as appropriate funding becomes available.

The SC section of the linac is designed for ions with the lowest charge-to-mass ratio q/A = 1/66 to achieve the stripping energy ~1 MeV/u for the heaviest ions[2] and it is based on interdigital drift-tube SC niobium cavities. This type of SC cavities has been used at PII for two decades and can typically provide ~(3-4) MV/m of accelerating fields in this velocity range. Progress in electromagnetic and mechanical design tools, fabrication technology and RF surface processing techniques related to TEM-class SC cavities suggests that the accelerating gradients ~8 MV/m are entirely feasible. With these high accelerating gradients, a total of 39 SC interdigital four-gap resonators, in three classes, are required for the first four cryostats of the new injector linac. The three resonator classes have matched velocities of 0.017c, 0.026c, and 0.038c and are similar in concept to the resonators now used in PII, but with significantly improved design details. Using modern technology for design, fabrication and processing of SC cavities will significantly reduce the cost of the post-accelerator compared to the original estimate made for the RIA project.

The low charge-state beams require stronger transverse focusing than is used in existing SC ion linacs. A FODO focusing lattice composed from SC quadrupole magnets is proposed. SC quads with the effective length of 15 cm, 30 mm aperture diameter and moderate gradients below 100 T/m are required.

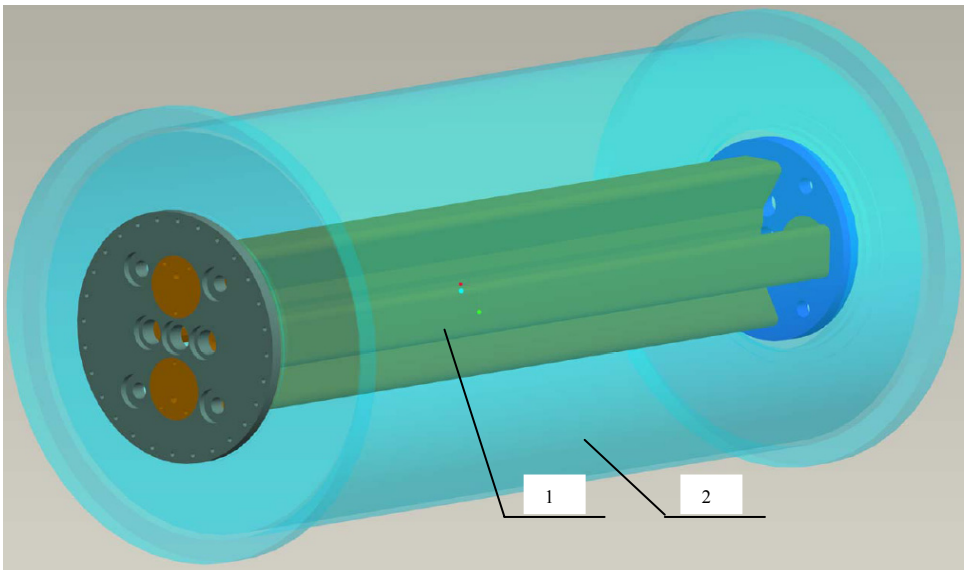

Fig. III-26. Engineering model of the new set of RFQ vanes (1) in the vacuum tank of the existing 12 MHz RFQ (2).

Beam dynamics end-to-end simulations of the post-accelerator have been performed and reported in reference.[2] Recently we have updated the design of the SC section. Figure III-27 shows rms and full envelopes of the ion beam with q/A = 1/66 in the SC section of the linac. The proposed FODO focusing structure and SC cavities with 20-mm aperture diameter provide normalized transverse acceptance of 0.2 π μm. The expected emittances downstream of the high-resolution mass-separator are less than 0.05 π μm.

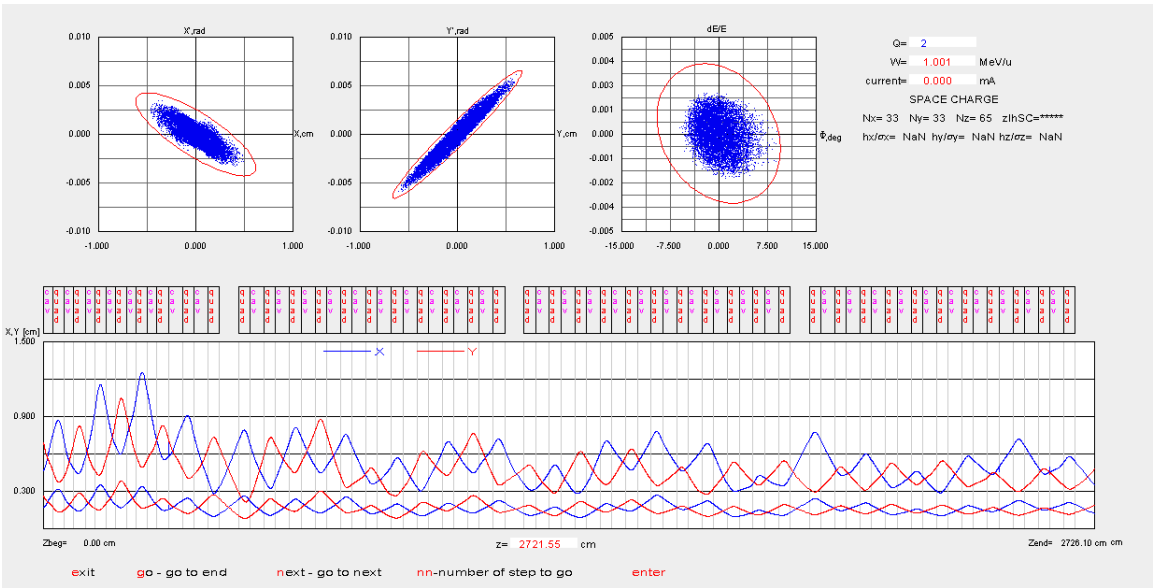

Fig. III-27. Beam rms and full envelops in the SC section of the low-q linac and phase space plots of the accelerated ions with q/A = 1/66.

[1]K. W. Shepard and W. C. Sellyey. Proceedings of the LINAC 96, p. 68.
[2]P. N. Ostroumov, V. N. Aseev, and A. A. Kolomiets, Heavy-Ion Beam Dynamics in the RIA Post-Accelerator, Proceedings of the PAC-2005, p. 3301.

b.9. Realistic Corrective Steering in the Front-End of the Fermilab Proton Driver Linac

(B. Mustapha, P. N. Ostroumov, and V. N. Aseev)

When considering element misalignment errors in an accelerator it is often required to apply corrective beam steering to compensate for these errors and periodically re-center the beam position and angle to avoid beam loss. A realistic correction procedure would use the reading from beam position monitors (BPM's) and adjust the strengths of the correctors (dipole coils) to re-center the beam. The number and location of BPM's and correctors should in principle be carefully studied during the design phase of an accelerator. After describing the correction procedure implemented into the beam dynamics code TRACK[1] we present the results of its application to the front-end of the Fermilab proton driver (FNAL-PD) linac.

We consider an accelerator section with N_m BPM's and N_c correctors. To simplify the discussion we consider only the correction of the horizontal beam position (x). The formalism could be generalized to include the vertical beam position (y) and the horizontal and vertical beam divergences or angles (x' and y'). In order to be able to correct the beam center we should first determine the response function of the BPM's to the correctors. Such a response function could be written in matrix form as: F (C) = M where C is the vector of strengths of the N_c correctors and M is the vector of beam positions measured on the N_m BPM's. In the ideal case without any misalignments or measurement errors we should have $M = M_0 = 0$ because the beam should be centered on all BPM's and $C = C_0 = 0$ because we should not need any correction. In this case the response function is $F = F_0$ such that F_0 (0) = 0 and it should be linear for small deviations about the beam axis: $F_0(C) = A \times C = M$, where A is a $N_c * N_m$ matrix. For the case with misalignment errors before applying corrections (C = 0) the beam should not be centered on most BPM's and we have F (0) = B where B is the vector of beam position measured on the N_m BPM's before correction. Notice that B would depend from the actual misalignment of all the elements in the considered section. So the general form of the monitors response function to the correctors is $F(C) = A \times C + B = M$ where B is purely coming from misalignment errors whereas A is independent from misalignment. The response function is now reduced to the response matrix A and the vector B characterizing the actual misalignment. Reading the BPM's before correction (C = 0) we can determine the vector B. By switching on one corrector (i_c) at a time we should be able to determine the response of every BPM (i_m) downstream using: $A(i_c,i_m) = (M(i_m)-B(i_m))/C(i_c)$. The upstream BPM's should not be affected. Knowing the response function $A \times C + B = M$ we can determine the set of corrector strengths C required to re-center the beam on all BPM's (M = 0). This could in principle be fulfilled by solving the matrix equation $A \times C + B = 0$ for C. For arbitrary N_m and N_c, which may lead to multiple solutions for $N_c > N_m$ or an over-determined problem for $N_c < N_m$, and to be able to set an upper limit for correctors strengths and to include measurement errors for BPM's, the solution is better performed using least-square minimization. The function to minimize in this case is:

$$f(C_{i_c}, i_c = 1, N_c) = \sum_{i_m=1}^{N_m} \frac{(\sum_{i_c=1}^{N_c} A_{i_c i_m} * C_{i_c} + B_{i_m})^2}{\sigma_{BPM}^{\ 2}}; for \left| C_{i_c} \right| \le C_{\max}$$

This procedure was implemented for the beam positions (x and y) and divergences (x' and y') into the code TRACK using the minimization package MINUIT[2] of the CERN Library. The procedure was successfully applied to the front-end of the FNAL-PD linac shown on Fig. III-28. After multiple iterations, the appropriate number and location of BPM's and correctors were found. Figure III-29 shows the location of correctors and monitors for different linac sections. The correction procedure is then applied for up to 200 different sets of randomly generated misalignment errors. Figure III-30 shows beam positions and divergences along the linac front-end before and after correction. We clearly see the reduction in the spread (largest deviation from center) of the beam positions and angles. Figure III-31 shows the effect of correction on the transverse beam emittances and envelopes. Figure III-32 shows the distribution of integrated field strength (B*L) required for the correction. A maximum value of B*L = 1250 Gs*cm should be enough for effective correction. Figure III-33 shows the effect of the BPM's measurements errors on the quality of the correction. For appropriate and effective correction a BPM error of $\sigma_{BPM} \sim 30$ μm is required.

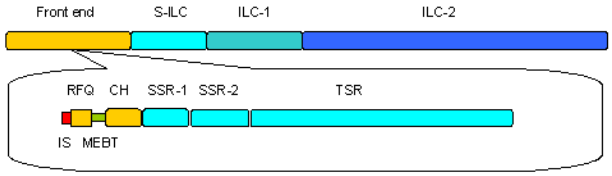

Fig. III-28. Schematic layout of the FNAL-PD linac showing more details about the front-end.

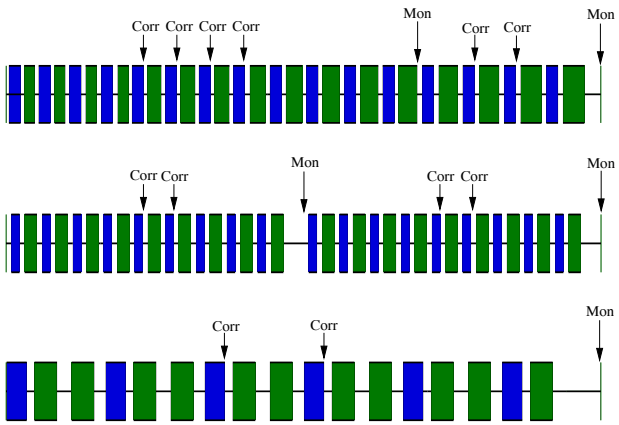

Fig. III-29. Number and location of correctors and monitors for appropriate correction in the room-temperature section (CH: top), in the first single-spoke section (SSR-1: middle) and in the second single-spoke section (SSR-2: bottom).

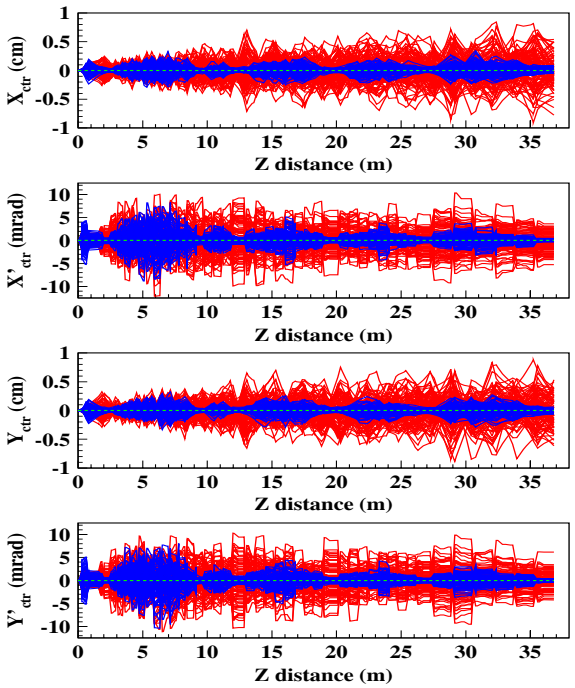

Fig. III-30. Beam central transverse positions and angles along the front-end of the FNAL PD linac (up to SSR-2) before (red) and after (blue) correction for 200 different sets of misalignment errors.

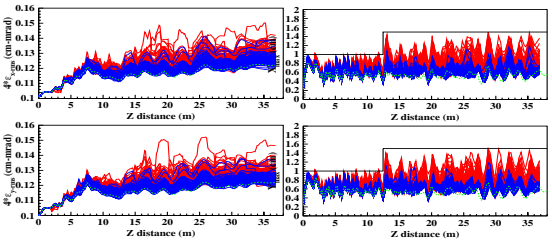

Fig. III-31. Beam transverse emittances (left) and envelopes (right) along the front-end of the FNAL-PD linac (up to SSR-2) before (red) and after (blue) correction for 200 different sets of misalignment errors.

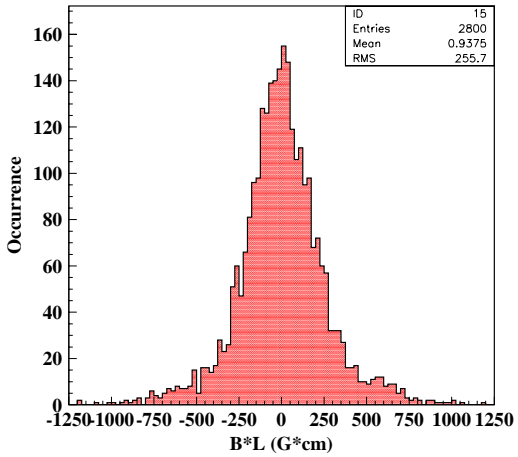

Fig. III-32. Correctors integrated field strengths used in the correction procedure for the front-end of the FNAL-PD linac.

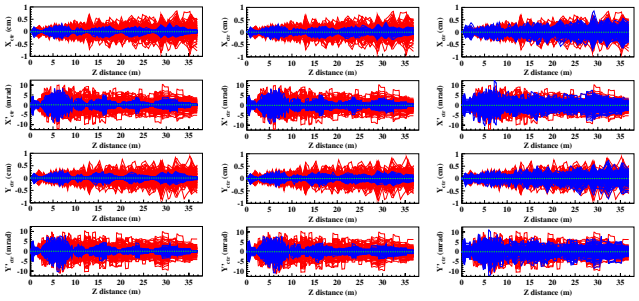

Fig. III-33. Effect of BPM measurement errors on the effectiveness of the correction procedure. The left plot is for σ_{BPM} = 10 μm, the center is for σ_{BPM} = 30 μm and the right for σ_{BPM} = 100 μm.

[1]"TRACK, the New Beam Dynamics Code", V. N. Aseev *et al*., in Proceedings of PAC-05.
[2]MINUIT–Function Minimization and Error Analysis, CERN Program Library Long Writeup D506.

b.10. First Track Simulations of the SNS Linac (B. Mustapha, J. Xu, V. N. Aseev, P. N. Ostroumov, D. Jeon,* and S. D. Henderson*)

In this collaborative effort between ANL and ORNL, we meant to expand the domain of applicability of the code TRACK[1] to new elements not previously included such as long Drift Tube Linac (DTL) and to benchmark the code against the commissioning data from the SNS linac. This work constitutes a first of many developmental steps towards the realization of the concept of the "Model Driven Accelerator", where

TRACK could be used to fully support machine operations in the SNS linac or any future facility based on linear accelerators.

The SNS accelerator facility[2] is designed to provide a 1 GeV, 1.4 MW proton beam to a liquid mercury target for neutron production. The accelerator complex consists of a H^- injector capable of producing 38 mA peak current, a 1 GeV linac, an accumulator ring and associated beam transport lines to experimental areas. The linac consists of a 2.5 MeV, 38mA H^- front-end injector, a six-tank 402.5 MHz DTL to accelerate the beam to 87 MeV, a four-module 805 MHz Coupled Cavity Linac (CCL) to accelerate the beam to 187 MeV, and a superconducting linac (SRF) to accelerate the beam to 1 GeV. Figure III-34 shows a schematic layout of the SNS linac.

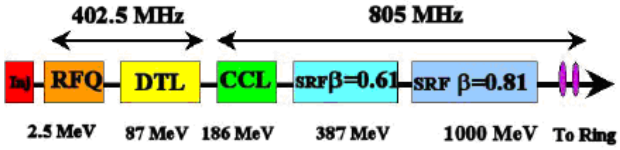

Fig. III-34. Schematic layout of the SNS linac.

The DTL section is composed of 6 tanks with a total of 216 cells to accelerate the beam from 2.5 MeV to 87 MeV. Each DTL tank is driven by a separate 402.5 MHz, 2.5-MW klystron. The focusing is provided by permanent magnet quadrupoles (PMQs) positioned within specific drift tubes. The focusing lattice is FFODDO where every third drift tube is kept empty for possible beam diagnostic devices. The cell length is equal to $\beta\lambda$ and the transverse focusing period length is $6\beta\lambda$. Before being able to simulate the DTL using TRACK, three major steps need to be performed. They are:

- Preparation of 3D electromagnetic fields for every cell including fringe fields.
- Building the lattice with the exact dimensions (length and aperture) as well as electric and magnetic field strengths for every cell.
- Implementation of a special tracking routine for the DTL where a whole DTL tank is considered as a single element with many cells.

Every DTL cell contains an accelerating RF gap and one or two PMQs as shown in Fig. III-35.

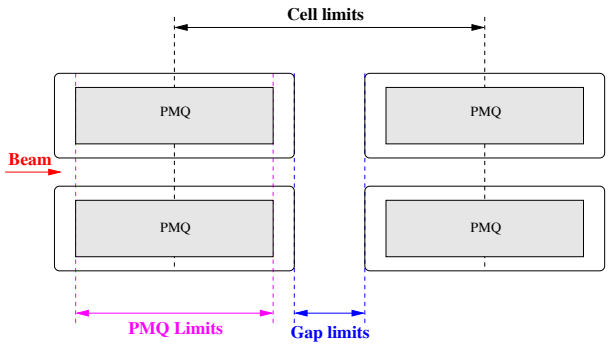

Fig. III-35. Approximate geometry of a DTL cell.

2D electric field (E) tables for the RF gaps are computed using Superfish.[3] Using the cylindrical symmetry we can determine the 3D E-field at any point within the aperture. Figure III-36 shows the E-field components in the first cell along the Z axis at X = Ra/2 and Y = Ra/4 where Ra = 1.25 cm is the aperture radius of the DTL.

The magnetic field (B) from the PMQs is calculated using the field formula's used in Trace-3D[4] for Bx and By whereas the Bz component is taken from the original paper by Halbach.[5] The results of the formulas were confirmed using EM-studio for the exact geometry and material properties of the PMQ. Figure III-37 shows the B-field components for the same conditions as Fig. III-36 (first cell at X = Ra/2 and

Y = Ra/4) where the first PMQ has a field gradient G = -3.7 kG/cm and the second with G = 0 (empty drift tube).

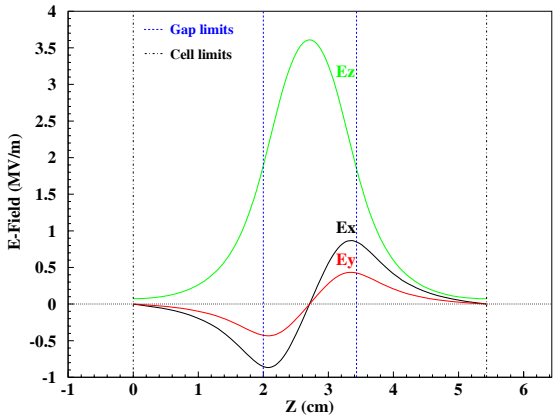

Fig. III-36. Electric field components in a DTL cell.

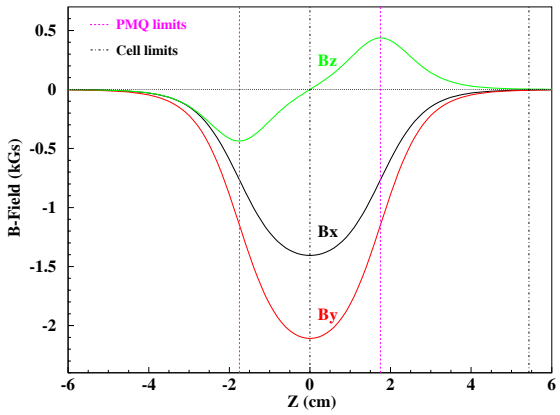

Fig. III-37. Magnetic field components in a DTL cell.

In TRACK's main lattice input a DTL tank is represented by a single line specifying the total length, a harmonic number, a global E-field scaling factor, the input phase, the number of cells and a file number with more detailed cell information. The cell information file contains the length, aperture, E-field strength, B-field strength for both PMQs for every cell in the tank (1 line per cell). In this way we have the flexibility of changing any parameter which is especially important when we want to input measured values for field strengths. Because every DTL tank is driven by a single klystron, no phase setting is allowed for individual cells for which the phases are set by the geometrical design. The DTL tracking routine is based on the existing RFQ routine described in Ref. 6. When the beam enters a new cell, the corresponding field data are loaded and the tracking performed by integrating the equation of motion for every particle in the 3D external and internal space charge fields.

Figure III-38 and Fig. III-39 show a detailed comparison between TRACK and PARMILA[7] simulations results for the DTL section (MEBT + 6 Tanks). In this case, a 38 mA H^- beam is simulated by tracking 10^5 particles. The E and B field strengths are set to the experimentally measured values. A good overall agreement is obtained; the differences could be explained by the fringe fields from the PMQs and a possible difference in the space charge calculations. As discussed earlier, fringe fields could cause a beam mismatch which is visible on the transverse beam parameters in Fig. III-38. Starting from the second DTL tank (Z ~ 14 m) we notice a longitudinal mismatch on TRACK results. We believe that this difference is due to a phase ramping procedure used in PARMILA to adjust the phases of the first and

last cells in a DTL tank to ensure phase matching between successive tanks. This procedure is not directly reflected on the design geometry used as input to TRACK. This phase mismatch is responsible for producing a more pronounced beam tail on the phase space plots of Fig. III-39.

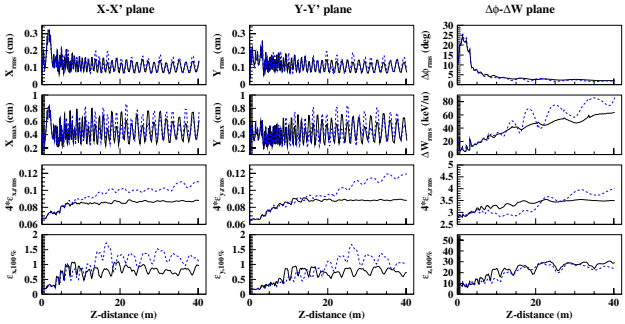

Fig. III-38. Comparison of PARMILA and TRACK simulation results of the SNS-DTL section. The plots show and compare the evolution of most important beam parameters along the DTL. The solid-black curves correspond to PARMILA and the dashed-blue curves to TRACK.

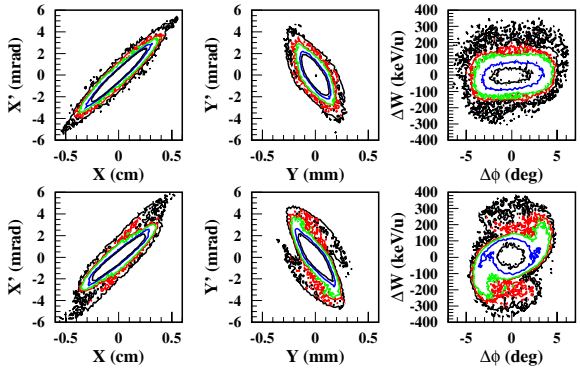

Fig. III-39. Comparison of phase space plots at the exit of the SNS-DTL section obtained using PARMILA and TRACK. The top plots are from PARMILA and the bottom ones are from TRACK. The colored contours represent different levels of particle density.

---

*Oak Ridge National Laboratory.

[1]V. N. Aseev *et al*., Proceedings of the PAC-05 Conference, Knoxville, TN, May 16-20, 2005.
[2]N. Holtkamp, Proceedings of the PAC-03 Conference, Portland, OR, May 12-16, 2003.
[3]J. H. Billen and L. M. Young, Poisson-Superfish Manual, Report LA-UR-96-1834, Los Alamos, 1996 (Revised 2005).
[4]K. R. Crandall, TRACE-3D Manual, Report LA-11054-MS, Los Alamos, 1987.
[5]K. Halbach, Nucl. Instrum. Methods **187**, 109-117 (1981).
[6]P. N. Ostroumov, V. N. Aseev, and A. A. Kolomiets, J. of Instr., JINST **1**, P04002, 2006.
[7]J. H. Billen and H. Takeda, PARMILA Manual, Report LA-UR-98-4478, Los Alamos, 1998 (Revised 2004).

b.11. Automatic Transverse Tuning of a Multiple-Charge-State Heavy-Ion Beam

(B. Mustapha and P. N. Ostroumov)

In most existing accelerators, beam tuning or retuning after an element failure or to change the beam parameters or specie is usually done manually step by step. This is due to the lack of a realistic model of the

machine that could fully support the machine operations which often results in excessive time wasted in beam tuning. The ultimate goal of this effort is to produce automatic and realistic beam tuning tools that could be incorporated into a realistic beam dynamics code which could be used for machine operations. This problem is especially important for SC linacs due to the presence of several different focusing lattice structures.

Extensive end-to-end beam dynamics simulations of the RIA driver linac[1] using the beam dynamics code TRACK[2] and including all sources of machine errors and detailed beam loss analysis showed that the losses could be significantly reduced for a fine-tuned linac. For this purpose we have developed an automatic longitudinal tuning procedure for multiple charge state heavy-ion beams.[3] For a complete tuning tool, we have recently developed an automatic transverse tuning procedure to produce smooth transverse beam dynamics by minimizing the RMS beam sizes after each focusing period. In addition to improving an existing tune, this powerful automatic beam tuning tool can be used to retune the linac and restore the beam after one or more element failures and to develop new tunes for ion beams with different Q/A ratios.

The transverse tuning procedure consists of producing smooth transverse beam dynamics by optimizing the field strengths in the focusing elements. This is done by minimizing the fluctuations in RMS beam sizes along the considered section. Large fluctuations in the RMS beam sizes are usually induced by mismatch between sub-sections of the linac which could eventually lead to beam losses. This method is general and should produce good results for both regular (periodic) or non regular accelerating structures. The function to minimize in this case is:

$$F = X^0_{rms} + \sum_i \frac{(X^i_{rms} - X^0_{rms})^2}{\Delta X^2_{rms}} + Y^0_{rms} + \sum_i \frac{(Y^i_{rms} - Y^0_{rms})^2}{\Delta Y^2_{rms}}$$

where X^0_{rms} and Y^0_{rms} are the RMS beam sizes at the entrance of the section or after the first focusing period, the sum index i runs over the focusing periods in a given section and ΔX_{rms} and ΔY_{rms} are the allowed errors on the RMS beam sizes. In the case of a multiple charge state beam we use the parameters of the total beam. The procedure could very well be used for a single charge state beam. A similar procedure could be implemented to smooth out the longitudinal beam parameters, if needed. The minimization is performed using the CERN-LIB optimization package MINUIT[4] modified to consider a large number of fit parameters. The fit parameters in this case are the magnetic field strengths of all focusing elements in the section.

Figure III-40 shows the X- and Y-rms beam sizes before and after applying the automatic tuning procedure. We clearly notice the reduction in the fluctuations of the RMS beam sizes; the low-frequency oscillations due to beam mismatch were removed after applying the tuning procedure. In this case, the tuning is done for a two-charge state uranium beam in the first section of the RIA driver linac by tracking a small number of particles (typically 100 for each charge state) using the code TRACK. Space charge forces are negligible in this case. The matrix approach like in TRACE-3D[5] did not produce good results because of significant deviations when performing full beam dynamics simulations using realistic 3D fields. Tuning is done better by tracking particles through realistic 3D and space charge fields. In the case where space charge forces should be included, the typical number of particles would be at least 10^5. Since the optimization process involves multiple iterations, large scale computing will be required.

[1] P. N. Ostroumov, V. N. Aseev, and B. Mustapha, Phys. Rev. ST. Accel. Beams **7**, 090101 (2004).
[2] "TRACK, The New Beam Dynamics Code", V. N. Aseev *et al*., in Proceedings of the PAC-05.
[3] B. Mustapha and P. N. Ostroumov, Phys. Rev. ST. Accel. Beams **8**, 090101 (2005).
[4] MINUIT–Function Minimization and Error Analysis, CERN Program Library Long Writeup D506.
[5] K. R. Crandall, TRACE-3D Manual, Report LA-11054-MS, Los Alamos, 1987.

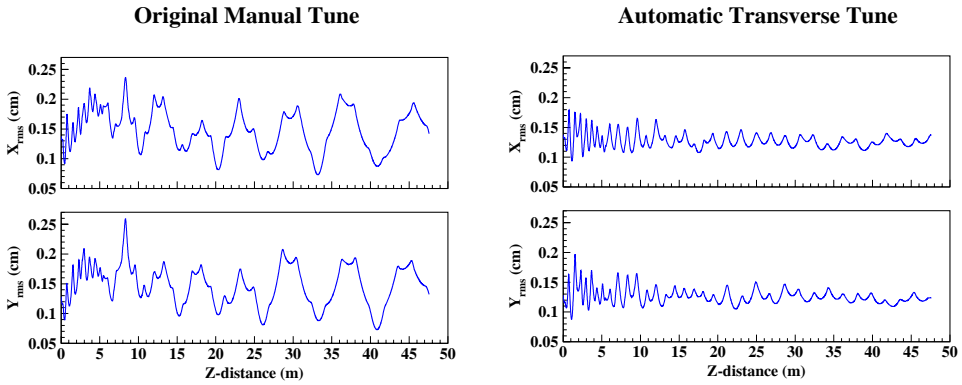

Fig. III-40. X- and Y-rms beam sizes before and after applying the automatic transverse tuning procedure. The beam is a two-charge state uranium beam in the first section of the RIA driver linac.

C. RARE ISOTOPE PRODUCTION AND SEPARATION

c.1. Development of a Windowless Liquid Lithium Stripper (J. A. Nolen, Y. Momozaki,* C. B. Reed*)

Windowless Liquid Lithium Stripper Overview

This section summarizes the on-going development of windowless liquid lithium strippers for advanced exotic beam facilities and other high current heavy ion accelerators that can withstand the large power density deposited by the intense heavy ion beams. The objective of the current phase of the work is to develop a film thickness diagnostic that can be used to initially measure the flowing film thickness and, later in the operating stripper system, to provide real time feedback of the film thickness for a variety of uses. Liquid lithium is considered a primary candidate for a stripper for high atomic number heavy ion beams in high intensity driver linacs because it has good nuclear physics properties in stripping electrons from beams such as uranium in the 10-20 MeV/u energy regime and good thermal properties in removing very high heat loads while maintaining sufficiently low vapor pressure. Preliminary nuclear physics calculations indicate that liquid lithium films in the range of 10-20 μm thick are required. In addition, preliminary thermal calculations show that the film velocity needs to be at $\gtrsim$ 50 m/s. To measure the exact thickness of a flowing liquid lithium film, a special diagnostic technique must be developed and demonstrated in high temperature (~350° C), at high vacuum (~10^{-7} - 10^{-8} Torr), in contact with lithium vapor, and with possible exposure to lithium splashing.

Previous work found that measuring the transmission of a low energy electron beam through the liquid lithium thin film was the best approach to measure the film thickness. A layout of the measurement setup was determined; critical components in the setup include an electron gun with appropriate energy and current output, beam transfer line, beam steering, focusing and bending devices, electron collector, precision current meter, and controller. An electron gun of ~30 keV maximum energy is needed to penetrate advanced exotic beam accelerator strippers which may require liquid lithium thin film thicknesses in the range of ~10 μm to 20+ μm. A suitable e-gun was identified and the procurement package prepared.

Formation of the film and factors affecting its stability and appearance were also studied. High speed (6 k and 12 k frames/sec) digital video movies were recorded of both the startup and steady state flow of the film. Figure III-41 identifies the basic elements of the thin film system. In Fig. III-42, one can see the initial film formation and, for example, the detrimental role played by the very large puddle of lithium clinging to the deflector plate.

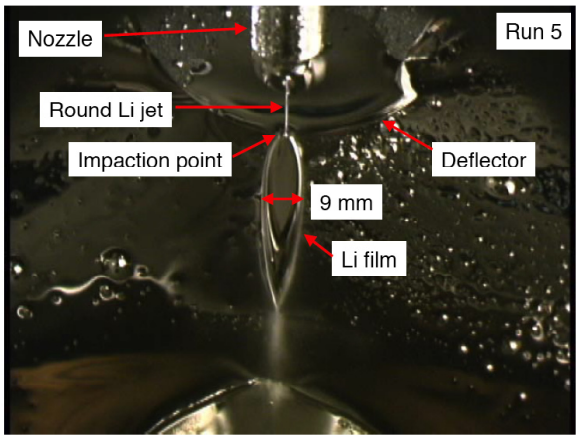

Fig. III-41. Liquid lithium thin film.

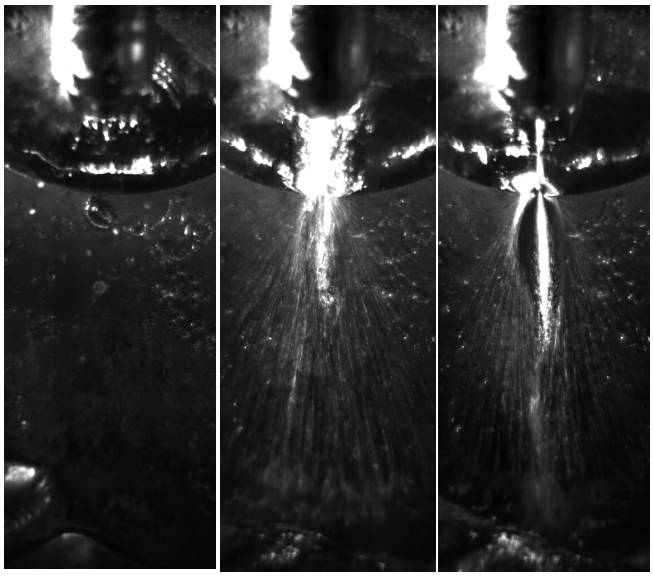

Fig. III-42. HS video clips of film formation.

Thermal Analysis of a Second Stripper for the Rare Isotope Accelerator

Thermal analysis calculations were made on the second stripper to be used in the driver linac of the Rare Isotope Accelerator (RIA). Both liquid (Sodium) and solid (Titanium and Vanadium) stripper concepts were considered. These calculations were intended to provide basic information to evaluate the feasibility of liquid (thick film) and solid (rotating wheel) second strippers. Nuclear physics calculations to estimate the volumetric heat generation in the stripper material were performed by "LISE for Excel". In the thermal calculations, the strippers were modeled as a thin 2D plate with uniform heat generation within the beam spot. Then, temperature distributions were computed by assuming that the heat spreads conductively in the plate in the radial direction without radiative heat losses to surroundings.

A schematic of the second stripper is shown in Fig. III-43. The stripper was modeled as a slab moving at velocity v, which could be a liquid or a solid. An incident U beam at the charge state of 72+, flux of 4 particle μA, and energy of 85 MeV/nucleon passes through the stripper material and deposits some energy as heat within it. Expected beam diameter is 1 mm.

Introducing some simplifications into this problem made it possible to use an analytical solution for a heat conduction problem of a moving, solid body. Since the stripper is very thin, the problem may be treated as a 2-D problem (Pittaway, 1964). In this analysis, a heat source that had a Gaussian distribution was moving at the velocity, v m/s on a thin stripper material. The stripper has a constant, uniform, background temperature of T_∞. For simplicity, it was assumed that no heat transfer from the surfaces of the stripper takes place.

The initial background temperature for Na was taken to be 381 K. That is 10 K above the melting point of Na. Example results of the thermal calculations for the spatial temperature distribution of the Na film along the beamline for a Na film velocity of 10 m/s are shown in Fig. III-44. This figure shows that for a once-through Na stripper system, the calculated maximum temperatures of the Na film are ~1800 K for Na film velocity of 10 m/s. This temperature would cause excessive evaporation of Na, implying that a much higher velocity, ~ 30 - 50 m/s, is required.

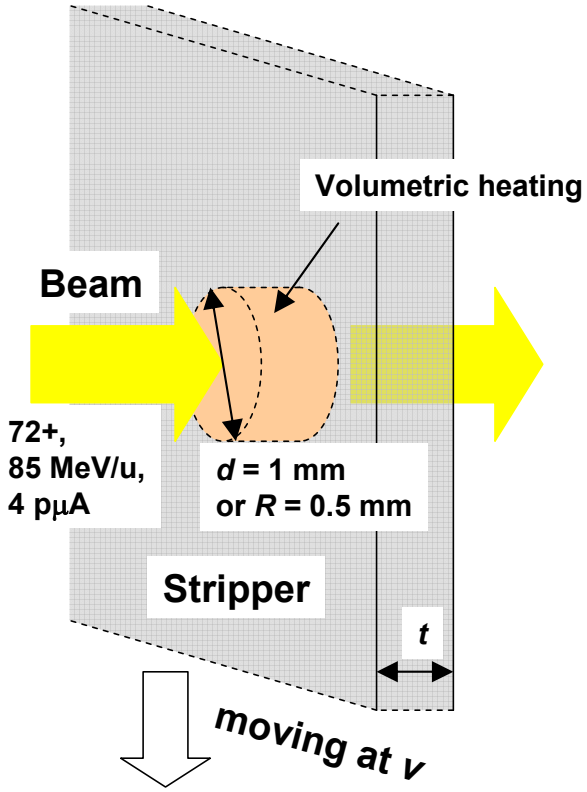

Fig. III-43. Schematic of second stripper.

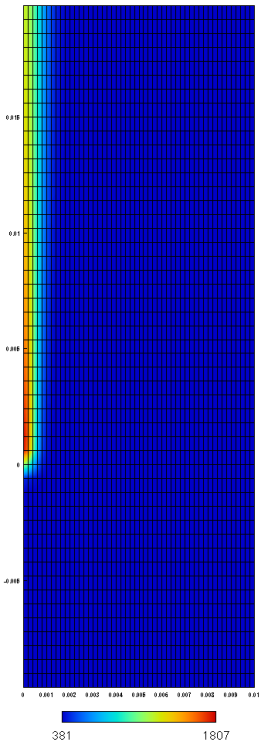

Fig. III-44. 2D spatial temperature distribution (Na at 10 m/s).

Collaboration with the Israeli Soreq/SARAF Group

In 2006, an opportunity to collaborate with the Israeli Soreq/SARAF group, who are building a high power thin lithium target, arose. The collaboration included our support in target design, assembly and commissioning, followed by our participation in high power testing of the target with intense proton beams. This will be the first test at the high power densities possible with this new facility (CW beams with the Bragg peak in the target) to investigate the onset of bubble formation inside a windowless lithium jet. This is considered a huge windfall since the Israeli's are paying for essentially all of the hardware. We provided immediate assistance to the Soreq/SARAF group on developing their high-power liquid-lithium target system in order to meet the scheduled Phase I completion of the SARAF accelerator. The on-line availability of the SARAF target system during phase one is scheduled only for the second six months of calendar year 2007. Then there will be a 1-2 year down period for the installation of the rest of the accelerator (Phase 2). The Soreq/SARAF (Phase 1) research combines a demonstrated technique, successfully and intensively used for nuclear astrophysics, with ANL's windowless liquid lithium target technology to reach higher fluxes than available up to now. The successful development and utilization of a liquid lithium target in real conditions of a physics experiment, not realized so far, is expected to bring a unique and invaluable experience for advanced exotic beam facilities before their implementation there. In 2006, several meetings at ANL and at Soreq were held to plan and discuss target system issues, and we began helping the Soreq/SARAF group in developing the infrastructure necessary (design, choice of materials, construction, safety reviews and training procedures) for a windowless liquid lithium target to be usable in the field for physics experiments. Also, two PhD students from The Hebrew University of Jerusalem were sent to ANL for six months at their expense to learn the engineering aspects of alkali metal technology and windowless target design and operation.

In summary, the aspects of the lithium target development at SARAF that are of great benefit to the US exotic beam programs are:

1. The practical installation and operation of a high-power liquid lithium target system in a nuclear physics/accelerator facility. Complete safety reviews and detailed operating procedures will be significant accomplishments.
2. Traps to control radiological contaminants such as ^{7}Be will be incorporated into the system and tested in practice.
3. At the beam currents available at SARAF (4 mA of protons) the power density at the Bragg peak inside the target will be higher than ever demonstrated previously in such targets. The practical limitations of such targets will be determined by the on-set of bubble formation within the target. Detailed simulations of this limit are very uncertain and this test will be an invaluable experimental demonstration and benchmark for such simulations.

We produced a number of EM pump designs coupled with estimated hydraulic characteristics of the SARAF target loop. These include yoke design, magnet and yoke material selection, pump duct design to minimize stress, stress analysis and handling the freeze-thaw issue. An example compact, inexpensive DC EM pump design is shown in Fig. III-45.

---

*Nuclear Engineering Division, Argonne National Laboratory.

[1]Claude B. Reed, Jerry A. Nolen, and Yoichi Momozaki, "A Liquid Lithium Thin Film Stripper for RIA", Seventh International Conference on Radioactive Nuclear Beams (RNB7), Cortina d'Ampezzo, Italy, July 3-7, (2006).
[2]Y. Momozaki and J. A. Nolen, "On a Thermal Analysis of a Second Stripper for Rare Isotope Accelerator," ANL-06/10, (2006).
[3]L. G. Pittaway, "The Temperature Distributions in Thin Foil and Semi-Infinite Targets Bombarded by an Electron beam," Brit. J. Appl. Phys. **15**, 967-982 (1964).

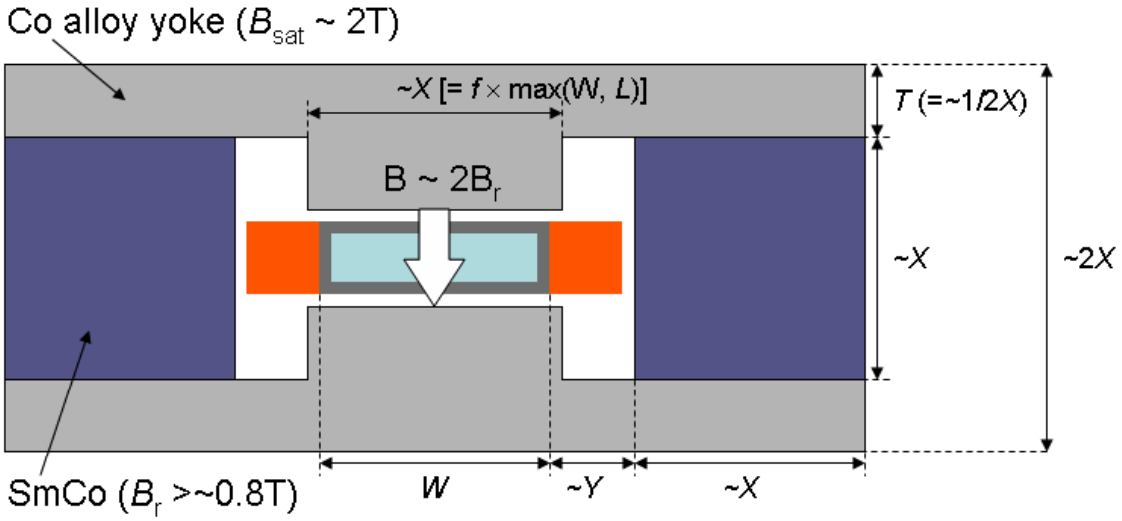

Fig, III-45. Example DC EM pump.

c.2. **Fragment Separator Design** (B. Erdelyi, J. Nolen, L. Bandura, and J. Maloney)

Using a combination of beam optics symmetry theories we have worked to design the optical layout for the fragment separator of an exotic isotope accelerator. The achievement of large acceptance and high resolution is a challenge in the presence of large aperture superconducting magnets. The primary motivation for the design was criteria for the fragment separator in the proposed Rare Isotope Accelerator (RIA), but the design methods which were developed can readily be applied to a much broader range of systems.

The design was developed by taking advantage of basic symmetries in the design layout, including the geometry of the components. The effects of the separator's components were calculated by determining a Taylor expansion for the transfer map for isotopes traveling from the beginning through the end of the fragment separator. At first order (*i.e.*, the terms with linear dependence on the initial 6-dimensional phase space vector) this map becomes a matrix. The components of the transfer map can be used to measure resolution and aberrations of the optical design for the separator.

Because no fields in the separator are explicitly time dependent and all components of the separator have geometric symmetry about the mid-plane above and below the optical axis, half of the terms in the transfer map are cancelled. Other less obvious symmetries were also considered, including the symplectic symmetry that arises from the Hamiltonian nature of the particle motion within the separator, and mirror symmetry about certain points in the separator. The combination of these symmetries allows explicit calculation of the minimum number of multipoles necessary to minimize the aberrations in the final beam.

The linear layout, depicted in Fig. III-46, consisted of two identical cells with dipoles and quadrupoles. Each cell maintains symmetry about the middle of the bending dipole. The system also focuses point-to-parallel and parallel-to-point at the middle of the dipole. Both the dispersive and achromatic images focus point-to-point and parallel-to-parallel. It was calculated by using a Mathematica notebook to determine the spacing of the magnetic components. COSY Infinity was used to calculate the final magnetic pole tip fields necessary to focus the system. The development of this design involved extensive testing of a variety of possible layout configurations seeking to maximize resolution while minimizing the maximum beam size anywhere in the system, and the quadrupole strengths.

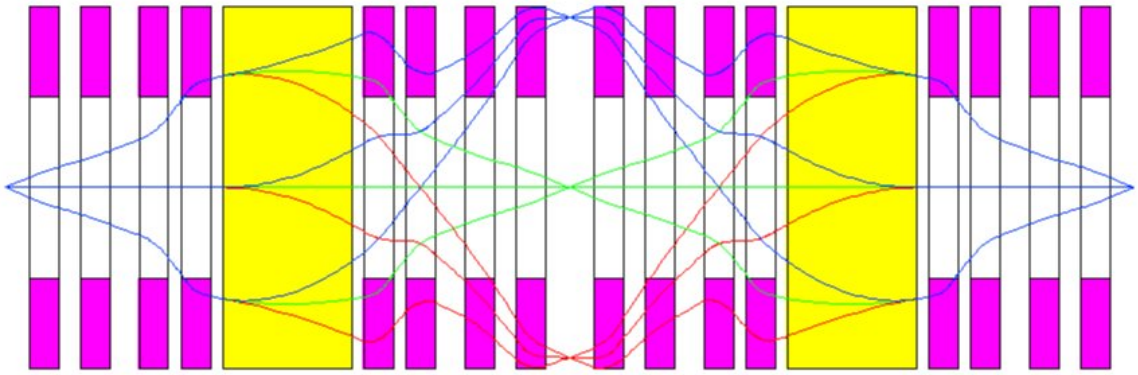

Fig. III-46. First order layout of the (first stage of the) proposed ion optics of the fragment separator.

After the linear layout system was designed, corrections had to be made for the higher order aberrations of the system, as well as the effect of fringe fields. Again, the use of symmetry theories, in particular the combination of mirror and symplectic symmetry, allowed determination of the minimum number of multipoles necessary to minimize the aberrations. We were able to show how aberrations in the optical system could be minimized by minimizing an explicit list of transfer map coefficients. The final layout, shown in Fig. III-47, successfully minimized all aberrations through third order. The residual aberrations were calculated through fifth order to show that their effect was minimal.

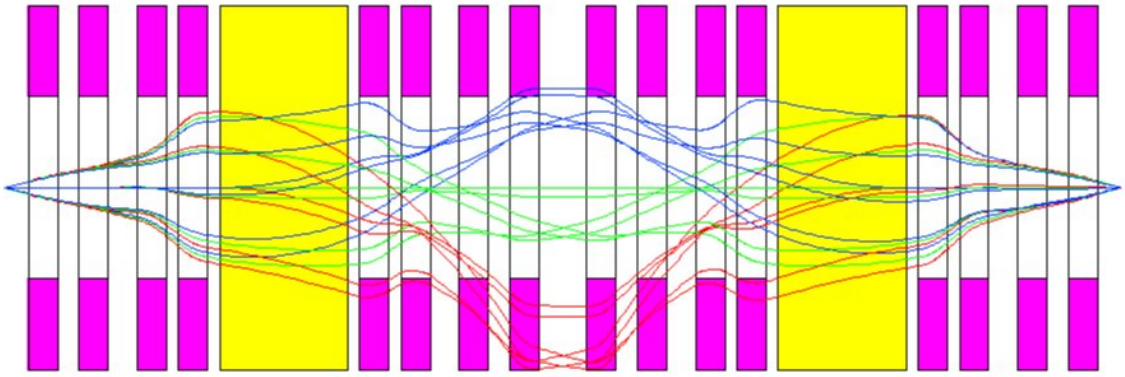

Fig. III-47. Third order layout of the (first stage of the) proposed ion optics of the fragment separator.

Additionally, we have been working on a modified layout using the principles from our original research which could be used to separate isotopes such as ^{15}O. This system, shown in Fig. III-48, also utilizes the same basic symmetries as the original design, but also minimizes aberrations at the dispersive image at higher orders.

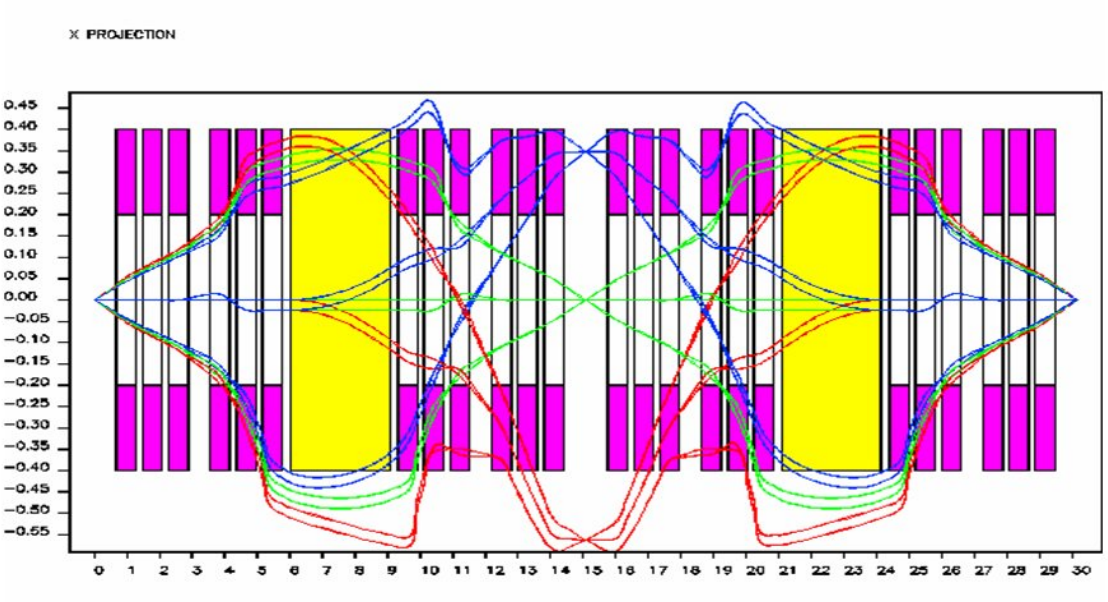

Fig. III-48. Second order alternate layout of the (first stage of the) proposed ion optics of the fragment separator.

c.3. Effects of the Wedge Absorber in Fragment Separators (B. Erdelyi, J. Nolen, L. Bandura, and J. Maloney)

Next-generation fragment separators for the study of exotic nuclei possess some design challenges due to the large emittances that result from the reaction kinematics in the target. In order to achieve separation in mass and charge, an absorber wedge must be used. As isotopes pass through the wedge, the amount of energy loss varies according to the isotope's specific mass and charge. This ensures that only one species is selected at the end of the fragment separator. In addition to complications resulting from the beam interactions in the target, the introduction of an absorber wedge into the fragment separator creates undesirable optical effects that must be eliminated. A computational framework to model these beam-material interactions and their effects on the operation of the fragment separator has been developed and implemented.

We have used COSY Infinity to model the beam-material interactions in the target and absorber in combination with the charged particle optics. COSY Infinity is a general purpose nonlinear dynamics code based on Differential Algebra (DA). We have integrated several stand-alone codes into COSY, which were necessary to look at energy loss and other nuclear physics processes. The codes we have utilized are EPAX for calculation of fragmentation cross sections, GLOBAL for charge state evolution of the beam, and ATIMA for energy loss and energy and angular straggling within the target and absorber. These codes are now available as simple calls to intrinsic functions within COSY.

A fission model has been developed to accurately model the dynamics of the secondary beam in the fragment separator and to correctly predict the cross sections of the fission products from a uranium primary beam at various energies. The fission and fragmentation database has been constructed from data generated by the nuclear physics code MCNPX. Production cross sections were provided for four primary beam energies and polynomial interpolations were used to obtain the cross sections of all isotopes in the 200-1500 MeV/u energy regime. In order to accurately model the beam dynamics in the fragment separator, the kinematics of the fission products, upon emergence from the target, were needed. In Fig. III-49, the phase space coordinates of ^{132}Sn particles produced by a 200 MeV/u ^{238}U beam in a carbon target are shown. The coordinates of all fission products are represented by similar "fuzzy" spherical shells. Several data points from MCNPX were collected and polynomial interpolations in mass, charge, and energy were used to obtain the initial coordinates of any secondary beam.

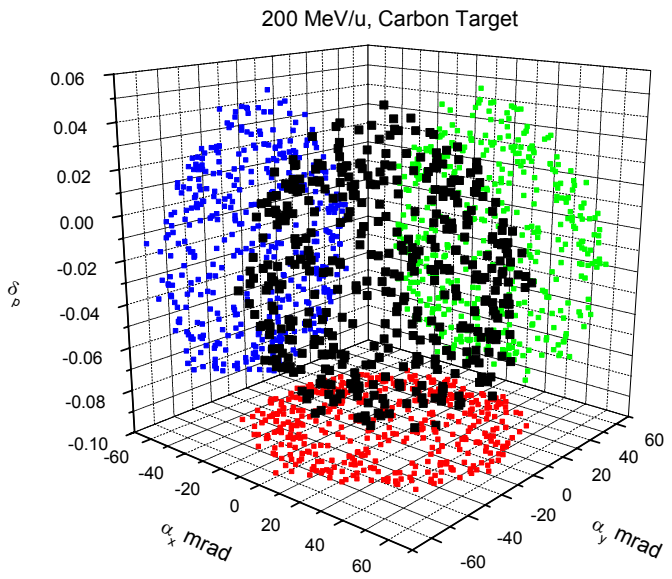

Fig. III-49. Initial coordinates of ^{132}Sn produced by 200 MeV/u ^{238}U on ^{12}C target.

A detailed study of the optical effects induced by the introduction of the absorber into the fragment separator has been performed. Using an unshaped absorber, we have analyzed how the magnification and dispersion change as functions of absorber thickness and projectile energy. The ideal thickness and shape of the absorber have been calculated such to maximize resolution and transmission for a 400 MeV/u ^{132}Sn beam. Figure III-50 shows the resolution of the fragment separator as a function of the absorber thickness. We have also investigated the dependence of resolution on initial beam emittance.

As an unshaped absorber produces aberrations in an otherwise low-aberration separator, higher order shaping of the entrance and exit surfaces is needed for their correction. Without shape correction, aberrations due to even a thin wedge can be on the order of several centimeters. Using optimizers from within COSY, we have fit the higher order surface coefficients such to minimize aberrations in the horizontal plane. We have succeeded in cancelling all of the aberrations (<1 mm) to third order for a wedge that is optimized for transmission and resolution.

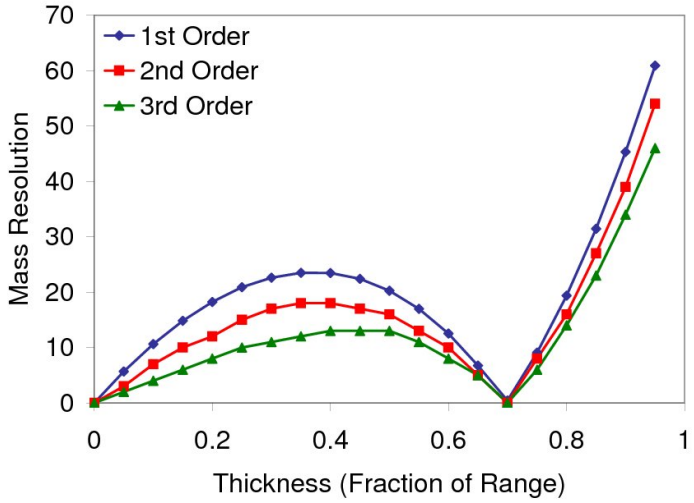

Fig. III-50. Mass resolution of fragment separator at 400 MeV/u.

Two modes have been implemented in order to look at different effects of the absorber. In "map mode" the deterministic effects are easily modeled. When the absorber is viewed as an optical element, the map approach can capture the average energy loss of a particle which is dependent on the projectile-absorber material combination, the energy of the reference particle, the shape of the absorber and the initial conditions of the particle. In map mode the optimization of the wedge shape to minimize aberrations in the system is fast.

In "Monte-Carlo mode" one may track all isotopes produced in the target and wedge. In this mode we divide the target and wedge into thin slices. For each slice, the incident particle sees a drift with energy loss. At the end of the slice, new particles can be created and primary particles are deleted. Coordinates must be assigned to the new particles based on the parent particle. For new particles which are not produced by a uranium nucleus, the new coordinates are determined by invoking the "fireball method". If the parent particle is uranium, then coordinates are found by interpolation using the fission database. It should be noted that MC mode also incorporates all of the features of map mode. Since MC mode allows us to track all isotopes in the fragment separator, we will perform separation purity studies by this approach.

c.4. Large Aperture Magnet Maps to Optics Maps (S. Manikonda, J. Nolen, M. Berz,* and K. Makino*)

Next-generation radioactive beam facilities like the proposed AEBL facility in the U.S. require the use of large aperture air-core type superconducting quadrupole magnets. Since the charged particle beams used in such facilities are wider in the dispersive plane than the transverse plane, it is cost efficient to utilize magnets with elliptic cross sections. We have proposed a new design for a quadrupole magnet with an elliptic cross section and with tunable higher order multipoles.

The design consists of eighteen superconducting racetrack coils placed on two hollow concentric rhombic prism support structures, with the ratio of the diagonals of the rhombus equal to 2. The cross section view showing the arrangement of the current coils on the support structure is shown in Fig. III-51. The positioning of the coils in the first quadrant is given in Table III-3. The signs "+" and "–" indicate the direction of the current to produce a positive multipole terms. The superconducting racetrack coils on the inner rhombic prism produce quadrupole and octupole fields. The racetrack coils on the outer rhombic prism produce hexapole and decapole fields, and also allow for a limited dipole field for correction purposes. The length of the magnet is 1m.

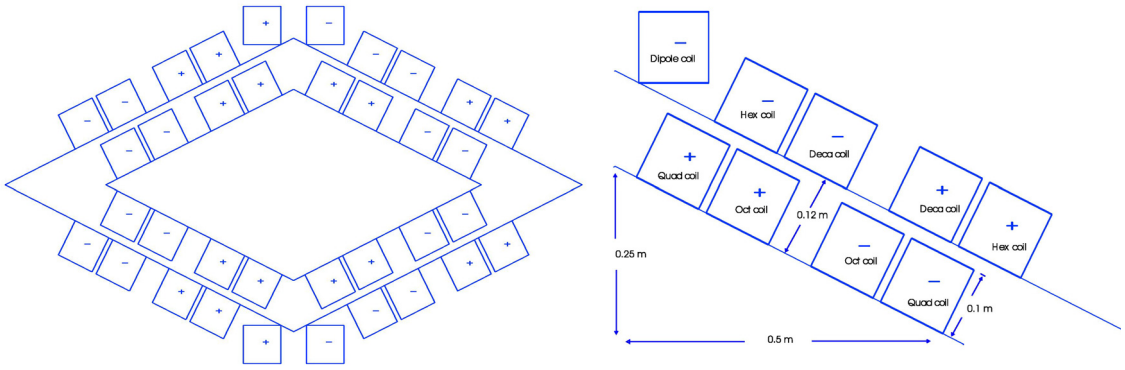

Fig. III-51. The cross section view of the full magnet and coil description in the first quadrant.

In order to study the proposed design new numerical tools to compute the multipole expansion of the magnetic field starting from the Biot-Savart law and Ampere's law have been implemented using the Differential Algebraic (DA) framework available in the code COSY Infinity. Some of the features of these tools are:

- Racetrack type current coil and infinitely long current wire of rectangular cross section have been implemented to do the 3D and 2D design of air-core type magnets.

- The computation of high-order multipole decomposition of the field is done using the DA techniques. Using orders around 10, accuracy of about 14 digits can be achieved using these tools.

- The currents and geometric design factors can be set as parameters for the field computation. This leads to high-order parameter dependent local expansion of the magnetic field, which can be used to study and further optimize the design.

- The multipole decomposition of the field obtained from these tools can be combined with the existing DA based transfer map extraction tools in the code COSY Infinity. Fringe fields can now be treated exactly and no approximation by the analytic Enge model is needed.

Table III-3. The center position of the coils in the first quadrant.

Coil Description	**Position of Coils**	
	X (m)	**Y (m)**
Inner Coils		
Quadrupole (-)	0.4473	0.8222E-01
Octupole (-)	0.3473	0.1322
Octupole (+)	0.1973	0.2072
Quadrupole (+)	0.9736E-01	0.2572
Outer Coils		
Hexapole (+)	0.5591	0.1604
Decapole (+)	0.4591	0.2104
Decapole (-)	0.3091	0.2854
Hexapole (-)	0.2091	0.3354
Dipole Corrector (-)	0.8385E-01	0.4172

The feasible range of multipole strengths that the proposed magnet can achieve is shown in Fig. III-52. The strengths are computed at the horizontal half aperture and the current density was varied between $\pm 10^8 A/m^2$.

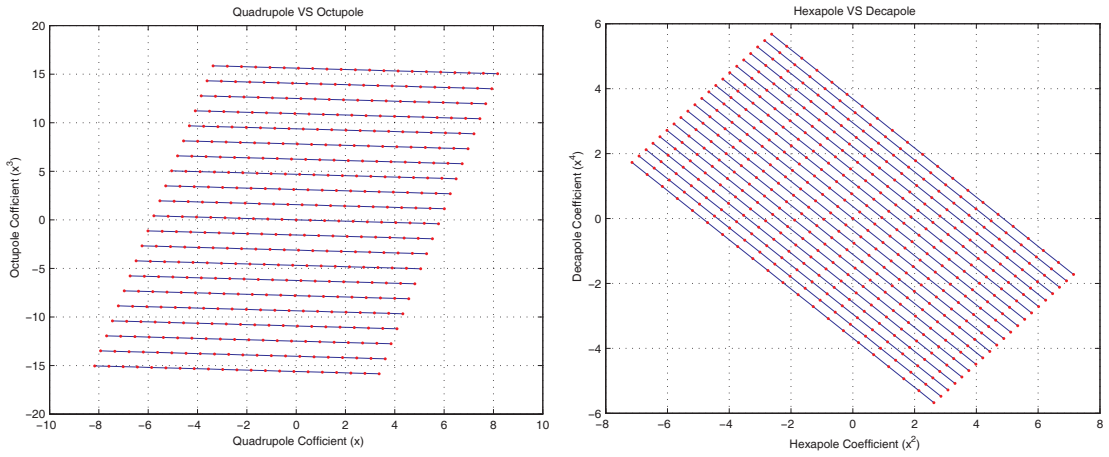

Fig. III-52. The operational plots for different multipoles.

The magnetic field on the central cross section of the magnet is shown in the Fig. III-53. As expected, the magnetic field is purely transverse ($B_z = 0$) here. The y-component of the magnetic field on the mid plane of

the magnet, showing the fringe field region, is plotted in Fig. III-54.

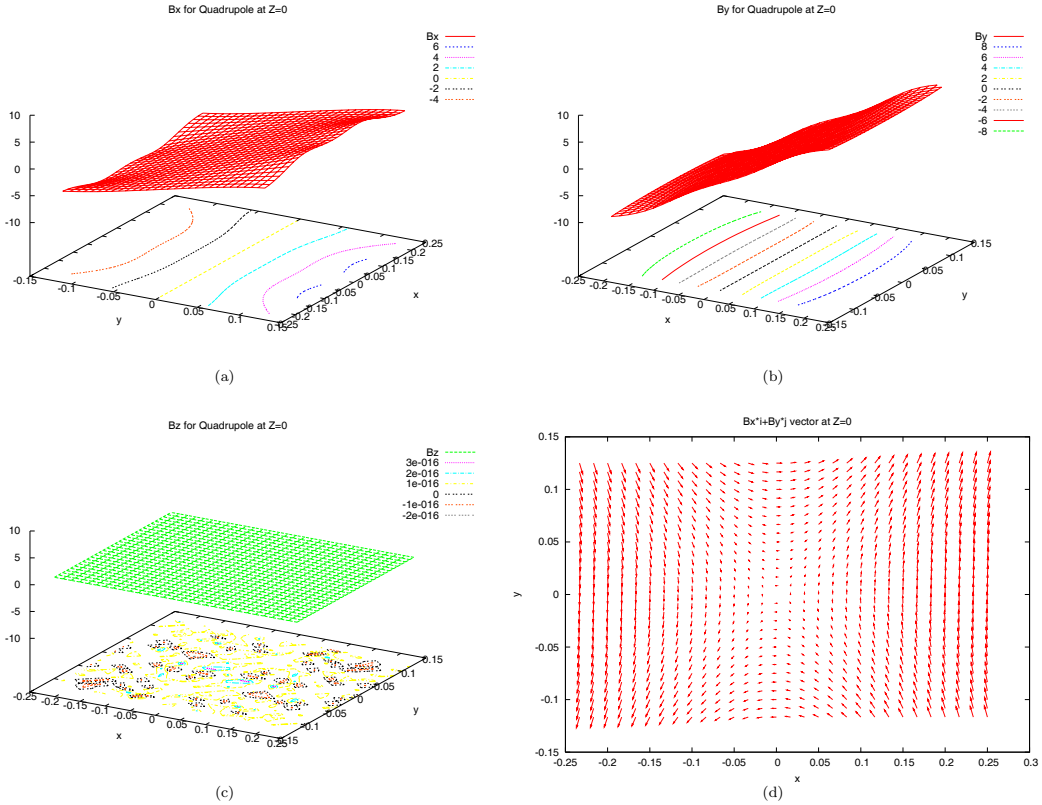

Fig. III-53. The magnetic field on the central cross section of the magnet (z = 0m).

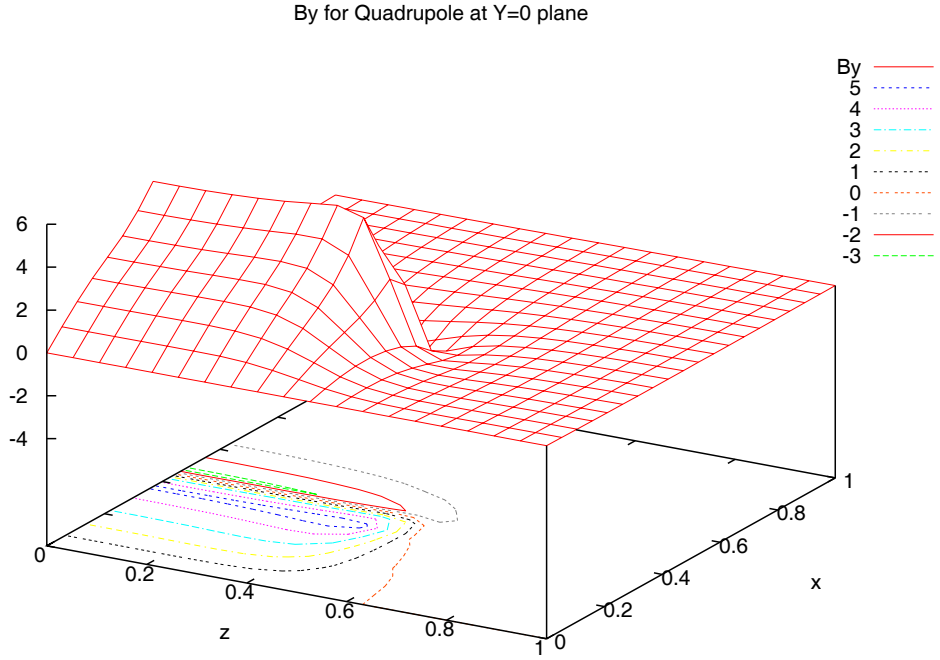

Fig. III-54. The plot of y-component of magnetic field on the midplane.

*Michigan State University.

c.5. Development of Uranium Carbide Material for High Power ISOL Applications

(J. P. Greene, J. A. Nolen, and T. Burtseva*)

One option as a high power isotope separator on-line (ISOL) production target proposed for the Advanced Exotic Beam Laboratory (AEBL) will be one based on fission from uranium or a compound of uranium to produce ion species far from stability.[1] The two-step target design employs neutrons first generated in a cooled, refractory, primary target which then induce fission in a surrounding assembly of uranium carbide.

The prototype target design was done by TechSource, Inc.[2] with the fine-grained, high thermal conductivity UC_2 target material to be supplied by Argonne National Laboratory (ANL). The primary target will be a liquid cooled tungsten cylinder, irradiated by the AEBL driver beam. The small energy deposition rate in the surrounding UC_2 secondary target material is not sufficient to heat the target to the desired operating conditions (1600 to 2100 C) necessary to promote effective release of fission products. Thermal conductivities on the order of 2 W/m-K (or greater) over the operating temperature range are required for a viable secondary target design.

The thermal conductivity measurements are carried out on sample disks prepared using UC_2 powder together with carbon (ratio of 8:1) in the form of exfoliated graphite obtained through Superior Graphite which avoids the need for a binder. Densities of 5 g/cc and greater have been achieved, meeting design specifications.

These thin sample pellets then have their thermal conductivity measured using the method of electron bombardment.[4] The sample is heated on the bottom face by a vertical electron beam source installed within a vacuum evaporator. After achieving thermal equilibrium, the temperature of both faces of the sample was measured with the aid of a two-color pyrometer. Modifications to the original design were recently performed adding ceramic rod supports and an intermediate tungsten collimator installed beneath the pellet support to prevent beam halo from hitting the Ta sample holder. New measurements were performed of the thermal conductivities for our UC_2 samples which exhibit properties comparable to values found in the literature. A thermal analysis was made on these heated disks using the code FlexPDE,[5] solving the heat flow partial differential equations and extracting the thermal conductivity as a check of the method.

As the original material used for this research is no longer commercially available, an effort was immediately mounted for preparation in-house by the method of arc melting.[3] Recently, alternative commercial sources for uranium carbide supply have come to our attention. One company, IBI Labs, which was contacted after the last collaboration meeting at Oak Ridge National Laboratory (ORNL), has provided us with a supply of commercially available UC_2 material having a grain size down to -325 mesh. This material will be fashioned into disks for thermal conductivity determinations and also release measurements. A photomicrograph of this new material is seen in Fig. III-55.

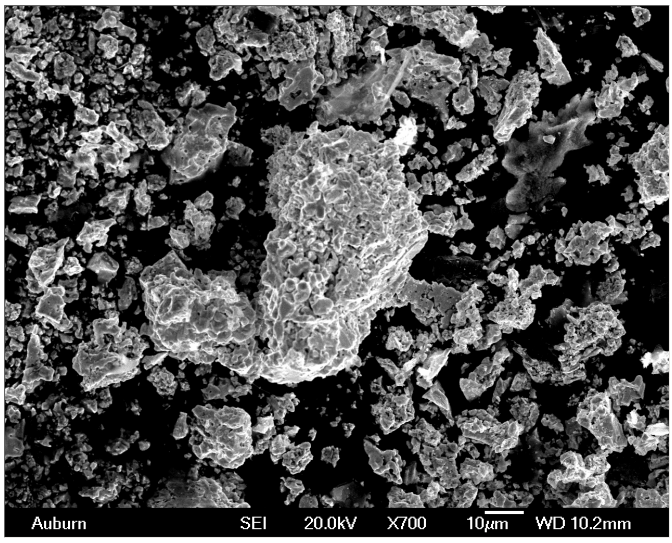

Fig. III-55. Photomicrograph of the -325 mesh uranium carbide powder purchased from IBI Labs.

Another avenue of manufacture has been undertaken by Refrac Systems using the method of hydriding, starting with depleted metal reacted in a hydrogen furnace. Over 3 kg of clean depleted uranium metal plate was shipped to Refrac Systems with the reacted product combined with fine graphite powder for the manufacture of UC_2. Enough uranium carbide material has now been manufactured to meet the requirements for the TechSource target design. In addition, as part of the compaction/carbonization process several disks having significantly higher densities (in the range of 8-11 g/cc) were prepared and are now being characterized for thermal properties and radioactive release. One of the prepared target disks is shown in Fig. III-56.

The desired release of the fission products produced under sample irradiation is also being explored as a function of density. The target/ion source (UNISOR) facility is being used for characterization of the secondary target material release properties. We are working closely with Dan Stracener and Ken Carter at ORNL and UC_2 manufactured from our fine grain size material has been shipped there for these measurements. Analysis of the experimental data on the release properties of radioactive ions from this intermediate density, smaller grain size pellets is being performed. This work is presently ongoing as we are awaiting beam time when available.

With verification of the thermal properties coupled with new data from ORNL on the release properties eventually from the high density material, we hope to move towards fabricating actual secondary target disks using custom designed dies and available large area press.

As an alternate method to make the large diameter disks needed for the actual target, we are investigating the use of a electrocompaction process that was recently demonstrated by an ANL/Superior Graphite collaboration. Under an agreement between the two parties, the ANL Physics Division has now taken possession of the equipment and is presently developing the required radiation safety documentation with the Energy Technology Division to operate it using uranium carbide. With Superior Graphite personnel, large diameter sample disks of WC/exfoliated graphite have been successfully pressed to high density as a demonstration of the process. It is believed that the densities and thermal conductivity achieved for UC_2 samples using this process will be sufficient for a prototype high-power ISOL target, including a tilted spallation target for manufacture and testing under actual experimental conditions.

---

*Energy Technology Division, Argonne National Laboratory.

[1]Report to ATLAS Users Facility, ANL-ATLAS-99-1, March (1999).
[2]W. Talbert *et al*., TechSource, Inc. (SBIR Grant).
[3]J. Crane, F. B. Litton, and H. S. Kalish, Arc Skull Melting and Casting of Uranium Carbide, ASM Trans. Quarterly **56**, 176 (1963).
[4]J. P. Greene, A. Levand, J. Nolen, and T. Burtseva, Nucl. Phys. **A746**, 425c-428c (2004).
[5]FlexPDE 4.2.7s (student version) www.pdesolutions.com.

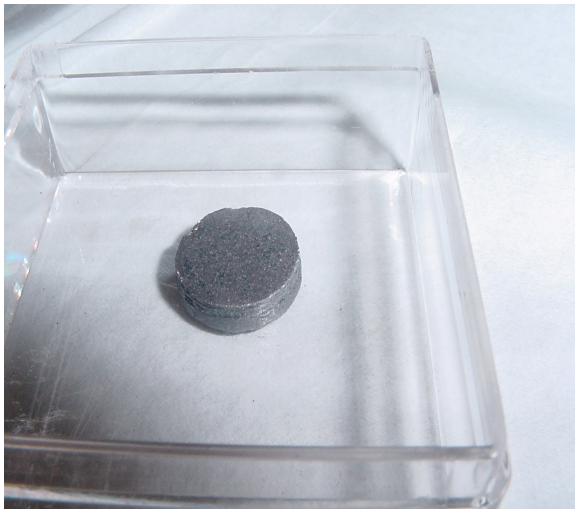

Fig. III-56. Picture of a high-density uranium carbide sample produced by Refrac, Inc.

c.6. A Study of the Cyclotron Gas Stopper Concept (M. Sternberg and G. Savard*)

The proposed cyclotron gas-stopping scheme (see Fig. III-57) for the efficient thermalization of intense rare isotope beams has been examined. Simulations expand on previous studies completed by Bollen *et al*.[1] and expose many complications of such an apparatus arising from physical effects either not accounted or not accounted properly for in previous work. Below is a schematic of the device, as proposed by Bollen *et al*.

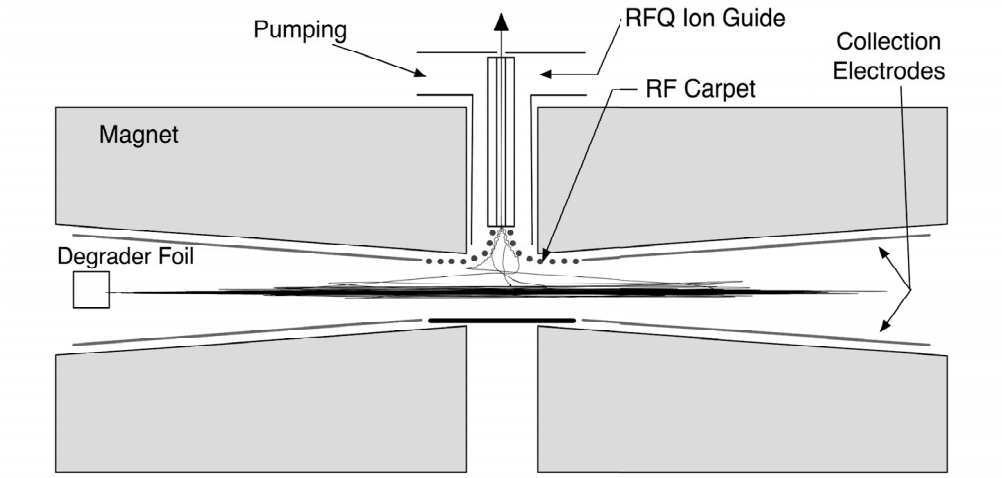

Fig III-57. Schematic layout of the proposed cyclotron catcher concept.

The proposed design uses a gas-filled weakly focusing cyclotron magnet with a 4 cm pole gap to thermalize energetic beams produced by fragmentation. After passing the ions through a degrader foil they can become confined within the cylindrical gas-filled magnetic region where current gas-stopping techniques can be used to cool ions to thermal energies using 10 mbar of high purity He. As the ions collide with and ionize the He gas they lose energy and their orbits within the magnet field shrink about the center of the magnet causing them to stop finally within a small cylindrical region in the center of the magnet. Simulations by Bollen *et al.* have shown this method to produce a clear separation between the He^+ ions concentrated in a donut shaped region surrounding the center and the cooled ions in the center within a 4 cm pole gap. It has been suggested that such a technique may be able to overcome space charge limitations inherent in other gas-cell designs by removing the highly concentrated He ions with a ring of charge collection electrodes allowing for operations at greater beam intensities, while the cooled ions in the middle could be extracted with the use of a DC gradient combined with an RF carpet followed by an RFQ-ion guide.

Such simulations suggested a large possible improvement on currently allowed beam intensities. However, these simulations failed to properly include many physical phenomena that were either neglected, mistreated, or improperly determined to be negligible. Of particular concern was their assertion that, "these [small angle scattering and energy straggling] effects are relatively small for ions stopping in helium and are small compared to the initial beam parameters." While the effects of energy straggling are very small, simulations preformed in SRIM suggest an average lateral stopping range of 37 cm for the test case used by Bollen *et al.* and it is not immediately clear that the effects of multiple scattering could be neglected when stopping ions within a 4 cm pole gap.

Our approach was to first reproduce the results of Bollen *et al*. then systematically improve on these simulations by:

- Correcting the charge-changing collision method used in the paper.
- Including proper charge state of ions in solids for beam exiting the degrader.
- Adding angular straggling.

- Performing simulations with larger phase-space for the incoming beam.

- Investigating alternative means of focusing.

Figure III-58 shows a plot of our results for stopping efficiency as a function of pole gap for the design proposed by Bollen *et al*. using two different models for the cyclotron's B-field. As one can see, the originally proposed cyclotron gas-stopper geometry with a 4 cm pole gap was found to have a near null efficiency (the original study reported a 100% stopping efficiency), with the largest loss in efficiencies coming from the inclusion of angular straggling and properly treating charge-state straggling. We extended these simulations to devices with modified geometry and a much larger pole gap and could achieve a stopping efficiency approaching roughly 90%, but at the expense of many engineering difficulties. The advantages that were, however, incorrectly predicted in previous simulations for high intensity operation of this device are severely compromised. In addition, we have demonstrated the validity of our simulation methods by reproducing experimental data from experiments involving ion collisions in gas-filled magnets. These results have been submitted for publication in NIM.

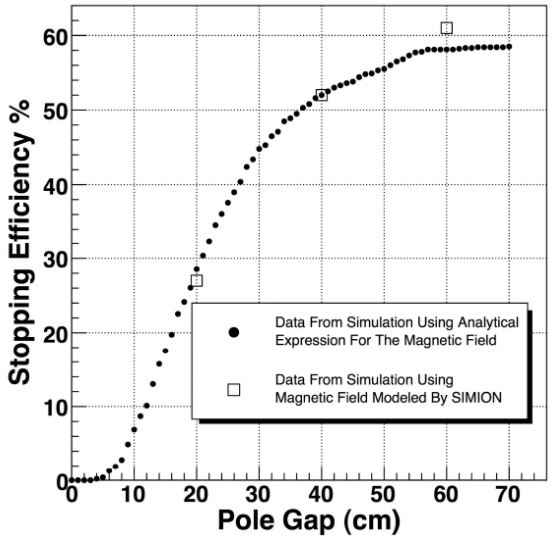

Fig. III-58. Calculated stopping efficiency as a function of the magnet pole gap.

_____

*Argonne National Laboratory and University of Chicago.

[1]G. Bollen *et al*., Nucl. Instrum. Methods **A550**, 27 (2005).

c.7. The High-Intensity AEBL/RIA Gas Catcher Test at ATLAS (G. Savard, J. Clark,* S. Gerbick, J. P. Greene, A. Levand, N. Scielzo, K. S. Sharma,† M. Sternberg, and B. J. Zabransky)

Both theoretical and experimental work has continued on the RIA prototype gas catcher and resulted in a breakthrough in performance at high intensity for such devices. Detailed calculations we performed identified radial losses due to positive space charge build up in the gas catcher as the main loss mechanism in high intensity operation. The incoming ions create ion-electron pairs by losing energy while they slow down. The electrons have higher drift velocity in the gas and are removed quickly. The remaining positive ions, mostly helium, remain behind and their space charge repels the positive radioactive ions which must then move in the combined DC fields from the electrodes and the space charge distribution. At low and moderate intensity, the ions reach the RF cone and are rechanneled to the nozzle and extracted; this is one of the great advantages over the DC only approach where there is no recovery mechanism and these ions are lost

even at fairly low intensity. At the highest intensities, however, the radioactive ions can be lost radially even before they get to the RF cone. To overcome this difficulty, we added an RF structure similar to that in the RF cone along the body of the gas catcher in regions where medium ionization is present and developed a novel structure for operation in the highest ionization regions. The complex electrodes for these body RF sections were built, chemically polished, cleaned and assembled together with their resonating RF feeding system and used to replace the existing electrodes in the AEBL/RIA prototype body sections.

In parallel to these efforts, the high-intensity beamline in construction in experimental area II at ATLAS to test high-intensity operation of the RIA/AEBL gas catcher by reproducing beam properties expected after the final degrader behind a RIA-type fragment separator was completed. This beamline utilizes a high-power rotating target for isotope production and a large bore superconducting solenoid to refocus all isotopes produced at an angle below 10 degrees to the entrance of the gas catcher. A movable zero-degree beamstop lets through scattered tails of the beam so that RIA-like ionization densities can be reached inside the gas catcher. This new beamline was commissioned in August 2006.

The RIA gas catcher prototype, retrofitted with the new RF body sections combined with the existing large RF cone, was installed in the new high-intensity beamline in experimental area II at ATLAS (see Fig. III-59) and connected to the diagnostics line from the CPT Penning trap injection system. A 25 cm diameter all-metal thin window is used to isolate the beamline vacuum from the gas catcher high purity helium gas. The modified gas catcher was first tested with fission products from a ^{252}Cf source with which the device was shown to operate properly and the body RF sections shown to be effective at focusing radioactive ions. Even at low intensity, the body RF was shown to increase the extracted radioactive ion yield by about 7% over the nominal 45% efficiency obtained under previous operating conditions. This increase is believed to be coming from fission products stopped very close to the body electrodes that were lost under the previous configuration where no RF repulsion along these electrodes was available to counteract fringe field effects. A first high intensity test of the gas catcher took place in September 2006 with activity from a fission source extracted from the gas catcher system being measured while ions from the new beamline were simultaneously injected into the gas catcher. Initial results indicate that the efficiency of the gas catcher under these conditions was reduced by 2% with an incoming ion flux of 3×10^7 per second, the maximum ion flux we could obtain from the new beamline in this initial run. This very positive result validated our approach and a second test where activity from the incoming beam was monitored as a function of intensity, with intensity in the $10^7 - 10^9$ ions/second range, took place at the end of 2006. Figure III-60 summarizes the results of this test.

The results from the initial high-intensity test shown in Fig. III-60 indicate that the device, with its new RF focusing structures, can operate without loss in efficiency at incoming ion intensity up to 10^8 ions per second and still has an efficiency of about 10% at 10^9 incoming ions per second. This represents successful operation at about four orders of magnitude higher intensity than previously demonstrated and within shooting distance of the original RIA goal of 20% efficiency at 10^9 ions per second. This is the first demonstration of operation in a regime anywhere close to that required at AEBL/RIA and the further refinement that will be incorporated in the coming year should allow us to reach or surpass this goal.

*Yale University, †University of Manitoba, Winnipeg, Manitoba.

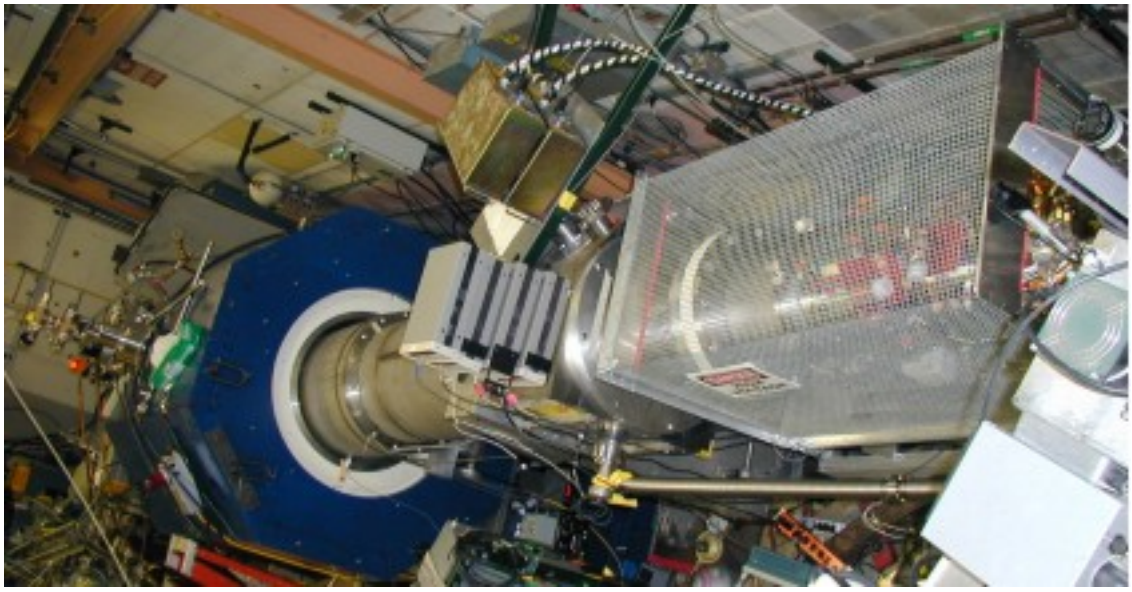

Fig. III-59. Aerial view of the large gas catcher inside its high-voltage shielding cage (on the right) in location at the end of the new beamline built to reproduce the ion properties expected after the final degrader in a RIA-type fragment separator. The main optical element in that beamline is a 65 cm bore superconducting solenoid shown in blue at the left of the picture.

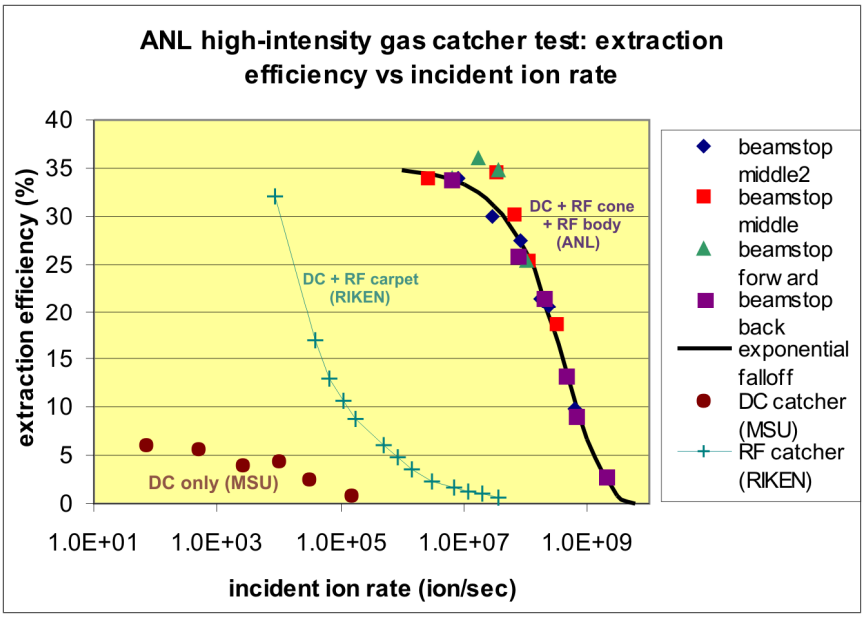

Fig. III-60. Efficiency for the extraction of the stopped radioactive ions versus the incoming ion rate. The addition of the new RF focusing structures allows successful operation at four or more orders of magnitude higher intensity than other approaches used so far.

IV. MEDIUM-ENERGY NUCLEAR PHYSICS RESEARCH

OVERVIEW

The overall goals of the Medium-Energy Physics research program in the Argonne Physics Division are to test our understanding of the structure of hadrons and nuclei and provide tests of the Standard Model. In addition, we develop and exploit new technologies for high-impact applications in nuclear physics as well as other national priorities. In order to test our understanding of the structure of hadrons and the structure of nuclei within the framework of quantum chromodynamics, the medium-energy research program emphasizes the study of nucleons and nuclei on a relatively short distance scale. Because the electromagnetic interaction provides an accurate, well-understood probe of these phenomena, primary emphasis is placed on experiments involving electron scattering, real photons and Drell-Yan processes. The electron beams of the Thomas Jefferson National Accelerator Facility (JLab) are ideally suited for studies of nuclei at hadronic scales and represent one center of the experimental program. Staff members have had a key role in the development of experimental equipment and development of the scientific program at JLab. During the past year, the MEP group had a major responsibility for four new proposals for the 12-GeV physics program. We have continued to develop the optical trap program and have applied this new technique to the study of neutron-rich light nuclei and began preparations for the search for a non-zero electric dipole moment in a nucleus.

Recently, staff members have focused increasingly on studies of the nucleon and the search for exotic phenomena. Preparations were begun for a super-Rosenbluth measurement for electron-proton elastic scattering at JLab. In the past year, analyses were completed for the search for pentaquark partners and for polarization in deuteron photodisintegration; while preliminary analyses were completed for the EMC effect in light nuclei, the $x > 1$ experiment in nuclei, and for transparency in ρ electroproduction in nuclei.

The HERMES experiment in the HERA electron ring at DESY-Hamburg has two novel features: (1) polarized electron scattering from internal polarized or unpolarized atomic gas targets, and (2) a dual-radiator ring imaging Cerenkov counter (RICH). Deep inelastic scattering has been measured with polarized electrons on polarized hydrogen, deuterium and ^{3}He. Argonne has concentrated on the hadron particle identification of HERMES, a unique capability compared to other spin structure experiments. In 1999 and under Argonne leadership, the RICH was brought into operation at the design specifications to provide complete hadron identification in the experiment. In recent months, HERMES entered its final year of operation. During its last year HERMES plans a program of measurements for unpolarized targets. These results are expected to provide new and significant data for deeply virtual Compton scattering as well as accurate d/u ratios in the valence region.

Measurements of high mass virtual photon production in high-energy proton-induced reactions have determined the flavor dependence of the sea of antiquarks in the nucleon. These measurements gave insight into the origin of the nucleon sea. In the same experiment, the high-x absolute Drell-Yan cross sections were measured. During the past year the angular distribution of the Drell-Yan process in free proton-proton scattering was determined as a constraint on the Boer-Mulders structure function of the proton. In Fiscal Year 2001, a new initiative was approved by the FNAL PAC to continue these measurements with much higher luminosity at the FNAL Main Injector. These Drell-Yan experiments not only provide the best means to measure anti-quark distributions in the nucleon and nuclei, but represent an outstanding opportunity to perform these measurements at an ideal proton beam energy of 120 GeV. During the past year, the FNAL PAC re-affirmed the importance of these Drell-Yan measurements. In addition, a technical, cost and schedule review of the Drell-Yan project was conducted during the past year.

The technology of laser atom traps provides a unique environment for the study of nuclear and atomic systems and represents a powerful new method that is opening up exciting new opportunities in a variety of fields, including nuclear physics. In particular, the group has continued the development and improvement in efficiency of a high-sensitivity magneto-optical trap for rare, unstable isotopes of krypton as a means for dating ancient groundwater. In 2004, a highlight was the optical trapping of single atoms of ^{6}He and performing precision laser spectroscopy on the individual atoms to determine the charge radius of ^{6}He nuclei. During the past year, the helium atom trap efficiency was improved by more than an order of magnitude. The helium trap was successfully moved and brought into operation at GANIL in preparation for the ^{8}He charge radius measurement.

Preparations for the search for an electric dipole moment (EDM) of ^{225}Ra are in progress. The ultimate goal is to search for a non-zero EDM for ^{225}Ra and improve the sensitivity for nuclear EDM searches by approximately two orders of magnitude. This test of time-reversal symmetry represents an outstanding opportunity to search for new physics beyond the Standard Model. Not only were radium-225 atoms successfully optically trapped, but the beneficial effect of blackbody radiation on the trap was discovered.

A. HADRON PROPERTIES

a.1. Precision Measurements of the Proton Electromagnetic Form Factors and Two-Photon Exchange Effects (J. Arrington, K. Hafidi, R. J. Holt, P. E. Reimer, P. Solvignon, and the JLab E05-017 Collaboration)

Polarization transfer measurements of the proton form factors showed a significant difference between the charge and magnetization distributions of the proton. These results contradict previous Rosenbluth separation measurements, and the explanation is now believed to be due to two-photon exchange (TPE) corrections. While these corrections are small, typically 5% or less, they have a significant impact on the Rosenbluth extraction of G_{Ep}.

We have been trying to better understand the TPE corrections and to provide better extractions of the nucleon form factors. A review article on nucleon form factors was prepared and published in collaboration with Craig Roberts of the theory group.[1] We have also completed and are about to submit a detailed extraction of the form factors, including TPE corrections.[2] Finally, we have been studying the possible effects on TPE corrections on other exclusive processes, such as the extraction of the pion form factor, the measurement of the strangeness form factors of the nucleon through parity violating electron-proton scattering, and the impact of the electromagnetic form factors on neutrino scattering measurements.[3,4]

We also have a significant experimental program aimed at better understanding two-photon exchange. JLab Experiment E01-001[5] used a modified technique to make an extremely high precision Rosenbluth extraction of G_{Ep}/G_{Mp}. This conclusively demonstrates the disagreement between the techniques, and provided a measure of the size of the TPE effects needed to explain the disagreement. A new measurement, E05-017,[6] is underway at JLab. These new data will provide information on the size of the TPE corrections at larger Q^2 than previous measurements, as well as providing much greater sensitivity to deviations from the linear cross section dependence associated with pure one-photon exchange. In addition, the measurement will reach values of Q^2 where the contribution of the electric form factor is extremely small, allowing for a clean separation of the magnetic form factor and the TPE corrections. These data will allow for more reliable corrections at large Q^2 as well as reducing the uncertainty associated with TPE calculations at lower Q^2.

A more direct way of isolating the TPE corrections is a comparison of positron-proton and electron-proton scattering. Such data provide some evidence for two-photon exchange corrections,[7] and we have two new experiments that will make improved comparisons of positron-proton and electron-proton scattering.[8,9] Figure IV-1 shows the proposed scheme for generation of a secondary mixed positron/electron beam in Hall B. For the JLab measurement, a test run was completed in Hall B in October 2006. We demonstrated a significant decrease in the background rates with modifications to the physical layout of the photon tagging system, as well as an improved shielding configuration. We were able to run with luminosities that allowed us to observe and reconstruct positron-proton and electron-proton elastic scattering using the secondary combined electron/positron beam. As a result, a full proposal was submitted and approved by the JLab PAC, and is expected to run in 2008-2009. For the Novosibirsk measurement, there will be a run in summer 2007, which will commission the new internal hydrogen target and the additional calorimetry added to the large angle detectors.

Finally, we also participated in new polarization transfer measurements at low momenta,[10] taken as calibration for recent polarization measurements on deuterium. This demonstrated the ability to make extremely high precision measurements in this region, which has led to a proposal (PR07-004, conditionally approved) to improve the precision and Q^2 coverage of this measurements in the region of low Q^2, where there is a gap between the extremely precise Rosenbluth measurements for $Q^2 < 0.1$ GeV^2, and polarization transfer measurements at $Q^2 > 1$ GeV^2. In addition, we will participate in the upcoming high Q^2 form factor measurements (E04-108) and TPE studies (E04-109) using polarization transfer.

---

[1] J. Arrington, C. D. Roberts, and J. M. Zanotti, J. Phys. G: Nucl. Part. Phys. **34**, S23 (2007).
[2] J. Arrington and W. Melnitchouk, to be submitted to Phys. Rev. C.

[3]J. Arrington and I. Sick, submitted to Phys. Rev. C, arXiv:nucl-th/0612079 (2006).
[4]R. Bradford, A. Bodek, H. Budd, and J. Arrington, Nucl. Phys. Proc. Suppl. 159:127 (2006), arXiv:hep-ex/0602017.
[5]JLab experiment E01-001, "New Measurement of G_E/G_M for the Proton", J. Arrington and R. Segel, spokespersons.
[6]JLab experiment E05-017, "A Measurement of Two-Photon Exchange in Unpolarized Elastic Electron-Proton Scattering", J. Arrington, spokesperson.
[7]J. Arrington, Phys. Rev. C **69**, 032201(R) (2004).
[8]J. Arrington *et al.*, nucl-ex/0408020.
[9]JLab experiment E06-116, "Beyond the Born Approximation: A Precise Comparison of Positron-Proton and Electron-Proton Elastic Scattering in CLAS," A. Afanasev, J. Arrington, W. K. Brooks, K. Joo, B. A. Raue, and L. B. Weinstein, spokespersons.
[10]G. Ron *et al.*, arXiv:0706.0128 (2007).

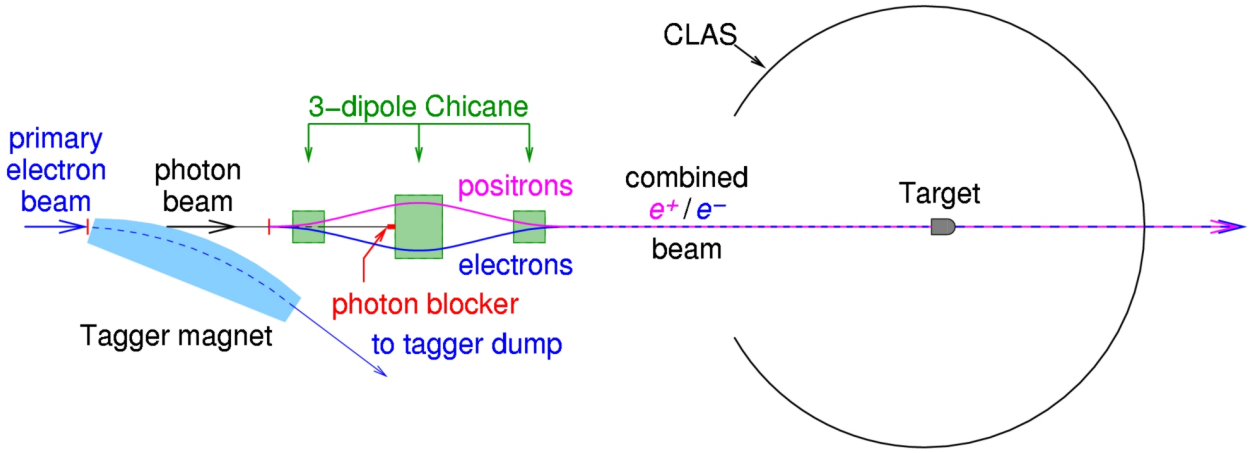

Fig IV-1. Overview of the secondary production of the mixed positron/electron beam in Hall B at JLab.

a.2. Parity Violating Electron-Proton Scattering and the Strangeness Content of the Nucleon (J. Arrington, K. Hafidi, P. E. Reimer, X. Zheng, and the JLab E99-115, E00-114, and E05-109 Collaborations)

Given precise knowledge of the nucleon electromagnetic form factors, parity violating electron-proton scattering can be used to probe the nucleon strange quark form factors. In 2004, the HAPPEX collaboration made a high precision measurement of parity violating *e-p* scattering at $Q^2 = 0.1$ GeV^2, as a measure of the strangeness contribution to the magnetic moment of the proton. In addition, elastic scattering from ^{4}He was measured, which provides a clean measure of the strangeness radius of the proton. The results have been published[1] and indicate that G_{Es} and G_{Ms} are smaller than previously believed at $Q^2 = 0.1$ GeV^2. A proposal to extend these measurements to higher precision at $Q^2 = 0.5$ GeV^2 (E05-109) was approved.

While the parity violating asymmetry is largely insensitive to the effects of two-photon exchange,[2] the isolation of the strange quark contribution requires precise knowledge of the electromagnetic form factors. An analysis of low-Q^2 nucleon form factors, including two-photon exchange effects from the calculation of Blunden *et al.*,[3] was recently completed.[4] We provide a prescription for a consistent analysis of the parity violating elastic scattering measurements, accounting for TPE corrections and correlations between the different measurements of the electromagnetic form factors. As part of this work, we provide parameterizations and uncertainties for the low-Q^2 form factors of the proton and neutron, appropriate for use in other experiments that require high precision knowledge of the low Q^2 form factors. This will also provide the foundation for a full flavor decomposition of the nucleon form factors into their contributions from

up, down, and strange quarks.

[1]A. Acha *et al.*, Phys. Rev. Lett. **98**, 032301 (2007).
[2]A. Afanasev and C. E. Carlson, Phys. Rev. Lett. **94**, 212301 (2005).
[3]P. G. Blunden, W. Melnitchouk, and J. A. Tjon, Phys. Rev. Lett. **91**, 142304 (2003).
[4]J. Arrington and I. Sick, submitted to Phys. Rev. C, arXiv:nucl-th/0612079 (2006).

a.3. The Charged Pion Form Factor (J. Arrington, K. Hafidi, R. J. Holt, P. E. Reimer, E. C. Schulte, X. Zheng, and the JLab E01-004 and E01-107 Collaborations)

While studies of hadron structure typically focus on the proton, which is easily accessible experimentally, the complicated structure of a three light-quark system makes modeling of the proton in realistic, QCD-based framework, extremely difficult. On the other hand, while the pion is more difficult to access experimentally, it's structure is simpler, and can in some cases provide a better meeting ground between theory and experiment in the study of QCD. Calculations led by C. Roberts of the Argonne theory group using the Dyson-Schwinger equations provide realistic representations of the QCD dynamics which can make predictions for both the pion form factors and the pion structure function, which provide complementary information on the pion structure.

Experiment E01-004 extended measurements of the pion form factor to 2.5 GeV^2. These results were recently published[1] as was a more detailed analysis[2] of the earlier JLab measurement.[3] In addition, it was possible to extract the pion form factor using calibration data from the pion color transparency measurement, E07-107. A draft has been prepared that includes both the extraction of the pion form factor, and as study of the separated longitudinal and transverse cross sections.

Figure IV-2 shows the preliminary results from E07-107, along with the previous world's data. These measurements can be used to test models of hadron structure in a simpler system than the nucleon, where more advanced calculations can be performed.

[1]T. Horn *et al.*, Phys. Rev. Lett. **97**, 192001 (2006).
[2]J. Volmer *et al.,* Phys. Rev. Lett. **86**, 1713 (2001).
[3]V. Tadevosyan *et al.,* Phys. Rev. C **75**, 055205 (2007).

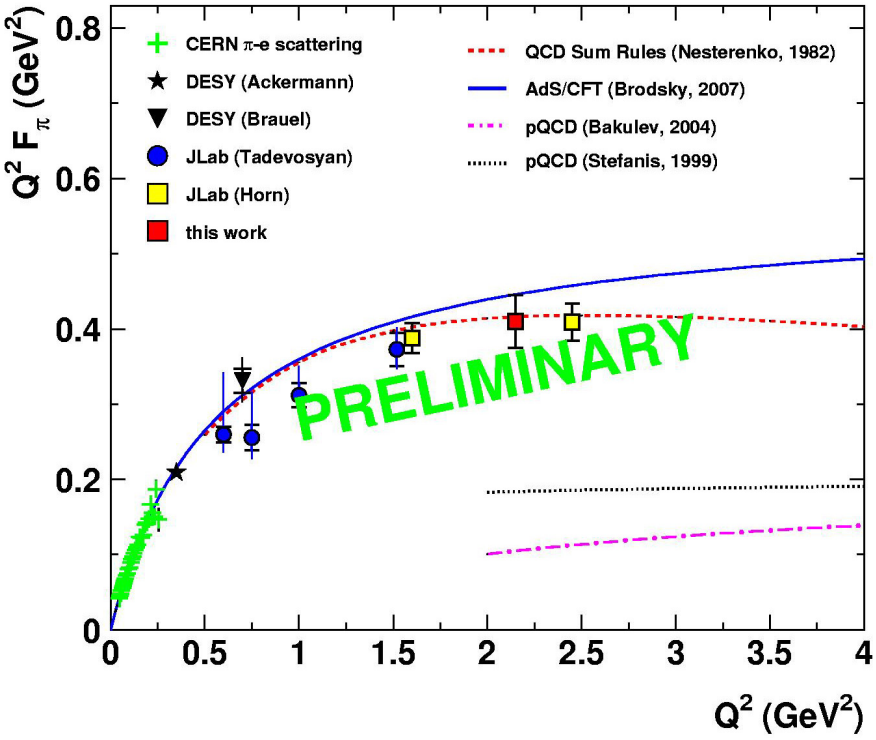

Fig. IV-2. World's data on the pion form factor, including preliminary JLab E07-107 results.

a.4. Duality and Separated Structure Functions of Nucleons and Nuclei (J. Arrington, D. Gaskell, D. F. Geesaman, K. Hafidi, R. J. Holt, D. H. Potterveld, P. E. Reimer, E. C. Schulte, P. Solvignon, X. Zheng, and the JLab E94-110, E99-118, E00-002, E00-108, E00-116, E04-001, E06-009 Collaborations)

Inclusive electron scattering in the deeply inelastic scattering (DIS) regime allows us to extract the quark distributions in nucleons or nuclei. In the resonance region, the simple picture of electron-quark scattering is not valid and the scattering is better understood in terms of resonance excitations and pion electroproduction. The unpolarized structure function has been measured precisely in both regions,[1,2] and the data show precise quark-hadron duality. In this case, duality results in the observation that the structure function at lower energies shows resonance structure, but when averaged over the resonances, reproduces the DIS structure function when taken as a function of the Nachtmann scaling variable, ξ. Using ξ provides an approximate treatment of target mass corrections, although additional studies using explicit treatment of these corrections yields the same conclusions.

Recently, such measurements have been extended to both the longitudinal and transverse separated structure functions, and to semi-inclusive pion electroproduction. For the proton and deuteron separated structure functions, the initial resonance region results (E94-110) have been reanalyzed after finding a potential model dependence in the analysis. The final results did not change significantly, and the initial paper[3] has been updated and resubmitted. In addition, an analysis of the separated DIS structure functions at low Q^2 (E99-118) have been finalized and published.[4] Additional studies of the resonance region structure functions, one focused on extremely low x values (E00-002) and one making precise measurements of duality at high x and Q^2 (E00-116) are close to having final results. Measurements looking at the separated structure functions for deuterium and nuclear targets (E04-001 and E06-009), aimed to study duality in nuclei and provide cross sections at low x and Q^2 as input to upcoming neutrino scattering measurements were started in 2005, and additional data is currently being taken.

The results from the semi-inclusive measurement, E00-116, were finalized and published.[5] They show duality in pion electroproduction over a significant range in x and z, at relatively low Q^2, indicating that duality is a global phenomenon, and providing significant evidence that factorization should hold fairly precisely for higher energy measurements planned for the 12 GeV upgrade.

[1]E. D. Bloom and F. J. Gilman, Phys. Rev. Lett. **25**, 1140 (1970).
[2]I. Niculescu *et al.*, Phys. Rev. Lett. **85**, 1182 (2000).
[3]Y. Liang *et al.*, nucl-ex/0410027 (2004).
[4]V. Tvaskis *et al.*, Phys. Rev. Lett. **98**, 142301 (2007).
[5]T. Navasadyan *et al.*, Phys. Rev. Lett. **98**, 022001 (2007).

a.5. Search for Additional Pentaquark States at JLab (P. E. Reimer, J. Arrington, K. Hafidi, E. C. Schulte, X. Zheng, and the JLab E04-012 Collaboration)

All experimental observed hadrons can be placed into two categories: mesons with valence quark-antiquark pair mesons ($\bar{q}q$) and baryons composed of three valence quarks (qqq). These are, however, not the only configurations of quarks and antiquarks allowed by the underlying theory, Quantum Chromodynamics and other configurations not fitting into the meson and baryon framework are known as "exotics". One possible exotic configuration is the pentaquark state with four quarks and an antiquark ($qqqq\bar{q}$). Recently, experimental evidence and theoretical work have suggested the existence of a pentaquark state, known as the Θ^+ with a mass near 1540 MeV. Within the Chiral Soliton model, the Θ^+ is a member of a set of 10 pentaquark states known as an antidecuplet. Using Hall A at JLab, E04-012[1] looked for evidence of an exotic isospin partner state, the Θ^{++}, in the H(e,e'K^-)X reaction, as well as the Σ^0 and N^0 members of the antidecuplet in the reactions H(e,e'K^+)X and H(e,e'π^+)X, by reconstructing the missing mass of the system. Although the Σ^0 and N^0 states are not explicitly exotic, the discovery of a narrow state would be a valuable confirmation of the existence of an antidecuplet of states. The experiment used collected data in May and June, 2004, using the HRS spectrometers to detect the scattered electron and the K^-, and K^+ and π^+ respectively. No evidence for any narrow resonances within the candidate regions. The cross section upper limits, σ_{max}, depend on the exact mass and width of the resonance. In the relevant mass regions and a maximum width of Γ = 10 MeV at 90% confidence, $\sigma_{max}(\Theta^{++}) < 4.0$ nb/sr, $\sigma_{max}(\Sigma^0) < 17.5$ nb/sr and $\sigma_{max}(N^0) < 10.0$ nb/sr,[2] with lower limits on σ_{max} for narrower resonances.

[1]J. P. Chen *et al.*, "High Resolution Study of the 1540 Exotic State," Proposal 04012 to the JLab PAC, P. E. Reimer, and B. Wojtsekhowski, spokespersons, December 2, 2003.
[2]Y. Qiang, Phys. Rev. C (to appear) arXiv: hep-ex/0609025.

B. HADRONS IN THE NUCLEAR MEDIUM

b.1. Measurement of the EMC Effect in Very Light Nuclei

(J. Arrington, L. El Fassi, K. Hafidi, R. J. Holt, D. H. Potterveld, P. E. Reimer, E. C. Schulte, P. Solvignon, X. Zheng, and the JLab E03-103 Collaboration)

For more than twenty years, it has been known that the quark momentum distribution of nuclei is not simply the sum of the quark distributions of its constituent protons and neutrons. The structure function is suppressed in heavy nuclei at large values of x (corresponding to large quark momenta), and enhanced at lower x values. Measurements to date indicate that the overall form of this modification is the same for all nuclei, but the magnitude of the enhancement and suppression is larger for heavier nuclei. Many attempts have been made to explain the EMC effect, but none of the proposed models can fully reproduce the observed modifications, and there is still no consensus on which effect or combination explain the data.

Experiment E03-103[1] ran in Hall C in late 2004 and measured the EMC effect for ^{3}He, ^{4}He, and a series of heavier nuclei. Because ^{4}He has an anomalously large density for a light nucleus, it is the most sensitive test to determine if the EMC effect scales with A or with nuclear density. More importantly, these measurements of the EMC effect can be compared to exact few body calculations. If the EMC effect is caused by few nucleon interactions, the universal shape observed in heavy nuclei may be a result of a saturation of the effect, and the shape may be different in few-body nuclei. Several calculations[2] predict that the x-dependence will be significantly different in these few-body nuclei. By making precise measurements in light nuclei, we will be able to distinguish between different models of the EMC effect based on their predictions for few-body nuclei.

Preliminary results are shown in Fig. IV-3. These results suggest that the EMC effect in ^{4}He is nearly identical to that of ^{12}C, suggesting that nuclear dependence of the EMC effect scales with density. The ^{3}He results suggest a larger effect than one would assume based on a density-scaling model. However, the ^{3}He result has a large isoscalar correction, which is model dependent, especially at large Q^2. The correction applied to the preliminary results is not from the best extraction of the neutron structure function, but it is consistent with what was used for the heavy nuclei in from previous measurements. By varying the n/p model, we change both the ^{3}He and heavy nuclei results in opposite ways, and can thus use these data to study the tradeoff between neutron cross section model and A-dependence of the extracted nuclear effects.

Finally, a measurement of $A \leq 4$ nuclei will help constrain models of the EMC effect in deuterium. Models of nuclear effects in deuterium and ^{3}He must be used to extract information on neutron structure, and a high precision measurement including ^{1}H, ^{2}H, ^{3}He, and ^{4}He will give a single set of data that can be used to evaluate these models in several light nuclei. This will help to quantify the model dependence of the neutron structure functions inferred from measurements on ^{2}H and ^{3}He. We are working with members of the Argonne theory group to perform a global comparison of the realistic few-body calculations with existing data on the proton and deuteron, as well as our new results on ^{3}He and ^{4}He.

---

[1] JLab experiment E03-103, "A Precise Measurement of the Nuclear Dependence of the EMC Effect in Light Nuclei", J. Arrington and D. Gaskell, spokespersons.

[2] G. I. Smirnov *et al.*, Eur. Phys. J. C **10**, 239 (1999); V. V. Burov *et al.,* Phys. Lett. **B466**, 1 (1999); I. R. Afnan *et al.*, Phys. Rev. C **68**, 035201 (2003); O. Benhar, private communication.

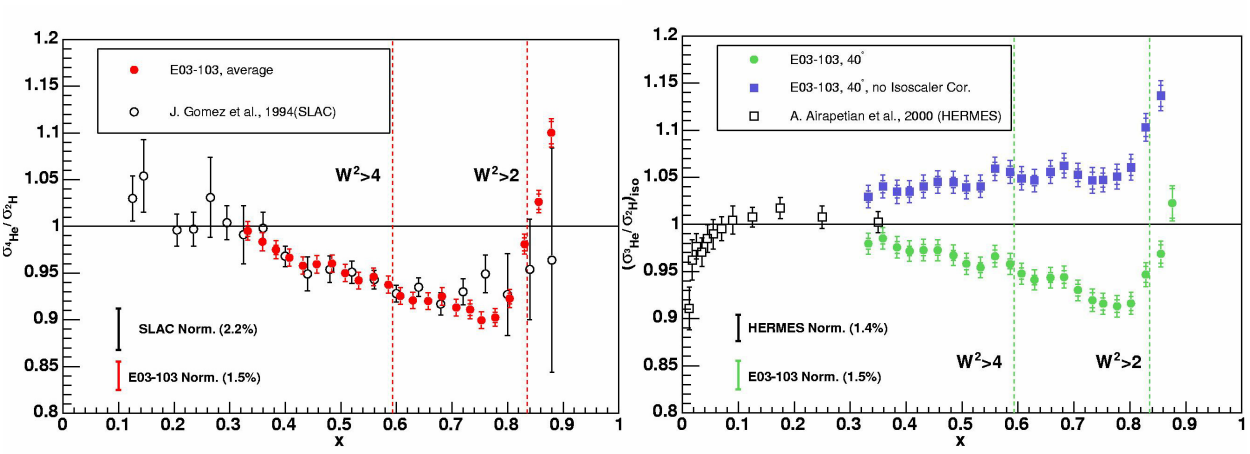

Fig. IV-3. Preliminary EMC ratio for ^{4}He and ^{3}He. Hollow points are previous data, solid points are the E03-103 preliminary results showing only the statistical uncertainties. For ^{3}He, the blue squares are the raw ^{3}He/^{2}H ratio, while the green circles show the ratio after applying the isoscalar correction due to the excess proton.

b.2. Search for the Onset of Color Transparency: JLab E02-110 Experiment (K. Hafidi, J. Arrington, L. El Fassi, D. F. Geesaman, R. J. Holt, B. Mustapha, D. H. Potterveld, P. E. Reimer, and the JLab Hall-B Collaboration)

According to QCD, point colorless systems, such as those produced in exclusive processes at high Q^2 have quite small transverse sizes. Therefore, they are expected to travel through nuclear matter experiencing very little attenuation. This phenomenon is known as Color Transparency (CT). An analogous mechanism is well known in QED: the interaction cross section of an electric dipole is proportional to its square size. As a result, the cross section vanishes for objects with very small electric dipole moments. Since color in QCD is equivalent to the charge in QED, the cross section of a color-neutral dipole, as formed by a pair of oppositely colored quarks for instance, is also predicted to vanish for small sized hadrons. Color transparency cannot be explained by Glauber theory and calls upon quark degrees of freedom. Earlier measurements were mainly focused on quasi-elastic hadronic (p, $2p$)[1] and leptonic (e,e'p)[2] scattering from nuclear targets. None of these experiments were able to produce evidence for CT up to $Q^2 \sim 8$ GeV^2. The strongest evidence for CT so far comes from Fermilab experiment E791 on the A-dependence of coherent diffractive dissociation of 500 GeV/c pions into dijets.[3] A recent measurement performed by the HERMES collaboration using exclusive ρ^0 electroproduction from nitrogen adds further evidence for the existence of CT.[4]

The main goal of E02-110 experiment[5] is to search for the onset of CT in the incoherent diffractive ρ^0 electro and photoproduction on deuterium, carbon and copper. In this process, the virtual photon fluctuates into $q\bar{q}$ pair which travels through the nuclear medium evolving from its small initial state with a transverse size proportional to $1/Q$, to a "normal size" vector meson detected in the final state. Therefore, by increasing the value of Q^2 one can squeeze the size of the produced $q\bar{q}$ wave packet. The photon fluctuation can propagate over a distance which is known as the coherence length l_c. The coherence length can be estimated relying on the uncertainty principle and Lorentz time dilatation as $l_c = 2\upsilon/\left(Q^2 + M^2_{q\bar{q}}\right)$, where ν is the energy of the virtual photon and $M_{q\bar{q}}$ is the mass of $q\bar{q}$ pair dominated by the ρ^0 mass in the case of the exclusive ρ^0 electroproduction. What is measured in the reaction is how transparent the nucleus appears to "small size" ρ^0 by taking the ratio of the nuclear per-nucleon (σ_A/A) to the free nucleon (σ_N) cross sections, which is called nuclear transparency $T_A = \sigma_A/A\sigma_N$. Consequently, the signature of CT is an increase in the nuclear transparency T_A with increasing hardness (Q^2) of the reaction. Recent theoretical calculations by Kopeliovich *et al.*,[6] predicted an increase of more than 40% at $Q^2 \sim 4$ GeV^2. However, one should be careful about other effects that can imitate this signal. Indeed, measurements by HERMES have shown that T_A increases when l_c varies from long to short compared to

the size of the nucleus for moderate l_c values. This so-called coherence length effect (CL) can mock the signal of CT and should be under control to avoid confusing it with the CT effect. Therefore, the experiment E02-110 intends to measure the Q^2 dependence of the transparency T_A for small l_c values where no CL effect is expected.

The experiment was performed using the CEBAF Large Acceptance Spectrometer (CLAS)[7] in Hall B at Jefferson Lab. The data were taken with both 4 and 5 GeV electron beams incident on 2 cm liquid deuterium target and a solid target (0.4 mm thick ^{56}Fe and 1.72 mm thick ^{12}C) simultaneously to reduce systematic uncertainties. In these measurements we are interested in the scattered electron and the two pions from the ρ^0 decay in the low t region below 0.5 GeV^2. Figure IV-4 shows the normalized invariant mass of the two charged pions for hydrogen, deuterium and iron. A clean ρ^0 peak is obtained for the three targets. The Q^2 dependence of the pion absorption is found to be of the order of 7%. The background contributing to the ρ^0 peak which is mainly coming from Δ^{++}, Δ^0 and the non resonant background was subtracted using Genova Monte Carlo. The data was also corrected for Radiative corrections using DIFFRAD[8] code. As shown in Fig. IV-5, no CL dependence was found for Fe data. Preliminary results for Fe and C are expected soon.

[1]A. S. Carroll *et al.*, Phys. Rev. Lett. **61,** 1698 (1988); Y. Mardor *et al.*, Phys. Rev. Lett. **81**, 5085 (1998); A. Leksanov *et al.*, Phys. Rev. Lett. **87**, 212301 (2001).
[2]N. C. R. Makins *et al.*, Phys. Rev. Lett. **72**, 1986 (1994); T. G. O'Neill *et al.*, Phys. Lett. **B351**, 87 (1995); D. Abbott *et al.*, Phys. Rev. Lett. **80**, 5072 (1998); K. Garrow *et al.*, Phys. Rev. C **66**, 044613 (2002).
[3]E. M. Aitala *et al.*, Phys. Rev. Lett. **86**, 4773 (2001).
[4]A. Airapetian *et al.*, Phys. Rev. Lett. **90**, 052501 (2003).
[5]JLab experiment E02-110, "Q^2 Dependence of Nuclear Transparency for Incoherent ρ^0 Electroproduction," K. Hafidi, B. Mustapha, and M. Holtrop, spokespersons.
[6]B. Kopeliovich *et al.*, Phys. Rev. C **65**, 035201 (2002).
[7]B. Mecking *et al.*, Nucl. Instrum. Methods **A503/3**, 513 (2003).
[8]I. Akushevich, Eur. Phys. J. C **8**, 457 (1999); Website: www.jlab.org/RC.

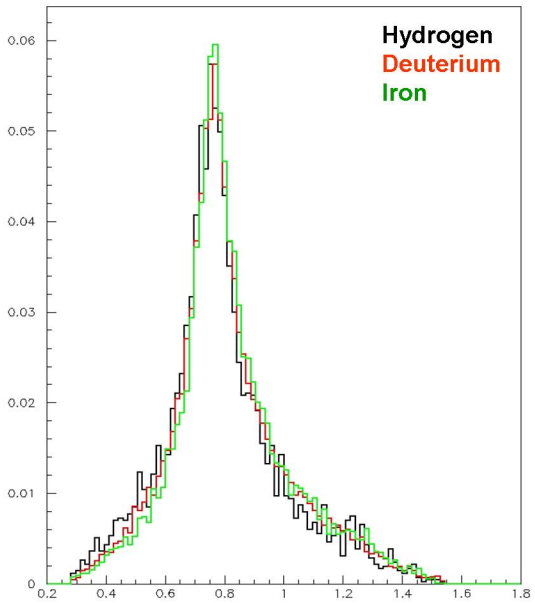

Fig. IV-4. Normalized π^+ π^- invariant Mass for ^{1}H, ^{2}H and ^{56}Fe targets.

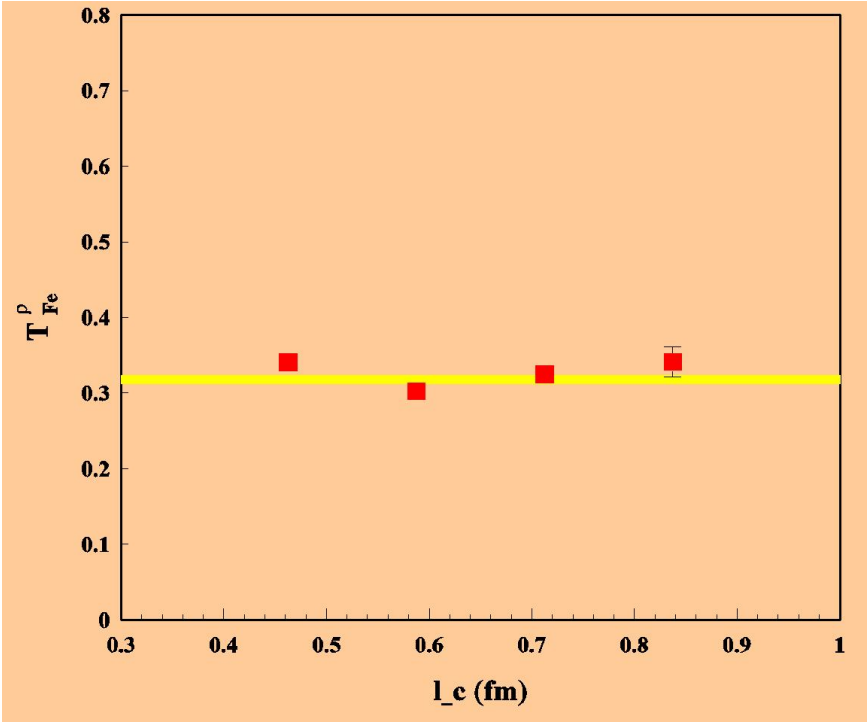

Fig. IV-5. Fe nuclear transparency as a function of l_c for 5 GeV electron beam.

b.3. Study of Color Transparency in Exclusive Vector Meson Electroproduction Off Nuclei: JLab E12-06-106 Experiment (K. Hafidi, J. Arrington, L. El Fassi, D. F. Geesaman, R. J. Holt, B. Mustapha, D. H. Potterveld, P. E. Reimer, and the JLab Hall-B Collaboration)

The nature of hadronic interactions can be investigated *via* tests of the prediction of "color transparency". Color transparency (CT) is one of few direct manifestations of the underlying color degrees-of-freedom in nuclear physics. Under the right conditions, two quarks, each of which (alone) would have interacted very strongly with nuclear matter, could from an object that passes undisturbed through the nuclear medium. A similar phenomenon occurs in QED, where an e^+e^- pair of small size has a small cross section determined by its electric dipole moment. In QCD, a $q\bar{q}$ or qqq system with a small color dipole moment is predicted to have similar reduced interactions due to the cancellation of the color fields of the quarks. Color transparency can be observed experimentally by measuring a reduced attenuation of particles as they exit a nucleus. These transparency measurements will allow us to study the necessary ingredients: formation of small sized configuration, the reduced color interactions of these configurations, and the evolution of these exotic configurations back into ordinary hadrons.

The E12-06-106 experiment[1] is a natural extension of the E02-110[2] experiment performed within CLAS detector using a 5 GeV electron beam. The E02-06-106 experiment will use 11 GeV electron beam and the CLAS12 detector. Its main goal is to study CT in the incoherent diffractive vector meson electroproduction on deuterium, C, Fe and Sn. In this process, the virtual photon with a four momentum Q, fluctuates into $q\bar{q}$ pair which travels through the nuclear medium evolving from its small initial state with a transverse size proportional to $1/Q$, to a "normal size" vector meson detected in the final state. Therefore, by increasing the value of Q^2 one can squeeze the size of the produced $q\bar{q}$ wave packet. JLab 12 GeV upgrade will allow for significant increase in the momentum and energy transfer involved in the reaction. Therefore, one expects to produce smaller configurations that live longer; the optimum parameters for CT studies. Figure IV-6 shows the expected errors bars of the nuclear transparency $T_A = \sigma_A/A\sigma_N$ for Fe target, extending the previous measurements into the very

important higher Q^2 region up to 5.5 GeV^2. The curve is a theoretical calculation by Kopeliovich *et al.*[3] The same accuracy is expected for C and Sn targets.

[1]JLab experiment E12-06-106, "Study of Color Transparency in Exclusive Vector Meson Electroproduction Off Nuclei," K. Hafidi, L. El Fassi, B. Mustapha, and M. Holtrop, spokespersons.
[2]JLab experiment E02-110, "Q^2 Dependence of Nuclear Transparency for Incoherent ρ^0 Electroproduction," K. Hafidi, B. Mustapha, and M. Holtrop, spokespersons.
[3]B. Kopeliovich *et al.*, Phys. Rev. C **65**, 035201 (2002).

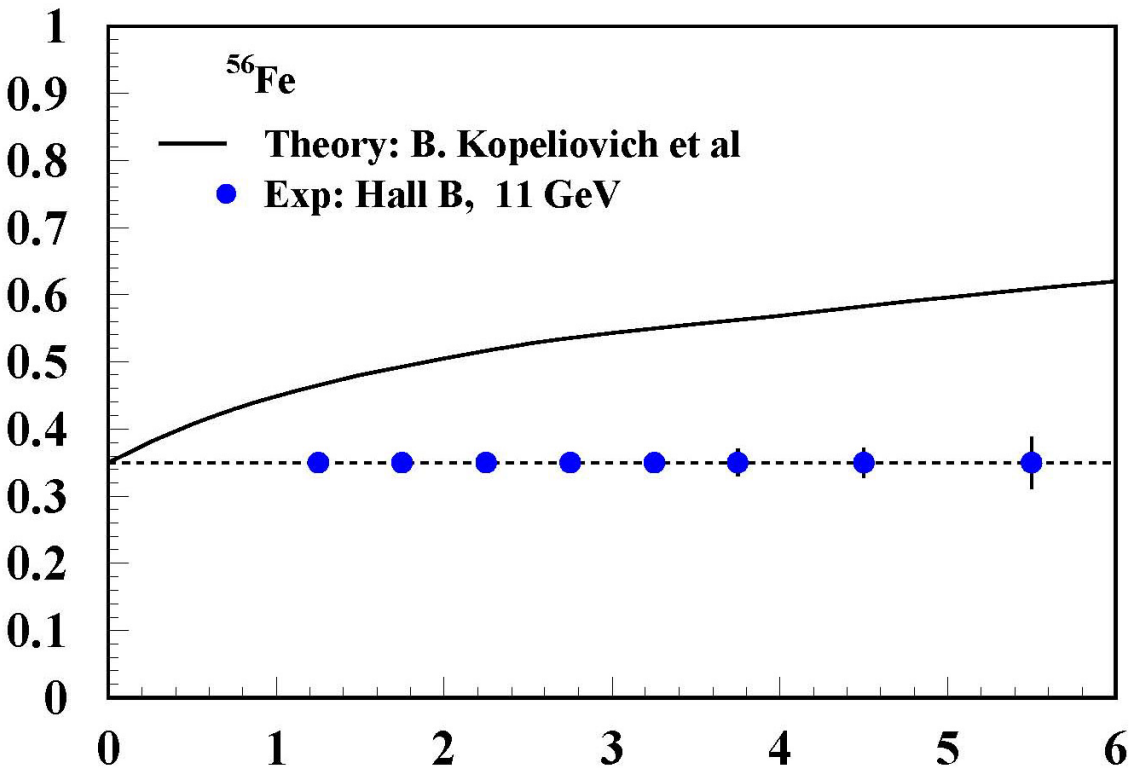

Fig. IV-6. Expected error bars for the Fe nuclear transparency. The solid curve is the model prediction by Kopeliovich et al.[3]

b.4. Search for Color Transparency in Pion Electroproduction (J. Arrington, L. El Fassi, X. Zheng, and the JLab E01-107 Collaboration)

Argonne also participated in an experiment to search for color transparency in pion electroproduction. Measurements were made for the A($e,e'\pi$) reaction from ^{2}H, ^{12}C, ^{63}Cu, and ^{197}Au over a range in Q^2. As with production of vector mesons, color transparency is expected to set at lower Q^2 than in the case of A(e,e'p) measurements, and there is some hint of color transparency in pion photoproduction for similar pion momenta.[1]

Experiment E01-107 was performed at Jefferson Lab Hall C in late 2004. The experiment measured the exclusive electroproduction of pions from nuclei by detecting the scattered electron and the knocked out pions in coincidence. The nuclear transparency is extracted by comparing the pion production from heavy nuclei to that from deuterium. The analysis of the data is complete and the results show a Q^2 dependence that is consistent with color transparency. A draft showing the extracted transparency as a function of A and Q^2 has been completed and is being circulated among the collaboration. A separate paper, detailing the separated structure function and addressing issues related to the pion electroproduction reaction mechanism is also

being circulated.

[1]D. Dutta *et al.*, Phys. Rev. C **68**, 021001 (2003).

b.5. Dynamics of Hadronization from Nuclear Semi-Inclusive Deep-Inelastic Scattering: JLab E02-104 Experiment (K. Hafidi, J. Arrington, L. El Fassi, D. F. Geesaman, R. J. Holt, S. Johnston, G. Larsen, B. Mustapha, D. H. Potterveld, P. E. Reimer, and the JLab Hall-B Collaboration)

Hadronization is the mechanism by which the quark, when ejected from a nucleon neutralizes its color to from many hadrons in the final state. The description of hadronization in terms of fragmentation functions is known in the vacuum, but the physical information on its dynamics is still a mystery. The time-space evolution of the hadron formation is unknown due to the fact that it is a non perturbative process and, therefore, is hard to calculate at the most fundamental level. Unfortunately, Lattice QCD calculations are not yet helpful in this matter. To access this dynamic, the nucleus will play the role of the detector since the production length is comparable with the nuclear size. The nuclear environment provides a unique opportunity to look at the early stage of hadronization a few Fermi from the origin. Therefore, by studying the properties of leading particles emerging from deep inelastic scattering (DIS) on a range of nuclei, important information on the characteristic time distance-scales of hadronization can be determined as a function of several variables.

A primary experimental observable is the hadronic multiplicity ratio:

$$R_M^h(z,\nu,p_T^2,Q^2)=\left\{\frac{N_h^{DIS}(z,\nu,p_T^2,Q^2)}{N_e^{DIS}(\nu,Q^2)}\right\}_A \Bigg/ \left\{\frac{N_h^{DIS}(z,\nu,p_T^2,Q^2)}{N_e^{DIS}(\nu,Q^2)}\right\}_D$$

N_h^{DIS} and N_e^{DIS} denote the number of hadrons and electrons measured in DIS kinematics, ν is the virtual photon energy, $z = E_h/\nu$ is the fraction of the photon energy carried by the hadron, Q^2 is the four-momentum transfer, and p_T is the transverse momentum of the hadron relative to the virtual photon direction. The second experimental quantity is called the transverse momentum broadening $\langle \Delta p_T^2 \rangle = \langle p_T^2 \rangle_A - \langle p_T^2 \rangle_D$, where $\langle p_T^2 \rangle$ is the p_T^2 averaged. The dependence of the multiplicity ratio on several kinematical variables offers a wealth of information on quark propagation in the nuclear medium and hadron formation. Studying the transition from high to low ν dependence is correlated with the transition from quark propagation to hadron propagation in nuclei while the z dependence controls the broadening effects. In addition, the transverse momentum broadening provides valuable information on the parton energy loss which is believed to play an important role in predicting signatures of the quark gluon plasma at RHIC[1] through the phenomenon of jet quenching.[2]

[1]J. Adams *et al.,* (STAR collaboration), Phys. Lett. **B616**, 8 (2005).
[2]Xin-Nian Wang, Phys. Lett. **B579**, 299 (2004).

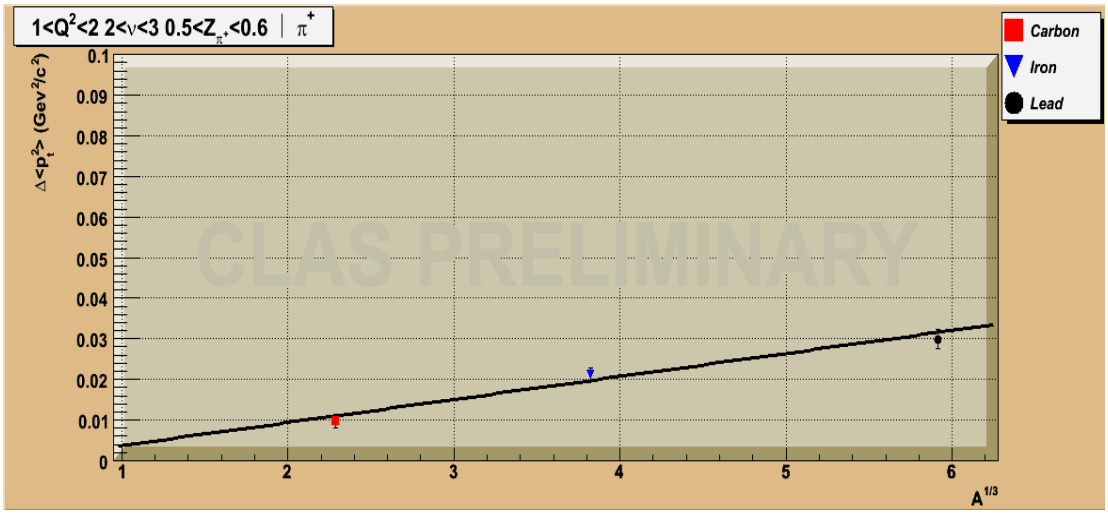

Fig. IV-7. Preliminary π^+ data from CLAS EG2 run for Δp_T^2 vs. $A^{1/3}$ for carbon, iron and lead for one bin in Q^2, z, and ν. The line is a linear fit.

Jefferson Lab offers unique capabilities to study hadron production in DIS. Measurements with the CEBAF Large Acceptance Spectrometer (CLAS) provide data on the widest possible range of nuclear target masses at high luminosity. Data at 5 GeV were taken in 2003 with 10^{34} $cm^{-2}s^{-1}$ luminosity using two targets simultaneously on (the liquid deuterium target and one solid target; alternating between C, Fe and Pb) to reduce systematic errors in the multiplicity ratio. Figure IV-7 shows preliminary π^+ data from the CLAS EG2 experiment at 5.0 GeV. These data are for z from 0.5 to 0.6, Q^2 from 1 to 2 GeV^2 and ν from 2 to 3 GeV. The plot shows a linear behavior of the transverse momentum broadening as a function of the nuclear radius within the statistical uncertainties. These are the first direct and precise measurements of p_T broadening on several nuclei, confirming that the quark energy loss has a quadratic dependence on the quark path length in the nuclear medium in this kinematical regime. This is consistent with the non Abelian analog of the LPM effect in QED.[1] An example of preliminary hadronic multiplicity ratio results is given in Fig. IV-8. The plot is for Q^2 from 1 to 1.25 GeV^2 and ν from 2.2 to 3 GeV for C, Fe and Pb. The high statistics collected in this experiment allow measuring the multiplicity ratio with significantly smaller uncertainties than HERMES experiment.[2]

[1] B. Z. Kopeliovich, J. Nemchik, E. Predazzi, and A. Hayashigaki, Nucl. Phys. **A740**, 212 (2004).
[2] A. Airapetian *et al*., (HERMES Collaboration), Eur. Phys. J. C **20**, 479 (2001).

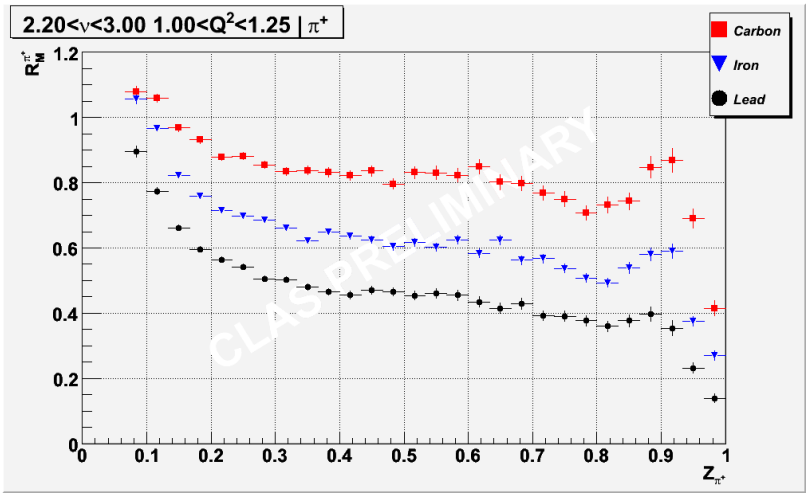

Fig. IV-8. Preliminary data from the CLAS EG2 run for the hadronic multiplicity ratio $R_M^{\pi^+}$ for positive pions in carbon (top), iron, and lead (bottom).

b.6. Quark Propagation and Hadron Formation: JLab E12-06-117 Experiment

(K. Hafidi, J. Arrington, L. El Fassi, D. F. Geesaman, R. J. Holt, S. Johnston, G. Larsen, B. Mustapha, D. H. Potterveld, P. E. Reimer and the JLab Hall-B Collaboration)

The properties of isolated quarks are generally experimentally inaccessible due to quark confinement in hadrons. In hard interactions, such as in deep inelastic scattering, the struck quark in a nucleon must separate from the rest of the residual system. When this separation distance is comparable to nuclear radii, it is possible to study the properties of the propagating quark by varying the radii of nuclear targets and observing modifications of the final hadronic states. The time interval (called the formation time) over which the struck quark transforms into a new hadron can be characterized as a function of multiple variables. This provides completely new information on how the color field of the hadron is restored in real time through the fundamental process of gluon emission. If the formation time is much smaller than the nuclear transit time, then the hadron that carries the struck quark will strongly interact with the nuclear medium. If on the other hand, the formation time is much longer than the nuclear transit time, then the formed hadron will not interact with the nuclear medium. In this way, hadron absorption by nuclei can be used to estimate the time scales of the hadron of the hadronization process. The observable that is used to quantify this absorption is the hadronic multiplicity radio:

$$R_M^h(z,\nu,p_T^2,Q^2)=\left\{\frac{N_h^{DIS}(z,\nu,p_T^2,Q^2)}{N_e^{DIS}(\nu,Q^2)}\right\}_A \Bigg/ \left\{\frac{N_h^{DIS}(z,\nu,p_T^2,Q^2)}{N_e^{DIS}(\nu,Q^2)}\right\}_D$$

N_h^{DIS} and N_e^{DIS} denote the number of hadrons and electrons measured in DIS kinematics, ν is the virtual photon energy, $z = E_h/\nu$ is the fraction of the photon energy carried by the hadron, Q^2 is the four-momentum transfer, and p_T is the transverse momentum of the hadron relative to the virtual photon direction. The second experimental quantity is called the transverse momentum broadening $\langle \Delta p_T^2 \rangle = \langle p_T^2 \rangle_A - \langle p_T^2 \rangle_D$, where $\langle p_T^2 \rangle$ is the p_T^2 averaged. The dependence of the multiplicity ratio on several kinematical variables offers a wealth of information on quark propagation in the nuclear medium and hadron formation. Studying the transition from high to low ν dependence is correlated with the transition from quark propagation to hadron propagation in nuclei while the z dependence controls the broadening effects. In addition, the transverse momentum broadening provides valuable information on the parton energy loss which is believed to play an important role in predicting signatures of the quark gluon plasma at RHIC[1] through the phenomenon of jet quenching.[2]

The E12-06-117 experiment presents a broad program to determine the mechanism of confinement in forming systems. It will use 11 GeV electron beam and CLAS12 detector. From these measurements, the quark production time will be determined and hadron formation times will be extracted for a series of 15 hadrons.

These measurements will provide two to three orders of magnitude more data than any previous measurement in this energy range, and will include a much larger collection of hadron species. The availability of 11 GeV beam in combination with the high rate capability of CLAS12 allows access to the ranges in ν, Q^2 and p_T, that are crucially needed to determine the production time and to isolate the correct physical picture. These data will enable the multi-dimensional analysis that is crucial for discriminating between the competing models for these observables. By producing a high-statistics (see Fig. IV-9), multi-dimensional analysis, the models with the correct physical picture can be validated and significant new information on the mechanism of QCD confinement in forming systems will be obtained.

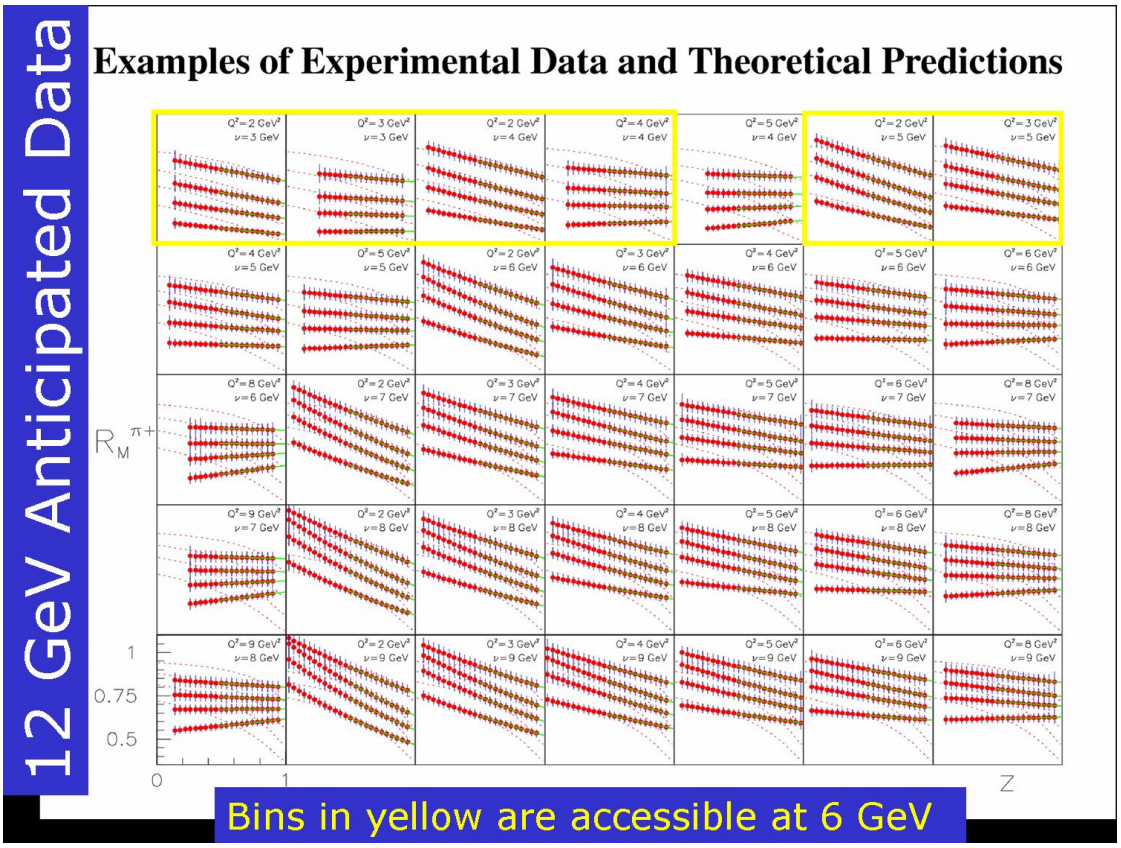

Fig. IV-9. Z dependence of the hadronic multiplicity ratio for (top to bottom in each plot) ^{14}N, ^{40}Ar, ^{84}Kr, ^{197}Au for 35 bins in ν and Q^2. The solid line is a gluon bremsstrahlung model[3] calculation for $z > 0.5$ for pions. The dotted line shows the parameterization based on HERMES 27 GeV data,[4] which is independent of Q^2.

[1]J. Adams *et al.*, (STAR Collaboration), Phys. Lett. **B616**, 8 (2005).
[2]Xin-Nian Wang, Phys. Lett. **B579**, 299 (2004).
[3]B. Z. Kopeliovich, J. Nemchik, E. Predazzi, and A. Hayashigaki, Nucl. Phys. **A740**, 212 (2004).
[4]A. Airapetian *et al.*, (HERMES Collaboration), Eur. Phys. J C **20**, 479 (2001).

b.7. Measurement of High Momentum Nucleons in Nuclei (J. Arrington, L. El Fassi, K. Hafidi, R. J. Holt, D. H. Potterveld, P. E. Reimer, E. C. Schulte, P. Solvignon, X. Zheng, and the JLab E02-019 Collaboration)

Inclusive scattering from nuclei at low energy transfer (corresponding to $x > 1$) is dominated by quasielastic scattering from nucleons in the nucleus. As the energy transfer decreases, the scattering probes nucleons of increasing momentum allowing us to map out the distribution of high momentum nucleons. Because the high momentum nucleons are dominantly generated by short-range correlations (SRCs), these data allow us to examine the strength of two-nucleon and multi-nucleon correlations in heavy nuclei.

Experiment E02-019[1] ran in late 2004 and measured inclusive scattering at large Q^2 over a broad range in x. The high Q^2 values in this experiment should simplify the extraction of the high momentum components, as effects such as final state interactions are reduced at large Q^2. The measurement focused on ^{2}H, ^{3}He, and ^{4}He, but data were also taken on several heavier nuclei. Measurements with few-body nuclei allow contact with theoretical calculations via essentially "exact" calculations for few-body systems. Data on heavy nuclei can then be used to constrain the high momentum components of their spectral functions, as well as allowing an extrapolation to infinite nuclear matter.

We are working with Fritz Coester and T.-S. Harry Lee from the Theory Group to extract information on the neutron structure and nuclear effects on few-body nuclei. With a realistic calculation of the deuteron, a comparison of proton and deuteron results from this and previous high-Q^2 measurements allows one to extract the ratio of neutron to proton cross sections. One can then take this extracted neutron structure function and calculate the ^{3}He and ^{4}He structure functions, both at $x > 1$, which is sensitive to the spectral function used, and for $x < 1$, which tests the nuclear effects in the calculation.

Direct comparisons[2] of heavy nuclei to deuterium at large x will allow us to map out the strength of two-nucleon correlations in both light and heavy nuclei. Just as the ratio of heavy nuclei to deuterium at $x \gtrsim 1.5$ shows that the distribution in heavy nuclei is dominated by two-nucleon correlations, similar ratios of heavy nuclei to ^{3}He at $x \gtrsim 2.5$ provide a measure of the strength of three-nucleon correlations.

Beyond probing nucleon distributions and short-range correlations, these data fill in a significant void in our knowledge of nuclear structure functions. Data at large x are important in the study of scaling and duality in nuclei.[3] In addition, the structure function at $x > 1$ must be included in studies of the energy-momentum sum rule and analysis of the QCD moments.[4]

[1] JLab experiment E02-019, "Inclusive Scattering from Nuclei at x > 1 and High Q^2 with a 6 GeV Beam," J. Arrington, D. B. Day, A. F. Lung, and B. W. Filippone, spokespersons.
[2] J. Arrington, D. B. Day, D. Higinbotham, and P. Solvignon, "Precision Measurements of Scattering from Three-Nucleon Short Range Correlations in Hall A at $1.6 < Q^2 < 1.9$ GeV^2".
[3] J. Arrington, R. Ent, C. E. Keppel, J. Mammei, and I. Niculescu, Phys. Rev. C **73**, 035205 (2006).
[4] I. Niculescu, J. Arrington, R. Ent, and C. E. Keppel, Phys. Rev. C **73**, 045206 (2006).

b.8. Short Range Correlations in Nuclei (J. Arrington, P. Solvignon, and the JLab E01-015 Collaboration)

While inclusive measurements at large x are sensitive to short range correlations in nuclei, previous measurements have been limited. The first extracted ratios from SLAC[1] required combining data from deuterium and nuclear targets from different experiments, requiring interpolation of the cross sections, and increasing the systematic uncertainties compared to direct ratio measurements. Measurements using CLAS[2,3] at Jefferson Lab were able to improve on this, but were only able to take ratios to ^{3}He, and were limited to relatively low Q^2 values. This was the first precision extraction for the ratio in the three-nucleon correlation region, but the Q^2 value was relatively low, and there was no way to determine if these data are in the scaling region.

While E02-019 measured these ratios at higher Q^2 with both deuterium and ^{3}He targets, the data for the highest

x values was somewhat limited. For this experiment, we used short (4 cm) He targets, and the subtraction of the contribution from the Al endcaps becomes very large as one approaches $x = 3$, the kinematic endpoint for scattering from ^{3}He. To improve on this, we submitted an informal proposal[4] for a short measurement in Hall A, designed to run with two to three days of beamtime during the present or upcoming running using the 20 cm ^{3}He targets in Hall A. By reducing the relative contribution from the endcaps and moving to slightly lower Q^2, we should be able to obtain high precision ratios in a minimal amount of time. The experiment was tentatively scheduled to run during the summer of 2007, but delays in the schedule mean that we will most likely have to wait until running later in the year.

While inclusive scattering provides the greatest sensitivity and kinematic range for such measurements, coincidence measurements can provide more detailed information about the structure of the correlations. Another measurements in Hall A at Jefferson Lab used two-nucleon knockout measurements, A(*e,e*'pN), to study the isospin-dependence of the correlations. Initial results for the two-proton knockout channel have been analyzed and submitted.[5] Preliminary results for the comparison of pn to pp channels suggests that the correlations in this kinematic region are strongly dominated by pn correlations, which are a factor of five or more larger than pp SRCs. This was explained in terms of the tensor structure of the two-nucleon interaction.[6] Using the Argonne theory group's variation Monte Carlo calculation for the structure of few-body nuclei, it was shown that the for the region of nucleon momentum probed in the experiment, 300-600 MeV/c, the SRCs are dominated by *n-p* pairs, due to the tensor force which is important for the *n-p* pairs, which largely in deuteron-like states.

[1]L. L. Frankfurt, M. I. Strikman, D. B. Day, and M. Sargsian, Phys. Rev. C **48**, 2451 (1993).
[2]K. Egiyan *et al.*, Phys. Rev. C **68**, 014313 (2003).
[3]K. Egiyan *et al.*, Phys. Rev. Lett. **96**, 082501 (2006).
[4]J. Arrington, D. B. Day, D. Higinbotham, and P. Solvignon, "Precision Measurements of Scattering from Three-Nucleon Short Range Correlations in Hall A at $1.6 < Q^2 < 1.9$ GeV^2".
[5]R. Shneor *et al.*, nucl-ex/0703023 (2007), submitted to Phys. Rev. Lett.
[6]R. Schiavilla *et al.*, Phys. Rev. Lett. **98**, 132501 (2007).

b.9. Mapping Out the Distribution of Super-Fast Quarks in Nuclei (J. Arrington, K. Hafidi, R. Holt, P. Reimer, P. Solvignon, and the JLab E12-06-105 Collaboration)

While previous measurements of inclusive scattering at $x > 1$ at energies up to 6 GeV allow us to study high momentum nucleons and short range correlations, higher energy measurements will allow us to study extremely high momentum quarks, which allow us to study non-hadronic degrees of freedom in nuclei, and look for signs of modification of the internal structure of the nucleons at high density.

A 12 GeV proposal[1] was submitted and approved to PAC30, to extend inclusive measurements at $x > 1$ to higher energy. At these energies, the scattering is no longer dominated by quasielastic scattering from individual nucleons, but by scattering from super-fast quarks. The highest momentum quarks come from the high-*x* quarks in the highest momentum nucleons. These high momentum nucleons are generated by short range *N-N* interactions and in conventional models, the strength above $x = 1.2$ is very small and falls of extremely rapidly. However if there is significant interaction between the quarks in these highly overlapping nucleons, it is much easier for the quarks in the nucleons to share momentum, and the distribution of these super-fast quarks increases dramatically. This is an extremely sensitive way to look for nuclear effects at high density that involve a breakdown of the individual nucleons' identities.

Such modification of the nucleon internal structure has been suggested as a possible explanation (or at least contribution) to the EMC effect. An example of this is the suggestion that a pair of overlapping nucleons spend some fraction of the time in a 6-quark bag, rather than remaining as two separated objects whose internal degrees of freedom (quarks) do not interact. Figure IV-10 shows the calculated structure function for a deuteron assuming that the structure function is simply the convolution of the proton and neutron structure functions (dashed red line), and assuming that there is a 5% contribution from a 6-quark bag state (solid blue line). In the region of the EMC effect, $0.3 < x < 0.9$, the inclusion of the 6q bag contribution

modifies the structure function by at most a few percent (left panel). However, for $x > 1$, the admixture of a 6q bag contribution increases the structure function by an order of magnitude or more (right panel). This behavior is not sensitive only to the presence of a 6-quark component. Any new mechanism by which quarks in the nucleons can directly exchange momentum when the nucleons have significant overlap will yield a significant excess in the distribution of quarks at $x > 1$.

The solid blue points in the right had plot show projected measurements and uncertainties (on the scale of the size of the points) for the 12 GeV measurement. The data will not be entirely in the DIS regime, but we expect to be sensitive to the quark distributions up to $x = 1.2$-1.3 or higher, more than enough to see a significant signal from such non-hadronic components to the nuclear wavefunction.

[1]JLab experiment E12-06-105, "Inclusive Scattering from Nuclei at $x > 1$ in the Quasielastic and Deeply Inelastic Regimes," J. Arrington and D. B. Day, spokespersons.

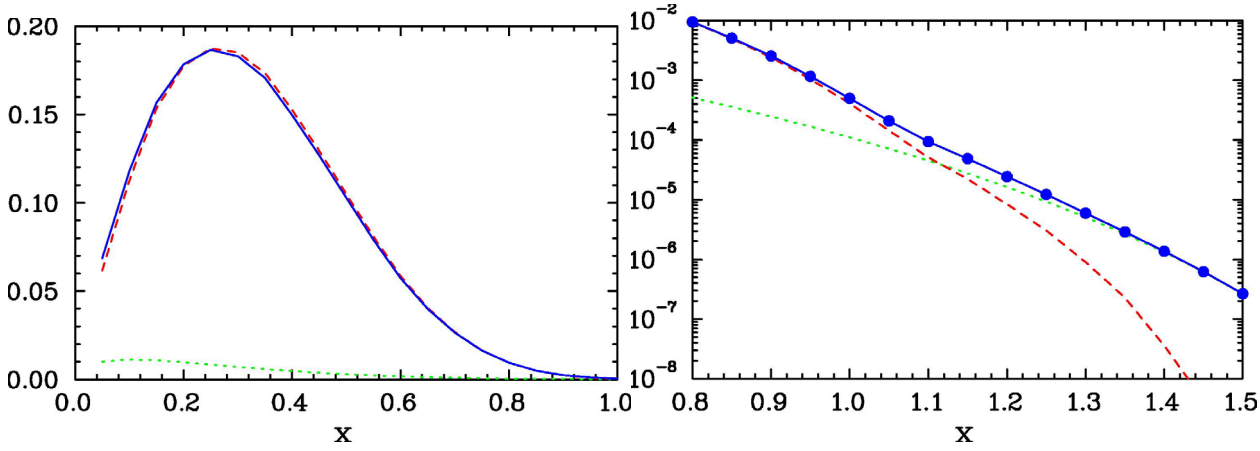

Fig. IV-10. Structure function for deuterium calculated as a convolution of the proton and neutron quark distributions (dashed red line), and with the inclusion of a 5% contribution from a 6-quark bag configuration (solid blue line). The calculated structure function is only for the valence quarks. The dashed green line shows the contribution of the 6-quark bag.

C. QUARK STRUCTURE OF MATTER

c.1. Studies of Nucleon Spin Structure and Related Measurements of Deep-Inelastic Scattering at HERA (H. E. Jackson, A. El Alaoui, K. G. Bailey, T. P. O'Connor, P. E. Reimer, Y. Sanjiev, and the HERMES Collaboration)

With the termination of operations at the HERA accelerator on July 1, 2007, the HERMES experiment will end over a decade of experimental measurements directed at probing the partonic structure of the proton. HERMES, HERA measurement of spin, is an international collaboration of 30 institutions which was formed to address a basic question of hadron structure. How do the spins of its constituent quarks combine with the spin of the glue and the angular momentum of the partons to give the proton its spin of 1/2? The HERMES experiment uses polarized internal targets in the HERA 30 GeV e^+/e^- storage ring at the DESY Laboratory. Although semi-inclusive deep-inelastic scattering (DIS) in which an identified hadron is observed in coincidence with the scattered lepton is emphasized, the program includes measurements of polarized inclusive cross sections which have established a new standard of precision, as well as studies of parton propagation in nuclear matter using data accumulated with unpolarized DIS. The HERMES program has and continues to produce a rich spectrum of new results on the partonic structure of hadrons.

A major milestone in the HERMES program was the completion of a quark-flavor decomposition of the spin of the proton based on measurements of semi-inclusive double spin asymmetries[1] which avoids the need for use of data from hyperon decay and the assumption of SU(3) symmetry. The data provided the first separate determinations of the polarizations of the up, down, and strange quarks. They show that the largest contribution to the nucleon spin comes from the valence region, while contrary to previous indications, the polarizations of the sea quarks are all consistent with zero. To probe the properties of the quark sea in more detail, a novel technique has been developed to measure directly the polarization of the strange quark sea using inclusive and semi-inclusive charged kaons asymmetries for a deuteron target. To increase the sensitivity and precision of the flavor decomposition, HERMES is expanding the database in this analysis to include neutral pions and kaons. A final full flavor decomposition of expanded scope including all HERMES measurements is planned. During the final running period in 2006-2007 HERMES is exploring the possibilities of probing the parton angular momenta by measuring spin asymmetries in hard exclusive reactions which leave the target nucleon intact.

The intense interest in these exclusive processes stems from their description in terms of Generalized Parton Distributions (GPDs) which are expected to provide access to the quark total angular momentum content of the nucleon. HERMES already has studied several exclusive reactions, including exclusive production of charged and neutral pions, and of ρ mesons. Recent measurements of deeply virtual Compton scattering (DVCS) include the first measurements of a beam-charge asymmetry. However, these measurements have been limited by the relatively poor missing mass resolution for real photons which is dominated by the resolution of the HERMES calorimeter. To improve the exclusivity of the events the collaboration decided to install a recoil detector around the storage cell target used in the HERA ring. Construction and installation of the detector was completed in 2006. The commissioning was completed in early 2007, and the remaining beam time until final shutdown is devoted to exploitation of this instrument. It will provide an order of magnitude improvement in resolution, in addition to higher acceptance and background rejection. Exploitation of this new capability is the highest priority for the beam time which remains. The enhanced selectivity of these measurements will provide a unique opportunity to assess the promise of GPDs as the next step in understanding the spin structure of the nucleon.

A major effort continues to study the third structure function, transversity, required to describe nucleon spin structure in leading order. Because it is odd under chirality transformations, it can only be probed by processes involving additional chiral-odd structure, such as chiral-odd fragmentation in semi-inclusive DIS. Data taken during HERA Run II with a transversely polarized target provide access to transversity and probe other effects of transverse motion of the quarks including measurement of the Sivers function which describes distribution of unpolarized quarks as a function of their transverse momentum distribution. This function must vanish in the absence of quark orbital angular momentum. The new data set which

includes results for neutral pions and charged kaons is of much greater statistical precision than that which was the basis for the first observation[2] of the Collins and Sivers asymmetries reported by HERMES.

A unique opportunity to explore a number of topics in unpolarized DIS is provided by dedicated running exclusively for HERMES during the last hour of each fill of the HERA e^+/e^- storage ring. Because the target density is limited during this period only a beam lifetime much shorter than normal, measurements can be made with very high luminosities. Studies of quark propagation in nuclear matter including measurements of the ratio of multiplicities for selected hadron types in heavy targets to those in deuterium continue. Data on the multiplicities measured for proton and deuteron targets currently under analysis provide accurate measurements of quark fragmentation functions specifically at HERMES kinematics, and test factorization. Charged-pion production in semi-inclusive DIS(SIDIS) on hydrogen and deuterium targets has been used to extract the ratio of u valence to d valence quarks in the proton. Hard exclusive electroproduction of charged pions have been measured and their production cross sections compared with predictions of models generated by generalized parton distributions.

The HERA accelerator will continue operations through July 1, 2007. Every effort is being made to maximize the impact of the beam time that remains. Highlights of recent results are presented below.

[1]A. Airapetian *et al.*, Phys. Rev. D **71**, 012003 (2005).
[2]A. Airapetian *et al.*, Phys. Rev. Lett. **94**, 012002 (2005).

c.1.1. Commissioning and Operation of the HERMES Recoil Detector (H. E. Jackson, A. El Alaoui, K. G. Bailey, T. P. O'Connor, P. E. Reimer, Y. Sanjiev, and the HERMES Collaboration)

The partonic structure of the nucleon has been traditionally described in terms of Parton Distribution Functions (PDFs) of the parton's momentum as a function of the nucleon's "infinite momentum". In the context of the rapid theoretical developments of the last decade, PDFs have been subsumed within Generalized Parton Distributions (GPDs) which relate directly to exclusive processes that involve at least one additional vertex, yet leave the target nucleon intact. PDFs and nucleon elastic form factors appear as kinematic limits and moments of GPDs, respectively. Strong interest in the formalism of GPDs and their experimental constraint emerged when GPDs were found to possess properties related to the total (including orbital) angular momentum carried by the quarks in the nucleon. Exclusive deep virtual Compton scattering (DVCS) is the simplest example of a reaction which is described by GPDs. Certain measurable asymmetries attributed to the interference between DVCS and Bethe Heitler processes provide constraints on GPDs. HERMES has already measured transverse-target-spin azimuthal asymmetries for the first time. By comparing the results with model calculations using GPDs it has been possible to place model-dependent constraints on the total angular momentum carried by the quarks.

However, the energy resolution for the electrons/positrons and the photons of the existing HERMES spectrometer is not sufficient to isolate a clean sample of the exclusive process, and the spectrometer has no acceptance for the detection of the recoil particles at large angles. To alleviate these limitations, a recoil detector has been designed to upgrade the spectrometer to study specifically exclusive DVCS. Its objectives are positive identification of recoiling protons, measurement of the momenta of these particles to improve the resolution of the transverse momentum, and improved rejection of non-exclusive background events. The detector is shown in Fig. IV-11. It consists of three components: a silicon detector surrounding the target cell inside the beam vacuum, a scintillating fiber tracker and a photon detector with three layers of tungsten and scintillator bars in three different orientations. All three detectors are located inside a solenoidal magnet which provides a 1 T longitudinal magnetic field to trap beam generated low energy electrons. The detector was installed and commissioned in 2006 and has been in routine operation since September of 2006. Data taking will continue until the HERA shutdown on July 1, 2007.

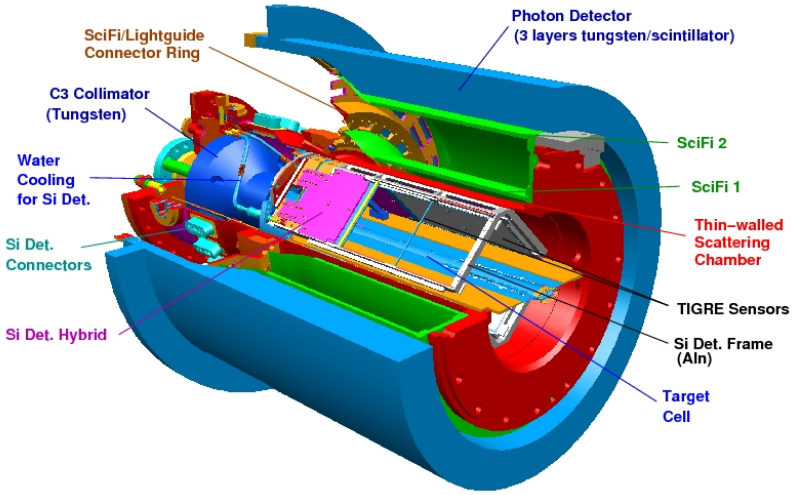

Fig. IV-11. Schematic overview of the HERMES Recoil Detector.

c.1.2. Strange Quark Parton Distributions in the Proton from Semi-Inclusive Deep-Inelastic Scattering on the Deuteron (H. E. Jackson, A. El Alaoui, K. G. Bailey, T. P. O'Connor, P. E. Reimer, Y. Sanjiev, and the HERMES Collaboration)

The internal structure of the nucleon is embodied in parton distributions of its constituent quarks and gluons. The spin-averaged parton distribution functions (PDFs) $q(x)$ of quarks and antiquarks of flavors $q = (u,d,s)$ describe the parton momentum distributions, where x is the dimensionless Bjorken scaling variable representing the momentum fraction of the target carried by the parton in the frame where the target has "infinite" momentum. They are sums of the number densities of the partons, $q(x) = q^+(x)\ [q^-(x)]$, with their spins in the same [opposite] direction as the nucleon. The differences, or helicity distributions, $\Delta q(x) = q^+(x) - q^-(x)$ describe the flavor dependent contributions of the constituent partons to the spin of the nucleon. The features of the parton distributions reflect the QCD dynamics of the constituents at the confinement scale. Strange quarks are of special interest as purely sea objects which reflect directly properties of the nucleon sea.

In the absence of significant experimental constraints, current global QCD analyses of PDFs assume the strange quark and antiquark momentum distributions $s(x)$ and $\bar{s}(x)$ to be given by $s(x) = \bar{s}(x) = r[\bar{u}(x) + \bar{d}(x)]/2$ with $r \approx 1$ at some low factorization scale. Much of the information on the helicity distributions of strange quarks is based on analysis of inclusive deeply inelastic scattering (DIS) and hyperon decay under the assumption of SU(3) symmetry among the structures of the octet baryons. In these inclusive experiments the first moment of the helicity distribution for strange quark was one of the principal results. The strange quark sea was observed to have a substantial negative polarization. The violation of the Ellis-Jaffe sum rule, a characteristic feature of the inclusive experiments was attributed to this negative polarization. In contrast to the inclusive measurements, recent data from semi-inclusive DIS at HERMES[1] suggest that the strange sea is unpolarized. A full 5 flavor decomposition using data from proton and deuteron targets, although not sensitive to the $\Delta\bar{s}(x)$, yielded $\Delta s = 0.028 \pm 0.033 \pm 0.009$ for the first moment of the strange quark helicity density. A separate extraction from DIS data on the deuteron alone gave $\Delta s + \Delta\bar{s} = 0.129 \pm 0.042 \pm 0.129$ where the large systematic error reflected lack of knowledge of kaon fragmentation functions.

HERMES is carrying out a new isoscalar extraction of both $s(x) + \bar{s}(x)$ and $\Delta s(x) + \Delta\bar{s}(x)$ which is based on data obtained from polarized DIS on a deuterium target. Because strange quarks carry no isospin the strange seas in the proton and the neutron are identical. In the deuteron, an isoscalar target, the fragmentation process in DIS can be described without any assumptions regarding isospin dependent fragmentation. Aside from isospin symmetry between the proton and the neutron, the only symmetry assumed is charge-conjugation invariance in fragmentation. The data for the analysis were recorded with a longitudinally nuclear-polarized deuteron gas target internal to the E = 27.6 GeV HERA

positron storage ring. Scattered beam leptons and coincident hadrons are detected by the HERMES spectrometer. Leptons are identified with an efficiency exceeding 98% and a hadron contamination of less than 1% using an electromagnetic calorimeter, a transition-radiation detector, a preshower scintillation counter and a Cerenkov detector. Charged kaons are identified using a dual-radiator ring-imaging Cerenkov detector. Events were selected subject to the kinematic requirements $Q^2 > 1$ GeV^2, $W^2 > 10$ GeV^2 and $y < 0.85$, where W is the invariant mass of the photon-nucleon system, and $y = \nu/E$. Coincident hadrons were accepted if $0.2 < z < 0.8$ and $x_F \approx 2p_L/W > 0.1$, where p_L is the longitudinal momentum of the hadron with respect to the virtual photon direction in the photon-nucleon center of mass frame.

Analysis of the data is nearly complete. Inclusive and semi-inclusive-charged-kaon spin asymmetries have been analyzed to extract the LO parton distributions of the strange sea in the proton. The partial moment of the non strange fragmentation function needed for the LO analysis has been extracted directly from the same data. The momentum densities are softer than previously assumed. The helicity densities are consistent with zero and the moment octet axial combination is observed to be substantially less than the axial charge extracted from hyperon decays under the assumption of SU(3) symmetry.

[1]A. Airapetian *et al.*, Phys. Rev. D **71**, 012003 (2005).

c.1.3. Inclusive Longitudinal Spin Asymmetries for the Proton and Deuteron

(H. E. Jackson, A. El Alaoui, K. G. Bailey, T. P. O'Connor, P. E. Reimer, Y. Sanjiev, and the HERMES Collaboration)

Using inclusive longitudinal spin asymmetries HERMES has measured the spin structure function $g_1(x,Q^2)$ of the proton and the deuteron in the kinematic range $0.0041 < x < 0.90$ and 0.18 GeV^2 $< Q^2 < 20$ GeV^2. The final result for $g_1(x,Q^2)$ from all data taken with longitudinally polarized hydrogen and deuterium targets is presented in Fig. IV-12, left panel. The statistical precision of the proton data is comparable to that of the hitherto most precise data from SLAC and CERN in the same x range, while the deuteron data provide the most precise determination of $g_1^d(x,Q^2)$ compared to previous measurements. The right panel of Fig. IV-12 shows the integrals of $g_1^{p,d,n,NS}$ over the range $0.021 < x < 0.9$, corresponding to the event selection $Q^2 > 1$ GeV^2, as a function of the low-x limit integration evaluated at $Q_0^2 = 5$ GeV^2 for $x < 0.04$, $g_1^d(x,Q^2)$ becomes compatible with zero and its measured integral shows saturation. Based on the

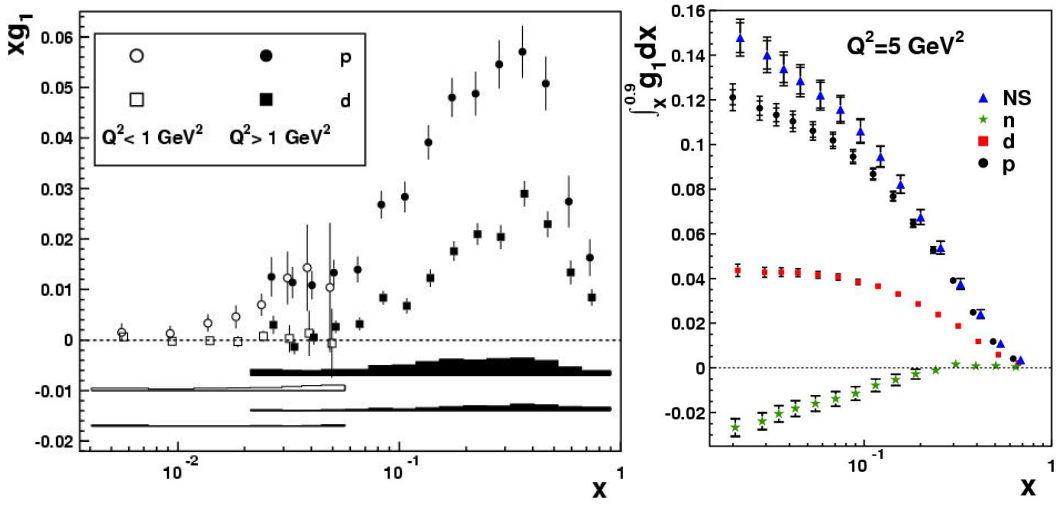

Fig. IV-12. HERMES results for xg_1 vs x for the proton and the deuteron (left) and the integrals of $g_1^{p,d,n,NS}$ over the range $0.021 < x < 0.9$ as a function of the low-x limit of integration.

assumed saturation of the integral of $g_1^d(x,Q^2)$, the flavor-singlet axial charge has been determined in the $\overline{\text{MS}}$ scheme at $Q_0^2 = 5$ GeV^2 using only the integral of $g_1^d(x,Q^2)$ and the axial charge a_8 as inputs giving $a_0 = 0.330 \pm 0.011(\text{theo.}) \pm 0.025(\text{exp.}) \pm 0.028(\text{evol.})$. In this factorization scheme, the result can be interpreted as the contribution $\Delta\Sigma$ of quark spins to the spin of the nucleon. The data, therefore, suggest that the quark helicities contribute a substantial fraction to the nucleon helicity, but there is still a need for a major contribution from gluons and/or angular momentum.

c.1.4. Collins and Sivers Asymmetries for Charged Pions and Kaons with a Transversely Polarized Target (H. E. Jackson, A. El Alaoui, K. G. Bailey, T. P. O'Connor, P. E. Reimer, Y. Sanjiev, and the HERMES Collaboration)

At leading twist, the quark structure of the nucleon is described by three parton distribution functions: the momentum distribution $q(x,Q^2)$, the known helicity distribution $\Delta q(x,Q^2)$, and the unknown transversity distribution $\delta(x,Q^2)$. In the helicity basis, transversity is related to a quark-nucleon forward scattering amplitude involving helicity flip of both nucleon and quark. Because it is chiral-odd it cannot be probed in inclusive measurements. At HERMES transversity in conjunction with the chiral-odd Collins fragmentation function is accessible in azimuthal single-spin asymmetries (SSA) in semi-inclusive DIS in a transversely polarized target. The Collins fragmentation function describes the correlation between the transverse polarization of the struck quark and the transverse momentum of the hadron produced. The Sivers mechanism can also produce a SSA. The T-odd Sivers distribution function describes the correlation between the transverse polarization of the nucleon and the transverse momentum of the quarks within. A non-zero Sivers effect signals a nucleon spin flip without quark helicity flip, which must therefore involve orbital angular momentum inside the nucleon.

HERMES has already published data[1] on a transversely polarized target which allowed extraction of Collins and Sivers moments for charged pions. Measurements with a transversely polarized target allow one to distinguish between the Collins and Sivers processes. The characteristic signature of the Collins (Sivers) effect is a $\sin(\varphi + \varphi_S)$ [$\sin(\varphi - \varphi_S)$] modulation of the cross section in the distribution of the azimuthal angle φ of the pion around the virtual photon direction and relative to the lepton scattering plane, and φ_S, the angle between the scattering plane and the transverse spin component of the target nucleon. In the years 2002-2005 HERMES has taken data with a transversely polarized target. The azimuthal asymmetries are evaluated in two dimensions (φ and φ_S) and the amplitudes for the Collins and Sivers processes were extracted simultaneously. Preliminary results for charged pions and kaons, based on the data taken in the years 2002-2004 which correspond to about 30% of the total statistics and supersede the published result[1] are shown in Fig. IV-13. The average Collins amplitude is positive for π^+ and negative for π^- with a magnitude for π^- comparable to or larger than the one for π^+. One explanation could be a substantial magnitude for the disfavored Collins fragmentation function with an opposite sign to the favored one. These non-zero Collins asymmetries provide clear evidence for the existence of both the transversity distribution and the Collins fragmentation function. The significant positive Sivers amplitudes for π^+ and K^+ provide the first evidence for a *T*-odd parton distribution function in leptoproduction and imply a non-vanishing orbital angular momentum of the quarks inside the nucleon.

[1] A. Airapetian *et al.*, Phys. Rev. Lett. **94**, 012002 (2005).

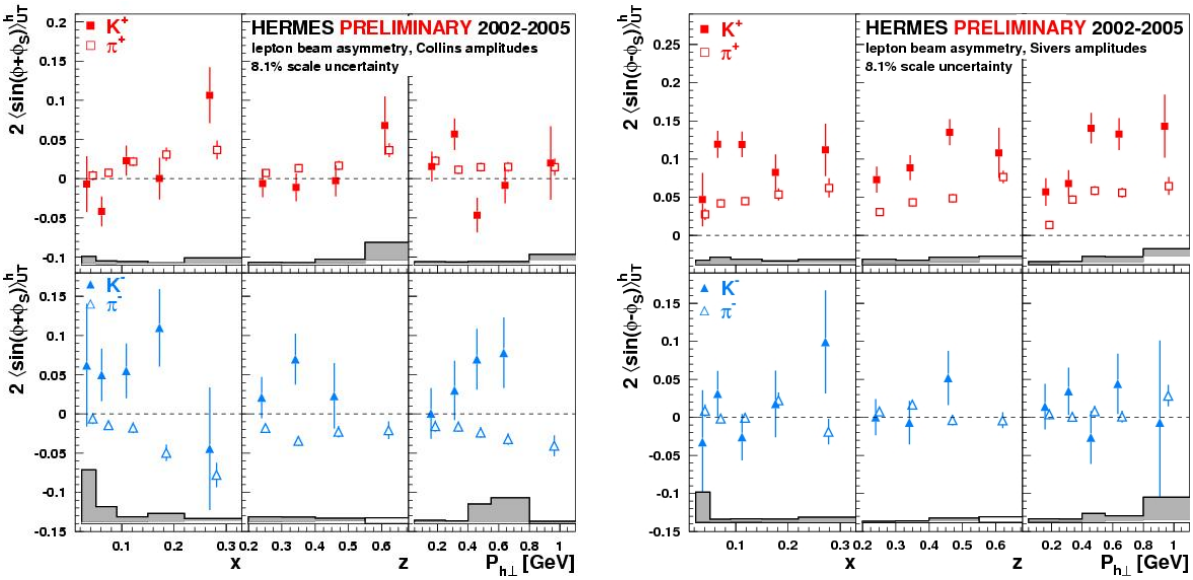

Fig. IV-13. Measured Collins moments (left) and Sivers moments (right) of charged pions and kaons obtained with a transversely polarized target. The error band represents the maximal systematic uncertainties in the measurement.

c.1.5. Transverse Target-Spin Asymmetries in Deeply-Virtual Compton Scattering at HERMES (H. E. Jackson, A. El Alaoui, K. G. Bailey, T. P. O'Connor, P. Reimer, Y. Sanjiev, and the HERMES Collaboration)

An exciting new field has opened with measurements of hard exclusive production of mesons and real photons (Deep Virtual Compton Scattering, DVCS). The parton correlation functions (known as Generalized Parton Distributions, GPDs) accessible in these processes are related to the total angular momentum of the quarks contributing to the spin of the nucleon. Thus, with prior knowledge of the spin contribution of the quarks from other experiments, the orbital angular momentum carried by the quarks may become accessible. Such studies appear to mark a major advance in unraveling the spin structure of the nucleon. DVCS provides the cleanest access to GPDs. DVCS amplitudes can be determined through a measurement of the interference between the DVCS and Bethe Heitler (BH) processes, in which the photon is radiated from a parton and from the lepton, respectively. Measuring the φ-dependence of a cross section asymmetry with respect to the charge (spin) of the lepton beam provides information about the real (imaginary) part of the DVCS amplitude.

HERMES has already measured azimuthal asymmetries with respect to the beam helicity,[1] and to the target helicity[2] and w.r.t. the beam charge.[3] New results have been obtained for the beam-spin asymmetry measured on nuclear targets. A very exciting observable is the DVCS transverse target-spin asymmetry (TTSA) shown in Fig. IV-14 as obtained from the HERMES data accumulated in 2002-2004 using a transversely polarized hydrogen target. This asymmetry provides direct access to the total angular momentum $J_{u,d}$ within a certain GPD model that parameterizes the GPDs using J_u and J_d as free parameters. In this particular GPD model, the data favor a non-zero value of J_u of order of 0.4 assuming $J_d = 0$.

[1]HERMES Collaboration, A. Airapetian *et al.*, Phys. Rev. Lett. **87**, 182001 (2001).
[2]M. Kopytin (for the HERMES Collaboration), AIP Conf. Proc. **792**, 424-427 (2005).
[3]HERMES Collaboration, A. Airapetian *et al.*, hep-ex/0605108.

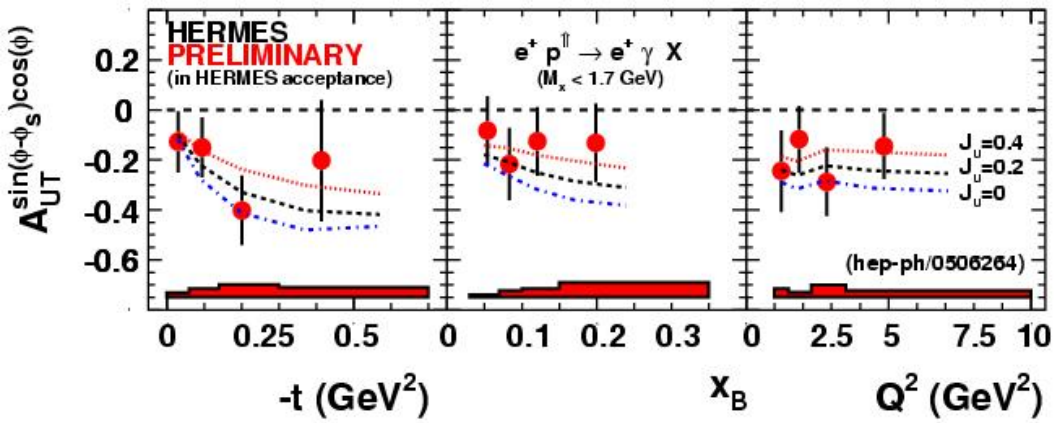

Fig. IV-14. HERMES results for the transverse target asymmetry in DVCS compared to GPD model calculations (see text)

c.1.6. Determination of the Gluon Polarization from High-p_T Hadron Electroproduction

(H. E. Jackson, A. El Alaoui, K. G. Bailey, T. P. O'Connor, P. Reimer, Y. Sanjiev, and the HERMES Collaboration)

A direct model dependent extraction of $\Delta g/g$ has been performed by studying charged hadron production at large transverse momenta p_T relative to the direction of the virtual photon. The high statistics data sample of antitagged (vetoed by the beam particle) inclusive charged hadrons was used. To relate the measured longitudinal double-spin asymmetry to the gluon polarization $\Delta g/g$, information on the relative contributions of the various subprocesses to the inclusive hadron production cross section, their asymmetries and variation with p_T was obtained from detailed Monte Carlo simulation using Pythia 6.2 and parameterizations of the spin dependent parton distributions of the nucleon and the photon. This information is used to obtain the signal asymmetry which still contains a convolution of $\Delta g(x)/g(x)$ with the hard subprocess cross section. Two methods have been applied to extract the average $\langle \Delta g/g \rangle (p_T)$ from the signal asymmetry using different assumptions on the shape of $\Delta g(x)/g(x)$. Method I assumes that $\Delta g(x)/g(x)$ is constant in the measured range of x while Method II employs a functional form for $\Delta g(x)/g(x)$. A value of $\Delta g/g = 0.071 \pm 0.034$ (stat.) ± 0.010 (sys-exp) ± 0.127 (sys-models) has been obtained for $\langle x \rangle = 0.22$ and $\langle \mu^2 \rangle = 1.35$ GeV^2. This result is shown in Fig. IV-15 together with previous determinations of $\Delta g/g$ and is compared there with several different parameterizations obtained from NLO-QCD fits. The data favor a very small $\Delta g/g$ or one with a node near $x \approx 0.1$.

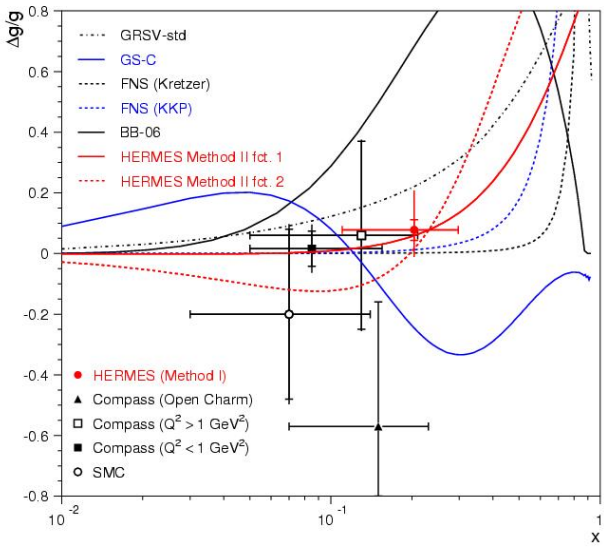

Fig. IV-15. HERMES results for Δg/g compared with a compilation of world data. The curves represent two fit functions from Method II (see text) and the results of several NLO-QCD fits.

c.1.7. Hadronization in Semi-Inclusive Deep-Inelastic Scattering on Nuclei (H. E. Jackson, A. El Alaoui, K. G. Bailey, T. P. O'Connor, P. Reimer, Y. Sanjiev, and the HERMES Collaboration)

A series of semi-inclusive deep-inelastic scattering measurements on deuterium, helium, neon, krypton, and xenon targets has been performed in order to study quark hadronization. The data were collected with the HERMES detector at the DESY HERA accelerator using a 27.6 GeV positron or electron beam. Hadron multiplicities on nucleus A relative to those on the deuteron R^h_A were determined for pions, kaons and protons of all charges as a function of the virtual-photon energy υ, the fraction of this energy transferred to the hadron z, the photon virtuality Q^2, and the hadron transverse momentum squared p_T^2. The data reveal a systematic decrease of R^h_A with the mass number A for each hadron type h. Furthermore, R^h_A increases (decreases) with increasing values of $\upsilon(z)$, increases slightly with increasing Q^2, and is almost independent of p_T^2, except at large values of p_T^2. For pions two-dimensional distributions have also been obtained. These indicate that the dependences of R^π_A on υ and z can largely be described as a dependence on a single variable L_c, which is a combination of υ and z. The dependence on L_c suggests in which kinematic conditions partonic and hadronic mechanisms may be dominant. The behavior of R^π_A at large p_T^2 constitutes tentative evidence for a partonic energy-loss mechanism. The A-dependence of R^h_A has also been investigated as a function of υ,z, and L_c. It follows approximately an A^α with $\alpha \approx 0.5$-0.6. A report of this work is in press (Nucl. Phys. B).

c.2.1. Drell-Yan Measurements with 120 GeV Protons, FNAL E906 (P. E. Reimer, D. F. Geesaman, J. Arrington, K. Hafidi, R. J. Holt, D. H. Potterveld and the FNAL E906 Collaboration)

Although many of the properties of the proton may be attributed to its three valence quarks, it is, in fact, much more complicated, with over 50% of its momentum carried by the non-valence (sea) quarks and gluons. To

understand the structure of the proton, it is necessary to understand the sea quarks, their origins and their interactions with the gluons that bind the proton together. The Fermilab E906 experiment is specifically designed to use Drell-Yan scattering to probe the sea quarks of the proton.[1,2]

The Drell-Yan mechanism provides a powerful tool to study the structure of the proton at the quark level. In Drell-Yan scattering a quark (or antiquark) in the proton beam annihilates with an antiquark (or quark) in the target, resulting in the production of a virtual photon that decays into a pair of leptons, which are detected in the spectrometer. The kinematics of the detected leptons can be used to select interactions between beam valence quarks and target antiquarks. This was successfully exploited by Fermilab E866/NuSea using an 800 GeV/c proton beam provided new insight into the antiquark sea in the proton[3,4] and nuclear dependence phenomena.[5] Fermilab E906 has been approved by Fermilab to extend Drell-Yan measurements to larger values of Bjorken-x using the new 120 GeV Main Injector at Fermilab.

Vacuum polarization accounts for the creation of a flavor symmetric sea. Previous E866 Drell-Yan data, however, exhibit a large asymmetry between $\bar{d}$ and $\bar{u}$ for $x < 0.25$, clearly indicating a non-perturbative origin to the sea. Above $x > 0.28$ these data, albeit with poor statistical uncertainty, indicate the ratio $\bar{d}/\bar{u}$ returns to unity. This result dramatically changed the sea quark parton distribution fits and was completely unpredicted by meson cloud and other non-perturbative models. The return of $\bar{d}/\bar{u}$ to unity clearly signals a change in the mechanism by which the sea is generated.[3,4,6] The current parton distributions now reproduce the previous Drell-Yan data for $0.28 < x < 0.3$, but parameterize $\bar{d}/\bar{u} < 1$ as x increases above 0.3. This is not expected by *any* models of the proton and is simply indicative of the complete lack of data. Fermilab E906 will determine $\bar{d}/\bar{u}$ and $\bar{d} - \bar{u}$ for $0.1 \leq x \leq 0.45$, encompassing the non-perturbative region and extending well into the region where the sea appears to return to symmetry, as shown in Fig. IV-16.

Very little is known about the regime in which only one parton carries much of proton's momentum – different theoretical treatments prescribe different behaviors as $x \rightarrow 1$ and very little data is available to serve as a guide. Through the partons in the beam proton, Fermilab E906 will access these distributions. The Drell-Yan cross section is dominated by the distribution of $4u(x) + d(x)$ as $x \rightarrow 1$. E906 will extend the data provided by Fermilab E866 to higher x and provide much more precise *proton* data than is currently available.

Models based on the hypothesis that nuclear binding in governed by the exchange of mesons have been used to quite successfully describe the nuclear force. Given the success of these models, it is natural to look for direct experimental evidence for the presence of these mesons in nuclei. Thus far, however, no direct evidence has been found.[7] If present, these mesons will lead to an enhancement of antiquarks in the nucleus. Drell-Yan is ideally suited to measure this enhancement. Fermilab E906 will collect data using nuclear targets, in addition to hydrogen and deuterium to look for these effects.

From deep inelastic scattering (DIS) experiments, we know that the quark level structure of a nucleon with in a nucleus *is* different from that of a free nucleon. In the range $0.10 < x < 0.25$, a surplus of quarks (approximately 2-4%) in nuclei, known as antishadowing, is clearly observed in DIS data. To understand these phenomena, it is important to determine if it is a general property of the quark and antiquark distributions, or just a property of the valence or sea quarks. Drell-Yan, with its ability to measure sea-only quark effects, is the ideal reaction in which to measure this. Early Drell-Yan data indicate that this surplus might not be present[7] but with poor statistical uncertainty (3-5%). Fermilab E906's measurements will clearly determine if there is antishadowing in the sea, with statistical uncertainties of less than 1% throughout this region (see Fig. IV-16).

Using the same nuclear target data, Fermilab E906 will also study the propagation of colored partons in strongly interacting, cold nuclear matter. By comparing the Drell-Yan yields from different nuclear targets and looking for apparent shifts in the beam parton's momentum distributions between nuclei, E906 will be able to measure the beam parton's energy loss. Previous Drell-Yan studies have placed upper limits on parton energy loss.[8] With increased sensitivity from the 120 GeV beam and better statistical accuracy, Fermilab E906 will turn these upper limits into measurements. These measurements will aid in the understanding of jet suppression data from RHIC.

FNAL E906 is able to make these improvements over previous measurements because of the lower beam energy available at the Fermilab Main Injector. For fixed x_{beam} and x_{target} the cross section scales as the inverse of the beam energy. Thus a factor of seven more events for the same integrated luminosity can be achieved. At the same time, the primary background to

the measurement, muons from J/ψ decays, decreases with decreasing beam energy, allowing for an increase in instantaneous luminosity by another factor of seven. These two factors combine to provide roughly 50 times more events for the same beam time.

FNAL E906 has been approved by the Fermilab PAC and will begin collecting data in late 2009. Much of the reconfigured spectrometer will come from detector elements recycled from the E866 Drell-Yan spectrometer. To increase the rate and triggering capabilities of the spectrometer, some new detectors will be fabricated. In addition, because of the significantly different kinematics of the 120 GeV experiment, the new spectrometer will require new coils to be fabricated for the first magnet in the spectrometer to focus the Drell-Yan muons. Current efforts are focused on the design of the coils of the new magnet, which is almost complete.

[1]J. Arrington *et al.,* (Fermilab E906 Collaboration), "Drell-Yan Measurements of Nucleon and Nuclear Structure with the Fermilab Main Injector: E906," Proposal Update to the Fermilab PAC, September 29, 2006.
[2]L. D. Isenhower *et al.,* (Fermilab E906 Collaboration), "Proposal for Drell-Yan Measurements of Nucleon and Nuclear Structure with the FNAL Main Injector," Proposal to the Fermilab PAC, April 1, 2001.
[3]E. A. Hawker *et al.,* (Fermilab E866/NuSea Collaboration), Phys. Rev. Lett. **80**, 3715 (1998).
[4]R. S. Towell *et al.,* (Fermilab E866/NuSea Collaboration), Phys. Rev. D **64**, 05202 (2001).
[5]M. J. Leitch *et al.,* (Fermilab E866/NuSea Collaboration), Phys. Rev. Lett. **84**, 3256 (2000).
[6]J.-C. Peng *et al.,* (Fermilab E866/NuSea Collaboration), Phys. Rev. D **58** 092004 (1998).
[7]D. M. Alde *et al.,* Phys. Rev. Lett. **64**, 2479 (1990).
[8]M. A. Vasiliev *et al.,* (Fermilab E866/NuSea Collaboration), Phys. Rev. Lett. **83**, 2304 (1999).

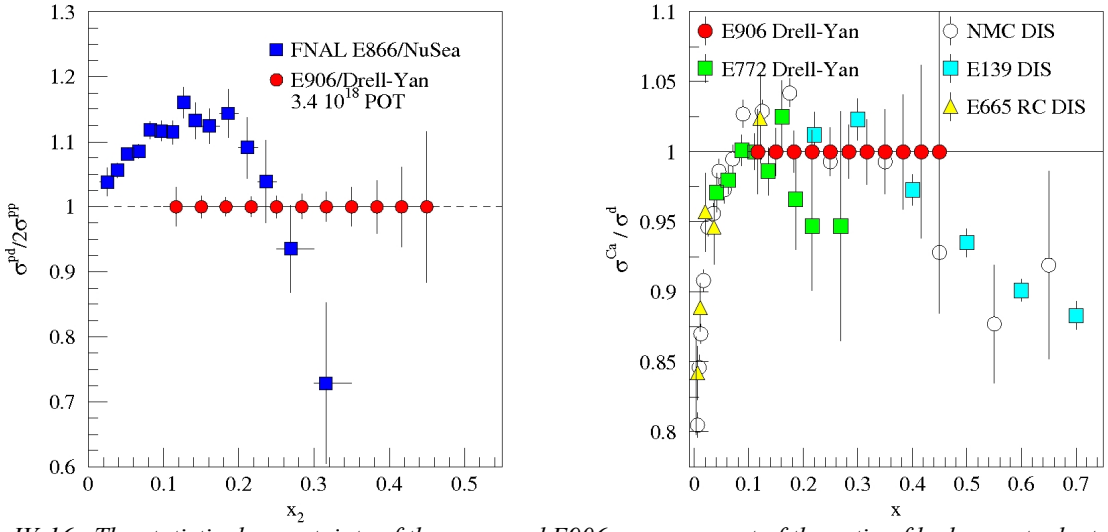

Fig. IV-16. The statistical uncertainty of the proposed E906 measurement of the ratio of hydrogen to deuterium cross sections (arbitrarily plotted at 1) compared with the E866 measurements of the same quantity (left). The statistical uncertainty of E906's measurement of the ratio of deuterium to Calcium cross sections (arbitrarily plotted at 1) compared with previous Drell-Yan and deep inelastic scattering (DIS) measurements (right).

c.2.2. Measurement of the Drell-Yan Angular Distributions (P. E. Reimer, D. F. Geesaman, S. B. Kaufman, N. C. R. Makins, B. A. Mueller and the FNAL E866/NuSea Collaboration)

In leading order QCD, the Drell-Yan process is the annihilation of a quark-antiquark pair into a virtual photon. The virtual photon then decays into a lepton-antilepton pair that is detected. The general expression for the angular distribution for Drell-Yan scattering is given by

$$d\sigma \sim 1 + \lambda \cos^2\theta + \mu \sin 2\theta \cos\varphi + \upsilon/2 \sin^2\theta \cos 2\varphi.$$

Theoretically, for massless quarks or a transversely polarized virtual photon in a reference frame with θ defined relative to the quark-antiquark annihilation axis, $\lambda = 1$ and $\mu = \upsilon = 0$. More generally, in any reference frame, the Lam-Tung rule, $1 - \lambda = 2\upsilon$, is expected to hold.

Experimentally, these angular distributions have only been studied in pion-induced Drell-Yan scattering experiments using nuclear targets. In both cases, the data indicate the Lam-Tung rule is violated and sizeable $\cos 2\varphi$ contributions to the angular distributions were observed. These results were more pronounced at large transverse momentum (p_T).

We have studied 800 GeV proton-induced Drell-Yan data collected by Fermilab E866/NuSea. The angular distributions from these data reveal no significant $\cos 2\varphi$ dependence, and within statistical uncertainties, the Lam-Tung sum rule is valid.[1] The lack of any observed effect can be used to constrain the *sea-quark* transverse-momentum-dependent Boer-Mulders structure function $h_1^{\perp}$. We are also studying the possibilities of more precise measurements of the angular distributions with future Drell-Yan experiments such as Fermilab E906.

[1]L. Zhu *et al.,* (E866/NuSea Collaboration), "Measurement of Angular Distributions of Drell-Yan Dimuons in $p + d$ Interactions at 800 GeV/c," submitted to Phys. Rev. Lett., arXiv: hep-ex/0609005.

c.3. 12-GeV Proposal to Determine the d/u Ratio in the Proton at High *x* (R. J. Holt, D. F. Geesaman, J. Arrington, K. Hafidi, R. J. Holt, D. H. Potterveld, and the JLab Hall A Collaboration)

A proposal was presented to the first 12-GeV JLab PAC to perform deep inelastic scattering from the ^{3}H and ^{3}He mirror nuclei.[1] The proposed experiment will provide first measurements of the EMC effect in ^{3}H, a determination of the ratio of the neutron to proton inelastic structure functions, and the ratio of the down to up quark distributions in the proton at relatively large Bjorken *x*. The F_2^n/F_2^p ratio will be extracted from the measurement of the inelastic cross section ratio of the two mirror nuclei. This ratio is expected[2] to be nearly free of nuclear effects, which have plagued previous extractions from deuteron structure function data. The d/u ratio at high *x* is particularly sensitive to the underlying quark structure of the nucleon.[3] These data will provide a stringent test of non-perturbative QCD-based models of the nucleon. The nucleon structure function data at high *x* are also essential to understand the QCD background expected at high-energy colliders such as the LHC. The expected data quality from this proposed experiment are indicated in Fig. IV-17.

Experiment E12-06-018 was conditionally approved by the JLab PAC 30. The condition was essentially a successful safety review of the tritium target design. Efforts are underway to design a safe 5000 Ci cooled-gas tritium target for this experiment.

[1]G. G. Petratos *et al.*, (JLab MARATHON Collaboration), "Measurement of the F2n.F2p, d/u Ratios, and A = 3 EMC Effect in the Deep Inelastic Scattering from the Tritium and Helium Mirror Nuclei", JLab PR12-06-118.
[2]I. R. Afnan *et al*., Phys. Rev. C **68**, 35201 (2003).
[3]N. Isgur, Phys. Rev. D **59**, 34013 (1999); S. J. Brodsky, M. Burkardt, and I. Schmidt, Nucl. Phys. **B441**, 197 (1995); W. Melnitchouk and A. W. Thomas, Phys. Lett. **B377**, 11 (1996).

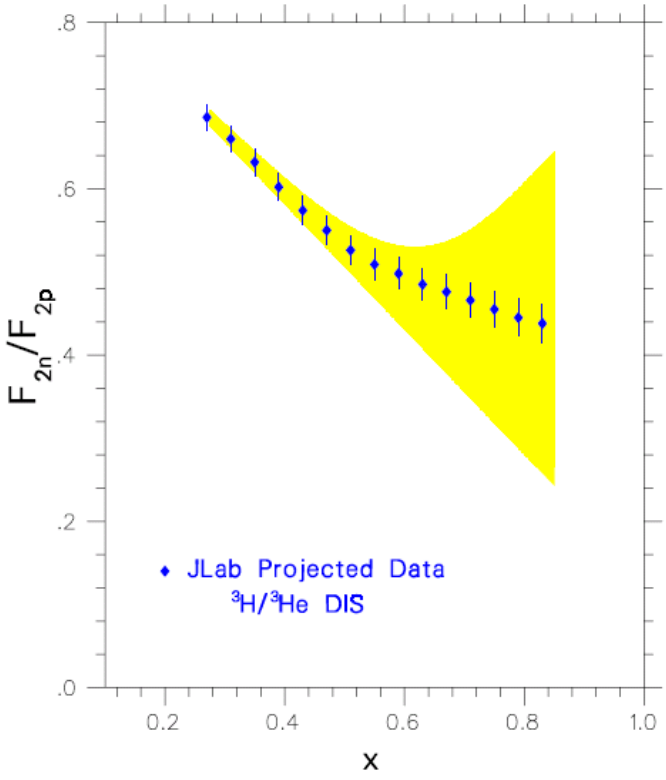

Fig. IV-17. Expected data for the ratio as a function of Bjorken x. The yellow band indicates the present uncertainty in the ratio from previous extraction of the ratio from deep inelastic scattering data from the proton and the deuteron.

D. FUNDAMENTAL SYMMETRIES IN NUCLEI

d.1. Laser Trapping of the Octupole-Deformed ^{225}Ra with Repumping by Black-Body Radiation (J. R. Guest, I. Ahmad, K. Bailey, J. P. Greene, R. J. Holt, Z.-T. Lu, T. P. O'Connor, and J. W. Wang)

Permanent electric dipole moments (EDMs) in atoms or molecules are a signature of Time (T)-and Parity (P)-violation and represent an important window onto physics beyond the Standard Model. We are developing a next-generation EDM search around laser-cooled and -trapped ^{225}Ra ($t_{1/2}$ = 15 d) atoms. Due to octupole deformation of the nucleus, ^{225}Ra is predicted to be two to three orders of magnitude more sensitive to T-violating interactions than ^{199}Hg (stable), which currently sets the most stringent limits in the nuclear sector. The scheme is to collect ^{225}Ra atoms in a magneto-optical trap (MOT), and then transfer the sample to an optical dipole trap where the atoms will be polarized by optical pumping and the EDM measurement will be performed.

In 2005, we showed for the first time that radium atoms can be laser-cooled and trapped. The feasibility was demonstrated on the long-lived ^{226}Ra ($t_{1/2}$ = 1600 yr). Building upon this success, in 2006 we succeeded in laser-trapping of ^{225}Ra,[1] the candidate isotope for the EDM experiment now under development. Using a ~1 mCi of ^{225}Ra (~25 ng) purchased from the ORNL Isotope Program, we realized a trap loading rate of 20 atoms per second, and a trap loading efficiency of 7×10^{-7}. Improvements including a longer transverse cooling region and a much higher vacuum (10^{-11} Torr) in the trap chamber are being implemented so that the number of ^{225}Ra atoms in the trap can reach 1×10^4 for an EDM measurement.

We have performed precision laser spectroscopy on the trapped ^{225}Ra and ^{226}Ra atoms (Fig. IV-18), and measured the isotope shifts and hyperfine structures of the transitions relevant to the control of atoms. Figure IV-19 shows the spectroscopy study on the repump transition, $6d\ ^3D_1 - 7p\ ^1P_1$, at 1429 nm. The hyperfine structure A-coefficients of ^{225}Ra have been determined to be 4687.7 ± -1.5 MHz for the $6d\ ^3D_1$ level, and 2797.3 ± 1.5 MHz for the $7p\ ^1P_1$ level.

As indicated by the spectrum inset in Fig. IV-18, room-temperature blackbody radiation can also redistribute population between the $^3P_1$, $^3D_2$, $^3D_1$, and $^3P_0$ levels. This effect was discovered in the course of our trapping experiment, and has been demonstrated by observing the slow transfer on the milli-seconds scale of population among the levels while the lasers are turned off. In practice, this blackbody mechanism eases the requirements on the repumping laser fields because atoms which decay from the $^3D_1$ level to the metastable $^3P_0$ level will be recycled to the $^3D_1$ level by the thermal radiation and be exposed to the repumping laser again. This is particularly significant for the trapping of ^{225}Ra, which can be efficiently repumped by exciting from only one of the hyperfine manifolds. To our knowledge, this is the first demonstration that blackbody radiation can serve as an effective repump source. This mechanism may find more uses in laser-trapping of other elements with complex structure.

---

[1] J. R. Guest, N. D. Scielzo, I. Ahmad, K. Bailey, J. P. Greene, R. J. Holt, Z.-T. Lu, T. P. O'Connor, and D. H. Potterveld, Phys. Rev. Lett. **98**, 093001 (2007).

[2] N. D. Scielzo, J. R. Guest, E. C. Schulte, I. Ahmad, K. Bailey, D. L. Bowers, R. J. Holt, Z.-T. Lu, T. P. O'Connor, and D. H. Potterveld, Phys. Rev. A **73**, 010501(R) (2006).

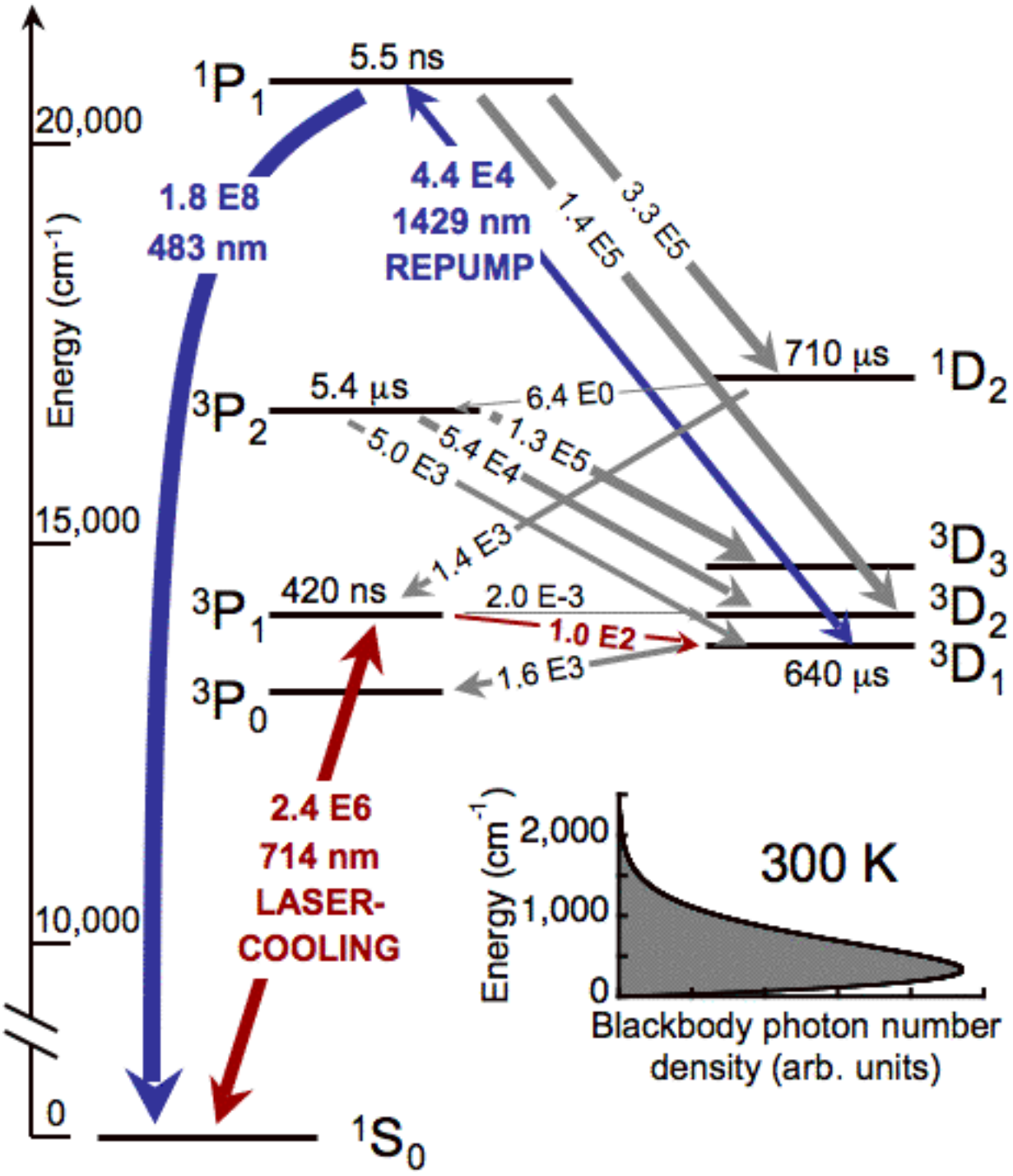

Fig. IV-18. Energy level diagram and decay rates for radium. Energies are indicated at the left, and calculated decay rates are shown ($^3P_1$ lifetime comes from experiment).[2] The room-temperature (300 K) blackbody photon number density is shown on the same energy scale in the inset.

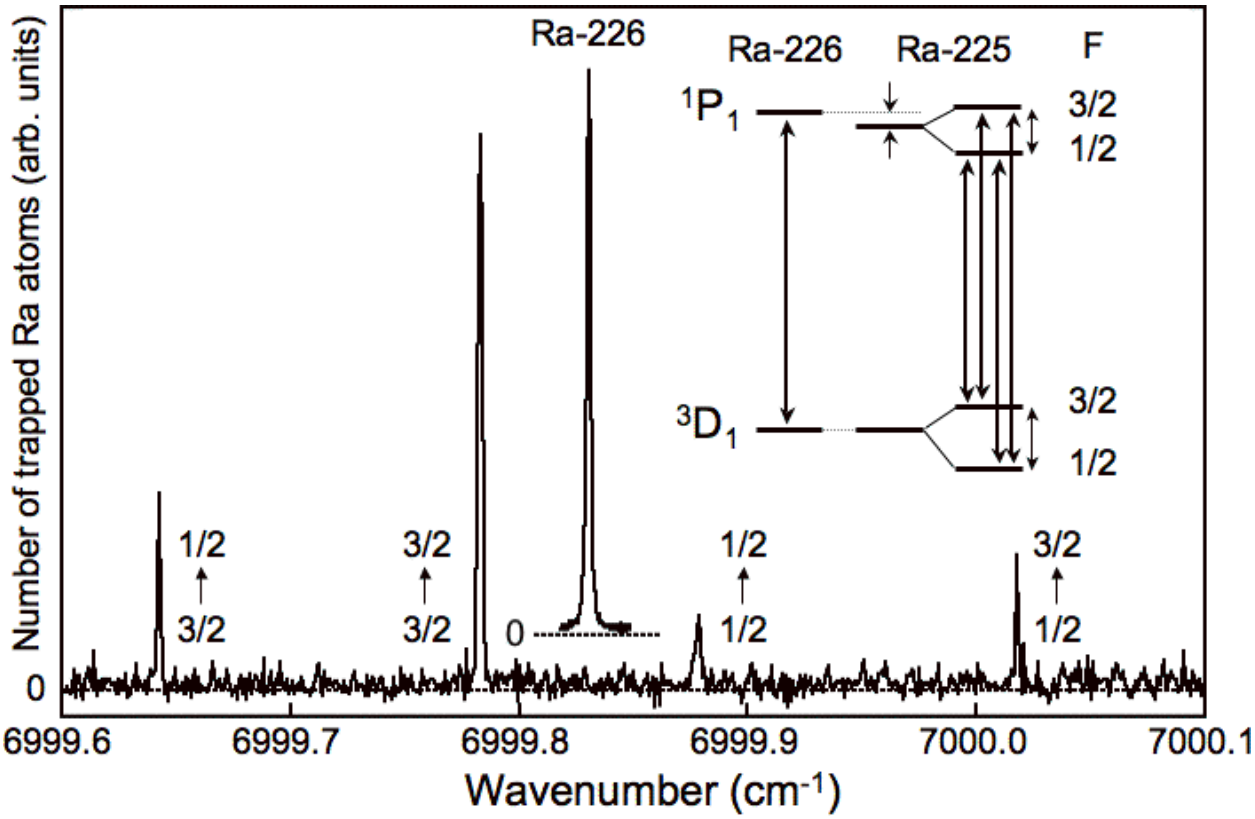

Fig. IV-19. Number of ^{225}Ra and ^{226}Ra atoms in the trap, as measured by fluorescence at 714 nm, vs. the wavenumber of the 1429 nm repump laser recorded by the wavemeter. The ^{225}Ra data are scaled by 100 to compare to ^{226}Ra, which is offset on the vertical scale for clarity. The repump resonances are indicated in the inset level schematic.

d.2. Measurement of $sin^2\theta_W$ Through Parity Violation in Deep-Inelastic Scattering (PV DIS) on Deuterium (P. E. Reimer, X. Zheng, J. Arrington, K. Hafidi, R. J. Holt, H. E. Jackson, and D. H. Potterveld)

In the Standard Model of the electro-weak interaction, $sin^2\theta_W$ represents the relative strength of the weak and electromagnetic forces. The Standard Model predicts the observed value $sin^2\theta_W$ will vary (or run) as a function of Q^2, the energy squared at which it is probed, due to radiative corrections. At $Q^2 = M_z^2$ (the mass of the Z-boson) $sin^2\theta_W$ is well measured; for $Q^2 < M_z^2$, however, only a few measurements exist. One way to probe $sin^2\theta_W$ at lower Q^2 is by measuring the parity violating (PV) asymmetry in polarized deep inelastic scattering (DIS). The asymmetry (A_d) is relatively large ($A_d \approx 10^{-4}\ Q^2$), making it experimentally quite accessible. The sensitivity to $sin^2\theta_W$ is through the product of the axial Z-electron and vector Z-quark couplings (C_{1q}) and the product of the vector Z-electron and axial Z-quark couplings (C_{2q}). A program of DIS parity violation measurement at Jefferson Lab with both 6 and 11 GeV electron beams is being developed.

A preliminary measurement at JLab with a 6 GeV beam has been approved (E05-007).[1] These data will provide a measurement of ($2C_{2u} - C_{2d}$). Current experimental knowledge of this quantity has an uncertainty of 180%, and is subject to model dependence in their interpretation. The complete measurement at 6 GeV will reduce this uncertainty by a factor of five. In addition, the 6 GeV experiment will explore the contribution of higher-twist effects to the asymmetry, providing crucial guidance to interpreting this data and future PV-DIS measurement with the 12 GeV upgrade to JLab. As a critical step toward the realization of this experiment, a scaler-based counting DAQ has been

designed and will be tested in the next year with beam at JLab.

Once the JLab 12 GeV upgrade is completed, a measurement of both $sin^2\theta_W$ and $(2C_{2u} - C_{2d})$ will be completed using the baseline equipment. A Letter of Intent was submitted to the JLab PAC as a stand alone measurement in Hall C[2] and a full proposal is being developed for this measurement. Because of the large parity violating asymmetry, this measurement can be completed with only two to three weeks of beam time and will provide a measurement of $\delta sin^2\theta_W/sin^2\theta_W = \pm$ *0.26% (stat)* $\pm$ *0.36% (sys)*, competitive with other off measurements below M_z^2.

Finally, investigations are underway construct a large-acceptance solenoid-based spectrometer to use DIS-Parity to not only measure $sin^2\theta_W$ but also probe parton distributions at large-x. This spectrometer would also take advantage of the 11 GeV polarized electron beam at JLab.

[1]J. Arrington *et al.*, "$\vec{e}$ -^{2}H Parity Violating Deep Inelastic Scattering at CEBAF 6 GeV," proposal 05007 to the JLab PAC, P. E. Reimer and X. Zheng, spokespersons, December 6, 2004.
[2]J. Arrington *et al*., "Precision Measurement of the Parity-Violating Asymmetry in Deep Inelastic Scattering Off Deuterium Using Baseline 12 GeV Equipment in Hall C," Letter of Intent submitted to the JLab PAC, K. Paschke, P. E. Reimer, and X. Zheng spokespersons, July 9, 2006.

E. ATOM TRAP TRACE ANALYSIS

e.1. Measuring the Nuclear Charge Radius of ^{8}He[1]

(P. Mueller, K. Bailey, R. J. Holt, R. V. F. Janssens, Z.-T. Lu, T. P. O'Connor, J. P. Schiffer, I. Sulai, L.-B. Wang,* M.-G. Saint Laurent,† J.-Ch. Thomas,† A. C. C. Villari,† O. Naviliat-Cuncic,‡ and X. Flechard‡)

Experimental and theoretical investigations of light nuclei play a complementary role in nuclear physics. A major progress in the theoretical description of nuclei has been the success of *ab-initio* calculations in accurately describing the properties of the lightest nuclei. At the same time, experimental investigations of light nuclei concentrate on precision measurements of these properties to serve as benchmarks for theoretical calculations. These experiments often take advantage of newly developed techniques as well as the highest possible production yields available at online facilities for the short-lived isotopes of interest.

In this line of experiments, we have been concentrating to perform precision measurements of the nuclear charge radius of the two short-lived isotopes of helium, ^{6}He and ^{8}He. Both isotopes exhibit a nuclear structure with a loosely bound neutron halo around a ^{4}He-like core. The charge radius provides a measure of the correlation of the halo neutrons and gives insight into nuclear binding in very neutron rich systems. In particular, it probes the isospin dependence of the three nucleon potentials that are a key component of the *ab-initio* calculations.

Previously, we have determined the nuclear charge radius of ^{6}He with a relative uncertainty of 0.7%.[2] The experiment was based on a measurement of the atomic isotope shift between ^{6}He and ^{4}He using high resolution laser spectroscopy of single helium atoms cooled and confined in a magneto-optical trap. The resulting rms charge radius value of 2.054(14) fm corroborated the neutron halo structure of ^{6}He and verified the strong correlation between the halo neutrons predicted by theory.

Currently, we are working towards extending our technique to also measure the nuclear charge radius of ^{8}He, which has the highest neutron-to-proton ratio of all known nuclei. The main experimental challenge of this effort is the production of ^{8}He with sufficient yield and its efficient detection with the laser spectroscopic setup.

We have selected the GANIL facility (Grand Accelerateur National d'Ion Lourds) in Caen, France as the online source for our ^{8}He experiment. At GANIL ^{8}He is produced by impinging a ~70 MeV/u ^{13}C beam of up to 2.2 pμA current on a carbon target optimized for helium isotope production. The helium is subsequently ionized, mass separated and delivered into the experimental area as a low energy (~20 keV) ion beam with a ^{8}He flux of up to 6×10^5 s^{-1}. In addition, the overall detection efficiency of the spectroscopic setup was improved by up to a factor of 20 as compared to the ^{6}He measurement through a number of experimental refinements.

In January 2007 the laser spectroscopic setup was moved from Argonne to GANIL and was subsequently reinstalled and commissioned during the time period from February to May 2007. A new helium neutralizer and transfer line was tested during a "parasitic" online run in April 2007 with a relatively low yield of ~200 ^{8}He/s available in this mode. The transfer efficiency for ^{8}He from the ion beam to the atomic beam apparatus was measured to be 25% in agreement with expectations. Currently, the optimization of the trap efficiency and the calibration of the isotope shift measurement are under way to prepare for a full online ^{8}He run scheduled from June 12th to June 19th 2007.

*Los Alamos National Laboratory, †Grand Accelerateur National D'Ion Lourd (GANIL), Caen, France, ‡Laboratoire de Physique Corpusculaire (LPC), Caen, France.

[1] Project homepage: http://www-mep.phy.anl.gov/atta/.

[2] L.-B. Wang *et al.*, Phys. Rev Lett. **93**, 142501 (2004).

e.2. ATTA-3: The Next-Generation Instrument for ^{81}Kr-Dating

(Y. Ding, K. Bailey, A. M. Davis,* R. W. Dunford,† S.-M. Hu,‡ Z.-T. Lu, P. Mueller, T. P. O'Connor, N. C. Sturchio,§ and L. Young†)

We have made a breakthrough in the optical excitation of Kr that will allow us to complete the development of the next-generation instrument, ATTA-3, with an efficiency leading to a 100-fold reduction in sample size. This reduction in sample size will help make ATTA an essential analytical instrument in earth sciences.

Due to the lack of a cw, narrow-bandwidth laser at 124 nm, laser trapping of krypton atoms can only be realized with atoms at the metastable $5s[3/2]^0_2$ level (Fig. IV-20). In ATTA-2, the excitation of Kr atoms to the metastable level is done by colliding atoms and electrons in a plasma discharge, which poses a serious limitation to the analyzer. The discharge source has a low excitation efficiency (Kr*/Kr ~ 10^{-4}); the collision process causes the atomic beam to diverge; in the plasma, Kr^+ ions are slowly imbedded into surfaces, causing a loss of sample, only to re-emerge later in subsequent analyses, and thereby inducing cross-sample contamination; moreover, a discharge requires a certain minimum gas pressure to operate, which raises the minimum amount of sample needed to support the operation of the discharge.

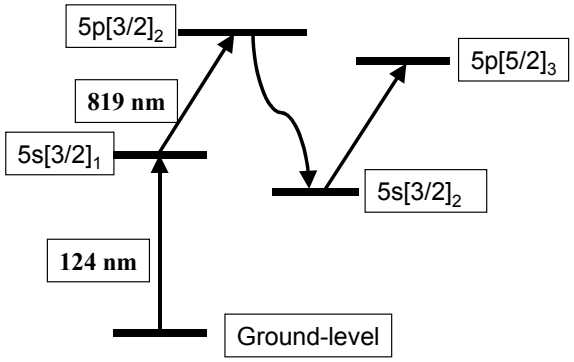

Fig. IV-20. Atomic energy diagram of Kr. The new optical excitation scheme (124 nm + 819 nm) is shown.

In order to avoid these problems and improve both the atom counting rate and counting efficiency, we have been investigating alternative sources of metastable Kr* atoms. It had been previously demonstrated that Kr atoms can be transferred from the ground level to the metastable level via a two-photon excitation process (Fig. IV-20): excitation with a vacuum ultraviolet photon at 124 nm and an infrared photon at 819 nm, followed by a spontaneous decay at 760 nm.[1] All three transitions are of the allowed E1 type. Based on this scheme, we have recently realized, for the first time, a beam of metastable Kr* atoms produced by photon excitation.[2] In the experiment, a vacuum ultraviolet Kr lamp was used to generate the 124 nm photons that are resonant with Kr atoms at the ground level. The 819 nm light was supplied by a diode laser system. At the optimum lamp and laser conditions, the metastable Kr* beam has reached a flux comparable to that produced with a RF-discharge in ATTA-2. With better engineering controls such as a liquid-nitrogen-cooled Kr atom source and a longer optical excitation path, we believe that a higher Kr* beam intensity can be reached. This optical production scheme is a clean and efficient way of producing a well-collimated beam of metastable Kr* atoms, and will enable the analysis of small sample size required by many geochemical and cosmochemical applications.

*University of Chicago, †Chemistry Division, Argonne National Laboratory, ‡Hefei National Laboratory, Anhui, China, University of Science and Technology of China, Hefei, Anhui, China, §University of Illinois at Chicago.

[1]L. Young *et al*., J. Phys. **B35**, 2985 (2002).
[2]Y. Ding *et al*., Rev. Sci. Instrum. **78**, 023103 (2007).

V. THEORETICAL PHYSICS

OVERVIEW

Our research addresses the key questions that comprise the Nation's nuclear physics agenda. We place heavy emphasis on the prediction of phenomena accessible at Argonne's ATLAS facility, at JLab, and at other laboratories; and on anticipating and planning for a future rare isotope beam facility (FRIB). In theoretical and computational nuclear astrophysics our program addresses such issues as the origin of the elements from hydrogen through the actinides and the nature of the basic mechanisms of supernova explosions, and serves to identify critical nuclear parameters and systematic properties to be explored with an advanced exotic beam laboratory. We employ quantum chromodynamics to explore hadron properties: in vacuum, as relevant to programs such as those pursued at JLab; and in-medium, as appropriate to the early universe, compact astrophysical objects, and the RHIC program. Dynamical coupled-channel models are developed to investigate the structure of nucleon resonances by using meson production data from; *e.g.*, JLab, Bonn and Mainz, and also to predict neutrino-nucleus reaction cross sections necessary for analyzing the data from experiments measuring neutrino properties. The structure of atomic nuclei is explored in *ab-initio* many-body calculations based on the realistic two- and three-nucleon potentials we have constructed. These potentials give excellent fits to nucleon-nucleon elastic scattering data and the properties of light nuclei. We use quantum Monte Carlo methods to, *e.g.*, compute nucleon-nucleus scattering phase shifts, transition amplitudes, and a variety of electroweak reactions important to astrophysics. Our nuclear structure and reaction program includes: coupled-channels calculations of heavy-ion reactions near the Coulomb barrier; studies of breakup reactions involving nuclei far from stability, the determination of radiative capture rates from Coulomb dissociation experiments, and studies of the effects of *np*-pairing on nuclei near the proton dripline and of the heaviest elements, using many-body wavefunctions. Our programs provide much of the scientific basis for the drive to physics with rare isotopes. Additional research in the Group focuses on: atomic and neutron physics; fundamental quantum mechanics; quantum computing; and tests of fundamental symmetries and theories unifying all the forces of nature, and the search for a spatial or temporal variation in Nature's basic parameters. The pioneering development and use of massively parallel numerical simulations using hardware at Argonne and elsewhere is a major component of the Group's research.

A. NUCLEAR DYNAMICS WITH SUBNUCLEONIC DEGREES OF FREEDOM

The objective of this research program is: to investigate the role of quark-gluon degrees of freedom in hadron structure and interactions, and in nuclear dynamics; to explore the properties and phase structure of hot, dense Quantum Chromodynamics (QCD) and its possible consequences for the structure of compact astrophysical objects; to develop theoretical methods and tools to place reliable constraints on the variation of Nature's fundamental parameters and physics beyond the Standard Model; the development and application of reaction theories for use in exploring hadron structure using the data from meson and nucleon-resonance production experiments at modern experimental facilities; and to investigate relations of Poincaré covariant dynamics specified by mass operators to complementary dynamics specified by Green functions.

At the level of quark-gluon degrees of freedom, the Dyson-Schwinger equations (DSEs) provide a Poincaré covariant, nonperturbative method for studying QCD in the continuum. A hallmark of present-day DSE applications in hadron physics is the existence of a symmetry preserving truncation that enables the simultaneous exploration of phenomena such as: confinement, dynamical chiral symmetry breaking, and bound state structure and interactions. In addition, the DSEs provide a generating tool for perturbation theory and hence yield model-independent results for the ultraviolet behavior of strong interaction observables. This means that model studies facilitate the use of physical processes to constrain the long-range behavior of the interaction between light-quarks in QCD, which is poorly understood and whose elucidation is a key goal of modern experimental programs. The last year saw numerous noteworthy applications and successes. For example, we presented arguments which support a view that chiral perturbation theory is inapplicable for pion-like meson masses greater than $m_{0^-} \sim 0.45$ GeV; that a unique signal for the restoration of chiral symmetry via excitation of mesons is equality between the pole residues for $0^{-+}(nS)$ and $0^{++}(nS)$ states when n, the radial quantum number, is large; that chiral symmetry and its dynamical breakdown in QCD even place constraints on properties of mesons composed of two heavy-quarks; and we also provided a prediction for the ratio of neutron electric and magnetic form factors.

At the level of meson and baryon degrees of freedom, we continue our effort to develop a dynamical coupled-channels model for use in analyzing the very extensive set of data for electromagnetic meson production reactions. A primary objective is the development of an interpretation for this data in terms of the quark-gluon substructure of nucleon resonances (N^*). We aim to draw the connection between this data and the predictions made by QCD-based hadron models and numerical simulations of lattice-regularized QCD. In the past year we completed a major stage of this project by determining the hadronic interactions in the model by fitting pion-nucleon scattering data up to 2 GeV. We predicted the effect of a meson cloud on the form factors describing the transition to all known low-lying nucleon resonances. Methods for determining the resonance parameters from the partial-wave amplitudes were developed. We also made progress on projects focused on η and ω photoproduction, which aim at discovering highly excited resonances with masses close to 2 GeV. In addition, we continued to play a leading role in directing operations of the Excited Baryon Analysis Center (EBAC) at Jefferson Laboratory.

Relativistic quantum dynamics requires a unitary representation of space-time symmetries (Poincaré group) and localization of states, such that states localized in relatively space-like regions are causally independent. We have recently focused on the application and elucidation of complementary mathematical representations of hadron phenomena, and on a consistent treatment of medium energy electromagnetic few-body processes.

a.1. Space-Time Variation of Strong Interactions and Fine Structure Constant

(V. V. Flambaum*)

Grand Unification Models suggest that the fundamental masses ($m_{electron}$, m_{quark}) and the strong interaction scale Λ_{QCD} may vary much faster than the QED fine structure constant α. A number of theoretical and experimental papers devoted to temporal variation of m/Λ_{QCD} were recently published. There is some evidence for this parameter variation in Big Bang nucleosynthesis, quasar absorption spectra and Oklo natural nuclear reactor data. The need for an interpretation of these measurements and the search for new, enhanced effects have created a topical field of research: strong interaction calculations of the dependence of nuclear parameters on quark masses. We have been active in this area.

We showed[1] that the relative effects of a variation in α and m_{quark}/Λ_{QCD} are enhanced by 5-6 orders-of-magnitude in a very narrow ultraviolet transition between the ground and first excited state in ^{229}Th (energy ~5 eV). An experiment capitalizing on this can potentially improve sensitivity to a variation in Nature's fundamental parameters by 7-10 orders-of-magnitude (exposing a variation of up to 10^{-23}/year).

We demonstrated[2] that atomic scattering lengths, which can be measured in Bose-Einstein condensate and Feshbach molecule experiments, are extremely sensitive to the variation of Nature's fundamental constants, in particular, to the electron-to-proton mass ratio (m_e/m_p). Based on a single- and two-channel scattering model, we showed how this variation in the mass ratio is communicated to the scattering length. Our results suggest that a variation in m_e/m_p on the level of $10^{-11} \sim 10^{-13}$ can be detected near a narrow magnetic or an optical Feshbach resonance by monitoring the scattering length on the 1% level. The formulae we have derived may also be used to estimate the isotopic shift in the scattering length.

We calculated[3] the dependence of nuclear magnetic moments on the current-quark masses, including an estimate of the effect of spin-spin interactions, and obtained limits on the variation of α and (m_{quark}/Λ_{QCD}) by using recent atomic clock experiments that examine the hyperfine transitions in H, Rb, Cs, Yb^+ and Hg^+ and the optical transition in H, Hg^+ and Yb^+.

We found[4] that the relative effect of a variation in α on microwave transitions between very close and narrow rotational-hyperfine levels may be enhanced by 2-3 orders-of-magnitude in diatomic molecules with unpaired electrons, such as LaS, LaO, LuS, LuO, YbF, and similar molecular ions. The enhancement results from cancellation between the hyperfine and rotational intervals.

*Argonne Fellow, Physics Division, and University of New South Wales, Sydney, Australia.

[1]V. V. Flambaum, Phys. Rev. Lett. **97**, 092502 (2006).
[2]C. Chin and V. V. Flambaum, Phys. Rev. Lett. **96**, 230801 (2006).
[3]V. V. Flambaum and A. F. Tedesco, Phys. Rev. C **73**, 055501 (2006).
[4]V. V. Flambaum, Phys. Rev. A **73**, 034101 (2006); V. V. Flambaum and M.G. Kozlov, Phys. Rev. Lett., to appear.

a.2. Coulomb Problem for Vector Bosons

(V. V. Flambaum* and M. Yu. Kuchiev†)

There is a difficulty with the Coulomb problem for vector bosons. Indeed, soon after Proca formulated a theory for vector particles it became clear that it produces inadequate results for the Coulomb problem. This inspired Corben and Schwinger to modify Proca's theory, tuning the Lagrangian and the equations of motion so as to force the vector boson's gyromagnetic ratio to acquire the value $g = 2$. (N.B. $g = 2$ is the

Standard Model value for $W_{\pm}$). They obtained a simple Sommerfeld-type formula for the spectrum valid up to $Z\alpha = 1/2$.

However, the problem has not completely disappeared: for $j = 0$ states the charge of the boson localized in the vicinity of the attractive Coulomb center remains infinite. We re-derived[1] these results for the spectrum and wavefunction starting from the Standard Model and then displayed a clear way to properly formulate the Coulomb problem for vector particles. Our main observation is that the polarization of the QED vacuum has a profound impact on the problem, forcing the density of charge of a vector boson to decrease exponentially at the origin thus making the Coulomb problem stable and well defined.

At first glance this result may be surprising because the vacuum polarization increases the strength of the attractive field at the origin. Moreover, the vacuum polarization for spinor and scalar particles in the Coulomb field is known to produce only small, perturbative effects. In contrast, we find for the vector particle a *strong reduction* in its charge density near the origin. To grasp the physical mechanism involved it is necessary to notice that the equation of motion for vector particles contains a particular term, which has no counterparts for scalars and spinors; namely, the last term in the following equation:

$$(\partial^2 + m^2)\, W^{\mu} + 2ie\, F^{\mu\nu}\, W_{\nu} + (ie/m^2)\, \partial^{\mu} (j_{\nu} W^{\nu}) = 0$$

This additional term is responsible for a strong repulsion arising from the vacuum polarization and makes the Coulomb problem stable. The effective potential becomes large and positive when $r \rightarrow 0$; *viz*., $U(r) \approx Z^2\alpha^3\beta/(m^2 r^4)$.

Here the factor β is the lowest coefficient of the Gell-Mann-Low function. Both the Standard Model and experimental data indicate that $\beta > 0$, presumably, up to the Grand Unification limit. Hence the vacuum polarization results in an intense repulsion near the origin for even arbitrarily small values of $Z^2\alpha^3$.

The wavefunction decreases exponentially at small distances: $\varphi(r) \sim \exp(-Z\alpha\,(\alpha\beta)^{1/2}/[\,m\,r])$, so that the charge density of the W-boson also decreases exponentially at the origin. Thus, accounting for the QED vacuum polarization eliminates the difficulty related to the infinite charge of a vector boson located at the Coulomb center.

For small Z the energy shift of discrete energy levels owing to the vacuum polarization is found to be small, which makes the Sommerfeld formula applicable for the spectrum of vector bosons.

In addition we have recently found that the charge density of a positively charged vector boson, *e.g.*, the W^+-boson, may be negative.[2] The effect manifests itself even for a free propagation; when the energy of the W-boson is higher than $\sqrt{2}m$ and the standing-wave is considered. The charge density of W also changes sign in the vicinity of a Coulomb center. For an arbitrary vector boson, this effect depends on the g-factor. We traced the origin of this surprising effect to the electric quadrupole moment and spin-orbit interaction of vector particles; their contributions to the current have a polarization nature. The corresponding charge density $\mu_{Pol} = -\nabla P$, where P is an effective polarization vector that depends on the quadrupole moment and spin-orbit interaction. The density oscillates in space, producing zero contribution to the total charge.

---

*Argonne Fellow, Physics Division, and University of New South Wales, Sydney, Australia, †University of New South Wales, Sydney, Australia.

[1]M. Yu. Kuchiev and V. V. Flambaum, Mod. Phys. Lett. A **21**, 781 (2006).
[2]V. V. Flambaum and M. Yu. Kuchiev, Phys. Rev. Lett. **98**, 181805 (2007).

a.3. Quark Deconfinement in Neutron Star Cores: The Effects of Spin-Down

(P. Jaikumar, J. Staff,* and R. Ouyed†)

We studied the role of spin-down of isolated neutron stars in driving quark deconfinement in its high-density core. We concluded that light neutron stars (≤ 1.6 solar massive neutron stars (≥ 1.8 solar masses) can enter a quark phase only if they are spinning faster than about 3 milliseconds as observed now.

We created sequences of neutron star models using numerical methods developed specifically to treat rapidly rotating neutron stars. We obtained typical timescales to reach quark deconfinement in the core of neutron stars that are born with Keplerian frequencies.

We found this time to be least for equations of state that support the largest minimum mass at zero spin, unless the moment of inertia is very high. For each equation of state, we also determined the minimum and maximum neutron star masses, as well as the current minimum spin periods that will allow for deconfinement in a Hubble time via spin-down only.

Our results directly address the issue of forming a quark star in the spin-down epoch of a neutron star, and present a window in mass and spin-periods in which observers are likely to discover quark stars. They also suggest that the existence of quark stars is predicated upon having a low deconfinement threshold of less than five-times the saturation density of nuclear matter.

An article describing this work was published.[1]

[*]Purdue University, †University of Calgary, Alberta, Canada.
[1]J. Staff, R. Ouyed, and P. Jaikumar, Astrophys. J. Lett. **645**, L145-L148 (2006).

a.4. Quark Matter in Neutron Stars: An Aperçu (P. Jaikumar, S. Reddy,* and A. W. Steiner†)

Deconfined quark matter may exist in a stable phase in the interior of a neutron star, where densities are as much as five times that of nuclei. We reevaluated the possibility for the existence of deconfined quark matter in the light of recent observations that, for the first time, determined the mass and radius of the same neutron star; *viz*., the X-ray binary EXO 0748-676. We concluded that the rather large inferred values of mass and radius of this object conflicts with a scenario in which significant softening occurs owing to a phase transition to quark matter at high density. However, strange stars that are made entirely of quark matter and hybrid stars that are composed of a quark core with a relatively stiff equation of state remain viable.

We reviewed recent observations of thermally emitting neutron stars, whose surface temperatures are accurately known, in order to determine if rapid neutrino cooling processes characteristic of quark matter could operate in such stars. We found that the data do not support any rapid cooling mechanism; instead, they are satisfactorily explained by neutrino emission in superfluid nucleonic matter. However, a cold neutron star in the supernova remnant 3C58 and the growing number of such remnants with low observed luminosity may well suggest that some neutron stars require a rapid cooling mechanism.

Based on a broad evaluation of transient phenomena in neutron stars, taken together with mass-radius and spin-period measurements, we emphasized the need to understand the long-term evolution of neutron stars within a consistent picture. In particular, we pointed out that it would be premature to rule out quark matter in neutron stars on the basis of mass-radius measurements alone.

An article describing this work was published.[1]

*Los Alamos National Laboratory, †Michigan State University.
[1]P. Jaikumar, S. Reddy, and A. W. Steiner, Mod. Phys. Lett. A **21**, 1965 (2006).

a.5. Surface Structure of Quark Stars with Magnetic Fields (P. Jaikumar)

Bare quark stars are a proposed class of compact stars that are composed entirely of deconfined quark matter. An observational confirmation of their existence would be conclusive evidence of quark deconfinement at large baryon densities, a phenomena anticipated from Quantum Chromodynamics (QCD). We outlined the main observational characteristics of bare quark stars as determined by their photon luminosity, including the effects of a strong magnetic field at the surface.

We studied the modifications of a quark star's surface charge distribution owing to a magnetic field in a force-free approximation, employing a Thomas-Fermi model to solve the Poisson equation. We found an exponentially decaying charge distribution at large distance from the surface, contrary to the *1/r* fall off in the non-magnetic case. For magnetic fields $B \sim 10^{14}$ G, or more, quantization of electrons into Landau orbits was found to significantly affect the charge distribution.

We showed that the flux and the spectrum of photons from quark stars is determined by e^+e^- pair-emission at high temperatures ($T > 10^9$ K) and by bremsstrahlung and other $2 \rightarrow 3$ processes for $T < 10^9$ K. The resulting non-thermal spectrum is different from that of a cooling neutron star, allowing for an observational distinction to be made. It was established that strong magnetic fields of $B \sim 10^{14}$ G or more induce a collective response of the surface material that strongly diminishes the reflectivity from the unmagnetized case and also polarizes the emitted photons.

An article describing this work was published.[1]

[1]P. Jaikumar, Pramana-Indian J. of Phys. **67**, 937 (2007).

a.6. Nucleosynthesis in Decompressing Neutron Star Matter (P. Jaikumar, B. Meyer,* K. Otsuki,† and R. Ouyed‡)

The rapid neutron capture process (*r*-process) makes approximately half of the heavy elements above ^{56}Fe. The astrophysical site for the *r*-process is not yet known with any certainty, although Type-II supernovae are the most promising candidates. We proposed an alternative site: decompressing neutron-rich material from the surface of a neutron star that undergoes a quark-hadron phase transition. We performed network calculations that are adapted to decompression and which match to dynamical *r*-process calculations at densities below neutron drip (4×10^{11} g/cc).

We studied the sensitivity of the final abundance pattern of heavy elements to heating from nuclear reactions and expansion timescale of the ejecta. We found that heating was an essential factor in producing the prominent peaks of the *r*-process and that a slow expansion rate of the ejecta was able to best reproduce the observed relative abundance of *r*-process elements in our galaxy, as shown in Fig.V-1.

We estimated the frequency of decompression events in our galaxy and found it to be significantly smaller than that of Type II supernovae but comparable to binary neutron star mergers. We highlighted the distinguishing features of the decompression scenario by contrasting it with conventional nucleosynthesis sites such as Type II supernovae and neutron star mergers, especially in the context of heavy-element compositions of extremely metal-deficient stars.

An article describing this work was submitted.

*Clemson University, †University of Chicago, ‡University of Calgary, Alberta, Canada.

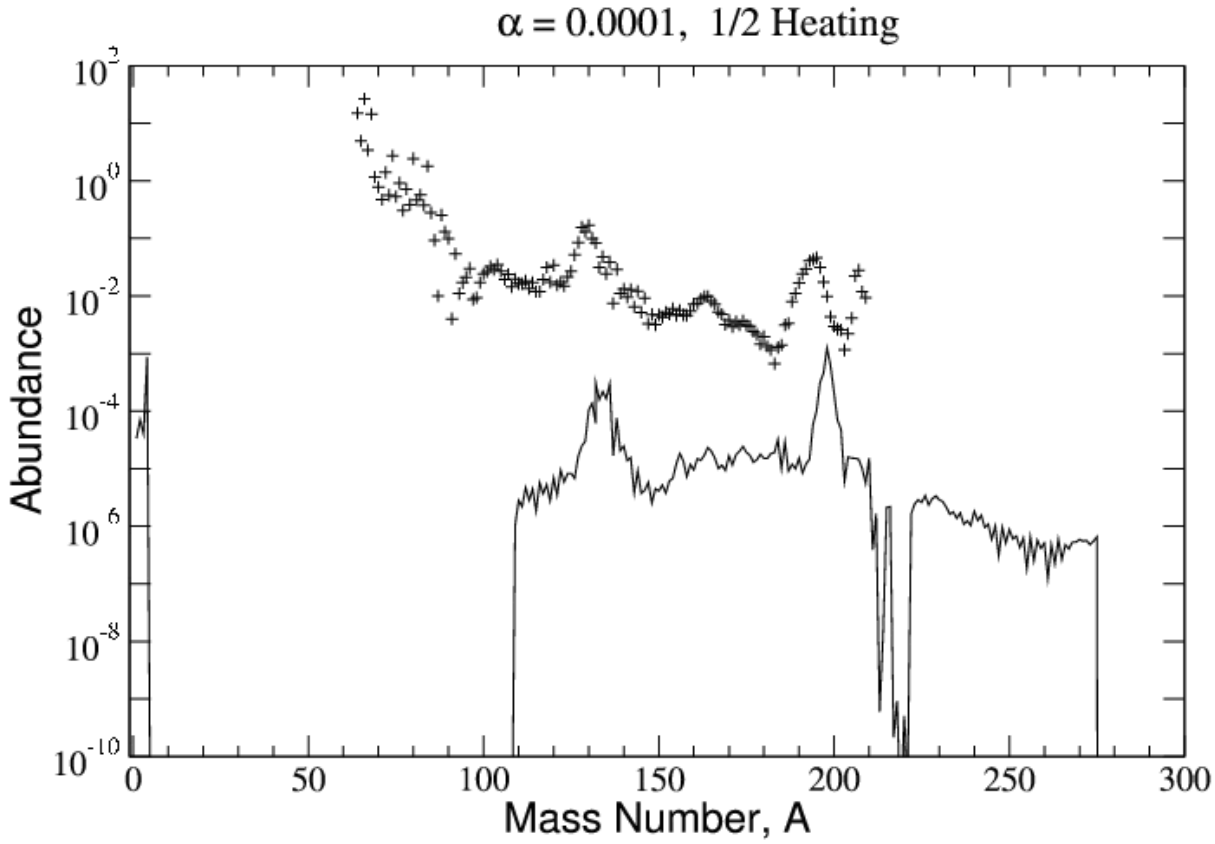

Fig. V-1. The final abundance distribution as a function of mass number in a decompression calculation for the slowest parameterized ejecta expansion rate α = 0.0001 and 50% local energy deposition from nuclear reactions.

a.7. Nucleon Weak and Strong Form Factors (C. D. Roberts, S. V. Wright, and A. Höll*)

The framework we have developed for the Poincaré covariant study of nucleon electromagnetic form factors can naturally also be employed to calculate weak and strong form factors of the nucleon, which are sensitive to different aspects of quark-nuclear physics and should prove useful, *e.g.*, in constraining coupled-channel models for medium-energy production reactions on the nucleon.

We obtained preliminary results in the chiral limit for three such form factors: the axial-vector, $G_A(Q^2)$, and pseudoscalar, $G_P(Q^2)$, nucleon form factors, which appear in the axial-vector--nucleon current, and the pion-nucleon coupling, $g_{\pi NN}(Q^2)$. These first calculations were based on an axial-vector nucleon vertex constructed from components that are necessary but not sufficient to ensure fulfillment of the axial-vector Ward-Takahashi identity for on-shell nucleons. Work on improvement is underway.

An article describing these results was published.[1]

*Universität Rostock, Germany.

[1] A. Höll, C. D. Roberts, and S. V. Wright, AIP Conf. Proc. **857**, 46 (2006).

a.8. Dynamical Chiral Symmetry Breaking and a Critical Mass (M. S. Bhagwat, C. D. Roberts, S. V. Wright, L. Chang,* and Y.-X. Liu†)

Dynamical chiral symmetry breaking (DCSB) is the creation, via interactions with the gauge field alone, of a fermion mass gap: whose magnitude exceeds, perhaps by a great amount, the mass-scale in the action set by the fermion's bare mass; and which persists when that bare-mass-scale vanishes, namely, in the chiral limit. It is fundamentally important in strong interaction physics. For example, DCSB is responsible for the generation of large constituent-like masses for dressed-quarks in QCD. This is a longstanding prediction of Dyson-Schwinger equation (DSE) studies, which has recently been confirmed in numerical simulations of lattice-regularized QCD. DCSB is also the keystone in the realization of Goldstone's theorem through pseudoscalar mesons in QCD, and thereby the remarkably small value of the ratio of π- and ρ-meson masses, and the weak ππ interaction at low energies. A large body of efficacious QCD phenomenology is built on an appreciation of the importance of DCSB. Nevertheless, not all facets of DCSB have been elucidated. We uncovered novel aspects of the interplay between explicit and dynamical chiral symmetry breaking.

On a bounded interval of current-quark mass, $D(m) = \{m \mid 0 \leq m < m_{cr}\}$, realistic models of QCD's gap equation can simultaneously admit two inequivalent dynamical chiral symmetry breaking (DCSB) solutions for the dressed-quark mass-function, $M_{\pm}(p^2)$, and a solution that is unambiguously connected with the realization of chiral symmetry in the Wigner mode, $M_W(p^2)$. The DCSB solutions are distinguished by their value at the origin: $M_+(p^2) > 0$ and $M_-(p^2) < 0$. In the ultraviolet all three solutions coincide with the running current-quark mass.

The pointwise values of all solutions evolve continuously with current-quark mass within $D(m)$. However, things change at the upper boundary. The M_W solution, whose chiral limit value is perturbative in the coupling, becomes identical to the essentially nonperturbative solution M_- that is actually characteristic of DCSB. Moreover, both disappear for $m > m_{cr}$, a domain whereupon the current-quark mass is large enough to completely destabilize these solutions. Only the positive M_+ solution exists on this domain. Furthermore, we demonstrated that the upper boundary of $D(m)$ also defines the radius of convergence for an expansion of M_+ in current-quark mass around its DCSB chiral-limit form.

The pointwise values of all solutions evolve continuously with current-quark mass within $D(m)$. However, things change at the upper boundary. The M_W solution, whose chiral limit value is perturbative in the coupling, becomes identical to the essentially nonperturbative solution M_- that is actually characteristic of DCSB. Moreover, both disappear for $m > m_{cr}$, a domain whereupon the current-quark mass is large enough to completely destabilize these solutions. Only the positive M_+ solution exists on this domain. Furthermore, we demonstrated that the upper boundary of $D(m)$ also defines the radius of convergence for an expansion of M_+ in current-quark mass around its DCSB chiral-limit form, see Fig. V-2.

Thus one has the coalescing of two qualitatively distinct solutions at m_{cr}, the persistence of only one essentially nonperturbative solution for $m > m_{cr}$ plus the breakdown of a chiral expansion for this solution, and, as we also showed, the simultaneous loss of a well-defined mass-dependent quark condensate. This behavior supports an interpretation of m_{cr} as the upper bound on the domain within which a perturbative expansion of physical quantities in the current-quark mass around their chiral-limit values can uniformly be valid. In a phenomenologically efficacious renormalization-group-improved rainbow-ladder truncation of QCD's DSEs, the critical current-quark mass corresponds to a mass $m_{0^-} \sim 0.45$ GeV for a pseudoscalar meson constituted of equal mass current-quarks. (NB. Irrespective of the current-mass of the other constituent, a meson containing one current-quark whose mass exceeds m_{cr} is never within the domain of uniform convergence.) This scale also marks the boundary below which observables should exhibit that curvature as a function of pion-like pseudoscalar-meson mass which is characteristic of chiral effective theories. This work was published.[1]

*Peking University, Beijing, China, †Peking University, Beijing, China; The Key Laboratory of Heavy Ion Physics, Ministry of Education, Beijing, China; Center of Theoretical Nuclear Physics, National Laboratory of Heavy Ion Accelerator, Lanzhou, China.

[1]L. Chang, Y.-X. Liu, M. S. Bhagwat, C. D. Roberts, and S. V. Wright, Phys. Rev. C **75**, 015201 (2007).

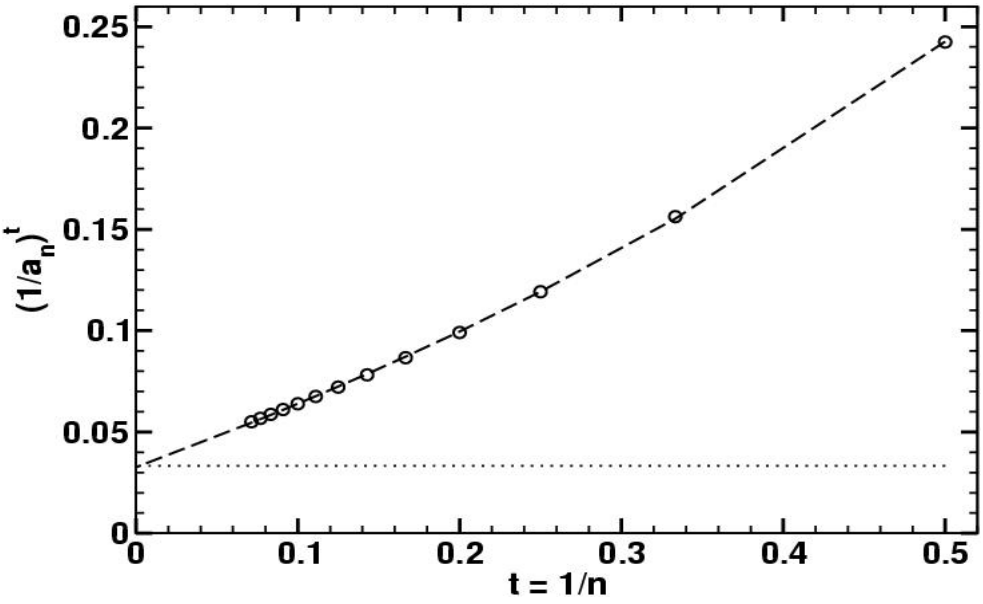

Fig. V-2. Reciprocal of the n-th roots of the coefficients in a chiral expansion of the DCSB solution, M_+, around $m = 0$, as a function of $t = 1/n$, where n is the order of the expansion. Dotted curve – $m_{cr} = 0.033$ (in units of model's mass-scale). Dashed curve – [1,1] Padé approximant, from which one can infer the chiral expansion's radius of convergence; viz., the ordinate intercept.

a.9. Studies of Meson Properties (M. S. Bhagwat, C. D. Roberts, S. V. Wright, A. Höll,* A. Krassnigg,† and P. Maris‡)

We examined properties of pseudoscalar and scalar mesons using a practical and symmetry preserving truncation of QCD's Dyson-Schwinger equations.

One study[1] provided a comparison between properties of ground and radially excited mesons via a calculation of the dependence on current-quark mass of the masses and leptonic decay constants for these systems. We obtained, *e.g.*, predictions for the mass and leptonic decay constant of the first radial excitation of the kaon: namely, $m_{K(1460)} = 1.52 \pm 0.12$ and $f_{K(1460)} \sim 10\, f_{\pi(1300)}$, where $\pi(1300)$ is the pion's first radial excitation; and the mass of the $\chi_{c0}(2P)$ meson; *viz*., *3.88* GeV. Moreover, we found that up till the *c*-quark mass, the ordering of meson masses is

$$0^{-+}(1S) < 0^{++}(1S) < 0^{-+}(2S) < 0^{++}(2S).$$

In a related investigation[2] we recalled that it has been conjectured that DCSB notwithstanding, the properties of highly excited pseudoscalar and scalar mesons exhibit a pattern that is consistent with a Wigner realization of chiral symmetry. These mesons appear as poles in QCD's inhomogeneous pseudoscalar and scalar vertex functions. Such poles are characterized in part by gauge-invariant residues. We argued that a unique signal of the truth of this conjecture is equality between the pole residues for $0^{-+}(nS)$ and $0^{++}(nS)$ states when *n*, the radial quantum number, is large; *i.e*.,

$$\rho_{\pi^n} = \rho_{\sigma^n}, \text{ for } n \text{ large.}$$

We were also able to prove[3] that chiral symmetry and its dynamical breakdown in QCD place constraints on properties of mesons composed of two heavy-quarks, one of which is an identity relating the gauge invariant residues of these states in the inhomogeneous pseudovector and pseudoscalar vertex functions, mentioned above, in the heavy-quark limit; *viz*.,

$$\rho_{\pi^n}(QQ) = f_{\pi^n}(QQ)\, m_{\pi^n}(QQ) \text{ for } m_Q \to \infty.$$

In illustrating this identity, we established that the leptonic decay constants for vector and pseudoscalar

heavy-heavy mesons both increase linearly with current-quark mass on a domain that begins at approximately twice the *c*-quark mass. This is the result one would obtain for heavy-quarks bound by a Coulomb potential. It therefore suggests that the properties of truly heavy-heavy mesons are determined primarily by the one-gluon exchange potential in QCD and hence, importantly, they are not sensitive to the confinement potential.

Within a Poincaré covariant framework it makes sense to discuss quark orbital angular momentum since, while it is not a Poincaré invariant, if absent in a particular frame, it will inevitably appear in another frame related via a Poincaré transformation. This constraint and feature of covariance is the reason that the Bethe-Salpeter wavefunction for mesons (and the Faddeev wavefunctions for baryons) is a matrix-valued function with a rich structure. We exhibited[3] the rest-frame angular momentum content of a pseudoscalar meson and its current-quark-mass-dependence. In the neighborhood of the chiral limit, there is a material $L = 1$ component, which can be characterized by a mixing angle of 35°. The angle decreases with increasing current-quark mass. As measured by this mixing angle, at a given bound state mass the $L = 1$ admixture is roughly 15% greater in the first radial excitation. However, measured as a function of current-quark mass, the situation is reversed: the angle in the excited state is approximately 1/2 that in the ground state and the ratio increases toward one with increasing current-quark mass. Figure V-3 illustrates these results, which are qualitatively model-independent.

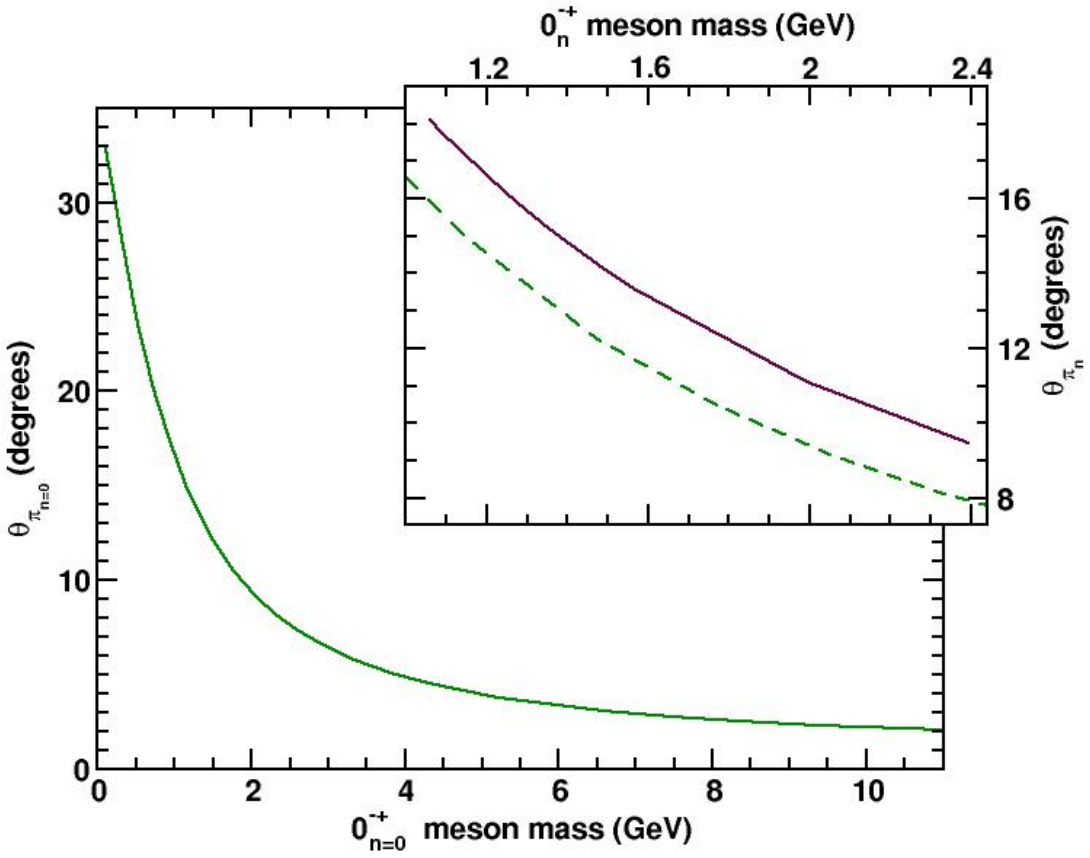

Fig. V-3. Main frame: $\theta_{\pi 0}$, which gauges the rest-frame admixture of L = 1 components in the ground state 0^{-+} meson's Bethe-Salpeter wavefunction, plotted as a function of the meson's mass. Inset: Solid curve -- analogue, $\theta_{\pi 1}$ for the first excited state; dashed curve, $\theta_{\pi 0}$ for comparison. In the chiral limit the ground state pseudoscalar is naturally massless whereas the calculated mass of the first excited state is 1.04 GeV.

Studies such as we have described in this subsection and their refinement through comparison with extant and forthcoming data are an essential precursor to the reliable prediction of properties of hybrid and exotic hadrons.

*Universität Rostock, Germany, †Karl-Franzens-Universität Graz, Austria, ‡University of Pittsburgh.
[1]A. Krassnigg, C. D. Roberts, and S. V. Wright, Int. J. Mod. Phys. A **22**, 424 (2007).
[2]M. S. Bhagwat, A. Höll, A. Krassnigg, and C. D. Roberts*, Theory and Phenomenology of Hadrons,* Nucl. Phys. **A790**, 10 (2007).
[3]M. S. Bhagwat, A. Krassnigg, P. Maris, and C. D. Roberts*,* Eur. Phys. J. A **31**, 630 (2007).

a.10. Schwinger Functions and Light-Quark Bound States (M. Bhagwat, C. D. Roberts, S. V. Wright, A. Höll,* and A. Krassnigg†)

The probability measure plays a crucial role in quantum field theory. In Euclidean space a theory's generating functional can truly be expressed in terms of a probability measure and the properties of such measures make it likely that the rigorous definition of interacting quantum field theories is possible in that case. However, in Minkowski space the probability density becomes a probability *amplitude*, through the appearance of "*i"* in the exponent, and that precludes the formulation of a measure theory.

The moments of a probability measure are *n*-point Schwinger functions. They correspond to vacuum expectation values of Euclidean fields and may loosely be termed Euclidean space Green functions. When certain conditions are met, analytic continuation of the Schwinger functions yields the Wightman functions and one may prove the reconstruction theorem; namely, the complete content of a quantum field theory is recovered from the Wightman functions. This is the basis for the contemporary belief that the evaluation of a theory's Schwinger functions is equivalent to solving that theory.

While that may be true in principle one must nonetheless develop practical means by which to extract physical information from the Schwinger functions. The challenge may be illustrated by noting that complete knowledge of a two-point Schwinger function in momentum space corresponds only to direct knowledge of the expectation value at spacelike momenta. A physical particle pole can only appear at timelike momentum. Locating such a pole therefore requires that all the conditions be met for a unique analytic continuation. If the Schwinger function is known only at a discrete set of points; *i.e*., on a set of measure zero, then that is strictly impossible. In this common instance all that is really possible are constrained inference and an estimation of the inherent error.

For us a context for these observations is the problem of determining the spectrum of QCD. Much has been learnt about the two-point Schwinger functions for quarks, gluons and ghosts. However, the pointwise behavior of the continuation of these functions to timelike momenta is uncertain. These two-point functions appear in the kernels of the Bethe-Salpeter equations whose solutions provide information about the properties of color-singlet hadrons. The study of ground state mesons in the pseudoscalar and vector channels has met with success. A present challenge is the extension to excited states in these and other channels, and to channels in which the ground state lies above *1* GeV. A veracious analytic continuation of two-point Schwinger functions becomes increasingly important as the bound-state mass becomes larger. The possibility that this continuation might be absent poses the question: can reliable information about bound state properties be obtained directly from the Schwinger functions?

Another context for this question is the numerical simulation of lattice-regularized QCD. That approach is grounded on the Euclidean space functional integral. Schwinger functions are all that it can directly provide. Hence, it can only be useful if methods are found so that the question can be answered in the affirmative.

We analyzed the capacity of Schwinger functions to yield information about bound states, and established that for the ground state in a given channel the mass and residue are accessible via rudimentary methods. When the mass-splitting between the first and second excited states is not significantly smaller than that between the ground and first excited states, these

methods may also reliably provide the same information about the first excited state, so long as the Schwinger function under consideration does actually possess the analytic properties assumed of it. However, simple methods cannot provide dependable information about more massive states in a given channel.

Indeed, there is no easy way to extract such information. An approach based on a correlator matrix can be successful but only if the operators are carefully constructed so as to have large overlap with states of interest in a given channel and statistical errors can be made small; *viz*., ~1%. While it is possible in principle to satisfy these constraints, doing so is labor intensive and time consuming. That is, nevertheless, justified in the absence of model-dependence.

We posed the question of whether, in the context of bound-state studies in which model assumptions are made regarding the nature of the long-range interaction between light quarks, labor can be saved and/or accuracy gained by working solely with Schwinger functions. Our analysis suggested strongly that the answer is *no*. In their formulation the studies of this type explicitly define an analytic continuation of a model into the complex plane. Hence, all momenta are directly accessible. We saw clearly that it is not possible to avoid model artifacts by pretending ignorance of this. Thus, nothing is gained by solving a complex of DSEs for the Schwinger functions associated with numerous carefully tuned interpolating fields. Moreover, capitalizing on the feature that all momenta are directly accessible is the most efficient manner by which to test and improve the model input, and, thereby, to relate experimental data on bound state properties to information about the interaction between light quarks. This is further emphasized by the fact that because excited states are unstable they are characterized by complex pole positions.

An article describing this work was accepted for publication.[1]

---

*Universität Rostock, Germany, †Karl-Franzens-Universität Graz, Austria.

[1]M. Bhagwat, A. Höll, A. Krassnigg, C. D. Roberts, and S. V. Wright, Few Body Systems **40**, 209 (2007).

a.11. Nucleon Electromagnetic Form Factors (J. Arrington, M. Bhagwat, C. D. Roberts, A. Höll,* A. Krassnigg,† and J. M. Zanotti‡)

Elastic electromagnetic nucleon form factors have long provided vital information about the structure and composition of these most basic elements of nuclear physics. The form factors are a measurable and physical manifestation of the nature of the nucleons' constituents and the dynamics that binds them together. Accurate form factor data obtained in recent years using modern experimental facilities has spurred a significant re-evaluation of the nucleon and pictures of its structure; *e.g.*, the role of quark orbital angular momentum, the scale at which perturbative QCD effects should become evident, the strangeness content, and meson-cloud effects. In a review article, we provided a succinct survey of the experimental studies and theoretical interpretation of nucleon electro-magnetic form factors.[1]

As described therein, a modern approach to the study of baryons is based on a Poincaré covariant Faddeev equation, which may be viewed as one of the collection of DSEs and an analogue of the Bethe-Salpeter equation that is well-suited to the study of mesons. A merit of the Poincaré covariant Faddeev equation is that a veracious understanding of the structure of dressed-quarks and -gluons is straightforwardly incorporated; namely, effects owing to and arising from the strong momentum-dependence of these propagators are realized and exhibited. This momentum-dependence, which explains, *e.g.*, the connection between constituent- and current-quark masses, was predicted by Dyson-Schwinger equation studies.

However, the study of baryons using this approach is not at a level of sophistication comparable to that of mesons. It is actually at roughly the same stage as was the study of mesons more than a decade ago; namely, model-building and phenomenology constrained and informed by the best available hadron physics theory.

Notwithstanding this, important predictions are being made. For example, Fig. V-4 shows the calculated[2] ratio

$$\mu_n \, G_{En}(Q^2)/G_{Mn}(Q^2).$$

(NB. The analogous proton ratio was calculated earlier and it passes through zero at $Q^2 \approx 6.5$ GeV^2. This is a prediction that will soon be tested by experiment at JLab.) For the neutron, it is noteworthy that in the

neighborhood of $Q^2 = 0$

$$\mu_n \, G_{En}(Q^2)/G_{Mn}(Q^2) = -(r^2_n/6)\, Q^2,$$

where r^2_n is the neutron's mean-square electric radius. Our calculation shows this to be a good approximation for $|r^2_n|\, Q^2 < 1$, a result which is consistent with the data. The calculated curve omitted pion-loop effects from the current and therefore underestimated the magnitude of r^2_n. This is apparent in the figure. It is thus evident that, just as we found in earlier studies of the proton, the small Q^2 behavior of this ratio is materially affected by the neutron's pion cloud.

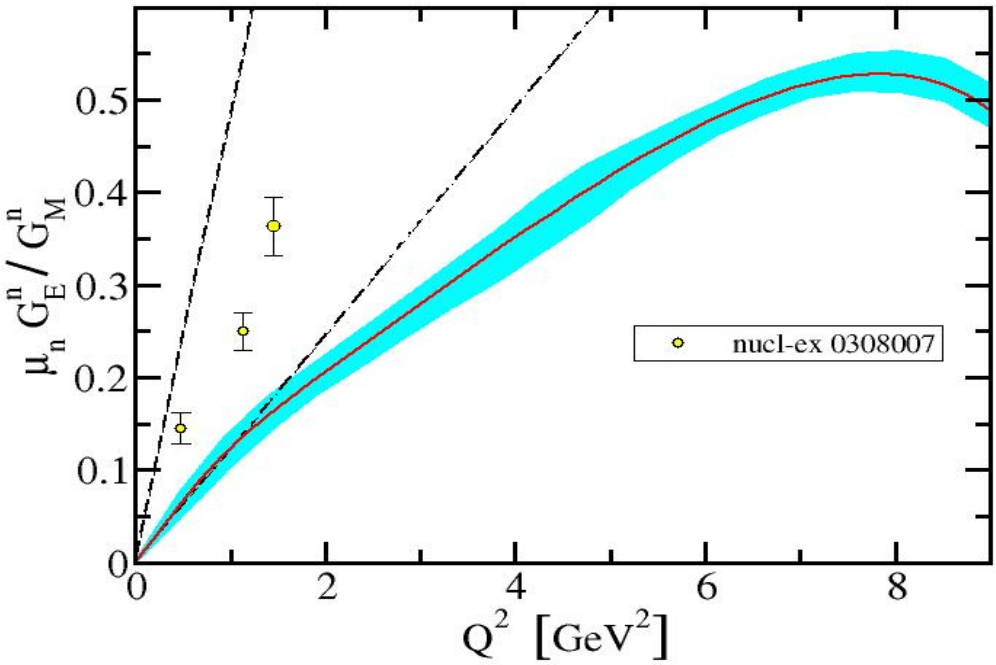

Fig. V-4. Solid curve – calculated result for $\mu_n \, G_{En}(Q^2)/G_{Mn}(Q^2)$. The band shows the response of the ratio to changes in model parameters and also reflects Monte Carlo -integration error. Dashed curve – $|r^2_n/6|_{expt.}\, Q^2$; dash-dot curve – $|r^2_n/6|_{calc.}\, Q^2$. Data from R. Madey et al., Phys. Rev. Lett. ***91****, 122002 (2003).*

Pseudoscalar mesons are not pointlike and, therefore, their contributions to form factors diminish in magnitude with increasing Q^2. It follows, therefore, that the evolution of $\mu_n \, G_{En}(Q^2)/G_{Mn}(Q^2)$ on $Q^2 > 2$ GeV^2, is primarily determined by the quark-core of the neutron. This calculation predicts that the ratio will continue to increase steadily until $Q^2 > 8$ GeV^2, which is a very different result to that for the proton. Data from JLab that is currently being analyzed will test this prediction out to $Q^2 > 3.5$ GeV^2.

In developing an understanding of these results, we returned to the observation that in a Poincaré covariant treatment the quark core of a nucleon is necessarily described by a Faddeev amplitude with nonzero quark orbital angular momentum. This is why the amplitude is a matrix-valued function with a rich structure that, in a baryons' rest frame, corresponds to a relativistic wavefunction with *s*-wave, *p*-wave and even *d*-wave components. The figure illustrates that while there is some quantitative sensitivity to the model parameters, the gross features of the form factors are primarily governed by correlations expressed in the nucleon's Faddeev amplitude and, in particular, by the amount of intrinsic quark orbital angular momentum. The nature of the kernel in the Faddeev equation specifies just how much quark orbital angular momentum is present in a baryon's rest frame.

*University of Rostock, Germany, †Karl-Franzens-Universität Graz, Austria, ‡University of Edinburgh, United Kingdom.
[1]J. Arrington, C. D. Roberts, and J. M. Zanotti, J. Phys. G **34**, S23-S52 (2007).
[2]M. S. Bhagwat, A. Höll, A. Krassnigg, and C. D. Roberts, *Theory and Phenomenology of Hadrons,* Nucl. Phys. **A790**, 10 (2007).

a.12. Semileptonic Decays of Heavy Ω Baryons in a Quark Model (M. Pervin, W. Roberts* and S. Capstick*)

The semileptonic decays of Ω_c and Ω_b baryons were treated in the framework of a constituent quark model. The form factors as well as the rates for the semileptonic heavy Ω decays were calculated within this model.

Analytic formulae were obtained for the form factors of Ω_b in the decays to ground states and a number of excited states of Ω_c. A modified fit of non-relativistic and semirelativistic Hamiltonians generated configuration-mixed baryon wavefunctions from the known masses and the measured $\Lambda^+_c \to \Lambda e^+ \nu$ rate, with wavefunctions expanded in both harmonic oscillator and Sturmian bases. We obtained general agreement with the leading-order constraints of heavy-quark effective theory. Using these configuration-mixed wavefunctions, the decay rates for Ω_b to pairs of ground and excited Ω_c states related by heavy-quark symmetry are, to a good approximation, in the ratios expected from heavy-quark effective theory. We also calculated numerous branching ratios for other decay modes; *e.g.*, $\Omega_c \to \Omega$, and provided evidence that our results have only modest model-dependence.

An article describing these results was published.[1]

*Florida State University.
[1]M. Pervin, W. Roberts, and S. Capstick, Phys. Rev. C **74**, 025205 (2006).

a.13. Ξ Baryons in a Constituent Quark Model (M. Pervin and W. Roberts*)

The study of hyperon properties can provide important insight into two questions of crucial interest in hadron physics; *viz.*, what are the relevant degrees of freedom in a baryon; and what is the mechanism of confinement? In order to understand the symmetries and dynamics of the strong interaction, the expected multiplet structure of the baryons must be established experimentally. For this, details of their excitation spectrum are crucial.

In this work we studied the multistrange (Ξs and Ωs) baryon spectrum using a non-relativistic quark model. The experimentally known states [*Ξ(1318)*, *Ξ(1530)*, *Ξ(1823)*, *Ω(1672)*] are well reproduced by our model, while we predicted the mass and spin-parity assignments for a number of the less-well-known states, such as the *Ξ(1690)*. The predictions for the spin-parity of multistrange baryons are very useful since, even for the "well-known" states, many of the quantum numbers have still not been measured.

*Florida State University.

a.14. Dynamical Coupled-Channel Model of πN Scattering in the $W \leq 2$ GeV Nucleon Resonance Region (T.-S. H. Lee, B. Julia-Diaz,* A. Matsuyama,† and T. Sato‡)

As a first step to analyze the electromagnetic meson production reactions in the nucleon resonance region, the parameters of the hadronic interactions of a dynamical coupled-channel model, developed in Ref. 1, are determined by fitting the πN scattering data up to invariant mass $W = 2$ GeV. The channels included in the calculations are πN, ηN and $\pi\pi N$ which has $\pi\Delta$, ρN, and σN resonant components. The non-resonant meson-baryon interactions of the model are derived from a set of Lagrangians by using a unitary

transformation method. One or two bare excited nucleon states in each of S, P, D, and F partial waves are included to generate the resonant amplitudes in the fits. The predicted total cross sections of πN reactions and $\pi N \rightarrow \eta N$ reactions are in good agreement with the data.

Some of our results are shown in Figs. V-5 and V-6 for the πN amplitudes and in Fig.V-7 for the predicted total cross sections.

*University of Barcelona, Spain, †Shizuoka University, Japan, ‡Osaka University, Japan.

[1]A. Matsuyama, T. Sato, and T.-S. H. Lee, Physics Reports **439**, 193 (2007).

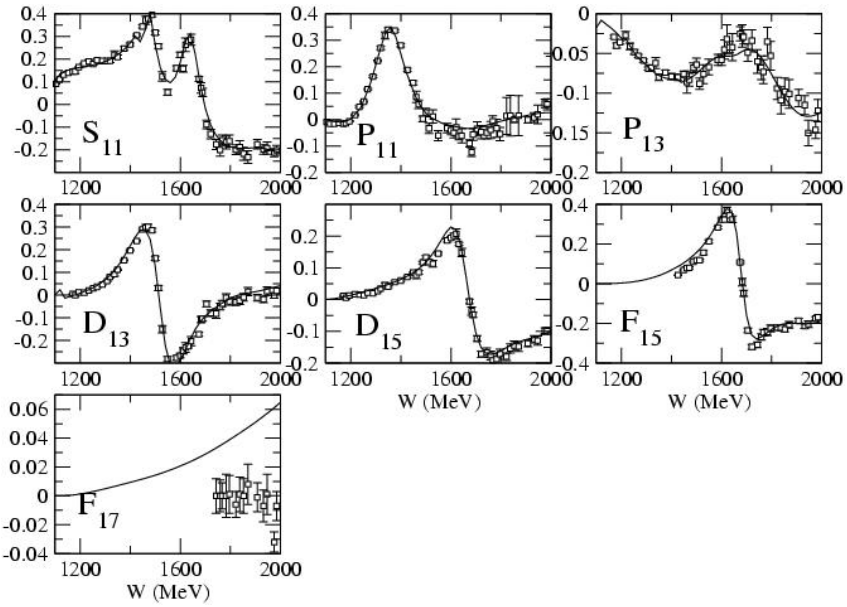

Fig. V-5. Real parts of the calculated πN partial wave amplitudes of isospin T = 1/2 are compared with the energy independent solutions of SAID.

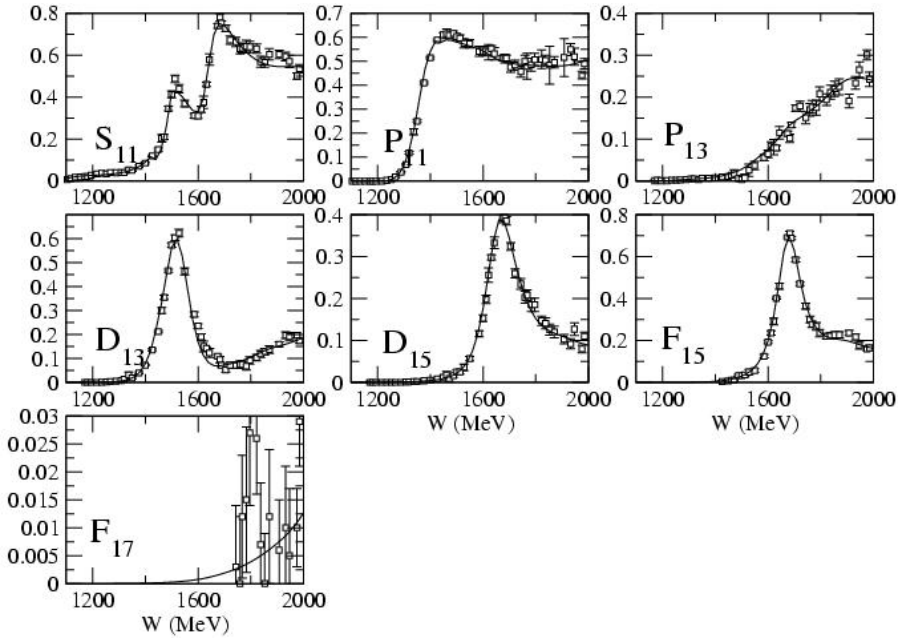

Fig. V-6. Imaginary parts of the calculated πN partial wave amplitudes of isospin T = 1/2 are compared with the energy independent solutions of SAID.

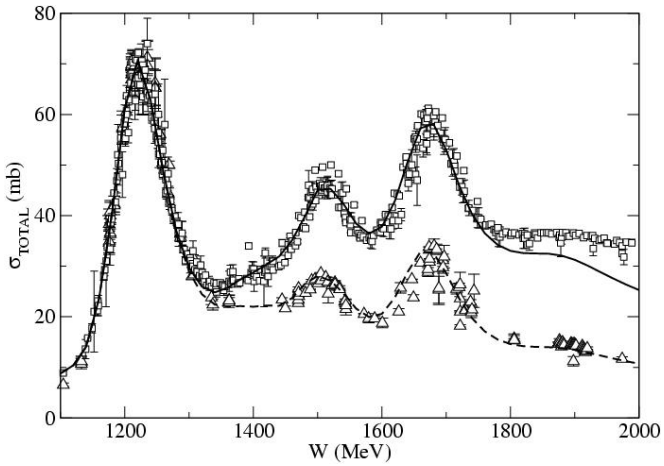

Fig. V-7. The predicted total cross sections of the $\pi^- p \rightarrow X$ (solid curve) and $\pi^- p \rightarrow \pi^- p + \pi^0 n$ (dashed curve) reactions are compared with the data.

a.15. Extraction and Interpretation of $\gamma N \rightarrow \Delta$ Form Factors within a Dynamical Model

(T.-S. H. Lee, B. Julia-Diaz,* T. Sato,† and C. Smith§)

Within the dynamical model of Ref. 1 we have performed an analysis of recent data of pion electroproduction reactions at energies near the $\Delta(1232)$ resonance. Figure V-8 shows the extracted Q^2-dependence of the meson cloud effects on the magnetic $\gamma N \rightarrow \Delta$ transition form factor. We have found that the extracted bare form factor (dashed curve) is close to the predictions of relativistic constituent quark models. The predictions from the lattice QCD calculations are only in very qualitative agreement with the extracted dressed form factors (solid curves).

*University of Barcelona, Spain, †Osaka University, Japan, §University of Virginia.

[1]T. Sato and T.-S. H. Lee, Phys. Rev. C **54**, 2660 (1996); Phys. Rev. C **63**, 055201 (2001).

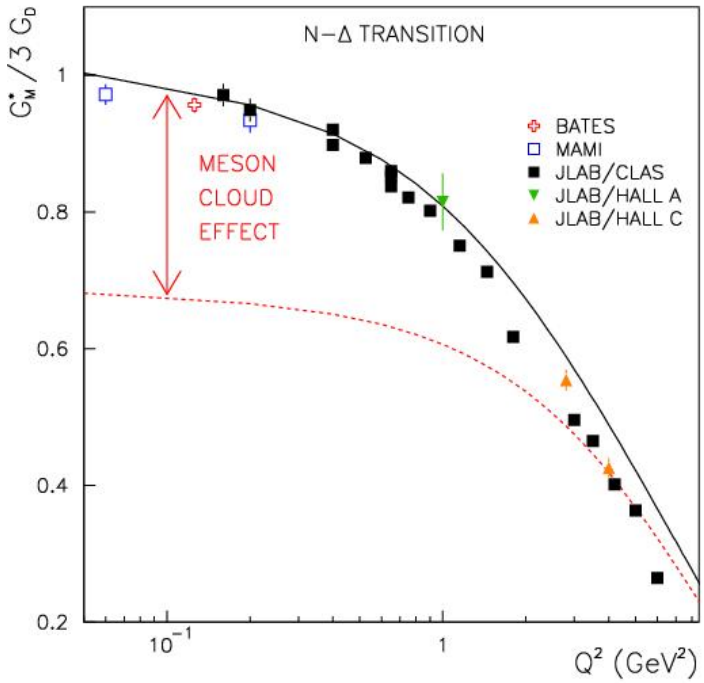

Fig. V-8. The extracted magnetic $\gamma N \rightarrow \Delta$ transition form factors.

a.16. Dynamical Coupled-Channel Analysis of π Electroproduction (T.-S. H. Lee, B. Julia-Diaz,* A. Matsuyama,† T. Sato,‡ and C. Smith§)

With the πN model constructed in Section a.14, we are now investigating π electroproduction reactions within the dynamical coupled-channel model of Ref. 1. The main focus is to extract the $\gamma N \rightarrow N^*$ form factors for testing the predictions from QCD-inspired hadron models and lattice QCD. As a first step, we have predicted the meson cloud effects on $\gamma N \rightarrow N^*$ (1440) form factors. Comparing with the empirical values extracted by the CLAS collaboration, we have found that meson cloud effects account for about 30% for the Roper $N^*(1440)$ resonance. The importance of the coupled-channel off-shell effects at short distances has been demonstrated.

Our current effort is to determine the $\gamma N \rightarrow N^*$ form factors for all of the known low-lying N^* with mass below 1.6 GeV. This is being done by developing a code to fit the differential cross section data of all of the available data of $p(e,e'\pi^0)p$ and $p(e,e'\pi^+)n$ reactions in the W = 1.1-1.7 GeV and Q^2 = *0-6* (GeV/c)^2 region.

*University of Barcelona, Spain, †Shizuoka University, Japan, ‡Osaka University, Japan, §University of Virginia.
[1]A. Matsuyama, T. Sato, and T.-S. H. Lee, Physics Reports **439**, 193 (2007).

a.17. Speed-Plot and Time-Delayed Methods for Extracting Resonance Parameters (T.-S. H. Lee, O. Suzuki,* and T. Sato*)

Speed-plot method proposed by Hohler and Time-delayed method originated from Wigner have been commonly used to extract the resonance parameters from the empirical partial-wave amplitudes. However, the validity of these methods for the coupled-channel cases have not been well investigated. Within several exactly soluble models, we reveal that these two methods give poles on different Riemann sheets and clarify the conditions under which we can safely apply these methods. We are currently applying these

methods to extract the poles from the πN scattering amplitudes generated from the dynamical coupled-channel model described in Section a.14. We are also developing theoretical interpretations of the extracted poles; in particular on their relations with the predictions from hadron models and lattice QCD.

*Osaka University, Japan.

a.18. On the Sign of the π-ρ-ω Coupling Constant (T.-S. H. Lee, K. Nakayama,* Y. Oh,* and J. Haidenbauer†)

It is shown that the relative sign between the $NN\omega$ and π-ρ-ω coupling constants can be determined most sensitively from ω production processes in NN collisions. Our results from a distorted-wave impulse approximation calculation are shown in Fig. V-9. Clearly, the recent data favor the sign of the π-ρ-ω coupling constant which is opposite to that inferred from studies of the photoproduction reaction in combination with the vector meson dominance assumption. We are currently investigating the consequences of our results in predicting the ω photoproduction reactions.

*University of Georgia, †Jülich Research Center, Germany.

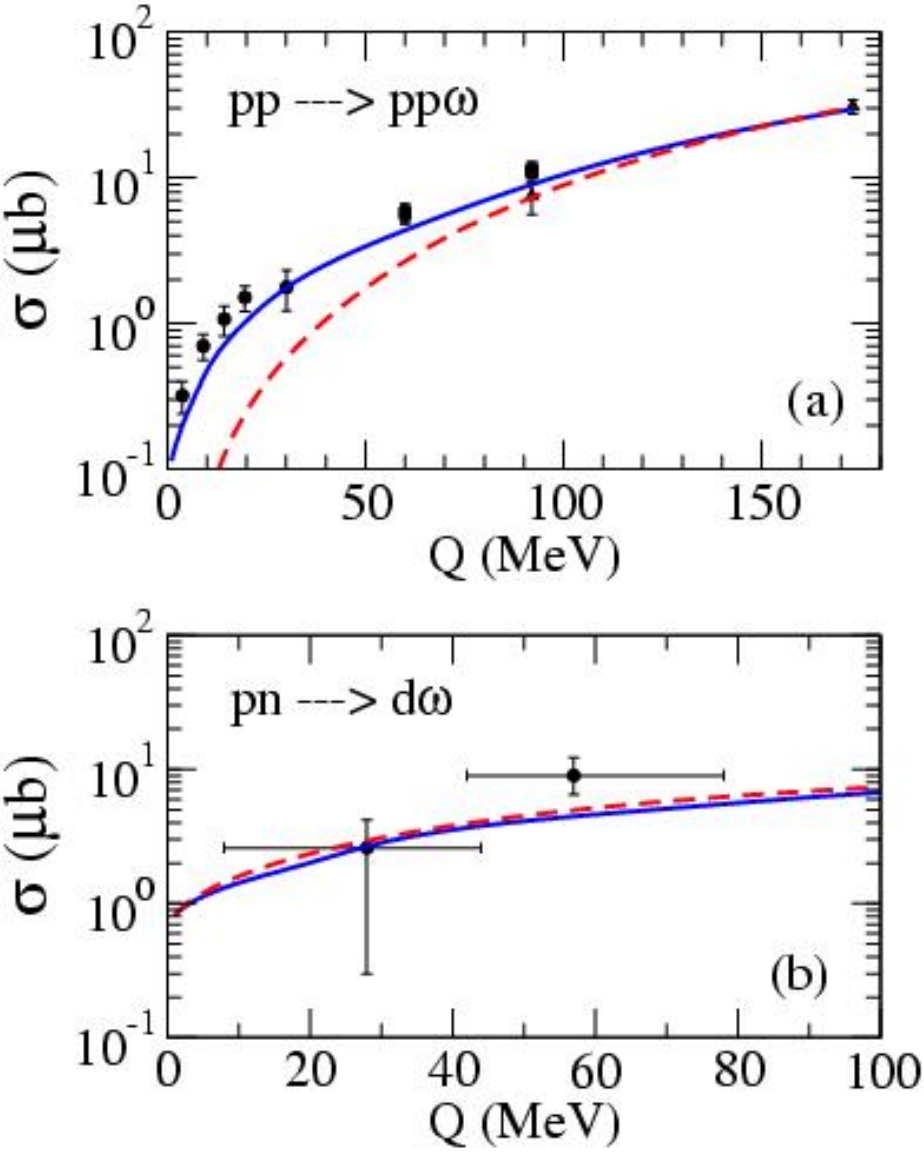

Fig. V-9. Total cross sections of ω production in NN collisions. The dashed curves are from the calculations using the sign of π-ρ-ω coupling conventionally determined by using the vector meson dominance assumption. The solid curves are obtained when the opposite sign is chosen.

B. NUCLEAR FORCES AND NUCLEAR SYSTEMS

The goal of this program is to achieve a description of nuclear systems ranging in size from deuterium and tritium to nuclear matter and neutron stars using a single parameterization of the nuclear forces. Aspects of our program include both the construction of two- and three-nucleon potentials and the development of many-body techniques for computing nuclear structure and reactions with these interactions. Detailed quantitative, computationally-intensive studies are essential parts of this program.

Quantum Monte Carlo (QMC) calculations of light ($A \leq 12$) nuclei with realistic interactions have been the main focus of our recent efforts. Our nonrelativistic Hamiltonian contains the accurate Argonne v_{18} two-nucleon (*NN*) potential, which includes charge-independence breaking terms, and either the Urbana IX three-nucleon (*NNN*) potential, or one of several Illinois *NNN* models. The QMC calculations include both variational (VMC) and Green's function (GFMC) methods. We begin with the construction of variational trial functions based on sums of single-particle determinants with the correct total quantum numbers, and then act on them with products of two- and three-body correlation operators. Energy expectation values are evaluated with Metropolis Monte Carlo integration and parameters in the trial functions are varied to minimize the energy. These optimized variational wavefunctions can then be used to study other nuclear properties. They also serve as a starting point for the GFMC calculations, which systematically remove higher excited-state components from the trial wavefunctions by propagation in imaginary time.

We are currently studying all $A \leq 10$ nuclei, including more than 100 ground or excited states, as well as ^{12}C. These are the first calculations to treat $A \geq 6$ nuclei directly with realistic *NN* and *NNN* interactions. In GFMC calculations, with our best Hamiltonian, we can reproduce most of the experimental ground- and excited-state energies to within *0.6* MeV.

Many excited states in the light nuclei are not particle stable and should be treated as scattering states, though until recently our efforts treated all of them as bound. A major effort was made in the last two years to extend our GFMC program to nucleon-nucleus scattering, and results for ^{5}He, or $n\alpha$ scattering are in press. These results demonstrate that we can make *ab-initio* calculations of the low-energy scattering cross section, and extract resonance energies and widths.

A new effort this year is to calculate electroweak M1, E2, and GT transition matrix elements in light nuclei. In previous years we had examined a number of transitions and form factors using VMC trial functions, but now we have developed the machinery to use the full GFMC propagated wavefunctions. Initial results have been obtained for a dozen transitions in $A = 6,7$ nuclei and good agreement with experiment is obtained in most cases. A major long term goal of the scattering and transition efforts is to use GFMC wavefunctions to predict reaction cross sections for astrophysics as part of the Theory Group's nuclear astrophysics effort.

We used our VMC wavefunctions to investigate the two-nucleon momentum distributions in ground states of light $A \leq 8$ nuclei as a function of the relative and center-of-mass momenta. We find an order-of-magnitude difference in the number of *np* and *pp* pairs with relative momenta

above *1.5* fm^{-1} when they have vanishing total momentum. This prediction can be tested in two-nucleon knockout electron-scattering experiments at JLab.

We also continued a systematic survey of cluster form factors and spectroscopic factors in the light *p*-shell nuclei using VMC wavefunctions. The correlations in these wavefunctions can provide significant quenching of spectroscopic factors compared to traditional shell-model calculations. A specific application was made for a new (d,^{3}He) experiment run at ATLAS. The calculated cluster form factors are used as input to the distorted-wave Born approximation (DWBA) program PTOLEMY, developed here many years ago, to provide the theoretical analysis of the experiments. We are also providing overlap calculations to experimental groups at MSU and TRIUMF.

Calculations with order 1% accuracy of the rms radii of helium isotopes are needed for comparison to experiment but had proven impossible to achieve. This year we made considerable progress in solving this problem and have provided a prediction for a measurement of the ^{8}He charge radius being made by Argonne experimentalists at GANIL.

A simple but useful guide for understanding the structure of light nuclei was formulated, based on counting the number of interacting pairs in different spin-isospin states for a given spatial symmetry and estimating the overall binding according to the spin-isospin operator expectation value taken from one-pion exchange. The overall binding of light nuclei, various aspects of their excitation structure, and clustering characteristics are all given a simple physical interpretation. This model correlates many of the results from our detailed QMC calculations of the last several years.

The influence of changes of fundamental physical constants on properties of nuclei is of considerable interest. We are studying how nuclear binding energies might change if the underlying nucleon and meson masses vary. This is done by making appropriate modifications of the nuclear Hamiltonian and carrying out VMC calculations for $A \leq 8$ nuclei. The specific predictions from DSE studies of how the hadron masses vary with the current-quark mass can be used as input, and in turn, the output may be used in astrophysical rate calculations to examine the consequences for primordial nucleosynthesis. These studies may also provide some useful insight into contemporary efforts to extract nucleon-nucleon scattering from lattice QCD calculations.

b.1. Quantum Monte Carlo Calculations of Light Nuclei Energies (S. C. Pieper, R. B. Wiringa, K. M. Nollett, and J. Carlson*)

We have been studying the ground states and excitation spectra of light nuclei as *A*-body problems with realistic nucleon-nucleon (*NN*) and three-nucleon (*NNN*) interactions using advanced quantum Monte Carlo (QMC) many-body methods. Our preferred Hamiltonian contains the Argonne v_{18} *NN* potential (AV18), which gives an excellent fit to elastic *NN* scattering data and deuteron properties, and the Illinois-2 *NNN* potential (IL2), which we have fit to binding energies of $A \leq 8$ nuclei. The QMC methods include both variational Monte Carlo (VMC), which gives an initial approximate solution to the many-body Schrodinger equation, and Green's function Monte Carlo (GFMC), which systematically improves on the VMC starting solution. The GFMC method produces absolute binding energies that are accurate at the 1-2% level.

The VMC calculations begin with the construction of an antisymmetric Jastrow trial wavefunction that includes single-particle orbits coupled to the desired *JM* values of the state of interest as well as pair and triplet correlations. A symmetrized product of two- and three-body spin, isospin, and tensor correlation operators (induced by the *NN* and *NNN* potentials) is applied to the Jastrow product to produce the full trial function. The wavefunction is diagonalized in the small basis of different spatial symmetry components to project out multiple states with the same quantum numbers.

In GFMC calculations an imaginary-time propagator, $exp[-(H-E_0)\tau]$, where H is the Hamiltonian, E_0 is an estimate of the eigenvalue, and τ is the imaginary time, is applied to the VMC trial function. The excited-state components of the trial function are damped out for large τ, leaving the exact lowest eigenfunction with the quantum numbers of the input VMC trial function. The expectation value of H is computed for a sequence of increasing values of τ to determine the convergence.

In 2006 we started work on new versions of the Illinois *NNN* potentials. The IL2 parameters we currently use were published in 2001. Since then we have made a number of improvements in the GFMC propagation and, with the improvements in computer speeds, are routinely doing calculations with much better statistics. This has revealed some difficulties in the IL2 parameters, particularly for ^{8}He. We are also including $A = 9$ and 10 nuclei in the fitting procedure for the first time. This work is still in progress.

We are part of the "Universal Nuclear Energy-Density Functional" collaboration in the DOE SciDAC program. Most of our work in that will be concerned with changes to the GFMC program to enable efficient ^{12}C calculations on parallel computers with 10,000's of processors. With other groups we will be making benchmark calculations of ^{12}C and other nuclei using various Hamiltonians. The first bench marks will be for ^{4,6,8}He and ^{6}Li using just a two-nucleon potential. However, realistic *NN* potentials do not bind ^{6,8}He without the addition of a *NNN* potential. To get around this difficulty, we have made small modifications to the ^{3}P components of the Argonne v_8' and a v_8' projection of the super-soft-core C potential so that the ^{6,8}He and ^{6}Li separation energies are close to the experimental values. A subroutine for these potentials is available at http://www.phy.anl.gov/theory/research/av18/.

*Los Alamos National Laboratory.

b.2. Scattering Methods for Quantum Monte Carlo Calculations (K. M. Nollett, S. C. Pieper, R. B. Wiringa, J. Carlson,* and G. M. Hale*)

Our calculations of properties of light nuclei have concentrated on energies of discrete levels, because the quantum Monte Carlo methods have until recently required that unbound states be treated as bound states. We have, therefore, been restricted to bound or narrow states, and unable to compute the widths of resonances. A smaller amount of effort has gone into computing transition probabilities and radiative-capture cross sections using VMC wavefunctions, along with calculations of a few static nuclear properties like RMS radii.

It is desirable to expand the range of the QMC methods to include unbound states treated as such and the computation of phase shifts and reaction cross sections. This will greatly expand the number of observables against which the computational methods and potentials can be tested. It will also open the door to accurate quantitative predictions of reaction cross sections for astrophysics, at least in the light systems important for solar neutrinos, big-bang nucleosynthesis, and seeding the r-process in alpha-rich freeze-out.

We are developing methods to compute unbound states, using an R-matrix-like boundary condition to specify the state being computed. As a first application, we have computed low-energy phase shifts in the first three partial waves in ^{4}He-neutron scattering.[1] In VMC, the boundary condition is set as a condition on the correlation between the ^{4}He nucleus and the last neutron. In GFMC, the boundary condition is enforced through a method of images that enforces a specified logarithmic derivative in the wavefunction normal to a specified surface of fixed ^{4}He-n separation (*9 fm* in most of our calculations). Useful calculations require an accuracy of about *50* keV or better. This in turn requires careful work to eliminate dependence of the result on the GFMC path constraint, the starting wavefunction, and the radius at which the boundary condition is imposed.

Results after carefully controlling these sources of error

are shown in Fig. V-10 below for the $J^\pi = 3/2^-$ and $J^\pi = 1/2^-$ *p*-wave and the $J^\pi = 1/2^+$ *s*-wave scattering partial waves. The results for three different choices of potential demonstrate the importance of the three-nucleon interaction in this system: the AV18 two-nucleon interaction alone provides less splitting between the *p*-waves than observed, while including the most up-to-date three-nucleon interaction (Illinois-2) produces good agreement with measured phase shifts.

This work opens the door to several additional calculations in light nuclei, particularly neutron resonances, states in ^{4}H, and the ^{7}Be(p,γ)^{8}B radiative capture reaction.

*Los Alamos National Laboratory.

[1]K. M. Nollett, S. C. Pieper, R. B. Wiringa, J. Carlson, and G. M. Hale, Phys. Rev. Lett. **99**, 022502 (2007).

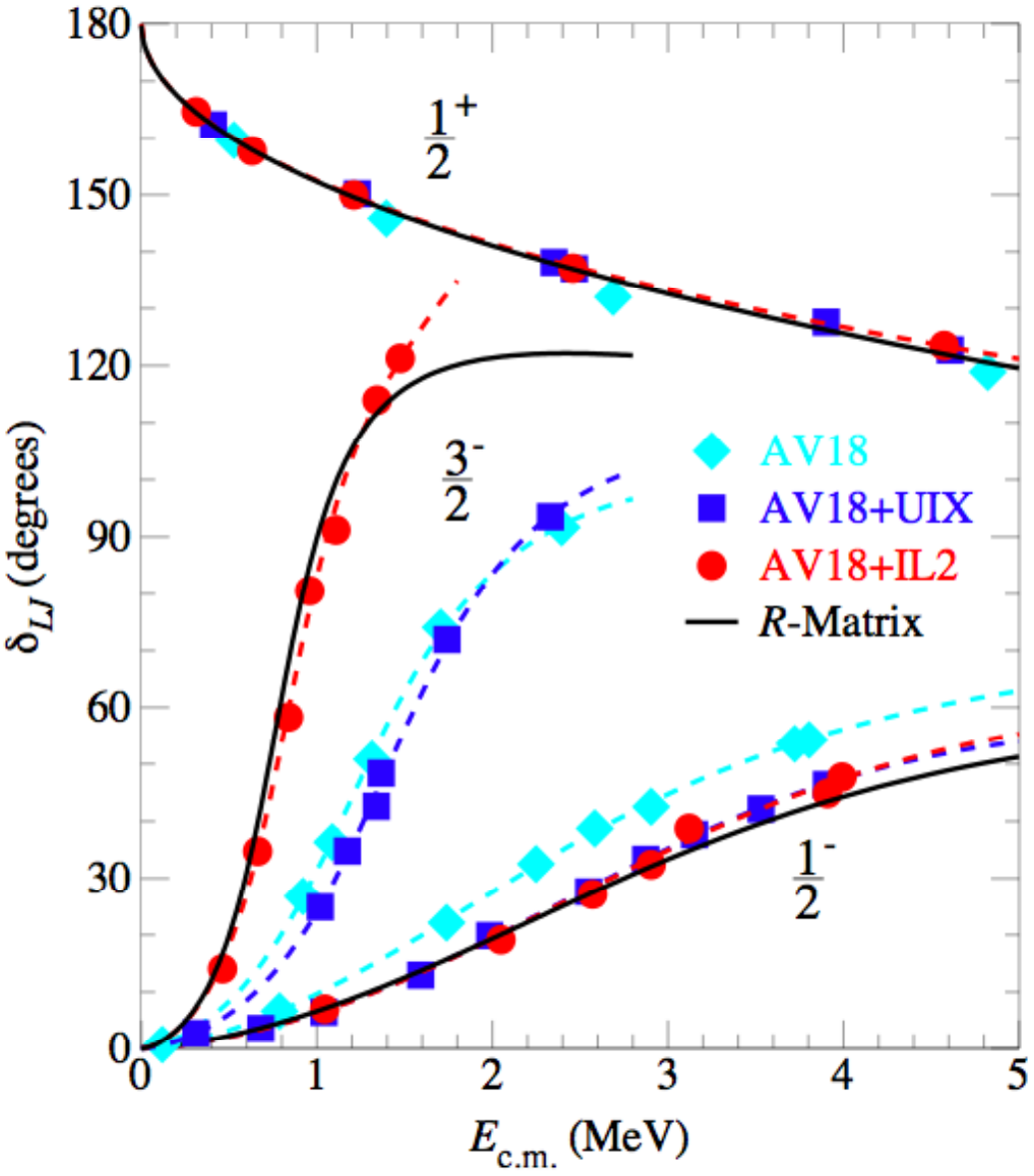

Fig. V-10. Phase shifts for ^{4}He-neutron scattering with three different potentials, broken down by partial wave. Solid curves are an R-matrix fit to the measured cross sections. Filled symbols joined by dashed curves are results of GFMC calculations.

b.3. Spectroscopic Factors and Cluster Form Factors of Light Nuclei (R. B. Wiringa, S. C. Pieper, and D. Kurath)

The cluster form factor is defined as the overlap between A-body and $(A-1)$-body nuclear states, either in configuration or momentum space, $\langle (A-1)_J | a_j | A_{J'} \rangle$, where a_j is a nucleon annihilation operator. It is a very useful quantity in analyzing pickup reactions such as (p,d), where $A_{J'}$ is a ground state, or stripping reactions such as (d,p), where $(A-1)_J$ is a ground state, or nucleon-knockout reactions such as $(e,e'p)$. The cluster form factor can be folded into a DWBA calculation to help extract experimental information. The spectroscopic factor S is just the normalization of this wavefunction overlap, and provides a simple characterization of nuclear structure aspects of such reactions.

We have been calculating the cluster form factors and spectroscopic factors for all $A \leq 10$ nuclei using VMC wavefunctions from the AV18+UIX Hamiltonian. The spectroscopic factors are being compared to predictions from the Cohen-Kurath (CK) shell model.[1] The CK spectroscopic factors for transitions between stable nuclei were first published in 1967, but many additional transitions are now experimentally accessible with the advent of rare-isotope beams at Argonne, MSU, and other facilities.

Two specific applications were made in 2005 as part of experiments carried out at ATLAS: a study of the ^{9}Li spectrum using the ^{8}Li(d,p) reaction, and a study of the ^{7}He spectrum using the ^{6}He(d,p) reaction. This year we participated in a follow-on experiment on ^{7}He using the ^{8}Li$(d,^3$He$)$ reaction. The VMC cluster overlaps between the ground state of ^{8}Li and the ground and low-lying excited states in ^{7}He were calculated and used as input to the DWBA program PTOLEMY to obtain differential cross sections. The VMC overlaps predict a specific overall normalization. We also made VMC calculations of the $\langle d|a_j|^3\text{He}\rangle$ and $\langle d|a_j|t\rangle$ overlaps to improve PTOLEMY calculations of $(d,^3$He$)$ and (d,t) reactions. A paper on the experiment is being prepared for publication.

In addition, we have been providing overlap calculations to other experimental groups at both MSU and TRIUMF.

[1] S. Cohen and D. Kurath, Nucl. Phys. **A101**, 1 (1967).

b.4. Calculations of RMS Radii of Helium Isotopes (S. C. Pieper, R. B. Wiringa, and J. Carlson*)

In October 2004, a group led by the Physics Division's Zheng-Tian Lu published a measurement, with better than 1% accuracy, of the rms charge radius of ^{6}He. The measurement prompted us to attempt a correspondingly accurate calculation of the ^{6}He point proton and neutron rms radii. This has proved significantly more difficult than we originally anticipated, but the work is nearing completion.

We first had to improve the GFMC propagation to obtain reliable densities in the neutron halo of ^{6}He. Even with these improvements we find that GFMC calculations made with different starting wavefunctions can result in binding energies that differ by *50* to *100* keV. Although this is only 0.2% to 0.3% of the binding energy, it is 5% to 10% of the separation energy to ^{4}He plus two neutrons and the rms radius can be significantly changed. Thus, in practice, all we can do is produce a narrow band of rms radius versus separation energy. We find that many different calculations, including ones for different Hamiltonians, even those without NNN potentials, lie in this band. The band reproduces the experimental rms radius at the experimental separation energy.

We have made similar calculations for ^{8}He, lithium isotopes, and other $A = 9$ and *10* nuclei for which rms radii are measured or should be experimentally accessible. Lu's group is in the process of measuring the charge radius of ^{8}He; at the experimental ^{8}He to ^{6}He separation energy, our band of calculated values predicts a charge radius of 1.94(3) fm, which is 0.11 fm smaller than the ^{6}He value.

*Los Alamos National Laboratory.

b.5. Pair Counting, Pion-Exchange Forces, and the Structure of Light Nuclei (R. B. Wiringa)

A simple but useful guide for understanding the structure of light nuclei has been formulated. It is based on counting the number of interacting pairs in different spin-isospin (*ST*) states for a given spatial symmetry and estimating the overall binding according to the sum of $\sigma_i \cdot \sigma_j$ $\tau_i \cdot \tau_j$ expectation values. This choice is motivated by long-range one-pion exchange (OPE), which in the microscopic quantum Monte Carlo (QMC) calculations gives about 75% of the net potential energy, although most of the contribution comes from the tensor component of the OPE potential rather than the spin-isospin part. This operator conveys a key feature of *NN* forces, namely that they are moderately attractive in (*ST*) = (*10*) and (*01*) pairs, slightly repulsive in (*11*) pairs, and very repulsive in (*00*) pairs.

The number of pairs of different (*ST*) combinations, $P_A(ST)$ for a given nuclear state can be obtained knowing the total spin, isospin, and spatial symmetry. The energy estimate is

$$E_{OPE} = C[9P_A(00)-3P_A(01)-3P_A(10)+P_A(11)]$$

where *C* is a scale factor in units of energy. With this estimate, the binding energy of the deuteron, triton, and alpha are *-3 C*, *-9 C*, and *-18 C*, respectively. This is actually a good estimate of the relative potential energies obtained in our QMC calculations, but not of the total binding because the positive kinetic energy contribution grows less rapidly. However, in the *p*-shell something like a virial theorem is established, with the ratio of kinetic to potential energy having a fairly constant value *0.76-0.80*, so E_{OPE} does become a binding energy estimator.

As nucleons are added in the *p*-shell, they essentially decouple from the *s*-shell, in that the contribution to E_{OPE} from pairs where one nucleon is in the *s*-shell and one in the *p*-shell vanishes. Thus the energy prediction for ^{5}He is *-18 C*, the same as for ^{4}He, indicating that the relative stability will be determined by finer details of the force and requirements of Fermi statistics. In general, the energies of *p*-shell nuclei are predicted to be basically the energy of their sub-cluster components, which helps explain why light nuclei show considerable clustering. This feature is also seen in the QMC calculations with the full AV18 *NN* potential; much of the cluster-cluster binding is provided by adding an *NNN* potential. The model also explains why mixing of different spatial symmetries in ground states increases as T increases across isobars.

In the *p*-shell, each nucleus has many excited states arising from different spin and spatial symmetry combinations. The $P_A(ST)$ for each state is easily evaluated and the above energy estimate used to study the excitation spectrum. When various spatial symmetry states can combine to give a specific total spin, those combinations that have the least amount of very repulsive (*00*) pairs will lie lowest. For example, in ^{7}Li the states that are predominantly 4P[421] symmetry are below those with 2P[421] symmetry, because they have more (*11*) pairs and fewer (*00*) pairs. It can also be used to predict orderings of some *sd*-shell intruder states.

A paper describing this concept was submitted and published in 2006.[1]

[1] R. B. Wiringa, Phys. Rev. C **73**, 034317 (2006).

b.6. Tensor Forces and the Ground State Structure of Nuclei (R. B. Wiringa, S. C. Pieper, R. Schiavilla,* and J. Carlson†)

We have calculated a variety of two-nucleon momentum distributions in the ground states of light nuclei with mass number $A \leq 8$ using variational Monte Carlo wavefunctions derived from a realistic Hamiltonian with two- and three-nucleon potentials. These include distributions that are a function of either the relative momenta *q* between the pair or the center-of-mass momenta *Q* of the pair. A special case is the relative momentum distribution when the center-of-mass of the pair is zero. Interestingly, we find the momentum distribution of *np* pairs is much larger than that of *pp* pairs for values of the relative momentum in the range *1.5-3* fm^{-1} and vanishing total momentum. This is illustrated in Fig. V-11 for nuclei from ^{3}He to ^{8}Be. This order of magnitude difference has a universal character originating from the tensor components present in any realistic nucleon-nucleon potential. The correlations induced by the tensor force strongly

influence the structure of *np* pairs, which are predominantly in deuteron-like states, building up a significant tail in the momentum distribution beyond *1.5 fm*$^{-1}$. In contrast, the *pp* pairs, which are mostly in $^1S_0$ states, have a minimum in the momentum distribution around *2 fm*$^{-1}$. We predict these features should be easily observable in two-nucleon knock-out processes, such as A(*e,e*'np) and A(*e,e*'pp), and there is some preliminary evidence from experiments at Brookhaven and JLab to support this idea. A letter on this work was submitted and has been published.[1]

*Thomas Jefferson National Accelerator Facility, †Los Alamos National Laboratory.

[1]R. Schiavilla, R. B. Wiringa, S. C. Pieper, and J. Carlson, Phys. Rev. Lett. **98**, 132501 (2007).

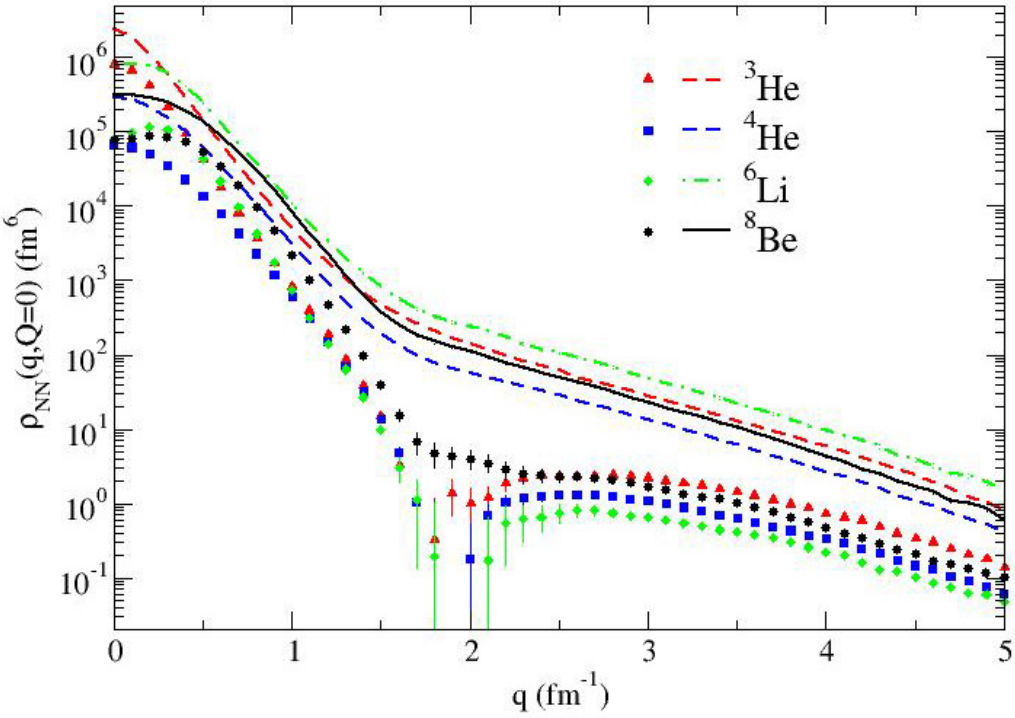

Fig. V-11. The np (lines) and pp (symbols) momentum distributions in various nuclei as functions of the relative momentum q at vanishing total pair momentum Q.

b.7. Quantum Monte Carlo Calculations of Electroweak Transition Matrix Elements

(M. Pervin, S. C. Pieper, and R. B. Wiringa)

We have been making quantum Monte Carlo calculations of M1, E2, and GT transition matrix elements in light nuclei. Variational Monte Carlo (VMC) calculations have been made in past years for electromagnetic form factors in ^{6}Li, transition densities in ^{7}Li, and weak decays of ^{6}He and ^{7}Be. Reasonable agreement with experiment at the ~10% level was obtained using wavefunctions generated from the AV18+UIX Hamiltonian. Now we are performing more precise Green's function Monte Carlo (GFMC) calculations with wavefunctions generated from the improved AV18+IL2 Hamiltonian. To the best of our knowledge, these are the first GFMC calculations of off-diagonal matrix-elements ever.

The matrix elements are extrapolated from mixed estimates that bracket the relevant electroweak operator between a variational trial state and a GFMC propagated wavefunction. Because they are off-diagonal terms, two mixed estimates are required for each transition, with a VMC initial (final) state paired with a GFMC final (initial) state. At present, we have

calculated more than a dozen M1, E2, and GT transitions between states of ^{6}He, ^{6}Li, ^{7}Li, and ^{7}Be. We find the B(E2) strengths, which depend sensitively upon the radius of the nucleus, are larger and closer to experimental values with the GFMC calculations compared to the older VMC results. However, the B(M1) and B(GT) strengths do not evolve much going from VMC to GFMC, although they do generally move closer to experiment. An example of the evolution of an E2 matrix element with the propagation of the GFMC wavefunction in imaginary time is shown in Fig. V-12.

A paper on the $A = 6,7$ calculations is in preparation. We will extend these calculations to larger nuclei in the next year, and have already made some preliminary studies in $A = 8$ nuclei.

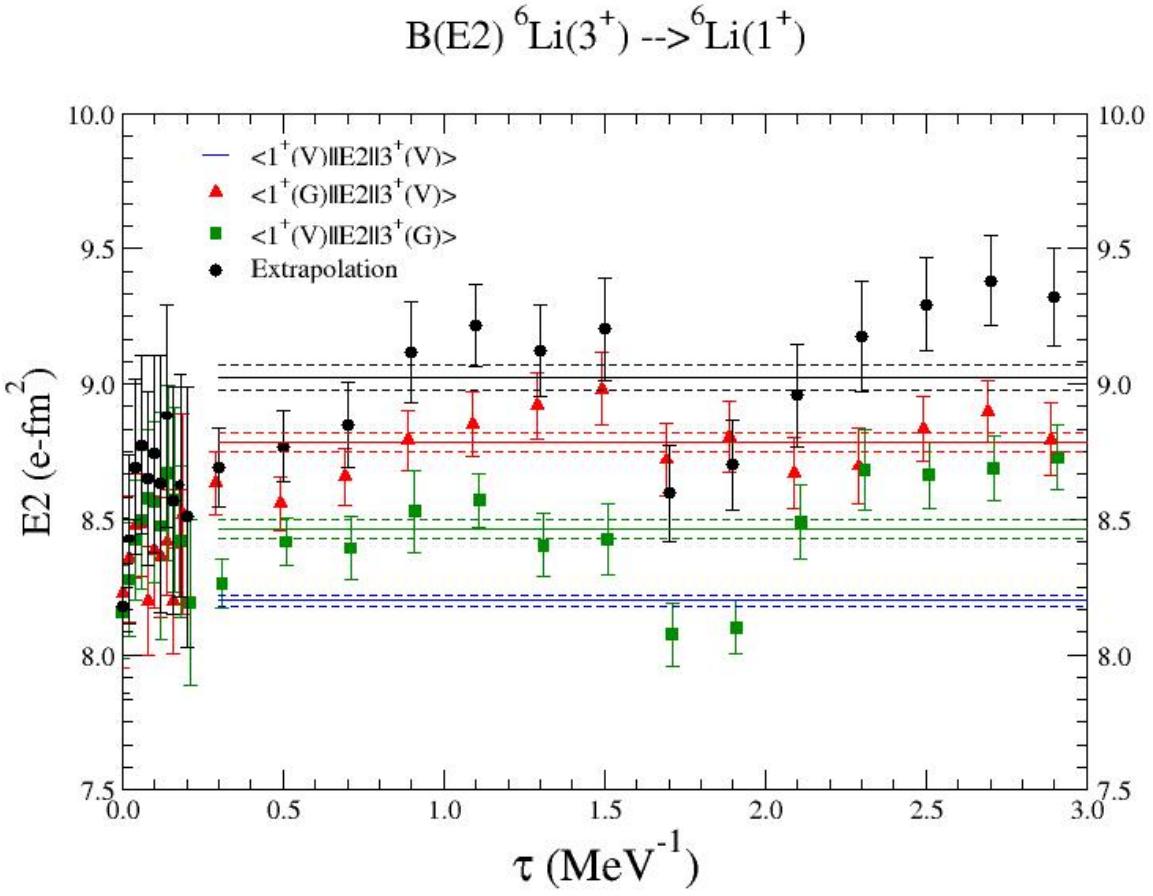

Fig.V-12. The VMC matrix element, GFMC mixed estimates, and extrapolated final result for the E2 transition from the first excited state to the ground state in ^{6}Li ($3^{+} \rightarrow 1^{+}$).

b.8. Quantum Monte Carlo Calculations of Isospin-Mixing Matrix Elements in ^{8}Be

(R. B. Wiringa, S. C. Pieper, and M. Pervin)

There are three pairs of states in the spectrum of ^{8}Be that show considerable isospin-mixing, the second and third 2^{+} states at 16.6 and 16.9 MeV, being the most famous. These isospin-mixed states come from blending the $T = 1$ isobaric analog of the ^{8}Li ground state with the second $T = 0$ excited state. There are also fairly close 1+ and 3+ pairs at slightly higher energies in the ^{8}Be spectrum. The isospin-mixing matrix elements that connect these pairs of states, $E_{01}(J) = \langle \Psi(J^{+};0)|H|\Psi(J^{+};1)\rangle$, were computed several years ago using VMC wavefunctions from the AV18+UIX Hamiltonian, which has kinetic, Coulomb,

magnetic moment, and strong charge-symmetry-breaking (CSB) contributions. However, the results underpredicted the values deduced from transition rate experiments.

Using the new methods described above, we are now recalculating these matrix elements using GFMC wavefunctions for the AV18+IL2 Hamiltonian. We find that the matrix element for the 2^+ states goes from *-107* keV in VMC to *-115* keV in GFMC, compared to the experimental value of *-144* keV. Two thirds of the calculated result is from Coulomb and one third from the other terms, so this is a sensitive place to test our knowledge of CSB interactions.

The $A = 8$ system is also of considerable interest as a laboratory for studying the conservation of the vector current (CVC) and the absence of second-class currents, which should be exact symmetries in the limit of good isospin. Experiments involve the weak decays of the 2^+ ground states of ^{8}Li and ^{8}B and the electromagnetic decay of the isospin-mixed 2^+ states in ^{8}Be to the broad first 2^+ state in ^{8}Be at *3* MeV. It is important to know how much T = 1 contamination is present in this latter state; our initial GFMC calculation gives a very small $E_{01} = -6$ keV, implying very small contamination.

b.9. Dependence of Nuclear Binding on Hadronic Mass Variation (V. V. Flambaum* and R. B. Wiringa)

We are studying how the binding of light ($A \leq 8$) nuclei depends on possible variations of hadronic masses, including meson, nucleon, and nucleon-resonance masses. Small variations in hadronic masses may have occurred over time; the present results could help evaluate consequent changes in primordial nucleosynthesis. Larger variations may be relevant to current attempts to extrapolate properties of nucleon-nucleon interactions from lattice QCD calculations.

We carry out this study by isolating the hadronic mass dependence in three different Hamiltonians based on different nucleon-nucleon potentials. We use the Argonne *v14* and Argonne *v28* potentials of 1984, and the Argonne *v18* potential of 1995 accompanied by the Urbana IX three-nucleon potential. The AV14 and AV18 are standard *NN* potentials, while the AV28 adds explicit Δ degrees of freedom. We calculate the energies of the $^1S_0$ virtual bound state and the deuteron for these potentials by direct solution of the two-body equations, and the energies of $A = 3$-*8* nuclei using variational Monte Carlo methods.

Results are presented as derivatives of the energy with respect to the different masses so they can be combined with different predictions of the hadronic mass-dependence on the underlying quark masses. As an example, we have used a particular set of relations obtained from a Dyson-Schwinger study of hadron masses and sigma terms.[1] In this case we find that nuclear binding decreases moderately rapidly as the quark mass increases, with the deuteron becoming unbound when the pion mass is increased by ~50%. In the other direction, the singlet state becomes bound if the pion mass is decreased by ~10%. However, the deuteron always lies below the singlet state for the range of quark masses we consider, in disagreement with some lowest-order effective field theory predictions.

---

*Argonne Fellow, Physics Division, and University of New South Wales, Sydney, Australia.

[1]V. V. Flambaum, A. Höll, P. Jaikumar, C. D. Roberts, and S. V. Wright, Few-Body Syst. **38**, 31 (2006).

C. NUCLEAR ASTROPHYSICS

The objective of this research program is to investigate nuclear processes that take place in stars, in the big bang, and in interstellar and intergalactic space. Nuclear phenomena are ubiquitous in the universe. The stars shine by nuclear energy, and the chemical compositions observed in the solar system and elsewhere are the results of nuclear processes that occurred in the big bang and inside the many generations of stars that have formed and evolved since then. Many astrophysical phenomena may only be understood by a combination of nuclear physics with methods more familiar to astrophysicists.

A particularly important problem is to determine rates for the nuclear reactions that occur in astrophysical environments. There are many applications (for example, the rapid neutron capture process) where large contributions from theoretical nuclear physics – particularly masses and cross sections – will always be necessary as input, and we maintain research interests in these areas. We have applied advances in the theoretical descriptions of light nuclei to compute cross sections important for considerations of big-bang nucleosynthesis, the solar neutrino flux, and seeding of the *r*-process. This work continues in close connection with our other work on light nuclei, and the main goals at present are to improve the wave functions and computational methods as described in Section b.2. In the last year, we have participated in work to improve the computational methods used to compute weak-interaction rates important for the collapse and subsequent supernova explosions of massive stars.

Understanding nucleosynthesis and energy generation in a particular astrophysical environment requires calculations of nuclear reaction networks. Even for cases in which the detailed astrophysical phenomena can only be understood from difficult calculations coupling a reaction network and hydrodynamics, simpler network calculations can identify the crucial reactions and other nuclear properties to be determined by more detailed theoretical and experimental work. Ongoing work in this area involves big-bang nucleosynthesis, nuclear burning in low-mass stars, and photon-nucleus reactions in high-energy cosmic rays.

A major goal of nucleosynthesis studies is to determine the specific physical conditions that gave rise to abundance patterns seen in nature: what mix of different kinds of stellar environments gave rise to observed chemical compositions? Large amounts of important new data on abundance patterns are now being collected, with important evidence arising from low-metallicity stars in our own galaxy, absorption-line systems backlit by distant quasars, and primitive inclusions and pre-solar grains embedded in meteorites. These data contain important clues about the nucleosynthetic history of the universe, both locally and globally, and the effort to disentangle the clues into information on stellar sources and galactic chemical evolution is necessarily coupled to our work on nucleosynthesis.

In addition, studies are underway of electroweak reaction rates relevant to astrophysical processes in dense nuclear matter. These are a part of our attempt to predict observable features of quark matter in compact astrophysical objects.

The subjects of nucleosynthesis and chemical evolution is today becoming increasingly important as probes of the star formation history of the Cosmos itself. The primordial

compositions of the first stars/first stellar generations reflect that of the Universe as it emerged from the cosmological Big Bang: hydrogen, deuterium, ^{3}He, ^{4}He, and ^{7}Li. Within galaxies, stars and supernovae play the dominant role in synthesizing the elements from carbon through uranium and in returning heavy-element-enriched matter to the interstellar gas from which subsequent generations of stars are formed. This history is written in the compositions of the stars and gas in our Galaxy and other galaxies as a function of time ("metallicity"). The contributions both from massive starts ($M > 10\ M_{\odot}$) and associated Type II supernovae and from thermonuclear (Type Ia) supernovae are particularly noteworthy. Observational studies with large aperture ground-based telescopes are now providing increasing amounts of information concerning both the compositions of the oldest stars in our Galaxy and nearby galaxies and the spectroscopic properties of gas clouds at high red shifts. Argonne researchers are involved with such projects as an outgrowth of their association with the Joint Institute of Nuclear Astrophysics (JINA). Our studies of the nuclear processes participating in nucleosynthesis, of the natures of the sites in which nucleosynthesis proceeds, and of the compositions of the stellar components of our Galaxy and other galaxies as a function of time (redshift) serve to inform us of the natures of the earliest stellar population of galaxies and the Cosmos.

c.1. Sedimentation and Type I X-Ray Bursts at Low Accretion Rates (J. W. Truran,* F. Peng,† and E. F. Brown‡)

Type I X-ray bursts are understood to involve hydrogen/helium thermonuclear runaways occurring on the surfaces of accreting neutron stars in short period binary systems. Neutron stars, with their strong surface gravity, have interestingly short timescales for the sedimentation of heavy elements. Motivated by observations of Type I X-ray bursts from sources with extremely low persistent accretion luminosities, $L_X < 10^{36}$ ergs s^{-1} ($\sim 0.01\ L_{Edd}$), we have studied how sedimentation effects the distribution of isotopes and the ignition of H and He in the envelope of an accreting neutron star. For local mass accretion rates $dm/dt < 10^{-2}\ (dm/dt)_{Edd}$ (for which the ignition of H is unstable), where $(dm/dt)_{Edd} = 8.8 \times 10^{4}$ g cm^{-2} s^{-1}, the helium and CNO elements settle out of the accreted fuel layer before the temperature is reached at which H would ignite. Using one-zone calculations of the thermonuclear burning, we identify a range of accretion rates for which the unstable ignition of hydrogen does not trigger unstable helium burning. This range depends on the emergent flux from reactions in the deep neutron star crust; for $F = 0.1$ MeV $((dm/dt)/m_u)$, the range is $3 \times 10^{-3}\ (dm/dt)_{Edd} \leq dm/dt \leq 10^{-2}\ (dm/dt)_{Edd}$. We speculate that sources accreting in this range will build up a massive He layer that later produces an energetic and long X-ray burst. At mass accretion rates lower than this range, we find that the hydrogen flash leads to a strong mixed H/He flash. Surprisingly, even at accretion rates $dm/dt \geq 0.1\ (dm/dt)_{Edd}$, although the H and He do not completely segregate, the H abundance at the base of the accumulated layer is still reduced. While following the evolution of the X-ray burst is beyond the scope of this introductory paper, we note that the reduced proton-to-seed ratio favors the production of ^{12}C, an important ingredient for subsequent superbursts.

---

*Argonne National Laboratory and University of Chicago, †California Institute of Technology, ‡Michigan State University.

[1]F. Peng, E. F. Brown, and J. W. Truran, ApJ **654**, 1022, (2007).

c.2. Flame Evolution for the Deflagration Phase in Type Ia Supernova Simulations

(J. W. Truran,* A. C. Calder,† D. M. Townsley,† O. E. B. Messer,†,‡ I. R. Seitenzahl,† F. Peng,† N. Vladimirova,† E. F. Brown,§ S. Asida,¶ and D. Q. Lamb†)

Type Ia supernovae (SNe) are bright explosions characterized by a lack of hydrogen spectral features and strong silicon P Cygni features near maximum light. The currently favored interpretation is the disruption of a near-Chandrasekhar-mass C/O white dwarf by a thermonuclear runaway. These events are fascinating in and of themselves and are important both for their contribution to the cosmic abundance of iron-peak elements and for their role as standard candles.

Models of Type Ia SNe necessarily involve a mechanism for incinerating the star by a thermonuclear runaway, and the nature of this mechanism is the subject of contemporary research. In the explosion, a thermonuclear flame propagates through the C/O fuel of the white dwarf as either a subsonic deflagration front or a supersonic detonation wave and releases sufficient energy to unbind the star. However, models involving either a pure deflagration or a pure detonation have traditionally been unable to provide an explanation for both the observed expansion velocities and the spectra produced by ejecta that is rich in both intermediate-mass and iron-peak elements.

There has been considerable progress recently in hydrodynamic simulations of deflagrations of C/O white dwarfs that model the entire star. This is a complicated endeavor, predominantly due to the vast range of length scales: the laminar flame width is $\sim 10^{-3} - 10$ cm, some 8 to 12 orders of magnitude smaller than the stellar radius. Because the computational requirements for simulations with these disparate scales demand resources well beyond current capabilities, multidimensional Type Ia models must make use of an appropriate sub-grid-scale model for the evolution of the thermonuclear burning front. Moreover, large-scale simulations are very demanding of computational resources, and it is not feasible at present to include enough isotopes to allow for directly computing the reaction kinetics. A realistic model must, nevertheless, accurately describe the nuclear energy that is released, the timescale on which it is released, and the compositional changes that occur in the flame. In addition, the burned material continues to evolve after the passage of the flame due to both weak interactions and hydrodynamic evolution, and realistic simulations must describe this "post-flame" evolution.

Our efforts in this regard involved a group of JINA researchers at the University of Chicago and Argonne National Laboratory working closely with the supernova simulation group at the FLASH Center at the University of Chicago to implement a state-of-the-art, efficient, accurate model of the nuclear burning in the diffusive flame and, after its passage, during the deflagration of a white dwarf star in a Type Ia Supernova. Such a flame model is essential for using computer simulations of the explosion to understand systematic trends in the brightness of these events, which are being heavily used to probe the expansion history of the universe. The involvement of JINA and ANL researchers has resulted in the best possible modeling of both the strong and weak nuclear interaction physics necessary to follow the early phases of the explosion, and to enable high-quality nucleosynthesis to be accomplished simultaneously with detailed hydrodynamic study of SNe Ia explosion mechanisms. In addition to the FLASH group, Type Ia supernova simulations by groups worldwide will benefit from the in-depth study of SNe Ia energetics made possible by the involvement of JINA and ANL researchers. For example, during the course of this work, we successfully matched a screened nuclear network calculation and a Coulomb-corrected nuclear statistical equilibrium calculation, a novel accomplishment in this section of literature.

Two significant papers addressing these issues have emerged from these studies: Calder *et al*., (ApJ **656**, 313, 2007) and Townsley *et al.,* (ApJ, in press, 2007). The Calder *et al.* paper presents a study of the nuclear burning that occurs during C/O deflagrations, with the goal of providing a realistic flame model for simulations of Type Ia supernovae. Our flame model builds on the advection-diffusion-reaction model of Khokhlov and includes electron screening and Coulomb corrections to the equation of state in a self-consistent way. We calibrate this model flame – its energetics and timescales for energy release and neutronization – with self-heating reaction network calculations that include both these Coulomb effects and up-to-date weak interactions. The burned material evolves post-flame due to both weak interactions and hydrodynamic changes in density and temperature. We develop a scheme to follow the evolution, including neutronization, of the NSE state subsequent to the passage of the flame front. As a result, our model flame is suitable for deflagration simulations over a

wide range of initial central densities and can track the temperature and electron fraction of the burned material through the explosion and into the expansion of the ejecta. The Townsley *et al.* paper reports the development of an improved method for tracking the nuclear flame. A simplified 3-stage burning model and a non-static ash state are integrated with an artificially thickened ADR flame front in order to provide an accurate but efficient representation of the energy release and (electron capture induced) neutronization in and after the unresolvable flame.

The importance of such detailed considerations of the consequences of nuclear burning and neutronization via electron captures is to provide an accurate determination of the ^{56}Ni abundance in the ejecta of a Type Ia supernova. For a value of $Y_e \approx 0.5$, the matter in nuclear statistical equilibrium following expansion and cooling is dominated by the self-conjugate nucleus ^{56}Ni. At high densities, however, electron captures on both protons and heavy nuclei effect neutronization of the matter and Y_e falls below *0.5*. Such neutron enrichment favors neutron-rich isotopes at the expense of ^{56}Ni. Since the brightness of SNe Ia at maximum is a direct function of the mass of ^{56}Ni ejected, an accurate determination of the composition of the ejecta is critical to the use of SNe Ia as distance indicators.

*Argonne National Laboratory and University of Chicago, †University of Chicago, ‡Oak Ridge National Laboratory, §Michigan State University, ¶The Hebrew University of Jerusalem, Israel.

c.3. 2-D Hydrodynamic Studies of Novae (J. W. Truran,* S. A. Glasner,† and E. Livne†)

Classical novae are a manifestation of thermonuclear runaway in accreted hydrogen-rich shells on the surfaces of white dwarfs in close binary systems. Compelling observational data indicate that the material ejected by some novae can be significantly enriched in C, N, O, or O, Ne, by <30% by mass. It was recognized early that such levels of envelope enrichment could best be explained by dredge-up of some of the underlying white dwarf matter, prior to the final stages of the thermonuclear runaway. The question of how this enrichment is realized has, however, challenged theory now for several decades, and constitutes a major roadblock to our understanding of the nova phenomenon. The three commonly recognized mechanisms for such enrichment involve: (1) diffusion, (2) gravity wave driven mixing, and (3) convective overshoot. In earlier work, researchers at the Flash Center at the University of Chicago and Argonne National Laboratory explored the possibility that the required mixing and dredge-up could result from a resonant interaction between large-scale shear flows in the accreted envelope and interfacial gravity waves. From a suite of two-dimensional simulations, we obtained a measure of the rate of mixing and the maximum mixed mass as a function of the wind velocity. The levels of envelope enrichment achieved via this mechanism were found to be quite compatible with those levels determined observationally to characterize the ejecta of classical novae.

In ongoing studies, Argonne National Laboratory and University of Chicago researchers are considering an alternative mechanism for such mixing - driven by convective undershooting which might be expected to accompany the final stages of nova thermonuclear runaways as discussed below.

The standard model for the outbursts of novae, as we have noted, involves a hydrogen thermonuclear runaway on the surface of an accreting white dwarf in a short period binary system. While one-dimensional studies have allowed us to understand the gross features of nova explosions, it is apparent that multidimensional simulations will ultimately be required. Over the past two years, Ami Glasner and Eli Livne (The Hebrew University of Jerusalem) and Truran have been involved with 2-D calculations of the late stages of the evolution to runaway – from the onset of convection to the runaway. For this study, a 1D hydrostatic fully convective ideal profile, for which the convective flux was defined according to the Mixing Length Theory, was used as an initial model. Previous multidimensional studies of nova thermonuclear runaways (TNR) were able to simulate only the final stages, for which the timescales are very short (10 to 200 seconds), such that only the last stages of the ignition phase and the runaway to peak temperature/luminosity (from a temperature *100 K* to peak) could be investigated. The degree of mixing of matter from the underlying white dwarf into the envelope during the course of the runaway was therefore difficult to estimate. Typically, the initial model was taken from 1-D simulations at a stage where convection and nuclear burning had already started, at a

temperature of approximately 10^8 *K*. A major question with this approach is the degree to which the results obtained are dependent on the choice of initial conditions. In general, the point at which the onset of convection occurs is when the temperature at the base of the envelope is of order 3×10^7 *K*, hundreds of seconds prior to the final stages of the runaway. Building on improvements in the hydro solver and better computational resources, we are now able to resolve scales that are already unstable to the shear Kelvin-Helmholtz (KH) instability, thus improving the credibility of the results concerning undershoot mixing. The time scales considered range from a phase close to the onset of convection, when the temperature at the base of the envelope is about 5×10^7 *K*, to the runaway itself. A comparison of the evolution for simulations at initial temperatures over a range of temperatures $3\text{-}9 \times 10^7$ *K* provides a measure of convergence of these results and their consistency with regard to the consequences of runaway. We observe a universal behavior in which multi-D effects give rise to mixing that shortens the timescale to thermonuclear runaway and yields an overall level of mixing of order 30-40 percent by mass. A paper reporting our results will appear later this year.[1]

---

*University of Chicago and Argonne National Laboratory, †The Hebrew University of Jerusalem, Israel.

[1]S. A. Glasner, E. Livne, and J. W. Truran, ApJ, in press, 2007.

c.4. *r*-Process Synthesis of the Heaviest Elements

(J. W. Truran,* K.-L. Kratz,† K. Farouqi,‡ B. Pfeiffer,† C. Sneden,§ J. J. Cowan,¶ K. Otsuki,‡ and I. Seitenzahl‡)

The origin of heavy elements in explosive environments by neutron capture processes represents one of the most challenging problems in nuclear astrophysics today. Truran and his students and postdocs at the University of Chicago are actively involved in many aspects of this research.

Abundances of heavier elements (barium and beyond) in many neutron-capture-element-rich halo stars accurately replicate the solar system r-process pattern. However, abundances of lighter neutron-capture elements in these same stars are not consistent with the solar system pattern. These comparisons suggest contributions from two distinct types of *r*-process synthesis events, a so-called main *r*-process for the elements above the second *r*-process peak (at mass number $A \sim 130\text{-}140$) and a weak *r*-process for the lighter neutron-capture elements. We have performed *r*-process theoretical predictions to further explore the implications of the solar and stellar observations. We find that the isotopic composition of barium and the elemental Ba/Eu abundance ratios in *r*-process-rich low-metallicity stars can only be matched by computations in which the neutron densities are in the range $23 \lesssim \log n_n \lesssim 28$, values typical of the main *r*-process. For *r*-process conditions that successfully generate the heavy element pattern extending down to $A = 135$, the relative abundance of ^{129}I produced in this mass region appears to be at least ~90% of the observed solar value. Finally, in the neutron number density ranges required for production of the observed solar/stellar third *r*-process-peak ($A \sim 195$), the predicted abundances of interpeak element hafnium ($Z = 72$, $A \sim 177\text{-}180$) follow closely those of third-peak elements and lead. Hf, observable from the ground and close in mass number to the third *r*-process-peak elements, might also be used as part of a new nuclear chronometer pair, Th/Hf, for stellar age determinations.[1]

An important and not yet fully investigated aspect of *r*-process nucleosynthesis is the question of fission and fission cycling and its impact on the final *r*-process abundance distributions. The relevance of fission cycling is strongly suggested by the extraordinary robustness of the observed *r*-process patterns in the very oldest stars in our Galaxy. This question is being investigated by researchers at the University of Chicago and Argonne National Laboratory. The rapid neutron capture process (*r*-process) synthesizes roughly 50% of all elements past the Fe-peak and all of the actinides. While even the site of the *r*-process remains unknown (the high entropy shell surrounding a proto-neutron star left behind by a core collapse supernovae and, to a lesser degree, neutron star mergers being currently the most promising ones), the endpoint of the *r*-process is even more uncertain. In and beyond the actinide region, fission (beta delayed, spontaneous, neutron- and neutrino induced) competes with beta decays and neutron captures, providing a way to cycle the *r*- process, as the fragments constitute new seed nuclei. However, fission barriers are strongly dependent on the mass models used, leaving the fission rates highly uncertain. The role of neutrino induced fission is even

more uncertain, since the neutrino luminosity and spectrum at the *r*-process site are unknown. If the timescales are right, a quasi steady flow of nuclei can be achieved. Abundance yields of steady flow *r*-process calculations are not sensitive to the details of the expansion, but to the nuclear microphysics, thus providing an attractive explanation of the robust nature of the strong *r*-process. Do steady flow calculations reproduce the strong *r*-process pattern? Another attractive feature of fission cycling is that it could explain the weak *r*-process component without invoking a second r-process site. Fission fragments end up in the region $50 < Z < 60$, producing a robust yield for higher Z elements, lighter elements, however, would not experience the equalizing effect of fission cycling and remain more sensitive to other parameters such as the expansion timescale. Kaori Otsuki and collaborators at Chicago and Michigan State University are currently working on implementing an improved treatment of fission into dynamical *r*-process studies.

*University of Chicago and Argonne National Laboratory, †University of Mainz, Germany, ‡University of Chicago, §University of Texas, ¶University of Oklahoma.

[1]K.-L. Kratz *et al*., ApJ **662**, 39 (2007).

D. NUCLEAR STRUCTURE AND HEAVY-ION REACTIONS

This research focuses on nuclear structure in unusual regimes such as nuclei near the proton and neutron driplines, deformed nuclei with strong octupole correlations, and superdeformed nuclei at high spin. We also study heavy-ion reactions near the Coulomb barrier. Much of this work is closely tied to experiments performed at ATLAS and at radioactive beam facilities.

Our studies of heavy-ion reactions include coupled-channels calculations of fusion reactions, elastic and inelastic scattering, and few nucleon transfer reactions. The calculated fusion cross sections are usually quite sensitive to the structure and the radii of the reacting nuclei, and it is often possible to reproduce the measurements fairly well by including couplings to one- and two-phonon excitations of the low-lying quadrupole and octupole modes. However, it is very challenging to reproduce the high precision fusion data that have become available in recent years. Calculations are also challenging for very heavy systems where couplings to multi-phonon excitations and multi-nucleon transfer channels can influence the fusion.

Another difficulty in the description of heavy-ion fusion reactions occurs at energies far below the Coulomb barrier, where the measured fusion cross sections fall off steeply with decreasing energy. The fall off is so steep in many cases that the S factor for fusion develops a maximum at low energy. This hindrance of the fusion is expected to be an entrance channel phenomenon because it occurs at a rather high excitation energy of the compound nucleus. We have shown that the fusion hindrance can be explained in the coupled-channels approach by using an ion-ion potential that has a shallow pocket in the entrance channel. We have applied this model and analyzed the fusion data for several of the heavy-ion systems that exhibit the fusion hindrance at low energy.

We have tested our three-body models of two-neutron halo nuclei against recent measurements of the charge radius and dipole response of ^{11}Li. Both measurements are probes of the core-dineutron distance in ^{11}Li. The distance we extract from the dipole response is slightly smaller than the value obtained from the charge radius measurement. The discrepancy is of the order of 1.5σ. Our interpretation of both measurements is that the s-wave component in the two-neutron halo ground state must be fairly large.

We are continuing the development of a program for calculating many-body variational wavefunctions. This approach puts pairing and particle-hole interactions on an equal footing. These wavefunctions strictly conserve particle-number and parity. Particle number and parity are projected before variation. In studies of nuclides near the $N = Z$ line, we also project states of good Q, the number parity of $T = 0$ pairs, before variation. This treatment explains many of the unusual features of nuclei having almost equal numbers of protons and neutrons, such as the Wigner energy anomaly, in a simple way. It also explains a similar anomaly for odd-mass nuclides near the $N = Z$ line.

We have developed a code for configuration mixing of the wavefunctions used to describe *n-p* pairing. We have applied these wavefunctions to explore *n-p* pair transfer probabilities in $N = Z$ nuclides. We find that this quantity is very sensitive to $T = 0$ and $T = 1$ correlations in the many-body wavefunction. Experimental studies of the pair transfer probability in ^{44}Ti will establish

the magnitude of $T = 0$ pairing interaction correlations in nuclei near the $N = Z$ line. Using realistic single-particle energies for nuclei in this mass region, we have made a refined estimate of the pair transfer probability to the $T = 0$ and $T = 1$ states in ^{44}Ti.

We are developing a method that goes beyond the usual configuration mixing approach. We utilize the power of the variational method in combination with the configuration interaction method. The method determines an optimal improvement to a wavefunction with a given number of configurations. We have applied the method to the pairing force interaction and to the *n-p* pairing interaction problem. In both cases, the results are extremely good. In the pairing case, which we studied in detail, this new approach gave well over 99.9% of the total correlation energy. In the past year, we have extended this method to cylindrically symmetric deformed nuclei, described by a Hamiltonian with particle-hole plus pairing interactions. We are finding that it is quite feasible, in terms of computer resources, to extend this variational approach to the more general interaction.

The low-lying states of odd mass nuclei provide a good test of the parametrizations of single particle potentials. Study of the spectroscopy of the heavy elements is particularly interesting, as it gives insights into the potentials that are relevant to the structure of super-heavy elements. In a collaborative effort with the experimental spectroscopy group at Argonne, we have analyzed low-lying neutron and proton single particle states in the mass 250 region. We have studied neutron single-particle states in ^{247}Cm and ^{251}Cf, as well as proton single particle states in ^{249}Bk, and determined single-particle potentials that are consistent with these analyses. The study of ^{251}Cf is particularly important as it has 153 neutrons, giving information on the neutron single particle states above the deformed gap at 152 neutrons. Nine single particle states have been identified in this nuclide. These studies constrain potentials that are used to describe superheavy elements. The same approach should prove useful for constraining potentials used to describe new regions of nuclides studied with the CARIBU facility.

d.1. Signature of Shallow Potentials in Deep Sub-Barrier Fusion Reactions (H. Esbensen and Ş. Mişicu*)

We have completed our calculations of nuclear potentials for a series of heavy-ion systems.[1] The calculations are based on the M3Y double-folding potential and include corrections for exchange and a repulsive term, which is calibrated to simulate the effect of nuclear incompressibility. We refer to the potential as the M3Y+repulsion potential. The repulsive term is an essential ingredient in producing a shallow pocket and a relatively thick barrier in the entrance channel potential between two heavy ions. We find that this kind of potential explains in a natural way the hindrance of low-energy fusion which has been observed for ^{28}Si + ^{64}Ni, ^{64}Ni + ^{64}Ni, ^{58}Ni + ^{58}Ni, ^{64}Ni + ^{89}Y, and ^{64}Ni + ^{100}Mo systems (see Ref. 2 for a recent review).

The fusion hindrance phenomenon is characterized by the energy E_s, where the S factor develops a maximum at low energies. Our calculations of the potential pocket show that the minimum of the pocket, V_{min}, correlates nicely with E_s. This is illustrated in Fig. V-13. It is seen that E_s is typically 3-5 MeV above the minimum of the pocket, whereas the minimum of the pocket (triangles) is some 8-15 MeV below the Coulomb barrier.

We use real potentials in the coupled-channels calculations we have performed and we describe the fusion by ingoing-wave boundary conditions, which we impose at the minimum of the pocket. Thus the calculated fusion cross section will vanish at energies that are below the minimum of the pocket. Fusion should in principle still be possible at energies below the pocket because the compound nucleus exists at even

lower energies. However, the fusion is expected to be strongly hindered at such low energies and it would require a much more complicated dynamics to describe it. We note that the fusion/absorption cross section would not have vanished below the pocket if we had applied a complex potential in our calculations. We were unfortunately not able to reproduce the low-energy data when we used a complex potential so we were forced to abandon that approach.

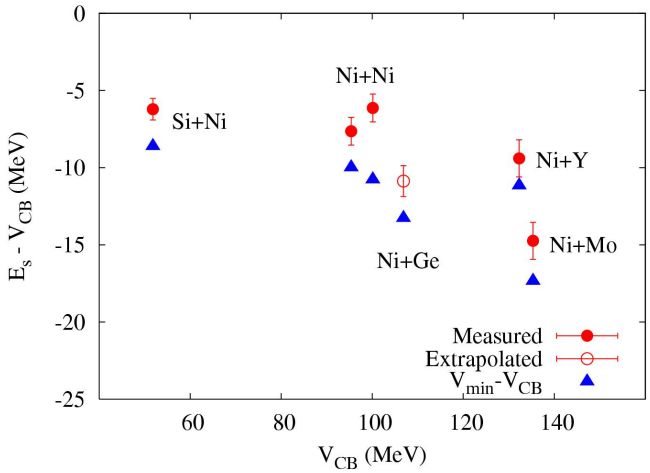

Fig. V-13. The energy E_s where the S factor for fusion develops a maximum (solid points) is compared to the minimum V_{min} of the potential pocket (triangles) for the heavy-ion systems discussed in the text. The open circle is an extrapolated value of E_s for the ^{64}Ni + ^{74}Ge system.

Another signature of a shallow pocket in entrance channel potential (in addition to the fusion hindrance discussed above) is a narrowing of the spin distribution for fusion when the center-of-mass energy is below the critical energy E_s. A narrower spin distribution implies a reduction in the multiplicity of γ-rays emitted from the compound nucleus.

An interesting feature of applying the M3Y+repulsion potential is that the calculated fusion cross section is suppressed at high energies compared with calculations that are based on the more conventional Akyüz-Winther potential. Moreover, the suppression helps in explaining the energy dependence of the data at high energies as illustrated in Fig. V-14.

This work has been published.[1]

---

*National Institute of Nuclear Physics, Bucharest, Romania.

[1]Ş. Mişicu and H. Esbensen, Phys. Rev. C **75**, 034606 (2007).
[2]C. L. Jiang *et al.*, Phys. Rev. C **73**, 014613 (2006); Phys. Lett. **B640**, 18 (2006).
[3]M. Beckerman *et al.*, Phys. Rev. C **25**, 837 (1982).
[4]C. L. Jiang *et al.*, Phys. Rev. Lett. **93**, 012701 (2004).

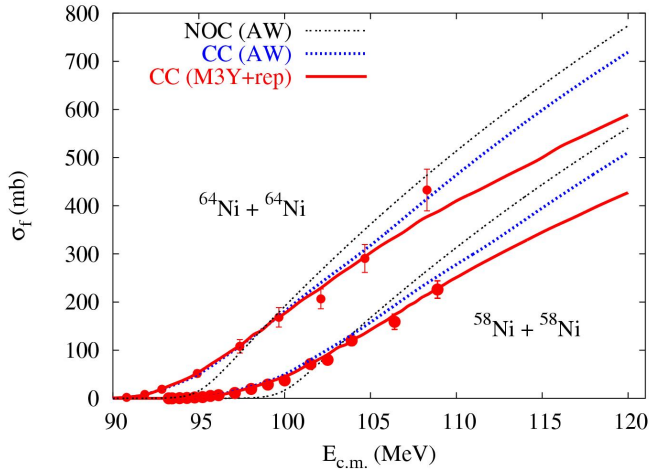

Fig. V-14. Fusion cross sections for ^{58}Ni + ^{58}Ni[3] and ^{64}Ni + ^{64}Ni.[4] The coupled-channels calculations that are based on the M3Y+repulsion potential (solid curves) reproduce the data, whereas the cross sections obtained with the AW potential (dashed curves), with (CC) and without (NOC) the effect of couplings, are steeper.

d.2. Coupled-Channels Analysis of ^{16}O + ^{208}Pb Fusion Reactions (H. Esbensen and Ş. Mişicu*)

The hindrance of heavy-ion fusion at extreme subbarrier energies, which has been observed at Argonne in several medium heavy systems (Si + Ni, Ni + Ni, Ni + Y, Ni + Mo),[1] was recently observed in the very asymmetric system ^{16}O + ^{208}Pb.[2] The hindrance phenomenon[1] is characterized by the development of a maximum in the *S* factor at low energy, and the new data confirm this behavior as illustrated in Fig. V-15a. The open circles are the old fusion data.[3] The solid points are the new data[2] which show a very broad maximum of the *S* factor at low energy.

We have analyzed the ^{16}O + ^{208}Pb fusion data by coupled-channels calculations. We use the M3Y double-folding potential which has been corrected for the influence of the nuclear incompressibility. This type of potential has been very successful in explaining the hindrance in the low-energy ^{64}Ni + ^{64}Ni fusion data[4] so it is natural to test whether a similar potential can explain the ^{16}O + ^{208}Pb fusion data. The total ion-ion potential we obtain is shown by the solid curve in Fig. V-15b. It has a rather shallow pocket and a much thicker Coulomb barrier than obtained with the more conventional Akyüz-Winther (AW) potential. The lowest dashed curve in Fig. V-15b is the entrance channel potential we obtain for the M3Y double-folding potential without the correction for nuclear incompressibility. This potential is unrealistic because it produces a pocket that is even deeper than the ground state of the compound nucleus. The ground state energy of the compound nucleus is indicated in the figure by the thick horizontal line.

We calculate the fusion cross section in coupled-channels calculations by imposing ingoing-wave boundary conditions at the position of the minimum of the pocket. The calculated fusion cross section will therefore vanish at energies that are below the minimum of pocket, which is 65.1 MeV in this case. The results we obtain in different calculations are shown in the *S* factor representation in Fig. V-15a. They all show, as expected, a very dramatic fall off as the energy approaches 65 MeV. The bottom curve (NOC) is the result we obtain in the no-coupling limit. The next curve (Excitations) shows the effect of couplings to low-lying surface modes in projectile and target. It has a narrow peak at very low energy, which is enhanced by a factor of 30 compared to the no-coupling (NOC) limit.

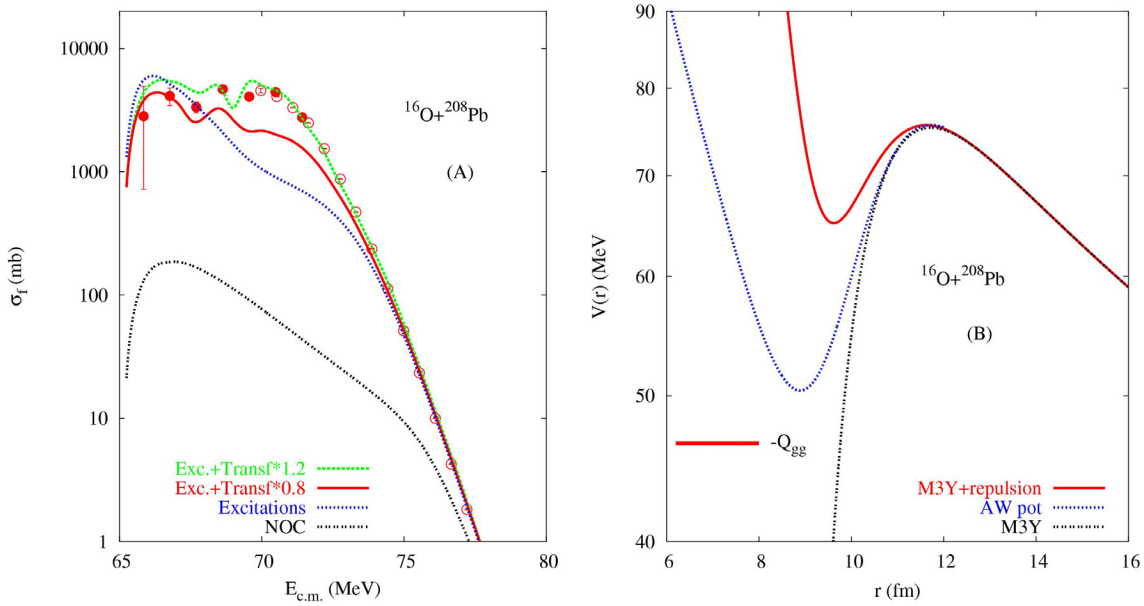

Fig. V-15. The left panel shows the S factor for the $^{16}O + ^{208}Pb$ fusion cross sections discussed in the text. The data are from Refs. 2 and 3. The right panel shows the total ion-ion potential that was used in the calculations (solid curve, M3Y+repulsion). It is compared to the total ion-ion potentials obtained from the AW potential, and from the pure M3Y double-folding potential.

Finally, we show in Fig. V-15a the results we obtain when we include couplings to the (^{16}O,^{17}O) one-neutron pickup in addition to low-lying surface modes. The solid curve is based on a realistic coupling strength for the one-neutron pickup, whereas the strength for the top dashed (green) curve was inflated by 50%, in order to be able to simulate the effect of other transfer channels. It is seen that this rough estimate is in remarkably good agreement with the low energy fusion data. Thus, it is the combination of a shallow potential pocket and couplings to transfer channels that makes it possible to explain the broad maximum of the measured low-energy *S* factor.

We also investigate other aspects of $^{16}O + ^{208}Pb$ reactions at energies near the Coulomb barrier, in order to see how realistic our model calculations are. Thus we want to see how well our coupled-channels calculations can account for the total reaction cross section and the elastic scattering data. This work is in progress.

---

*National Institute of Nuclear Physics, Bucharest, Romania.

[1]C. L. Jiang *et al*., Phys. Rev. C **73**, 014613 (2006); Phys. Lett. **B640**, 18 (2006).
[2]M. Dasgupta, D. J. Hinde, C. Low, and J. O. Newton, AIP Conf. Proc. **853** (2007).
[3]C. R. Morton *et al.*, Phys. Rev. C **60**, 044608 (1999).
[4] Ş. Mişicu and H. Esbensen, Phys. Rev. Lett. **96**, 112701 (2006).

d.3. Coupled-Channels Analysis of $^{48}Ca + ^{90,96}Zr$ Fusion Reactions (H. Esbensen and C. L. Jiang)

A common problem in the analysis of heavy-ion fusion experiments is the difficulty in reproducing all of the data points, both at low and high energies. In order to make a good fit to the data, it is often necessary to

adjust the parameters of the ion-ion potential. The radius and the depth of the potential, for example, are sensitive parameters for determining the height of the Coulomb barrier, and small adjustments of these parameters are well justified. Another example on a parameter that is sometimes adjusted is the diffuseness of the ion-ion potential. Although the value of this parameter is well determined empirically or from double-folding potentials, it is sometimes chosen to be very large, in order to be able to reproduce the fusion data at high energy.[1]

In an effort to understand what causes the need for using a large diffuseness, we decided to reanalyze a recent measurement, namely, the fusion of ^{48}Ca + ^{90,98}Zr.[2] The previous analysis[2] showed that the low energy ^{48}Ca + ^{90}Zr fusion data could be reproduced with a realistic diffuseness of the ion-ion potential but the high energy data were then suppressed compared to the calculated cross section. The ^{48}Ca + ^{96}Zr data, on the other hand, could only be reproduced with a diffuseness of the ion-ion potential that was 25% larger than the empirical value.

Our analysis shows that the ^{48}Ca + ^{96}Zr fusion data can be reproduced fairly well when we use a conventional ion-ion potential, such as the Akyüz-Winther potential. The results we obtain are compared to the data in Fig. V-16. The high-energy data (panel B) are suppressed when compared to the no-coupling (NOC) calculation but the data are nicely reproduced by the coupled-channels calculation, both at high and low energies. There is some indication of a problem at low energies (panel A), where the logarithmic slope of the data is larger than predicted by the calculation. Apart from that, we are able to make a good fit to the data using a "normal" diffuseness of the ion-ion potential. This was achieved by using coupling strengths that differ slightly from those used in the original analysis.[2]

The ^{48}Ca + ^{90}Zr data can also be reproduced fairly accurately by the coupled-channels calculations, except at the highest energies where the data are suppressed. This is consistent with the conclusion of Ref. 2. However, when we include one- and two-proton transfer channels, with positive *Q*-values, we are able to reproduce the data over the entire energy range. Thus, we conclude that the use of a large diffuseness can sometimes be avoided by considering the uncertainty in the empirical coupling strengths, or by including other reaction channels (such as transfer) in the adopted coupling scheme.

The only puzzle of the original analysis[2] that remains is the large logarithmic slope of the low-energy ^{48}Ca + ^{96}Zr fusion data. We suspect that this indicates the onset of the hindrance, which has been observed in the fusion of other heavy-ion systems. More measurements at smaller cross sections are needed in order to confirm this expectation. It is also of interest to apply the M3Y+repulsion double-folding potential[3] in the coupled-channels calculations in order to be able to remove this last puzzle. This work is in progress.

[1] O. Newton *et al.*, Phys. Rev. C **70**, 024605 (2004).
[2] A. M. Stefanini *et al.*, Phys. Rev. C **73**, 034606 (2006).
[3] Ş. Mişicu and H. Esbensen, Phys. Rev. Lett. **96**, 112701 (2006).

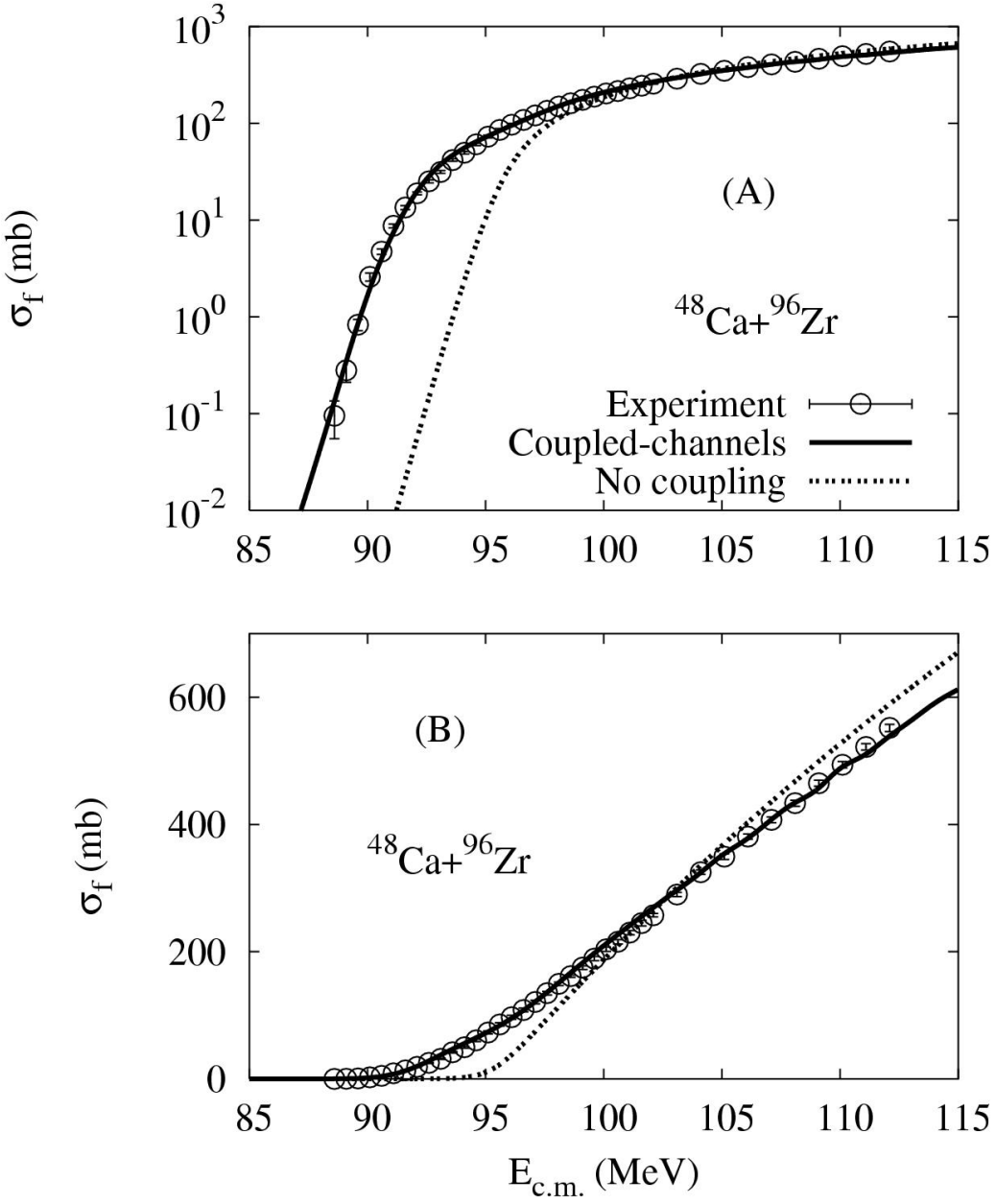

Fig. V-16. Calculated fusion cross sections for ^{48}Ca + ^{96}Zr are compared to the data.[1] The solid curve is the coupled-channels result. The dashed curve was obtained without any couplings. The top part (A) is a logarithmic plot whereas (B) shows a linear plot of the cross sections.

d.4. Charge Radius and Dipole Response of ^{11}Li (H. Esbensen, P. Mueller, K. Hagino,* and H. Sagawa†)

The dipole strength of ^{11}Li has now been measured accurately up to 3 MeV in the ^{9}Li + n + n three-body final state. The measurement was performed at RIKEN at 70 MeV/nucleon on a Pb target.[1] The data are shown

in Fig. V-17 and they are compared to the prediction of a three-body model which we developed about 15 years ago.[2] The data show a strong peak near 300 keV which is reproduced surprisingly well by the calculated distribution (solid curve). The calculation includes the effect of the final state *nn* interaction to all orders and also the experimental energy resolution. Without the final state *nn* interaction (dashed curve) we are not able to reproduce the data.

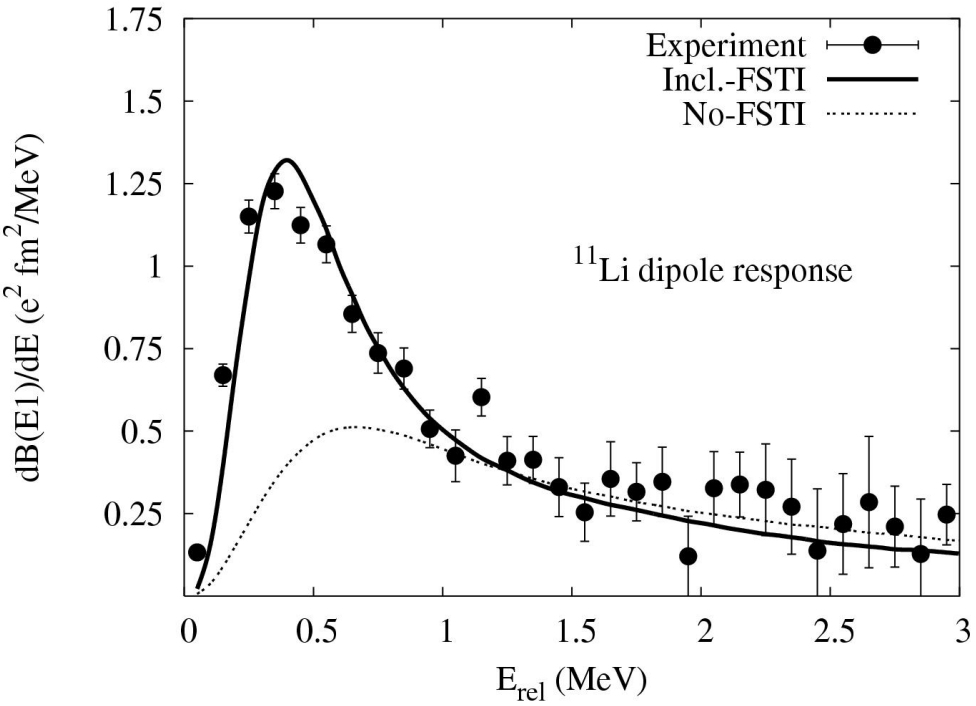

Fig. V-17. The measured dipole response of ^{11}Li[1] is compared to the calculated distribution[2] with (solid) and without (dashed curve) the effect of the final state neutron-neutron interaction.

The charge radius of ^{11}Li was recently measured at ISAC using laser spectroscopy.[3] It is of interest to see whether the measured charge radius can be explained by the same three-body model that reproduces the measured dipole response,[1] or whether the core polarization is so strong that a three-body model is unrealistic. The fact that the measured quadrupole moments of ^{11}Li and ^{9}Li are in good agreement (within the 15% experimental uncertainty) suggests that the effect of core polarization must be small. In a three-body model of ^{11}Li we assume that the core nucleus is identical to a free ^{9}Li nucleus. The difference between the mean square charge radii of ^{11}Li and ^{9}Li can, therefore, be expressed in terms of corrections that are caused by the valence neutrons,

$$\delta\left\langle r_{ch}^2\right\rangle = \left\langle r_{ch}^r\left(^{11}Li\right)\right\rangle - \left\langle r_{ch}^2\left(^{9}Li\right)\right\rangle = \left(\frac{2}{11}\right)^2\left\langle r_{c,2n}^2\right\rangle + \frac{2R_n^2}{Z} + \left\langle r^2\right\rangle_{2n}^{so}.$$

The first term is the main correction, which is due to the center-of-mass motion of the core nucleus in the presence of the two valence neutrons. It has here been expressed in terms of $\langle r^2_{c,2n}\rangle$, which is the mean square distance between the core and the dineutron, *i.e.*, the center of mass of the two valence neutrons. The second term is due to the non-zero, mean-square charge radius of a neutron, $R_n^2 = -0.1161(22)\ fm^2$, and the last term, $\langle r^2\rangle^{so}_{2n}$, is due to the spin-orbit charge density of the two valence neutrons.

The total dipole strength that was measured up to 3 MeV is $1.42 \pm 0.18\ e^2fm^2$. The calculated strength for the same energy range is $1.26\ e^2fm^2$, and the calculated mean-square core-dineutron distance is $24.35\ fm^2$. Using simple scaling we therefore estimate that the mean square core-dineutron distance associated with the dipole response is $27.4 \pm 3.5\ fm^2$. Inserting this estimate into the equation above, together with the other two corrections, we obtain the value $\delta\langle r^2_{ch}\rangle = 0.89 \pm 0.18\ e^2fm^2$.

The difference between the mean square charge radii of ^{11}Li and ^{9}Li which we obtain from the laser spectroscopy measurement,[3] after applying the revised atomic physics corrections obtained in Ref. 4, is $\delta\langle r^2_{ch}\rangle = 1.10 \pm 0.08\ fm^2$. The agreement with the value we estimated from the dipole response measurement is not perfect; the difference is $0.21 \pm 0.14\ fm^2$, which is a 1.5σ discrepancy. It remains to be seen what causes this discrepancy. An obvious candidate is core polarization, which is beyond the level of a three-body model.

We have also explored what are the implications of the two measurements for the structure of the two neutron halo ground state. Both measurements favor a fairly large *s*-wave component, namely, about 25% according to the dipole strength and up toward 50% according to the charge radius measurement. This is in qualitative agreement with the interpretation of other measurements, such as the β-decay and the momentum distributions of the fragment in ^{11}Li breakup reactions. This work has been submitted for publication.

*Tohoku University, Japan, †University of Aizu, Japan.

[1]T. Nakamura *et al*., Phys. Rev. Lett. **96**, 252502 (2006).
[2]H. Esbensen and G. F. Bertsch, Nucl. Phys. **A542**, 310 (1992).
[3]R. Sanchez *et al*., Phys. Rev. Lett. **96,** 033002 (2006).
[4]M. Puchalski *et al.*, Phys. Rev. Lett. **97**, 133001 (2006).

d.5. Mean Field and Many Body Wavefunctions (R. R. Chasman)

We are continuing our long term effort to develop programs for calculating many-body variational wavefunctions. In our approach, pairing and particle-hole two-body interactions are treated on an equal footing.

In this approach, the complexity of the wavefunctions depends only on the number of levels included in the valence space. In these wavefunctions, we strictly conserve particle number and parity; projecting states of good particle number and parity before carrying out the variational calculations. By including an independent amplitude for the four particle configuration consisting of two neutrons and two protons in the same J_z sub-state, we can now explain several of the unusual features of nuclides near the $N = Z$ line, such as the Wigner energy anomaly, in a very simple way. Most of it arises from the large interaction strength between nucleons in the same orbital. Similarly, we find that the inclusion of a three nucleon amplitude in odd-mass configurations accounts well for the extra correlation energy in such nuclides near the $N = Z$ line.

The major limitation of shell model calculations is that the number of configurations becomes unmanageable as the valence space is increased. The wavefunctions that we are developing contain large numbers of configurations, *e.g.*, 10^{22} configurations in the wavefunctions that we use for Hamiltonians that include *n-p* pairing interactions. However, these wavefunctions are product wavefunctions and the number of independent amplitudes is quite small, *e.g.*, 150 independent amplitudes in a wavefunction that has 10^{22} configurations. To fully utilize this simple wavefunction structure, a systematic approach to configuration interaction is needed. We have recently developed such an approach by extending the variational method for use in the context of configuration interaction calculations.

Many of the techniques that we have developed to treat *n-p* (neutron-proton) pairing can be profitably applied to Hamiltonians that contain particle-hole interactions in addition to pairing interactions. We are in the process of developing a code to handle particle-hole interactions in addition to pairing.

d.6. Variational Approach to Configuration Interaction (R. R. Chasman)

Methods for the systematic improvement of solutions to quantum-mechanical problems play an essential role in the accurate theoretical description of physical phenomena. We are developing[1] a class of many-body wavefunctions that are a product of terms. Each of the terms in the product is, in turn, a sum of terms. In such a case, the number of independent variational amplitudes is orders of magnitude smaller than the number of configurations in the wavefunction. In a simple pairing interaction, in a system with 32 doubly degenerate levels and 16 pairs of nucleons, there are approximately 10^9 configurations, but the BCS solution for this problem has only 32 independent amplitudes. For the *n-p* pairing Hamiltonian that we have studied, there are roughly 10^{22} configurations for a half-filled system with 30 four-fold degenerate levels, each capable of holding two neutrons and two protons. In our product wavefunction, there are just 150 independent amplitudes.

In a model system with pairing and particle-hole interactions, having enough levels to adequately describe the deformed actinides, there are roughly 10^{29} configurations for a nuclide with half-filled neutron and proton shells. The wavefunctions that we use for such nuclides are also a product of sums. Each of the terms in the product is a sum over all configurations that can be built from the orbitals having a fixed value of $|\Omega|$, which is the projection of angular momentum on the nuclear symmetry axis for a deformed nucleus. For a spherical nucleus, $|\Omega|$ is $|j_z|$. The number of independent amplitudes in this model actinide system is roughly 1.2×10^4.

We have found that such product solutions can be systematically improved by combining the approach of configuration interaction with the variational method. The basic idea is to take linear combinations of wavefunctions, all with the same general structure, to construct more accurate solutions. We start with a variational solution of the given product form. We then calculate amplitudes for a second wavefunction having exactly the same form. The amplitudes of the second wavefunction are determined variationally as the optimal improvement to the original wavefunction for a wavefunction of that form. A third wavefunction is then calculated as the optimal improvement on the first two wavefunctions. The method can be continued indefinitely.

There are exact solutions available for a pairing Hamiltonian with constant matrix elements. We tested our approach by comparing our results with the exact energy for the model pairing Hamiltonian. We got agreement to *1 keV*, by taking 80 basis states. Using only 40 basis states, the error is just *3 keV*. In the case of the *n-p* pairing Hamiltonian, there are no exact solutions available. We found that the wavefunction with 80 basis states improves the binding energy by *1 MeV* relative to the wavefunction consisting of a single optimized state.

Our major effort, in the past year, has been to extend this variational approach to a Hamiltonian with pairing and particle-hole interactions. We are developing such a code and it runs reasonably quickly. We obtain 25 of the optimal variational wavefunctions on a laptop (1.7 GHz uniprocessor) in two hours, using 200 iterations to calculate each variational wavefunction. We are working to further improve the efficiency of this code.

The usual stumbling block to adding more and more wavefunctions in configuration interaction calculations is that, at some point, the overlap between the added wavefunction and those already in place approaches 1 and there is no improvement in the energy. Our variational approach does not have the problem of overlap pileup.

[1] R. R. Chasman, Phys. Rev. Lett. **95**, 262501 (2005).

d.7. Neutron-Proton Pairing (R. R. Chasman)

We have developed[1-3] a treatment of neutron-proton pairing that explains many features of nuclear structure seen near the $N = Z$ line. Our many-body treatment includes *n-p* pairing, as well as like particle pairing. We do a full projection of neutron and proton particle number before the variational calculation. We also found that there is a new quantum number that holds exactly for collective states; *i.e.*, those states in which no levels are blocked. This new quantum number (Q) is the number parity of the $T = 0$ and $T = 1$ *n-p* pairs. Fixing the number parity of one *n-p* mode fixes the other, because we conserve proton number and neutron

number exactly. This number parity is closely related to the isospin quantum number. These collective states are the ground states for $N = Z$ nuclides. We project Q before doing a variational calculation. The form of our variational wavefunction includes an explicit amplitude for "alpha like" correlations in each level as well as the usual amplitudes for *n-n*, *p-p* and *n-p* pairs. Similarly in odd mass nuclei, we have explicit amplitudes for ^{3}He and ^{3}H like correlations. We have added terms to the *n-p* pairing interaction that allow pairs of particles in the same orbitals, giving states with maximum angular momentum. Because of the exclusion principle, these must be *n-p* pairs and $T = 0$.

In odd-odd $N = Z$ nuclei, the ground state is a degenerate doublet, consisting of a $Q = 0$ and $Q = 1$ state, when the $T = 0$ and $T = 1$ pairing strengths are equal. The splitting of this ground state doublet affords some information about the relative strengths of the $T = 0$ and $T = 1$ pairing strengths. In even-even nuclei, there is a large splitting between the 0^+ $T = 1$ ground state and the 1^+ $T = 0$ excited state. Our model explains this feature in a transparent way. Most of the excitation energy owes to the breaking of a quartet and the single particle excitation energy involved in making a $T = 0$ pair. In the odd-odd $N = Z$ nuclei case, neither of these effects applies for the $T = 0$ state.

The Wigner energy is the extra binding energy of $N = Z$ even-even nuclei relative to neighboring nuclei. Our approach explains the magnitude of the Wigner energy very well. It arises from the extra pairing energy involved in creating a quartet of nucleons in the same orbital. There is a similar increase in the correlation energy of odd-mass nuclei having one less nucleon than an $N = Z$ nucleus. Our model gives a ratio of 1/2 for the two energy anomalies. We have made an analysis of experimental binding energies and find a ratio in good agreement with this prediction.

Our detailed calculations of the dependence of the binding energies on the relative strengths of the $T = 0$ and $T = 1$ pairing strengths shows that the differences are small as a function of the variation of the relative strengths. Other observables are needed to establish the magnitude of $T = 0$ correlations in nuclei. To that end, we have carried out a calculation of the *n-p* pair transfer spectroscopic factor using single-particle level spacings that are appropriate for ^{44}Ti, for which ^{2}H pair transfer studies are being carried out. In our calculation, the initial state is the ground state of ^{44}Ti, an even-even $N = Z$ nuclide and the final states are the lowest $T = 1$ and $T = 0$ states in the neighboring odd-odd $(Z + 1, N + 1)$ nucleus ^{46}V. The spectroscopic probability factors show a considerable sensitivity to the relative strengths of the $T = 0$ and $T = 1$ pairing strengths. In Fig. V-18, we show the spectroscopic factors for $T = 0$ and $T = 1$ pair transfer probabilities to states in ^{46}V. A 15% reduction of the $T = 0$ pairing strength gives roughly a 40% reduction in the ratios of $T = 0/T = 1$ pair transfer probability spectroscopic factor. This reduction of 15% of the $T = 0$ pairing strength gives an excitation energy for the 1^+ state in agreement with experiment. In the lower portion of the figure, we display the excitation energy of the 1^+ state as a function of the $T = 0$ pairing strength, keeping a fixed $T = 1$ pairing strength.

[1]R. R. Chasman, Phys. Lett. **B524**, 81 (2002).
[2]R. R. Chasman, Phys. Lett. **B553**, 204 (2003).
[3]R. R. Chasman, Phys. Lett. **B577**, 47 (2003).

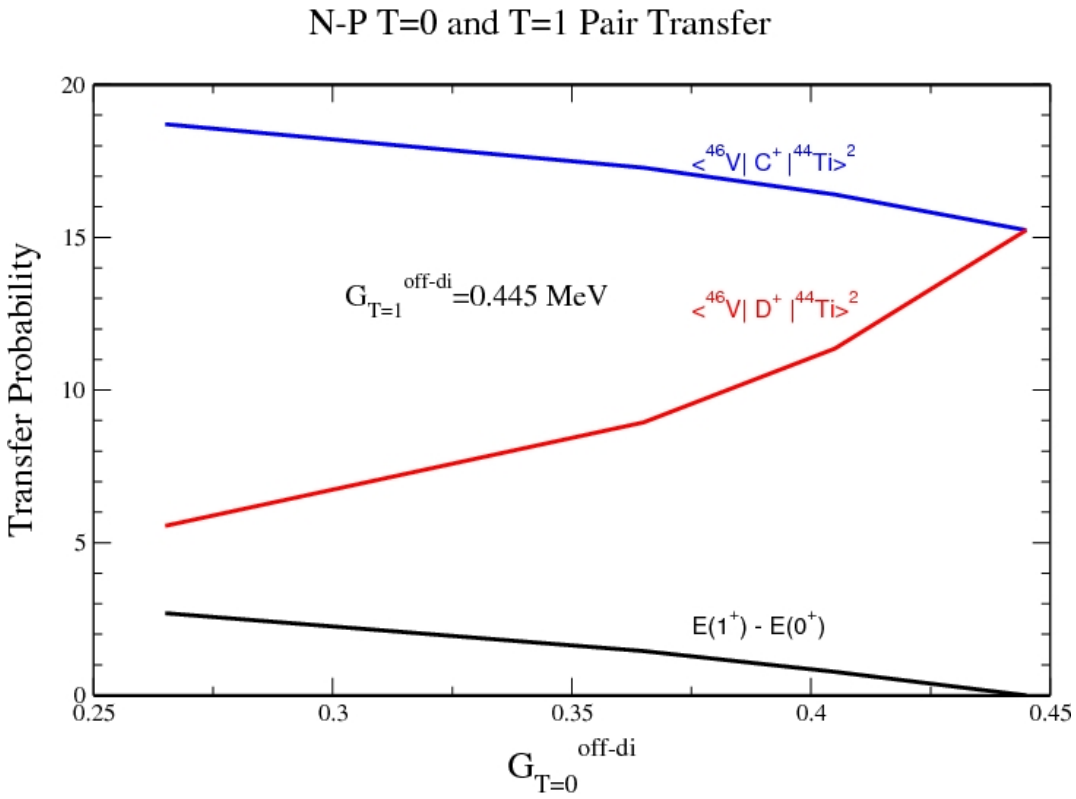

Fig. V-18. Spectroscopic Factors for T = 0 and T = 1 n-p pair transfer. The T = 1 pairing interaction matrix element is held constant. The transfer probabilities are shown as a function of the T = 0 pairing strength. See text for more details.

d.8. Energy Levels of the Heavy Elements (I. Ahmad and R. R. Chasman)

The study of single-particle states in the heavy elements is a long-term collaborative project. The low-lying states in odd-mass nuclides provide a good test of the parametrizations of single particle models. Vibrational admixtures are usually small for these states. The single-particle energy level spacings in the heavy elements provide useful guidance for single-particle potentials that are appropriate for super-heavy elements. Seven single-particle states have been identified[1] in ^{247}Cm, so this nuclide provides a good test of neutron single particle potentials. The study[2] of ^{251}Cf is particularly important as it has 153 neutrons, giving information on the neutron single particle states above the deformed gap at 152 neutrons. Nine single particle states have been identified in this nuclide. Eight single-particle levels have been identified[3] in ^{249}Bk. This provides a very good test of proton single-particle potentials in the very heavy elements. When pairing effects are extracted[4] from the observed levels in ^{247}Cm, ^{251}Cf and ^{249}Bk, the orderings and spacings of levels are in good agreement with the levels obtained from our parametrization of a deformed Woods-Saxon potential. These analyses will provide useful constraints on other parametrizations of superheavy potentials.

[1] I. Ahmad *et al*., Phys. Rev. C **68**, 044306 (2003).
[2] I. Ahmad *et al*., Phys. Rev. C **72**, 054308 (2005).
[3] I. Ahmad *et al*., Phys. Rev. C **71**, 054305 (2005).
[4] R. R. Chasman, Phys. Rev. C **14**, 1935 (1976).

E. ATOMIC THEORY AND FUNDAMENTAL QUANTUM MECHANICS

In addition to research on hadron and nuclear physics, and nuclear astrophysics, we also conduct research in atomic physics, neutron physics, and quantum computing.

Work in atomic physics includes the studies of interactions of electrons or high-energy photons with matter, in support of experiments performed at Argonne's Advanced Photon Source (APS). Theoretical studies are being conducted on the physics of the photoeffect and Compton scattering by bound electrons, focusing on topics selected in view of basic importance, timeliness, and potential in applications. Comprehensive surveys of photo-interaction data for silicon and graphite are underway. Some of the results are useful for underpinning cross sections and stopping power for charged-particle interactions, namely, basic data for radiation physics.

Ongoing theoretical work in support of a new experiment to measure the neutron electric-dipole moment (EDM) is currently focusing mostly on issues relating to the penetration of neutrons into a perfect silicon crystal in the Bragg reflection process. Preliminary reflectivity measurements at the NIST reactor have been performed and the main instrumental issues appear to have been identified. An experiment to measure the interaction of the neutron's known magnetic dipole moment with the crystalline electric field, intended both to test the principle of the EDM experiment and to calibrate the electric field, is planned for late in 2006.

Work was completed on representations of complex rational numbers as states of finite strings of two types of qubits, one for real and one for imaginary numbers. These rational string states representations were extended to a representation of real and complex numbers by defining Cauchy sequences of the rational string states. The definition of the Cauchy condition, which mirrored that used in mathematical analysis, was given for sequences of states of the form $|\, \underline{s_n} \rangle$, where $\underline{s_n}: \{1,\ldots,n\} \rightarrow \{0,1\}$ is a *0 - 1* valued function, and extended to linear superpositions of sequences of these states. Much of the work to show that (equivalence classes) of these state sequences represent real and complex numbers consists in verifying that definitions of addition and multiplication and their inverses have the requisite properties and that the set is complete (the set is closed under taking of limits).

e.1. Interactions of Photons with Matter (M. Inokuti and D. Y. Smith*)

In support of experiments in atomic and condensed-matter physics with the use of synchrotron radiation, theoretical studies are being conducted on the physics of photo-absorption and Compton scattering, focusing on topics selected in view of basic importance, timeliness, and potential applications.

One theme of long-term studies has been the use of dispersion relations and sum rules for indices of response of matter over the entire range of photon energies. An application is the evaluation of the mean excitation energy for stopping power. New results are 164 ± 2 *eV* for silicon, and 77 ± 4 *eV* for graphite.[1]

*University of Vermont.

[1] D. Y. Smith, M. Inokuti, W. Karstens, and E. Shiles, Nucl. Instrum. Methods **B250**, 1 (2006).

e.2. Interactions of Charged Particles with Matter (M. Inokuti)

Stopping power, the total yield of ionization, and its statistical fluctuations are examples of quantities describing the penetration of charged particles through matter and are important to applications such as the detection of particles and the analysis of their charges and kinetic energies. The understanding of those quantities in terms of individual collisions and associated cross sections remains a major challenge and is the goal of our continuing effort. A recent publication[1] concerns the evaluation of the mean excitation energies, namely, the *I* values, in the Bethe stopping-power formula from the oscillator-strength spectra for 9 atoms and 23 molecules that are treated by Berkowitz.[2]

Extensive work for the International Commission on Radiation Units and Measurements (ICRU) continues on the editing of its reports and on physical data such as stopping powers and various interaction cross sections.

The main line of Inokuti's life-long study concerns interactions of energetic charged particles with matter and consequent changes in the structure and properties of matter. This topic forms a basis for particle detection and analysis in experimental nuclear and particle physics, as well as for mechanistic considerations in radiation chemistry and biology, and in materials science. I am writing a manuscript for a monograph entitled "Principles of Radiation Physics". The book will be a comprehensive presentation of my major observations and findings in about 600 printed pages.

[1] S. Kamakura, N. Sakamoto, H. Ogawa, H. Tsuchida, and M. Inokuti, J. Appl. Phys. **100**, 064905 (2006).
[2] J. Berkowitz, *Atomic and Molecular Photoabsorption. Absolute Total Cross Sections* (Academic Press 2002).

e.3. A Bragg Scattering Method to Search for the Neutron Electric Dipole Moment (M. Peshkin, M. Arif,* T. W. Dombeck,† D. S. Hussey,* D. Jacobson,* H. Kaiser,‡ D. Koetke,§ and R. K. Smither¶)

The goal of this experiment is to search for the neutron electric dipole moment by observing the precession of the neutron's spin polarization in the atomic electric fields when neutrons are Bragg reflected from a perfect silicon crystal. The anticipated rotation in a single reflection is a few microradians. By causing the neutrons to undergo some 20,000 successive reflections as they drift down a slot cut into the crystal, we anticipate achieving a sensitivity of a few times 10^{-27} e-cm, comparable with the sensitivity sought in the next round of ultra-cold-neutron experiments, but with significantly different systematic errors. Our experiments are being carried at out the reactor at the NIST Center for Neutron Research, in Gaithersburg, MD.

In 2006, NIST commenced construction of a dedicated beamline and experimental area for this experiment. That construction is expected to be completed in early summer 2007. At that time we will measure the reflectivity and geometrical properties of an improved slotted silicon crystal currently being prepared at Argonne. We have previously shown experimentally that the reflectivity of a properly prepared silicon surface is greater than 0.9999. In 2007 we plan to measure the reflectivity or raise its lower bound.

We are currently preparing for an experiment to measure the interaction of the neutron's magnetic dipole moment (MDM) with the atomic electric fields by the same technique, making use of the Schwinger interaction between an electric field and a moving MDM, the latter appearing as an effective EDM. The MDM experiment will serve as a proof of principle and exploration of systematic errors for the EDM experiment, and it will also serve as a necessary calibration of the effective electric fields experienced by the neutrons in the EDM experiment. Technical details of the MDM experiment are given in a NIST report "Technical Report on the Status of the Measurement of Neutron Schwinger Scattering in Silicon," dated January 17, 2007. The MDM experiment is being done in collaboration with F. Wietfeldt of Tulane University.

We are currently procuring a set of Helmholtz coils to achieve the magnetic field quality needed for the Schwinger experiment. We have on hand, or on order, all of the necessary polarization handling equipment (polarizer, Heusler analyzer crystal, spin rotation coils, etc.). We expect to use these in 2007 to investigate the effects of neutron penetration into the crystal in Bragg scattering and begin preliminary measurements and

calibrations.

*National Institute of Standards and Technology †University of Hawaii, ‡University of Indiana, §Valparaiso University, ¶Advanced Photon Source User Program, Argonne National Laboratory.

e.4. Quantum Theory Representations of Real and Complex Numbers[1,2] (P. Benioff)

As part of a long term project of working towards a coherent theory of physics and mathematics together, work was completed on a quantum representation of real and complex numbers as equivalence classes of Cauchy sequences of states of qubit strings that represent real and imaginary rational numbers. Complex rational number states are represented by four types of annihilation creation operators for four different types of qubits on an integer lattice; $a^{\dagger}_{i,j}$, $b^{\dagger}_{i,j}$, $c^{\dagger}_{\gamma,0}$, $d^{\dagger}_{\delta,0}$. Here i = 0,1, j is an integer, and δ,γ, = +,-. Complex rational string states are represented by $|\gamma,s;\delta,t> = c^{\dagger}_{\gamma,0}\ a^{\dagger}_{s(l),l.}\ a^{\dagger}_{s(u),u}\ d^{\dagger}_{\delta,0}\ \ b^{\dagger}_{t(k),k}\ \ b^{\dagger}_{t(v),v}\ |0>$. Here s and t are 0,1 valued functions on the respective integer intervals [l,u] and [k,v], γ,δ give the signs of the real and imaginary components and |0> is the qubit vacuum state. Also, $l \leq 0 \leq u$ and $k \leq 0 \leq v$. Quantum representations of real and complex numbers are defined as equivalence classes of sequences $\{|\gamma_n,s_n>$: n = 0,1,…} and $\{|\gamma_n,s_n;\delta_n,t_n>$: n = 0,1,…} of qubit string states that satisfy the Cauchy condition. This definition was also extended to apply to sequences of superpositions of states of the form $\Sigma_{\gamma,s,\delta,t}\ c_{\gamma,s,\delta,t}\ |\gamma,s;\delta,t>$.

The above description was expanded by considering gauge transformations of the real and complex rational number representations and the corresponding transformed representations of real and complex numbers. If $U:I \rightarrow U(2)$ is a function from the integers I to the group U(2), then the action of U on a state $|\gamma,s;\delta,t>$ gives the state $U|\gamma,s;\delta,t> = |\gamma_U,s_U;\delta_U,t_U>$. This state represents the same complex rational number in the transformed representation as $|\gamma,s;\delta,t>$ does in the original representation. One can now define Cauchy sequences of these transformed states to obtain another quantum representation R_U, C_U, of the real and complex numbers. It is clear that for each gauge U, one has quantum representations of the real and complex numbers. All these representations are isomorphic, yet they are distinct. One can show that there is a sense in which a real number in R_U, is orthogonal to "the same" real number in $R_{U'}$ where U' is another gauge transformation.

[1]P. Benioff, *Fields of Iterated Quantum Reference Frames Based on Gauge Transformations of Rational String States*, arXiv preprint quant-ph/0604135.
[2]P. Benioff, *Fields of Quantum Reference Frames Based on Different Representations of Rational Numbers as States of Qubit Strings*, arXiv preprint quant-ph/0611139.

e.5. Fields of Iterated Reference Frames Based on Quantum Theory Representations of Real and Complex Numbers[1,2] (P. Benioff)

These representations yield interesting structures when one considers the fact that real and complex numbers form the base of all physical theories, and of space time if space time is represented as a 4-tuple of real numbers. Let F denote a reference frame based on R, C, which are the usual real and complex numbers that are considered, by an observer in F, as "given" and with no structure beyond that required by the relevant axiom sets. F is defined to contain all physical theories as mathematical structures based on R, C, and space time as R^4 if it is represented as a 4-tuple of real numbers. The above description of quantum representations, R_U, C_U, takes place in F where the relevant theories used in the description of R_U, C_U, are based on R, C. Since R_U, C_U, are representations of the real and complex numbers, they can also serve as the base of physical theories. This gives a frame F_U, which is a collection of all physical theories as mathematical structures based on R_U, C_U. There are many such frames, one for each U. Each F_U is equivalent as the theories in each frame are equivalent. Also, an observer in F_U sees R_U, C_U as given and with no structure. The structure of R_U, C_U is visible to an observer in F.

This structure of frames emanating from frames can be iterated leading to fields of iterated reference frames

with a genealogical structure. There are several possibilities for the structure: a finite number of iterations, a one way infinite number, a two way infinite number, and a cyclic structure. Figure V-19 is a schematic of two iterations with an ancestor frame F and two progeny generations.

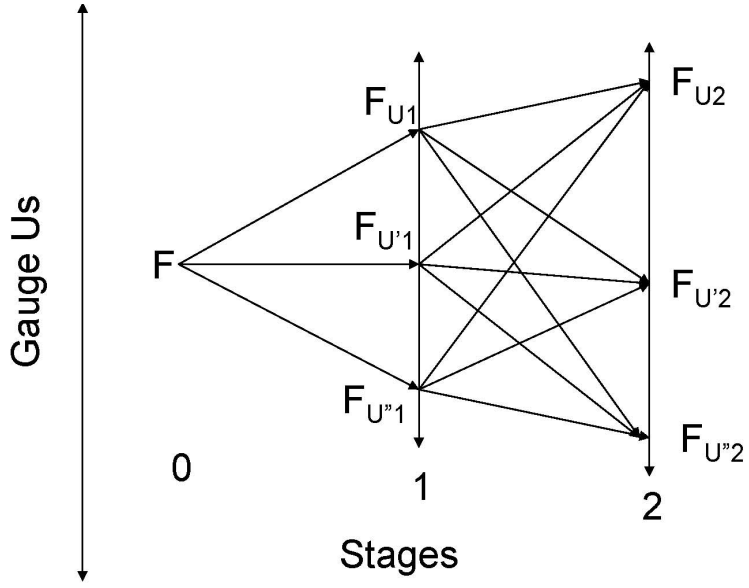

Fig. V-19. Three iteration stages of frames coming from frames. Only three frames of the infinitely many, one for each gauge U, are shown at stages 1 and 2. The arrows connecting the frames show the iteration direction of frames coming from frames.

The connection of the frame field to physics is important. Since there is no evidence of many different universes with the structure of the field, one needs to find a way to collapse the field. One method to collapse the different F_U in each generation is to use gauge invariant representations of qubit states. This can be done by letting qubit states correspond to the irreducible representation subspaces of SU(2). This still leaves the generations intact. Clearly, there is much work to do towards the goal of a coherent theory of physics and mathematics.

---

[1]P. Benioff, *Fields of Iterated Quantum Reference Frames Based on Gauge Transformations of Rational String States*, arXiv preprint quant-ph/0604135.

[2]P. Benioff, *Fields of Quantum Reference Frames Based on Different Representations of Rational Numbers as States of Qubit Strings*, arXiv preprint quant-ph/0611139.

F. OTHER ACTIVITIES

f.1. Third ANL/MSU/INT/JINA Rare Isotope Accelerator Workshop (H. Esbensen, K. M. Nollett, and C. D. Roberts)

This meeting was primarily organized by the Argonne Theory Group and was held in the Physics Division from April 4-7, 2006. It is one of a series of workshops that are hosted in a rotating fashion among the sponsoring institutions. The series was established to explore, explain and support the case for an advanced exotic beam facility from a theoretical-physics perspective, and to encourage the theoretical work that will be needed to interpret experiments once such a facility is built.

An advanced exotic beam facility is vital for the future of low-energy nuclear physics and will produce advances: in understanding the nature of nuclei and nuclear matter; in explaining the origins of the chemical elements and the workings of stars; and in testing the standard model of particle physics. Both the community and DOE remain firmly committed to such a facility.

The first two meetings in this series focused on specific areas of nuclear theory. The topic of the first, held at the Institute for Nuclear Theory (INT), was the astrophysical *r*-process. The second, held at Michigan State University (MSU), concentrated on the present state of nuclear reaction theory. Owing to the timing of this third meeting, we wanted the presentations, the discussions and, indeed, the proceedings volume[1] to cover a broader range of topics in current nuclear theory. Sessions were organized on: dynamic symmetries in nuclei; fundamental symmetries; nuclear structure; and nuclear astrophysics. We recruited a collection of speakers to give a thorough overview of topics at the leading edge of nuclear theory and asked them to respond to the following question: "What questions does your research pose that only an exotic beam facility can answer?"

The picture which emerged from the presentations is that progress is being made in a broad range of distinct but overlapping areas within nuclear theory. This is captured in the contributions to the proceedings volume, which span a wide range of topics, from the lightest nuclei to some of the heaviest, from *ab initio* to phenomenological approaches, from "pure" nuclear physics to challenging astrophysical problems that require proper accounting for nuclear properties. An expansion of the range of measurable nuclear properties beyond present capabilities will present new constraints and new challenges for the theoretical approaches discussed.

We set aside thirty minutes at the end of each session for discussion in an open forum; these discussions were often lively. Such discussion, with broad representation from across the nuclear physics community, is important to maintain theory on a trajectory that will both support and profit from experiments at the next generation of experimental facilities.

[1] *Opportunities with Exotic Beams,* edited by T. Duguet, H. Esbensen, K. M. Nollett, and C. D. Roberts (World Scientific, New Jersey, 2007).

f.2. Nineteenth Annual Midwest Theory Get-Together (C. D. Roberts)

The Theory Group hosted the nineteenth Annual Midwest Theory Get-Together on October 13-14, 2006. Nuclear theorists from seventeen Midwest universities and ANL met to learn about the research goals and foci of different individuals and groups throughout the region. While the organizational duties rotate amongst the participants, Argonne is the regular host site because of its meeting facilities and central location. The organizer for 2006 was Stefan Frauendorf from the University of Notre Dame. The meeting provides a good chance for students to broaden their outlook and get some practical speaking experience in a friendly atmosphere. The format is informal, with an agenda of talks being volunteered at the beginning of the meeting. In 2006 we had forty-five registered participants: faculty, postdocs and students. Over the Friday afternoon and Saturday morning twenty-nine presentations were made, covering topics such as: *ab-initio* studies of masses and scattering based on nuclear Hamiltonians; effective field theories;

fundamental quantum mechanics; hadron physics, parton distribution functions and QCD; the nuclear shell model, nuclear pairing and nucleon matter; nuclear and quark astrophysics; quantum Monte Carlo methods; relativistic heavy ion collisions; and relativistic quantum mechanics for few body systems. It was a successful event.

VI. OTHER EDUCATIONAL AND COMMUNITY OUTREACH ACTIVITIES

OVERVIEW

Education remains a key part of our mission, especially training young nuclear physicists for the next generation of research, stewardship and homeland security. We are involved in many programs, including education at undergraduate, graduate, and post-doctoral level. We are also involved in using our expertise and capabilities to support programs in local Universities and in our community.

a.1. Minority Program (B. Zeidman)

The primary aim of the minority program is increasing the number and quality of minority participants in physics and other sciences. This involves ongoing interactions with minority students and faculty during visits to colleges and universities with substantial minority populations and a number of other activities. Among these efforts is inclusion of qualified scientists and students from minority institutions in research being performed by ANL scientists; e.g., collaborations on experiments, short-term appointments, and internships, such as SRP and SULI. In addition, attendance at meetings of minority organizations and visits to educational institutions provide chances for individual interactions and discussion of a wide variety of topics, e.g., research opportunities at ANL and other DOE laboratories, graduate education, internships, employment possibilities, etc., that influence choices of major field and career development.

The strongest interactions with minority students result from visits to minority institutions where it is possible to have discussions in depth with individual students. During the academic year, the program involves recruiting trips to schools with substantial minority populations, many having been visited in prior years. Included in these visits are seminars that discuss research performed by the Physics Division, particularly in the Medium Energy and Heavy Ion programs. Since ANL experiments at JLab include collaborators (both faculty and student) from some of these universities, (e.g., Florida International University, Hampton University, North Carolina A&T University, Southern University, New Orleans, UTEP) some members of the audience are often active participants in the research being discussed. Inasmuch as many students from these colleges may also have been at ANL as participants in the SRP and SULI programs, it is possible to make direct connections between the research being discussed and persons present or known to the audience. SRP and SULI students recruited under the programs performed research in several ANL divisions other than PHY during the past year, *e.g.* APS, HEP. Institutions recently visited include: Clark-Atlanta University; Morehouse; Spelman; North Carolina A&T; North Carolina Central; Hampton; Norfolk State; University of Texas-El Paso; New Mexico State; Lincoln; Howard University; Morgan State; Fisk; Vanderbilt; Southern University; and Dillard University.

b.1. ANL Summer School Experience in Physics

(S. M. Fischer, C. J. Lister, A. Hecht, R. V. F. Janssens, P. Mueller, N. Patel, D. Peterson, R. Scott, D. Haskel,* and G. McMichael†)

In order to increase the exposure of young high school students in Chicago to science and scientific careers, a one week summer school was organized in the Physics Division. The aim was to involve and encourage students, particularly from minority groups, who may not have considered a scientific career. The pilot program included students from the Hyman Rickover Naval Academy. Eight top students from 9th grade were selected by competition. The students had completed a year-long course in introductory physics. They came to Argonne each day, and were involved in a variety of projects: hands on experiments, talks about physics, talks with scientists about their careers, and tours of experimental facilities throughout the laboratory. Dr. Rosner gave the graduation awards. Figure VI-1 is a photograph of the graduation ceremony.

This program was successful and has the potential to grow in scope, mainly by having two parallel programs running, one in the Chemistry Division and one in Physics, with a mixture of 9th and 10th grade students. In the future, we hope the program will encompass additional Chicago high schools.

*Advanced Photon Source, Argonne National Laboratory, †Intense Pulsed Neutron Source, Argonne National Laboratory.

Fig. VI-1. Students from the "Summer School Experience" with Susan Fischer (left), their teacher Dereck Svelnys, and Kim Lister.

STAFF MEMBERS OF THE PHYSICS DIVISION

Listed below is the staff of the Physics Division for the year ending December 31, 2006. The program headings indicate only the individual's current primary activity.

SCIENTIFIC STAFF

EXPERIMENTAL NUCLEAR PHYSICS STAFF

Regular Staff

John R. Arrington, Ph.D., California Institute of Technology, 1998
Birger B. Back, Ph.D., University of Copenhagen, Denmark, 1974
Michael P. Carpenter, Ph.D., University of Tennessee-Knoxville, 1987
¶‡ Cary N. Davids, Ph.D., California Institute of Technology, 1967
§ Bela Erdelyi, Ph.D., Michigan State University, 2001
* Susan M. Fischer, Ph.D., University of Notre Dame, 1994
¶¶ Donald F. Geesaman, Ph.D., State University of New York-Stony Brook, 1976
Kawtar Hafidi, Ph.D., University of Paris XI, France, 1999
‡‡ Walter F. Henning, Ph.D., Technical University of Munich, Germany, 1968
§§ Roy J. Holt, Ph.D., Yale University, 1972
** Robert V. F. Janssens, Ph.D., University Catholique de Louvain, Belgium, 1978
Michael P. Kelly, Ph.D., University of Washington-Seattle, 1999
Teng Lek Khoo, Ph.D., McMaster University, Canada, 1972
Torben Lauritsen, Ph.D., State University of New York-Stony Brook, 1990
Christopher J. Lister, Ph.D., University of Liverpool, United Kingdom, 1977
⊕ Zheng-tian Lu, Ph.D., University of California-Berkeley, 1994
¤¤ Brahim Mustapha, Ph.D., University of Paris XI, France, 1999
• Jerry A. Nolen, Jr., Ph.D., Princeton University, 1965
Petr N. Ostroumov, Ph.D., Moscow Engineering and Physical Institute, Russia, 1982
Richard C. Pardo, Ph.D., University of Texas-Austin, 1976
David H. Potterveld, Ph.D., California Institute of Technology, 1988
Karl Ernst Rehm, Ph.D., Technical University of Munich, Germany, 1973
Paul E. Reimer, Ph.D., University of Illinois at Urbana-Champaign, 1996
⊕⊕ Guy Savard, Ph.D., McGill University, Canada, 1988
¶¤ John P. Schiffer, Ph.D., Yale University, 1954
Dariusz Seweryniak, Ph.D., Uppsala University, Sweden, 1994
¶ Kenneth W. Shepard, Ph.D., Stanford University, 1970
Kenneth M. Teh, Ph.D., Vanderbilt University, 1988

---

‡ Adjunct Professor, Vanderbilt University
§ Joint appointment with Northern Illinois University
* Continuous appointment with DePaul University
¶¶ Director of the Physics Division
‡‡ On leave of absence at GSI-Darmstadt, Germany
§§ Adjunct Professor, University of Illinois at Urbana-Champaign
** Associate Director of the Physics Division. Adjunct Professor at Michigan State University, Vanderbilt University, and University of Notre Dame
⊕ Professor Coterminous, University of Chicago
¤¤ Term Appointment
• Director of the ATLAS Facility. Adjunct Professor, Michigan State University
⊕⊕ Professor Coterminous, University of Chicago and Adjunct Professor, University of Manitoba, Canada
¶ Retired September 2006
¤ Professor Emeritus, University of Chicago

Special Appointments

Irshad Ahmad, Ph.D., University of California-Berkeley, 1966
Lowell M. Bollinger, Ph.D., Cornell University, 1951
Cary N. Davids, Ph.D., California Institute of Technology, 1967
Cheng-lie Jiang, Ph.D., China Institute of Atomic Energy, China, 1960
William J. Childs, Ph.D., University of Michigan, 1956
Donald S. Gemmell, Ph.D., Australian National University, Australia, 1960
Harold E. Jackson, Jr., Ph.D., Cornell University, 1959
* Michael Paul, Ph.D., The Hebrew University of Jerusalem, Israel, 1973
John P. Schiffer, Ph.D., Yale University, 1954
Kenneth W. Shepard, Ph.D., Stanford University, 1970
¤ Ben Zeidman, Ph.D., Washington University, 1957

THEORETICAL NUCLEAR PHYSICS STAFF

Regular Staff

Henning Esbensen, Ph.D., University of Aarhus, Denmark, 1977
Tsung-Shung Harry Lee, Ph.D., University of Pittsburgh, 1973
Kenneth Nollet, Ph.D., University of Chicago, 2000
Steven C. Pieper, Ph.D., University of Illinois at Urbana-Champaign, 1970
Craig D. Roberts, Ph.D., Flinders University of South Australia, Australia, 1989
‡ James W. Truran, Ph.D., Yale University, 1965
Robert B. Wiringa, Ph.D., University of Illinois at Urbana-Champaign, 1978

Special Appointments

Paul Benioff, Ph.D., University of California-Berkeley, 1959
Richard R. Chasman, Ph.D., University of California-Berkeley, 1959
Fritz Coester, Ph.D., University of Zurich, Switzerland, 1944
Mitio Inokuti, Ph.D., University of Tokyo, Japan, 1962
Dieter Kurath, Ph.D., University of Chicago, 1951
Malcolm H. Macfarlane, Ph.D., University of Rochester, 1955
§ Vijay Pandharipande, Ph.D., University of Bombay, India, 1969
Murray Peshkin, Ph.D., Cornell University, 1951

---

* Special Term Appointee from The Hebrew University of Jerusalem, Israel
¤ Special Term Appointee. Adjunct Professor, Hampton University
‡ Joint appointment with the University of Chicago
§ Special Term Appointee from the University of Illinois at Urbana-Champaign (deceased January 2006)

TEMPORARY APPOINTMENTS

Mandar Bhagwat (Kent State University)
Theoretical physics studies
(January 2006 -)

Yun Ding (the University of Chicago)
Medium-energy physics studies
(January 2006 -)

Sebastian Gros (the University of Liverpool, United Kingdom)
Research at ATLAS
(May 2005 -)

* Jeffrey R. Guest (the University of Michigan)
Medium-energy physics studies
(August 2004 -)

Prashanth Jaikumar (McGill University, Canada)
Theoretical physics studies
(September 2004 - September 2006)

Shashikant Manikonda (Michigan State University)
Research at ATLAS
(December 2006 -)

† Peter Mueller (Johannes Gutenberg-University, Germany)
Medium-energy physics studies
(July 2004 -)

Donald A. Peterson (Oregon St. University)
Research at ATLAS
(January 2004 -)

Muslema Pervin (Florida State University)
Theoretical physics studies
(January 2006 -)

Andrew Robinson (the University of Edinburg, United Kingdom)
Research at ATLAS
(May 2005 -)

Nicholas D. Scielzo (the University of California-Berkeley)
Medium-energy physics studies
(July 2003 - October 2006)

Hariprakash Sharma (the University of Manitoba, Canada)
Research at ATLAS
(July 2004 - July 2006)

---

* Argonne Scholar-AHCPF (Arthur Holly Compton Postdoctoral Fellowship)
† Argonne Scholar-WFLPF (Willard Frank Libby Postdoctoral Fellowship)

Patricia Solvignon (Temple University)
Medium-energy physics studies
(July 2006 -)

Tao Sun (Michigan State University)
Medium-energy physics studies
(October 2006 -)

Xiaodong Tang (Texas A&M University)
Research at ATLAS
(May 2003 - July 2006)

Stewart V. Wright (the University of Liverpool, United Kingdom)
Theoretical physics studies
(September 2004 - July 2006)

Jin Xu (Brown University)
Research at ATLAS
(August 2005 -)

Shaofei Zhu (the University of Notre Dame)
Research at ATLAS
(January 2004 - December 2006)

TECHNICAL AND ENGINEERING STAFF

(and areas of activity)

Kevin G. Bailey (B.S., University of Nebraska, 1989)
Technical assistance, medium-energy physics

Donald Barnett
ATLAS operations

* John M. Bogaty (A.A.S., DeVry University, 1961)
Electrical systems, ATLAS operation and development

Lee Kevin Carlquist (A.S., College of DuPage, 1986)
ATLAS operations

* Benny E. Clifft (A.S.E.E., DeVry University, 1959)
Electrical systems, ATLAS operation and development

* Donald Cyborski
Computer operations

Alex Deriy (B.S., University of Illinois-Chicago, 1988)
ATLAS operations

Gregory Devane
ATLAS operations

* Special Term Appointee

* Joseph Falout (B.S.M.E., University of Illinois, 1970)
Experimental equipment design

Joel Fuerst (M.S.M.E., Northwestern University, 1990)
Cryogenic development at ATLAS

Scott M. Gerbick (B.S., Purdue University, 2003)
ATLAS experimental equipment maintenance, technical assistance, low-energy physics

John P. Greene (M.S., DePaul University, 1982)
Target preparation

** Ray E. Harden (A.A.S., Milwaukee School of Engineering, 1957)
ATLAS operations

* Dale J. Henderson (B.S., Elmhurst College, 1951)
Detector development, technical assistance, low-energy physics

* Jack Jagger
Consulting engineer, medium-energy physics

Robert Jenkins
ATLAS operations

** Mark Kedzie
ATLAS experimental equipment development

** David Kurth
Graphic specialist

Anthony Krupa (A.A.S.-E.E.T., Purdue University, 1987)
ATLAS operations

Anthony Levand (B.S.M.E., University of Illinois at Urbana-Champaign, 1986)
Experimental equipment design at ATLAS

Eric Lindert (B.S., University of Wisconsin-Milwaukee, 1992)
ATLAS operations

* Paul Markovich (B.S., Purdue University, 1972)
Surface chemistry, ATLAS development and operation

Stephen MacDonald
Cryogenics engineer, ATLAS development and operation

* Bruce Millar
ATLAS operations

Floyd Munson, Jr. (A.A.S., DeVry University 1966; B.S., Lewis University, 1993)
Control system for ATLAS

---

* Special Term Appointee
** Terminated (September 2006)

Thomas P. Mullen (B.S., Marquette University, 1966)
Division ESH/QA engineer

Bruce G. Nardi (A.A.S., Morton Jr. College, 1967; A.A.S. DeVry University, 1969)
Electronics design and maintenance

Tom O'Connor (M.S., DePaul University, 1995)
Technical assistance, medium-energy physics

Donald Phillips (A.S., DeVry University, 1974)
ATLAS operations

* John Phillips (M.S., University of Illinois-Chicago, 1986)
Consulting ESH/QA engineer

Maria Power (M.S., Illinois Institute of Technology, 1993)
Technical assistance, ATLAS control system

John Rohrer (A.A.S., Triton College, 1987)
Experimental equipment support, low-energy physics

Robert Scott (B.S., University of Illinois-Chicago, 1995)
ATLAS operations

Sergey Sharamentov (M.S., Moscow Engineering Physical Institute, 1976)
Electrical systems, ATLAS operation and development

Brent R. Shumard (B.S., University of Valparaiso, 2002)
Detector development, technical assistance, low-energy physics

* James R. Specht (A.A.S., DeVry University, 1964)
Cryogenics engineer, ATLAS development and operation

Matthew Sternberg (B.S.C., University of Oregon)
Low-energy research at ATLAS
(October 2006 –)

** Philip Strickhorn (B.S., DeVry University, 1990)
Electrical and technical assistance, ATLAS operations

Richard Vondrasek (B.S., University of Chicago, 1990)
ATLAS ECR source

* Loren Weber (M.S., Northern Illinois University, 1974)
ATLAS operations

Philip R. Wilt (Johnstown Technical School, 1973)
Electronics design and maintenance

Bruce J. Zabransky (M.S., University of Illinois-Chicago, 1973)
Mechanical engineer

---

* Special Term Appointee
** Terminated (September 2006)

Gary P. Zinkann (B.S., DeVry University, 1975)
ATLAS operations supervisor

ADMINISTRATIVE STAFF

* Allan Bernstein (M.B.A., Rosary College, 1986)
* James E. Nelson (B.A., University of Illinois-Chicago, 1975)
** Barbara Fletcher (B.A., DePaul University, 1998)
Janet Bergman, Administrative Secretary
Jeannie Glover, Administrative Secretary
Debra Morrison, Administrative Secretary
§ Amy Randich, High School Student
Elizabeth Rizzo, Administrative Assistant
Colleen Tobolic, Administrative Secretary
Barbara Weller, Administrative Secretary

_____
* Assistant Director of the Physics Division
** Executive Secretary
§ Terminated (September 2006)

VISITORS AND STUDENTS

Long-Term Visitors (at Argonne more than 4 months)

Vladislav Asseev (Institute for Nuclear Research of the Russian Academy of Sciences, Russia)
Accelerator development
(October 2003 - November 2006)

* Van D Bistrow (University of Chicago)
Medium-energy physics
(July 2005 - June 2006)

** Victor Flambaum (University of South Wales, Australia)
Theoretical physics studies
(August 2005 -)

William Karstens (Saint Michaels College)
Theoretical physics studies
(July 2003 -)

Andrei Kolomiets (Institute of Theoretical and Experimental Physics, Russia)
Research at ATLAS
(April 2004 - April 2006)

Sergey Kondrashev (Moscow Engineering Physics Institute, Russia)
Research at ATLAS
(November 2006 -)

_____
* Guest Faculty Research Participant
** Argonne Fellow

† Serban Misicu (Horia Hulubei National Institute of Physics & Nuclear Engineering, Romania)
Theoretical physics studies)
(October 2005 - March 2006)

Short-Term Visitors (at ANL for less than 4 months at a time)

Masato Asai (Japan Atomic Energy Research Institute, Japan)
Low-energy research at ATLAS
(March 2006 - July 2006)

* Thomas Dombeck (University of Hawaii)
Theoretical studies
(August 2006 -)

* Christopher Fasano (Monmouth College)
Theoretical studies
(February 1999 -)

Ntombizonke Kheswa (iThemba Labs, South Africa)
Low-energy research at ATLAS
(April 2006 - May 2006)

Rachid Nouicer (University of Chicago)
Low-energy research at ATLAS
(April 1998 - January 2006)

Shuiming Hu (University of Science and Technology, China)
Medium-energy physics
(March 2006 - May 2006)

Timur Kulevoy (Institute of Theoretical and Experimental Physics, Russia)
Theoretical studies
(March 2006 - June 2006)

* Eugene Shiles (University of Vermont)
Theoretical physics studies
(August 2002 -)

* David Smith (University of Vermont)
Theoretical physics studies
(February 2002 -)

Resident Graduate Students

Laura Bandura (Northern Illinois University)
Low-energy research at ATLAS
(January 2006 –)

Zachary Conway (University of Illinois at Urbana-Champaign)
Research at ATLAS
(June 2003 -)

---

† Fulbright Fellow
* Guest Faculty Research Participant

Jennifer Fallis (University of Manitoba, Canada)
Low-energy research at ATLAS
(January 2006 –)

Daniel Lascar (Northwester University)
Low-energy research at ATLAS
(January 2006 –)

Gang Li (McGill University, Canada)
Low-energy research at ATLAS
(August 2006 –)

Nidhi Patel (Colorado School of Mines)
Research at ATLAS
(May 2005 -)

Mahuya Sengupta (Michigan State University)
Research at ATLAS
(November 2005 -)

Jin Wang (University of Chicago)
Medium-energy physics
(May 2006 –)

Guest Graduate Students

Lamiaa El Fassi (Mohammed V University, Morocco)
Medium-energy physics
(September 2003 -)

Nkemdilim Ezeife (University of Chicago)
Medium-energy physics
(July 2006 - August 2006)

Jennifer Fallis (University of Manitoba, Canada)
Low-energy research at ATLAS
(May 2005 – August 2005)

Gitai Feinberg (The Hebrew University of Jerusalem, Israel)
Research at ATLAS
(May 2006 -)

Nathan Hoteling (University of Maryland)
Research at ATLAS
(February 2003 -)

Shlomi Halfon (The Hebrew University of Jerusalem, Israel)
Research at ATLAS
(May 2006 -)

Louis Jisonna (Northwestern University)
Low-energy research at ATLAS
(June 2000 -)

James Maloney (Northern Illinois University)
Research at ATLAS
(June 2006 -)

Iouri Sanjiev (St. Petersburg Nuclear Physics Institute, Russia)
Medium-energy physics
(January 2006 -)

Ibrahim Sulai (University of Chicago)
Medium-energy physics
(June 2005 -)

Jie Sun (University of Notre Dame)
Theoretical physics studies
(May 2006 - August 2006)

Tout Wang (University of Toronto, Canada)
Low-energy research at ATLAS
(May 2006 – September 2006)

Undergraduate Students

Andrew Bump (DeVry University)
Shane Caldwell (DePaul University)
John Carr (University of Illinois-Chicago)
Robert Carrier (St. Xavier University)
Mark Chantell (University of Chicago)
David Danaher (Monmouth College)
Alan Davila (University of Texas-El Paso)
Christopher Deatrick (Western Michigan University)
Mark Durante (North Central College)
Steven Fazzio (Macalester College)
Daniel Fiorino (DePaul University)
David Grayson (University of Illinois at Urbana-Champaign)
Tomas Hernandez (University of Texas-El Paso)
Sereres Johnston (Andrews University)
Jason Kozemczak (Greenville College)
Grant Larsen (University of Chicago)
Roman Mongado (DeVry University)
Patrick McCormack (North Central College)
Holly Nolan (North Central College)
Elena Poklonskaya (St. Petersburg Electrotechnical University (LETI), Russia)
Ida Sefer (North Central College)
Matthew Sternberg (University of Oregon)

LOW-ENERGY NUCLEAR PHYSICS RESEARCH

$^{40}Ca(\alpha,\gamma)^{44}Ti$ Reaction in the Energy Regime of Supernova Nucleosynthesis
H. Nassar, M. Paul, I. Ahmad, Y. Ben-Dov, J. Caggiano, S. Ghelberg, S. Goriely, J. P. Greene, M. Hass, A. Heger, A. Heinz, D. J. Henderson, R. V. F. Janssens, C. L. Jiang, Y. Kashiv, B. S. Nara Singh, A. Ofan, R. C. Pardo, T. Pennington, K. E. Rehm, G. Savard, R. Scott, and R. Vondrasek
Phys. Rev. Lett. **96**, 041102/1-4 (2006)

Breakdown of *K*-Selection in ^{178}Hf
A. B. Hayes, D. Cline, C. Y. Wu, J. Ai, H. Amro, C. Beausang, R. F. Casten, J. Gerl, A. A. Hecht, A. Heinz, R. Hughes, R. V. F. Janssens, C. J. Lister, A. O. Macchiavelli, D. A. Meyer, E. F. Moore, P. Napiorkowski, R. C. Pardo, Ch. Schlegel, D. Seweryniak, M. W. Simon, J. Srebrny, R. Teng, K. Vetter, and H. J. Wollersheim
Phys. Rev. Lett. **96**, 042505/1-4 (2006)

Stabilization of Nuclear Isovector Valence-Shell Excitations
G. Rainovski, N. Pietralla, T. Ahn, C. J. Lister, R. V. F. Janssens, M. P. Carpenter, S. Zhu, and C. J. Barton III
Phys. Rev. Lett. **96**, 122501/1-4 (2006)

System Size and Centrality Dependence of Charged Hadron Transverse Momentum Spectra in Au + Au and Cu + Cu Collisions from $\sqrt{s_{NN}}$ = 62.4 to 200 GeV
B. B. Back *et al*. (PHOBOS Collaboration)
Phys. Rev. Lett. **96**, 212301/1-4 (2006)

Energy Dependence of Direct Flow Over a Wide Range of Pseudorapidity in Au + Au Collisions at RHIC
B. B. Back *et al*. (PHOBOS Collaboration)
Phys. Rev. Lett. **97**, 012301/1-4 (2006)

K-Isomers in ^{254}No: Probing Single Particle Energies and Pairing Strengths in the Heaviest Nuclei
S. K. Tandel, T. L. Khoo, D. Seweryniak, G. Mukherjee, I. Ahmad, B. Back, R. Blinstrup, P. A. Butler, M. P. Carpenter, J. Chapman, P. Chowdhury, C. N. Davids, P. T. Greenlees, A. A. Hecht, A. Heinz, R.-D. Herzberg, P. Ikin, R. V. F. Janssens, G. D. Jones, F. G. Kondev, T. Lauritsen, C. J. Lister, E. F. Moore, D. Peterson, P. Reiter, U. S. Tandel, X. F. Wang, and S. F. Zhu
Phys. Rev. Lett. **97**, 082502/1-4 (2006)

Anomalous Isomeric Decays in ^{174}Lu as a Probe of *K* Mixing and Interactions in Deformed Nuclei
G. D. Dracoulis, F. G. Kondev, G. J. Lane, A. P. Byrne, T. R. McGoram, T. Kibédi, I. Ahmad, M. P. Carpenter, R. V. F. Janssens, T. Lauritsen C. J. Lister, D. Seweryniak, P. Chowdhury, and S. K. Tandel
Phys. Rev. Lett. **97**, 122501/1-4 (2006)

Isospin Symmetry of Odd-Odd Mirror Nuclei: Identification of Excited States in $N = Z - 2$ ^{48}Mn
M. A. Bentley, C. Chandler, M. J. Taylor, J. R. Brown, M. P. Carpenter, C. Davids, J. Ekman, S. J. Freeman, P. E. Garrett, G. Hammond, R. V. F. Janssens, S. M. Lenzi, C. J. Lister, R. du Rietz, and D. Seweryniak
Phys. Rev. Lett. **97**, 132501/1-4 (2006)

Two-Quasiparticle *K*-Isomers and Pairing Strengths in the Neutron-Rich Isotopes ^{174}Er and ^{172}Er
G. D. Dracoulis, G. J. Lane, F. G. Kondev, A. P. Byrne, R. O. Hughes, P. Nieminen, H. Watanabe, M. P. Carpenter, R. V. F. Janssens, T. Lauritsen, D. Seweryniak, S. Zhu, P. Chowdhury, and F. R. Xu
Phys. Lett. **B635**, 200-206 (2006)

First Evidence of Fusion Hindrance for a Small *Q*-Value System
C. L. Jiang, B. B. Back, H. Esbensen, R. V. F. Janssens, S. Mişicu, K. E. Rehm, P. Collon, C. N. Davids, J. Greene, D. J. Henderson, L. Jisonna, S. Kurtz, C. J. Lister, M. Notani, M. Paul, R. Pardo, D. Peterson, D. Seweryniak, B. Shumard, X. D. Tang, I. Tanihata, X. Wang, and S. Zhu
Phys. Lett. **B640**, 18-22 (2006)

Transverse Momentum and Rapidity Dependence of Hanbury-Brown-Twiss Correlations in Au + Au Collisions at $\sqrt{s_{NN}}$ = 62.4 and 200 GeV

B. B. Back *et al*. (PHOBOS Collaboration)
Phys. Rev. C **73**, 031901(R)/1-5 (2006)

α Decay of ^{105}Te

D. Seweryniak, K. Starosta, C. N. Davids, S. Gros, A. A. Hecht, N. Hoteling, T. L. Khoo, K. Lagergren, G. Lotay, D. Peterson, A. Robinson, C. Vaman, W. B. Walters, P. J. Woods, and S. Zhu
Phys. Rev. C **73**, 061301(R)/1-3 (2006)

First Observation of Excited States in ^{114}Cs: Spectroscopy of the Yrast $\nu(h_{11/2}) \otimes \pi(h_{11/2})$ Band

J. F. Smith, A. M. Fletcher, C. J. Chiara, M. P. Carpenter, H. J. Chantler, C. N. Davids, J. L. Durell, D. B. Fossan, S. J. Freeman, R. V. F. Janssens, T. Koike, F. G. Kondev, D. R. LaFosse, J. C. Lisle, D. Patel, E. S. Paul, W. Reviol, D. G. Sarantites, D. Seweryniak, K. Starosta, R. Wadsworth, and A. N. Wilson
Phys. Rev. C **73**, 061303(R)/1-5 (2006)

Variation with Mass of $B(E3; 0_1^+ \rightarrow 3_1^-)$ Transition Rates in A = 124-134 Even-Mass Xenon Nuclei

W. F. Mueller, M. P. Carpenter, J. A. Church, D. C. Dinca, A. Gade, T. Glasmacher, D. T. Henderson, Z. Hu, R. V. F. Janssens, A. F. Lisetskiy, C. J. Lister, E. F. Moore, T. O. Pennington, B. C. Perry, I. Wiedenhöver, K. L. Yurkewicz, V. G. Zelevinsky, and H. Zwahlen
Phys. Rev. C **73**, 014316/1-5 (2006)

Systematics of Heavy-Ion Fusion Hindrance at Extreme Sub-Barrier Energies

C. L. Jiang, B. B. Back, H. Esbensen, R. V. F. Janssens, and K. E. Rehm
Phys. Rev. C **73**, 014613/1-5 (2006)

Erratum: Structure of Two-, Four-, and Six-Quasiparticle Isomers in ^{174}Yb and *K*-Forbidden Decays
[Phys. Rev. C **71**, 044326 (2005)]

G. D. Dracoulis, G. J. Lane, F. G. Kondev, A. P. Byrne, T. Kibédi, H. Watanabe, I. Ahmad, M. P. Carpenter, S. J. Freeman, R. V. F. Janssens, N. J. Hammond, T. Lauritsen, C. J. Lister, G. Mukherjee, D. Seweryniak, P. Chowdhury, and S. K. Tandel
Phys. Rev. C **73**, 019901(E) (2006)

The ^{8}B Neutrino Spectrum

W. T. Winter, S. J. Freedman, K. E. Rehm, and J. P. Schiffer
Phys. Rev. C **73**, 025503/1-15 (2006)

Near-Yrast Structure of the ^{109}Mo Nucleus

W. Urban, Ch. Droste, T. Rzaca-Urban, Zlomaniec, J. L. Durell, A. G. Smith, B. J. Varley, and I. Ahmad
Phys. Rev. C **73**, 037302/1-4 (2006)

Spectroscopy of the Odd-Odd *fp*-Shell Nucleus ^{52}Sc from Secondary Fragmentation

A. Gade, R. V. F. Janssens, D. Bazin, B. A. Brown, C. M. Campbell, M. P. Carpenter, J. M. Cook, A. N. Deacon. C.-D. Dinca, S. J. Freeman, T. Glasmacher, B. P. Kay, P. F. Mantica, W. F. Mueller, J. R. Terry, and S. Zhu
Phys. Rev. C **73**, 037309/1-4 (2006)

High-*K* Isomers and Rotational Structures in ^{174}W

S. K. Tandel, P. Chowdhury, E. H. Seabury, I. Ahmad, M. P. Carpenter, S. M. Fischer, R. V. F. Janssens, T. L. Khoo, T. Lauritsen, C. J. Lister, D. Seweryniak, and Y. R. Shimizu
Phys. Rev. C **73**, 044306/1-19 (2006)

Half-Life and Spin of $^{60}Mn^{g}$

S. N. Liddick, P. F. Mantica, B. A. Brown, M. P. Carpenter, A. D. Davies, M. Horoi, R. V. F. Janssens, A. C. Morton, W. F. Mueller, J. Pavan, H. Schatz, A. Stolz, S. L. Tabor, B. E. Tomlin, and M. Wiedeking
Phys. Rev. C **73**, 044322/1-5 (2006)

Single-Particle and Collective Degrees of Freedom in ^{101}Zr and $^{103,105}Mo$

R. Orlandi, A. G. Smith, D. Patel, G. S. Simpson, R. M. Wall, J. F. Smith, O. J. Onakanmi, I. Ahmad, J. P. Greene, M. P. Carpenter, T. Lauritsen, C. J. Lister, R. V. F. Janssens, F. G. Kondev, D. Seweryniak, B. J. P. Gall, O. Dorveaux, and A. E. Stuchbery
Phys. Rev. C **73**, 054310/1-12 (2006)

Reevaluation of the $^{30}P(p,\gamma)^{31}S$ Astrophysical Reaction Rate from a Study of the $T = 1/2$ Mirror Nuclei, ^{31}S and ^{31}P

D. G. Jenkins, A. Meadowcroft, C. J. Lister, M. P. Carpenter, P. Chowdhury, N. J. Hammond, R. V. F. Janssens, T. L. Khoo, T. Lauritsen, D. Seweryniak, T. Davinson, P. J. Woods, A. Jokinen, H. Penttila, G. Martínez-Pinedo, and J. José
Phys. Rev. C **73**, 065802/1-8 (2006)

Forward-Backward Multiplicity Correlations in $\sqrt{s_{NN}}$ = 200 GeV Au + Au Collisions

B. B. Back *et al*. (PHOBOS Collaboration)
Phys. Rev. C **74**, 011901(R)/1-5 (2006)

Cross-Shell Excitation in Two-Proton Knockout: Structure of ^{52}Ca

A. Gade, R. V. F. Janssens, D. Bazin, R. Broda, B. A. Brown, C. M. Campbell, M. P. Carpenter, J. M. Cook, A. N. Deacon, D.-C. Dinca, B. Fornal, S. J. Freeman, T. Glasmacher, P. G. Hansen, B. P. Kay, P. F. Mantica, W. F. Mueller, J. R. Terry, J. A. Tostevin, and S. Zhu
Phys. Rev. C **74**, 021302(R)/1-4 (2006)

Centrality and Energy Dependence of Charged-Particle Multiplicities in Heavy Ion Collisions in the Context of Elementary Reactions

B. B. Back (for the PHOBOS Collaboration)
Phys. Rev. C **74**, 021902(R)/1-4 (2006)

Decay Modes of ^{250}No

D. Peterson, B. B. Back, R. V. F. Janssens, T. L. Khoo, C. J. Lister, D. Seweryniak, I. Ahmad, M. P. Carpenter, C. N. Davids, A. A. Hecht, C. L. Jiang, T. Lauritsen, X. Wang, S. Zhu, F. G. Kondev, A. Heinz, J. Qian, R. Winkler, P. Chowdhury, S. K. Tandel, and U. S. Tandel
Phys. Rev. C **74**, 014316/1-9 (2006)

Excited States and Signature Inversion in ^{116}Cs

J. F. Smith, C. J. Chiara, M. P. Carpenter, C. N. Davids, M. Devlin, D. B. Fossan, S. J. Freeman, R. V. F. Janssens, D. R. LaFosse, D. G. Sarantites, D. Seweryniak, K. Starosta, R. Wadsworth, A. N. Wilson, and R. Wyss
Phys. Rev. C **74**, 034310/1-10 (2006)

Multiple Octupole-Type Band Structures in ^{220}Th: Reflection-Asymmetric Tidal Waves?

W. Reviol, C. J. Chiara, M. Montero, D. G. Sarantites, O. L. Pechenaya, M. P. Carpenter, R. V. F. Janssens, T. L. Khoo, T. Lauritsen, C. J. Lister, D. Seweryniak, S. Zhu, and S. G. Frauendorf
Phys. Rev. C **74**, 044305/1-8 (2006)

One-Neutron Knockout in the Vicinity of the $N = 32$ Sub-Shell Closure: $^{9}Be(^{57}Cr,^{56}Cr + \gamma)X$

A. Gade, R. V. F. Janssens, D. Bazin, B. A. Brown, C. M. Campbell, M. P. Carpenter, J. M. Cook, A. N. Deacon, D.-C. Dinca, S. J. Freeman, T. Glasmacher, M. Horoi, B. P. Kay, P. F. Mantica, W. F. Mueller, J. R. Terry, J. A. Tostevin, and S. Zhu
Phys. Rev. C **74**, 047302/1-4 (2006)

$T = 1$ States in ^{74}Rb and Their ^{74}Kr Analogs
S. M. Fischer, C. J. Lister, N. J. Hammond, R. V. F. Janssens, T. L. Khoo, T. Lauritsen, E. F. Moore, D. Seweryniak, S. Sinha, D. P. Balamuth, P. A. Hausladen, D. G. Sarantites, W. Reviol, P. Chowdhury, S. D. Paul, C. Baktash, and C.-H. Yu
Phys. Rev. C **74**, 054304/1-10 (2006)

Multiple Band Structures in ^{169}Ta
D. J. Hartley, W. H. Mohr, J. R. Vanhoy, M. A. Riley, A. Aguilar, C. Teal, R. V. F. Janssens, M. P. Carpenter, A. A. Hecht, T. Lauritsen, E. F. Moore, S. Zhu, F. G. Kondev, M. K. Djongolov, M. Danchev, L. L. Riedinger, G. B. Hagemann, G. Sletten, P. Chowdhury, S. K. Tandel, W. C. Ma, and S. W. Ødegård
Phys. Rev. C **74**, 054314/1-16 (2006)

Triaxiality in ^{105}Mo and ^{107}Mo from the Low to Intermediate Spin Region
J. A. Pinston, W. Urban, Ch. Droste, T. Rzaca-Urban, J. Genevey, G. Simpson, J. L. Durell, A. G. Smith, B. J. Varley, and I. Ahmad
Phys. Rev. C **74**, 064304/1-10 (2006)

Yrast Structure of ^{64}Fe
N. Hoteling, W. B. Walters, R. V. F. Janssens, R. Broda, M. P. Carpenter, B. Fornal, A. A. Hecht, M. Hjorth-Jensen, W. Królas, T. Lauritsen, T. Pawlat, D. Seweryniak, X. Wang, A. Wohr, J. Wrzesinski, and S. Zhu
Phys. Rev. C **74**, 064313/1-6 (2006)

Level Structure of the Neutron-Rich ^{56,58,60}Cr Isotopes: Single-Particle and Collective Aspects
S. Zhu, A. N. Deacon, S. J. Freeman, R. V. F. Janssens, B. Fornal, M. Honma, F. R. Xu, R. Broda, I. R. Calderin, M. P. Carpenter, P. Chowdhury, F. G. Kondev, W. Królas, T. Lauritsen, S. N. Liddick, C. J. Lister, P. F. Mantica, T. Pawlat, D. Seweryniak, J. F. Smith, S. L. Tabor, B. E. Tomlin, B. J. Varley, and J. Wrzesiński
Phys. Rev. C **74**, 064315/1-15 (2006)

Improved Measurement of the ^{44}Ti Half-Life from a 14-Year Long Study
I. Ahmad, J. P. Greene, E. F. Moore, S. Ghelberg, A. Ofan, M. Paul, and W. Kutschera
Phys. Rev. C **74**, 065803/1-8 (2006)

Double *K*-Shell Photoionization of Silver
E. P. Kanter, I. Ahmad, R. W. Dunford, D. S. Gemmell, B. Krässig, S. H. Southworth, and L. Young
Phys. Rev. A **73**, 022708/1-11 (2006)

Production Cross-Sections of Protactinium and Thorium Isotopes Produced in Fragmentation of ^{238}U at 1 A GeV
J. Kurcewicz, Z. Liu, M. Pfützner, P. J. Woods, C. Mazzocchi, K.-H. Schmidt, A. Kelić, F. Attallah, E. Badura, C. N. Davids, T. Davinson, J. Döring, H. Geissel, M. Gòrska, R. Grzywacz, M. Hellström, Z. Janas, M. Karny, A. Korgul, I. Mukha, C. Plettner, A. Robinson, E. Roeckl, K. Rykaczewski, K. Schmidt, D. Seweryniak, K. Sümmerer, and H. Weick
Nucl. Phys. **A767**, 1-12 (2006)

X-Ray Binaries
H. Schatz and K. E. Rehm
Nucl. Phys. **A777**, 601-622 (2006)

Gamma-Ray Spectroscopy of the Doubly Magic Nucleus ^{56}Ni
E. K. Johansson, D. Rudolph, J. Ekman, C. Fahlander, C. Andreoiu, M. A. Bentley, M. P. Carpenter, R. J. Charity, R. M. Clark, P. Fallon, R. V. F. Janssens, F. G. Kondev, T. L. Khoo, T. Lauritsen, A. O. Macchiavelli, W. Reviol, D. G. Sarantites, D. Seweryniak, C. E. Svensson, and S. J. Williams
Eur. Phys. J. A **27**, 157-165 (2006)

Physics of a Rare Isotope Accelerator
D. F. Geesaman, C. K. Gelbke, R. V. F. Janssens, and B. M. Sherrill
Ann. Rev. Nucl. and Part. Sci. **56**, 53-92 (2006)

New Information on the $T_{1/2}$ = 47 s Isomer in the ^{136}I Nucleus
W. Urban, M. Saha Sarkar, S. Sarkar, T. Rzaca-Urban, J. L. Durell, A. G. Smith, J. A. Genevey, J. A. Pinston, G. S. Simpson, and I. Ahmad
Eur. Phys. J. A **27**, 257-262 (2006)

Development of a Detection Method for ^{244}Pu by Resonance Ionization Mass Spectrometry
A. Ofan, I. Ahmad, J. P. Greene, M. Paul, and M. R. Savina
New Astronomy Reviews **50**, 640-643 (2006)

A New Evaporator System for Target Preparation at Argonne National Laboratory
John P. Greene, Janelle Neubauer, and Dino Deligiannis
Proceedings of the 22nd World Conference of the International Nuclear Target Development Society, Gaithersburg, MD, October 19-22, 2004; Nucl. Instrum. Methods **A561**, 58-61 (2006)

Oxide Targets for GAMMASPHERE
J. P. Greene, K. Lister, and S. Fischer
Proceedings of the 22nd World Conference of the International Nuclear Target Development Society, Gaithersburg, MD, October 19-22, 2004; Nucl. Instrum. Methods **A561**, 104-106 (2006)

Identification of Nilsson States in Transcurium Nuclei
I. Ahmad
Proceedings of the International Conference on Finite Fermionic Systems: Nilsson Model 50 Years, Lund, Sweden, June 14-18, 2005; Phys. Scr. **T125**, 78-81 (2006)

Observation of States Beyond Band Termination in ^{156,157,158}Er and Strongly Deformed Structures in ^{173,174,175}Hf
M. A. Riley, M. K. Djongolov, A. O. Evans, D. J. Hartley, R. V. F. Janssens, E. S. Paul, A. Pipidis, J. Simpson, A. A. Aguilar, D. E. Appelbe, C. R. Bingham, D. B. Campbell, M. P. Carpenter, P. Chowdhury, P. T. W. Choy, R. M. Clark, M. Cromaz, D. M. Cullen, M. Danchev, G. D. Dracoulis, P. Fallon, A. Görgen, G. B. Hagemann, D. T. Joss, J. Goon, R. A. Kaye, T. L. Khoo, F. G. Kondev, R. W. Laird, K. Lagergren, T. Lauritsen, A. O. Macchiavelli, B. McClain, E. F. Moore, G. Mukherjee, E. Ngijoi-Yogo, P. J. Nolan, H. I. Park, L. L. Riedinger, G. Sletten, S. K. Tandel, P. M. Walker, D. Ward, I. Ragnarsson, F. Saríc, and Jing-ye Zhang
Proceedings of the International Conference on Finite Fermionic Systems: Nilsson Model 50 Years, Lund, Sweden, June 14-18, 2005; Phys. Scr. **T125**, 123-126 (2006)

Lifetime Measurements in $N = Z$ ^{72}Kr
C. Andreoiu, C. E. Svensson, R. A. E. Austin, M. P. Carpenter, D. Dashdorj, P. Finlay, S. J. Freeman, P. E. Garrett, A. Görgen, J. Greene, G. F. Grinyer, B. Hyland, D. Jenkins, F. Johnston-Theasby, P. Joshi, A. O. Macchiavelli, F. Moore, G. Mukherjee, A. A. Phillips, W. Reviol, D. G. Sarantites, M. A. Schumaker, D. Seweryniak, M. B. Smith, J. J. Valiente-Dobón, and R. Wadsworth
Proceedings of the International Conference on Finite Fermionic Systems: Nilsson Model 50 Years, Lund, Sweden, June 14-18, 2005; Phys. Scr. **T125**, 127-129 (2006)

New Results from the PHOBOS Experiment
G. Roland (for the PHOBOS Collaboration)
Proceedings of the 18th International Conference on Ultra-Relativistic Nucleus-Nucleus Collisions, Budapest, Hungary, August 4-9, 2005; Nucl. Phys. **A774**, 113-128 (2006)

Particle Production at Very Low and Intermediate Transverse Momenta in d + Au and Au + Au Collisions
Adam Trzupek (for the PHOBOS Collaboration)
Proceedings of the 18th International Conference on Ultra-Relativistic Nucleus-Nucleus Collisions, Budapest, Hungary, August 4-9, 2005; Nucl. Phys. **A774**, 469-472 (2006)

System Size, Energy and Pseudorapidity Dependence of Directed and Elliptic Flow at RHIC
S. Manley (for the PHOBOS Collaboration)
Proceedings of the 18th International Conference on Ultra-Relativistic Nucleus-Nucleus Collisions, Budapest, Hungary, August 4-9, 2005; Nucl. Phys. **A774**, 523-526 (2006)

Forward-Backward Multiplicity Correlations in $\sqrt{s_{NN}}$ 200 GeV Au + Au Collisions
Peter Steinberg (for the PHOBOS Collaboration)
Proceedings of the 18th International Conference on Ultra-Relativistic Nucleus-Nucleus Collisions, Budapest, Hungary, August 4-9, 2005; Nucl. Phys. **A774**, 631-634 (2006)

Correlations and Fluctuations Over a Broad Range in Pseudorapidity Using the PHOBOS Detector
G. S. F. Stephans (for the PHOBOS Collaboration)
Proceedings of the 18th International Conference on Ultra-Relativistic Nucleus-Nucleus Collisions, Budapest, Hungary, August 4-9, 2005; Nucl. Phys. **A774**, 639-642 (2006)

In-Beam γ-Spectroscopy of Low-Spin Mixed-Symmetry States of ^{138}Ce with Gammasphere in Singles-Mode
N. Pietralla, G. Rainovski, T. Ahn, M. P. Carpenter, R. V. F. Janssens, C. J. Lister, and S. Zhu
Proceedings of the 12th International Conference on Capture Gamma-Ray Spectroscopy and Related Topics (CGS 12), Notre Dame, IN, September 4-9, 2005, eds. Andreas Woehr and Ani Aprahamian, AIP Conference Proceedings **819**, 11-15 (2006)

Violations of *K*-Conservation in ^{178}Hf
A. B. Hayes, D. Cline, C. Y. Wu, J. Ai, H. Amro, C. Beausang, R. F. Casten, J. Gerl, A. A. Hecht, A. Heinz, R. Hughes, R. V. F. Janssens, C. J. Lister, A. O. Macchiavelli, D. A. Meyer, E. F. Moore, P. Napiorkowski, R. C. Pardo, Ch. Schlegel, D. Seweryniak, M. W. Simon, J. Srebmy, R. Teng, K. Vetter, and H. J. Wollersheim
Proceedings of the 12th International Conference on Capture Gamma-Ray Spectroscopy and Related Topics (CGS 12), Notre Dame, IN, September 4-9, 2005, eds. Andreas Woehr and Ani Aprahamian, AIP Conference Proceedings **819**, 24-29 (2006)

Search for Enhanced Alpha Preformation in the N = Z + 1 Nuclei ^{113}Ba, ^{109}Xe, ^{105}Te
A. A. Hecht, C. J. Lister, C. N. Davids, A. Heinz, N. Hoteling, C. Mazzocchi, J. Palombo, D. Seweryniak, J. Shergur, M. Stoyer, W. B. Walters, P. J. Woods, and S. Zhu
Proceedings of the 12th International Conference on Capture Gamma-Ray Spectroscopy and Related Topics (CGS 12), Notre Dame, IN, September 4-9, 2005, eds. Andreas Woehr and Ani Aprahamian, AIP Conference Proceedings **819**, 355-359 (2006)

Rotational Damping, Ridges and the Quasi-Continuum of γ Rays in ^{152}Dy
T. Lauritsen, R. V. F. Janssens, T. L. Khoo, I. Ahmad, M. P. Carpenter, K. G. Kondev, C. J. Lister, E. F. Moore, D. Seweryniak, S. Zhu, T. Dössing, B. Herskind, A. M. Heinz, D. G. Jenkins, R. M. Clark, P. Fallon, A. O. Macchiavelli, D. Ward, G. Lane, P. Chowdhury, A. Korichi, A. Lopez-Martens, and A. J. Larabee
Proceedings of the 12th International Conference on Capture Gamma-Ray Spectroscopy and Related Topics (CGS 12), Notre Dame, IN, September 4-9, 2005, eds. Andreas Woehr and Ani Aprahamian, AIP Conference Proceedings **819**, 459-463 (2006)

Light Nuclei Studied with Nucleon Transfer Reactions Using Exotic Beams
A. H. Wuosmaa, K. E. Rehm, J. P. Greene, D. J. Henderson, R. V. F. Janssens, C. L. Jiang, L. Jisonna, E. F. Moore, R. C. Pardo, M. Paul, D. Peterson, S. C. Pieper, G. Savard, J. P. Schiffer, R. E. Segel, S. Sinha, X. Tang, and R. B. Wiringa
Proceedings of the International Conference on Frontiers in Nuclear Structure, Astrophysics, and Reactions (FINUSTAR), Kos, Greece, September 12-17, 2005, eds. S. V. Harissopulos, P. Demetriou, and R. Julin, AIP Conference Proceedings **831**, 332-336 (2006)

Heavy-Ion Fusion Hindrance at Extreme Sub-Barrier Energies
C. L. Jiang, B. B. Back, H. Esbensen, R. V. F. Janssens, S. Misicu, K. E. Rehm, P. Collon, C. N. Davids, J. Greene, D. J. Henderson, L. Jisonna, S. Kurtz, C. J. Lister, M. Notani, M. Paul, R. Pardo, D. Peterson, D. Seweryniak, B. Shumard, X. D. Tang, X. Wang, and S. Zhu
Proceedings of the International Conference on Reaction Mechanisms and Nuclear Structure at the Coulomb Barrier (Fusion06), San Servolo Island, Venice, Italy, March 19-23, 2006, AIP Conference Proceedings **853**, 63-38 (2006)

Decay Modes of Narrow Molecular Resonances
S. Courtin, F. Haas, M.-D. Salsac, D. Lebhertz, A. Michalon, C. Beck, M. Rousseau, A. Sanchez I Zafra, D. G. Jenkins, R. G. Glover, P. E. Kent, D. Hutcheon, C. Davis, J. E. Pearson and the Dragon Collaboration, and C. J. Lister
Proceedings of the International Conference on Reaction Mechanisms and Nuclear Structure at the Coulomb Barrier (Fusion06), San Servolo Island, Venice, Italy, March 19-23, 2006, AIP Conference Proceedings **853**, 134-139 (2006)

Fusion-Fission of $^{16}O + ^{197}Au$ at Sub-Barrier Energies
B. B. Back, C. L. Jiang, R. V. F. Janssens, D. J. Henderson, B. R. Shumard, C. J. Lister, D. Peterson, K. E. Rehm, I. Tanihata, X. Tang, X. F. Wang, and S. Zhu
Proceedings of the International Conference on Reaction Mechanisms and Nuclear Structure at the Coulomb Barrier (FusionN06), San Servolo Island, Venice, Italy, March 19-23, 2006, AIP Conference Proceedings **853**, 331-335 (2006)

Microsecond and Nanosecond Isomers Populated in Fission Reactions
G. A. Jones, P. M. Walker, Zs. Podolyák, P. H. Regan, S. J. Williams, M. P. Carpenter, J. J. Carroll, R. S. Chakrawarthy, P. Chowdhury, I. J. Cullen, G. D. Dracoulis, A. B. Garnsworthy, G. Hackman, R. V. F. Janssens, T. L. Khoo, F. G. Kondev, G. J. Lane, Z. Liu, D. Seweryniak, N. J. Thompson, and S. Zhu
Proceedings of the International Conference on Reaction Mechanisms and Nuclear Structure at the Coulomb Barrier (Fusion06), San Servolo Island, Venice, Italy, March 19-23, 2006, AIP Conference Proceedings **853**, 342-349 (2006)

Reaction Studies in Nuclear Astrophysics
K. E. Rehm
Proceedings of the International Conference on Reaction Mechanisms and Nuclear Structure at the Coulomb Barrier (Fusion06), San Servolo Island, Venice, Italy, March 19-23, 2006, AIP Conference Proceedings **853**, 350-357 (2006)

Proton Drip Line Spectroscopy with Gammasphere and the FMA
M. P. Carpenter
Proceedings of the Conference on Nuclei at the Limits (NS06), Oak Ridge, TN, July 24-28, 2006, Book of Abstracts, p. 18 (2006)

Approaching ^{98}Ni Along the N = 50 Line Utilizing Deep Inelastic Reactions
M. P. Carpenter, R. V. F. Janssens, S. Zhu, B. Fornal, R. Broda, A. Galindo-Uribarri, N. Hoteling, A. Ibanez, T. L. Khoo, F. G. Kondev, T. Lauritsen, C. J. Lister, E. Padilla-Rodal, D. Seweryniak, J. P. Ureggo-Blanco, and X. Wang
Proceedings of the Conference on Nuclei at the Limits (NS06), Oak Ridge, TN, July 24-28, 2006, Book of Abstracts, p. 19 (2006)

Triple Shape Coexistence in ^{181}Tl
M. P. Carpenter, F. G. Kondev, R. V. F. Janssens, D. Seweryniak, G. Mukherjee, I. Ahmad, C. N. Davids, S. M. Fischer, S. Freeman, G. Jones, N. Hammond, D. J. Jenkins, T. L. Khoo, A. J. Larabee, T. Lauritsen, N. Liechty, C. J. Lister, E. F. Moore, P. Raddon, S. Sinha, and R. Wadsworth
Proceedings of the Conference on Nuclei at the Limits (NS06), Oak Ridge, TN, July 24-28, 2006, Book of Abstracts, p. 20 (2006)

Probing *sd-pf* Cross-Shell Interactions via Terminating Configurations in N ≈ Z Scandium Isotopes
C. J. Chiara, M. Devlin, E. Ideguchi, F. Lerma, W. Reviol, S. K. Ryu, D. G. Sarantites, C. Baktash, A. Galindo-Uribarri, G. Stoitcheva, D. Rudolph, D. R. LaFosse, M. P. Carpenter, R. V. F. Janssens, T. Lauritsen, C. J. Lister, P. Reiter, D. Seweryniak, P. Fallon, A. Görgen, A. O. Macchiavelli, and W. Satuła
Proceedings of the Conference on Nuclei at the Limits (NS06), Oak Ridge, TN, July 24-28, 2006, Book of Abstracts, p. 24 (2006)

Alpha-Gamma Angular Correlations Using Novel Position-Sensitive Detectors
P. Chowdhury, C. M. Wilson, R. Gramer, S. K. Tandel, N. J. Hammond, C. J. Lister, S. M. Fischer, E. F. Moore, K. M. Teh, M. McClish, K. S. Shah, and R. Farrell
Proceedings of the Conference on Nuclei at the Limits (NS06), Oak Ridge, TN, July 24-28, 2006, Book of Abstracts, p. 25 (2006)

A New Alpha-Decaying High-Spin Isomer in the Very Neutron-Deficient Nucleus, ^{158}Ta
I. G. Darby, J. Uusitalo, D. T. Joss, R. D. Page, J. Simpson, K. Andgren, B. Cederwall, S. Eeckhaudt, T. Grahn, C. Gray-Jones, P. T. Greenlees, B. Hadinia, P. M. Jones, R. Julin, S. Juutinen, M. Leino, A.-P. Leppänen, M. Nyman, J. Pakarinen, P. Rahkila, J. Sarén, M. Sandzelius, C. Scholey, D. Seweryniak, and D. D. Warner
Proceedings of the Conference on Nuclei at the Limits (NS06), Oak Ridge, TN, July 24-28, 2006, Book of Abstracts, p. 30 (2006)

Superdeformation and High-Spin Spectroscopy Studies on ^{174}Hf
M. K. Djongolov, D. J. Hartley, L. L. Riedinger, G. B. Hagemann, R. V. F. Janssens, F. G. Kondev, E. F. Moore, M. A. Riley, A. Aguillar, C. R. Bingham, D. B. Campbell, M. P. Carpenter, P. Chowdhury, M. Cromaz, D. M. Cullen, M. Danchev, G. D. Dracoulis, P. Fallon, J. Goon, R. A. Kaye, T. L. Khoo, R. W. Laird, T. Lauritsen, A. O. Macchiavelli, B. McClain, G. Mukherjee, E. Ngijoi-Yogo, H. I. Park, G. Sletten, S. K. Tandel, P. M. Walker, and Jing-ye Zhang
Proceedings of the Conference on Nuclei at the Limits (NS06), Oak Ridge, TN, July 24-28, 2006, Book of Abstracts, p. 37 (2006)

Multi-Quasiparticle Isomers and K-Conservation Paths in Stable and Neutron-Rich Yb and Lu Isotopes
G. D. Dracoulis, G. J. Lane, F. G. Kondev, A. P. Byrne, T. Kibedi, R. O. Hughes, H. Watanabe, P. Nieminen, M. P. Carpenter, R. V. F. Janssens, T. Lauritsen, C. J. Lister, D. Seweryniak, S. Zhu, and P. Chowdhury
Proceedings of the Conference on Nuclei at the Limits (NS06), Oak Ridge, TN, July 24-28, 2006, Book of Abstracts, p. 39 (2006)

New T = 1 and T = 0 States in N = Z ^{74}Rb and the np Pairing Gap
S. M. Fischer, C. J. Lister, P. Chowdhury, N. J. Hammond, R. V. F. Janssens, T. L. Khoo, F. G. Kondev, T. Lauritsen, E. F. Moore, D. Seweryniak, S. Sinha, D. P. Balamuth, P. A. Hausladen, D. G. Sarantites, W. Reviol, S. D. Paul, and C. Baktash
Proceedings of the Conference on Nuclei at the Limits (NS06), Oak Ridge, TN, July 24-28, 2006, Book of Abstracts, p. 45 (2006)

Proton Cross-Shell Excitations: The Study of ^{52}Ca
A. Gade, R. V. F. Janssens, D. Bazin, R. Broda, B. A. Brown, C. M. Campbell, M. P. Carpenter, J. M. Cook, A. N. Deacon, D.-C. Dinca, B. Fornal, S. J. Freeman, T. Glasmacher, P. G. Hansen, B. P. Kay, P. F. Mantica, J. R. Terry, S. J. Freeman, T. Glasmacher, P. G. Hansen, B. P. Kay, P. F. Mantica, J. R. Terry, J. A. Tostevin, and S. Zhu
Proceedings of the Conference on Nuclei at the Limits (NS06), Oak Ridge, TN, July 24-28, 2006, Book of Abstracts, p. 52 (2006)

Internal Conversion Coefficient Measurements of Transitions in ^{167}Lu
G. Gürdal, C. W. Beausang, D. S. Brenner, H. Ai, M. Carpenter, R. F. Casten, B. Crider, D. J. Hartley, A. A. Hecht, R. V. F. Janssens, A. Heinz, T. Lauritsen, C. J. Lister, R. Raabe, J. X. Saladin, D. Seweryniak, E. Williams, and S. Zhu
Proceedings of the Conference on Nuclei at the Limits (NS06), Oak Ridge, TN, July 24-28, 2006, Book of Abstracts, p. 63 (2006)

Decay of the *r*-Process Waiting Point Nucleus ^{138}Sn and Adjacent Nuclei
A. A. Hecht, J. Shergur, A. Wöhr, W. B. Walters, K.-L. Kratz, N. Hoteling, B. A. Brown, B. Pfeiffer, O. Arndt, J. Cederkall, S. Hennrich, O. Keller, L. M. Fraile, P. Hoff, A. Joinet, U. Köster, and M. A. Stoyer
Proceedings of the Conference on Nuclei at the Limits (NS06), Oak Ridge, TN, July 24-28, 2006, Book of Abstracts, p. 68 (2006)

On the Role of the $g_{9/2}$ Neutron Orbital in the Structure of Fe Isotopes Toward N = 40
N. Hoteling, W. B. Walters, A. A. Hecht, M. Carpenter, R. Janssens, T. Lauritsen, D. Seweryniak, X. Wang, S. Zhu, R. Broda, B. Fornal, W. Krolas, and J. Wrzesinski
Proceedings of the Conference on Nuclei at the Limits (NS06), Oak Ridge, TN, July 24-28, 2006, Book of Abstracts, p. 73 (2006)

Superdeformation in Nuclei: Order Embedded in Chaos
T. L. Khoo
Proceedings of the Conference on Nuclei at the Limits (NS06), Oak Ridge, TN, July 24-28, 2006, Book of Abstracts, p. 81 (2006)

Identification of the $(\pi h_{11/2})^{-}2 \otimes (\nu i_{13/2})^{-}2$, $I^{\pi} = 22^{+}$ Isomer in ^{204}Hg
G. J. Lane, K. H. Maier, B. Fornal, M. Rejmund, R. Broda, A. P. Byrne, M. P. Carpenter, G. D. Dracoulis, R. V. F. Janssens, and J. Wrzesiński
Proceedings of the Conference on Nuclei at the Limits (NS06), Oak Ridge, TN, July 24-28, 2006, Book of Abstracts, p. 86 (2006)

High-K Multi-Quasiparticle States and Anomalous γ-Ray Decays in ^{184}W
G. J. Lane, J. T. Werner, G. D. Dracoulis, F. G. Kondev, A. P. Byrne, R. O. Hughes, H. Watanabe, P. Nieminen, M. P. Carpenter, R. V. F. Janssens, T. Lauritsen, D. Seweryniak, S. Zhu, and P. Chowdhury
Proceedings of the Conference on Nuclei at the Limits (NS06), Oak Ridge, TN, July 24-28, 2006, Book of Abstracts, p. 87 (2006)

Rotational Damping, Ridges and the Quasicontinuum of γ Rays in ^{152}Dy
T. Lauritsen, R. V. F. Janssens, T. L. Khoo, I. Ahmad, M. P. Carpenter, P. Chowdhury, T. Dossing, P. Fallon, A. M. Heinz, B. Herskind, D. G. Jenkins, F. G. Kondev, A. Korichi, A. J. Larabee, C. J. Lister, A. Lopez-Martens, A. O. Macchiavelli, E. F. Moore, D. Seweryniak, D. Ward, and S. Zhu
Proceedings of the Conference on Nuclei at the Limits (NS06), Oak Ridge, TN, July 24-28, 2006, Book of Abstracts, p. 89 (2006)

Strongly Deformed Bands in ^{163}Tm: Particle Excitation *vs*. Wobbling?
N. S. Pattabiraman, Y. Gu, S. Frauendorf, U. Garg, T. Li, B. K. Nayak, X. Wang, S. Zhu, S. S. Ghugre, R. V. F. Janssens, R. S. Chakrawarthy, M. Whithead, A. O. Macchiavelli, and D. Ward
Proceedings of the Conference on Nuclei at the Limits (NS06), Oak Ridge, TN, July 24-28, 2006, Book of Abstracts, p. 124 (2006)

New Superdeformed Bands in ^{131,132}Ce
E. S. Paul, A. O. Evans, B. M. McGuirk, A. J. Boston, L. Nelson, P. J. Nolan, K. Lagergren, W. T. Cluff, A. Pipidis, M. A. Riley, D. T. Joss, J. Simpson, F. Johnson-Theasby, R. Wadsworth, G. Rainovski, K. Starosta, M. P. Carpenter, A. A. Hecht, R. V. F. Janssens, F. G. Kondev, T. Lauritsen, E. F. Moore, S. Zhu, and I. Ragnarsson
Proceedings of the Conference on Nuclei at the Limits (NS06), Oak Ridge, TN, July 24-28, 2006, Book of Abstracts, p. 126 (2006)

Alpha Decay of ^{257}Rf
J. Qian, A. Heinz, R. Winkler, J. Vinson, A. B. Gamsworthy, R. V. F. Janssens, D. Peterson, D. Seweryniak, M. Asai, B. Back, M. P. Carpenter, G. Savard, A. A. Hecht, C.-L. Jiang, T. L. Khoo, F. G. Kondev, T. Lauritsen, C. J. Lister, A. Robinson, X. Wang, and S. Zhu
Proceedings of the Conference on Nuclei at the Limits (NS06), Oak Ridge, TN, July 24-28, 2006, Book of Abstracts, p. 131 (2006)

Test of Nuclear Chirality in ^{104}Rh by Study of the Electromagnetic Transitions Properties
G. Rainovski, T. Ahn, M. P. Carpenter, A. Costin, M. Danchev, A. Dewald, R. V. F. Janssens, T. Koike, C. J. Lister, O. Möller, N. Pietralla, C. Vaman, R. Wadsworth, and S. Zhu
Proceedings of the Conference on Nuclei at the Limits (NS06), Oak Ridge, TN, July 24-28, 2006, Book of Abstracts, p. 134 (2006)

The "Octupole Transitional" Nuclei ^{219,220}Th
W. Reviol, C. J. Chiara, D. G. Sarantites, O. L. Pechenaya, M. P. Carpenter, R. V. F. Janssens, T. L. Khoo, C. J. Lister, D. Seweryniak, S. Zhu, and S. G. Frauendorf
Proceedings of the Conference on Nuclei at the Limits (NS06), Oak Ridge, TN, July 24-28, 2006, Book of Abstracts, p. 136 (2006)

Ground State Proton Radioactivity from ^{121}Pr
A. P. Robinson, P. J. Woods, C. N. Davids, D. Seweryniak, M. P. Carpenter, A. Hecht, R. V. F. Janssens, D. Peterson, S. Sinha, W. B. Walters, and S. Zhu
Proceedings of the Conference on Nuclei at the Limits (NS06), Oak Ridge, TN, July 24-28, 2006, Book of Abstracts, p. 138 (2006)

Multi-Quasiparticle States in ^{254}No: K-Conservation, Single Particle Energies and Pairing Strengths
S. K. Tandel, T. L. Khoo, D. Seweryniak, G. Mukherjee, I. Ahmad, B. Back, R. Blinstrup, P. A. Butler, M. P. Carpenter, J. Chapman, P. Chowdhury, C. N. Davids, P. T. Greenlees, A. A. Hecht, A. Heinz, R.-D. Herzberg, P. Ikin, R. V. F. Janssens, G. D. Jones, F. G. Kondev, T. Lauritsen, C. J. Lister, E. F. Moore, D. Peterson, P. Reiter, U. S. Tandel, X. Wang, and S. Zhu
Proceedings of the Conference on Nuclei at the Limits (NS06), Oak Ridge, TN, July 24-28, 2006, Book of Abstracts, p. 167 (2006)

Delayed Alignments and Search for Oblate Rotation in Neutron-Rich Hf Nuclei
U. S. Tandel, P. Chowdhury, S. K. Tandel, D. Cline, C. Y. Wu, M. P. Carpenter, R. V. F. Janssens, T. L. Khoo, T. Lauritsen, C. J. Lister, D. Seweryniak, and S. Zhu
Proceedings of the Conference on Nuclei at the Limits (NS06), Oak Ridge, TN, July 24-28, 2006, Book of Abstracts, p. 168 (2006)

Configurations and Decay Hindrances of High-K States in ^{180}Hf
S. K. Tandel, P. Chowdhury, M. P. Carpenter, A. Deacon, S. J. Freeman, N. J. Hammond, R. V. F. Janssens, G. D. Jones, T. L. Khoo, F. G. Kondev, T. Lauritsen, C. J. Lister, E. F. Moore, D. Seweryniak, J. F. Smith, and S. Zhu
Proceedings of the Conference on Nuclei at the Limits (NS06), Oak Ridge, TN, July 24-28, 2006, Book of Abstracts, p. 169 (2006)

Multi-Quasiparticle States in ^{254}No: K-Conservation, Single Particle Energies and Pairing Strengths
S. K. Tandel, T. L. Khoo, D. Seweryniak, G. Mukherjee, I. Ahmad, B. Back, R. Blinstrup, P. A. Butler, M. P. Carpenter, J. Chapman, P. Chowdhury, C. N. Davids, P. T. Greenlees, A. A. Hecht, A. Heinz, R.-D. Herzberg, P. Ikin, R. V. F. Janssens, G. D. Jones, F. G. Kondev, T. Lauritsen, C. J. Lister, E. F. Moore, D. Peterson, P. Reiter, U. S. Tandel, X. Wang, and S. Zhu
Proceedings of the Conference on Nuclei at the Limits (NS06), Oak Ridge, TN, July 24-28, 2006, Book of Abstracts, p. 170 (2006)

New Spectroscopic Studies of the N = Z Nuclei ^{74}Rb, ^{76}Sr and ^{78}Y
R. Wadsworth, B. S. Nara Singh, A. N. Steer, D. G. Jenkins, P. Davies, R. Glover, N. S. Pattabiraman, T. Grahn, P. T. Greenlees, P. Jones, R. Julin, M. Leino, M. Nyman, J. Pakarinen, P. Rahkila, C. Scholey, J. Sorri, J. Uusitalo, P. A. Butler, M. Dimmock, R.-D. Herzberg, D. T. Joss, R. D. Page, J. Thomson, R. Lemmon, J. Simpson, B. Blank, B. Cederwall, B. Hadinia, M. Sandzelius, A. V. Afanasjev, C. Andreoiu, P. E. Garrett, C. E. Svensson, R. A. E. Austin, M. P. Carpenter, F. Moore, D. Seweryniak, A. O. Macchiavelli, D. Ward, W. Reviol, D. Sarantites, and A. Gorgen
Proceedings of the Conference on Nuclei at the Limits (NS06), Oak Ridge, TN, July 24-28, 2006, Book of Abstracts, p. 182 (2006)

Strength of Octupole Correlations in the Actinides
X. Wang, S. Zhu, R. V. F. Janssens, I. Wiedenhöver, M. P. Carpenter, I. Ahmad, S. J. Freeman, J. P. Greene, T. L. Khoo, F. G. Kondev, T. Lauritsen, C. J. Lister, D. Seweryniak, U. Garg, A. Bernstein, P. Wilson, E. Diffenderfer, C. Teal, A. Larabee, and B. Meredith
Proceedings of the Conference on Nuclei at the Limits (NS06), Oak Ridge, TN, July 24-28, 2006, Book of Abstracts, p. 183 (2006)

Study of Neutron-Rich sd-pf Shell Nuclei Using Multi-Nucleon Transfer Reactions
M. Wiedeking, E. Rodriguez-Vieitez, P. Fallon, R. M. Clark, M. Cromaz, M. Descovich, I-Y. Lee, M.-A. Deleplanque, A. O. Macchiavelli, F. S. Stephens, D. Ward, M. P. Carpenter, R. V. F. Janssens, X. Wang, S. Zhu, D. Cline, R. Teng, and C. Y. Wu
Proceedings of the Conference on Nuclei at the Limits (NS06), Oak Ridge, TN, July 24-28, 2006, Book of Abstracts, p. 186 (2006)

Triaxial Strongly Deformed Bands in ^{171,172}Hf?
Y. C. Zhang, W. C. Ma, M. P. Carpenter, P. Chowdhury, D. Cullen, M. K. Djongolov, G. B. Hagemann, D. J. Hartley, R. V. F. Janssens, T. L. Khoo, F. G. Kondev, T. Lauritsen, E. F. Moore, E. Ngijoi-Yogo, S. Odegard, S. V. Rigby, D. G. Roux, D. T. Scholes, J. A. Winger, R. B. Yadav, and S. Zhu
Proceedings of the Conference on Nuclei at the Limits (NS06), Oak Ridge, TN, July 24-28, 2006, Book of Abstracts, p. 195 (2006)

Deep Inelastic Reactions with CHICO: The Case of ^{48}Ca + ^{208}Pb
S. Zhu, R. V. F. Janssens, M. P. Carpenter, J. A. Becker, D. Cline, A. B. Hayes, A. Hecht, A. Gade, T. Lauritsen, C. J. Lister, R. Macri, D. Seweryniak, X. Wang, and C. Y Wu
Proceedings of the Conference on Nuclei at the Limits (NS06), Oak Ridge, TN, July 24-28, 2006, Book of Abstracts, p. 197 (2006)

Structure of the Even-Even Neutron-Rich ^{56,58,60}Cr Isotopes
S. Zhu, A. N. Deacon, R. V. F. Janssens, S. J. Freeman, R. Broda, M. P. Carpenter, I. R. Calderin, B. Fornal, T. Lauritsen, C. J. Lister, D. Seweryniak, J. F. Smith, S. L. Tabor, and B. J. Varley
Proceedings of the Conference on Nuclei at the Limits (NS06), Oak Ridge, TN, July 24-28, 2006, Book of Abstracts, p. 198 (2006)

Reaction Studies with Light, Unstable Nuclei
K. Ernst Rehm
2006 Annual Meeting of the Division of Nuclear Physics of the American Physical Society, Nashville, TN, October 25-28, 2006; Bull. Am. Phys. Soc. **51**, 10 (2006)

High Spin Structure in Neutron Rich Zn Isotopes
A. A. Hecht, N. Hoteling, W. B. Walters, M. P. Carpenter, R. V. F. Janssens, T. Lauritsen, D. Seweryniak, X. Wang, S. Zhu, B. Fornal, R. Broda, W. Krolas, J. Wrzesinski, A. Woehr, N. J. Stone, and J. Stone
2006 Annual Meeting of the Division of Nuclear Physics of the American Physical Society, Nashville, TN, October 25-28, 2006; Bull. Am. Phys. Soc. **51**, 36 (2006)

Update on the Structure of N-Rich $^{52-56}$Ti
S. Zhu, R. V. F. Janssens, M. P. Carpenter, S. Freeman, B. Fornal, A. Deacon, B. Kay, J. Kozemczak, A. Larabee, T. Lauritsen, A. Robinson, D. Seweryniak, J. Smith, D. Steppenbeck, and X. Wang
2006 Annual Meeting of the Division of Nuclear Physics of the American Physical Society, Nashville, TN, October 25-28, 2006; Bull. Am. Phys. Soc. **51**, 36 (2006)

A New Measurement of the E1 Component of the ^{12}C $(\alpha,\gamma)^{16}$O Reaction
X. D. Tang, M. Notani, K. E. Rehm, I. Ahmad, J. Greene, A. A. Hecht, D. Henderson, R. V. F. Janssens, C. L. Jiang, E. F. Moore, N. Patel, R. C. Pardo, G. Savard, J. P. Schiffer, S. Sinha, M. Paul, L. Jisonna, R. E. Segel, C. Brune, A. Champagne, and A. Wuosmaa
2006 Annual Meeting of the Division of Nuclear Physics of the American Physical Society, Nashville, TN, October 25-28, 2006; Bull. Am. Phys. Soc. **51**, 39 (2006)

Alpha-Gamma Coincidence Spectroscopy Using a Si PSAPD and Ge DSSD Combination
C. M. Wilson, P. Chowdhury, R. Gramer, S. K. Tandel, N. J. Hammond, C. J. Lister, S. M. Fischer, E. F. Moore, K. M. Teh, L. McClish, K. S. Shah, and R. Farrell
2006 Annual Meeting of the Division of Nuclear Physics of the American Physical Society, Nashville, TN, October 25-28, 2006; Bull. Am. Phys. Soc. **51**, 84 (2006)

Internal Conversion Coefficient Measurements of Transitions in ^{167}Lu
G. Gürdal, C. W. Beausang, D. S. Brenner, H. Ai, R. F. Casten, A. Heinz, E. Williams, B. Crider, R. Raabe, D. J. Hartley, M. Carpenter, R. V. F. Janssens, T. Lauritsen, C. J. Lister, D. Seweryniak, S. Zhu, A. A. Hecht, and J. X. Saladin
2006 Annual Meeting of the Division of Nuclear Physics of the American Physical Society, Nashville, TN, October 25-28, 2006; Bull. Am. Phys. Soc. **51**, 89 (2006)

Quadrupole Moments of Normal Deformed and Triaxial Strongly Deformed Bands in ^{167}Lu
E. Ngijoi-Yogo, W. C. Ma, D. G. Roux, R. B. Yadav, Y. Zhang, G. B. Hagemann, C. R. Hansen, B. Herskind, G. Sletten, H. Amro, D. A. Meyer, G. Gürdal, C. W. Beausang, D. J. Hartley, C. Engelhardt, H. Hübel, A. Neusser, P. Bringel, M. P. Carpenter, T. L Khoo, T. Lauritsen, and E. F. Moore
2006 Annual Meeting of the Division of Nuclear Physics of the American Physical Society, Nashville, TN, October 25-28, 2006; Bull. Am. Phys. Soc. **51**, 89 (2006)

Four-, Six- and Eight-Quasiparticle Isomers in ^{174}Lu
F. G. Kondev, I. Ahmad, M. P. Carpenter, R. V. F. Janssens, T. Lauritsen, C. J. Lister, D. Seweryniak, G. D. Dracoulis, G. J. Lane, A. P. Byrne, T. Kibedi, P. Chowdhury, and S. K. Tandel
2006 Annual Meeting of the Division of Nuclear Physics of the American Physical Society, Nashville, TN, October 25-28, 2006; Bull. Am. Phys. Soc. **51**, 90 (2006)

Nucleon Alignment and Shape Competition at High Spin in ^{180}Hf
U. S. Tandel, P. Chowdhury, S. K. Tandel, S. Sheppard, D. Cline, C. Y. Wu, M. P. Carpenter, R. V. F. Janssens, T. L. Khoo, T. Lauritsen, C. J. Lister, D. Seweryniak, and S. Zhu
2006 Annual Meeting of the Division of Nuclear Physics of the American Physical Society, Nashville, TN, October 25-28, 2006; Bull. Am. Phys. Soc. **51**, 90 (2006)

Search for Highly Deformed Rotational Structures in Tungsten Isotopes
S. K. Tandel, A. J. Knox, U. S. Tandel, C. Parnell-Lampen, P. Chowdhury, D. J. Hartley, J.-Y. Zhang, M. P. Carpenter, R. V. F. Janssens, T. L. Khoo, T. Lauritsen, C. J. Lister, D. Seweryniak, X. Wang, and S. Zhu
2006 Annual Meeting of the Division of Nuclear Physics of the American Physical Society, Nashville, TN, October 25-28, 2006; Bull. Am. Phys. Soc. **51**, 90 (2006)

Alpha Decay of ^{257}Rf
J. Qian, A. Heinz, R. Winkler, J. Vinson, A. B. Gamsworthy, R. V. F. Janssens, D. Peterson, D. Seweryniak, B. Back, M. P. Carpenter, G. Savard, A. A. Hecht, C. L. Jiang, T. L. Khoo, F. G. Kondev, T. Lauritsen, C. J. Lister, A. Robinson, X. Wang, and S. Zhu
2006 Annual Meeting of the Division of Nuclear Physics of the American Physical Society, Nashville, TN, October 25-28, 2006; Bull. Am. Phys. Soc. **51**, 91 (2006)

Octupole Strength in the ^{238,240,242}Pu
X. Wang, S. Zhu, R. V. F. Janssens, M. P. Carpenter, I. Ahmad, J. P. Greene, T. L. Khoo, F. G. Kondev, T. Lauritsen, C. J. Lister, D. Seweryniak, S. J. Freeman, U. Garg, I. Wiedenhöver, A. Bernstein, P. Wilson, E. Diffenderfer, C. Teal, A. Larabee, and B. Meredith
2006 Annual Meeting of the Division of Nuclear Physics of the American Physical Society, Nashville, TN, October 25-28, 2006; Bull. Am. Phys. Soc. **51**, 91 (2006)

On Line Yield Measurements of UC Targets

H. K. Carter, E. H. Spejewski, A. Kronenberg, D. W. Stracener, W. Talbert, H.-H. Hsu, J. Nolen, J. Greene, and T. Burtseva

2006 Annual Meeting of the Division of Nuclear Physics of the American Physical Society, Nashville, TN, October 25-28, 2006; Bull. Am. Phys. Soc. **51**, 103 (2006)

Two-Quasiparticle States in ^{252,254}No and the Stability of Superheavy Nuclei

T. L. Khoo, S. K. Tandel, A. Robinson, D. Seweryniak, and F. G. Kondev

2006 Annual Meeting of the Division of Nuclear Physics of the American Physical Society, Nashville, TN, October 25-28, 2006; Bull. Am. Phys. Soc. **51**, 112 (2006)

OPERATION AND DEVELOPMENT OF ATLAS
and
ACCELERATOR PHYSICS AND EXOTIC BEAM TECHNOLOGY

Atomic Layer Deposition of W on Nanoporous Carbon Aerogels
J. W. Elam, J. A. Libera, M. J. Pellin, A. V. Zinovev, J. P. Greene, and J. A. Nolen
Appl. Phys. Lett. **89**, 053124/1-3 (2006)

Global Theory of Extended Generating Functions
Bela Erdelyi
Int. J. Pure and Appl. Math. **33**, 553-578 (2006)

Application of a New Procedure for Design of 325 MHz RFQ
P. N. Ostroumov, V. N. Aseev, and A. A. Kolomiets
Jrnl. of Instr. **1**, P04002 (2006)

Physics Design of the 8-GeV H-Minus Linac
P. N. Ostroumov
New Jrnl. of Phys. **8**, 281 (2006)

Computational Needs for the RIA Accelerator Systems
P. N. Ostroumov, J. A. Nolen, and B. Mustapha
Proceedings of the 8th International Computational Accelerator Physics Conference (ICAP-04), St. Petersburg, Russia, June 29-July 2, 2004; Nucl. Instrum. Methods **A558**, 25-31 (2006)

ECRIS Operation with Multiple Frequencies
R. C. Vondrasek, R. Scott, and R. C. Pardo
Proceedings of the 11th International Conference on Ion Sources (ICIS05), Caen, France, September 12-16, 2005; Rev. Sci. Instrum. **77**, 03A337/1-4 (2006)

Monte Carlo Beam Capture and Charge Breeding Simulation
J. S. Kim, C. Liu, D. H. Edgell, and R. Pardo
Proceedings of the 11th International Conference on Ion Sources (ICIS05), Caen, France, September 12-16, 2005; Rev. Sci. Instrum. **77**, 03B106/1-5 (2006)

The Rare Isotope Accelerator
D. F. Geesaman
Proceedings of the 34th ICFA Advanced Beam Dynamics Workshop on "High Power Superconducting Ion, Proton, and Multi-Species Linacs" (HPSL2005), Naperville, IL, May 22-24, 2005, p. OP5 (2006)

Error Simulations and Beam Loss Studies in the RIA Driver Linac
B. Mustapha, P. N. Ostroumov, and V. N. Aseev
Proceedings of the 34th ICFA Advanced Beam Dynamics Workshop on "High Power Superconducting Ion, Proton, and Multi-Species Linacs" (HPSL2005), Naperville, IL, May 22-24, 2005, pp. TP2/1-4 (2006)

Failure Mode and Recovery in the RIA Driver Linac
B. Mustapha and P. N. Ostroumov
Proceedings of the 34th ICFA Advanced Beam Dynamics Workshop on "High Power Superconducting Ion, Proton, and Multi-Species Linacs" (HPSL2005), Naperville, IL, May 22-24, 2005, pp.TWA4/1-5 (2006)

Availability Optimization of a High Power Driver
E. S. Lessner and P. N. Ostroumov
Proceedings of the 34th ICFA Advanced Beam Dynamics Workshop on "High Power Superconducting Ion, Proton, and Multi-Species Linacs" (HPSL2005), Naperville, IL, May 22-24, 2005, pp. TWA5/1-4 (2006)

Applications of Differential Algebraic Methods in Beam Physics
B. Erdelyi
Proceedings of the 34th ICFA Advanced Beam Dynamics Workshop on "High Power Superconducting Ion, Proton, and Multi-Species Linacs" (HPSL2005), Naperville, IL, May 22-24, 2005, pp. TWA6/1-4 (2006)

TRACK: The New Beam Dynamics Code
V. N. Assev, P. N. Ostroumov, E. S. Lessner, and B. Mustapha
Proceedings of the 34th ICFA Advanced Beam Dynamics Workshop on "High Power Superconducting Ion, Proton, and Multi-Species Linacs" (HPSL2005), Naperville, IL, May 22-24, 2005, pp. TWA8/1-4 (2006)

Remote Control of the ATLAS Superconducting Accelerator
F. H. Munson, R. C. Pardo, M. A. Power, R. C. Raffenetti, and R. J. Carrier
Proceedings of the 10th International Conference on Accelerator and Large Experimental Physics Control Systems (ICALEPCS2005), Geneva, Switzerland, October 10-14, 2005, pp. PO1.075-7/1-5 (2006)

Design of the Driver Linac for the Rare Isotope Accelerator
P. N. Ostroumov, J. A. Nolen, and K. W. Shepard
Proceedings of the 39th ICFA Advanced Beam Dynamics Workshop on "High Intensity High Brightness Hadron Beams" (HB2006), Tsukuba, Japan, May 29-June 2, 2006, pp. 89-93 (2006)

Design and Development of an 8-GeV Superconducting H-Linac
P. N. Ostroumov, G. Apollinari, G. W. Foster, and R. Webber
Proceedings of the 39th ICFA Advanced Beam Dynamics Workshop on "High Intensity High Brightness Hadron Beams" (HB2006) Tsukuba, Japan, May 29-June 2, 2006, pp. 134-136 (2006)

Superconducting Spoke Cavities
Mike Kelly
Proceedings of the 39th ICFA Advanced Beam Dynamics Workshop on "High Intensity High Brightness Hadron Beams" (HB2006), Tsukuba, Japan, May 29-June 2, 2006, pp. 337-340 (2006)

Lattice Design in a Multi-GeV H-Minus Linac
P. N. Ostroumov and G. W. Foster
34th ICFA Advanced Beam Dynamics Workshop on "High Power Superconducting Ions, Proton, and Multi-Species Linacs" (HPSL2005), Naperville, IL, May 22-24, 2005, Abstract MWA2 (2006)

Design of the Driver Linac for the Rare Isotope Accelerator
P. N. Ostroumov, J. A. Nolen, and K. W. Shepard
39th ICFA Advanced Beam Dynamics Workshop on "High Intensity High Brightness Hadron Beams" (HB2006), Tsukuba, Japan, May 29-June 2, 2006, Abstract TUAY03 (2006)

Physics Design of a Multi-GeV Superconducting H-Minus Linac
P. N. Ostroumov, G. Apollinari, G. W. Foster, and R. Webber
39th ICFA Advanced Beam Dynamics Workshop on "High Intensity High Brightness Hadron Beams" (HB2006), Tsukuba, Japan, May 29-June 2, 2006, Abstract TUBY02 (2006)

Shielding Design for the CARIBU Project
Eugene Moore, Samuel Baker, Richard Pardo, Guy Savard, and the CARIBU Collaboration
2006 Annual Meeting of the Division of Nuclear Physics of the American Physical Society, Nashville, TN, October 25-28, 2006; Bull. Am. Phys. Soc. **51**, 85 (2006)

MEDIUM-ENERGY NUCLEAR PHYSICS RESEARCH

Double-Hadron Leptoproduction in the Nuclear Medium
A. Airapetian *et al*. (HERMES Collaboration)
Phys. Rev. Lett. **96**, 162301/1-5 (2006)

Search for the Θ^+ Pentaquark in the $\gamma d \to \Lambda n K^+$ Reaction Measured with CLAS
S. Niccolai *et al*. (CLAS Collaboration)
Phys. Rev. Lett. **97**, 032001/1-6 (2006)

Measurement of Deeply Virtual Compton Scattering with a Polarized Proton Target
S. Chen *et al*. (CLAS Collaboration)
Phys. Rev. Lett. **97**, 072002/1-6 (2006)

Search for Θ^{++} Pentaquarks in the Exclusive Reaction $\gamma p \to K^+K^- p$
V. Kubarovsky *et al*. (CLAS Collaboration)
Phys. Rev. Lett. **97**, 102001/1-5 (2006)

Determination of the Pion Charge Form Factor at $Q^2 = 1.60$ and 2.45 $(\mathrm{GeV/c})^2$
T. Horn *et al*. (Jefferson Lab F_π Collaboration)
Phys. Rev. Lett. **97**, 192001/1-4 (2006)

Measurement of the x- and Q^2-Dependence of the Asymmetry A_1 on the Nucleon
K. V. Dharmawardane *et al*. (CLAS Collaboration)
Phys. Lett. **B641**, 11-17 (2006)

Measurement of the Lifetimes of the Lowest $^3P_1$ State of Neutral Ba and Ra
N. D. Scielzo, J. R. Guest, E. C. Schulte, I. Ahmad, K. Bailey, D. L. Bowers, R. J. Holt, Z.-T. Lu, T. P. O'Connor, and D. H. Potterveld
Phys. Rev. A **73**, 010501(R)/1-4 (2006)

Experimental Constraints on Nonlinearities Induced by Two-Photon Effects in Elastic and Inelastic Rosenbluth Separations
V. Tvaskis, J. Arrington, M. E. Christy, R. Ent, C. E. Keppel, Y. Liang, and G. Vittorini
Phys. Rev. C **73**, 025206/1-6 (2006)

Low-Q Scaling, Duality, and the EMC Effect
J. Arrington, R. Ent, C. E. Keppel, J. Mammei, and I. Niculescu
Phys. Rev. C **73**, 035205/1-6 (2006)

Moments of Nuclear and Nucleon Structure Functions at Low Q^2 and the Momentum Sum Rule
I. Niculescu, J. Arrington, R. Ent, and C. E. Keppel
Phys. Rev. C **73**, 045206/1-5 (2006)

Search for the Θ^+ Pentaquark in the Reactions $\gamma p \to \bar{K}^0 K^+ n$ and $\gamma p \to \bar{K}^0 K^0 p$
R. DeVita *et al*. (CLAS Collaboration)
Phys. Rev. D **74**, 032001/1-16 (2006)

Longitudinal Spin Transfer to the Λ Hyperon in Semi-Inclusive Deep-Inelastic Scattering
A. Airapetian *et al*.
Phys. Rev. D **74**, 072004/1-11 (2006)

Beam of Metastable Krypton Atoms Extracted from a Microwave-Driven Discharge
Y. Ding, K. Bailey, A. M. Davis, S.-M. Hu, Z.-T. Lu, and T. P. O'Connor
Rev. Sci. Instrum. **77**, 126105/1-2 (2006)

A New Parameterization of the Nucleon Elastic Form Factors
R. Bradford, A. Bodek, H. Budd, and J. Arrington
Proceedings of the 4th International Workshop on Neutrino-Nucleus Interactions in the Few-GeV Region, Okayama, Japan, September 26-29, 2005; Nucl. Phys. **B159**, 127-132 (2006)

Measurement of ΔS in the Nucleon at HERMES from Semi-Inclusive DIS
H. E. Jackson (on behalf of the HERMES Collaboration)
Proceedings of the 17th International Conference on Particles and Nuclei (PANIC'05), Santa Fe, NM, October 23-30, 2005, eds. Peter D. Barnes, Martin D. Cooper, Robert A. Eisenstein, Hubert van Hecke, and Gerard J. Stephenson, AIP Conference Proceedings **842**, 363-365 (2006)

Opportunities with Drell-Yan Scattering: Probing the Sea Quark Distributions of the Proton
P. E. Reimer (on behalf of the Fermilab E866 and E906 Collaborations)
Proceedings of the 17th International Conference on Particles and Nuclei (PANIC'05), Santa Fe, NM, October 23-30, 2005, eds. Peter D. Barnes, Martin D. Cooper, Robert A. Eisenstein, Hubert van Hecke, and Gerard J. Stephenson, AIP Conference Proceedings **842**, 369-371 (2006)

Progress Towards Laser Trapping of ^{225}Ra for an Electric Dipole Moment Measurement
N. D. Scielzo, I. Ahmad, K. Bailey, D. L. Bowers, J. R. Guest, R. J. Holt, Z.-T. Lu, T. P. O'Connor, D. H. Potterveld, and E. C. Schulte
Proceedings of the 17th International Conference on Particles and Nuclei (PANIC'05), Santa Fe, NM, October 23-30, 2005, eds. Peter D. Barnes, Martin D. Cooper, Robert A. Eisenstein, Hubert van Hecke, and Gerard J. Stephenson, AIP Conference Proceedings **842**, 787-789 (2006)

Laser-Trapping of Radium and the Path to a Next Generation Electric Dipole Moment Measurement
J. R. Guest, N. D. Scielzo, I. Ahmad, K. Bailey, J. P. Greene, R. J. Holt, Z.-T. Lu, T. P. O'Connor, D. H. Potterveld, and J. Wang
Proceedings of the 2006 International Conference on Trapped Charge Particles and Fundamental Physics, Tigh-Na-Mara, Parksville, BC, Canada, September 3-8, 2006, Book of Abstracts, p. 4 (2006)

Towards a Laser Spectroscopic Determination of the ^{8}He Nuclear Charge Radius
P. Mueller, K. Bailey, R. J. Holt, R. V. F. Janssens, Z.-T. Lu, T. P. O'Connor, J. P. Schiffer, I. Sulai, M.-G. Saint Laurent, J.-Ch. Thomas, A. C. C. Villari, O. Naviliat-Cuncic, X. Flechard, S.-M. Hu, G. W. F. Drake, and M. Paul
2006 Annual Meeting of the Division of Nuclear Physics of the American Physical Society, Nashville, TN, October 25-28, 2006; Bull. Am. Phys. Soc. **51**, 20 (2006)

Laser Trapping of Ra-225 and Ra-226 Progress Towards an Electric Dipole Moment Measurement
J. R. Guest, N. D. Scielzo, I. Ahmad, K. Bailey, J. P. Greene, R. J. Holt, Z.-T. Lu, T. P. O'Connor, and D. H. Potterveld
2006 Annual Meeting of the Division of Nuclear Physics of the American Physical Society, Nashville, TN, October 25-28, 2006; Bull. Am. Phys. Soc. **51**, 110 (2006)

THEORETICAL PHYSICS

Strange Star Surface: A Crust with Nuggets
Prashanth Jaikumar, Sanjay Reddy, and Andrew W. Steiner
Phys. Rev. Lett. **96**, 041101/1-4 (2006)

Hindrance of Heavy-Ion Fusion Due to Nuclear Incompressibility
S. Mişicu and H. Esbensen
Phys. Rev. Lett. **96**, 112701/1-4 (2006)

Pair Production and Optical Lasers
D. B. Blaschke, A. V. Prozorkevich, C. D. Roberts, S. M. Schmidt, and S. A. Smolyansky
Phys. Rev. Lett. **96**, 140401/1-4 (2006)

Reply to Comment by M. Gai
H. Esbensen, G. F. Bertsch, and K. A. Snover
Phys. Rev. Lett. **96**, 159202 (2006)

Calculation of Isotope Shifts and Relativistic Shifts in C I, C II, C III and C IV
J. C. Berengut, V. V. Flambaum, and M. G. Kozlov
Phys. Rev. A **73**, 012504/1-13 (2006)

Direct Urca Neutrino Rate in Color Superconducting Quark Matter
P. Jaikumar, C. D. Roberts, and A. Sedrakian
Phys. Rev. C **73**, 042801(R)/1-5 (2006)

From Finite Nuclei to the Nuclear Liquid Drop: Leptodermous Expansion Based on the Self-Consistent Mean-Field Theory
P.-G. Reinhard, M. Bender, W. Nazarewicz, and T. Vertse
Phys. Rev. C **73**, 014309/1-11 (2006)

Interplay of Compressional and Vortical Nuclear Currents in Overtones of the Isoscalar Giant Dipole Resonance
Şerban Mişicu
Phys. Rev. C **73**, 024301/1-12 (2006)

Pair Counting, Pion-Exchange Forces and the Structure of Light Nuclei
R. B. Wiringa
Phys. Rev. C **73**, 034317/1-11 (2006)

Global Study of Quadrupole Correlation Effects
M. Bender, G. F. Bertsch, and P.-H. Heenen
Phys. Rev. C **73**, 034322/1-26 (2006)

Dynamical Coupled-Channel Approach to Hadronic and Electromagnetic Kaon-Hyperon Production on the Proton
B. Juliá-Díaz, B. Saghai, T.-S. H. Lee, and F. Tabakin
Phys. Rev. C **73**, 055204/1-20 (2006)

Coulomb Problem for Vector Bosons
M. Yu. Kuchiev and V. V. Flambaum
Phys. Rev. D **73**, 093009/1-16 (2006)

Short-Lived Nuclei in the Early Solar System: Possible AGB Sources
G. J. Wasserburg, M. Busso, R. Gallino, and K. M. Nollett
Nucl. Phys. **A777**, 5-69 (2006)

Modern Theories of Low-Energy Astrophysical Reactions
L. E. Marcucci, Kenneth M. Nollett, R. Schiavilla, and R. B. Wiringa
Nucl. Phys. **A777**, 111-136 (2006)

Early Infrared Spectral Development of V1187 Scorpii (Nova Scorpii 2004 No. 2)
D. K. Lynch *et al*.
Astrophys. J. **638**, 987-1003 (2006)

From First Stars to the Spite Plateau: A Possible Reconciliation of Halo Stars Observations with Predictions from Big Bang Nucleosynthesis
L. Piau, T. C. Beers, D. S. Balsara, T. Sivarani, J. W. Truran, and J. W. Ferguson
Astrophys. J. **653**, 300-315 (2006)

Possible Evidence for "Dark Radiation" from Big Bang Nucleosynthesis Data
V. V. Flambaum and E. V. Shuryak
Europhys. Lett. **74**, 813-816 (2006)

Sigma Terms of Light-Quark Hadrons
V. V. Flambaum, A. Höll, P. Jaikumar, C. D. Roberts, and S. V. Wright
Few-Body Systems **38**, 31-51 (2006)

Spin-Zero Particles Must Be Bosons: A New Proof within Nonrelativistic Quantum Mechanics
M. Peshkin
Foundations of Physics **36**, 19-29 (2006)

Complex Rational Numbers in Quantum Mechanics
P. Benioff
Int. J. Mod. Phys. B **20**, 1730-1741 (2006)

Mean Excitation Energies for Stopping Power of Atoms and Molecules Evaluated from Oscillator-Strength Spectra
Sachie Kamakura, Naoki Sakamoto, Hidemi Ogawa, Hidetsugu Tsuchida, and Mitio Inokuti
J. Applied Phys. **100**, 064905/1-12 (2006)

Narrow Atomic Transitions with Enhanced Sensitivity to Variation of the Fine Structure Constant
E. J. Angstmann, V. A. Dzuba, V. V. Flambaum, A. Yu. Nevsky, and S. G. Karshenboim
J. Phys. B **39**, 1937-1944 (2006)

Coulomb Problem for Vector Bosons in Standard Model
Michael Kuchiev and Victor Flambaum
Modern Phys. Lett. A **21**, 781-788 (2006)

Probing Variations in Fundamental Constants with Radio and Optical Observations of Quasar Absorption Lines
P. Tzanavaris, J. K. Webb, M. T. Murphy, V. V. Flambaum, and S. J. Curran
Mon. Not. R. Astron. Soc. **374**, 634-646 (2007)

Pentaquark Θ^+ (1540) Production in $\gamma N \to K \overline{K} N$ Reactions
Yongseok Oh, K. Nakayama, and T.-S. H. Lee
Physics Reports **423**, 49-89 (2006)

Bethe's Contributions to Atomic and Molecular Physics
M. Inokuti and B. Bederson
Phys. Scr. **73**, C98-C106 (2006)

Mean Excitation Energy for the Stopping Power of Light Elements
D. Y. Smith, M. Inokuti, W. Karstens, and E. Shiles
Proceedings of the 13th International Conference on Radiation Effects in Insulators (REI-2005), Santa Fe, NM, August 28-September 2, 2005; Nucl. Instrum. Methods **B250**, 1-5 (2006)

Dynamical Model of Electroweak Pion Production in the Resonance Region
T. Sato, B. Szczerbinska, K. Kubodera, and T.-S. H. Lee
Proceedings of the 4th International Workshop on Neutrino-Nucleus Interactions in the Few-GeV Region, Okayama, Japan, September 26-29, 2005; Nucl. Phys. **B159**, 141-146 (2006)

Schwinger Functions and Light-Quark Bound States, and Sigma Terms
A. Höll, P. Maris, C. D. Roberts, and S. V. Wright
Proceedings of the Cairns Topical Workshop on Light-Cone QCD and Nonperturbative Hadron Physics (LC 2005), Cairns, Australia, July 7-15, 2005; Nucl. Phys. **B161**, 87-44 (2006)

Surface Structure of Quark Stars with Magnetic Fields
P. Jaikumar
Proceedings of the 9th Workshop on High Energy Physics Phenomenology (WHEPP-9), Bhubaneswar, India, January 3-14, 2006; Pramana - J. Phys. **67**, 937-949 (2006)

Radiative Capture Versus Coulomb Dissociation
H. Esbensen
Proceedings of the 12th International Conference on Capture Gamma-Ray Spectroscopy and Related Topics (CGS 12), Notre Dame, IN, September 4-9, 2005, eds. Andreas Woehr and Ani Aprahamian, AIP Conference Proceedings **819**, 518-522 (2006)

Sensitivity to Multiphonon Excitations and Incompressibility in Fusion Reactions
H. Esbensen and S. Mişicu
Proceedings of the International Conference on Reaction Mechanisms and Nuclear Structure at the Coulomb Barrier (Fusion06), San Servolo Island, Venice, Italy, March 19-23, 2006, AIP Conference Proceedings **853**, 13-20 (2006)

A Perspective on Hadron Physics
A. Höll, C. D. Roberts, and S. V. Wright
Proceedings of the Xth Mexican Workshop on Particles and Fields, Morelia, Michoácan, Mexico, November 7-12, 2005, eds. Adnan Bashir, Victor Villanueva, Luis Villaseñor, Miguel A. Pérez, and Luis Urrutia, AIP Conference Proceedings **857**, 46-61 (2006)

Variation of Fundamental Constants
V. V. Flambaum
Proceedings of the XX International Conference on Atomic Physics (ICAP 2006), Innsbruck, Austria, July 16-21, 2006, eds. Christian Roos, Hartmut Häffner, and Rainer Blatt, AIP Conference Proceedings **869**, 29-36 (2006)

Models for Extracting *N** Parameters from Meson-Baryon Reactions
T.-S. H. Lee
Proceedings of the Workshop on the Physics of Excited Nucleons (NSTAR2005), Tallahassee, FL, October 12-15, 2005, eds. S. Capstick, V. Crede, and P. Eugenio (World Scientific 2006) pp. 1-15

Quantum Monte Carlo Studies of Bound and Unbound Nuclear States
Kenneth M. Nollett
Conference on Nuclei at the Limits (NS06), Oak Ridge, TN, July 24-28, 2006, Book of Abstracts, p. 115 (2006)

Scattering and Reactions in Ab Initio Nuclear Theory
Kenneth M. Nollett
2006 Annual Meeting of the Division of Nuclear Physics of the American Physical Society, Nashville, TN, October 25-28, 2006; Bull. Am. Phys. Soc. **51**, 10 (2006)

Ab Initio Calculations of Electroweak Matrix Elements
Muslema Pervin, R. B. Wiringa, Steven C. Pieper, and Kenneth M. Nollett
2006 Annual Meeting of the Division of Nuclear Physics of the American Physical Society, Nashville, TN, October 25-28, 2006; Bull. Am. Phys. Soc. **51**, 20 (2006)

A Unitary and Relativistic Model for $\pi\eta N$ and $\pi\pi N$ Photoproduction
Alvin Kiswandhi, Simon Capstick, and T.-S. Harry Lee
2006 Annual Meeting of the Division of Nuclear Physics of the American Physical Society, Nashville, TN, October 25-28, 2006; Bull. Am. Phys. Soc. **51**, 28 (2006)

N-Δ Transition Form Factors
Mandar S. Bhagwat
2006 Annual Meeting of the Division of Nuclear Physics of the American Physical Society, Nashville, TN, October 25-28, 2006; Bull. Am. Phys. Soc. **51**, 80 (2006)

Physics Division
Argonne National Laboratory
9700 South Cass Avenue, Bldg. 203
Argonne, IL 60439-4843

www.anl.gov

UChicago ▶
Argonne LLC

A U.S. Department of Energy laboratory
managed by UChicago Argonne, LLC